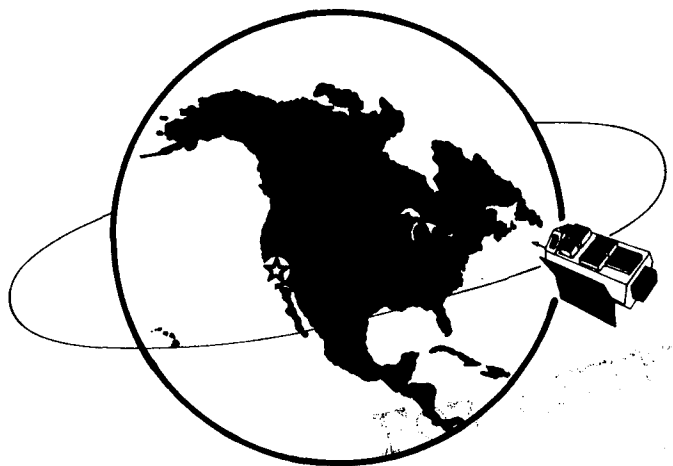


NASA CP-2376  
U.7

# 19TH INTERNATIONAL COSMIC RAY CONFERENCE

LA JOLLA, USA AUGUST 11-23, 1985

NASA-CP-2376-VOL-7  
19850027655



CONFERENCE  
PROGRAM  
SESSIONS  
VOL. 7

NOT TO BE TAKEN FROM THE BOOK

LIBRARY COPY

LIBRARY OF THE  
NASA  
GODDARD SPACE FLIGHT CENTER  
GREENBELT, MARYLAND  
20771



# 19TH INTERNATIONAL COSMIC RAY CONFERENCE

LA JOLLA, USA AUGUST 11-23, 1985

## CONFERENCE PAPERS



**HE**  
SESSIONS  
VOL. 7

**PUBLICATION COMMITTEE**

**F.C. Jones, Chm.**

**J. Adams**

**G.M. Mason**

**NASA Conference Publication 2376**

**Published by  
Scientific and Technical Information Branch  
National Aeronautics and Space Administration  
Washington, D.C. 20546**

**August 1985**

**For sale by the National Technical Information Service, Springfield, VA 22151**



## PREFACE

The 19th International Cosmic Ray Conference, under the auspices of the Cosmic Ray Commission of the International Union of Pure and Applied Physics, is being held on the campus of the University of California, San Diego, on 11 through 23 August 1985. In keeping with the tradition begun in 1971 by the Australian organizers of the 12th ICRC, the Proceedings of this conference are appearing in two sets of volumes. The first set, consisting of volumes 1 through 8, is being distributed to all participants at the beginning of the conference. This set contains the contributed papers. The second set, distributed after the conference, contains invited, rapporteur, and highlight papers. The papers are reproduced here exactly as they were received from the authors, without refereeing.

For the 19th ICRC, the scientific program was organized according to three major divisions-- OG (cosmic rays and gamma rays of Galactic Origin), SH (Solar and Heliosphere), and HE (High Energy). Technical papers are included in each of the three divisions.

This conference depended on funds from several agencies of the United States government, including major financial support from the National Aeronautics and Space Administration and support from the National Science Foundation, the Department of Energy, and the Air Force Geophysics Laboratory. Important financial support also came from the Center for Astrophysics and Space Sciences of the University of California, San Diego, from the California Space Institute of the University of California, from the Department of Physics and Astronomy of the University of Maryland, College park, from the International Union for Pure and Applied Physics, and from several corporate sponsors who will be acknowledged by name in the post-conference volumes.

We appreciate the confidence placed in the conference organizers by the Cosmic Ray Commission, and acknowledge with thanks the role of the Commission members in setting up the rules for the conference and in advising the organizers during its planning.

We are grateful to all of the members of the various organizing committees listed at the front of this volume. The three Program Committees went to great effort to organize a coherent scientific program and to schedule four parallel sessions with a minimum of conflicts. The Local Organizing Committee has worked long and hard to ensure efficient and hospitable accommodations for all the participants, both in the scientific sessions and outside them. The Publications Committee not only took great pains to assemble these volumes but also maintained an orderly data base of papers and authors which was extremely helpful to the program committees. The General Organizing Committee made important contributions of ideas and efforts to make the conference possible; this committee included international representation from all of North America, thus the departure from the traditional name of National Organizing Committee. And the entire effort was coordinated by the dedicated members of the Steering Committee.

Martin H. Israel, Chairman  
General Organizing Committee

August, 1985

## LETTER FROM THE EDITORS

This conference marks a departure from previous conferences in this series in that the publication of the Conference Papers was carried out an entire continent away from the activities of Local Organizing Committee. This posed some problems but, to the considerable surprise of the Publications Committee members, the one that was expected to be the most trouble turned out not to be significant. The overwhelming majority of those submitting papers and abstracts sent them to the correct address, not to La Jolla as was feared. We wish to thank our many authors for their alertness and commend them for handling a complicated situation so well.

There are eight volumes to be distributed to the conference participants in addition to the Conference Program and Author Index: three volumes for OG, two for SH and three for HE. the detailed makeup of these volumes is described in the prefaces written by the Scientific Program chairmen for their respective volumes. Out of some 1100 abstracts that were accepted by the Scientific Program Committees for inclusion in the conference some 929 papers were finally received in time for inclusion in the Conference Papers. This represents a response of approximately 84 percent, a modest improvement. Even if one excludes the 42 one page papers that should be considered as "confirming abstracts", even though there was no such formal category, the response was somewhat higher than that of recent years. We attribute this to the carrot of a later deadline than before coupled with the stick of there being no printing of post deadline contributed papers. We believe that this decision of the General Organizing Committee was a wise one. Of course invited, rapporteur, and highlight talks will be printed in volumes to be distributed to the participants after the conference as usual.

The Publications Committee had much generous help in performing its duties: from Goddard Space Flight Center we had the help of B. Glasser, L. Harris, E. Schronce, N. Smith, J. Esposito and T. Smith. From the Naval Research Laboratory we were helped by T. Mazzotta, and at the University of Maryland M. L. Snidow and J. Mucha gave much needed assistance. Special thanks are due to Caryl Short, the lone staff member of the Publications Committee. She maintained the computer data base, organized the abstracts as they arrived, and kept track of the papers themselves to see that the finally arrived in the right place at the right time. Without her help the job would have been far more difficult than it was.

PUBLICATIONS COMMITTEE

August, 1985

Frank C. Jones, Chm.  
Jim Adams  
Glen M. Mason

THE SESSIONS  
VOLUME VII

18th INTERNATIONAL COSMIC RAY CONFERENCE  
LA JOLLA, USA  
AUGUST 11-23, 1985

INTERNATIONAL UNION OF PURE AND APPLIED PHYSICS  
MEMBERS OF THE COMMISSION ON COSMIC RAYS OF IUPAP

A.E. Chudakov, Chm.	P.H. Fowler	T.O. Montmerle	B.V. Sreekantan
F.B. McDonald	D. Hovestadt	H. Moraal	K. Suga
G.C. Castagnoli	J. Kota	J.R. Prescott	J. Wdowczyk

STEERING COMMITTEE

F. McDonald, Chm.	T. Gaisser	F. Jones	R. Mewaldt
G. Burbage	M. Israel	R. Lingenfelter	L. Peterson
M. Forman			

GENERAL ORGANIZING COMMITTEE

M. Israel, Chm.	V. Jones	B. Price	J. Simpson
M. Bercovitch	S. Krimigis	R. Ramaty	E. Stone
P. Freier	J. Kurfess	F. Reines	D. Venkatesan
R. Gall	J. Lockwood	M. Shapiro	J. Waddington
R. Jokipii	P. Meyer	M. Shea	S. White
L. Jones			

PROGRAM COMMITTEES

<b>OG SESSIONS</b>	<b>SH SESSIONS</b>	<b>HE SESSIONS</b>	<b>PUBLICATIONS</b>
R. Mewaldt, Chm.	M. Forman, Chm.	T. Gaisser, Chm.	F. Jones, Chm.
G. Cassidy	H. Hudson	K. Lande	J. Adams
C. Fichtel	G. Mason	J. Linsley	G. Mason
A. Harding	B. McKibben	E. Loh	
J. Matteson	M. Pomerantz	G. Yodh	
D. Muller			
W. Webber			

LOCAL ORGANIZING COMMITTEE

L. Peterson, Chm.	A. Buffington	J. Linsley	O. Piccioni
G. Burbidge	M. Burbidge	K. Marti	M. Thiemens
R. Lingenfelter	W. Fillius	G. Masek	W. Thompson
R. Rothschild	R. Gall	J. Matteson	H. Ticho
J. Arnold	R. Gould	C. McIlwain	R. White
W. Baity	H. Hudson	R. Mewaldt	

Sponsored by

National Aeronautics and Space Administration

National Science Foundation

Department of Energy

Center for Astrophysics and Space Science, University of California, San Diego

California Space Institute, University of California

Department of Physics and Astronomy, University of Maryland, College Park

## Preface to HE Volumes

Papers contributed to the XIX International Cosmic Ray Conference were arranged into three major divisions: Origin and Galactic phenomena (OG), Solar and Heliospheric (SH), and High Energy (HE). The HE sessions at this conference comprise all the subjects formerly included in the muon and neutrino sessions (MN) and the extensive air shower sections (EA) as well as those on high energy interactions, new particle searches and emulsion chamber results, which were previously classified in HE. In addition, technical papers have not been classified separately, but have been inserted in appropriate subject sections. All the papers now classified as HE are contained in volumes 6, 7 and 8.

Volume 6 includes sessions HE1 (cross sections and interactions of particles and nuclei at high energy) and HE3 (emulsion chamber results). Extensive air shower papers (HE4) are in volume 7. Papers on muons and neutrinos (HE5), searches for new particles and processes (HE6) and some on new techniques (HE7) are in volume 8.

Altogether some 380 abstracts were received for the HE sections. These were divided into the 25 groups listed in the tables of contents of the HE volumes. (These groups correspond only approximately to the 26 contributed paper sessions at the conference.)

Four rapporteurs were selected to cover the subjects of the HE sessions:

L.W. Jones	High Energy Interactions and New Particle Searches (HE1 & HE6);
M. Shibata	Emulsion Chamber Observations and Interpretation (HE3);
R.W. Clay	Extensive Air Showers (HE4);
K. Sivaprasad	Muons and Neutrinos (HE5).

The written versions of the rapporteur talks are contained in the post-conference volume together with highlight and invited papers.

The work of arranging the HE program was shared by a committee consisting of

T.K. Gaisser (Bartol), Chairman  
K. Lande (Pennsylvania)  
E.C. Loh (Utah)  
J. Linsley (New Mexico)  
G.B. Yodh (Maryland)

This conference is the 19th in a series. Previous conferences in this series were held at:

Cracow, Poland	-	1947
Corno, Italy	-	1949
Bagneres-de-Bigorre, France	-	1953
Guanajuato, Mexico	-	1955
Varenna, Italy	-	1957
Moscow, USSR	-	1959
Kyoto, Japan	-	1961
Jaipur, India	-	1963
London, UK	-	1965
Calgary, Canada	-	1967
Budapest, Hungary	-	1969
Hobart, Australia	-	1971
Denver, USA	-	1973
Munchen, FRG	-	1975
Plovdiv, Bulgaria	-	1977
Kyoto, Japan	-	1979
Paris, France	-	1981
Bangalore, India	-	1983

---

HE 4.1  
EXTENSIVE AIR SHOWER THEORIES AND  
SIMULATIONS

---

PAPER CODE		PAGE
HE 4.1-2	ELECTRONS, MUONS AND HADRONS IN EXTENSIVE AIR SHOWERS AND HOW DO THEY DEPEND ON NUCLEAR INTERACTION MODEL (PART II)  JA WROTNIAK,GB YODH	1
HE 4.1-3	ANALYSIS OF EQUI-INTENSITY CURVES AND NU DISTRIBUTIONS OF EAS  G TANAHASHI	5
HE 4.1-5	ANALYSIS OF THE HADRONIC COMPONENT IN E. A. S. OBSERVED AT 700 G.CM**2 BY A SCALE BREAKING MODEL  J PROCUREUR,JN STAMENOV,PV STAVREV SZ USHEV	9
HE 4.1-7	ELECTRONS, MUONS AND HADRONS IN EXTENSIVE AIR SHOWERS AND HOW DO THEY DEPEND ON THE NUCLEAR INTERACTION MODEL (PART I)  JA WROTNIAK,GB YODH	12
HE 4.1-8	SIMULATION OF EAS PROPERTIES ON THE BASIS OF HIGH ENERGY INTERACTION MODEL DEDUCED FROM THE ACCELERATOR DATA  G KUBIAK,J SZABELSKI,J WADOWCZYK	16
HE 4.1-9	NEW ASPECTS IN NUCLEON-NUCLEUS COLLISIONS AND EAS PROPERTIES AROUND 10**6 GEV  JN CAPDEVIELLE,J GAWIN	20
HE 4.1-10	SMALL AIR SHOWERS AND COLLIDER PHYSICS  JN CAPDEVIELLE,J GAWIN,B GROCHALSKA	24

x  
VOLUME 7

- HE 4.1-11 HIGH ENERGY HADRONS IN EXTENSIVE AIR SHOWERS 28  
SC TONWAR
- HE 4.1-13 DEPENDENCE OF THE AVERAGE SPATIAL AND ENERGY CHARACTERISTICS OF THE HADRON-LEPTON CASCADE ON THE STRONG INTERACTION PARAMETERS AT SUPERHIGH ENERGIES 32  
NG BOYAADJIAN, PYU DALLAKYAN, AP GARYAKA  
EA MAMIDJANIAN
- HE 4.1-14 HADRONIC COMPONENTS OF EAS BY RIGOROUS SADDLE POINT METHOD IN THE ENERGY RANGE BETWEEN  $10^{*5}$  AND  $10^{*8}$  GEV 36  
M SINHA, S ROY
- HE 4.1-15 ABOUT THE INCREASE OF THE LARGE P1 PROCESSES FRACTION IN HA INTERACTIONS AT ENERGIES  $5 \cdot 10^{*14}$  -  $10^{*16}$  EV ACCORDING TO THE DATA ON EAS HADRONS 40  
TV DANILOVA, AG DUBOVY, AD ERLYKIN  
NM NESTEROVA, AP CHUBENKO
- HE 4.1-17 PHENOMENOLOGY OF SOFT HADRON INTERACTIONS AND THE RELEVANT EAS DATA 44  
NN KALMYKOV, GB KRISTIANSEN, MV MOTOVA
- HE 4.1-19 THE MAXIMUM DEPTH OF SHOWER WITH  $E_{SUB} > 10^{*17}$  EV ON AVERAGE CHARACTERISTICS OF EAS DIFFERENT COMPONENTS 48  
AV GLUSHKOV, NN EFIMOV, IT MAKAROV  
MI PRAVDIN, LG DEDENKO
- HE 4.1-20 SENSITIVITY OF DEPTH OF MAXIMUM AND ABSORPTION DEPTH OF EAS TO HADRON PRODUCTION MECHANISM 52  
RA ANTONOV, VI GALKIN, LA HEIN  
IP IVANENKO, BL KANEVSKY, VA KUZMIN



---

HE 4.2  
EXTENSIVE AIR SHOWER CORES AND DENSITY  
SPECTRA

---

PAPER CODE		PAGE
HE 4.2-1	A CRITICAL ANALYSIS OF AIR SHOWER STRUCTURE FUNCTIONS AND SIZE SPECTRUM MEASUREMENTS WITH THE NBU AIR SHOWER ARRAY  N CHAUDHURI,DK BASAK	56
HE 4.2-2	MEASUREMENT OF THE LOCAL DENSITY SPECTRUM  ZH LIU,JG LIU,GJ LI,GZ BAI,QX GENG J LING,WE HAZEN,ES HAZEN	60
HE 4.2-3	CHARACTER OF ENERGY FLOW IN AIR SHOWER CORE  K MIZUSHIMA,K ASAKIMORI,T MAEDA T KAMEDA,Y MISAKI	64
HE 4.2-4	OBSERVATION OF EAS USING A LARGE WATER TANK  K INOUE,H SAKUYAMA,N SUZUKI,T SUZUKI	68
HE 4.2-5	THE DEVELOPMENT OF AIR SHOWER IN THE IRON ABSORBER  M HAZAMA,S DAKE,K HARADA,M KAWAMOTO M SAKATA,T SUGIHARA	69
HE 4.2-6	APPLICATION OF PHOTODIODES TO THE DETECTION OF ELECTROMAGNETIC BURSTS  Y FUKUSHIMA,T SAITO,M SAKATA,M SHIMA Y YAMAMOTO	73
HE 4.2-9	CORE STRUCTURE OF EAS IN 10**15EV TO 10**17EV  T HARA,Y HATANO,N HAYASHIDA,T KIFUNE M NAGANO,G TANAHASHI	77

xii  
VOLUME 7

- HE 4.2-10 PARTICLE DISTRIBUTIONS IN  $\sim 10^{14}$  -  $10^{16}$  EV AIR SHOWER CORES AT SEA LEVEL 81  
AL HODSON, AG ASH, RM BULL
- HE 4.2-11 THEORETICAL STUDY OF EAS CORE STRUCTURE 85  
L POPOVA
- HE 4.2-15 MONTE CARLO SIMULATIONS OF ELECTRON LATERAL DISTRIBUTIONS IN THE CORE REGION  $10^{13}$  -  $10^{16}$  EV AIR SHOWERS 89  
AG ASH
- HE 4.2-16 COMPARISON OF SIMULATION RESULTS WITH SEA-LEVEL EXPERIMENTAL DATA ON  $10^{14}$  -  $10^{16}$  AIR SHOWER CORES 93  
AG ASH
- HE 4.2-18 PARTICLE DISTRIBUTION IN  $\sim 10^{13}$  -  $10^{16}$  EV AIR SHOWER CORES AT MOUNTAIN ALTITUDE AND COMPARISON WITH MONTE CARLO SIMULATIONS 94  
AG ASH
- HE 4.2-19 TSKHRA-TSKARD COMPLEX INTENDED FOR THE INVESTIGATION OF EAS SPATIAL CHARACTERISTICS NEAR AXIS 98  
YA GROMOV, YG VERBETSKI, DM KOTLYAREVSKI  
LP GARSEVANISHVILI, AA NOVALOV  
IV PAZIASHVILI, NS RUSISHVILI  
LS KHACHATURYAN, NG TATALASHVILI  
L KHACHATURYAN, GZ STEMANETYAN

---

HE 4.3  
EXTENSIVE AIR SHOWER MUONS AND ELECTRONS

---

PAPER CODE		PAGE
HE 4.3-1	A NEW STUDY OF SHOWER AGE DISTRIBUTION IN NEAR VERTICAL SHOWERS BY NBU AIR SHOWER ARRAY  N CHAUDHURI,DK BASAK,GC GOSWAMI,B GHOSH	101
HE 4.3-2	A NEW STUDY OF MUONS IN AIR SHOWERS BY NBU AIR SHOWER ARRAY  N CHAUDHURI,N MUKHERJEE,S SARKAR DK BASAK,B GHOSH	105
HE 4.3-3	LATERAL DISTRIBUTION OF ELECTRONS OF AIR SHOWERS  K ASAKIMORI,T MAEDA,T KAMEDA K MIZUSHIMA,Y MISAKI	107
HE 4.3-4	DETAILED STUDIES OF THE ELECTRON LATERAL DISTRIBUTION IN EXTENSIVE AIR SHOWERS WITH ENERGIES AROUND $10^{16}$ EV  T DZIKOWSKI,J GAWIN,J WADOWCZYK	111
HE 4.3-6	STUDY OF MUONS NEAR SHOWER CORES AT SEA LEVEL USING THE E594 NEUTRINO DETECTOR  JA GOODMAN,SC GUPTA,H FREUDENREICH K SIVAPRASAD,SC TONWAR,GB YODH RW ELLSWORTH,MC GOODMAN,D BOGERT R BURNSTEIN,R FISK,S FUESS,J MORFIN T OHSKA,J BOFILL,W BUSZA,R MAGAHIZ T MATTISON,A MUKHERJEE,L OSBORNE,R PITT L ROSENSON,A SANDACZ,M TARTAGLIA FE TAYLOR,R VERDIER,S WHITAKER,GB YEH B STRONGIN,M ABOLINS	114
HE 4.3-7	CORRELATION OF HIGH ENERGY MUONS WITH PRIMARY COMPOSITION IN EXTENSIVE AIR SHOWER  C CHO,S HIGASHI,N HIRAOKA,S OZAKI T SATO,T SUWADA,T TAKAHASHI,H UMEDA	115

xiv  
VOLUME 7

HE 4.3-8	MEASUREMENT OF LOW ENERGY MUONS IN EAS AT ENERGY REGION LARGER THAN $10^{17}$ EV	119
	Y MATSUBARA, T HARA, N HAYASHIDA, K KAMATA M NAGANO, H OHOKA, G TANAHASHI, T TESHIMA	
HE 4.3-9	MUON FLUCUATION STUDIES OF EAS $> 10^{17}$ EV	123
	PR BLAKE, M LUKSYS, WF NASH, AJ SEPHTON	
HE 4.3-10	AVERAGE FEATURES OF THE MUON COMPONENT OF EAS $\geq 10^{17}$ EV	127
	PR BLAKE, M LUKSYS, WF NASH, AJ SEPHTON	
HE 4.3-11	MEASUREMENT OF SHOWER ELECTRONS AND MUONS USING A SMALL AIR SHOWER ARRAY	131
	SK CHAN, LK NG	
HE 4.3-12	THE LONGITUDINAL DEVELOPMENT OF MUONS IN COSMIC RAY AIR SHOWERS AT ENERGIES $10^{15} - 10^{17}$ EV	135
	T CHEUNG, PK MACKEDOWN	
HE 4.3-13	TOPOLOGICAL ASPECTS OF AGE PARAMETER	139
	JN CAPDEVIELLE, J GAWIN	
HE 4.3-14	MONTE CARLO SIMULATION OF E.A.S. GENERATED BY $10^{14} - 10^{16}$ EV PROTONS	143
	EJ FENYVES, BC YUNN, T STANEV	
HE 4.3-15	LATERAL DISTRIBUTION OF CHARGED PARTICLES IN EAS	147
	LG DEDENKO, GV KULIKOV, VI SOLOVJEVA VP SULAKOV	

HE 4.3-16 LATERAL DISTRIBUTION OF HIGH ENERGY  
MUONS IN EAS OF SIZES  $N \text{ SUB } E \sim 10^{**5}$  AND  
 $N \text{ SUB } E \sim 10^{**6}$

151

YUN BAZHUTOV, GB ERMAKOV, YUA FOMIN  
VI ISAEV, ZV JAROCHKINA, NN KALMYKOV  
BA KHRENOV, GB KHRISTIENSEN, GV KULIKOV  
MV MOTOVA, IP PROSHKINA, VP RUKOVICHKIN  
VI SOLOVJEVA, VP SULAKOV, AV SHKURENKOV  
AV TRUBITSYN, VV VASHKEVICH

---

HE 4.4  
CERENKOV SIGNALS AND EXTENSIVE AIR  
SHOWER ENERGY CALIBRATION

---

PAPER CODE		PAGE
HE 4.4-1	ENERGY CALIBRATION OF THE FLY'S EYE DETECTOR  RM BALTRUSAITIS, GL CASSIDAY, R COOPER R ELBERT, PR GERHARDY, VD KOSLOV, EC LOH Y MIZUMOTO, P SOKOLSKY, D STECK	155
HE 4.4-2	THE STRUCTURE OF EAS AT $E > 0.1$ EEV  RM BALTRUSAITIS, GL CASSIDAY, R COOPER JW ELBERT, PR GERHARDY, EC LOH, Y MIZUMOTO P SOKOLSKY, D STECK	159
HE 4.4-4	STANDARD VALUE FOR THE RADIATION LENGTH IN AIR  J LINSLEY, J LINSLEY	163
HE 4.4-5	LONGITUDINAL TRIAL FUNCTIONS AND THE COSMIC RAY ENERGY SCALE  J LINSLEY	167
HE 4.4-7	EAS DEVELOPMENT CURVE AT ENERGY OF $10^{16}$ - $10^{18}$ EV MEASURED BY OPTICAL CERENKOV LIGHT  T HARA, M DAIGO, M HONDA, K KAMATA T KIFUNE, Y MIZUMOTO, M NAGANO, Y OHNO G TANAHASHI	171
HE 4.4-8	MISSING ENERGIES AT PAIR CREATION  AA EL-ELA, S HASSAN, ER BAGGE	175
HE 4.4-9	TRANSITION EFFECT OF AIR SHOWER PARTICLES IN PLASTIC SCINTILLATORS  K ASAKIMORI, T MAEDA, T KAMEDA K MIZUSHIMA, Y MISAKI	179

- HE 4.4-10 THE SYSTEM OF EAS TIME ANALYSIS 183  
AZ KHALAFYAN, VM MKHITARYAN, JS OGANEZOVA  
GL BASHINDJAGHYAN, NB SINEV, LI SARYCHEVA
- HE 4.4-13 ON THE DETERMINATION OF THE DEPTH OF EAS 187  
DEVELOPMENT MAXIMUM USING THE LATERAL  
DISTRIBUTION OF CERENKOV LIGHT AT  
DISTANCES < 150 M FROM EAS AXIS  
N ALIEV, T ALIMOV, M KAKHKHAROV  
BM MAKHMUDOV, N RAKHIMOVA, R TASHPULATOV  
NN KALMYKOV, GB KRISTIANSEN, VV PROSIN
- HE 4.4-14 STUDY OF THE ENERGY SPECTRUM OF PRIMARY 191  
COSMIC RAYS; EAS SIZE FLUCTUATIONS AT A  
FIXED PRIMARY ENERGY  
N ALIEV, T ALIMOV, N KAKHAROV, N KHAKIMOV  
N RAKHIMOVA, R TASHPULATOV  
GB KRISTIANSEN
- HE 4.4-15 STUDY OF THE SHOWER MAXIMUM DEPTH BY THE 195  
METHOD OF DETECTION OF THE EAS CERENKOV  
LIGHT PULSE SHAPE  
N ALIEV, T ALIMOV, M KAKHKHAROV  
N KHAKIMOV, BM MAKHMUDOV, N RAKHIMOVA  
R TASHPULATOV, GB KRISTIANSEN, VV PROSIN  
VYU ZHUKOV
- HE 4.4-16 ANALYSIS OF CERENKOV PULSES RECORDED 199  
SIMULTANEOUSLY AT TWO SITES  
DF LIEBING, JR PATTERSON
- HE 4.4-17 PRELIMINARY RESULTS OF THE CERENKOV EAS 203  
FLASHES OBSERVATIONS ON THE MULTIMIRROR  
INSTALLATION OF THE CRIMEAN  
ASTROPHYSICAL OBSERVATORY  
BM VLADIMIRSKY, YL ZYSKIN, YI NESHFOR  
AA STEPANIAN, VP FOMIN, VG SHITOV
- HE 4.4-18 THE EXPERIMENTAL CASCADE CURVES OF EAS 207  
AT  $E > 10^{17}$  EV OBTAINED BY THE METHOD  
OF DETECTION OF CERENKOV PULSE SHAPE  
YUA FOMIN, NN KALMYKOV, GB KRISTIANSEN  
MV MOTOVA, YUA NECHIN, VV PROSIN, VY ZHUKOV  
NN EFIMOV, VM GRIGORIEV, ES NIKIFOROVA

HE 4.4-19 LATERAL-ANGULAR AND TEMPORAL  
CHARACTERISTICS OF EAS OPTICAL RADIATION

211

TA CHUYKOVA, VI GALKIN, IP IVANENKO  
TM ROGANOVA



---

HE 4.5  
GAMMA-RAY AIR SHOWERS

---

PAPER CODE		PAGE
HE 4.5-1	THE IDENTIFICATION OF GAMMA-RAY INDUCED EAS  PR BLAKE,WF NASH	215
HE 4.5-3	MUONS IN GAMMA SHOWERS  T STANEV,CP VANKOV,F HALZEN	219
HE 4.5-4	MUON SPECTRUM IN AIR SHOWERS INITIATED BY GAMMA RAYS  SA STEPHENS,RE STREITMATTER	223
HE 4.5-5	DEVELOPMENT OF ELECTROMAGNETIC CASCADES IN THE ATMOSPHERE INCLUDING THE LANDAU-POMERANCHUK-MIGDAL EFFECT  RE STREITMATTER,SA STEPHENS	227
HE 4.5-6	ELECTROMAGNETIC AND MUONIC STRUCTURE OF SHOWERS INITIATED BY GAMMA-RAYS AND BY HADRONS  AMM HILLAS	231
HE 4.5-7	THE MUON CONTENT OF GAMMA-RAY SHOWERS  PG EDWARDS,RJ PROTHEROE	235
HE 4.5-9	THE HUMP IN THE CERENKOV LATERAL DISTRIBUTION OF GAMMA RAY SHOWERS  S SINHA,MVS RAO	239
HE 4.5-10	SIMULATION OF GAMMA-INITIATED SHOWERS  JN STAMENOV,K VANCOV,T VODENICHAROVA	243
HE 4.5-11	PHENOMENOLOGICAL CHARACTERISTICS OF ELECTRON COMPONENT IN GAMMA-QUANTA INITIATED SHOWERS  SI NIKOLSKY,JN STAMENOV,SZ USHEV	247

xx  
VOLUME 7

- |           |  |     |
|-----------|--|-----|
| HE 4.5-13 | A THREE-DIMENSIONAL MONTE CARLO<br>CALCULATION OF THE PHOTON INITIATED<br>SHOWERS AND KIEL RESULT    | 251 |
|           | A OKADA,Y MURAKI   |     |
| HE 4.5-14 | CONSTRUCTION OF A COSMIC RAY AIR SHOWER<br>TELESCOPE   | 252 |
|           | LK NG,SK CHAN  |     |
| HE 4.5-15 | AN UNDERGROUND COSMIC RAY MUON TELESCOPE<br>FOR OBSERVATION OF COSMIC RAY ANISOTROPY                 | 256 |
|           | YW LEE,LK NG   |     |
| HE 4.5-16 | NUCLEAR CASCADES IN ELECTROMAGNETIC<br>SHOWERS PRODUCED BY PRIMARY GAMMA-QUANTA<br>IN THE ATMOSPHERE | 260 |
|           | TV DANILOVA,AD ERLYKIN,AV MIRONOV<br>EI TUKISH   |     |

---

HE 4.6  
EXTENSIVE AIR SHOWER TECHNIQUES

---

PAPER CODE		PAGE
HE 4.6-2	ON THE POSSIBILITIES OF LARGE-SCALE RADIO AND FIBER OPTICS DETECTORS IN COSMIC RAYS  GA GUSEV, MA MARKOV, IM ZHELEZNYKH	264
HE 4.6-3	RADIO SIGNALS FROM VERY LARGE AIR SHOWERS  K SUGA, F KAKIMOTO, K NISHI	268
HE 4.6-4	ON THE PRODUCTION MECHANISM OF RADIO-PULSES FROM LARGE EXTENSIVE AIR SHOWERS  P DATTA, KM PATHAK	272
HE 4.6-5	A NEW STUDY ON THE EMISSION OF EM WAVES FROM LARGE EAS  KM PATHAK, GKD MAZUMDAR	276
HE 4.6-6	AIR FLUORESCENCE DETECTION OF LARGE AIR SHOWERS BELOW THE HORIZON  P HALVERSON, T BOWEN	280
HE 4.6-7	INVESTIGATION OF COSMIC RAYS IN VERY SHORT TIME SCALES  J PELTONEN, E VALTONEN, JJ TORSTI H ARVELA, M LUMME, M NIEMINEN, E VAINIKKA	284
HE 4.6-8	A FACILITY FOR INVESTIGATION OF MULTIPLE HADRONS AT COSMIC-RAY ENERGIES  E VALTONEN, JJ TORSTI, H ARVELA, M LUMME M NIEMINEN, J PELTONEN, E VAINIKKA	288
HE 4.6-9	A POSSIBLE EAS ARRAY ABOVE THE SOUDAN II DETECTOR  K SIVAPRASAD	292

HE 4.6-10	FAST SCINTILLATION COUNTER SYSTEM AND PERFORMANCE	293
	H SASAKI, A NISHIOKA, M KUSUNOSE T NAKATSUKA, T NAKATSUKA, T HORIKI Y HATANO	
HE 4.6-11	PERFORMANCE OF A LOCAL ELECTRON DENSITY TRIGGER TO SELECT EXTENSIVE AIR SHOWERS AT SEA LEVEL	297
	T ABBAS, J MADANI, F ASHTON	
HE 4.6-13	MICROPROCESSOR-BASED SINGLE PARTICLE CALIBRATION OF SCINTILLATION COUNTER	301
	GKD MAZUMDAR, KM PATHAK	
HE 4.6-14	SAMARKAND COMPLEX SET-UP FOR INVESTIGATION OF COSMIC RAY VARIATION IN THE ENERGY RANGE OF $7.10^{*}9 - 10^{*}15$ EV	304
	LI DORMAN, F VALIHODZHAEV, BM MAKHMUDOV N SIRODZHEV, R TASHPULATOV	
HE 4.6-15	RADIO WAVE EMITTED BY AN EXTENSIVE AIR SHOWERS IN 10 KHZ TO 1 MHZ REGION	308
	J NISHIMURA	

---

HE 4.7  
EXTENSIVE AIR SHOWER ARRIVAL TIMES AND  
MINI-ARRAYS

---

PAPER CODE		PAGE
HE 4.7-1	STRUCTURE OF THE SHOWER DISK OBSERVED AT MT. NORIKURA  H SASAKI, A NISHIOKA, N OHMORI, M KUSUNOSE T NAKATSUKA, T HORIKI, Y HATANO	312
HE 4.7-2	STRUCTURE OF AIR SHOWER DISK NEAR THE CORE  N INOUE, M KAWAMOTO, Y MISAKI, T MAEDA T TAKEUCHI, Y TOYODA	316
HE 4.7-3	PROPERTIES OF 10**18 - 10**19 EV EAS AT FAR CORE DISTANCE  M TESHIMA, M NAGANO, T HARA, Y HATANO N HAYASHIDA, CX HE, M HONDA, F ISHIKAWA K KAMATA, Y MATSUBARA, M MORI, H OHOKA G TANAHASHI	320
HE 4.7-4	LONGITUDINAL DEVELOPEMENT OF MUONS IN LARGE AIR SHOWERS STUDIED FROM THE ARRIVAL TIME DISTRIBUTIONS MEASURED AT 900M ABOVE SEA LEVEL  F KAKIMOTO, I TSUCHIMOTO, T ENOKI, K SUGA K NISHI	324
HE 4.7-5	ARRIVAL TIME DISTRIBUTIONS OF ELECTRONS IN AIR SHOWERS WITH PRIMARY ENERGIES ABOVE 10**18 EV OBSERVED AT 900M SEA LEVEL  F KAKIMOTO, I TSUCHIMOTO, T ENOKI, K SUGA K NISHI	328
HE 4.7-6	THE THICKNESS OF THE SHOWER DISC AS OBSERVED IN SHOWERS PRODUCED BY PRIMARIES ABOVE 10**19 EV  MA LAWRENCE, AA WATSON, AA WEST	332

HE 4.7-7	METHODS FOR ROOF-TOP MINI-ARRAYS	336
	WE HAZEN,ES HAZEN	
HE 4.7-8	EXPECTED RATES WITH MINI-ARRAYS FOR AIR SHOWERS	339
	WE HAZEN	
HE 4.7-9	FAST SCINTILLATION COUNTER PREAMPLIFIER FOR THE OBSERVATION OF LINSLEY EFFECT	343
	LK NG	
HE 4.7-10	A MINI-ARRAY FOR LARGE AIR SHOWERS	347
	LK NG,LK NG,SK CHAN,WE HAZEN,ES HAZEN	
HE 4.7-12	A NOTE ON SOME STATISTICAL PROPERTIES OF THE RISE TIME PARAMETERS USED IN MUON ARRIVAL TIME MEASURES	351
	DJ VAN DER WALT,EJ DE VILLIERS	
HE 4.7-13	SUB-LIMINAL PULSES FROM COSMIC RAY AIR SHOWERS	355
	J LINSLEY	
HE 4.7-14	THICKNESS OF THE PARTICLE SWARM IN COSMIC RAY AIR SHOWERS	359
	J LINSLEY	
HE 4.7-15	STUDY OF THE TIME-DIFFERENTIATED PARTICLE FLUX DENSITY AT VARIOUS DISTANCES FROM EAS AXIS	363
	VG ATRASHKEVICH,RJ CHERNYKH,YUA FOMIN GK GARIPOV,GB KHRISTIANSEN,BV KULIKOV AP LEBEDEV,SJ MATSENOV,VJ NAZAROV AA SILAEV,VJ SOLOVYEVA,VP SULAKOV AV TRUBITSYN,OV VEDENEEV	

ELECTRONS, MUONS AND HADRONS IN EXTENSIVE AIR SHOWERS  
AND HOW DO THEY DEPEND ON NUCLEAR INTERACTION MODEL  
(Part II)

J.A.Wrotniak and G.B.Yodh

Department of Physics and Astronomy  
University of Maryland  
College Park, MD 20742, U.S.A.

Here we present some of the results of Monte Carlo simulations of extensive air showers for nuclear interaction models as outlined in our contribution HE 4.1-7 to this Conference.

In the notation used below, numbers in brackets ( ) denote mean square errors in last decimal digit units. k, M, G, T and E stand for appropriate powers of 10. For the scarcity of place, the radial data on showers are not included.

Table 1. Average shower size at 1000 g/cm<sup>2</sup>

E[eV]	Primary protons					Primary iron	
	F-Y00	M-Y00	M-F00	M-F01	R-F01	FF-Y00	RM-F00
20 T	1.09(6)k		1.17(5)k			.25(1)k	.31(1)k
100 T	10.8(5)k	11.6(5)k	8.5(4)k	10.7(4)k	10.2(6)k	2.12(4)k	2.41(4)k
500 T	88(3)k		64(3)k			22.3(6)k	21.8(3)k
2 P	539(20)k		331(14)k			165(4)k	139(3)k
10 P	3.21(6)M	2.99(7)M	2.28(6)M	2.69(8)M	2.21(7)M	1.47(5)M	1.08(2)M
50 P	20.2(4)M		15.2(4)M			10.9(1)M	7.7(2)M
200 P	92(1)M		69(2)M			58(1)M	40(1)M
1 E	507(7)M	519(5)M	411(10)M	451(7)M	391(6)M	378(4)M	261(4)M

Table 2. Fluctuations of the shower size at 1000 g/cm<sup>2</sup> (s.d.of Log{base 10} Ne)

E[eV]	Primary protons					Primary iron	
	F-Y00	M-Y00	M-F00	M-F01	R-F01	FF-Y00	RM-F00
20 T	.42		.44			.13	.12
100 T	.33	.33	.34	.35	.34	.13	.13
500 T	.22		.26			.12	.10
2 P	.18		.19			.08	.07
10 P	.13	.14	.17	.19	.17	.07	.07
50 P	.10		.15			.05	.05
200 P	.07		.11			.04	.05
1 E	.06	.05	.09	.09	.09	.03	.04

Table 3. Average depth of shower maximum ( $g/cm^2$ )

E[eV]	Primary protons					Primary iron	
	F-Y00	M-Y00	M-F00	M-F01	R-F01	FF-Y00	RM-F00
20 T	486(6)		481(5)			307(2)	306(2)
100 T	557(7)	562(7)	521(6)	537(7)	532(8)	377(2)	368(2)
500 T	621(7)		570(6)			447(3)	433(2)
2 P	698(10)		602(7)			509(3)	481(3)
10 P	735(6)	712(6)	653(5)	671(6)	639(7)	583(4)	535(3)
50 P	801(8)		708(7)			643(3)	587(3)
200 P	> 865(8)		729(6)			701(4)	622(4)
1 E	> 920(8)	> 872(7)	777(10)	784(6)	742(4)	773(5)	669(4)

Table 4. Average shower size at maximum (exactly: geometric mean values)

E[eV]	Primary protons					Primary iron	
	F-Y00	M-Y00	M-F00	M-F01	R-F01	FF-Y00	RM-F00
20 T	10.6(1)k		10.9(1)k			7.82(4)k	7.50(3)k
100 T	56.9(7)k	56.0(7)k	58.3(6)k	65.2(7)k	63.7(8)k	40.9(2)k	39.6(2)k
500 T	289(3)k		310(3)k			225(1)k	223(1)k
2 P	1.15(2)M		1.26(2)M			957(4)M	982(4)k
10 P	5.74(5)M	6.01(6)M	6.55(4)M	6.95(5)M	7.18(6)M	5.12(2)M	5.38(2)M
50 P	28.8(3)M		33.3(3)M			26.2(1)M	28.8(2)M
200 P	111(2)M		134(1)M			106(1)M	118(1)M
1 E	552(9)M	614(5)M	662(7)M	703(5)M	726(3)M	530(3)M	610(2)M

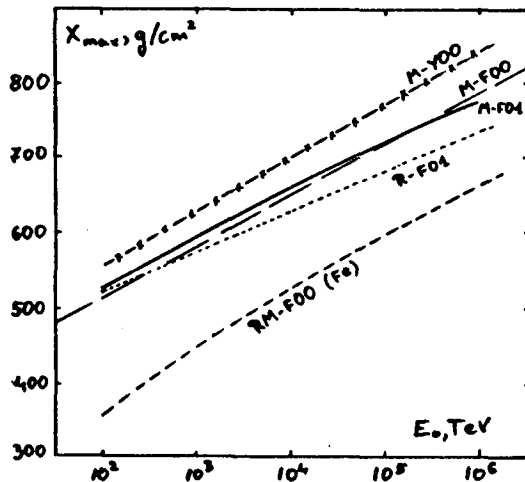


Fig.1. The depth of maximum for some of our models.

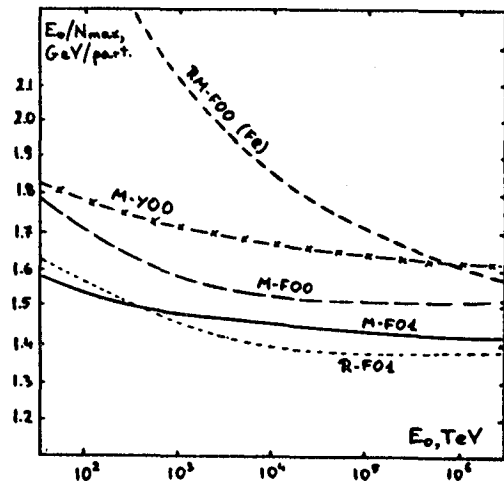


Fig.2. Energy per electron at the shower maximum.



Table 5. Fluctuations in shower size at maximum (s.d. of Log {base 10} Ne{max})

E[eV]	Primary protons					Primary iron	
	F-Y00	M-Y00	M-F00	M-F01	R-F01	FF-Y00	RM-F00
20 T	.10		.09			.032	.033
100 T	.08	.08	.08	.07	.07	.027	.029
500 T	.07		.06			.021	.022
2 P	.06		.05			.017	.014
10 P	.06	.06	.04	.05	.04	.015	.015
50 P	.06		.04			.014	.011
200 P	.07		.04			.009	.014
1 E	.07	.04	.04	.04	.02	.013	.008

Model M-F00 was also run at primary proton energy of 100 EeV (or  $10^{20}$  eV); 151 showers at 1000 g/cm<sup>2</sup> and 64 at 1400 g/cm<sup>2</sup> were simulated. Number of electrons at 1000 g/cm<sup>2</sup> was 59.5(5) G, its fluctuations .04, at maximum (average depth 906(5) g/cm<sup>2</sup>): 66.1(5) G and .024, respectively.

Table 6. The average muon number at 1000 g/cm<sup>2</sup>.

(a) at E &gt; 2 GeV

E[eV]	Primary protons					Primary iron	
	F-Y00	M-Y00	M-F00	M-F01	R-F01	FF-Y00	RM-F00
20 T	.36(1)k		.34(1)k			.64(1)k	.64(1)k
100 T	1.55(3)k	1.53(2)k	1.43(3)k	1.09(2)k	1.06(2)k	2.32(2)k	2.30(2)k
500 T	6.6(1)k		6.1(1)k			9.57(6)k	9.24(4)k
2 P	22.4(5)k		21.0(3)k			34.2(2)k	32.3(3)k
10 P	90(2)k	91(2)k	82(1)k	52.9(6)k	51.9(8)k	147.6(6)k	136.1(6)k
50 P	337(6)k		334(4)k			612(2)k	567(3)k
200 P	1.03(3)M		1.08(2)M			2.03(2)M	1.90(1)M
1 E	3.71(14)M	4.54(9)M	4.14(7)M	2.33(4)M	2.38(3)M	7.87(5)M	7.60(3)M

(b) at E &gt; 200 GeV

E[eV]	Primary protons					Primary iron	
	F-Y00	M-Y00	M-F00	M-F01	R-F01	FF-Y00	RM-F00
20 T	3.1		2.9			<.1	<.1
100 T	8.4	8.5	8.7	8.5	8.6	7.8	7.5
500 T	29		32			73	77
2 P	83		97			207	223
10 P	299	330	342	254	279	692	773
50 P	1.03 k		1.24 k			2.43 k	2.71 k
200 P	2.88 k		3.96 k			7.11 k	8.25 k
1 E	10.5 k	13.6 k	13.8 k	9.3 k	10.7 k	24.5 k	30.1 k

Table 7. The average hadron number above 2 GeV at 1000 g/cm<sup>2</sup>.

E[eV]	Primary protons					Primary iron	
	F-Y00	M-Y00	M-F00	M-F01	R-F01	FF-Y00	RM-F00
20 T	4.3(3)		4.8(3)			2.0(2)	4.2(3)
100 T	34(3)	38(3)	27(2)	17(2)	19(2)	11(1)	17(1)
500 T	244(11)		168(8)			88(3)	96(2)
2 P	1.33(6)k		701(32)			554(15)	500(13)
10 P	6.7(2)k	5.9(2)k	3.7(2)k	1.95(9)k	1.65(9)k	4.41(9)k	3.19(6)k
50 P	34(2)k		18.3(7)k			28.8(4)k	18.0(5)k
200 P	131(4)k		65(3)k			131(3)k	78(2)k
1 E	566(19)k	550(15)k	293(12)k	130(6)k	106(5)k	711(10)k	388(8)k

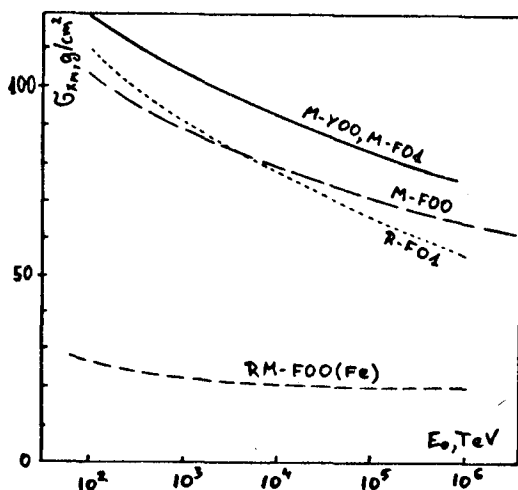


Fig.3. Fluctuations in the depth of maximum.

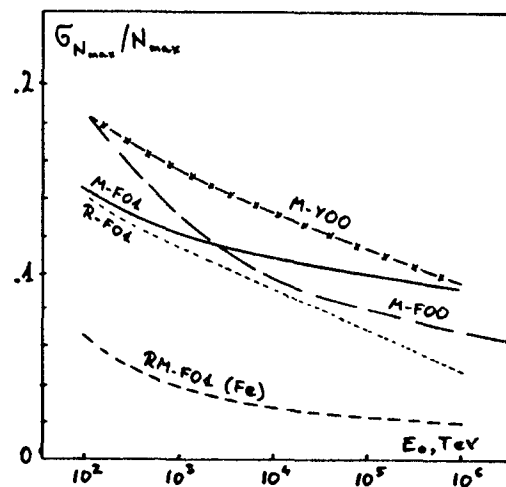


Fig.4. Relative fluctuations of the shower size at maximum.

[One more model was used for EAS generation: M-F10, with all features exactly like M-F00, but with quite different multiplicity distributions. All shower characteristics checked by us were in statistically good agreement between these models].

In principle, the data shown here should speak for themselves. We would like, however, conclude with three remarks:

- \* The most significant part of scaling violation effect is generated by the inclusion of rising cross-section.
- \* Among the models considered the lowest value for  $E_0/N[\max]$  is obtained when rapidly rising cross-section and charge exchange are both included (model R-F01). The value is still 1.38 GeV/electron.
- \* Except at the highest energies, the sensitivity to atomic mass of the primary is greater than to specific assumptions about multiple production.

ANALYSIS OF EQUI-INTENSITY CURVES AND  $N_{\mu}$  DISTRIBUTION OF EAS

G.TANAHASHI

Institute for Cosmic Ray Research, University of Tokyo  
Tanashi, Tokyo, 188 Japan

## ABSTRACT

The distribution of the number of muons in EAS and the equi-intensity curves of EAS are analyzed on the basis of Monte Carlo simulation of various cosmic ray composition and the interaction models. Problems in the two best combined models are discussed.

1. Introduction

Many analyses of EAS data have been reported to investigate the cosmic ray composition and their interaction. For example, the comprehensive work was reported by Gaisser et al(1) in 1978. After then, the equi-intensity data of Chacaltaya was revised(2) and the other data of Akeno experiment was added to it(3). Akeno experiment also gave a distribution of the number of muons(>1Gev) of EAS at fixed shower size with a good statistics(4). In this report we make an analysis of these data with use of the Monte Carlo simulation described in 2.

2. One dimensional simulation of EAS

Among the parameters used in the interaction model of the cosmic ray with the air nucleus, the collision m.f.p. is assumed to be  $\lambda = \lambda_0 / (1 + 0.07(\log E_0(\text{TeV}) + 1)^{1.5}) \text{gcm}^{-2}$  where  $\lambda_0 = 80$  and  $120$  for proton and pion interaction respectively, and  $E_0$  is the cosmic ray energy. The value of  $\lambda$  are shown in Fig.1 together with  $\sigma = 290.E_0(\text{TeV})^{0.06} \text{mb}$  obtained in the Akeno experiment(5). The assumptions of the other parameters are following.

The leading particle carries the energy  $E_s$  fluctuated uniformly between  $0-E_0$ . The partition of the rest of the energy between the fragmentation and the central region is half to half. The energy spectrum of the produced particles in the fragmentation is  $\exp(-E/E^*)$  where  $E^*$  is  $0.6E_s$  and  $E_s$  for proton and pion incident respectively. In the central region the spectrum is assumed to be a plateau shaped one whose energy spread is shown in Fig.2 for various models. Resultant multiplicity-energy relation, multiplicity distribution, scaling behavior and inclusive rapidity distribution are checked to fit the data of accelerator experiments. Produced particles are to be pions or kaons, and the proportion of the kaon production is to increase with the energy as  $0.05 \log E_0(\text{GeV})$ .

Interaction models shown in Fig.2 are used for the EAS calculation. They are SC(scaling), STD(standard, which is scaling + the extension of the central distribution in  $10^{14} \text{ev}$  to the higher energies), SC1/2(scaling + increasing multiplicity with  $E_0^{1/2}$  in the central region above  $10^{14} \text{ev}$ ), SCM(scaling + particles nearly at rest in CM system above  $10^{14} \text{ev}$ ) and CCM (no fragmentation particles and all particles nearly at rest in CM system above  $10^{14} \text{ev}$ ).

We have further two kinds, I and II, in each of the above models. I includes the generation of the high energy neutral pion as the leading particle, and the forward and backward symmetry of the produced particles in CM system. II includes no production of the energetic neutral pion as the leading, and the enhanced particle production in the backward three times more than the forward as the effect of target nucleus. The details

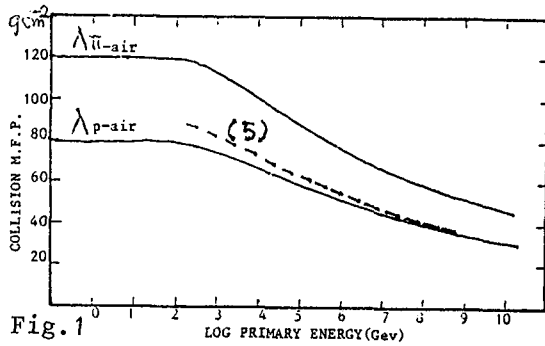


Fig. 1

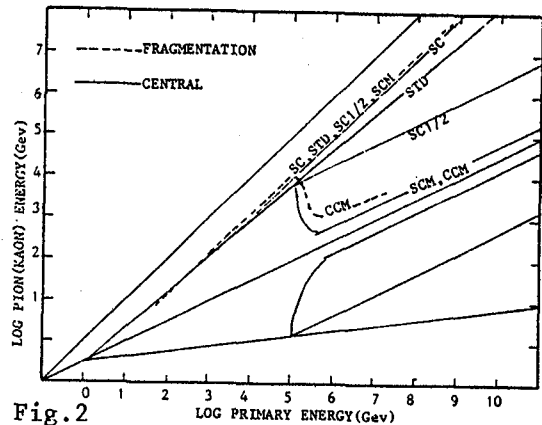


Fig. 2

of these assumptions will be described elsewhere.

The shower curves of electrons and muons of STD based on I, II are shown in Fig. 3. It is seen that the attenuation of particles between  $1000-1600 \text{ gcm}^{-2}$  is nearly exponential and has almost the same attenuation length ( $180-190 \text{ gcm}^{-2}$  in I and  $190-200 \text{ gcm}^{-2}$  in II) irrespective of the primary energies above  $10^{13} \text{ ev}$ . In the same figure, the shower curves of the constant cross section are also shown for the comparison. The reason that the attenuations are almost the same comes mainly from the increasing cross sections. The other result is that the muon content in II is almost 3 times larger than I's.

In Fig. 4 the shower curves of various models are shown in comparison. All of them are based on model I. It is found again the attenuation beyond  $1000 \text{ gcm}^{-2}$  are almost parallel. The difference among SC, STD and SC1/2 are very small, and this

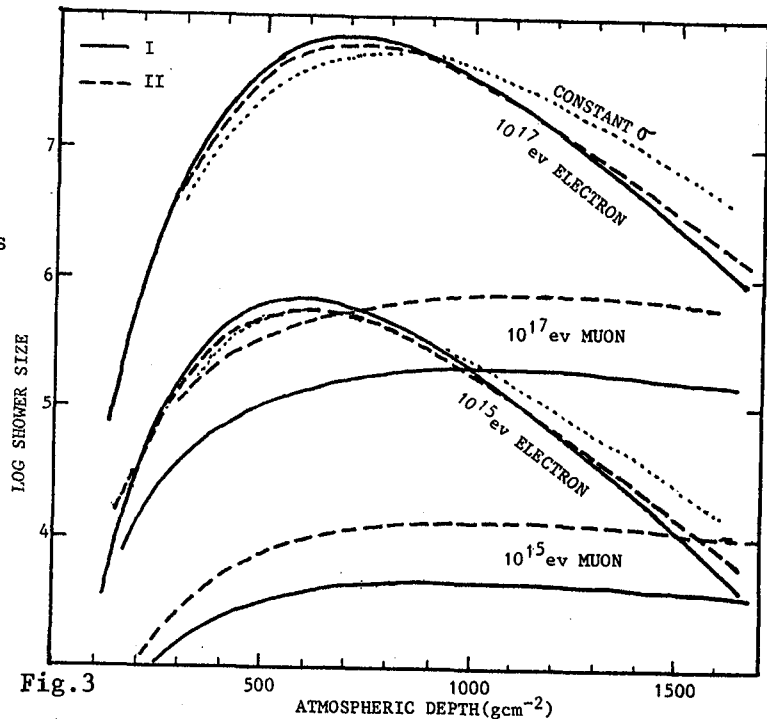


Fig. 3

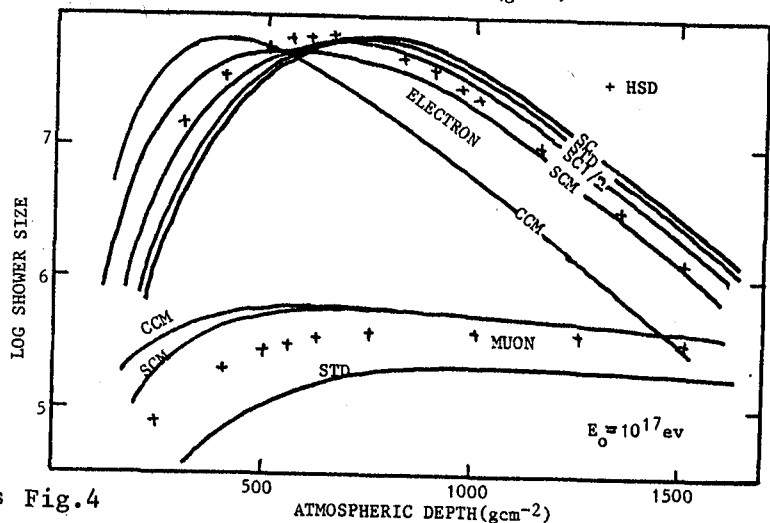


Fig. 4

means that the energy distribution in the central region does not affect much the shower curve except the extreme case like SCM. The crosses in the figure show the iron shower curve (HSD) based on the superposition of STD.

### 3. $N_{\mu}$ distribution of fixed $N_e$

The  $N_{\mu}$  distributions of EAS of different primary component (mass number  $A=1,4,15$  and  $50$ ) are calculated under the condition of fixed  $N_e$  assuming the primary integral energy spectrum to be  $E^{-2}$ . These  $N_{\mu}$  distributions include the error which comes into  $N_{\mu}$  in the course of the data reduction and also the error due to the possible fluctuation of muon lateral distribution. The distribution of  $A>4$  are almost due to these errors. These  $N_{\mu}$  distributions of each component are superposed to fit the experiment (5) as shown in Fig.5.

The conclusions obtained from this comparison are (i) low  $N_{\mu}$  tail requires the existence of proton showers more than

several % (ii) the  $N_{\mu}$  distribution of the proton shower must be as broad as in STD, that is, the very high multiplicity models are avoided because of their narrow distribution of  $N_{\mu}$  (iii) the average  $N_{\mu}$  of each component must be spread over more than

factor 3 for fixed  $N_e$ .

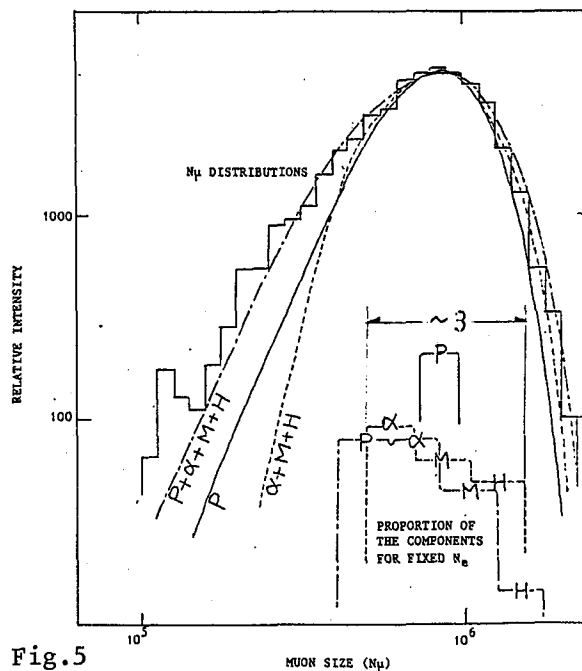


Fig.5

### 4. Equi-intensity curves of EAS

Equi-intensity curves of a mixed composition are related to each shower curves as follows. Assume that the shower curves are energy independent in the required energy region, that is  $N(E,x)=E \cdot N(x)$  where  $N(E,x)$  is the shower curve of energy  $E$  in depth of  $x$ . The intensity ratio of the heavy to the proton shower in fixed shower size is

$$\Delta(x) = (I_h/I_p)_{N_e} = (I_h/I_p)_E \cdot (N_h(x)/N_p(x))^{\gamma}$$

where  $k = (I_h/I_p)_E$  is the intensity ratio in fixed energy and  $\gamma$  is the integral exponent of the primary energy spectrum. Putting  $\gamma=2$ ,  $\Delta(x)$  can be calculated with use of the values of  $N_h(x)$ ,  $N_p(x)$  as the function of  $k$ . Equi-intensity curves  $\bar{N}(x)$  are obtained from

$$\bar{N}(x) = N_p(x) / (1 + \Delta(x)) + N_h(x) \cdot \Delta(x) / (1 + \Delta(x))$$

$\Delta(x)$  and  $\bar{N}(x)$  are calculated for the following combinations of the proton and the heavy showers.

proton shower	STD	STD	STD	SCM
heavy shower	HSD	SCM	CCM	CCM
notation	HSD/STD	SCM/STD	CCM/STD	CCM/SCM

The  $\bar{N}(x)$  are shown in Fig.6 for  $k=0.1, 1.0$  and  $10$  together with the experimental data (2) (3). In general, the attenuation length between  $800-1400 \text{ gcm}^{-2}$  are steeper than either prediction, but two cases (HSD/STD and  $k=10$ )

(CCM/SCM and  $k=0.1$ ) barely fit the experiment as shown in the figure in dotted curves after the normalization of the intensity. SCM/STD and CCM/STD do not fit because of too much difference of proton and heavy shower curves. This difference makes the composite curves flat.

### 5. Discussions and conclusion

Both two selected cases satisfy the requirement (i) in 3.

As for CCM/SCM, it is not clear whether (ii)(iii) are satisfied or not, but seems to be not. This model is introduced to approach the one which is proposed by Kakimoto et al(2) to explain the rapid development of EAS in high altitude observed by them. So the further progress of this experiment will test the model.

On the other hand, HSD/STD satisfies all the requirements (i)(ii)(iii) in 3. The problems of this model are the less content of muons in EAS and the slow development of the number of muons. The model needs about 2 times more muons. If we adopt model II instead of I, the number of muons increases but the attenuation length also increases apart further from the experiment. As for the slow development of muon in this model, we can scarcely fit the experiment by taking the number of muons of iron showers in  $600 \text{ g cm}^{-2}$  and of proton showers in  $1100 \text{ g cm}^{-2}$  (Fig.7). If the  $N_{\mu}$  difference of the proton and the heavy nucleus shower is larger in some model, such a model is better in this problem.

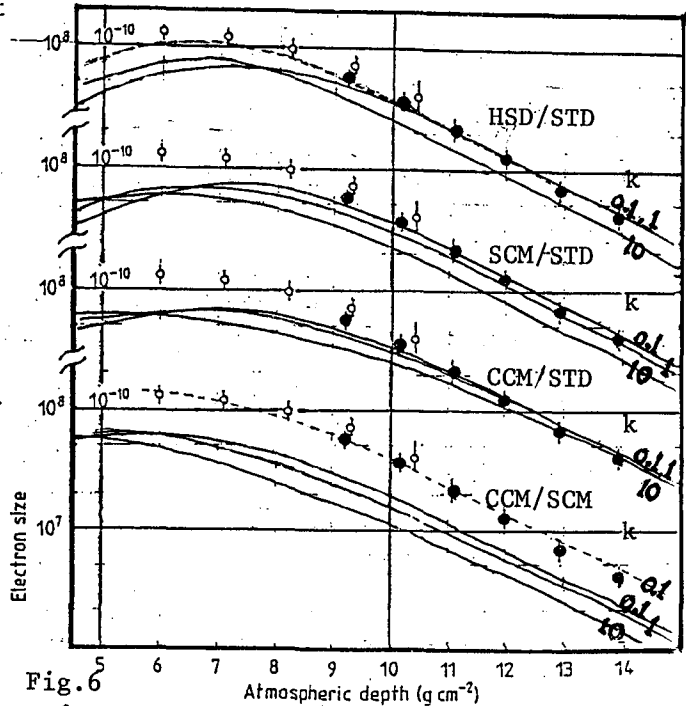


Fig.6

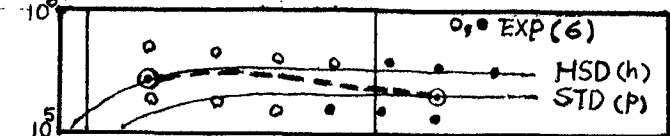


Fig.7

### Acknowledgements

The EAS simulation are done by FACOM 380 at the computer room, Institute for Nuclear Study, University of Tokyo.

### References

- (1) Gaisser, T.K. et al. Rev. Mod. Phys., 50, 859 1978
- (2) Kakimoto, F. et al. J. Phys. G; Nucl. Phys. 9, 339 1983
- (3) Nagano, M. et al. J. Phys. G; Nucl. Phys. 10, 1295 1984
- (4) Hara, T. et al. Proc. 18th ICRC(Banbalore), 11, 285 1983
- (5) Hara, T. et al. Phys. Rev. Lett. 50, 2058 1983
- (6) Hara, T. et al. Proc. 18th ICRC(Bangalore), 11, 281 1983

## ANALYSIS OF THE HADRON COMPONENT IN E.A.S.

OBSERVED AT 700 g.cm<sup>-2</sup> BY A SCALE BREAKING MODEL

J. Procureur

Laboratoire de Physique Théorique  
 Université de Bordeaux 1  
 rue du Solarium  
 33170 Gradignan (France)

J.N. Stamenov, P.V. Stavrev, S.Z. Ushev

Institute of nuclear research and nuclear energy  
 Bld. Lenin 72  
 Sofia (Bulgaria)

## ABSTRACT

The Tien Shan experimental results about the hadron component in E.A.S. with sizes  $10^4$ - $10^6$  are analysed with help of a scale breaking model. It is shown that the secondary particles multiplicity depends on the interaction energy stronger as predicted from accelerator experiments and the primary mass composition is rich on protons at energies  $10^5$ - $10^6$  GeV

1. Introduction Hadrons in extensive air showers provide direct informations about high energy interactions.

In the rule the biases pertaining to different shower array arrangements have a relative large influence for the basic phenomenological characteristics of the E.A.S. hadron component.

In this situation, the problem of the correct comparison between model calculated and experimental characteristics is of great importance for the reliability of the derived conclusions about the high energy interaction characteristics.

This is why we take carefully into account the triggering conditions of the Tien Shan array and the characteristic procedures for the statistical data treatment.

2. Method The characteristics of the E.A.S. hadron component were calculated on the basis of a scale breaking model under the assumption of a pure proton primary composition.

Details on the model of simulation are given in the proceedings of this conference (HE 5.4-8) and in ref (1).

The different observables computed from simulation charac-

terize the "pure development" of the showers.

Then, to be compared with the results obtained in Tien Shan experiment, pseudo-experimental values were determined with help of the IMEAT algorithm which takes into account all internal characteristics of this array.

By this way we obtained results for showers with fixed sizes  $10^4$ - $10^6$  and with average zenith angle  $\theta = 22^\circ$

### 3. Results

The dependences of hadron numbers  $N_h(>E_h)$  on the shower size were analysed in the size interval  $10^4$ - $10^6$  and at Tien Shan observation level.

Simulations were made for different threshold energies for the hadrons:  $E_h > 0.6$ ; 1 and 10 TeV.

It is seen in fig. 1 that the experimental dependences (2-4),  $N_h \sim N_e^\alpha$  for  $E_h > Tr$ , are much steeper than those predicted from the adopted Scale Breaking Model.

Their comparison

with the results obtained by Erlykin et al. (2) and the analysis of the both models show that the main reason for the discrepancies between the experimental and calculated curves lies in the adopted energy dependence of the secondary particles multiplicity:

$$\langle n_s \rangle = \alpha + \beta \ln s + \gamma (\ln s)^2 \quad (1)$$

For a better agreement with experiment, it is necessary to adopt a stronger energy dependence of the multiplicity. Indeed, our determination of  $\langle n_s \rangle$  coming from the p-p̄ collider is equivalent to  $E^{0.13}$  whereas the multiplicity used in ref. (2) takes into account the p-air interaction and is  $\langle n_s \rangle \propto E^{0.25}$ .

On fig. 2 are shown the integral energy spectra of hadrons for different fixed sizes and at observation level  $700 \text{ g.cm}^{-2}$

It is seen that the calculated integral spectra  $N_h(>E_h)$  become as expected harder with the rising of the size  $N_e$ .

The shape of the hadron energy spectra in E.A.S. is well described with calculation results, carried out with help of the used scale breaking model (1).

The correct agreement for the shape of these spectra is a good indication for the predominance of protons in the primary mass composition at energies  $10^5$ - $10^6$  GeV.

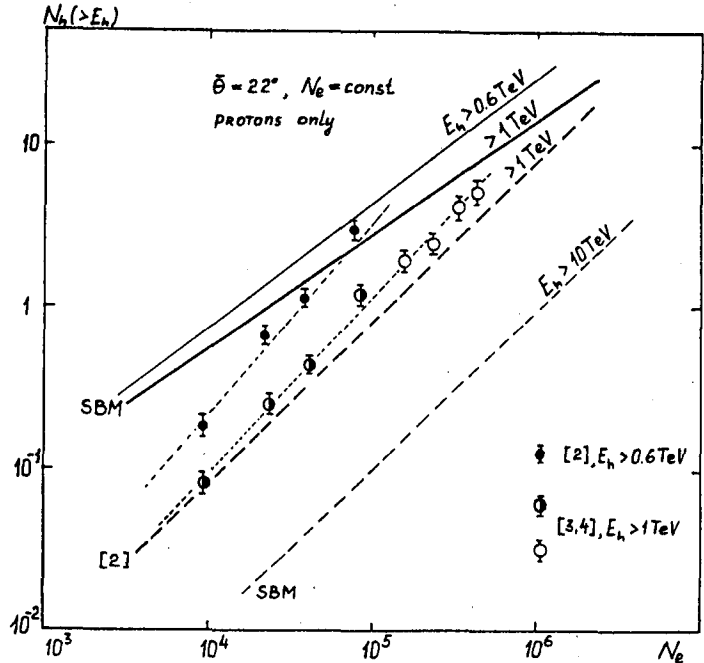


fig. 1



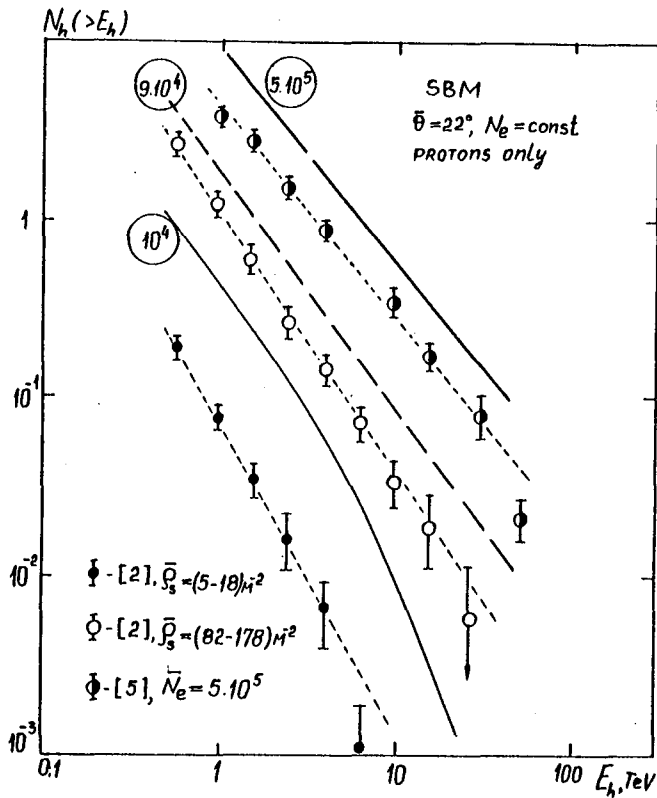


fig. 2

#### 4. Conclusions

The analysis of Tien Shan hadron component data on the basis of the used scale breaking model shows that the average multiplicity  $\langle n_s \rangle$  of secondary particles increases essentially more than predicted by the p-p collider,  $\langle n_s \rangle \propto E^{0.13}$ , under the supposition that the protons play the main role (5-6) in the primary mass composition for energies  $10^5$ - $10^6$  GeV.

#### References.

- (1) J. Procureur, J.N. Stamenov et al., 1985, to be published in J. Phys. G
- (2) T.V. Danilova et al., 1984, Moscow, preprint FIAN n° 14
- (3) V.S. Aseikin et al., 1982, Moscow, preprint FIAN n° 215
- (4) N.M. Nesterova, A.G. Dubovy, 1979, Proc. 16th ICCR, Kyoto, 8, 345
- (5) V.A. Romakhin, N.M. Nesterova, 1979, Trudy FIAN v 109, 77
- (6) J.N. Stamenov et al., 1983, Proc. 18th ICCR, Bangalore OG4-11

ELECTRONS, MUONS AND HADRONS IN EXTENSIVE AIR SHOWERS  
AND HOW DO THEY DEPEND ON NUCLEAR INTERACTION MODEL  
(Part I)

J.A.Wrotniak(\*) and G.B.Yodh

Department of Physics and Astronomy  
University of Maryland  
College Park, MD 20742, U.S.A.

We performed Monte Carlo simulations of extensive air showers, using a couple of different nuclear interaction models and obtaining a variety of shower characteristics. The discussion of these shows, that the sensitivity of observables to the primary mass spectrum is significantly stronger than to the interaction model, the latter being quite weak.

The interpretation of cosmic ray observation carried out at various depths in the atmosphere requires detailed simulations of the propagation of nuclear-electromagnetic cascades generated by primary cosmic rays in the atmosphere. These calculations demand quantitative prescription for the following inputs necessary to carry out the simulation:

1. Chemical composition and energy spectrum of primary cosmic rays beyond where direct measurements were made ( $>50$  TeV/nucleus);
2. Inclusive cross-sections for particle production in hadron-air nucleus collision at high energies - beyond (and not only, cf [1]) those available at SPS pp and Tevatron II;
3. High energy nucleus-nucleus cross-sections and fragmentation properties.

In addition, photons and electrons produced in the simulation tree must be propagated down to earth using electromagnetic theory and semi-empirical distribution functions. Thus the simulation is complex, multivariate enterprise. Quite often it is difficult to intercompare results from simulations of different groups because of not only disparity of the input,

---

(\*) On leave from Łódź University, Poland.

(\*\*) This work (and its continuation, HE 4.1-2) was supported in part by the U.S.National Science Foundation under Grant No. PHY 8207425

but also due to the simulation structure and algorithms.

In this paper together with HE 4.1-2 in this volume (see also [1]) we examine the sensitivity of air shower observations to changes in the interaction model and the nature of the primary by carrying out rather complete simulations over a wide energy range using the same program structure for shower generation, but changing the parameters, mostly one at a time, in the interaction models, for both proton and iron primaries. The energy range covered is from 20 TeV to 1 EeV ( $10^{21}$  eV). The interaction models vary from one with constant cross-section and scale invariant production distributions to a model with rapidly rising cross-section, large violation of scaling in both forward and central regions and charge exchange for the leading particle.

### Nuclear interaction models

Particle production distributions in p-air and meson-air collisions are approximated by p-p and meson-p collisions. Two basic models of our variety are briefly compared in Table 1; the corresponding inclusive cross-sections are shown in Figs. 1 and 2.

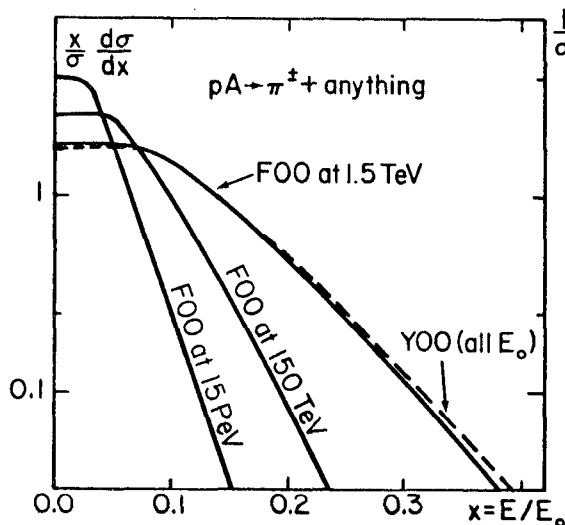


Fig. 1. The distributions of  $x = E/E_0$  for models used in our study.

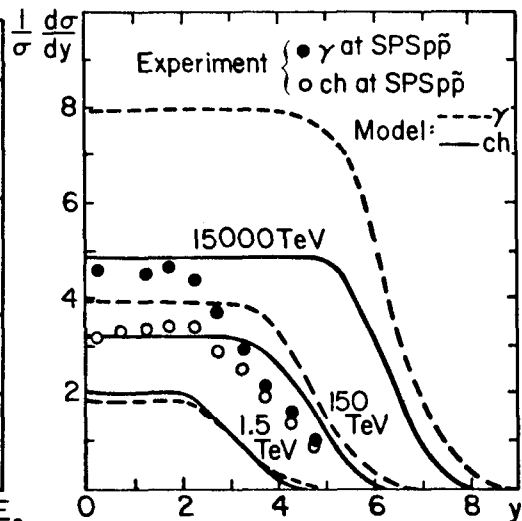


Fig. 2. The rapidity distributions compared with pseudorapidity data from SPSp̄p̄.

Some other models were tried out, too, in order to check effects due to some particular differences in the assumptions:

- \* M-Y00 - same as F-Y00, but the cross-sections in hadron-air interactions rise as in M-F00 (this is what the M before the hyphen means),

- \* M-F01 - adding a possibility of charge exchange to M-F00: interacting pion emerges from the collision with equal probabilities in any of three possible isospin states, and a kaon - in any of the four (the charge exchange possibility is denoted with the last "1" in the model notation),
- \* R-F01 - similar to M-F01, but with faster rise in cross sections: mean free paths for nucleons decrease in "M" case from 84 to 55 g/cm<sup>2</sup>, and in "R" - from 86 to 37 g/cm<sup>2</sup> between 1 TeV and 1 EeV.

Table 1 Comparison of features of two basic models used.

	Model F-Y00	Model M-F00
Mean free paths for inelastic interaction	Energy-independent: nucleons: 75 g/cm <sup>2</sup> pions: 110 g/cm <sup>2</sup> kaons: 130 g/cm <sup>2</sup>	Below 1 TeV nucleons: 84 g/cm <sup>2</sup> pions, kaons: 117 g/cm <sup>2</sup> Above 1 TeV $L(E) = L_0 / (1 + 0.0383 \cdot \ln E)$
Inelasticity	Uniform in (0,1) for nucleons and (1/3,1) for mesons	
Inclusive distributions in $x = E/E[\text{interaction}]$ for secondaries	Energy-independent: scaling extrapolation of the ISR data	Below 1 TeV as Y00; above: the functional shape is unchanged, but the scale x-value decreases as $1/E[\text{int}]^{1.25}$
Secondaries produced	Charged pions - 60% Neutral pions - 30% Charged kaons - 5% Neutral kaons - 5%	Below 1 TeV as Y00; above: the fractions of kaons and neutral pions increase with energy, reaching at 1EeV 6.8% (each) and 53.7%, respectively
Charge exchange of an interacting meson	None (i.e. the leading particle emerging from the interaction is always identical in kind to the interacting one)	
Transverse momenta	See [3]; irrelevant here, as we present only longitudinal EAS properties	

### Nucleus-Nucleus interactions

For nuclei other than protons the interaction cross-sections had to be assumed, as well as some nucleus interaction/fragmentation model. Once again, the detailed description of the fragmentation algorithm may be found in [3]; it is based on the data compiled in [4] by J.E. Nowicka et al. The mean free paths for nucleus-air interaction were assumed in two different ways:

- @ Energy-independent values [4] ranging from 37 g/cm<sup>2</sup> (alpha particles) to 16 g/cm<sup>2</sup> (iron). These were used for heavy nuclei-initiated EAS generated with model F-Y00,

therefore denoted as FF-Y00;

- @ R - rising cross-sections in Gaisser parametrization [2], consistent with "R" pA ones, e.g. for the iron group the mean free paths decrease from 12.2 to 10.6 g/cm<sup>2</sup> between 100 TeV and 1 EeV. These were used in combination with "M-" or "R-" models, therefore denoted as e.g. RM-F00 or RR-F01.

### Other simulation assumptions

For hadrons and muons three-dimensional Monte-Carlo simulation was performed down to the threshold energy of 2 GeV (1 GeV for pi-zeros). Photons and electrons emerging in the simulation tree were accounted for down to 170 MeV. However, the electromagnetic showers were followed the Monte-Carlo way only to a 200 GeV threshold; as soon as a photon or electron reached energy between 170 MeV and 200 GeV, the number of cascade electrons due to it was estimated from the Greissen formula. [This approach is more exact, than a non-Monte-Carlo treating of each electromagnetic shower from the very beginning].

The assumed cascade unit was 36.7 g/cm<sup>2</sup> and the critical energy - 84.2 MeV. (The c.u. value turned out to be quite important; changing it by just 1 g/cm<sup>2</sup> results in 6-7% change in 200 TeV shower sizes at sea level!). In the high-energy part (i.e. above 200 GeV) only pair creation, bremsstrahlung and Coulomb scattering were included into simulation.

As far as the main aim of this work was to check the model sensitivity, we limit this presentation to only vertical showers in the U.S. Standard atmosphere; the detection level was at the depth of 1000 g/cm<sup>2</sup>.

Above 1 PeV initial energy, the thinning technique invented by Hillas [5] was used (to save the CPU time); performed checks proved, that this did not affect either the average values or the width of fluctuations (at least those checked by us).

The review of results obtained as described here may be found in our contribution HE 4.1-2 to this Conference.

### References

1. J.A.Wrotniak and G.B.Yodh; HE 1.2-6 in the present volume
2. T.K.Gaisser et al.; 18th ICRC, Bangalore, 5, 174 [1983]
3. J.A.Wrotniak; SHOWERSIM/84, Univ.Md.Rep. PP 85-191 [1985]
4. J.E.Nowicka et al; Univ.Md.Rep. PP 85-190 [1985]
5. A.M.Hillas; 17th ICRC, Paris, 8, 193 [1981]

SIMULATION OF EAS PROPERTIES ON THE BASIS OF  
HIGH ENERGY INTERACTION MODEL DEDUCED FROM  
THE ACCELERATOR DATA

G.Kubiak, J.Szabelski and J.Wdowczyk  
Institute of Nuclear Studies  
90-950 LODZ 1, box 447  
POLAND

A.W.Wolfendale  
University of Durham, Durham DH1 3LE  
ENGLAND

1. Introduction. Calculations of extensive air showers in atmosphere have been performed using formulae describing p-p and p-air nucleus interactions presented elsewhere in this proceedings /HE 1.2-4/. The formulae fitted to the accelerator data have been extrapolated taking the same trend up to  $10^{16}$  eV. Above that energy it was assumed that the degree of scaling violation / $\alpha$ -parameter/ is saturating or even decreasing. The latter assumption follows from earlier work of some of us /Wdowczyk and Wolfendale, 1984/ where we found that without this restriction shower maxima at the highest energies are located too high in the atmosphere. Results of calculations have been compared with experimental data. The comparison was made separately for the curves obtained from the so called equal intensity cuts and for the Cerenkov data.

2. Method of calculations. In the first stage using Monte Carlo method there were calculated EAS longitudinal development curves for three different requirements. These requirements are: fixed primary energy, fixed size of shower at every observation level and fixed size at the sea level. Examples of the curves for proton primaries with energies around  $10^{16}$  eV are given in figure 1. In the next stage the curves calculated for fixed sizes at every observation level and for different primary masses are combined according to the assumed mass composition. The mass composition have been taken according to the two component model of the galactic cosmic rays /Wdowczyk, 1984, also see OG 5.4-6 this proceedings/.

3. Results. In figure 2. the longitudinal development curves are compared with experimental data. In figure 3. the position of the shower maxima obtained from the equal intensity cuts are compared with predictions /here the predictions are taken for fixed shower sizes at the observation levels/. Finally in figure 4. the data on shower maxima positions obtained from the Cerenkov observations are compared with the predictions /in that case the predictions are taken for the fixed size at sea level as the observations are performed usually at sea level/. Separately are shown curves obtained under the assumption that the scaling violation parameter  $\alpha = 0.25$  above  $10^{16}$  eV and

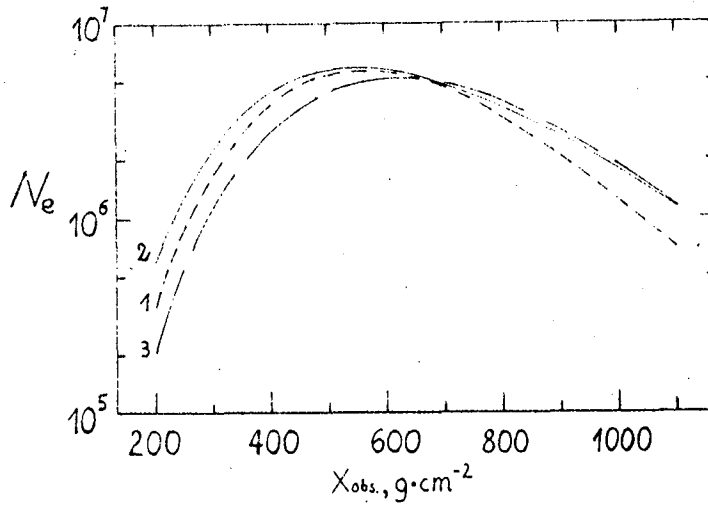


Fig.1. EAS longitudinal development curves. 1-fixed primary energy, 2-fixed size of the shower at every observation level, 3-fixed size at sea level.

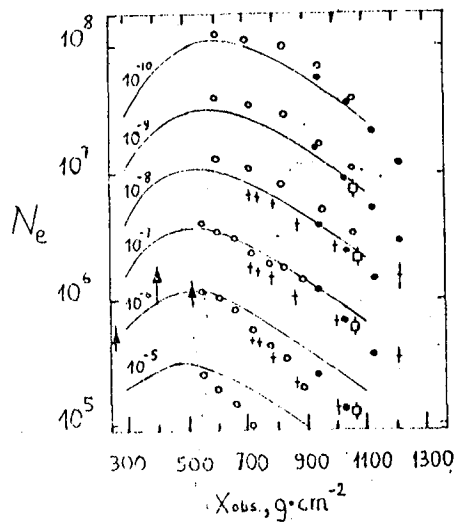


Fig.2. The longitudinal development of EAS in the atmosphere obtained for proton-air nucleus interactions compared with the experimental data, see J.Gawin et al., /1984/.

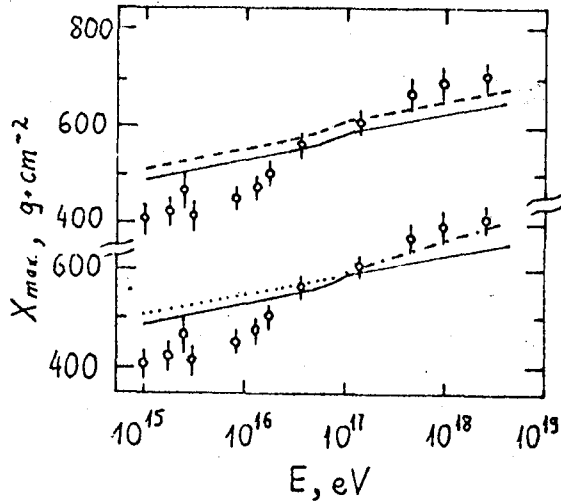


Fig.3. The positions of shower maxima. Calculations were performed with fixed shower sizes at every observation level. Experimental points are from equal intensity cuts. Predictions are from the following models: proton-proton interactions /---/, proton-air nucleus interactions with full mass composition /—/ and with primary protons only /..../, scaling sets for energies higher than  $1E16$  eV /-.-./.

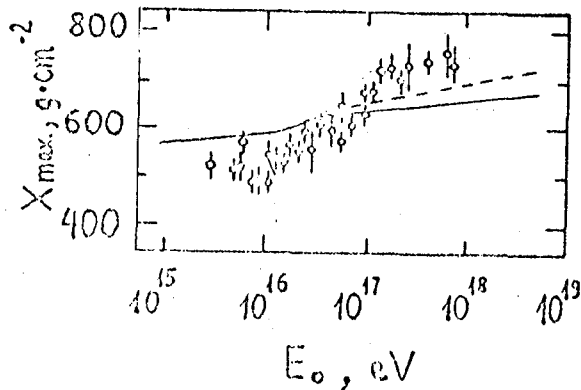


Fig.4. Predictions for the locations of shower maxima obtained with fixed size at sea level. Full line is for proton-air nucleus interactions with scale-breaking model, the dashed one is from the model with scaling for energies above  $1E16$  eV. The experimental points are from Cerenkov measurements.



assuming that effectively scaling sets at that energy.

In figures there are given results of calculations obtained with the formula for proton - air nucleus interactions. In figure 3. for comparison there is also shown the development curve obtained using formula for proton-proton interactions /we may say for a proton atmosphere/.

4. Conclusions. If we use the model based on direct extrapolation of the accelerator data the predicted variation of the shower maximum position is different than that obtained from the observations. The predicted positions of shower maxima are located too low at energies  $10^{15}$  -  $3 \times 10^{16}$  eV and too high for energies above. The situation can not be significantly improved by the variation of the primary particle mass as the used composition is already proton dominated at energies above  $10^{16}$  eV and reasonably heavy below that energy.

Practically sufficient improvement is obtained if it is assumed that some sort of scaling is introduced above  $10^{16}$  eV. By term of scaling we mean here that the multiplicity of the secondary particles at these energies saturates.

It seems extremely difficult to restore the agreement with the data at energies  $10^{15}$  -  $10^{16}$  eV. Introduction of heavy particles here is not only insufficient but also contradictory with other observations /for instance multiple muons/. It seems that the observations require an assumption about existence of some new feature at energies around few times  $10^{15}$  -  $10^{16}$  eV. That requirement is strengthened by the fact that the same tendency is observed both in the data obtained from the equal intensity cuts and those from the Cerenkov observations.

Important point which follows from the comparisons made in figures 3. and 4. is that the positions of shower maxima should be calculated differently for the case of the equal intensity cuts and for the case of the Cerenkov observations.

#### References

1. Gawin, J. et al., /1984/, Acta Universitatis Lodzianis, Folia Phisica 7, 59.
2. Wdowczyk, J., /1984/, Proceedings of the Int. School of Cosmic Ray Astrophysics, Erice, Sicily, November 4-15.
3. Wdowczyk, J., Wolfendale, A. W., /1984/, J. Phys., A: Nucl. Phys., 10, 257.

## NEW ASPECTS IN NUCLEON-NUCLEUS COLLISIONS

AND EAS PROPERTIES AROUND  $10^6$  GeV

J.N. Capdevielle

Laboratoire de Physique Théorique, Bordeaux, France

and

J. Gawin

Institute of Nuclear Studies, Lodz, Poland

1. Introduction

At energies higher than  $2 \cdot 10^5$  GeV, we have very few information on detailed properties of nucleon-nucleon collision ; the rare elements are coming from "jets", and, as non direct improvements from  $\gamma$ -ray families. The results exhibit some conflicting features, or, at least, very large fluctuations like copious production of  $\gamma$ -rays in opposition to Centauro-like events, sometimes suggest that phase transition to quark gluon plasma occurs in nucleus-nucleus collisions and even in nucleon-nucleus collision (1) (2). The multicluster phenomenological model (MPM) is here extrapolated for EAS simulation up to  $5 \cdot 10^6$  GeV to put in evidence some significant deviation between experimental data and prediction.

2. Extrapolation of short range order picture, nucleus-nucleus collision

The emission of small clusters from nucleon-nucleon collision is taken following (3) assuming always that the width of the plateau of rapidity is rising with  $\ln s$  (and also the height); the secondary particles are generated by decay of those clusters like in (4) but the truncated Poissonian distribution has been replaced by a Gaussian distribution. The width of this Gaussian has also been parametrized versus  $\ln s$  at ISR and  $\bar{p}$ -p energy and extrapolated in continuity of HE 4.1-9. The extension to p-air collision is also not different.

The most convenient was in this last case to generate directly the clusters from an inclined plateau, the rapidity of a cluster in CMS  $y_c$  being obtained from

$$\int_{-y_0}^{y_c} R(y) dy = \xi \int_{-y_0}^{y_0} R(y) dy$$

( $\xi$  simple random number) and decay those clusters like for nucleon-nucleon collision in center of mass system. About KNO violation and asymptotic limit for fluctuations of multiplicity, as well as correlation between  $\langle p \rangle$  and central rapidity density we assume strict continuity with the previous description at energies higher than  $2 \cdot 10^5$  GeV, as well as for proportion of different species  $K^\pm$ ,  $p, \bar{p}$  (taken as in ref. (1) of HE 4.1-9).

Nethertheless, we introduced here one variant in MPM concerning the production of secondary  $\eta$  mesons : herealso, a  $\ln s$  increase has been taken from the invariant mass distribution of the two-photon sample in UA2 experiment and the rate previously estimated

in ISR. In this version, about half of the photons produced in a collision of  $10^6$  GeV are coming from  $\eta$  mesons (fig. 1).

A typical characteristic of the multicluster phenomenological model is the constant decrease of total inelasticity  $\langle K \rangle$  for nucleon-nucleon collision (underlined in HE 4.1-9) and consequently for p-air collision (fig. 1), estimated by summation of the energy carried by secondaries in Laboratory system.

The extension to nucleus-nucleus collision follows ref.(6) in HE 4.1-9 : the plateau of rapidity is transformed like for p-nucleus, assuming an increase of multiplicity in collision of nuclei A and B

$$R \left( \frac{AB}{pp} \right) \sim \frac{1}{2} \langle \nu_A \rangle + \langle \nu_B \rangle = \frac{1}{2} P$$

B being the air constituent target nucleus. ( $\nu$  is defined as for p-nucleus and P is the number of participating nucleons). In the EAS Monte-Carlo simulation, we have treated separately the contribution coming directly from the participating nucleons and the contribution governed by the behaviour of the "spectators".

### 3. Comparison with experimental data

We obtain with 5 GeV muon in Tian-Shan a better agreement than with models previously used (fig.2, 4.1-9) ; muon content after  $10^6$  GeV deviates from MPM, but if we consider the version assuming  $\eta$  meson production the agreement is restored up to  $5 \cdot 10^6$  GeV. This can be explained by the larger number of  $\gamma$ 's produced in the  $\eta$  channels decay with lower individual energies than in  $\pi^0$  decay. The muon of 220 GeV are also in agreement with KGF data (fig. 3 HE 4.1-9) and Moscow data for muons of the same energy (5); the flattening in the experiment after  $N_e = 10^6$  is up to now not confirmed in Moscow and it could be an effect of the small statistics. Very good agreement is also obtained at Tian-Shan level for high energy hadrons, and also for the  $\langle E_{H,r} \rangle$  factor (fig. 2). Up to now,  $\langle E_{H,r} \rangle$  was decreasing with energy with a majority of models but in one case, including decrease of  $\langle K \rangle$  versus rising  $s$  (6). We note that in MPM this circumstance is also the cause of the large number of energetic hadrons surviving at Tian-Shan altitude.

Satisfactory situation appears also for maximum depth  $T_{\max}$  versus energy (fig. 3); for instance,  $T_{\max}$  near  $10^6$  GeV is measured near  $520 \text{ g.cm}^{-2}$  by Cerenkov method (5) when MPM gives  $550 \text{ g.cm}^{-2}$  for proton. We observe that the maximum depth from Cerenkov measurements is located at deeper altitude than in previous experiments with lower number of detectors and smaller resolution. If  $\eta$  meson production is assumed, the maximum depth decreases by about  $35 \text{ g.cm}^{-2}$ . Furthermore, very good agreement is obtained with the most recent data on  $T_{\max}$  measurements. (7).

### 4. Conclusion

If we consider the good agreement obtained with age parameter data in Akeno (HE 4.3-13), we can conclude that the multicluster phenomenological model gives an acceptable description of EAS data and can be extended at least at one decade higher than the  $\bar{p}$ -p energy. If we include  $\eta$  meson production, it can be even accepted at energies near  $10^7$  GeV. A rise of rapidity plateau in  $\ln s$  (simultaneously in width and height) appears sufficient and

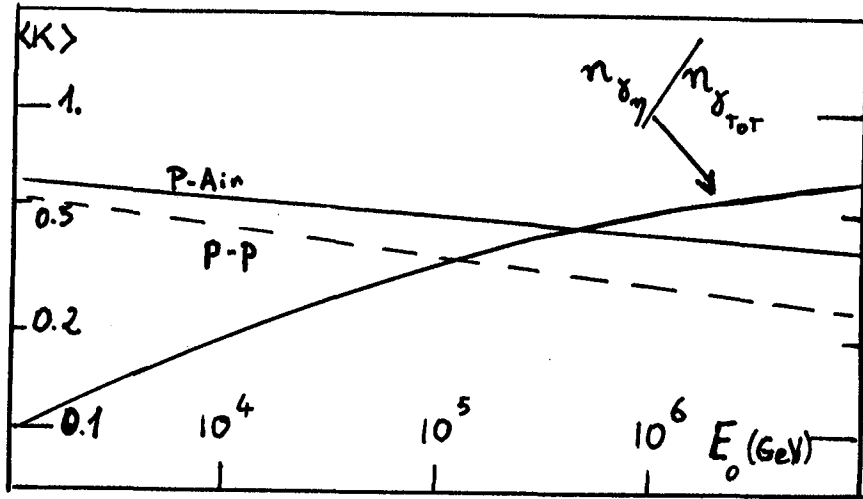


Fig. 1

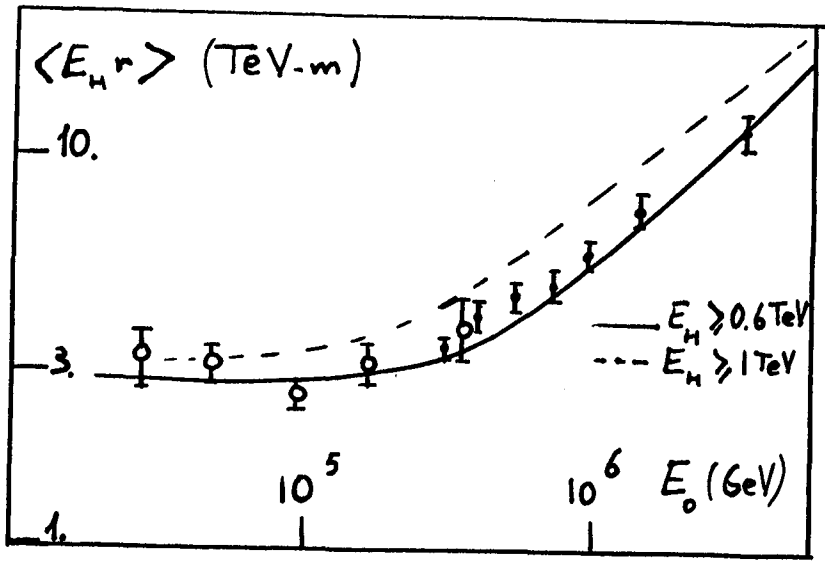


Fig. 2

differently with previous models we don't need any exotic change in composition or in multiplicity to explain in this kinematical range the experimental data. At least, it appears no necessity of any enhancement of heavy nuclei in primary component. A very large fraction of the rapidity plateau is compatible, and, may be, only in the central region we cannot exclude a more important rise of rapidity density.

### References

1. J.N. Capdevielle et al., 1984, J.Phys. G10, 705.
2. A. Faessler, 1983, Nucl.Phys. A400, 578c.
3. B. Degrange, 1985, private communication, Paris.
4. K. Alpgard et al., 1983, Phys.Lett. 123B, 108.
5. G.B. Kristiansen, 1984, private communication, Moscow.
6. A. Antonov et al., 1984, Proc.Symp. Cosmic ray and particle physics, Tokyo, 431.
7. N. Inoue et al., 1985, J.Phys. G11, 657.

x Thornton, ICRC 73, 9, 99

▽ Kristiansen, 85

Other points from Nagano, R.P. 83.

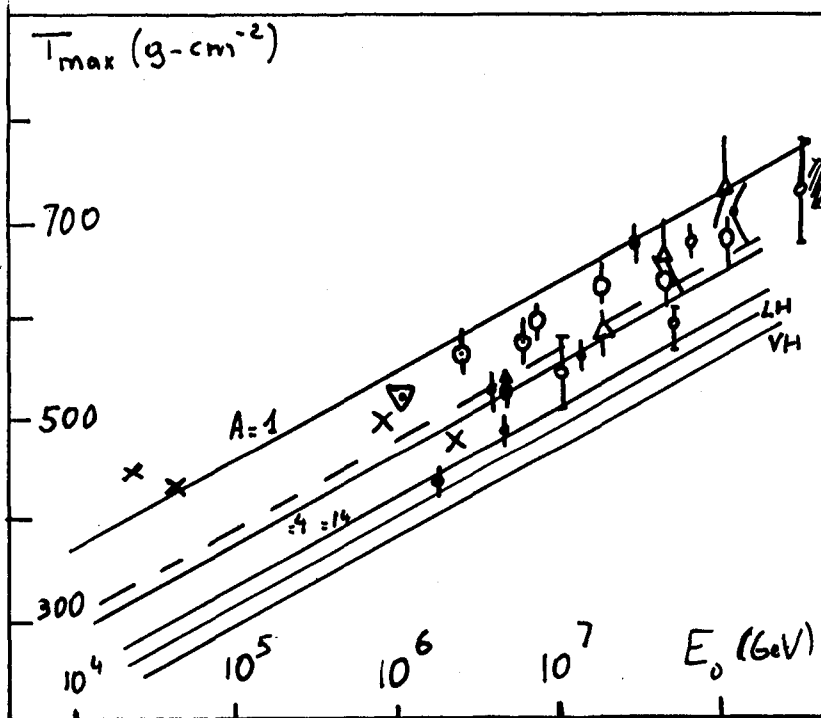


Fig. 3

## SMALL AIR SHOWERS AND COLLIDER PHYSICS

J.N. Capdevielle

Laboratoire de Physique Théorique, Bordeaux, France

and

J. Gawin, B. Grochalska

Institute of Nuclear Studies, Lodz, Poland

1. Introduction

At energies lower than  $2 \cdot 10^5$  GeV (in Lab. system), we have now more accurate information on nucleon-nucleon collision ( $\bar{p}$ -p collider (1)) and on primary composition (JACEE data (2)). The behaviour of those both basic elements in cosmic ray phenomenology from ISR energy suggests some tendencies for reasonable extrapolation in the next decade  $2 \cdot 10^5 - 2 \cdot 10^6$  GeV (paper HE 4.1-10).

Small showers in altitude, recorded in the decade  $2 \cdot 10^4 - 2 \cdot 10^5$  GeV offers a good tool to testify the validity of all the Monte-Carlo simulation analysis and appreciate how nucleon-air collision are different from nucleon-nucleon collisions.

2. Multicluster phenomenological model and nucleon-nucleus collision

The width and the height of the rapidity plateau are together assumed to rise with  $\ln s$ , in agreement with a total multiplicity proportional to  $\ln^2 s$ , taken as  $n_s = 0.127 \ln^2 s + 0.584 \ln s + 0.57$ . The proportion of secondary neutral is rising slightly more rapidly, on the opposite of other works assuming  $n_\gamma = n_s$ , following the numerical values quoted from UA5 and UA1 (1) (HE 5.1-5). For each individual collision we assume a uniform distribution of clusters, chosen randomly on the length of the available rapidity plateau. The short range clustering effect is obtained by the production in large number of small masses resonances decaying in  $\pi^+\pi^-$ ,  $\pi^+\pi^0$ , ... (K=2). We assumed a Gaussian distribution for the rapidity of the individual secondaries around the rapidity of corresponding cluster in center of mass system. The width of this normal distribution has been parametrized between ISR and collider energy, and the model gives a very good fit to the pseudo-rapidity distributions at  $E_{cm} = 53$  and  $540$  GeV.

Strong KNO violation is taken into account, in the sense shown in HE 5.1-5, with a better accuracy, treating the fluctuations of multiplicity like Erlang processes :

$$\Psi(z) \sim \frac{z^{\alpha-1}}{\Gamma(z)} e^{-\alpha z}$$

describing correctly the situation in all the dynamical range if  $\alpha = 100 aE^{-a}$  where  $a = 0.1042$  (E in GeV in laboratory system). The values  $\alpha = 6$  describes the low energy part, near Slattery behaviour and the very high energy corresponds to  $\alpha = 2$ , considered as an asymptotic KNO function in the "bremstrahlung analogy" approach to multiproduction.

For each individual collision the central density of rapidity  $\rho_0$  is estimated by counting the secondaries contained in  $2/3$  of the plateau length and the average  $\langle p_t \rangle$  is correlated with  $\rho_0$  (3)

according to

$$\langle p_t \rangle = \frac{C}{[-e^{-z} E_i(-z)]^\gamma}$$

( $C = 0.38 \text{ GeV/c}$ ,  $\gamma = \frac{1}{8}$  at 155 TeV and here  $z = \frac{\pi}{4} [n/\bar{n}(s)]^2$ ), the the invariant cross section being parametrized by the same formula for  $\pi$ 's and K's in function of the transverse mass  $m_T = \sqrt{m^2 + p_t^2}$ .

We observed that the model described up to here reproduced also the decrease of inelasticity by 30% between ISR and  $\bar{p}$ -p collider, after summation of the energies  $E_i = m_T \cosh y_i$  carried by individual secondaries ( $E_i$ ,  $y_i$  in Lab. system) (4).

The model is extended to hadron-air collision by introducing the number of participating nucleons  $\langle \nu \rangle = A (\sigma_{pp}^{\text{in}} / \sigma_{pp}^{\text{A}} = 1.325 + 0.0543 \ln E)$  established from hadron-nucleus data (5) with  $R_A = \langle n(pA) \rangle / \langle n(pp) \rangle \sim \frac{1}{2} (\langle \nu \rangle + 1)$ . Considering rapidity distribution normalized by rapidity distributions of p-p interactions of the same energy, we describe the rate

$$R(y) = \frac{(dn/dy)_{\text{p-Air}}}{(dn/dy)_{\text{p-p}}} \sim my + m_0$$

on plateau basis ( $m_0 = \rho_A / \rho_0$ ) and finally generate directly the clusters from the corresponding "inclined plateau"; the value  $R(y)$  obtained by the adapted Monte-Carlo procedure for all secondaries is shown on fig. 1 for 3000 p-air collisions with  $E = 10^6 \text{ GeV}$ .

For hadron-nucleus collision we adopt  $\langle p_t \rangle_{\text{p-A}} = \langle p_t \rangle_{\text{p-p}}$  as predicted by dual parton model (7) and fluctuations of multiplicity similar to p-p collisions. We refer hereafter this model as MPM (multicluster phenomenological model).

### 3. Comparison with Tian-Shan and KGF data (8,9)

Mixed component is taken as energy constant with 39.5% nucleons, 28.7%  $\alpha$ , 13.5% CNO, 11.5% LH, 6.9% iron groups, with  $\gamma = 2.7$  (2). The situation is shown in fig. 2 for MPM and nucleons, as well as for MPM and mixed. (The extension to nucleus-nucleus collision and the introduction of secondary  $\eta$ -mesons are discussed in HE 4.1-10), and also in fig. 3 for 220 GeV muons recorded in KGF (for nucleons primary only). The hadron behaviour versus size is shown on fig. 4 for  $E_H > 0.6 \text{ TeV}$  and  $E_H \geq 1 \text{ TeV}$  at Tian Shan level.

### 4. Conclusion

The multicluster phenomenological model, adapted to p-air collision is in surprising good agreement with EAS data at energy smaller than  $2 \cdot 10^7 \text{ GeV}$ ; this agreement is obtained without an increase of primary mass or multiplicity, even for higher energy muons in KGF (220 GeV) and high energy hadrons (0.6 to 1 TeV), suggesting agreement non only in central region, but in all the dynamical rapidity range.

5. Acknowledgements J.N.C. is indebted to Professor B. Degrange for drawing his attention on multicluster models.

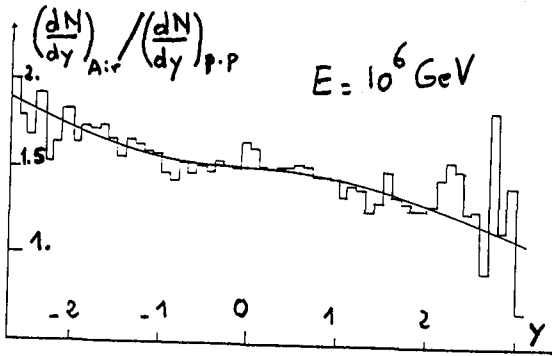


Fig. 1

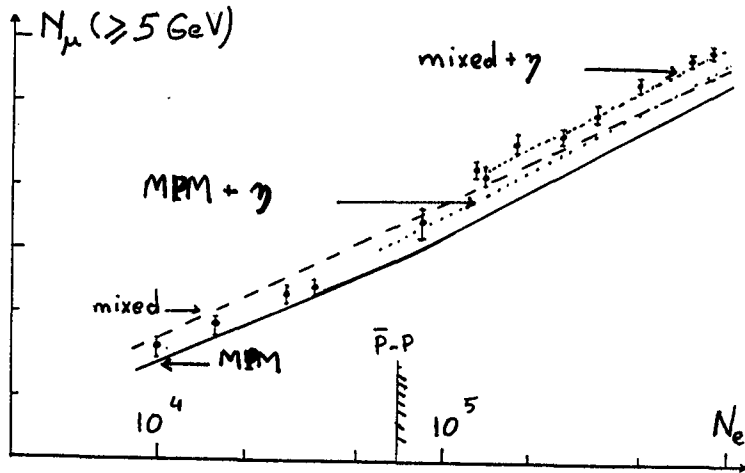


Fig. 2

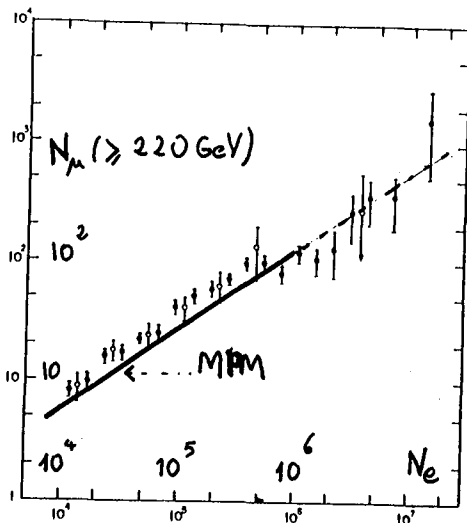


Fig. 3

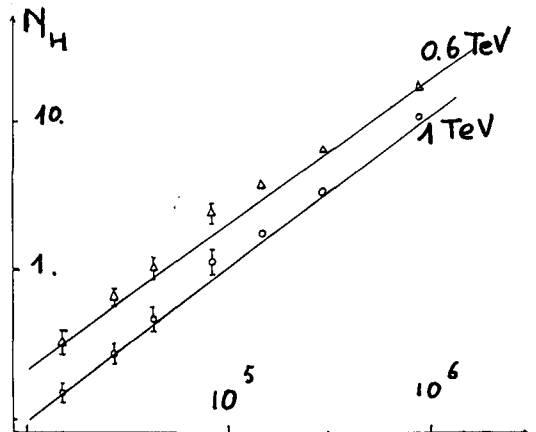


Fig. 4



References

1. P. Carlson, 1983, Proc. 17th Inter. Winter meeting on fundamental Physics, JEN Madrid, 11.
2. JACEE collaboration, 1984, Burnett T.H. et al., Int. Symp. Cosmic rays and particle Physics, Tokyo, 468.
3. S. Barshay, 1984, Phys.Rev. D29, 1010.
4. G.N. Fowler et al., 1984, Phys.Lett. 145B, 407.
5. J.E. Elias et al., 1980, Phys.Rev. D22, 13.
6. M.A. Faessler, 1984, CERN EP/84-165.
7. C. Pajares, 1983, Proc. 11th Int. Winter meeting on fundamental Physics, JEN Madrid, 257.
8. V. Aseikin et al., 81, 1982, FIAN reprint 178 and 215.
9. B.S. Acharya, 1983, Ph.D. Thesis, Tata Institute, Bombay.

## HIGH ENERGY HADRONS IN EXTENSIVE AIR SHOWERS

S.C. Tonwar

Tata Institute of Fundamental Research  
Homi Bhabha Marg, Colaba, Bombay-400 005  
India

## ABSTRACT

Experimental data on the high energy hadronic component in extensive air showers of energies  $\sim 10^{14}$ -  $10^{16}$  eV, when compared with expectations from Monte Carlo simulations have shown the observed showers to be deficient in high energy hadrons relative to simulated showers. We attempt here to understand these anomalous features with more accurate comparison of observations with expectations, taking into account the details of the experimental system. Results obtained from this analysis and their implications for the high energy physics of particle interactions at energies  $\sim 10^{15}$  eV are presented.

Studies on the characteristics of particle interactions at energies above those available at particle accelerators are being carried out either with emulsion chambers at mountain altitudes or through experiments on the high energy hadron component in extensive air showers. Results obtained on the hadron component in air showers of energies  $\sim 10^{14}$  -  $10^{16}$  eV over the last 15 years or so have presented a baffling picture. Initial attempts to interpret the observed characteristics of high energy hadron component in EAS were undermined by the apparent large differences between the results reported by different groups. However, during the last few years, our group<sup>1,2</sup> has been able to show that these differences are mostly due to instrumental factors and there indeed is a basic disagreement between the experimental results and the expectations from Monte Carlo simulations which use data available from CERN PP experiments. These disagreements relate to (i) the number of high energy hadrons per shower and (ii) the charged to neutral ratio among these hadrons. The present situation regarding the comparison between experimental results from four groups and our simulations<sup>1</sup> is shown in figure 1. It is seen from this figure that the most accurate measurements (represented by the line RHV) made using multiplate cloud chamber show the observed number of hadrons in a shower to be almost an order of magnitude smaller than the expected number. Electronic detectors (like single layer scintillators used as burst detectors), which integrate partially the energies of hadrons incident over the hadron detector, represented by lines RVS and BVS, expectedly overestimate the number compared to the measurements made with multiplate cloud chamber. Large area hadron calorimeters which integrate over the energies of the

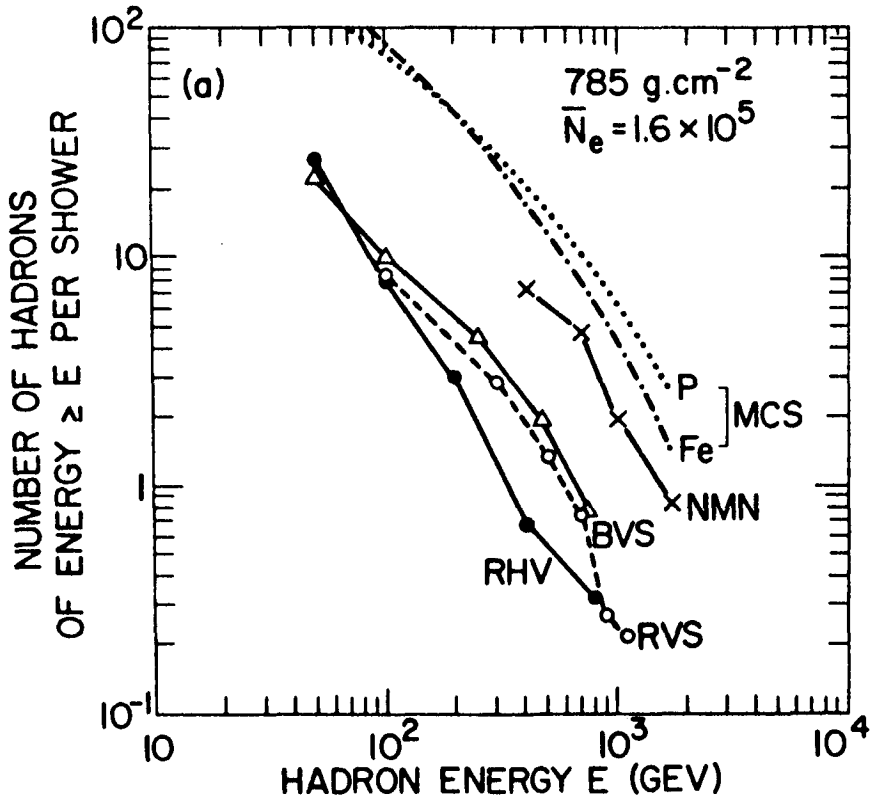


Figure 1 : Comparison of the observed integral energy spectrum for high energy hadrons in air showers of average size  $\sim 1.6 \times 10^5$  at mountain altitudes ( from reference 1)

hadrons incident over the detector fully, represented by the line MNM, give a much larger number for the high energy hadrons as expected.

It is clear from figure 1 that some major changes are required in interaction model at energies  $\sim 10^6$  GeV to account for this large discrepancy. A constraint on the range of models that can be proposed to account for this discrepancy is imposed by the observed charged to neutral ratio<sup>2</sup> for these high energy hadrons at mountain altitudes as shown in figure 2. It is seen from this figure that the observed C/N ratio is less than half of the value expected from simulations. Since charged pions constitute the largest component of the charged hadrons, protons and charged kaons being much smaller in number and neutrons and neutral kaons constitute most of the neutral hadrons, the results from C/N ratio suggest that dominance of pions among secondary particles may be less in interactions at air shower energies. Of course, another constraint on the range of models is imposed by the fact that observations on electron and muon components in air showers seem to agree well with expectations<sup>3</sup>. It should be remarked here that

our lack of firm knowledge of primary composition at air shower energies which plays a very significant role in interpretation of observations on electron and muon components, does not have any important role in the interpretation of data on high energy hadrons. It should also be noted that the discrepancies discussed above cannot be accounted in terms of experimental factors, e.g. energy resolution etc. The parameters that

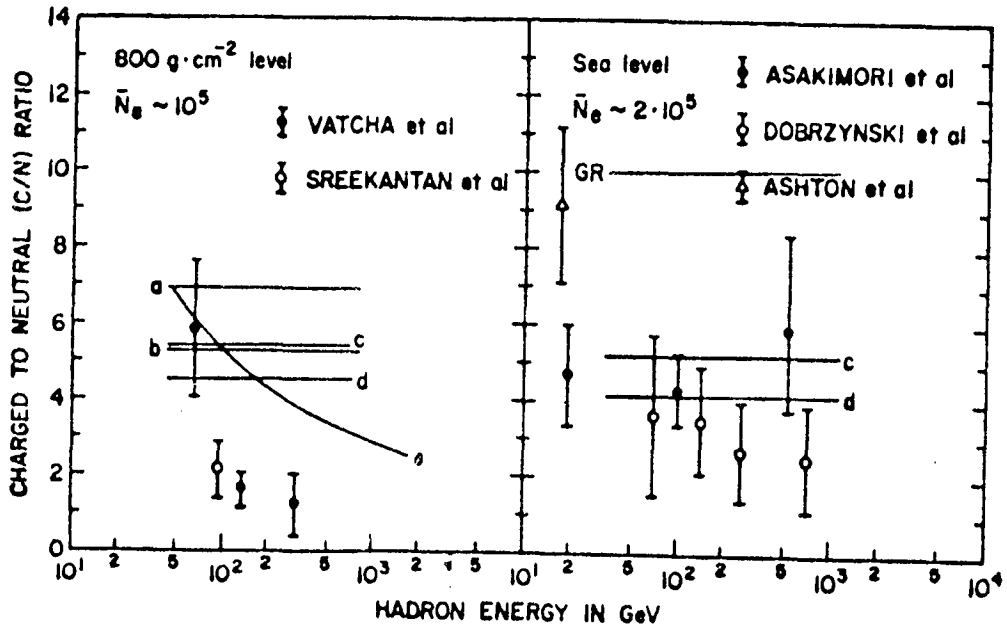


Figure 2: Comparison of the observed charged to neutral (C/N) ratio with expectations from simulations as a function of the hadron energy (from reference 2)

are readily available for changing the interaction model, without invoking an altogether new type of interaction such as suggested by the observations<sup>4</sup> of Chirons, Geminions, and Centauros, etc. type of events in emulsion chamber experiments at mountain altitudes, are (i) interaction cross-sections, (ii) composition of secondary particles, (iii) transverse momentum distributions, and (iv) longitudinal momentum distributions. Note that the average multiplicity as well as its distribution are essentially controlled by the forms of distributions for (iii) and (iv). The simulations already incorporate the increase in cross-sections<sup>5</sup> consistent with observations upto PP Collider energies and in fact are consistent with observations upto the highest energies  $\sim 10^{18}$  eV. Changing the composition of secondary particles towards lowering the pion content among secondaries and increasing the baryon content helps in reducing the C/N ratio but does not reduce the expected number of high energy hadrons significantly. The fact that large  $p_t$  tail and jets seem to play an important role at very high energies has already been

incorporated in the calculations, though not specifically as jets but as an energy dependent component of large  $p_t$  particles. It may also be noted here that consistency of the observed lateral distribution of hadrons with simulations approximately, poses some restraints on the range of large  $p_t$  cross-section that can be assumed. Softer  $x$  distribution is being tried in simulations at present and analysis is being carried out of showers simulated with various assumptions. Progress in this work will be discussed at the Conference.

#### ACKNOWLEDGEMENT

It is a pleasure to thank Prof. B.V. Sreekantan for many fruitful discussions.

#### REFERENCES:

1. Sreekantan, B.V., S.C. Tonwar, and P.R. Viswanath, Phys. Rev. D 28, 1050 (1983)
2. S.C. Tonwar, in Proton-Antiproton Collider Physics-1981, proceedings of the Workshop on Forward Collider Physics, Madison, eds. V.Barger, D.Cline, and F. Halzen ( AIP, New York, 1982), p.562.
3. G.B. Yodh et al, Phys. Rev. D 29, 892 (1984)
4. S. Hasegawa, Proceedings of International Symposium on Cosmic Rays and Particle Physics, Tokyo, 1984, eds. A. Ohsawa and T. Yuda (Institute for Cosmic Ray Research, Tokyo, 1984), p.718
5. S.C. Tonwar, preprint (1985).

DEPENDENCE OF THE AVERAGE SPATIAL AND ENERGY  
CHARACTERISTICS OF THE HADRON-LEPTON CASCADE  
ON THE STRONG INTERACTION PARAMETERS  
AT SUPERHIGH ENERGIES

N.G.BOYADJIAN, P.YU.DALLAKYAN, A.P.GARYAKA,  
E.A.MAMIDJANIAN

Yerevan Physics Institute, Markarian st. 2  
375036, Yerevan, Armenia, USSR

ABSTRACT

A method for calculating the average spatial and energy characteristics of hadron-lepton cascades in the atmosphere is described. The results of calculations for various strong interaction models of primary protons and nuclei are presented. The sensitivity of the experimentally observed EAS characteristics to variations of the elementary act parameters is analyzed.

The theoretical analysis of hadron-lepton cascade propagation in the atmosphere is possible at present by two methods: a) Monte-Carlo cascade simulation; b) solving the set of kinetic equations. Despite the advantages, the Monte-Carlo method is at the same time the most cumbersome and demands much computer time. The main drawback of the second method is that shower characteristics for fixed primary energy are obtained, whereas in the experiment the showers with fixed  $N_e$  are studied. However the comparison of the results obtained by both methods shows that the dependence of the average shower characteristics on the strong interaction parameters turns out to be qualitatively the same, while the quantitative difference is small. As an example of this, we may point out the conclusion that the average experimental characteristics of EAS can be described using the strong interaction model with increasing

cross sections, growing plateau in the pionization region and asymptotic scaling in the fragmentation region; this conclusion, being made from the solution of diffusion equations /1/, was confirmed by the Monte-Carlo simulation results /2/.

In the present paper we describe a method of solving the three-dimensional set of kinetic equations for shower components, based on the calculation of the contributions from the successive generations by Monte-Carlo evaluation of the corresponding multidimensional integrals.

The integral spectrum of the  $(i + 1)$ -th pion generation in EAS for depth  $Z$  and primary energy  $E_0$  can be presented in the form:

$$\Pi_{i+1}(>E, z) = \int \frac{dz'}{\lambda_\pi} e^{-\frac{z-z'}{\lambda_\pi}} \int_{E_{i+1} \geq E} \frac{d^3 p_{i+1}}{E_{i+1}} \frac{d^3 p_i}{E_i} * \quad (1)$$

$$* [N_i(\vec{p}_i, z) \int_{\pi N} (\vec{p}_{i+1}, \vec{p}_i) + \Pi_i(\vec{p}_i, z') \int_{\pi \pi} (\vec{p}_{i+1}, \vec{p}_i)]$$

where  $\Pi(>E, z)$ ,  $\Pi(\vec{p}, z)$  and  $N(\vec{p}, z)$  are the integral and differential momentum spectra of pions and nucleons at depth  $Z$ , and  $\int_{\pi N}(\vec{p}, \vec{p}_0)$  and  $\int_{\pi \pi}(\vec{p}, \vec{p}_0)$  are the invariant inclusive spectra of pion production in  $NA$  and  $\pi A$  interactions. The expressions for the nucleon and muon spectra can be written in the same manner. For Monte-Carlo computation of integral (1) a set of interaction depths in the atmosphere and particle momenta are randomly simulated. From the known momenta and depths, we calculate the distance from the shower axis to the particle's arrival point at the observation level. The value of the integrand is calculated for the simulated set. Further on, knowing the energy and the distance of the particle from the axis, we can obtain the integral and differential spectra over  $E$  and  $r$ . The spatial distribution function (SDF) of electrons is obtained multiplying the  $\gamma$ -production spectrum  $\Gamma(E, z, r)$  by the SDF for photon initiated

showers in the approximation of ref./3/. The accuracy of the calculation of the integral depends on the variance and the number of simulations of the integrand values. The integral was smoothed to minimize the dispersion. The method will be described in detail in a forthcoming paper.

This work presents the results of calculations for the models of multiple production. The first one is the so-called "standard" model of the scaling type, where the inclusive spectra are taken in the Hillas parametrization /4/, and  $\langle p_{\perp} \rangle = 0.37$  GeV. The second is the model of quark-gluon jets /5/, where the target nuclei effects are taken into account according to ref./6/. In this model, as is well known, there takes place the cross section rise, the plateau grows and the scaling is weakly violated in the fragmentation region. In this model the spectra differ quantitatively from those used earlier, mainly in the fragmentation region. The mean transverse momentum in this model increases logarithmically with energy.

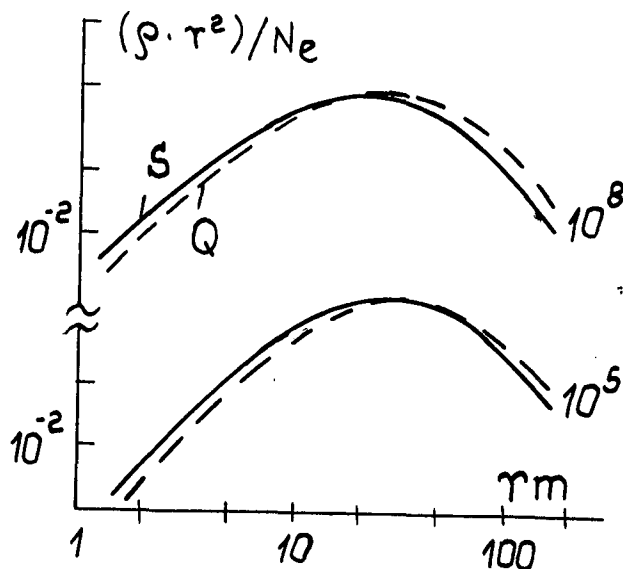


Fig. 1

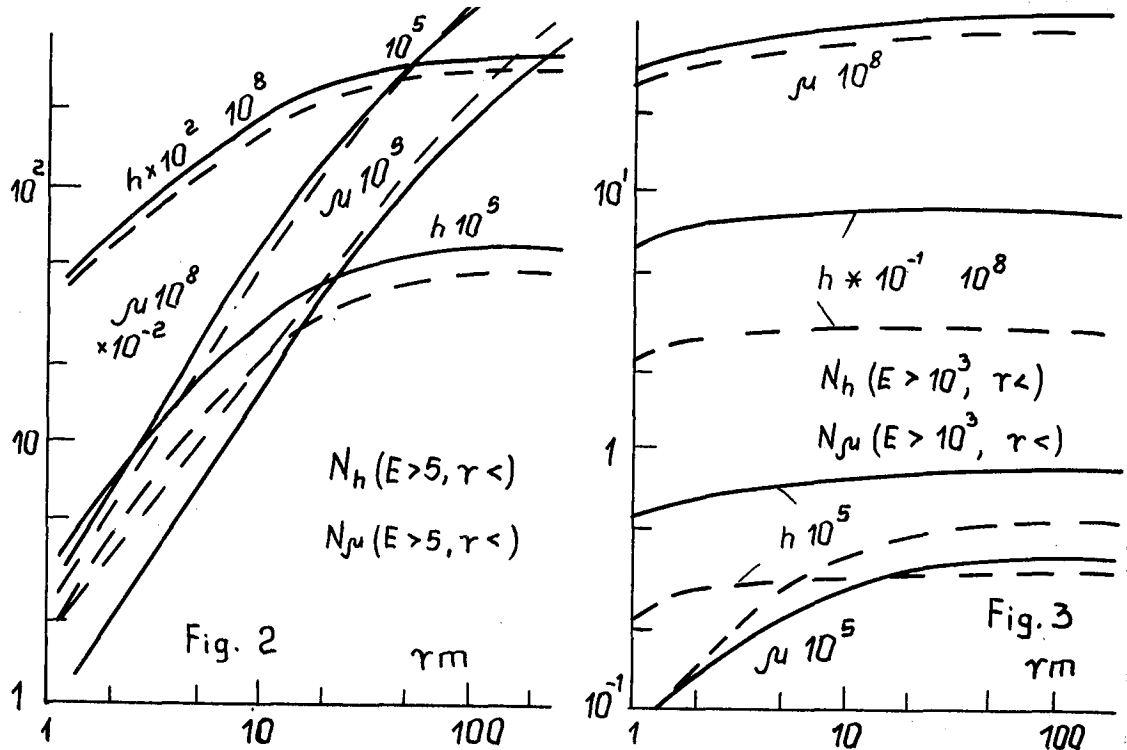
Figure 1 shows the radial distribution of  $\rho_e \cdot r^2 / N_e$ , where  $\rho_e(r)$  is the SDF at  $700 \text{ g/cm}^2$ . The figures near the curves denote the primary energy in GeV. S labels the "standard" model curve, Q - the models of the quark-gluon jets. The curves differ insignificantly, since the SDF of EAS is mostly due to the electromagnetic interactions. However in the model a more rapid energy dissipation takes place and

the SDF is a bit wider.

Figure 2 presents hadron and muon distribution in a circle of radius with  $E > 5$  GeV. The same is shown in



Fig.3 for an energy cut-off 1 TeV. The small energy particles number and the SDF show weak model dependence. As expected, the high-energy hadrons are concentrated in the narrow region near the shower axis. The same is true for high-energy muons. The SDF of high-energy hadrons is the most model-dependent characteristic. In the Q model the total number of muons with energy  $> 5$  GeV is greater than



in the S model, whereas the number of muons with  $E > 1$  TeV is almost the same but the SDF in the Q model is wider which is due to both rise of the cross section and the average transverse momentum. The total number of hadrons with  $E > 1$  TeV is larger in the S model as compared to that in the Q model by a factor of  $\sim 2.5$  in the range of  $E_0$  and  $r$ .

The authors are indebted to the participants of the ANI-84 workshop for useful discussions.

#### REFERENCES

- /1/ Boyadjian N.G. et al. Proc.17th ICRC, Paris, 1981, 6, 280.
- /2/ Kalmykov N., Khristiansen G. Proc.18th ICRC, 1983, 7, 330.
- /3/ Lagutin A.A. et al. Proc.16th ICRC, Kyoto, 1979, 7, 18.
- /4/ Hillas A. Proc. Workshop on Casc. Simul., Paris, 1981, p.13.
- /5/ Kaidalov A., Ter-Martirosian K. Yad.Fiz., 1984, 39, 545; 40, 211.
- /6/ Anisovich V.V. et al. Yad.Fiz., 1984, 39, 932.

HADRONIC COMPONENTS OF EAS BY RIGOROUS SADDLE POINT  
METHOD IN THE ENERGY RANGE BETWEEN  $10^5$  AND  $10^8$  GEV.

Malabika Sinha and Sisir Roy  
Indian Statistical Institute  
Calcutta 700035, India

Introduction : The study of hadronic components in the high energy range between  $10^5$  and  $10^8$  Gev exhibits by far the strongest mass sensitivity<sup>(1)</sup> since the primary energy spectrum as discussed by Linsley<sup>(2)</sup> and measured by many air shower experimental groups<sup>(3)</sup> indicates a change of slope from -1.7 to 2.0 in this energy range. This change of slope may be due to several reasons such as due to a genuine spectral feature of astrophysical origin, a confinement effect of galactic component or a rather rapid change of mass which problem has been attempted here to study in details.

Several attempts have already been done as discussed by Gridex<sup>(5)</sup>. Here, we shall analyse the hadronic components of EAS at this energy range within the scheme of a scale breaking model of multiparticle production<sup>(4)</sup>. We have used a modified rigorous saddle point method<sup>(5)</sup> to calculate the inverse Mellin transform of diffusion equations. The hadron spectra has been calculated for primary energy range from  $10^5$  to  $10^8$  Gev at sea-level as well as at mountain height at  $720 \text{ gm/m}^2$ .

Method : The integro-differential cascade equation for nucleon N and pions  $N_\pi$  are respectively given by

$$\frac{\partial N}{\partial y}(E, y) = - \frac{N(E, y)}{\lambda_{in}} + \int_E^{E_0} \frac{N(E', y)}{\lambda_{in}} W_{NN}(E', E) dE' \quad (1)$$

$$\begin{aligned} \frac{\partial N_\pi}{\partial y}(E, y) = & - \left( \frac{1}{\lambda_{in}} + \frac{B}{Ey} \right) N_\pi(E, y) + \int_E^{E_0} \frac{N(E', y)}{\lambda_{in}} W_{N\pi}(E, E') dE' \\ & + \int_E^{E_0} \frac{N_\pi(E', y)}{\lambda_{in}} W_{\pi\pi}(E', E) dE' \end{aligned} \quad (2)$$

For simplification, we have considered (i) the nucleon interaction length  $\lambda_N \approx$  pion interaction length  $\lambda_\pi$  at high energy<sup>(6)</sup>. (ii) Limiting fragmentation is assumed to hold for  $F_{NN}$ . The unknown function  $N_\pi(E, y)$  can be expressed in the form

$$N_\pi = n_\pi(E, y) e^{-y/\lambda_\pi} = n_\pi(E, y) e^{-y'} \quad (3)$$

$$\text{Let } \sigma_{in} = \sigma_{in} (1 + a \ln E/100) \quad (4)$$

$$\text{i.e. } \frac{1}{\lambda_{\pi}} = (1 + a \ln E/100) \text{ where } a \approx .037.$$

Initially, this rigorous saddle point method was proposed for scaling model(5) where

$$n_{\pi} + N_n = \frac{C_0}{E} \sqrt{\frac{\pi}{y'}} e^{y'} (g(s) - 1) - \bar{s}_0 \ln w \quad (5)$$

$$s_0 \text{ is given by } \left. \frac{dg}{ds} \right|_{s=s_0} = \frac{\ln w}{y'} \text{ and } \bar{s}_0 \text{ by } s_0 - ay' + 1$$

But according to our model the inclusive cross-section and the average multiplicity are given by

$$\frac{1}{\sigma_{in-el}} E \frac{d\sigma}{d^3p} \Big|_{pp \rightarrow \pi \bar{\pi}} \approx \frac{9}{\langle n \rangle_{\pi^-}} \cdot \frac{25}{4} \cdot \frac{1}{4\pi} \frac{f \rho \pi w}{16\pi^2} \exp \left[ - \frac{26.88}{\langle n \rangle_{\pi^-}} \cdot \frac{p_{\pi}^2}{(1-x)} \right] \exp \left[ - 2.38 \langle n \rangle_{\pi^-} x \right] \frac{mb}{\text{Gev}^2} \quad (6)$$

$$\text{where } \langle n \rangle_{\pi^+}^{pp} = \langle n \rangle_{\pi^-}^{pp} = \langle n \rangle_{\pi^0}^{pp} = 0.35 S^{\frac{1}{3}} (\text{Sin GeV}^2)$$

$$\text{Thus } F_{N\pi} = 1.06 e^{-2.38 \langle n \rangle_{\pi^-}} \cdot x$$

$$F_{N\pi} = 1.062 e^{-2.38 \times 5/9 \langle n \rangle_{\pi^-}} \cdot x \quad \text{Now at high energy we can write } F_{N\pi} = 1.06 e^{-2.38 \cdot 2^{\frac{1}{3}} x^{\frac{1}{3}} E_0^{\frac{1}{3}}} \quad (7)$$

where  $E/E' \sim E/E_0$ .

Here  $x$  be the Feynman scaling variable as used in the previous paper on saddle point method(5). So we can use the previous method to our case also. Now after some calculations it can be shown that  $s$  admits of an approximate representation in terms of gamma function i.e.

$$\left. \frac{dg}{ds} \right|_{s=s_0} = \frac{\ln w}{y'}$$

Here the following approximation has been taken for gamma function

$$(s) = 1 + a_1 (s-1) + a_2 (s-1)^2 + a_3 (s-1)^3 + a_4 (s-1)^4 + a_5 (s-1)^5$$

$$\text{where } a_1 = 0.5748, a_2 = 0.95123, a_3 = -0.699, a_4 = 0.4245, a_5 = -0.10106.$$

**Results :** In Fig.1, the several data are shown together with the hadron spectrum obtained by us from our model and also with that calculated by Grieder. These data cover a large size range centred around  $N_e = 10^7$  and this corresponds to primary energy  $10^6$  Gev. So different types of detecting system with large size window, explain this large dispersion of data.

But even with this dispersion we can emphasize from the comparison of these data with our prediction for iron and proton initiated showers of same total energy i.e.  $10^6$  Gev, that this energy range of primary spectrum can not be dominated by iron nuclei.

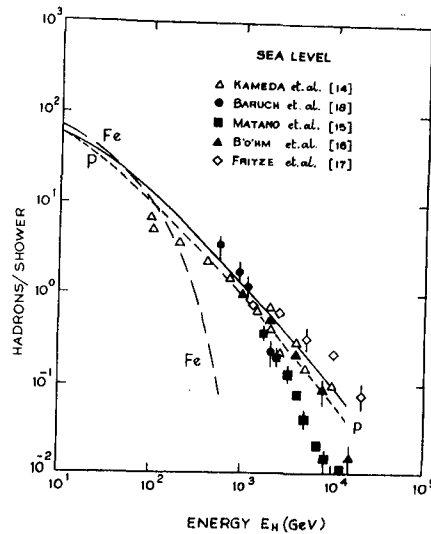


FIG. 1

Hadron energy spectra at sea level in proton initiated showers of  $10^6$  Gev primary energy obtained from our present work (solid line). Dashed and dot lines are from Grieder [1].

In Fig.2, we have compared the data obtained by Dubovy et al<sup>(7)</sup> at  $720 \text{ gm/m}^2$  which shows a nice agreement with our predicted hadron spectra with proton as primary particles whereas the spectra expected by taking heavy particle ( $\text{Fe} = 56$ ) as primary is showing a sharp cut off supporting our conclusion.

Now it is evident from the above results that in the critical energy region under consideration i.e. between  $10^5$  and  $10^8$  Gev, in particular around  $10^6$  Gev, is not dominated by iron primaries.

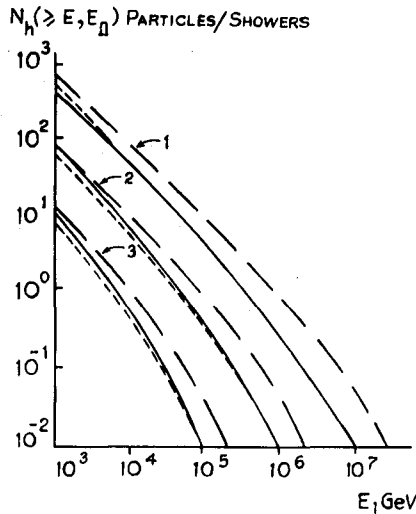


FIG. 2

Integrated energy spectra of hadrons in EAS as calculated for  $y = 720 \text{ gm/cm}^2$  and primary energy  $E$  (GeV)  $1-10^8$ ,  $2-10^7$ ,  $3-10^6$  and compared with those from Boyadzhyn et. al. [22] for  $a = a_\pi = 0$  (dashed curves),  $a_\pi = a_n = 0.03$  (dot curves) and prediction from present model (solid curves).

## References :

- 1] P.K.F. Grieder : 15th PICRC 8, 370 (Plodiv 1977).
- 2] J. Linsley : 18th PICRC, 12, 135 (Bangalore 1983), and references therein.
- 3] P.K.F. Grieder : 18th PICRC, EA 2-23, 328 (Bangalore, 1983).
- 4] P. Bandopadhyay et. al. Nuovo Cimento, 49A, 133 (1979) and references therein.
- 5] J. Sidhanta et. al. Phys. Rev. D 28, 1113 (1983).
- 6] J. Sidhanta and Rajkumar Roychoudhury, Z. Naturforsch 39a (1984).
- 7] A.G. Dubovy and N.M. Nestarova, Brief Communication on Physics No. 8, Phys., Inst., Acad., Sci. ( USSR ), 1978, p. 18.

ABOUT INCREASE OF THE LARGE  $p_{\perp}$  PROCESSES FRACTION IN  $hA$  INTERACTIONS AT ENERGIES  $5 \cdot 10^{14} - 10^{16}$  eV ACCORDING TO THE DATA ON E.A.S. HADRONS

Danilova T.V., Dubovy A.G., Erlykin A.D., Nesterova N.M., Chubenko A.P.

P.N. Lebedev Physical Institute, Moscow, 117924, USSR

The lateral distributions of EAS hadrons obtained at Tien-Shan array are compared with the simulations. The simulation data have been treated by the same way as experimental data, included the recording method. The comparison shows that the experimental hadron lateral distributions are wider than simulated ones. On the base of this result the conclusion is drawn that the fraction of processes with large  $p_{\perp}$  increases in hadron-air interactions at energies  $5 \cdot 10^{14} - 10^{16}$  eV compared with accelerator data in p-p interactions at lower energies.

Introduction. The hadron lateral distributions of EAS detected by Tien-Shan array /1/ ( $N_e \geq 1.3 \cdot 10^5$ ;  $p_0 = 690 \text{ g.cm}^{-2}$ ) were published previously /2,3/. It was found that the experimental distributions were wider than simulated ones and the difference increased with EAS size  $N_e$ . The more rapid rise with energy of the transverse momentum in hadron-air nuclei interactions has been assumed at primary energies  $E > 5 \cdot 10^{14}$  eV compared with the lower energies.

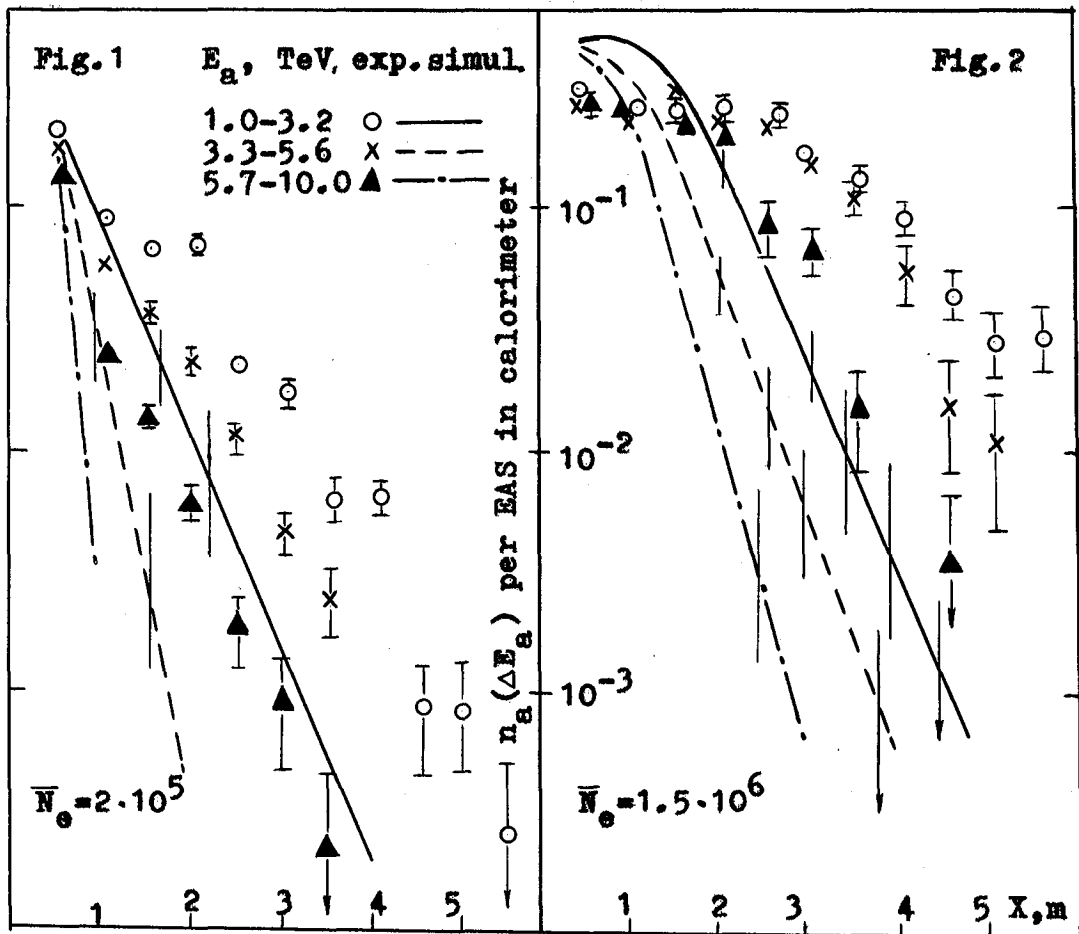
It is difficult to explain this result by variation of the primary mass composition, because calculations show a weak dependence of hadron lateral distribution at distances  $R=1,5-5$  m from EAS axis on primary composition.

Method. EAS electron-photon component parameters ( $N_e$ -size;  $X_0, Y_0$  - axis coordinates;  $\Theta, \varphi$  - zenith and azimuth angles;  $S$  - "age" and so on) have been determined by means of the multichannel scintillation and G.M. counter system. The energy and coordinates of hadrons have been determined by means of the ionization calorimeter ( $S_{tot} = 36 \text{ m}^2$ ). The descriptions of methods and accuracies were given in /1,2,3/.

The hadron density has been calculated as  $\rho_a(R) = N_a(R)/S$  for various distances  $R$ ; ( $N_a$  is the number of hadron cascades detected in the calorimeter;  $S(R, X_0, Y_0, \Theta, \varphi)$  is the area within the bounds of the calorimeter). The special simulation /3/ demonstrated the correctness of  $N_a(R)$  to  $\rho_a(R)$  restoration and the small influence of coordinate location inaccuracies. It is necessary to take into account the limited lateral resolution of hadron detectors (ionization chambers). It is possible that the hadron cascades in the calorimeter could be formed by several hadrons separated by distances smaller than the chamber size ( $0.25 \times 3$ )  $\text{m}^2$ .

In this report Tien-Shan experimental results on lateral distributions of hadron cascades in the calorimeter:

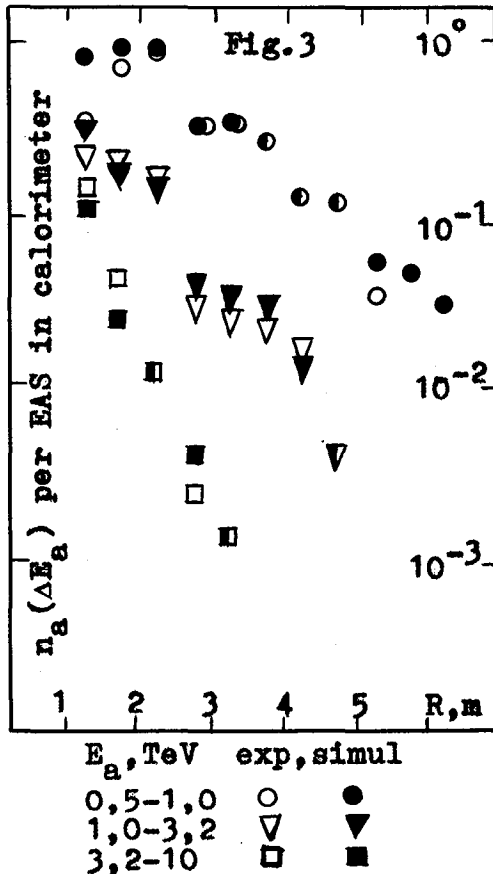
$N_a(R, \Delta E, N_e)$  are compared with the simulation data



based on atmospheric nuclear cascade model. The simulation data have been treated by the same way as experimental ones (selection, recording and processing criteria).

**Experiment.** On the base of  $\sim 5000$  EAS the dependence of hadron cascade number in calorimeter on  $R$  was obtained at distances  $R = 1-6$  m from axis in various intervals of energies  $E_a$  ( $\Delta E_a$ ) from 0.5 to 10 TeV and various intervals of  $N_0$ . The showers with axes passed through the upper plane of the calorimeter have been selected. EAS axis parameters ( $X_0$ ,  $Y_0$ ,  $\Theta$ ,  $\Psi$ ) were estimated by scintillation counters for the selection and after that they were corrected with the help of lateral parameters of hadron cascade with maximum energy. The cascade energy has been measured at 150-820 g.cm<sup>-2</sup> of Pb absorber in the calorimeter. The special calculation shows that this energy is equal to the energy of incident hadron on the average. The cascades which passed through the side chambers were not taken into account. The experimental results are presented in fig.1 and 2.

**Simulations.** The results of Monte-Carlo atmospheric nuclear cascade simulation were used to compare with the experiment. The detailed interaction characteristics at accelerator energies have been taken into consideration [4,5]. Previously the results of the calculation were checked by EAS expe-



perimental data at small  $N_e$  ( $E_0 = 10^{13} - 10^{14}$  eV). The energy dependence of the transverse dependence of the transverse momentum was taken as:  $p_{\perp} = 0.02 \lg E + 0.38$  for nucleons and  $p_{\perp} = 0.02 \lg E + 0.295$  for pions. Two versions of secondary particles energy spectrum were examined, where the "scaling" was preserved ( $\alpha = 0$ ) and it was violated ( $\alpha = 0.25$ ) /6/. The "normal" mixed primary composition was considered ( $\sim 40\%$  of protons). The simulation data for hadrons with the energy threshold  $E_a \geq 0.5$  TeV were used. At first, the distortion due to the limited lateral resolution of hadron detectors was analysed. Hadrons incident on the square of  $(0.25 \times 0.25)$  m<sup>2</sup> size have been combined to one cascade as in /7/. This size is equal to transverse size of ionization chambers in the experiment. The energy of the cascade was determined as the sum of energies of all hadrons in the square. The mu-

tual perpendicular chamber disposition at adjacent rows allows to select the cascades in this square.

In fig.3 the simulation results for the number of separate hadrons are compared with the number of hadron cascade in the calorimeter. The data are presented for showers of  $N_e = 6 \cdot 10^5$ ,  $\Theta < 45^\circ$  in three intervals of  $E_a$ :  $\Delta E_a = (0.5-1)$ ;  $(1-3.2)$ ;  $(3.2-10)$  TeV. The data in fig.3 show that the number of hadron cascades on  $(0.25 \times 0.25)$  m<sup>2</sup> square does not differ so much from separate hadron number at distances (1-5) m from axis.

The experimental and simulation result comparison. On the base of simulations one can conclude that the previous experimental data /2,3/ of hadron lateral distribution are not almost distorted by detection methods at distances  $R = 1-5$  m from the EAS axis.

In order to avoid the errors due to possible wrong identification of hadron cascades in two projections in the calorimeter, the new treatment of experimental and simulation data has been carried out by examination of only on X projection. In this case the total thickness of absorber above the chamber has been taken into account in the treatment of the experiment and the hadrons incident on the area  $(0.25 \times 3)$  m<sup>2</sup> (the size of the ionization chamber) are combined to cascades in simulation.



In fig.1,2 the experimental data on hadron cascade number  $n_0(X, \Delta E_a, N_e)$  passed through the calorimeter at different  $X$  distances are compared with the simulations for the version of "scaling" model treated by the same way as experimental ones. The data for three intervals of  $E$  are presented for two intervals of  $N_e$ :  $N_e = (1,3-3,2) \cdot 10^5$ ;  $N_e = 2 \cdot 10^5$  and  $N_e = (10-32) \cdot 10^5$ ;  $N_e = 1.5 \cdot 10^6$ . The experimental results are shown by figures, the simulated ones are by lines. It is seen from fig.1,2 the experimental distributions are wider than simulation ones. The preliminary additional calculation indicates: if hadrons with energies  $E_a < 0.5$  TeV are taken into account the result changes not so much.

Conclusions. The analysis of lateral-energy EAS hadron characteristics has been carried on the base of experimental statistical material several times greater than before /2,3/. Atmospheric nuclear cascade simulations made within assumption of "normal" weak rise of  $p_{\perp}(E)$  were carried out in the same conditions of detection and treatment as in the experiment. The comparison experimental and simulation results indicates the increase of large transverse momentum  $p_{\perp}(E)$  processes in hadron-air nuclear interactions at energies  $5 \cdot 10^{14} - 10^{16}$  eV compared with lower accelerator energies in p-p interactions. It permits one to assume that the fraction of hadron "jets" with large  $p_{\perp}$ , observed at accelerator experiments, increases with energy. This effect is predicted by QCD-theory /8/ in processes of deep inelastic scattering of partons. The special calculation is necessary to determine influence of these processes on the EAS hadron lateral distribution at  $E_0 > 5 \cdot 10^{14}$  eV. However, the approximate estimation has been carried out by us on the base of QCD-theory /8/ indicates to possibility to explain Tien-Shan experimental data by means of the large  $p_{\perp}$  "jet" production.

Acknowledgements. We would like to thank Romakhina N.S. for her help in treatment of data.

### References

1. A.D. Erlykin, N.M. Nesterova et.al. 9<sup>th</sup> ICRC, London, 1965, 2, 731
2. V.A. Romakhin, N.M. Nesterova, A.G. Dubovy 15<sup>th</sup> ICRC, Plovdiv, 1977, 8, 107
3. A.G. Dubovy, N.M. Nesterova, V.A. Romakhin Kratkie soob., Lebedev Institute, 1978, 10, 8
- 4,5. Danilova T.V., Erlykin A.D., Machavariani S.K. 17<sup>th</sup> ICRC, Paris, 1981, 6, 18<sup>th</sup> ICRC, Bangalore, 1983, 6, 78
6. Wdowczyk J., Wolfendale A.W. Nuovo Chim., 1979, 54A, N4, 433
7. Dubovy A.G., Dunaevsky A.M., Nesterova N.M. et al 17<sup>th</sup> ICRC, Paris, 1981, 6, 199.
8. Gribov L.V., Levin E.M., Ryskin M.G. Phys.Lett.B, 1983, 121, 65

PHENOMENOLOGY OF SOFT HADRON INTERACTIONS AND THE  
RELEVANT EAS DATA

N.N.Kalmykov, G.B.Khristiansen, M.V.Motova  
Institute of Nuclear Physics, Moscow State University,  
Moscow II7234, USSR

I.Introduction. The interpretation of the experimental data in superhigh energy cosmic rays requires the calculations using various models of elementary hadron interaction. One should prefer the models justified by accelerator data and giving definite predictions for superhigh energies. The model of quark-gluon pomeron strings (the QGPS model) satisfies this requirement.

2.Model of quark-gluon pomeron strings. The QGPS model combines the supercritical pomeron theory with the modern quark-gluon pattern of hadron interactions. (The term supercritical pomeron theory was used in the works /3,4/ where EAS calculations were first made in terms of the QGPS model) The QGPS model, called also the dual parton model /5,6/, allows at present to calculate all necessary characteristics of hadron-nucleon and hadron-nucleus interactions /7-9/.

The QGPS model gives a good agreement with experimental EAS data /3,4/ and describes also the main data on gamma-families /10/. The calculations in /3,4,10/ were made at  $\Delta = \alpha_p(0) - 1 = 0.07$  (see /1,2/), where  $\alpha_p(0)$  is the intercept of Regge pomeron trajectory. In this work we present the results of the EAS calculations in terms of the QGPS model with the parameters specified using the ISR and SPS data. The value of  $\Delta$  is now  $0.12 \pm 0.02$  /8/. That gives a stronger violation of scaling than  $\Delta = 0.07$ . Besides, the hadron-nucleus interactions are also treated in the QGPS model, so we don't need the additive quark model (AQM) that was used in /3,4/. It should be noted that values of function

$$R(x) = \left( \frac{1}{\sigma_{in}^{hA}} \times \frac{d\sigma^{hA}}{dx} \right) / \left( \frac{1}{\sigma_{in}^{hN}} \times \frac{d\sigma^{hN}}{dx} \right)$$

for AQM and QGPS models are the same with a good accuracy

(~10%).

3. Comparison with EAS data. Fig. I shows the inelastic nucleon cross-section in air calculated at  $\Delta=0.12$  in terms of the Glauber model. The result is almost the same as in work /3/ up to the energies of  $\sim 10^5$  GeV but the cross-section increases more rapidly at higher energies than at  $\Delta=0.07$ . The calculation results agree with the estimates obtained in cosmic ray experiments /II, I2/.

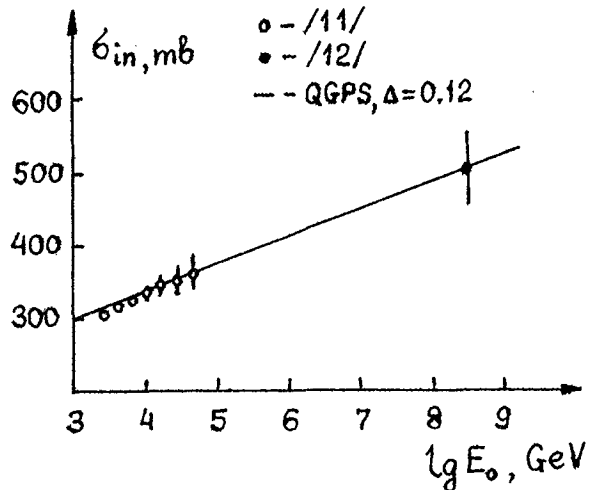


Fig.I. The inelastic nucleon cross-section in air.

Fig.2 shows the dependence of the  $>10$  GeV muon number  $N_M$  on the EAS electron size  $N_e$  at sea level. The model gives a good fit to experimental data if allowance is made for the complex primary composition (40% of protons and 15%

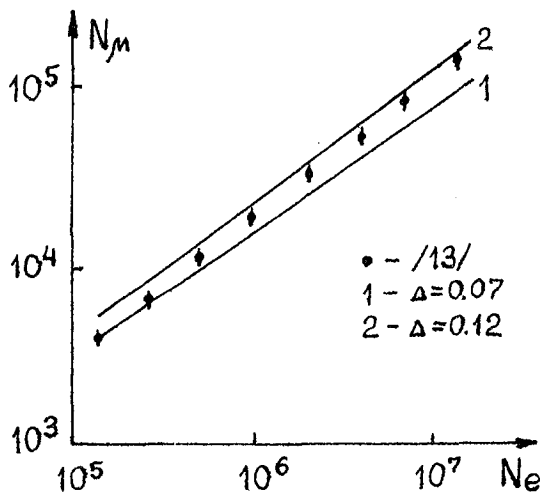


Fig.2. The number of  $>10$  GeV muons as function of the EAS electron number at sea level.

of fractions of nuclei with  $A=4, 15, 29$  and  $56$ ). The fit is better at  $\Delta=0.12$  than at  $\Delta=0.07$ . The small difference ( $\sim 0.05$ ) between the calculated and experimental values of  $\alpha$  in relation

$$N_M \sim N_e^\alpha$$

may be easily compensated considering the possible changes of the composition with energy in terms of the diffusion model /I3/ or the increase of the kaon and barion fractions of second-

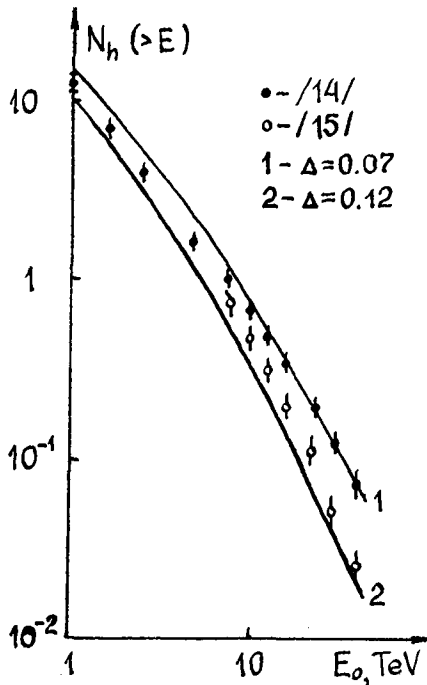


Fig.3. The energy spectrum of hadrons in EAS with  $N \approx 9 \cdot 10^5$  at mountain level.

energy (by  $10-20 \text{ g/cm}^2$ ) at different  $E_0$ , so the earlier conclusions concerning the agreement of the QGPS model predictions with experimental data /3,4,10/ remain valid.

Thus a certain variation of the QGPS model parameters improves the description of EAS experimental data as a whole.

daries as the energy increases /8/. A better agreement in the absolute values may be attained by slightly varying the primary cosmic ray composition.

Fig.3 shows the energy spectrum of EAS hadrons at mountain level and experimental data /14/. Considering that incidence of hadron groups onto EAS array causes difference between the hadron spectrum and measured spectrum of energies released in the ionization calorimeter at  $E_h \sim 10 \text{ TeV}$  /15/ one can claim that transition to  $\Delta=0.12$  improves the fit to experimental data.

The EAS maximum depth varies little as a function of primary energy

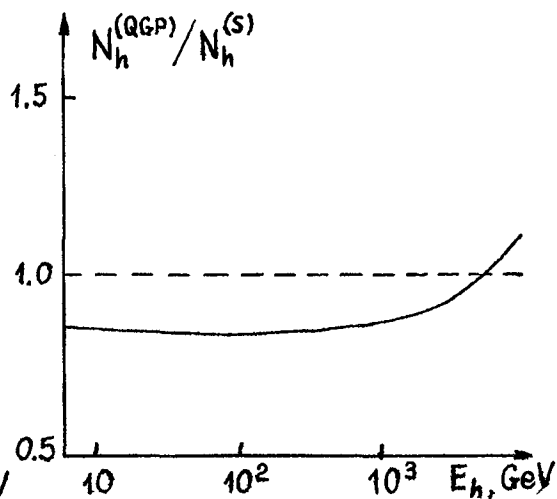
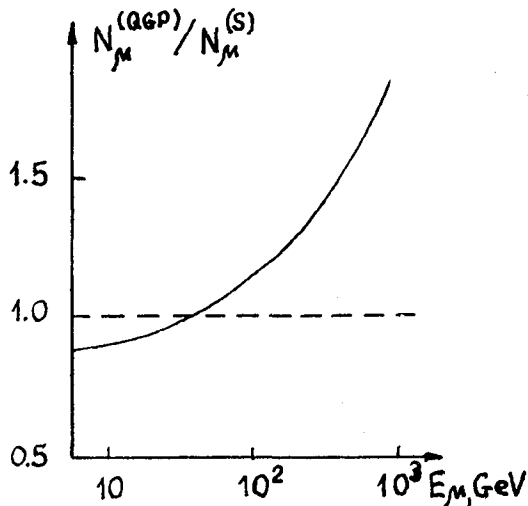


Fig.4. The sea-level energy spectra of muons and the mountain level energy spectra of hadrons in nucleus generated EAS.

4. Quark-gluon plasma. The possible production of quark-gluon plasma in nucleus-nucleus collisions has been intensively discussed since recently /16,17/. This model predicts significant cumulative effects (production of particles with energy  $> E_0/A$ ) and a large number of secondary kaons and barions. Fig.4 shows some characteristics of nucleus generated EAS ( $A=56$ ,  $E_0=10^6$  GeV) calculated in terms of quark-gluon plasma model /16,17/ the results being normalised to the traditional superposition model predictions. The calculations have shown that the shower maximum shifts as little as by  $20 \text{ g/cm}^2$ . The significant variations take place for hadron spectrum at energy region close to  $E_0/A$  and for muon spectrum at energies above 100 GeV. So to establish the existence of the quark-gluon plasma one should study hadron and muon spectra in nuclei generated showers at sufficiently high energies.

5. Acknowledgement. The authors are indebted to A.B.Kaidalov and Yu.M.Shabelsky for important discussions.

#### 6. References.

1. Kaidalov A.B., Phys.Lett., 1982, B116, 459.
2. Kaidalov A.B., Ter-Martirosyan K.A., Phys.Lett., 1982, B117, 247.
3. Kalmykov N.N., Khristiansen G.B., Pisma ZhETF, 1983, 37, 247.
4. Kalmykov N.N., Khristiansen G.B., Proc.18 ICCR, Bangalore, 1983, v.II, 330.
5. Capella A., Tran Thanh Van J., Z.Phys.C, 1983, 18, 85.
6. Aurenche P. et al., Z.Phys.C, 1984, 23, 67.
7. Kaidalov A.B., Ter-Martirosyan K.A., Sov.Nucl.Phys., 1984, 39, 1545; 1984, 40, 211.
8. Kaidalov A.B., Piskunova O.I., Preprint ITEP-I49, Moscow, 1984.
9. Kaidalov A.B., Preprint ITEP-II6, Moscow, 1984.
10. Kalmykov N.N. et al., Sov.Nucl.Phys., 1985, 41, 947.
11. Nam R.A. et al., Proc.18 ICCR, Bangalore, 1983, v.5, 336.
12. Cady R. et al., Proc.18 ICCR, Bangalore, 1983, v.II, 398.
13. Khristiansen G.B. et al., Cosmic rays of superhigh energies. Karl Thiernig Verlag, Munchen, 1980.
14. Nesterova N.M., Dubovy A.G., Proc.16 ICCR, Kyoto, 1979, v.8, 345.
15. Dubovy A.G. et al., Proc.18 ICCR, Bangalore, 1983, v.6, 163.
16. Anishetty R. et al., Phys.Rev.D, 1980, 22, 2793.
17. Elbert J.W., Stanev T., Proc.18 ICCR, Bangalore, 1983, v.5, 526.

THE MAXIMUM DEPTH OF SHOWER WITH  $E_0 > 10^{17}$  eV  
ON AVERAGE CHARACTERISTICS OF EAS DIFFERENT COMPONENTS

A.V.Glushkov, N.N.Efimov, I.T.Makarov, M.I.Pravdin

Institute of Cosmophysical Research & Aeronomy,  
Lenin Ave., 31, 677891 Yakutsk, USSR

L.G.Dedenko

Scientific-Research Institute of Nuclear Physics,  
Moscow, USSR

ABSTRACT

EAS development model independent method of the determination of a maximum depth of shower ( $X_m$ ) is considered.  $X_m$  values obtained on various EAS parameters are in a good agreement.

1. Introduction. Investigations of the shower maximum depth  $X_m$  are carried out at various arrays and by different methods but the significant scattering of the obtained data is still available (Table 1). A reason of most of discrepancies is mainly due to methodical difficulties associated with the transition from the observed EAS parameters  $P=P(X_m)$  to  $X_m$ . Thereby one had to use the theoretical conceptions on EAS development difficult to test experimentally.

2. Method. We considered one more method of  $X_m$  determination on the experimental data obtained at the Yakutsk EAS array. By computer calculations such parameters were found which are the functions of  $P=P(X_m/X)$  or  $P=P(X-X_m)$  type in wide limits of initial conditions:  $X=1020 \cdot \sec \theta$ . The calculations were carried out at various  $E_0$  and  $\theta$  on two, quite different models of EAS development. The first model corresponded to scaling [10], the second one - to scaling at  $E < 10^{14}$  eV

Table 1

Parameter	$E_0$	$X_m$	Work
$n_Q$	$1,6 \cdot 10^{17}$	$660 \pm 30$	[1]
$\tau_{1/2}(Q)$	$1,4 \cdot 10^{17}$	$700 \pm 15$	[2]
	$2 \cdot 10^{17}$	$681 \pm 20$	[3]
	$1,2 \cdot 10^{17}$	$706 \pm 36$	[4]
	$10^{17}$	$620 \pm 20$	[5]
	$10^{17}$	$545 \pm 20$	[5]
	$10^{17}$	$500 \pm 20$	[5]
	$2 \cdot 10^{17}$	$680 \pm 20$	[6]
LDF(Q)	$2 \cdot 10^{17}$	$627 \pm 20$	[7]
	$1,5 \cdot 10^{17}$	$600 \pm 50$	[8]
$\psi(\mu)$	$3 \cdot 10^{17}$	$684 \pm 30$	[9]
$lg(\rho_c/\rho_\mu)$	$3 \cdot 10^{17}$	$750 \pm 30$	[9]
LDF( $\rho_c$ )	$3 \cdot 10^{17}$	$609 \pm 3$	[9]

[10] and to  $n_s \sim E^{0,25}$  at  $E \geq 10^{14}$  eV. The cross-sections in inelastic processes on both models changed with energy according to [10]. The index of the LDF of electrons  $n_e$  at the distance interval  $R=200-600$  m from the shower core ( $\rho_e \sim R^{-n_e}$ ) and ratios of densities of the EAS Cerenkov light to electrons  $\lg(Q/\rho_e)$  and of electrons to muons  $\lg(\rho_e/\rho_\mu)$  at  $R=300$  m were considered. The above parameters are satisfactorily measured at the Yakutsk EAS array ( $\rho_e = \rho_s - \rho_\mu$ ).

3. Results. Calculation results at  $E_0 = 10^{17}-10^{18}$  eV and  $\theta = 16, 32$  and  $40^\circ$  are shown in Figs.1-3. From Fig.1 it is seen that  $n_e$  is unambiguously associated with  $X_m/X$  independently of  $E_0, \theta$  and characteristics of nuclear interactions. We use this peculiarity of electron LDF to find  $X_m$ :

$$X_m = \left( \frac{n_e - 2,11}{1,7} \right) \cdot X, \text{ g/cm}^2. \quad (1)$$

The obtained  $X_m$  are given in Table 2. The parameter  $\lg(Q/\rho_e)$  which is the function of  $X-X_m$  possesses the analogous feature (Fig.2).

$$X_m = X - 423(\lg \frac{Q}{\rho_e} - 0,88). \quad (2)$$

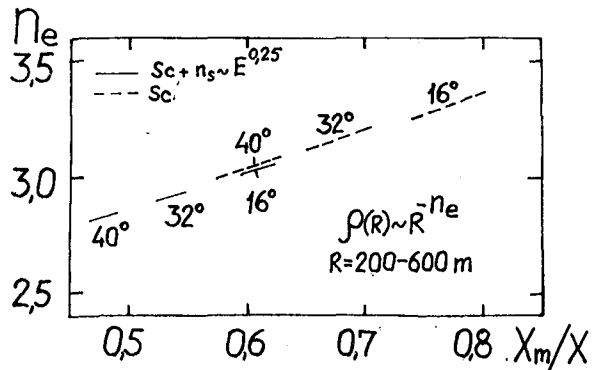


Fig.1

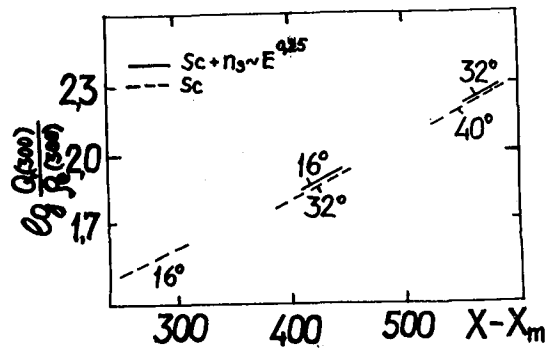


Fig.2

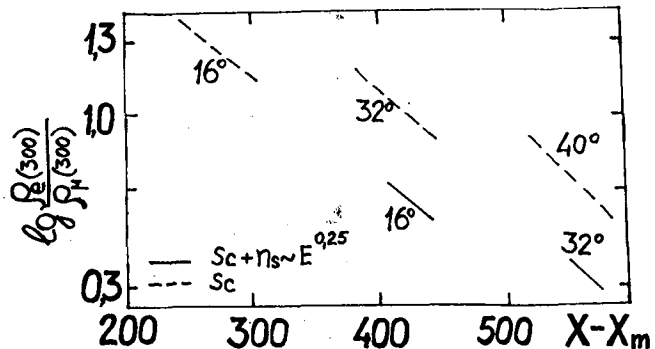


Fig.3

Table 2

$\lg E_0$	17,20	17,55	18,02	18,42	18,94
$X, \text{ g/cm}^2$	1060	1060	1070	1080	1060
$n_Q$	2,57	2,60	2,70	2,78	2,80
$X_m \pm \Delta X_m$	$660 \pm 30$	$675 \pm 30$	$725 \pm 30$	$765 \pm 30$	$755 \pm 40$
$n_e$	3,18	3,22	3,26	3,31	3,31
$X_m \pm \Delta X_m$	$665 \pm 60$	$690 \pm 60$	$720 \pm 60$	$760 \pm 60$	$750 \pm 60$
$\lg(Q/\rho_e)$	1,94	1,91	1,79	1,71	1,59
$X_m \pm \Delta X_m$	$615 \pm 30$	$625 \pm 30$	$685 \pm 40$	$730 \pm 40$	$760 \pm 45$
$\lg(\Phi/N_e)$	5,37	5,31	5,19	5,19	5,0
$X_m \pm \Delta X_m$	$640 \pm 40$	$665 \pm 40$	$725 \pm 40$	$735 \pm 40$	$800 \pm 40$
$\lg E_0$	-	17,56	17,91	18,39	18,79
$X, \text{ g/cm}^2$	-	1090	1080	1080	1080
$\lg(\rho_e/\rho_\mu)$	-	0,76	0,82	0,99	1,04
$X_m \pm \Delta X_m$	-	$670 \pm 20$	$670 \pm 20$	$715 \pm 20$	$725 \pm 25$
$\lg(N_e/N_\mu)$	-	1,17	1,28	1,47	1,54
$X_m \pm \Delta X_m$	-	$665 \pm 35$	$670 \pm 35$	$720 \pm 35$	$735 \pm 35$

As for  $\lg(\rho_e/\rho_\mu)$  the unambiguity condition due to the zenith angle is broken. Therefore the experimental and calculational data are needed to be compared at similar  $\theta$ .

The averaging of data in Table 2 results in the following expression:

$$X_m = (700 \pm 35) + (66 \pm 6)(\lg E_0 - 18), \text{ g/cm}^2. \quad (3)$$

Note that all the above parameters were experimentally obtained at fixed  $\rho_s$  (300) and calculations were also carried out under such condition. If to make calculations at fixed  $E_0$ , then  $X_m$  value becomes  $\sim 50 \text{ g/cm}^2$  less.

**4. Discussion.** The integral values  $\lg(\Phi/N_e)$  and  $\lg(N_e/N_\mu)$  are close to the parameters  $\lg(Q/\rho_e)$  and  $\lg(\rho_e/\rho_\mu)$ . Here  $\Phi$  is the total flux of the EAS Cerenkov light;  $N_\mu$  and  $N_e$  are the total numbers of muons and electrons. Their dependences on  $X-X_m$  are analogous to ones presented in Figs. 2 and 3.

Apply this method of the analysis of data to other arrays. One can do it without additional calculations with respect to the parameter  $\lg(\rho_c/\rho_\mu)$  [9], since it is similar to our parameter. According to [9] at  $R=300 \text{ m}$ ,  $E_0=10^{17} \text{ eV}$  and  $\theta \approx 15^\circ$  we have  $\lg(\rho_c/\rho_\mu)=0,3$ . To recount from  $\rho_c$  measured at the Haverah Park array to  $\rho_e$  at  $R=300 \text{ m}$  we



use the ratio  $\rho_e / \rho_c \approx 1,8$  [11]. Then  $\lg(\rho_e / \rho_\mu) \approx 0,58$  and from Fig.3 we find  $X_m \approx 620 \text{ g/cm}^2$ , i.e. much higher than in Table 1.

5. Conclusion. The analysis of various EAS components based on the method of "model independent" parameters yields  $X_m = 700 \pm 35 \text{ g/cm}^2$  at  $E_0 = 10^{18} \text{ eV}$  and at fixed  $\rho_s(300)$ .

### References

1. Efimov, N.N. et al., (1983), Proc. 18-th ICRC, Bangalore, vol.6, 176.
2. Kalmykov, N.N. et al., (1979), Proc.16-th ICRC, Kyoto, vol.9, 73.
3. Protheroe, R.J. and Turver, K.E. Nuovo Cimento, 51A, (1979), 277.
4. Thornton, B. and Clay, R., (1980), Phys.Rev.Lett., vol.45, 1463.
5. Inoue, N. et al., (1981), Proc.17-th ICRC, Paris, vol.11, 270.
6. Hammond, P.T. et al., (1978), Nuovo Cimento, 1C, 315.
7. Dyakonov, M.N. et al., (1981), Proc.17-th ICRC, Paris, vol.6, 106.
8. Hara, T. et al., (1981), Proc.17-th ICRC, Paris, vol.11, 277.
9. McComb, T.J.L. and Turver, K.E., (1982), Nucl.Phys., vol.8, 1119.
10. Hillas, A.M., (1979), Proc.16-th ICRC, Kyoto, vol.9, 13.
11. Kellermann, E.W. and Towers, L., (1969), Preprint, Univ.Leads.

SENSITIVITY OF DEPTH OF MAXIMUM AND ABSORPTION DEPTH OF EAS  
TO HADRON PRODUCTION MECHANISM

Antonov R.A., Galkin V.I., Hein L.A., Ivanenko I.P.,  
Kanevsky B.L., Kuzmin V.A.

Institute of Nuclear Physics, Moscow State University,  
Moscow 119899, USSR

Comparison of experimental data on depth of EAS development maximum in the atmosphere,  $t_m$ , and path of absorption,  $\lambda$ , in the lower atmosphere of EAS with fixed particle number in the energy region  $E_0 = 10^{15} - 10^{18}$  eV with the results of calculation show that these parameters are sensitive mainly to the inelastic interaction cross section and scaling violation in the fragmentation and pionization region. The data are explained in a unified manner within the framework of a model in which scaling is violated slightly in the fragmentation region and strongly in the pionization region at primary cosmic rays composition close to the "normal" one and a permanent increase of inelastic interaction cross section. It is shown that, while interpreting the experimental data, disregard of two methodical points causes a systematic shift in  $t_m$ : i) shower selection system; ii) EAS electron lateral distribution when performing the calculations on basis of which the transfer is made from the Cerenkov pulse FWHM to the depth of shower maximum,  $t_m$ .

Two models (I, II) [1] were used as basic ones in our simulation. In the both models, an increase in cross section of hadron-air nuclei interaction was taken in the form

$$\sigma_h^{in}(E_0) = \sigma_h^{in}(E') (1 + \alpha_h \ln(E_0/E')) \text{ where } E' = 100 \text{ GeV, } \alpha_h = 0.04.$$

In model I, at  $E_0 = 10^{14} - 10^{15}$  eV scaling is violated in both pionization and fragmentation regions, model II being quasi-scaling.

For a set of fixed values of  $E_0$  the double distributions over particle number at sea level and  $t_m$  were obtained. Using the Bialece theorem the distribution over  $E_0$  at fixed particle number was derived regarding the power-law primary energy spectrum ( $I(>E_0) \sim E_0^{-\lambda}$ ).

Table 1 lists the results of calculations for a 1030 g/cm<sup>2</sup> observation depth. For each version 100 showers were simulated. The values of the threshold energy  $E_{thr}$  of tracing a nuclear cascade are listed in Table 1. Mixed composition of primary radiation was regarded (see Table 2).

An examination of Table 1 shows that at a fixed particle number at sea level,  $N$ , the value  $t_m^{meas}$  is systematically overestimated regardless of a measurement method. The overestimate depends on  $E_0$  and the interval width  $\Delta N$ .  $E_0$  increasing up to  $\sim 10^{18} - 10^{19}$  eV, the overestimation decreases to zero.

Fig. 1 illustrates the difference of distributions over  $t_m$  in the case of a fixed primary energy and in the case

Table 1

E <sub>0</sub> , eV	E <sub>thr</sub> , GeV	Model I			Model II		
		$\bar{t}_m, \text{g/cm}^2$	$\bar{t}_m^{\text{meas}} - \bar{t}_m, \text{g/cm}^2$		$\bar{t}_m, \text{g/cm}^2$	$\bar{t}_m^{\text{meas}} - \bar{t}_m, \text{g/cm}^2$	
			$\gamma=1.7$	$\gamma=2.2$		$\gamma=1.7$	$\gamma=2.2$
10 <sup>14</sup>	5	427±7	+220	+240	467±9	+235	+251
10 <sup>15</sup>	5	490±7	+206	+226	541±8	+184	+210
10 <sup>15</sup>	10	485±7	+161	+181	---	---	---
3·10 <sup>15</sup>	5	520±7	---	---	---	---	---
10 <sup>16</sup>	5	---	---	---	618±8	+158	+170
10 <sup>17</sup>	50	---	---	---	667±15	+57	+67

Table 2

A	1	4	14	26	50-56
%	41	9	15	17	18

of a fixed particle number at observation level.

Table 3 compares results of Cerenkov light FWHM calculations regarding ( $\tau_2$ ) and disregarding ( $\tau_1$ ) shower lateral distribution. The latter approximation assumes all photons to be delayed as if they were emitted from the shower core. Further we present the values of differences between  $t_m$  evaluated using  $\tau_1$  and  $\tau_2$ : one can see that the use of  $t_m(\tau_1)$  dependence instead of  $t_m(\tau_2)$  leads to overestimation of  $t_m$ .

Fig.2 compares the summary of experimental data on  $t_m$  with the results of our calculation. At chemical composition close to the normal one the experimental data are well described by model I.

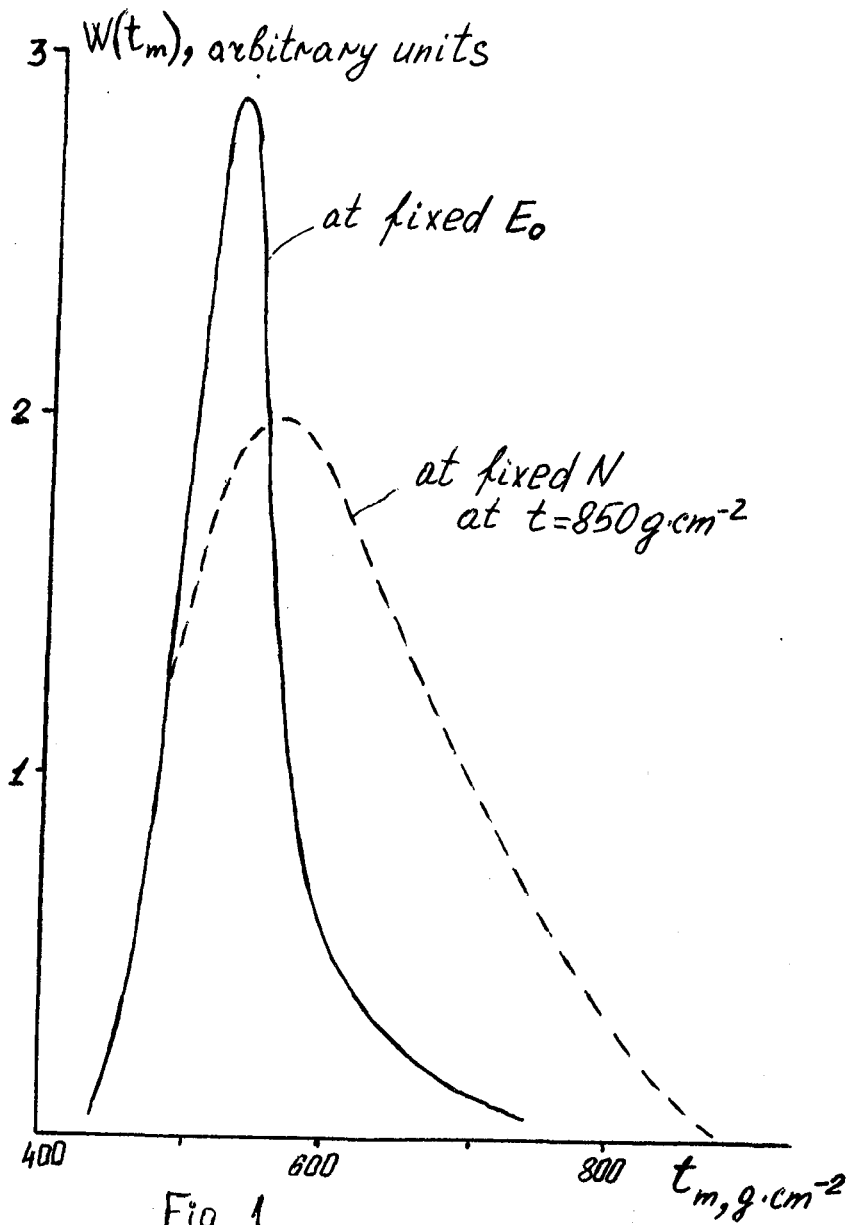
Table 3

E <sub>0</sub> , eV	R, m	$\tau_1, \text{ns}$	$\tau_2, \text{ns}$	$\Delta t = t_m(\tau_2) - t_m(\tau_1), \text{g/cm}^2$
10 <sup>15</sup>	200	8.5	4.1	110
10 <sup>15</sup>	300	25.2	16.9	90
10 <sup>15</sup>	400	40.6	33.9	50
10 <sup>17</sup>	200	19.5	13.2	150
10 <sup>17</sup>	400	54.3	63.4	50

Fig.3 presents the comparison of the experimental data from [3] on absorption path of EAS with fixed particle number N near sea level with our calculation. Calculation in terms of model I at  $\alpha_h \approx 0.04$  and "normal" composition is consistent with the experiment.

## References

1. Antonov R.A., Ivanenko I.P., Kuzmin V.A., Roganova T.M., Yadernaya Fizika, 1984, v.40, vyp. 5(11), 1222.
2. Ivanenko I.P., Kanevsky B.L., Roganova T.M., Pis'ma v JETP, 1978, 28, 704; Yadernaya Fizika, 1979, 29, 694; Preprint FIAN N 001, Moscow, 1979.
3. Nagano M. et al., J. Phys. G.: Nucl. Phys., 1984, 10, L235.



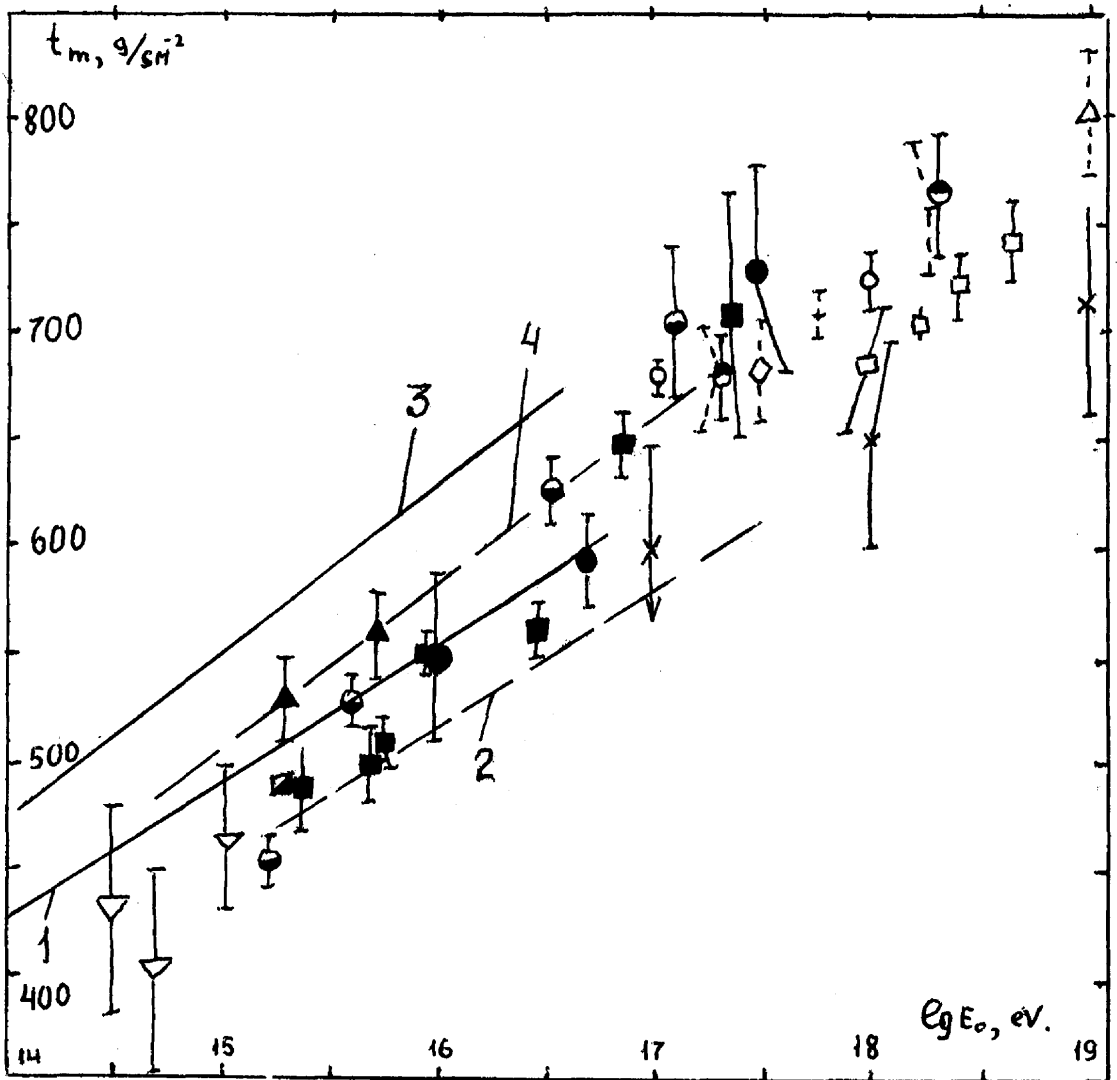
 $\lambda_{abs}$ 

Fig. 2.

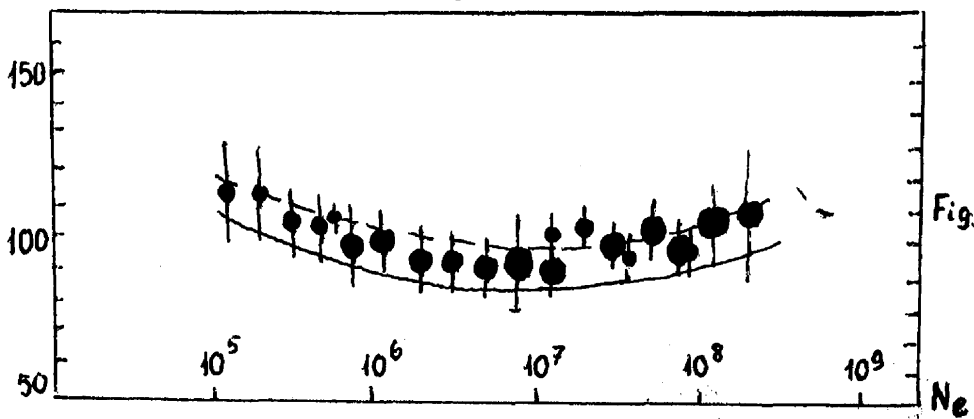


Fig. 3.

A CRITICAL ANALYSIS OF AIR SHOWER STRUCTURE  
FUNCTIONS AND SIZE SPECTRUM MEASUREMENTS  
WITH THE NBU AIR SHOWER ARRAY

N. Chaudhuri and D.K. Basak  
Department of Physics  
North Bengal University  
Darjeeling-734430, India

A total of 11,000 showers in the size range  $10^4$  to  $10^6$  particles so far detected by the NBU air shower array has been analysed using five different structure functions. A comparison of structure functions in terms (i) of shower size (ii) electron density at various core distances has been discussed to indicate the present status of structure functions in air shower analysis.

1. Introduction A small air shower array of 21 detectors has been set up at North Bengal University to cover shower size measurement in the range  $10^4$  to  $10^6$  particles. The shower sizes determined by taking any one of the different structure functions<sup>1-5</sup> for each set of observed showers show dispersion of individual shower sizes. It has been found that the lateral density distribution of electrons cannot be represented by a standard NKG function at all core distances with the single age parameter.

2. Methods The air shower array at NBU comprising 21 scintillation counters covers an area of  $900 \text{ m}^2$ . The detectors are of two different sizes. One is of  $25\text{cm} \times 50\text{cm}$  and the other is  $50\text{cm} \times 50\text{cm}$ . The layout of the array (Basak et al<sup>6</sup>) is based on the arrangement of detectors in a square symmetry. Each scintillator is of 5cm thickness mounted firmly on the box made of aluminium sheet. The small area detectors are placed near the centre of the array.

The analog pulses from all the 21 detectors are amplified first by preamplifiers each of gain  $\approx 30$  and are then sent to the main laboratory where they are again amplified by main amplifiers of appropriate gain. These pulses are then digitised with the help of analog-to-digital converter and the observed density information are printed on a paper tape.

### 3. Results

#### 3.1. The structure functions in terms of shower size

The observed density is corrected by considering the effect of transition in the scintillator material

and aluminium box using the formula of Asakimori et al<sup>7</sup> as given below

$$\Delta_c = \Delta_o / (1.192 - 0.136 \log r)$$

where  $\Delta_c$  is the corrected density and  $\Delta_o$  is the observed<sup>density</sup>, and  $r$  is the core distance in metre.

The structure functions in terms of shower sizes computed by taking NKG function and any one of the other structure functions for each observed shower are shown in Figs. 1 to 4. It is found that Fig. 1 shows the dispersion of individual shower sizes about the expected undeviated shower size line. However Fig. 4 shows a significant deviation between the expected and deviated line fitting the dispersion of the computed shower sizes using NKG and Hillas function. The important characteristics of air showers is the size spectrum which has been determined from the density distribution. The differential size spectrum can be represented by a power-law of the type

$$F(N_e) = (0.42 \pm 0.02) \times 10^{-8} (N_e/10^4)^{-2.51 \pm 0.01} \\ \text{m}^{-2} \text{sec}^{-1} \text{sr}^{-1} \text{particle}^{-1}.$$

It is important in the sense that if the size-primary energy relation is known, then the primary particle energy spectrum can be derived from the size spectrum.

### 3.2. The structure functions in terms of electron density distribution

The structure functions in terms of published electron density distribution functions<sup>1-5</sup> have been compared with the observed density distribution for different shower size and age values as shown in Figs. 5 and 6. We find that the observed electron density distribution follows the Hillas distribution more accurately than other density distribution functions.

4. Discussion The structure functions in terms of size indicate that the change of shower age from 1.2 to 1.1 (Figs. 1 to 4) causes a shift of core coordinates and a consequent decrease of shower size from Hillas function by about 35%. The use of distribution function by Lagutin et al<sup>4</sup> yields shower sizes somewhat smaller than those computed by NKG function, whereas in the electron density distribution, the Hillas function gives better distribution with observed density distribution. The differential size spectrum determined using the Hillas function gives an exponent of 2.51 for showers of size range  $10^4$  to  $10^6$  electrons.

5. Conclusions It can be concluded that the data on electron lateral distribution are in agreement with Hillas distribution function and the size spectrum obtained from Hillas function with average age of 1.2 compares well with the spectrum by KGF group<sup>8</sup> as

$$F(N_e) = (1.37 \pm 0.07) \times 10^{-8} (N_e/10^4)^{-2.42 \pm 0.02} \text{ m}^{-2} \text{ sec}^{-1} \text{ sr}^{-1} \text{ particle}^{-1}$$

6. Acknowledgements The authors are grateful to the Department of Atomic Energy, Govt. of India for the financial assistance for carrying out research work at North Bengal University.

### References

1. Greisen, K., (1960), Ann.Rev.Nucl.Sci., 10, 63.  
Nishimura, J. & Kamata, K., (1950), (1951), (1952),  
Prog.Theor.Phys. 5, 899, 6, 628, 7, 185.
2. Hillas, A.M. and Lapikens, J., (1977), Proc. 15th ICRC,  
Plovdiv, 8, 460.
3. Dedenko, L.G. et al, (1975), Proc. 14th ICRC, Munich  
8, 2731.
4. Lagutin, A.A. et al, (1979), Proc. 16th ICRC, Kyoto,  
7, 18.
5. Capdevielle, J.N. et al, (1983), Proc. 18th ICRC,  
Bangalore, 11, 307.
6. Basak, D.K. et al, (1984), Nucl.Intr.Meths., 227, 167.
7. Asakimori, K. et al, (1981), Proc. 17th ICRC, Paris,  
11, 301.
8. Rao, S. (1981), Ph.D. thesis, TIFR, University of Bombay,  
India.

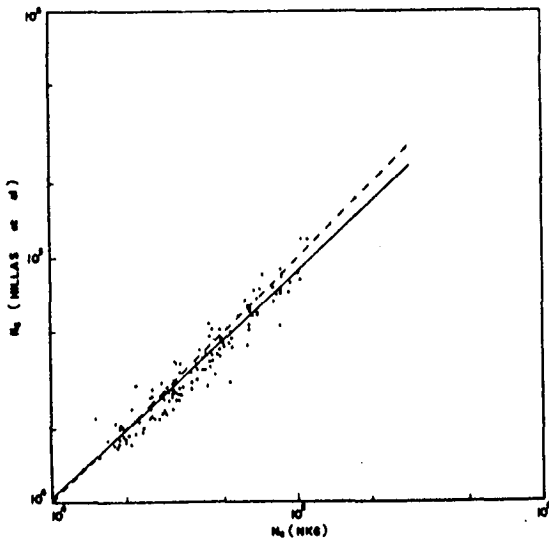


FIG. 1 THE DISPERSION OF SIZES OBTAINED FOR THE SAME SET OF SHOWERS USING THE FUNCTIONS OF HILLAS AND NKG FOR  $s = 1.3$ .

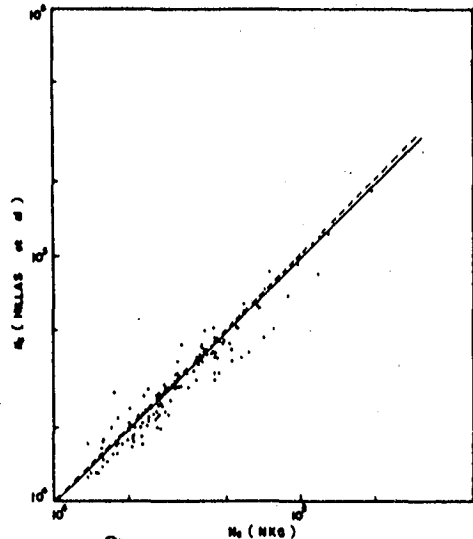


FIG. 2 THE DISPERSION OF SIZES OBTAINED FOR THE SAME SET OF SHOWERS USING THE FUNCTIONS OF HILLAS AND NKG FOR  $s = 1.3$ .



HE 4.2-1

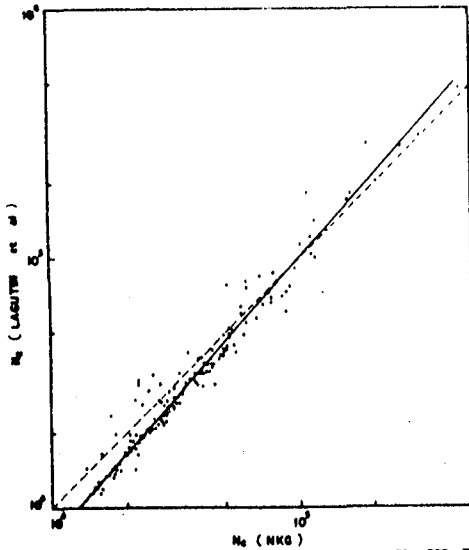


FIG. 3. THE DISPERSION OF SIZES OBTAINED FOR THE SAME SET OF SHOWERS USING THE FUNCTIONS OF LAGUTIN et al<sup>4</sup> AND NKG FOR  $s = 1.2$ .

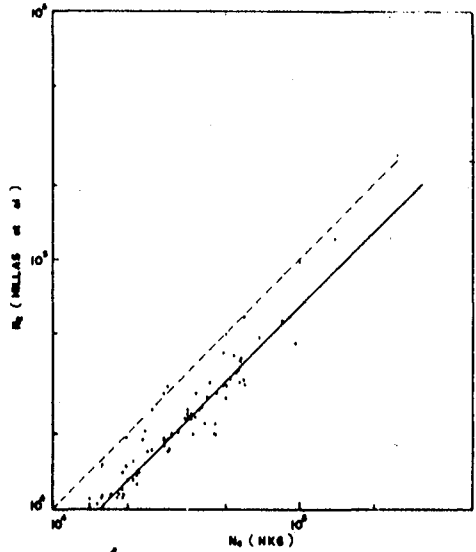


FIG. 4. THE DISPERSION OF SIZES OBTAINED FOR THE SAME SET OF SHOWERS USING THE FUNCTIONS OF MILLAS et al<sup>2</sup> AND NKG FOR  $s = 1.1$ .

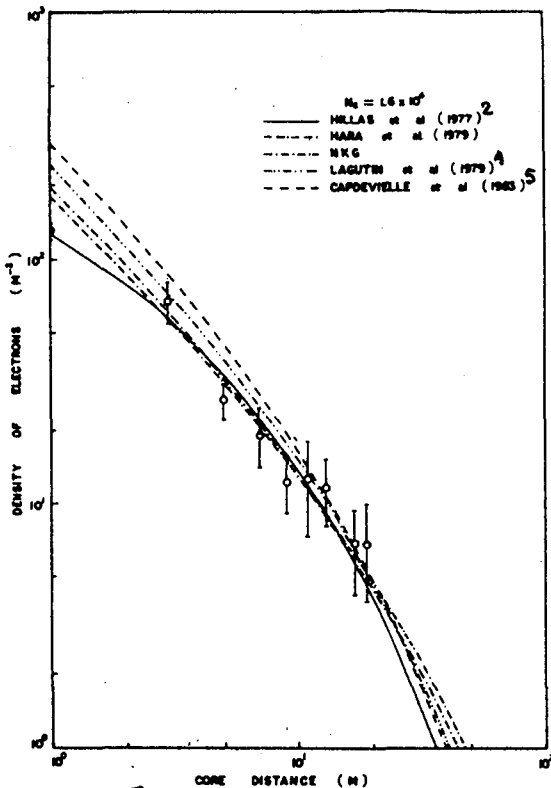


FIG. 5. COMPARISON OF OBSERVED LATERAL DISTRIBUTION OF ELECTRONS WITH THE THEORETICAL DISTRIBUTIONS ACCORDING TO VARIOUS STRUCTURE FUNCTIONS FOR  $N_0 = 1.6 \times 10^6$  &  $s = 1.0$ .

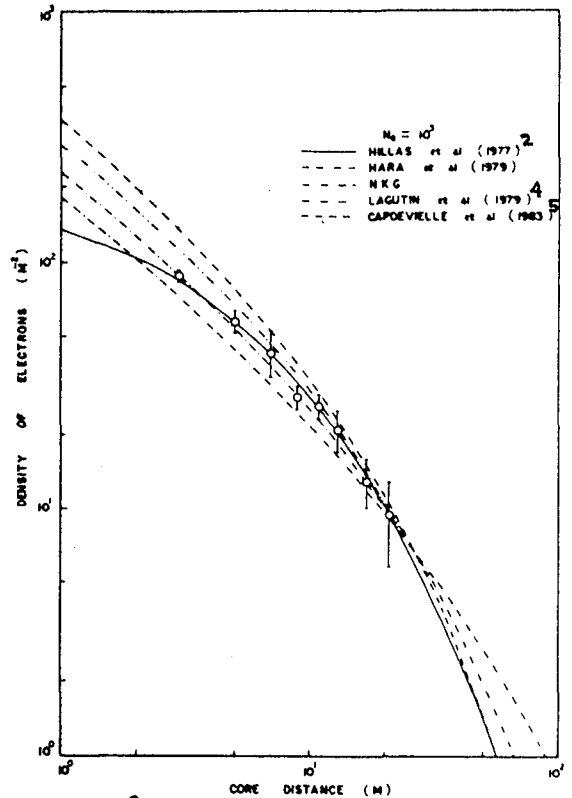


FIG. 6. COMPARISON OF OBSERVED LATERAL DISTRIBUTION OF ELECTRONS WITH THE THEORETICAL DISTRIBUTIONS ACCORDING TO VARIOUS STRUCTURE FUNCTIONS FOR  $N_0 = 10^7$  AND  $s = 1.2$ .

## MEASUREMENT OF THE LOCAL DENSITY SPECTRUM

Liu Z.H., Liu J.G. Li G.J.

Bai G.Z., Geng Q.X., Ling J.

Chongqing Institute of Architecture and Engineering  
Chongqing, People's Republic of China

Hazen W.E., Hazen E.S.

University of Michigan, Ann Arbor, Michigan, U.S.A.

## ABSTRACT

Since there is still disagreement among the results of various groups, we are doing a measurement of the local density spectrum with a close-packed array of four scintillators, each of area  $0.14 \text{ m}^2$ . Data are taken with conventional electronics, supervised by an on-line microcomputer. The data are stored on audio cassettes and analyzed with the aid of another microcomputer. Since we have four independent samples for each shower, uncertainties inherent in results from many earlier experiments can be minimized.

1. Introduction.

The local density spectrum provides important data for comparison with those from energy spectrum determinations and have some advantages from the experimental viewpoint. Although the measurements of density spectrum have been made for many years, there is still disagreements among the results of various groups. In order to get more detail and useful data of local partial density, some measurements and experimental plan have been made by our groups.

2. Method and experimental arrangement

The experimental arrangement consists of a small array of four plastic scintillators and a computerized

recording and analysing system. The area of each scintillator is  $0.14 \text{ m}^2$  and the thickness is 2.5 cm. The light signals are collected by a photomultiplier of model GDB-44 with a photocathode area of  $15.2 \text{ cm}^2$ . The scintillator is closed packed in a container of aluminum cone shell, and the inside surface of the container has been well polished, so the light of scintillator will be uniformly diffused.

The output from the scintillator counter has been calibrated against the response of a single particle to determine the particle number.

In order to obtain the correct value, the pre- and main amplifier has been well adjusted.

### 3. Computerized recording system.

Fig. 1 shows the associated recording and discriminating system.

The output signal from each photomultiplier are digitized through the electronics and transmitted to the computer's memory, therefore the data of each detector can be analysed separately. Use of the micro-computer offers advantages in data handling as well as provides overall system simplicity and flexibility.

### 4. Discussion.

Since we have four independent samples for each shower, uncertainties inherent in results from many earlier experiments can be minimized.

In the present measurement, only four scintillators have been operated, but it may be increased up to 8 photomultipliers.

### 5. Acknowledgements.

This work was supported by Chongqing Science and Technology Committee. We are grateful for the interest and support of Professor B.E.Wei, and we are also thank

up to 8  
PMT's

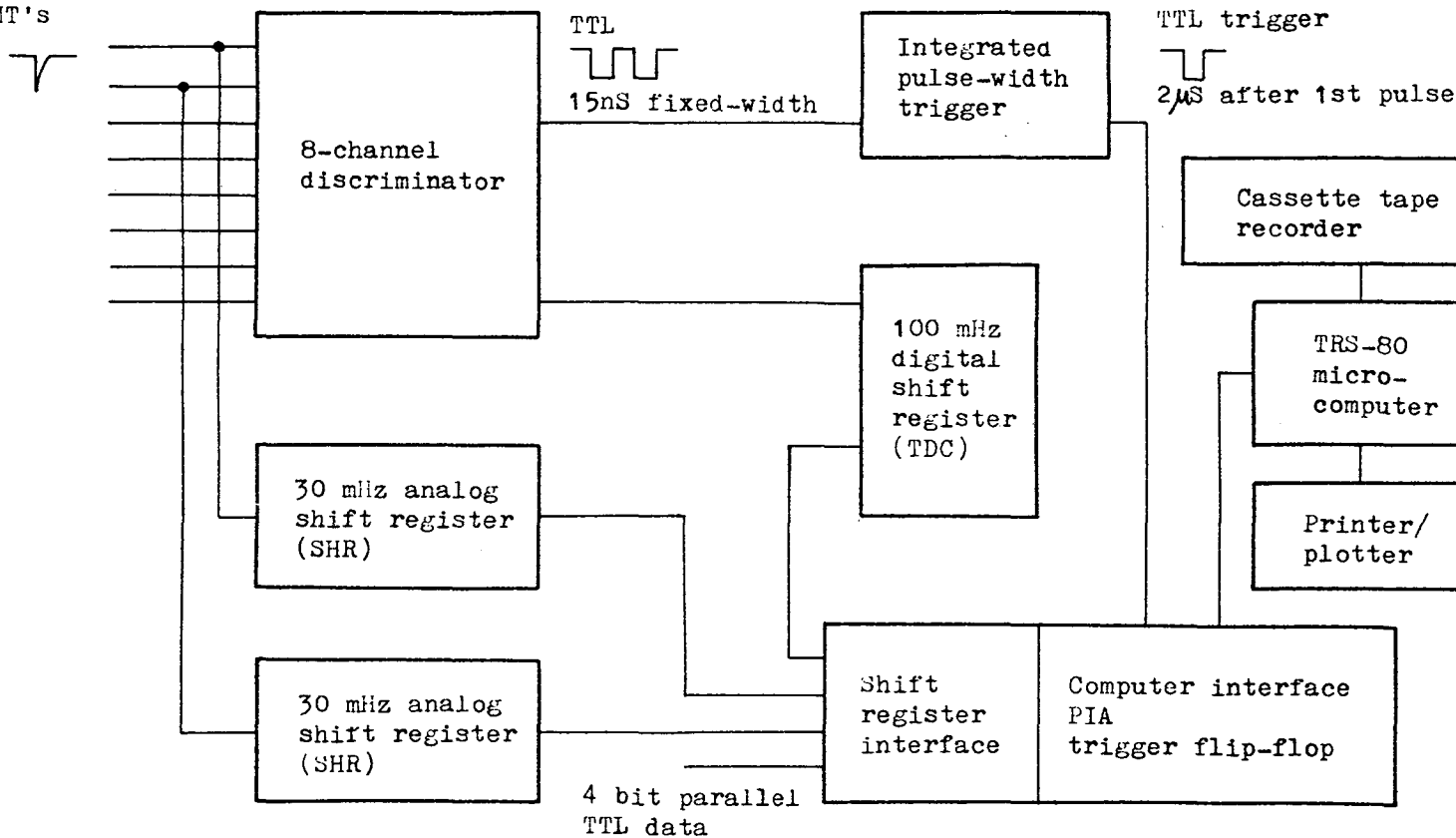


Fig. 1. Block Diagram of the Computerized Recording System

to Mr Y.H.Tam and Mr Y.F.Dai for valuable discussion.

References

- (1) Porter, M.R. et al., 17th ICRC, Conference Papers, Vol. 6, 308, 1981.
- (2) Hatano Y. et al., 16th ICRC, Conference Papers, Vol. 11, 161, 1979.
- (3) Hazen W.E. and Hazen E.S., 18th ICRC, Conference Papers, Vol. 6, 14, 1983.

## Character of Energy Flow in Air Shower Core

K.Mizushima

Kobe Women's Junior College, Chuo-Ku,  
Kobe 650, Japan

K.Asakimori and T.Maeda

Department of Physics, Kobe University  
Nada-Ku Kobe 657, Japan

T.Kameda

Kobe Women's University, Suma-Ku, Kobe 654, Japan

Y.Misaki

Research Center for Nuclear Physics,  
Osaka University, Ibaraki, Osaka 567, Japan

## ABSTRACT

Energy per charged particle near the core of air showers was measured by 9 energy flow detectors, which were the combination of Cerenkov counters and scintillators. Energy per particle of each detector was normalized to energy at 2m from the core. We obtained the following results as to the energy flow ;

- i) integral frequency distribution of mean energy per particle (averaged over 9 detectors) is composed of two groups separated distinctly,
- ii) Showers contained in one group show an anisotropy of arrival direction.

1 Introduction As it is clear that energy flow is an important parameter of air showers, we have pursued it from various points of view. Some results were reported elsewhere (1) (2). One of the most interesting results was the possible existence of an anisotropy of arrival direction seen among the showers having large relative deviation. However, number of the showers selected was small in the previous report, and so there lies a fear that the anisotropy is a pretense due to small samples. Also the criterion of large relative deviation was not clear enough. To confirm these points the experiment has been carried out, and the data analyzed augmented in number by twice and a half time compared to ones reported previously.

2 Experiment and Results Arrangement of nine energy flow detectors in the air shower array of Kobe University and the characteristics of them were reported in (1) and (2).

The measurement was carried out during the period from October 1981 to November, 1983. 2606 showers whose axes hit within 3m from the center of the assembly of energy flow detectors less

than  $30^\circ$  of zenith angle, were selected. We denote the energy flow in  $i$ -th Cerenkov counter by  $E_{0i}$ , where  $i=1,2,\dots,9$ , and put  $E_i = E_{0i}/N_i$ , where  $N_i$  is the number of charged particle measured by the scintillator just above the Cerenkov counter. Next, to obtain mean energy per charged particle at 2m from the axis,  $E_i$  is normalized at 2m using the average lateral distribution of energy flow which is approximately independent on shower size and on age for showers of size range  $10^5 \sim 10^6$ . Because of strict condition of selection ( $\theta \leq 30^\circ, r \leq 3m$ ) and characteristics of lateral distribution of  $E_i$ , errors induced in normalization are small. Each  $E_i$  normalized is ordered from maximum to minimum, and is expressed by  $E_{2i}$  ( $i=1,\dots,9$ ), where  $i=1$  corresponds to maximum, and  $i=9$  to minimum.

Using these  $E_{2i}$ , we put  $ME9 = \sum_{i=1}^9 E_{2i}/9$  and  $ME4 = \sum_{i=1}^4 E_{2i}/4$ .

Fig.1 shows the relation between  $ME9$  and size of showers. Showers of large value of  $ME9$  are found in region of smaller size ( $\leq 3 \times 10^5$ ). Fig.2 shows the integral spectra of  $ME9$ , corresponding to showers of different size region,  $10^5 \leq N < 1.5 \times 10^5$ ,  $1.5 \times 10^5 \leq N < 3 \times 10^5$ , and  $3 \times 10^5 \leq N$ , and we denote these spectra as SP1, SP2, and SP3 respectively.

If we approximate these spectra by power function, SP1 and SP2 have at least two different powers, suggesting that showers in the small size region have at least two different kinds of shower groups. Considering the bending point in SP1 and SP2 as critical energy, we divide showers into two groups and denote showers above the critical energy as H-group. Straight line in Fig.1 is the boundary of two groups. In Fig.3 are plotted arrival directions of showers H-group. They seem to show an anisotropy in the region of galactic north pole. Fig.4 shows the integral spectra in two regions of Right Ascension,  $12h \sim 16h$  and the remainder. From these two spectra the anisotropy occurs at  $ME9 \sim 0.9$  Gev and this value corresponds to the bending of SP1 and SP2 in Fig.2.

Fig.5 and Fig.6 show the relation between  $ME4$  and size of showers and that between  $ME4$  and age parameter. As  $ME4$  is interpreted to be energy flow of background particles, it is supposed to reflect the longitudinal development of air showers. The figures prove such interpretation to be right.

Fig.7 shows the relation between  $ME4$  and  $E_{21} - ME4$  (denote MAXE) in showers of different age regions. Detailed analysis of  $ME4$  and MAXE is now being carried out.

3 Discussion The criterion imposed vaguely on the boundary of large relative deviation previously is now clarified, and the boundary indicates the crossing point of two different groups. And in the group above the boundary (H-group) is seen an anisotropy to be exist. In spite of augmented data by factor 2.5, an anisotropy remains still in the region near the galactic north pole.

If the anisotropy found here is confirmed by further accumulation of data, and if H-group has any difference of characteristics from the remainder, it is safely said that H-group reflects some composition of the primary cosmic rays. It seems to be also interesting to study the relevance of the anisotropy mentioned here to that found in  $\mu$ -rich showers and N-rich ones.

Considering these items, we intend to investigate the characteristics of individual shower in H-group in detail.

#### References

- (1) Asakimori, K. et al.: 17th ICRC at Pris, 6(1981) 187.
- (2) Asakimori, K. et al.: 18th ICRC at Bangalore, EA 1.1-27

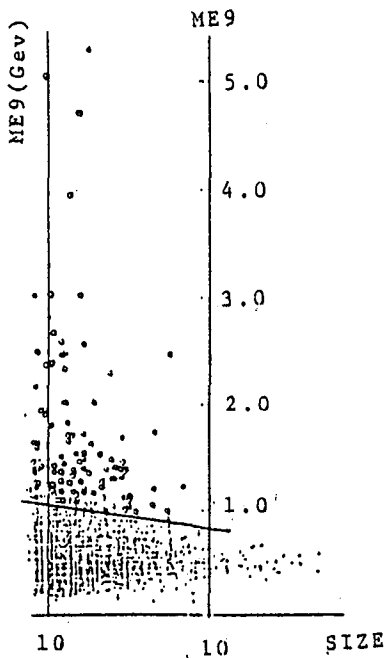


Fig. 1

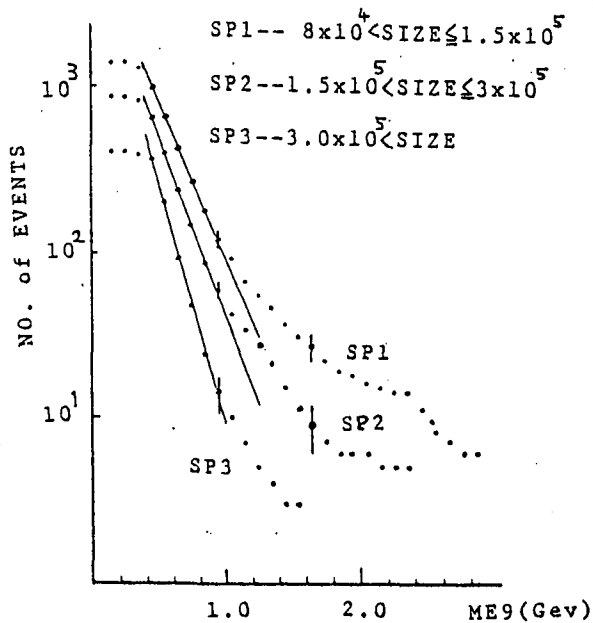


Fig. 2



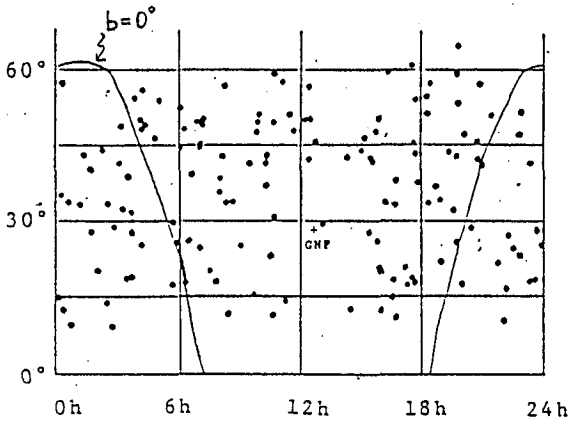


Fig. 3

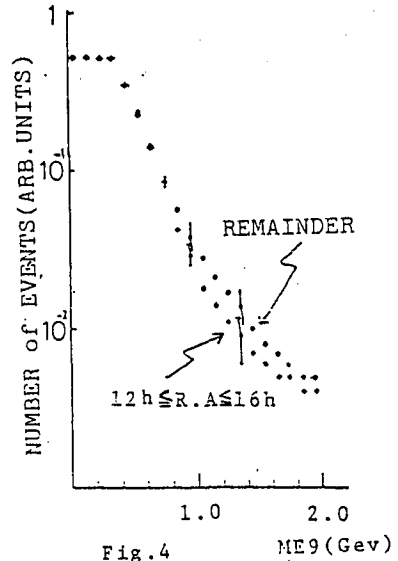


Fig. 4

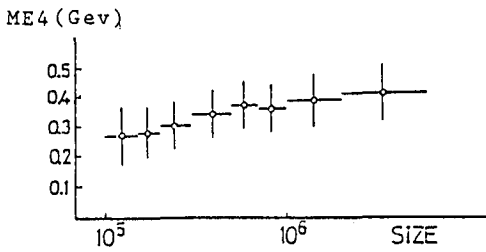


Fig. 5

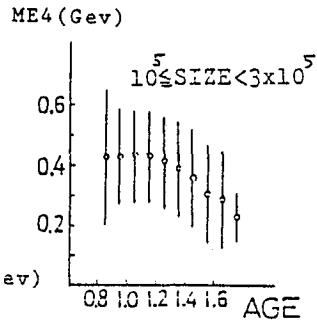


Fig. 6

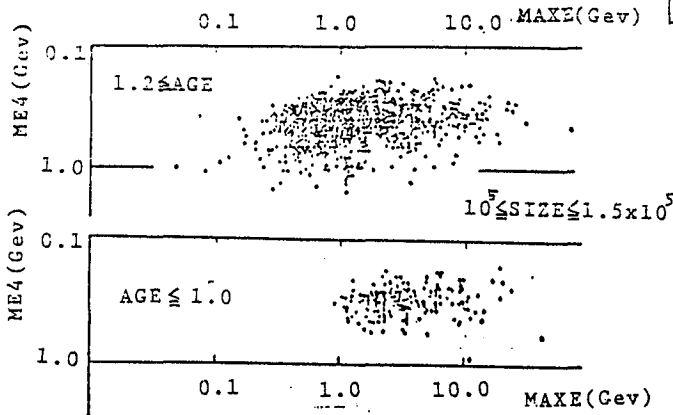


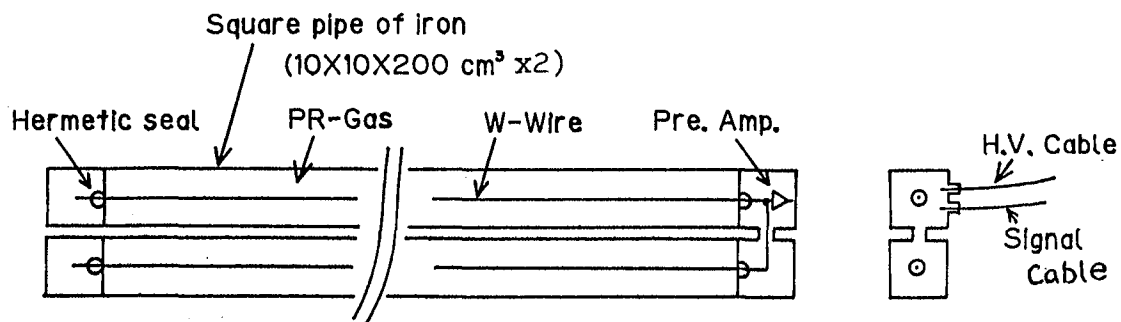
Fig. 7

## Observation of EAS using a large water tank

K. Inoue, H. Sakuyama, N. Suzuki and T. Suzuki

Department of Physics, Meisei University, Hino, Tokyo 191

Using a large water tank ( 30 m in diameter, 4.5 m in depth ) transition of EAS has been investigated at Taro ( 200 m above sea level ). There are set 150  $0.4 \text{ m}^2$  proportional counters to the bottom of the water tank. A conventional EAS array of 25 plastic scintillation detectors has been arranged within several tens meter from the water tank. Proportional counter (  $10 \times 10 \times 200 \text{ cm}^3 \times 2$  ) is made of a square shaped pipe of iron. Tungsten wire (  $100 \mu\text{m} \phi$  ) is tight stretched in the center of counter. A gas mixture of 90 % argon and 10 % methane is used at 760 mmHg. A set of proportional counter is shown in figure. About 3000 EAS have been obtained through 1 m of water since 1984.



## The Development of Air Shower in the Iron Absorber

M. Hazama:

Aichi Women's College, Nisshincho Aichi

S. Dake and K. Harada:

Department of Physics, Kobe University, Kobe

M. Kawamoto:

Natural Science, Kobe University, Kobe

M. Sakata and Y. Yamamoto:

Department of Physics, Konan University, Kobe

T. Sugihara:

College of Liberal Arts, Kobe University, Kobe

### ABSTRACT

The iron open-sandwich experiments to observe one dimensional development of individual air showers were carried out at Akeno Observatory. One dimensional energy flow, incident energy and production height of shower is estimated using the data of size and age obtained from the above experiment and simple calculation.

#### 1. Introduction.

In order to study the total development of individual air showers, two general methods to observe at different altitudes or to catch the generation gap of air showers from the difference of their arrival directions at the same altitude, have been used. But it is impossible to observe the longitudinal development of a shower and only able to grasp its average features.

The experiments to measure the particle density of each generation of a shower using the multiple detectors set top and bottom sandwiching some materials such as water, iron, lead etc. as absorber between them and arranged over the range of 3 - 7 m, mainly to study the longitudinal development of the central parts of an air shower, have been carried out. (1-4) But the cost of experiment increases when the sandwich type arrangement mentioned above is adopted to observe the total longitudinal development of individual air shower, because the whole range of lateral spread of an air shower must be covered with the detectors.

Now, the new observation method so called "open sandwich" has been proposed as follows. Some different kinds of air

shower arrays are arranged over the range enough to observe whole features of air shower.

The types of air shower array are classified by the thickness of the substance piled on the scintillation counter. The transition of the particle densities of an air shower is known when it passes through a substance by comparing the particle densities obtained from some different kinds of air shower arrays, and in the result the total longitudinal development of an air shower can be observed by the smaller number of detectors.

## 2. Experimental procedure.

Iron open sandwich experiment was carried out at station in Akeno Observatory (920g/cm<sup>2</sup>) for three months (December 1980 - March 1981). The array consists of 100 scintillation counters which covered an area of 50x50m<sup>2</sup>, they are 30 counters, on which 5 iron plates are laid (4.5cm iron thick and called 2Fe array), 28 counters 10 iron plates (9cm thick, 4Fe array) and 42 counters non iron plate (0Fe array) in which 4 counters to detect arrival direction are included. The unit area of 96 scintillation counters is 0.5m x 0.5m and of 4 detectors for arrival directions is 1m x 1m.

The air shower array was triggered by the condition of any six fold coincidence out of central eight scintillation counters discriminating of 6 particles per counter. Thus 12,070 air showers were obtained in the above observation period.

## 3.1 Analysis of air showers.

The coordinates of shower axis ( $X_c, Y_c$ ) and the set of the parameters size  $N_0$  and age  $S_0$  ( $N_0, S_0$ ) on top of the iron plate, where  $S_0$  denotes lateral spread of air shower, are determined by fitting lateral density distribution curve obtained from 0Fe data to the theoretical lateral curves (NKG lateral structure function) by means of the least square method.

Another two sets of size and age ( $N_2, S_2$ ) and ( $N_4, S_4$ ) for the axis of 0Fe array are also obtained by the same method as above using the data from 2Fe and 4Fe array respectively. The arrival direction (zenith angle  $\theta$ ) is determined by the difference of time arriving at the 4 counters to detect zenith angle.

1,308 air showers whose axes hit near the central part of the array and the parameters sizes and ages are determined with high precision, which are suitable for analysis, are selected and analyzed. They satisfy the following conditions:

$\theta < 30^\circ$ ,  $r = \sqrt{X_c^2 + Y_c^2} < 8.0 \text{ m}$ ,  $\sqrt{\sum dN_0(i)^2/42} < N_0$ ,  
 $\sqrt{\sum dN_2(i)^2/30} < N_2$ ,  $\sqrt{\sum dN_4(i)^2/28} < N_4$ , where  $dN_0(i)$ ,  $dN_2(i)$  and  $dN_4(i)$  are the difference between the number of particles detected by the  $i$ -th detector of 0Fe, 2Fe, or 4Fe array and one estimated as the value of  $i$ -th detector from the sets of parameters ( $N_0, S_0$ ), ( $N_2, S_2$ ) or ( $N_4, S_4$ ) respectively.

### 3.2 Models, energy and production height of air shower.

An air shower starts from the gamma rays decayed from neutral pi mesons which are produced when a primary cosmic ray interacts with an air nucleus. The number of gamma rays and the energy distribution of the gamma rays are assumed as follows.

In 1-gamma ray model (e1) 1 gamma ray is emitted and in CKP model (e2) the number and the energy of gamma ray follow CKP distribution. One third of incident energy transfers to electromagnetic cascade in both models. The age parameter of an air shower  $S_1$ , which denotes longitudinal development of air shower, can not to be measured directly.

From the experimental results that in electromagnetic cascade the age for lateral development agrees with the one for longitudinal development when they are measured in the range one Molliele unit, which presents order of lateral spread of air shower and about 91 m at Akeno,  $S_1$  is substituted for  $S_0$  in usual. However, they are essentially different to each other, then following two models about age parameter of individual air shower are assumed as  $S_1 = S_0 \dots (sa)$  and  $S_1 = S_0 + 0.2 \dots (sb)$ .

The combination of 2 models for energy distribution and 2 models for age makes the 4 models; (e1-sa), (e2-sa), (e1-sb) and (e2-sb) called model A, B, C and D respectively. The primary energy  $E_0$  and production height  $T$  of the air shower were determined by selecting the set of  $(E_0, T)$  which corresponds to the set of  $(N_0, S_1)$  obtained from calculation of electro magnetic cascade depending on models mentioned above, and yet agrees with experimental value.

### 3.3 Determination of energy flow.

The calculation for energy flow of the air shower has been carried out by the assumption that the electromagnetic component consists of electrons only because it has been difficult to know the energy distribution of gamma rays.

Now, new attempt to estimate the energy flow of electron or gamma ray individually has been made by giving each energy distribution based on electromagnetic cascade theory, and the age for electron or gamma rays is also determined separately. The energy distribution of electron or gamma ray composed of the shower, on top of the iron plate, is given by electromagnetic cascade theory respectively as follows,

$$N_e dE = A_e E^{-(1+S_e)} dE \quad \text{and}$$

$$N_g dE = A_g E^{-(1+S_g)} dE.$$

Where, age  $S_e$  is substituted for  $S_1$  assumed above, and age for gamma ray  $S_g$  is given by the set of  $(E_0, T)$  determined above.

## 4. Results and discussions

The energy determination of air shower ever been used is to multiply size  $N_0$  by the average energy which is obtained some simulations. (5) Age is taken into account as well as size

in this method. The present results agree with those published before in model A and B. (5) The average value of the ratio  $E_0$  to  $N_0$  and one of energy flow per electron  $E_f$  are in Table 1. The values of  $E_f$  are consistent with ones of other works. (6) The ratio  $N_4/N_2$  correlates with age  $S_0$  as shown in Fig. 1. Fig. 2 shows the correlation of mean energy per shower electron or total energy flow to  $S_0$  at Akeno altitude. The correlation between the ratio of total energy flow to incident energy  $E_f/E_0$  and  $S_0$  is shown in Fig. 3.

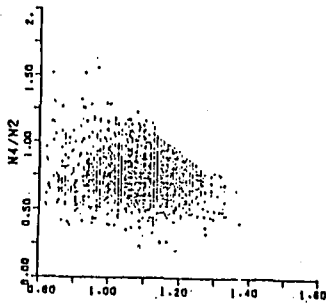


Fig. 1

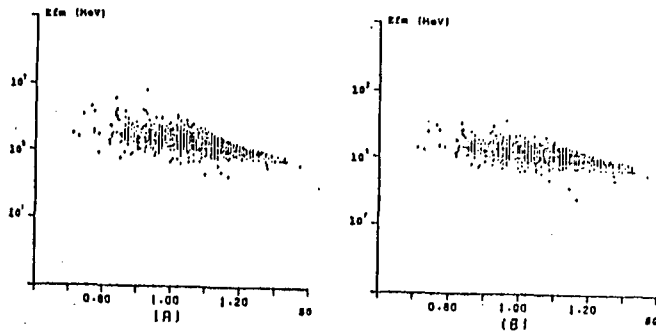


Fig. 2

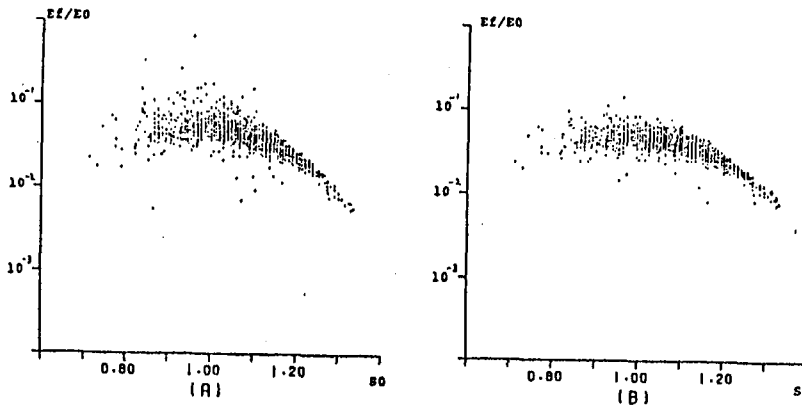


Fig. 3

model	$\langle E_0/N_0 \rangle$ (Gev)	$\langle E_f \rangle$ (Mev)
A	4.27	140
B	3.33	117

Table-1

## References

1. Y. Toyoda, J. Phys. Soc. Japan, 17(1962)415
2. S. Dake et al., Nuovo Cim., 41B(1977)55
3. Y. Matano et al., Acta Phys. Hungaricae 29 Suppl. 3(1970)451
4. S. Miyake et al., J. Phys. Soc. Japan., 18(1963)592
5. K. Kamata et al., ICR. Rep., 43(1984)3
6. G. Tanahashi et al., J. Phys. Soc. Japan, 20(1965)883

## Application of Photodiodes to the Detection of Electromagnetic Bursts

Fukushima, Y., Saito, To., Sakata, M., Shima, M., Yamamoto, Y.  
Department of Physics, Konan Univ., Higashinada, Kobe, 658, Japan.

### Abstract

A new type of photodiode + scintillator ( $1 \text{ m}^2 * 1 \text{ cm}$ ) detector is developed to detect the large electro-magnetic burst under a EX-chamber. The threshold burst size is found to be  $4.3 * 10^5$  particles at the center of the scintillator. Therefore a gamma-ray family of 10 TeV is detectable by it, when it is set under 14 r.l. of iron. In addition, a very fast (2.4 nsec width) and very bright (correspond to  $10^6$  particles) scintillation pulse has become available for this study.

### 1. Introduction.

Simultaneous observations of EAS and gamma-ray family have been made by two groups (1)(2). In these observations it is important, for successful joining of a EAS event with its corresponding gamma-ray family, to detect the distribution of electromagnetic cascade burst in the EAS core area. The burst distribution is detected by scintillation counter array beneath emulsion and X-ray film (EX) chambers. In our case (1), an unit burst detector is composed of a plastic scintillator ( $50 * 50 * 3 \text{ cm}^3$ ) and a 2" photomultiplier tube (PMT), and the detecting range for burst size is  $10^3 \sim 10^6$  particles/ $0.25 \text{ m}^2$ .

A new type of photodiode, recently developed, may be useful instead of PMT for detection of such a large burst. The sensitivity of the photodiode is not comparable to that of PMT as yet, detection of large size burst as these observation may be possible. Photodiode have many advantages in comparison with PMT : low cost, miniature size and high stability, and one can make burst detector covering large area with low cost.

Large burst events emit scintillation light of considerable luminosity and of very short duration of a few nsec. Then we, first of all, make a pulsed light source which emits very bright pulsed scintillation light of 2.4 nsec. It is obtained by irradiating plastic scintillator ultraviolet laser pulse of short width less than 1 nsec.

### 2. Pulsed Light Source and Light Response Checker.

Short ultraviolet light of 337.1 nm is made by the method of transverse excited nitrogen laser of Blumlein type (3). Figure 1 illustrates the cross sectional view of the laser device; the electrodes

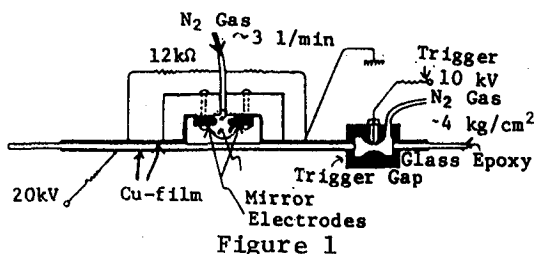


Figure 1

of which have a gap of 3 mm and length of 5 cm and is operated by 14 kV ~ 22 kV DC high voltage. The flow of  $\text{N}_2$  gas is about 3 l/min under the atmospheric pressure. From this laser oscillator about 10 different spectral lines are emitted and the 337.1 nm line is the most eminent in them. In order to cut off the visible lines we use a interference

filter of passing only (337±15) nm. The specifications of this device are presented in Table 1. The pulse shape of the 337.1 nm is detected by a biplaner photo tube (R1193U, Tr = 0.27 nsec, HAMAMATSU) and an oscilloscope (7904, 500 MHz, Tektronix). In Fig. 2(a), the shape of it is shown. Because of the limit of the oscilloscope's response the FWHM will be smaller than 0.9 nsec which is known from Fig. 2(a). The shape of a scintillation light made by the laser light is shown in Fig. 2(b), from which one can observe the pulse shape of real scintillation light of width 2.4 nsec. The stability of this laser output is less than 5% after preliminary heating of a half hour as is seen in Fig. 3.

Spectral Output	: 337.1 nm
Repetition Rate	: 3-40 Hz
Pulse Width	: ≤1 nsec
Output Stability	: 10 %
Beam Dimension	: 1.5*3 mm <sup>2</sup>
(At Exit)	(Vertical* Horizontal)
Beam Divergence	: 7.7*7.7 mrad <sup>2</sup>
(Half Angle)	
Trigger	: N <sub>2</sub> Gas Pressurized Spark Gap (-4 kg/cm <sup>2</sup> )

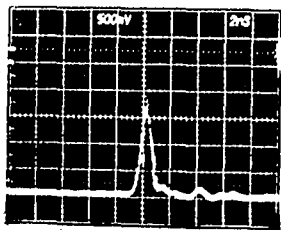


Figure 2(a)

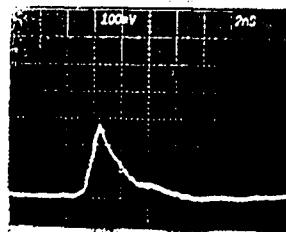


Figure 2(b)

0.5V/div., 2nsec/div. 0.1V/div., 2nsec/div.

Table 1

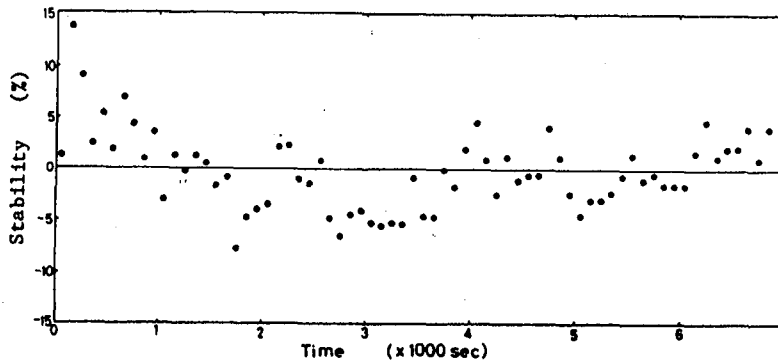
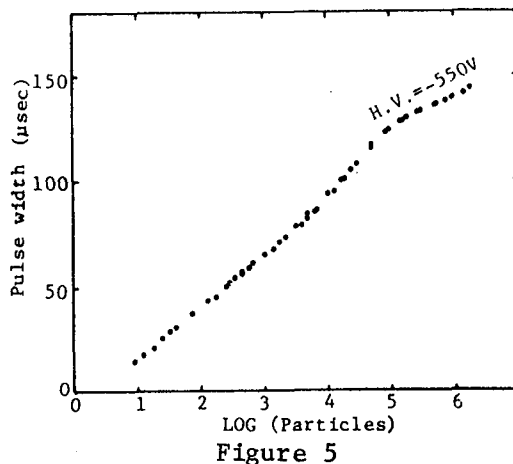
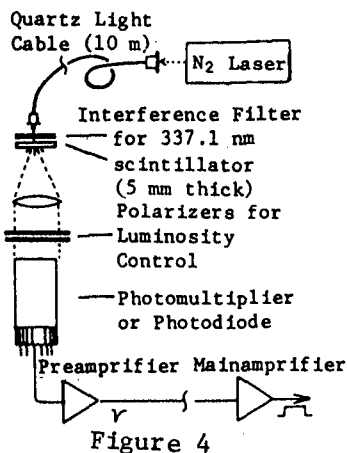


Figure 3

The laser oscillator is put in a noise shield box and only the pulsed light is derived through a quartz light cable. The strength of scintillation pulse is adjusted by two functions: one is the high voltage applied on the laser gap and the other is relative angle of polarizers as seen in Fig. 4, which we call 'light response checker' for PMT or photodiode. The plastic scintillator (5 mm thick), seen in Fig. 4, converts the 100% of the 337.1 nm to scintillation light.

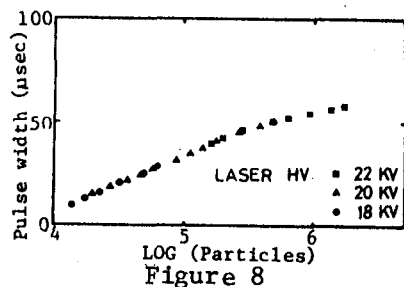
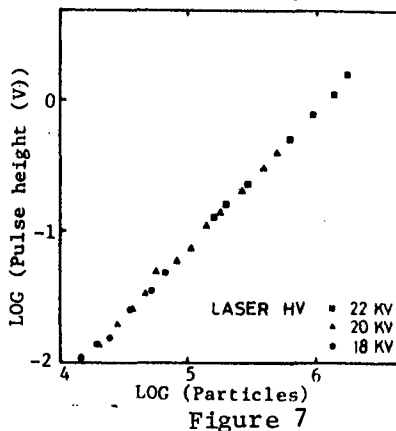
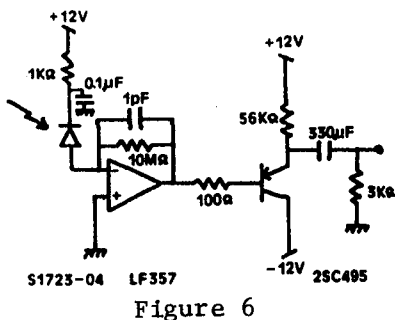
Figure 5 shows the response curve of PMT system which is composed of PMT, preamplifier and mainamplifier, where output of the mainamplifier is square wave and whose pulse width corresponds to logarithm of pulse height from preamplifier. In addition, the "number of particles" used as the unit of abscissa in Fig. 5 means the luminous intensity at the PMT window; intensity of "one particle" is given when a relativistic particle vertically traverse a scintillator of 3.5 cm thick set in a scintillator box of our standard use (1). From this figure it is found that the maximum luminosity generated by this light source is a few millions of particles.





### 3. Response of PIN Type Photodiodes.

We use PIN type photodiodes (S1723-01, HAMAMATSU) which have large sensitive area ( $10 \times 10 \text{ mm}^2$ ) and very high speed of response in both rise and decay times ( $T_r = 15 \text{ nsec}$ ). The preamplifier circuit for this photodiode is shown in Fig. 6, which has field effect transistor and function of current-voltage converter. Pulse height of the preamplifier shows a good linear relation with luminous intensity as shown in Fig. 7.



The output pulse width from the mainamplifier, the same type as used for PMT system, does not show a linear relation with them as shown in Fig. 8. From this result, however, we can conclude that this PIN photodiode-amplifier system is useful for detection of local burst size higher than a few  $10^4$  particles when we use it instead of PMT in the standard type scintillator box before mentioned.

### 4. A Burst Detector of $1 \text{ m}^2$ Unit Detected by Photodiodes.

An unit pack of photodiode and preamplifier is attached to the each corner of the scintillator whose size is  $100 \times 100 \times 1 \text{ cm}^3$ , and the whole unit is wrapped with aluminum foil as shown in Fig. 9. The uniformity of response is measured, as illustrated in Fig. 10. Numbers in the figure show the values of relative pulse heights of the preamplifier output,

where the same brightness of 337.1 nm laser pulse is directly put on each point of the scintillator, which is well fitted by  $R^{-1.55}$ , where R is distance between the photodiode and each point. This R-dependence is well interpreted by the following conditions that attenuation length is 1 m, a refractive index is 1.5, and a reflective index at the boundary is 0.97 in the scintillator.

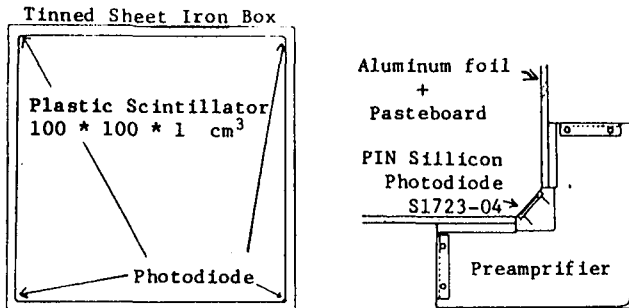


Figure 9

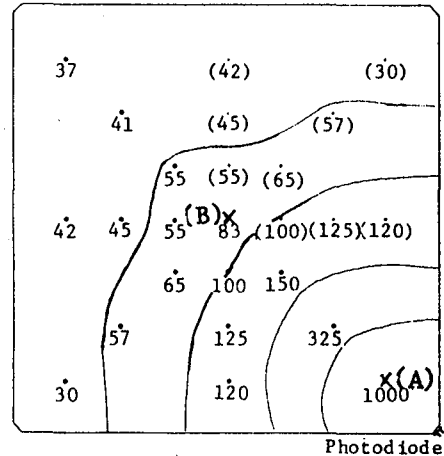


Figure 10

The threshold burst size, detectable by the photodiode system, is estimated as follows. First, a PMT (H.V. = -800 V) is attached to the 1 m<sup>2</sup> scintillator instead of the photodiode, and its output pulse height was measured for real single cosmic ray traversing the position (A), where the position (A) is shown in Fig. 10. Then this pulse height was found to be 4.5 mV. Secondly, when a certain intensity of 337.1 nm laser pulse is irradiated to the central position (B) as seen in Fig. 10, the output pulse height from the PMT was found to be saturated. At lower H.V. of PMT (-550 V), however, it was found to be 4.0 V. The ratio of decrease of output pulse height from the H.V. = -800 V to -550 V is 0.079, which has been observed for this PMT. On the other hand, the difference of response between the positions (A) and (B) was 1000 : 83 as seen in Fig. 10. Then the intensity of 337.1 nm laser in this irradiation is found to correspond to scintillation light of  $(4.0 \text{ V}) / ((0.0045 \text{ V}) * 0.079 * (83 / 1000)) = 1.3 * 10^5$  particles of real cosmic rays.

When the same laser light irradiated at the same point (B) is observed by the photodiode, the preamplifier output is found to be 24 mV. Because the threshold voltage of this photodiode-preamplifier system is 8 mV (S/N = 3), the threshold particle number for this system is  $1.3 * 10^5 * (8 \text{ mV} / 24 \text{ mV}) = 4.3 * 10^4$  particles at position (B). If this burst detector is set beneath a EX-chamber with 14 r.l. of iron, a burst of  $4.3 * 10^4$  electrons and positron will be generated by a cosmic gamma-ray of about 10 TeV, so that we can conclude that a gamma-ray family of  $\Sigma E_\gamma = 10 \text{ TeV}$ , at least, is detectable by this new burst detector.

#### References

- (1) Nakatsuka, T. et al., 18-th ICRC, Bangalore, 1983, conf. Vol. 11, 346.
- (2) Matano, T. et al., 18-th ICRC, Bangalore, 1983, conf. Vol. 11, 342.
- (3) Mitani, T. J. Appl. Phys. 52(5), May, 1981, P.3159

CORE STRUCTURE OF EAS IN  $10^{15}$ ev TO  $10^{17}$ ev

T.Hara, Y.Hatano, N.Hayashida, T.Kifune, M.Nagano and G.Tanahashi

Institute for Cosmic Ray Research, University of Tokyo  
Tanashi, Tokyo, 188 Japan

## ABSTRACT

With use of Akeno calorimeter, the attenuation of particles in concrete is analyzed as the function of the shower size of  $10^5$  to  $10^7$ . The attenuation length does not depend much on the shower size but depends a little on the shower age. The average value is  $\sim 150\text{gcm}^{-2}$  for  $s=0.5-0.85$  and  $\sim 140\text{gcm}^{-2}$  for  $s=0.85-1.15$ . These values and their fluctuations are consistent with the equi-intensity curves of EAS.

## 1. Introduction

Akeno calorimeter has an area of about  $10\text{m} \times 10\text{m}$  and has the proportional counter arrays at 5 different depths (0, 115, 230, 345 and  $633\text{gcm}^{-2}$  in concrete) with 10cm resolution in one dimension (1). We report the preliminary result of energy flow or the attenuation length measurement with use of the calorimeter. In this paper the attenuation length ( $\Lambda$ ) is defined as

$$\text{Energy flow} = \int_{x_0}^{\infty} N(x) dx = \int_{x_0}^{\infty} N(x_0) \exp(-x/\Lambda) dx$$

where  $\int$  ; the energy loss/particle. unit mass  
 $N(x)$  ; shower size in the depth  $x$   
 $x_0$  ; observation depth,  $930\text{gcm}^{-2}$  in Akeno

The data are of the latter half of 1982, and about 13,000 vertical showers are analyzed whose sizes are between  $10^5$  and several times of  $10^7$ . Only 3 shower cores hit the calorimeter area above the size of  $10^7$ .

## 2. Average attenuation length of EAS

The analysis is only for the vertical showers with  $\sec\theta=1.0-1.1$ . EAS data are sorted in the shower size ( $N$ ) bin of  $10^{5.0-5.5}$ ,  $10^{5.5-6.0}$ ,  $10^{6.0-6.5}$ ,  $10^{6.5-7.0}$  and  $>10^{7.0}$ , and also in the age ( $s$ ) bin of  $0.50-0.85$ ,  $0.85-1.15$  and  $1.15-1.50$ . The average lateral distribution of particles and the shower sizes in each concrete depth are determined in every combinations of the above sorting. Fig.1 shows the average local attenuation lengths as the function of core distance in  $N=10^{6.0-6.5}$  and in all  $s$ . They are defined in 1 replacing  $N(x)$  by  $\Delta(x)$ , the particle density in a unit of 10 proportional counters ( $5\text{m} \times 1\text{m}$ ). The average shower sizes in each concrete depth are obtained by integrating  $\Delta(x)$  over the core distance. They are shown in Fig.2. A systematic difference of the particle densities measured by the scintillation counters and by the proportional counters are corrected in the figure, that is  $\Delta_{\text{pc}}/\Delta_{\text{sc}}$  is about 1.5 at  $\Delta=10$ , 1.3 at  $\Delta=10^2$  and 1.15 at  $\Delta=10^3$ . The shower sizes are normalized within each size bin. The error bars only show the uncertainty due to the threshold of the counter output, and in most cases the true values are considered to be rather close to the lower limit. The data of size= $10^7$  and age= $0.85-1.15$  are not reliable because of the poor statistics of the core events.

The attenuation lengths from these transition data are  $150 \pm 10\text{gcm}^{-2}$  for  $s=0.50-0.85$  and  $140 \pm 10\text{gcm}^{-2}$  for  $s=0.85-1.15$ , and not much depend on the shower size. These values are smaller than  $\sim 180\text{gcm}^{-2}$  predicted for the proton showers of the standard interaction, and also for the iron showers

as shown in Fig.3(2), where "standard" means the increasing cross section as  $\sigma \propto E^{0.06}$ , Feynman scaling and the extrapolation of the known central energy distribution to the higher energies.

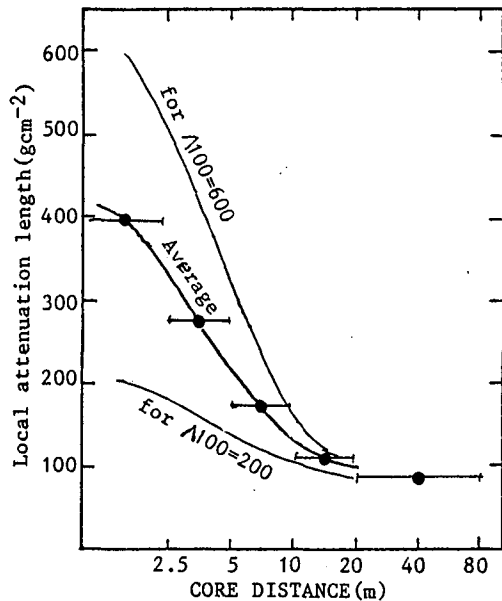


Fig.1

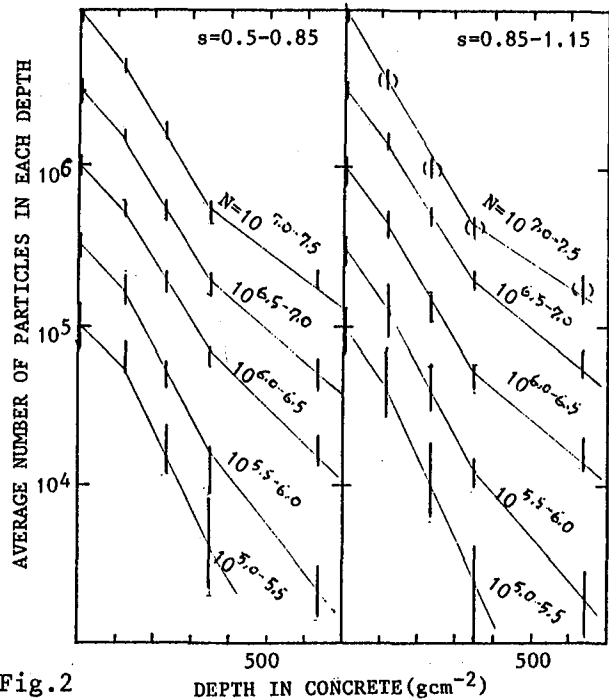


Fig.2

### 3. Relation of 3 attenuation lengths $\Lambda_E$ , $\Lambda_I$ , $\Lambda_N$

To see the consistency of the result with others, three attenuation lengths are taken into account. Their definitions are as follows.

(i)  $\Lambda_E$  of the fixed energy shower

$\Lambda_E$  is obtained from the shower calculation of the fixed energy, and in the case of the simulation, the average value of many showers is used.  $\Lambda_E$  is about  $180\text{gcm}^{-2}$  in  $10^{16}\text{ev}$  and in  $>950\text{gcm}^{-2}$  for the standard proton showers (Fig.3).

(ii)  $\Lambda_I$  of equi-intensity cut

$\Lambda_I$  is obtained from the equi-intensity cut of the size spectra in the different depths. The experimental value is  $160\text{--}170\text{gcm}^{-2}$  (3) in  $10^{16}\text{ev}$  to  $10^{17}\text{ev}$  and  $>950\text{gcm}^{-2}$ .

(iii)  $\Lambda_N$  of the fixed size in the fixed level

The attenuation length obtained in the calorimeter experiment is  $\Lambda_N$ .

The experimental value is  $140\text{--}150\text{gcm}^{-2}$  as described in 2.

In what follows we make a simple calculation of these  $\Lambda$ s to see how the cosmic ray composition affects these values. The composition is assumed to be two components, the proton and the heavy nuclei. Each shower curve is to be the exponential form, say  $N_p \cdot \exp(-x/\Lambda_p)$  for proton and  $N_h \cdot \exp(-x/\Lambda_h)$  for heavy nuclei.  $N_p = N_h = 10^9$ ,  $\Lambda_p = 180\text{gcm}^{-2}$  and  $\Lambda_h = 140\text{gcm}^{-2}$  in  $10^{16}\text{ev}$  as shown in Fig.3. The reason to adopt the small value of  $\Lambda_h$  is that the usual models of heavy nuclei shower can not give a appreciably smaller attenuation than the proton's. The fluctuations of the longitudinal development are ignored. The integral energy spectrum is to be  $E^{-2}$ , and the intensity ratio at the same energy  $k = I_h/I_p$  is to be a parameter of the calculation.  $\Lambda_E$ ,  $\Lambda_I$  and  $\Lambda_N$  are given as follows.

$$\Lambda = (x_2 - x_1) / \ln(N_1/N_2)$$

$$\text{for } \Lambda E, N_1/N_2 = (\exp(x_1 p + k) \cdot \exp(x_1 h)) / (\exp(x_2 p + k) \cdot \exp(x_2 h))$$

$$\text{for } \Lambda I, N_1/N_2 = ((\exp(x_1 p^2 + k) \cdot \exp(x_1 h^2)) / (\exp(x_2 p^2 + k) \cdot \exp(x_2 h^2)))^{0.5}$$

$$\text{for } \Lambda N, N_1/N_2 = (\exp(x_1 p^2 + k) \cdot \exp(x_1 h^2)) / (\exp(x_1 p) \cdot \exp(x_2 p + k) \cdot \exp(x_1 h) \cdot \exp(x_2 h))$$

where  $N_1$  and  $N_2$  are the shower size at the depth of  $x_1$  and  $x_2$  respectively and  $\exp_1 p = \exp(-x_1/\Lambda p)$ ,  $\exp_1 h = \exp(-x_1/\Lambda h)$ ,  $\exp_2 p = \exp(-x_2/\Lambda p)$ ,  $\exp_2 h = \exp(-x_2/\Lambda h)$ .

The relations between  $k$  and  $\Lambda$ s are shown in Fig.4. It is seen that  $\Lambda N$  has almost the same value as  $\Lambda I$  in the whole range of  $k$ . This means that the difference of  $\Lambda I$  (160-170  $\text{gcm}^{-2}$ ) and  $\Lambda N$  (140-150  $\text{gcm}^{-2}$ ) can not be explained by means of the different response of proton and heavy nuclei showers.

The other possible explanation is to attribute it to the fluctuation of the shower development. Fig.5 shows two distributions of simulated attenuation lengths of fixed energy and of fixed size for the proton showers. The positions of the distribution maximum are almost the same, but the average value of the fixed energy one is larger than that of the fixed size. As the attenuation length of fixed energy is nearly equal to that of the equi-intensity cut in single component showers, this can explain the difference provided that the primary cosmic rays contain a proper amount of protons.

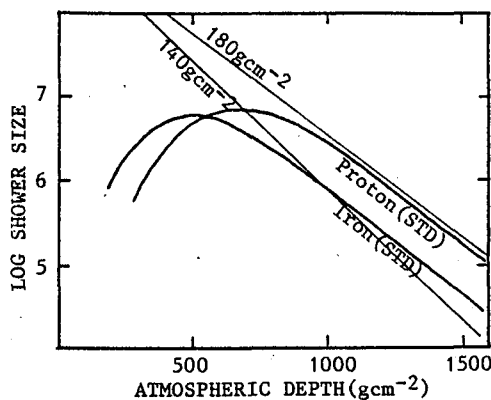


Fig.3

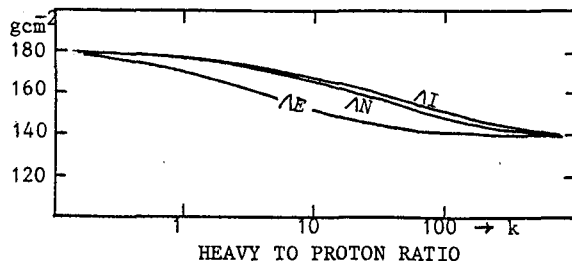


Fig.4

#### 4. Fluctuation of the attenuation length

The attenuation length of each shower can not be directly obtained from the data, and only "the attenuation length within  $10\text{m} \times 10\text{m} (\Lambda_{100})$ " are obtained. The histogram in Fig.6 shows the  $\Lambda_{100}$  distribution (bottom side scale) of the showers which hit the central part ( $5\text{m} \times 5\text{m}$ ) of the calorimeter. This kind of fluctuation decreases with the core distance, and gets remarkably smaller beyond 15m down to 80-90  $\text{gcm}^{-2}$ . So, for the core hitting showers, we can convert  $\Lambda_{100}$  to the attenuation length assuming the local attenuation lengths are continuous between 5m and 20m.

The conversion depends on how to interpolate the attenuation between 5m and 20m. The most gentle one is that the local attenuation lengths fluctuate around the average in proportion to the central  $\Lambda_{100}$  in the region above 80-90  $\text{gcm}^{-2}$  like the two curves in Fig.1. The attenuation lengths obtained with use of this conversion are shown in the top side scale of Fig.6. In the same figure, the distribution of the attenuation length is compared with the one simulated for proton showers (the same one in Fig.5). The observed distribution does not agree with the prediction. Some part of the disagreement may be the contribution of the heavy nuclei showers, but the further discussion needs the further detailed analysis, especially the improvement of  $\Lambda_{100}$  conversion to the attenuation length.

Fig.5

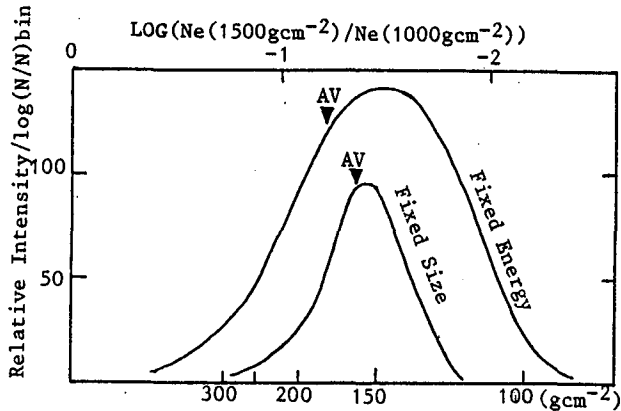
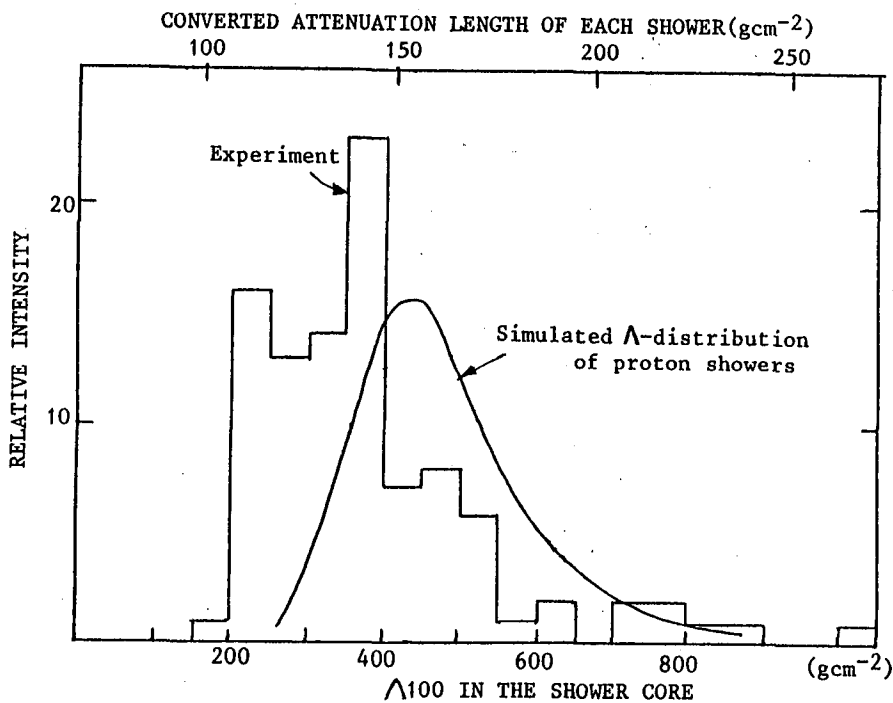


Fig.6



### Acknowledgements

The authors are indebted to the technical staffs in Akeno crew. The data reductions and the EAS simulation are done by FACOM 380 at the computer room, Institute for Nuclear Study, University of Tokyo.

### References

- (1) Hara, T. et al. Proc. 16th ICRC(kyoto), 8, 135 1979
- (2) Tanahashi, G. HE 4.1-3 in this conference
- (3) Nagano, M. et al. J. Phys. G; Nucl. Phys. 10, 1295, 1984

PARTICLE DISTRIBUTIONS IN  $\sim 10^{14} - 10^{16}$  eV AIR SHOWER CORES  
AT SEA LEVEL

A.L. Hodson\*, A.G. Ash\*, and R.M. Bull†

\*Department of Physics, University of Leeds, Leeds, U.K.

†Department of Physics, University of Nottingham, Nottingham, U.K.

ABSTRACT

At the Bangalore Conference we reported experimental evidence for the 'steepening' of the differential density spectra for known fixed distances (0, 1.0, 2.5 and 4.0 m) from the shower centres and for 'core flattening', the cores becoming flatter, on average, as the shower size (primary energy) increases. With improved statistics on 4192 cores, the previous results are exactly confirmed.

1. Introduction. At the Bangalore Conference we reported the first measurements of the differential density spectra for cosmic-ray air showers at known fixed distances from the centres of shower cores (Hodson et. al., 1983a) and also evidence that as the shower size increases the cores, on average, become flatter (Hodson et.al., 1983b). In this paper we report data on a total of 4192 shower cores, increasing the statistics previously available. The conclusions regarding 'steepening' of the density spectra and 'core flattening' given at Bangalore are confirmed and it is shown that the flattening effect extends to at least 2.5 m radius from the shower centre.

2. Data and results. The data on particle distributions near to the cores of  $10^{14} - 10^{16}$  eV air showers at Leeds (80 m above mean sea level,  $1020 \text{ g cm}^{-2}$ ) were obtained from a  $7 \text{ m} \times 5 \text{ m}$  array of discharge chambers. A particular feature of the apparatus is the precision (usually  $\sim 0.1 \text{ m}$ ) with which the centres of symmetry of the shower cores can be located. The experimental arrangement, triggering system, and data analysis were exactly as described in the above 1983 papers. An additional 1589 shower cores have now been analysed and the combined data are given in Figures 1 and 2.

Figure 1 shows the differential spectra for densities  $\rho(r)$  measured at  $r = 0, 1.0, 2.5,$  and  $4.0 \text{ m}$  from the shower centres. All four spectra are of a similar shape which may be approximated by two power law lines; all four spectra are consistent with a power law index of  $\sim -2$  at low densities before steepening to an index of  $\sim -3.5$  at high densities. Deviations from the  $-2$  power law at the lowest densities shown in Figure 1 are attributed to trigger and scanning bias. The 'central density' spectrum (Figure 1a) steepens at  $\rho(0) \sim 800 \text{ m}^{-2}$ ; for  $r = 1.0, 2.5,$  and  $4.0 \text{ m}$  the spectra steepen at lower density values. The 'join point' between the two power law lines occurs at about the same differential rate in each of the four spectra (horizontal dashed lines).

Figure 2 expresses the data on core flattening. The quantity  $\langle \rho(r) \rangle$  is defined as the average density for all shower cores in a particular interval of  $\rho(4.0)$ . The closer the ratio  $\langle \rho(r) \rangle / \langle \rho(r') \rangle$  is to unity, where  $r' < r$ , the flatter is the particle distribution in the region between  $r'$  and  $r$  from the shower centre. In the absence of data on the

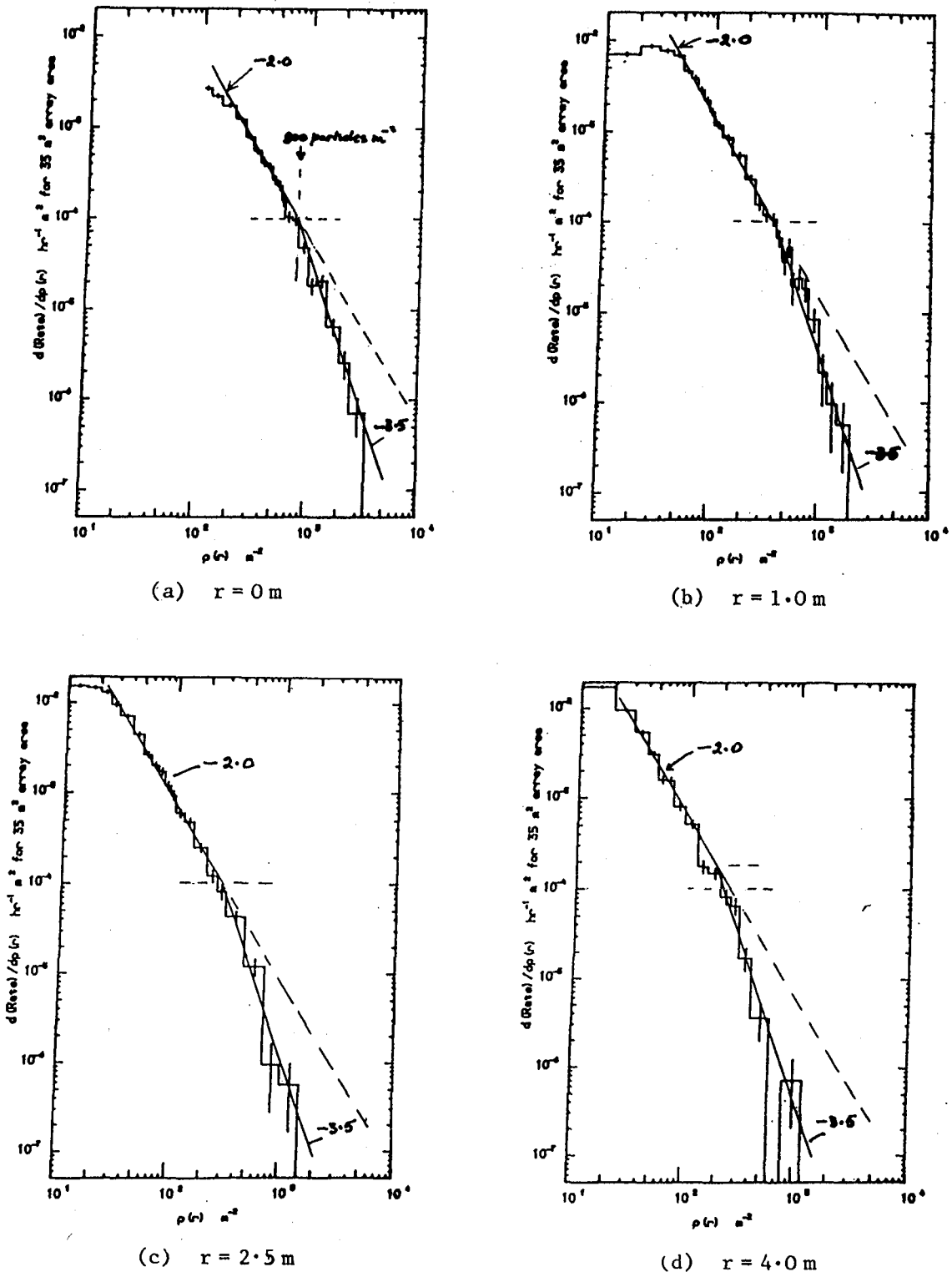
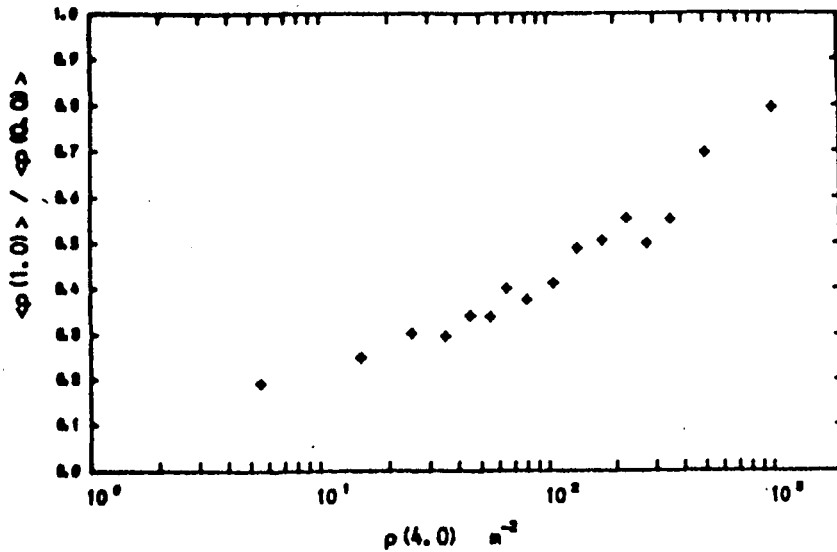


Figure 1. Experimental differential density spectra at known fixed distances ( $r$ ) from the shower centre.

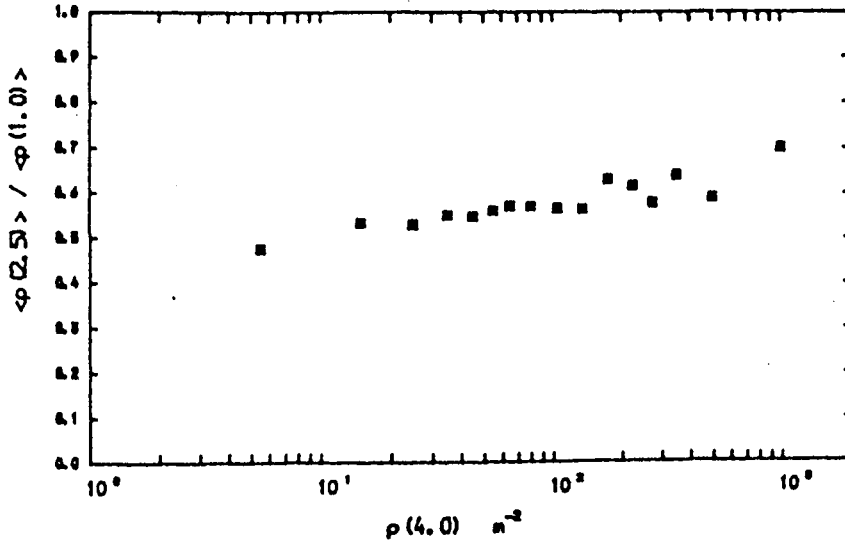
Total no. of shower cores: 4192;

Run time: 7033 hours





(a) 'Core flattening' between 0 and 1.0 m from the shower centre



(b) 'Core flattening' between 1.0 and 2.5 m

Figure 2. Data showing that the particle distribution in shower cores becomes flatter, on average, as the shower size increases.

(The ordinate is a measure of the flatness of the distribution; the abscissa is an approximate measure of shower size.)

densities of our showers at large distances, we take  $\rho(4.0)$  as a rough measure of shower size  $N$ . (Data from the Kiel air shower array (Bagge et al., 1979) suggest  $N \sim 2000 \times \rho(4.0)$ , where  $\rho(4.0)$  is expressed in particles  $m^{-2}$ .)

The dependence of  $\langle \rho(1.0) \rangle / \langle \rho(0) \rangle$  on  $\rho(4.0)$  is given in Figure 2a, that of  $\langle \rho(2.5) \rangle / \langle \rho(1.0) \rangle$  in Figure 2b. The upward trend towards unity in both Figures 2a and 2b shows that, on average, as the shower size (primary energy) increases the cores become flatter; the trend is less marked in Figure 2b but still clearly indicates a significant flattening out to at least 2.5 m from the shower centre.

The data given in this paper are well suited to comparison with predictions from Monte Carlo simulations. Details of such simulations and conclusions drawn are given by Ash (1985a,b).

Complementary to the present data are the results of a similar analysis by Ash (1985c) of photographs of air shower cores observed in the 20  $m^2$  discharge chamber array operated by Hazen et al. (1981) at Sacramento Peak (730  $g\ cm^{-2}$ ), New Mexico.

3. Acknowledgements. This work was supported by the Science and Engineering Research Council. We especially thank our film scanners, Mrs J Barker and Mrs J Wilson, for their painstaking work.

#### References

- Ash, A.G., 1985a, paper HE 4.2-15, this Conference  
 Ash, A.G., 1985b, paper HE 4.2-16, this Conference  
 Ash, A.G., 1985c, paper HE 4.2-18, this Conference  
 Bagge, E.R., Samorski, M., and Stamm, W., 1979, Conference Papers, 16th International Cosmic Ray Conference (Kyoto), 13, 260  
 Hazen, W.E., Hendel, A.Z., and Hazen, E.S., 1981, Conference Papers, 17th International Cosmic Ray Conference (Paris), 11, 350.  
 Hodson, A.L., Porter, M.R., Ash, A.G., and Bull, R.M., 1983a, Conference Papers, 18th International Cosmic Ray Conference (Bangalore), 6, 23  
 Hodson, A.L., Porter, M.R., Ash, A.G., and Bull, R.M., 1983b, *ibid.* 11, 201

## THEORETICAL STUDY OF EAS HADRONIC STRUCTURE

L. Popova

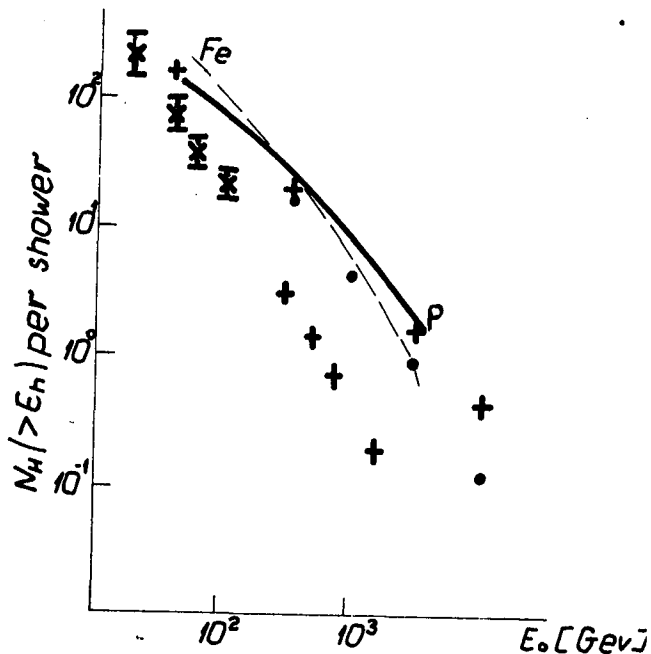
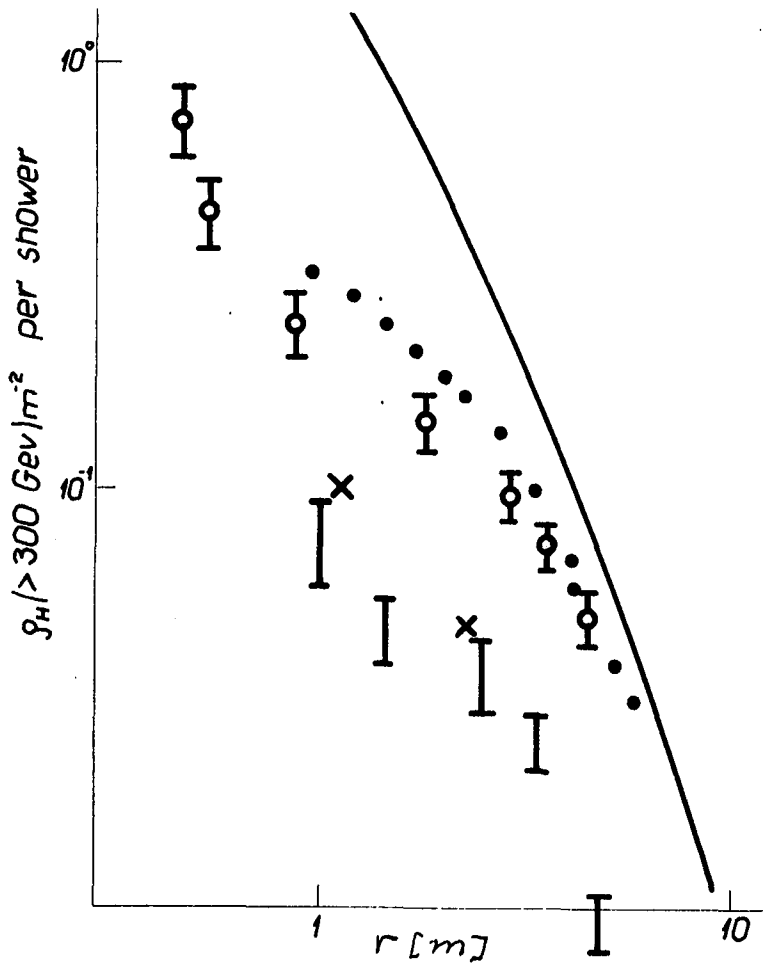
Institute of Nuclear Research and Nuclear Energy  
Bld. Lenin 72, Sofia, Bulgaria

1. General remarks on the experimental data The structure of EAS is determined mainly by the energetic hadrons. They are strongly collimated in the core of the shower and essential difficulties are encountered for resolution of individual hadrons. The properties for resolution are different of the variety of hadron detectors used in EAS experiments. This is the main reason making it difficult to obtain a general agreement between actually registered data with different detectors.

The most plausible source for disagreement is the uncertainty in determination of the energy of individual hadrons. A principal factor might be the incidence of multiple hadrons over large area detectors. Such measurements do not distinguish between events with one or more hadrons over the detectors and thus, provide an upper limit to the hadron energy flow<sup>/1/</sup>. For example, hadron measurements in Kolar Gold Fields<sup>/2/</sup> performed with a deep iron calorimeter, include leakage of energy flow in the energetic electron component which arrives through the top layers and, particularly, through the sides of the calorimeter for inclined showers. This is valid, to a lesser extent for the measurements at Tian Shan<sup>3,4,5/</sup> performed with smaller ionising detector. The measurements at Pic du Midi<sup>/6/</sup> with flash tube hodoscope were relatively less affected due to the thickness of the detectors. In the scintillator burst detectors, distortion in hadron energy due to multiple hadron incidence is expected to play a significant role even though the individual scintillators occupy relatively small area as in the case of Norikura experiment<sup>/7/</sup>.

Many efforts during the last few years were devoted to estimation of the effect from multihadron incidence<sup>/8/</sup>. The signals observed in Ooty experiment<sup>/8/</sup> with burst detectors were converted to hadron energy using conversion factor obtained with Monte Carlo simulations<sup>/1/</sup>. There was pointed out a reasonably good agreement between the results in Ooty experiment, and those from Pic du Midi<sup>/6/</sup>. Nevertheless, significant difference is observed with the calorimeter measurements<sup>2,3/</sup>. This situation is shown in fig.1 and 2, where we compared the experimental data of hadrons in EAS at different levels. All data are normalized assuming that the attenuation length of hadrons is  $350 \text{ g.cm}^{-2}$  <sup>/5/</sup>.

2. Analysis of the model calculations In the beginning we want to point out an unsuspected effect revealed from the theoretical investigations, e.g. the change in the assumptions about the main parameters of high energy interactions, as well as for the nature of the primary particles, are relatively slightly affecting the properties of hadronic component in EAS at mountain altitudes. For example, the lateral distribution of hadrons ( $E_h > 300 \text{ Gev}$ ) calculated by us on the basis of our new phenomenological model<sup>/10/</sup>, in which is assumed broken scaling variable  $x_s = x \cdot \sqrt{s}^u$ , is very similar to that



obtained by Grieder/<sup>11/</sup> assuming standard model with multiplicity  $n_s \sim E^{0.437}$  in the both extreme cases of proton and iron primary spectrum. Similar small effect from the change of interaction models on EAS hadrons with different energies and in wide range of shower sizes is observed in comparing our broken scaling model calculations with those of Kempa/<sup>12/</sup> assuming standard model with different multiplicity laws ( $n_s \sim E^{1/4}$  and  $n_s \sim E^{1/2}$ ). All those facts are showing that in general, the number of hadrons at mountain altitudes is not very sensitive to the change of multiplicity law.

By means of the results obtained recently by Sreekantan et al/<sup>16/</sup> with similar broken scaling model we can see in fig.3 the influence of the assumption about the energy spectrum of the secondary particles, characterized by the scaling violation parameter  $\alpha$ . They have assumed slight increase of  $\alpha$  that equalizes our parameter ( $\alpha = 0.13$  in Lab. system) at energies about  $2 \cdot 10^5$  Gev. The steeper shape of curve 2 can be connected with the larger coefficient of inelasticity (0.72) in pion collisions assumed by Sreekantan et al.

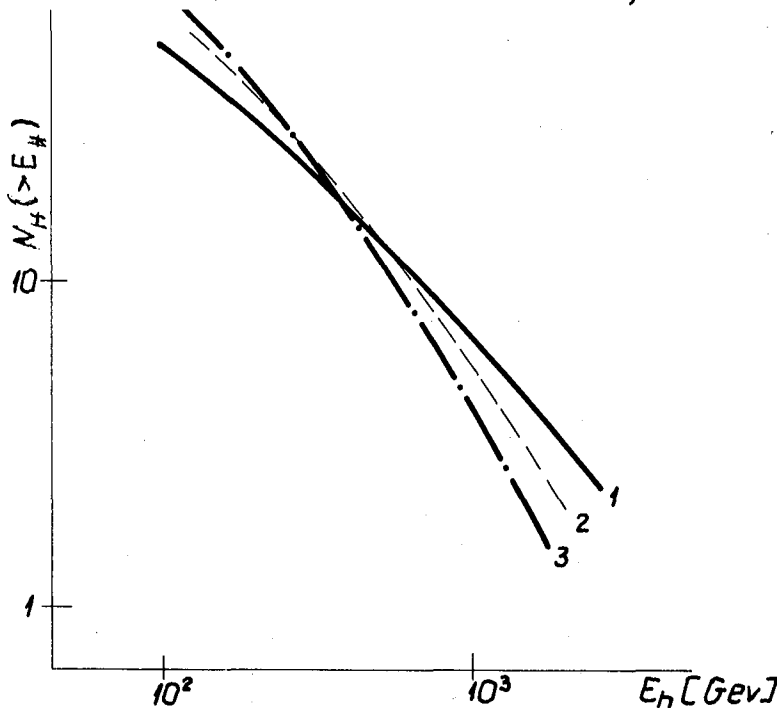


Fig.3 Comparison of the theoretical predictions for the energy spectrum of hadrons in EAS with size  $1.5 \cdot 10^5$  at  $785 \text{ g/cm}^2$  according to the present calculations for proton showers (1) with the estimations of Sreekantan et al/<sup>9/</sup> for proton (2) and iron (3) primary spectrum

Similar effect give the calculations of Danilova et al/<sup>13/</sup>. Assuming  $k_{\pi\text{-air}} = 0.84$  they obtain less number of hadrons in extensive showers (with a factor of 2) than we have calculated with  $k_{\pi\text{-air}} = 0.5$ . More essential is the effect from energy increase of the inelastic cross section. The number of hadrons calculated in/<sup>9/</sup> for  $\sigma_{\text{in}}^{\text{air}} = 260 + 11 \ln \frac{E}{1000} \text{ b}$  is about 2 times smaller than in the case of logarithmic increase of  $\sigma_{\text{in}}^{\text{air}}$  assumed in our calculations.

The effect of primary particle mass on the properties of hadron component is illustrated in both figures 2 and 3. We can see that even for the two extreme cases of pure proton and pure iron primary composition there is relatively small change in the energy spectrum of hadrons.

**3. Comparison with experimental data:** In fig.1 we have compared the results for hadron lateral distribution obtained in our calculations with broken scaling model and hadron densities compiled from different mountain experiments. It is seen that the slope of the theoretical curve differs from the experimental distribution. That difference is substantial near the core of showers, where the effect of multiple hadrons in hadronic detection is rather strong. Apart the apparatus effect, the observed disagreement can be due to the fact that in our model calculations we have neglected the possibility for appearance of secondary pions with large transverse momentum (above 1.4 Gev/c). In fact there is observed in accelerator experiments up to 2.105Gev slight decrease in the slope of  $p_T$ -distribution. Certainly, existence of such pions should cause a flatter lateral distribution of shower hadrons near the core. However, drastic change of  $p_T$ -distribution, needed to explain the contradiction in fig.1 was not observed over the entire range 0.2-10<sup>3</sup>Tev. It might be supposed that the rise of transverse momenta at 10<sup>3</sup>Tev could be attributed to only few secondary particles and jets/14,15/.

From the comparison with the experimental data in fig.2 we can see an apparent difference between the expected total number and the measurements with burst detectors. It is obvious that the model calculations are fitting the upper limit of hadronic flow detected with calorimeters.

**4. Conclusion** The above results allow us to conclude that we can get a better agreement with the average tendency of hadronic measurements if we assume in our new phenomenological model a larger coefficient of inelasticity and stronger energy increase of the total inelastic cross section in high energy pion interactions. Nevertheless, EAS data above 105Gev are revealing a faster development of hadronic cascades in the air than it can be expected by extrapolating the parameters of hadron interactions obtained in accelerator measurements.

#### References:

1. Tonwar S.C. and Sreekantan V. J.Phys. A4,866,1971
2. Chatterjee B.K. et al. Canad. J. of Phys. 16,8,136,1968
3. Romachin V. et al. Proc. 15 th ICRC, 8, 107,1977
4. Nesterova N.M. and Chubenko A.P. Proc. 16 ICRC, 8,346,1979
5. Nesterova N.M. and Dubovy A.C. Proc. 16 ICRC, 8,845,1979
6. Van Staa R. et al. J.Phys. A1,135,1974
7. Miyake S. et al. Proc. 16 ICRC, 13,165,1979
8. Vatcha R.H. and Sreekantan S.V. J.Phys. A6,1050,1057,1973
9. Sreekantan R.V. et al. Phys. Rev.(in press),1983
10. Popova L. Acta Universitatis Lodziensis,1984,Lodz, Poland
11. Grieder P.K. Proc. 17 ICRC 6, 288,1981
12. Kempa J. Nuovo Cimento 31, 568,1979
13. Danilova T.V. and Erlykin A.D. Preprint Number 15 of Lebedev Institute of Physics, Moscow,1984
14. Nikolski S.I. Journal of Theoretical and Experimental Physics: 51,80,1966
15. Brasil-Japan. Emulsion Chamber Collab.-AIP Conf.Proc.49, New York 145,1979.

MONTE CARLO SIMULATIONS OF ELECTRON LATERAL DISTRIBUTIONS  
IN THE CORE REGION OF  $10^{13}$  -  $10^{16}$  eV AIR SHOWERS

A.G. Ash

Department of Physics  
University of Leeds  
Leeds LS2 9JT  
U.K.

ABSTRACT

This paper contains details of computer models of shower development which have been used to investigate the experimental data on shower cores observed in the Leeds  $35\text{m}^2$  and Sacramento Peak (New Mexico)  $20\text{m}^2$  arrays of current-limited spark ("discharge") chambers. The simulations include predictions for primaries ranging from protons to iron nuclei (with heavy nuclei treated using both superposition and fragmentation models).

1. Introduction

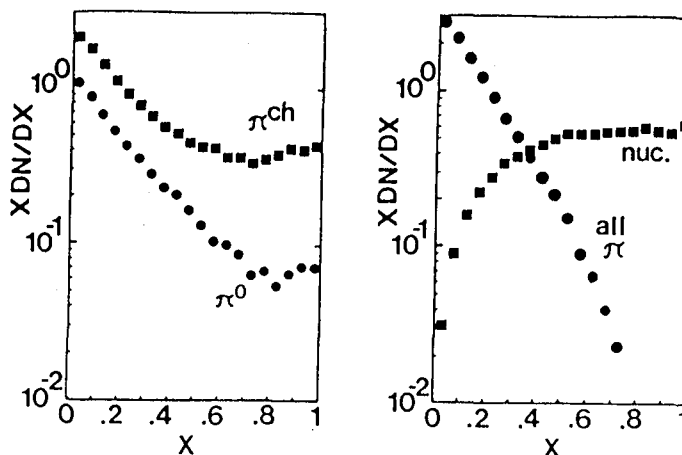
Analysis of photographs of  $10^{14}$  -  $10^{16}$  eV air shower cores in arrays of current-limited spark chambers at Leeds ( $1020\text{ g cm}^{-2}$ ) and Sacramento Peak ( $730\text{ g cm}^{-2}$ ) has provided data on particle distributions within a few metres of the shower axis in the form of density spectra and density averages measured at known fixed distances from the shower centre (Ash, 1985a, Hodson et al., 1983a,b, 1985). Comparison of these results with Monte Carlo simulation predictions by Ash (1985a,b) has demonstrated the failure of the scaling model. Details of the calculations are presented in this paper (see also Ash, 1984).

2. Hadron collision models

Simulation techniques based in the laboratory frame were used, and the models generated only pions and leading nucleons; nuclear target effects were neglected. The energy-splitting algorithms of Hillas (1981) were used to generate "radial scaling" secondary energy spectra in pion collisions (Fig.1a) and nucleon collisions (Fig.1b); except that for the latter, the flat leading nucleon spectrum given was replaced by a more accurate form (Hillas, 1979a): the elasticity  $X = E_{\text{nuc}}/E_0$  was sampled using  $X = 0.76a + 0.24a^4$  (instead of  $X = a$ ) where  $a$  is a random number (0.0....1.0). (If, as a result,  $E_{\text{nuc}}$  was less than the nucleon rest energy  $mc^2$  then  $E_{\text{nuc}} = mc^2$ ). For  $E_0 \gg mc^2$  the resulting average elasticity is equal to 0.42.

Transverse momenta were sampled from the energy-independent distribution  $h(p_t)dp_t \propto p_t e^{-p_t/p_0}$  with  $p_0$  equal to  $0.24\text{ GeV}/c$  for secondary pions (in both pion and nucleon collisions) and equal to  $0.28\text{ GeV}/c$  for leading nucleons. (If  $p_t > p$  then the secondary was considered to be going backwards and was dropped from the cascade.).

Mean free paths for nucleon-'air' nucleus collisions (Fig.2) based on nucleon-nucleon cross sections rising as  $\ln^2 s$  at high energy were as



(a) Pion collisions (b) Nucleon collisions

Fig. 1 Particle production spectra in simulated 100 GeV hadron-'air' nucleus collisions.  $X$  is the secondary energy divided by the projectile energy, both measured in the laboratory frame

given by Hillas (1979b); those for pion collisions were obtained by scaling up the nucleon mean free paths by (114/86) at all energies.

### 3. Nuclear fragmentation models

The "superposition model" was used i.e. a shower with primary mass number  $A$ , energy  $E_{\text{prim}}$ , was taken as a co-axial superposition of  $A$  proton showers with energy  $E_{\text{prim}}/A$ . A more realistic treatment of primaries

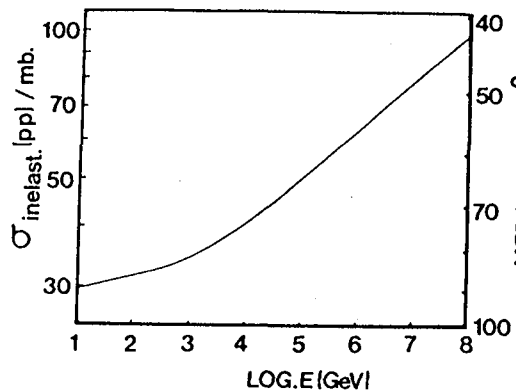


Fig. 2 Inelastic pp cross-sections and corresponding mean-free-paths in air used in simulations

ranging from helium nuclei to iron nuclei was given in the one-dimensional "fragmentation model" which is based mainly on emulsion data and follows quite closely the Bartol model (Gaisser et al., 1982) with which it is in good agreement for the average distribution in the atmosphere of the "first" inelastic collisions of primary nucleons. Excellent agreement with Freier and Waddington's (1975) simulation predictions of the average rate of release of nucleons from projectile nuclei as a function of atmospheric depth is obtained using the Cleghorn nucleus-nucleus cross sections, adopted by them, instead of the larger cross-sections of Gaisser et al. (1982) normally used.

### 4. Propagation model

A non-isothermal atmosphere was used. Coulomb scattering and ionisation loss ( $2.2 \text{ MeV per g cm}^{-2}$ ) were applied to hadrons, but were neglected for projectile nuclei in the "fragmentation model". Geomagnetic effects were neglected.



### 5. Electromagnetic cascade function

An average development function based on unpublished Monte Carlo calculations for photon-initiated cascades by A.M. Hillas was used. The electron density at  $1020 \text{ g cm}^{-2}$  (Leeds) for cascades due to vertical photons was

$$\rho(r) = \frac{1}{2\pi r} \frac{dn(r)}{dr} (1 + r/45)^{-3} \text{ m}^{-2} \quad \text{with} \quad n(r) = \frac{a}{\sqrt{y}} e^{t(1 + \ln f/0.72)}$$

$$\text{and} \quad a = 0.460/(1 + 0.380/x) \quad x = E.r/5.8093$$

$$f = 1 - 0.72(1 - y/t) \quad y = \ln(1 + 2.390x)$$

$E$  is the photon energy in GeV, and  $t$  is the vertical thickness (r.l.) between the photon production point ( $\pi^0$  decay) and the observation level. A radiation length of  $36.1 \text{ g cm}^{-2}$  was used. If a cascade was inclined this was taken into account by multiplying the density calculated from the formula by the cosine of the zenith angle and taking  $t$  equal to the slant thickness, and  $r$  equal to the perpendicular distance from the cascade axis.

The cascade function has been used directly for each photon (EMC Model I) or in conjunction with a simple Monte Carlo technique to simulate fluctuations in the formation of the first  $e^+e^-$  pair (EMC Model II).

Mountain level calculations involved rescaling the above electromagnetic cascade lateral distributions according to the lower air density.

### 6. Simulation of the electron distribution in the shower core

#### (a) Calculations for Leeds

A map of the core region was obtained by superposing electromagnetic cascades, taking into account the direction and location of their axes. In each shower simulation the shower primary was directed at the centre of a square of side  $10.2 \text{ m}$  located in the observation plane. The square was subdivided into  $(51)^2$  equal squares, and the counts of electrons deposited in each of them determined using the cascade function. Computing time consumed in doing this was saved by ranking photons so as to concentrate the most detailed calculations on photon cascades with the densest "cores", and by "thin sampling" (Hillas, 1981) of low energy hadrons. Calculations for photon energies down to  $1 \text{ GeV}$  from  $\pi^0$  decay could therefore be made on a routine basis.

After calculating the electron counts the simulation program searched for a shower centre (centre of symmetry) in the central  $(7.6)^2 \text{ m}^2$  of the mapping area (most of the shower centres, located to within  $\sim 5 \text{ cm}$ , fall within  $0.5 \text{ m}$  of the centre of the mapping area). The shower was discarded if a shower centre was not found in the "search area", and also if the electron density, averaged over  $2 \times 2$  adjacent square elements of the mapping area, did not exceed  $50 \text{ m}^{-2}$  somewhere in the mapping area.

If the shower was not discarded then densities at various radial distances from the shower centre were obtained, as in the experimental work (Hodson et al., 1983a,b, 1985), from counts made in an "annular

grid", in this case, "superposed" over the mapping area. The grid used consisted, as in the experiment, of a series of concentric circles, starting with a radius of 0.25 m and then with radii increasing in 0.5 m steps. For the above experimental work the annuli were divided into equal areas of  $\pi/16\text{m}^2$ . However for the simulations it was more convenient to divide the annuli angularly each into 16 sections ("sampling bins") by common radii from the centre. The difference between the two procedures is not significant: both give densities for the same radial widths.

Counts were obtained in the "sampling bins" with the "annular grid" centred on the shower centre. The central count, calculated by integrating the electron density over the area of the central bin, gave the density corresponding to the experimental central density  $\rho(0)$ . Counts in the annuli at 1.0, 2.5 and 4.0 m were derived from the mapping area counts and gave densities corresponding to the experimental densities  $\rho(1.0)$ ,  $\rho(2.5)$  and  $\rho(4.0)$  respectively. These results were supplemented by counts, determined as above, in the remaining annuli out to 4.5 m and by densities calculated at points in the mapping plane further out. The radial density distribution was thus sampled at intervals of 0.5 m out to 7.0 m from the shower centre.

#### (b) Calculations for Sacramento Peak

Both the calculations and the experimental analysis are made using the corresponding Leeds-level grids with dimensions in array space scaled up according to the lower air density found at mountain level.

#### 7. Construction of density spectra etc.

Predictions of the average lateral distribution and density spectra at fixed distances from the shower centre have been obtained for a wide choice of primary composition and energy spectra. A technique of weighting the simulated showers according to the primary fluxes assumed was used to obtain results for different primary energy spectra.

#### 8. Acknowledgements

The author thanks Dr A.M. Hillas for his help with this work, and the Science and Engineering Research Council for support in the form of a Post-Doctoral Research Fellowship.

#### References

- Ash, A.G., 1984, Ph.D.thesis, University of Leeds
- Ash, A.G., 1985a, paper HE4.2-18, this Conference
- Ash, A.G., 1985b, paper HE4.2-16, this Conference
- Freier, P.S. and Waddington, C.J., 1975, *Astrophys.Sp.Sci.*, 38, 419
- Gaisser, T.K. et al., 1982, *Phys.Rev.*, D25, 2341
- Hillas, A.M., 1979a, Haverah Park Note, September 1979
- Hillas, A.M., 1979b, 16th ICRC, Kyoto, 6, 13
- Hillas, A.M., 1981, 17th ICRC, Paris, 8, 193
- Hodson, A.L. et al., 1983a, 18th ICRC, Bangalore, 6, 23
- Hodson, A.L. et al., 1983b, 18th ICRC, Bangalore, 11, 201
- Hodson, A.L. et al., 1985, paper HE4.2-10, this Conference

COMPARISON OF SIMULATION RESULTS WITH SEA-LEVEL EXPERIMENTAL DATA  
ON  $10^{14} - 10^{16}$  eV AIR SHOWER CORES

A.G. Ash

Department of Physics, University of Leeds, Leeds LS2 9JT, U.K.

ABSTRACT

Simulation predictions for the Leeds 35 m<sup>2</sup> horizontal discharge chamber array for proton primaries with a  $\sim E^{-2.7}$  spectrum extrapolated from balloon data to  $10^{16}$  eV give power law  $\rho(r)$ -spectra with constant slope  $\sim -2$  consistent with the experimental data up to the point at which they steepen but overshooting them at higher densities, and at high shower sizes predicted cores which are significantly steeper than those observed. Further comparisons with results for heavy nuclei primaries (up to  $A = 56$ ) point to the inadequacy of changes in primary composition to account for the observed density spectra and 'core flattening', and the shower size spectrum together, and point, therefore, to the failure of the scaling interaction model at  $\sim 10^{15}$  eV primary energy.

PARTICLE DISTRIBUTIONS IN  $\sim 10^{13} - 10^{16}$  eV AIR SHOWER CORES AT MOUNTAIN ALTITUDE AND COMPARISONS WITH MONTE CARLO SIMULATIONS

A.G. Ash

Department of Physics, University of Leeds, Leeds LS2 9JT, U.K.

ABSTRACT

Photographs of 521 shower cores in an array of current-limited spark ('discharge') chambers at Sacramento Peak (2900m above sea level, 730 g cm<sup>-2</sup>), New Mexico, U.S.A., have been analysed and the results compared with similar data from Leeds (80m above sea level, 1020 g cm<sup>-2</sup>). It was found that the 'central' density differential spectrum is consistent with a power law index of -2 up to  $\sim 1500\text{m}^{-2}$  where it steepens, and that shower cores become flatter on average with increasing size.

Scaling model predictions for proton primaries with a  $\propto E^{-2.71}$  energy spectrum account well for the altitude dependence of the data at lower densities. However, deviations at higher densities indicate a change in hadron interaction characteristics between  $\sim \text{few} \times 10^{14}$  and  $10^{15}$  eV primary energy causing particles close to the shower axis to be spread further out.

1. Introduction. Experimental data on particle distributions within a few metres of the axes of air showers at Sacramento Peak (2900m above sea level, 730 g cm<sup>-2</sup>), New Mexico, U.S.A., are described. The data are the results of the author's analysis of photographs of showers in an array of current-limited spark chambers ('discharge' chambers) operated by Hazen et al. (1981). These photographs were originally obtained as part of a search for high- $p_t$  subcores.

The results are compared with similar data from the 35m<sup>2</sup> discharge chamber array at Leeds (80m above sea level, 1020 g cm<sup>-2</sup>) (Hodson et al., 1985) and predictions from Monte Carlo simulations.

2. Experimental Details. The array was housed under a canvas tent and was photographed from above using a small camera. During the experimental runs used as the basis for the present work the array consisted of 20 lm<sup>2</sup> discharge chambers (nearly identical to those used at Leeds) arranged into 4 parallel rows each of 5 chambers, with  $\sim 30\text{cm}$  gaps (walkways) between adjacent rows and the chambers in each row close-packed to give in most cases only  $\sim 3\text{cm}$  width of dead space between them. The trigger condition was a particle density  $\geq 50\text{m}^{-2}$  in a scintillator near the centre of the array in coincidence with at least one particle in a scintillator a few metres outside the array. The trigger rate was  $\sim 10\text{hr}^{-1}$ .

3. Analysis and Results. The methods of analysis of the shower photographs follow closely those of Hodson et al. (1983a,b) for the Leeds data. The photographs (negatives on 35mm film) were projected at a linear demagnification of 8 in array space and scanned by eye for cores. Core location and subsequent density measurements made use of an annular grid, superposed over the projected image, identical in pattern to that used for the Leeds photographs (see Hodson et al., 1983a) but with its dimensions (in array space) linearly scaled up by a factor  $s=(1020/730)$ . This was to take approximately into account the effect of the difference in air density on particle densities when comparing the data for Leeds and Sacramento Peak. As in Hodson et al. (1983a) the grid was used to determine a shower centre (centre of symmetry) for the particle distribution of each core located in the array area and, with the grid

centred on the shower centre, densities at various radial distances were determined. To reduce the effects of trigger bias and scanning bias the analysis excluded all showers with centres located in the walk-ways between the rows of chambers, those with centres falling in the 4 corner chambers and any in the remaining outer chambers with centres falling within 0.4m of the edge of the array. The total collecting area for shower cores was then equal to  $\approx 12\text{m}^2$ .

A count of discharges in the centre circle (radius 0.25sm) of the grid gave the 'central' density; when a walk-way overlapped part of the centre circle (maximum 50%) then symmetry was used to obtain the count for the whole of its area. Counts in the angular sections of the annuli at the scaled distances sm and 2.5sm gave densities at these distances. (In general, counts were made in only one randomly-selected section in each of these annuli.)

In the rest of this paper, observed particle densities per  $\text{m}^2$  (i.e. count/actual bin area in array space) are given, rather than densities scaled up by a factor  $s^2$ .

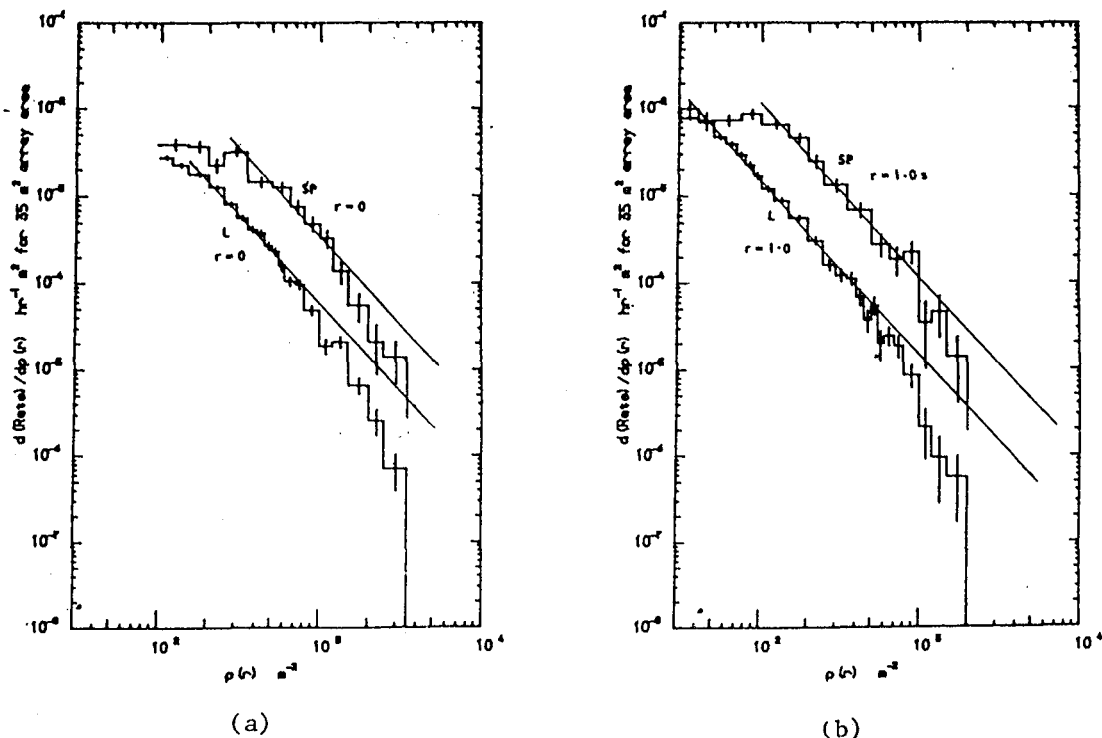


**Figure 1** Differential density spectra  $\rho(r)$  observed at Leeds (L) and Sacramento Peak (SP)

Figure 1 shows the differential density spectra for 521 cores at 0, 1.0s, and 2.5sm from the shower centre (normalised to a  $35\text{m}^2$  collecting area) as observed at Sacramento Peak, compared with the corresponding experimental data for Leeds. Power law lines of index -2 have been superposed on the spectra to show the steepening at high densities in the Leeds data (see Hodson et al., 1985) and for comparison with Sacramento Peak. (The deviations of the spectra from the -2 power law at low densities are due to trigger and scanning bias.) In Figure 1(a) there is evidence of a

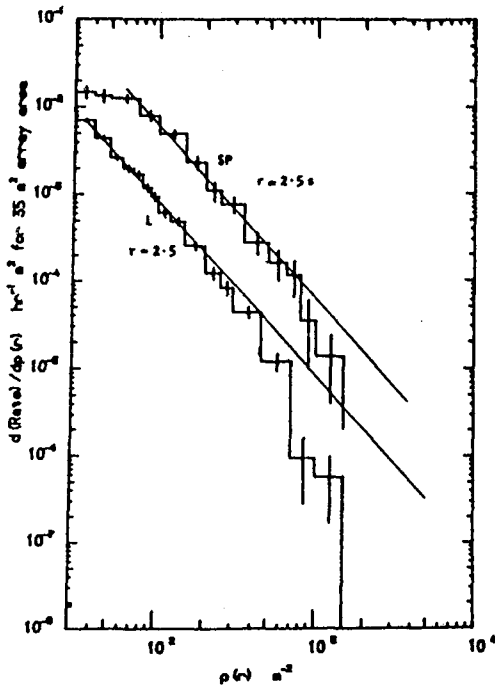
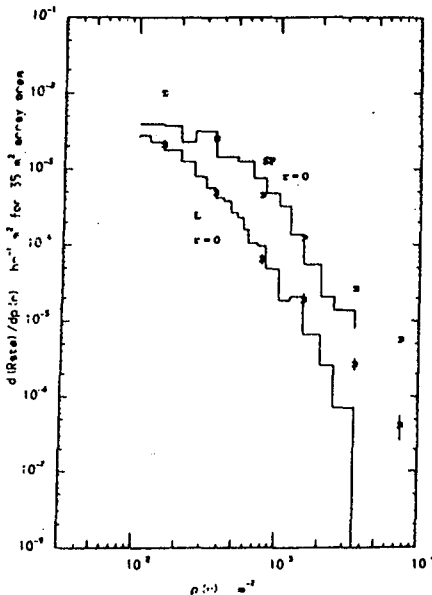


Figure 1(c)

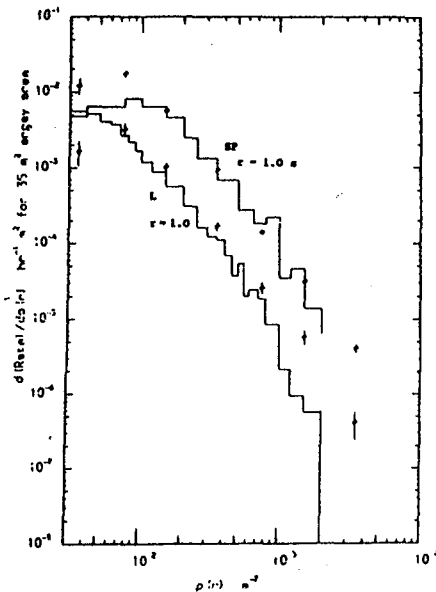
steepening from the  $-2$  power law in the Sacramento Peak  $\rho(0)$  spectrum at  $\sim 1.5 \cdot 10^3 \text{ m}^{-2}$ ; the spectra further out (Figures 1(b) and 1(c)) may also steepen around  $10^3 \text{ m}^{-2}$  but this is less clear.

Figure 3 gives a plot of core 'flatness',  $\langle \rho(1.0 \text{ s}) \rangle / \langle \rho(0) \rangle$ , versus  $\rho(2.5 \text{ s})$  (used as a measure of shower size, as  $\rho(4.0)$  in Hodson et al., 1985); this shows a tendency for shower cores to become flatter within  $s (= 1.4) \text{ m}$  as the showers become larger (as also reported for the Leeds data (Hodson et al., 1985)). Taking Figures 1 and 3 together, steep dense shower cores are observed at a lower rate than might be expected by extrapolation.

Figures 2 and 3 give comparisons with simulation predictions, after excluding all real and simulated showers with  $\rho(0) < 100 \text{ m}^{-2}$ , using scaling models (with EMC Model I) for proton



(a)



(b)

Figure 2 Comparison of observed differential density spectra (histograms) at Leeds (L) and Sacramento Peak (SP) with simulation predictions (points)

primaries, described by Ash (1985a). The full detailed core-mapping calculations were used for comparison with the Leeds data; for Sacramento Peak a simpler calculation was used, with the shower centre assumed to coincide with the shower axis. For the present purposes this

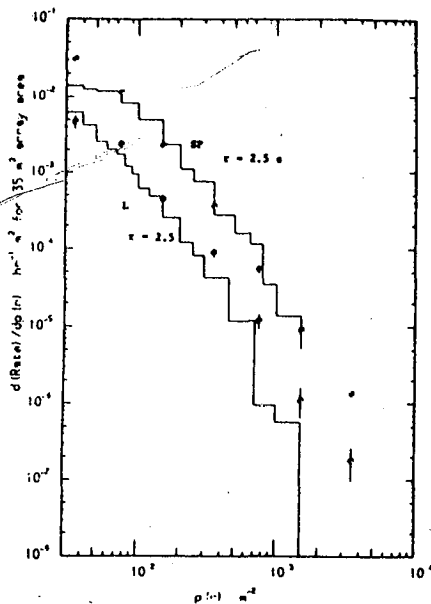


Figure 2(c)

The predictions agree well with the observed spectra both in slope and in absolute rates in the  $-2$  power law region, where proton showers would be expected to dominate the spectra. At higher densities, all the Leeds spectra and the Sacramento Peak  $\rho(0)$  spectrum are clearly steeper than those predicted.

Figure 3 shows that the predicted large proton showers have much steeper cores, on average, than those observed, as was also found for the Leeds data (Ash, 1985b).

**4. Discussion.** It is interesting to consider the mean primary energy  $\langle E \rangle$  of showers with a given  $\rho(r)$  at Sacramento Peak. At  $\rho(0) \approx 1.5 \times 10^3 \text{ m}^{-2}$  the proton simulations predict  $\langle E \rangle \approx 6 \times 10^{14} \text{ eV}$ ; if the steepening of the  $\rho(0)$  spectrum is due to a rapid increase in the slope of the proton primary energy spectrum then a clear steepening should also occur for similar values of  $\langle E \rangle$  in the density spectra further out. At 2.5 s and s m from the shower centre  $\langle E \rangle = 6 \times 10^{14} \text{ eV}$  corresponds to densities of  $\sim 200 \text{ m}^{-2}$  and  $400 \text{ m}^{-2}$  respectively; no steepening is evident at around these densities. This, together with the observed core flattening, lends support for a significant change in hadron interaction characteristics between primary energies of  $\sim$  a few  $\times 10^{14}$  and  $10^{15} \text{ eV}$ . A natural explanation might be found in a mechanism which spreads particles out from within  $\sim 1 \text{ m}$  of the shower centre. Complete understanding probably requires the combined effect of interaction changes plus some steepening in the proton energy spectrum.

**5. Acknowledgements.** Grateful thanks go to Professor W.F. Hazen for loan of the Sacramento Peak shower photographs, to Dr A.L. Hodson for help in preparing this paper, and to Dr A.M. Hillas for his advice. The Science and Engineering Research Council provided a Post-Doctoral Fellowship.

**References** (ICRC = International Cosmic Ray Conference)

- Ash, A.G., 1985a, paper HE 4.2-15, this Conference  
 Ash, A.G., 1985b, paper HE 4.2-16, this Conference  
 Hazen, W.E., Hendel, A.Z., and Hazen, E.S., 1981, 17th ICRC (Paris), 11, 350  
 Hodson, A.L., Porter, M.R., Ash, A.G., and Bull, R.M., 1983a, 18th ICRC (Bangalore), 6, 23  
 Hodson, A.L., Porter, M.R., Ash, A.G., and Bull, R.M., 1983b, *ibid*, 11, 201  
 Hodson, A.L., Ash, A.G., and Bull, R.M., 1985, paper HE 4.2-10, this Conference

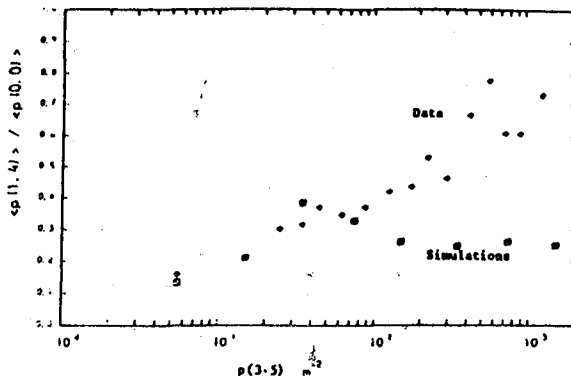


Figure 3 'Core flattening' at Sacramento Peak

difference is unimportant. The proton primary energy spectrum was  $dn/dE = 1.36 \times 10^4 E^{-2.71} \text{ GeV}^{-1} \text{ m}^{-1} \text{ sr}^{-1} \text{ s}^{-1}$ , consistent with balloon-based observations, here extrapolated to  $10^{16} \text{ eV}$ .

TSKHRA-TSKARO COMPLEX INTENDED FOR THE  
INVESTIGATIONS OF EAS SPATIAL CHARACTE-  
RISTICS NEAR AXIS

O.L.Berdzenishvili, Yu.G.Verbitski, Yu.A.Gromov,  
D.M.Kotlyarevski, A.A.Novalov, I.V.Paziashvili,  
N.S.Rusishvili, L.Sh.Khachaturyan, P.V.Tsomaya,  
Z.Sh.Sharvadze, G.Z.Stemanetyan

Institute of Physics, Academy of Sciences of the  
Georgian SSR, Tbilisi, USSR

Tskhra-Tskaro EAS complex located at the height of 2500 m above sea level is intended for a correlated investigation of three main components of the extended atmospheric showers (EAS) - hadron, muon and electron-proton ones - near the shower axis. This complex is aimed at the investigation of proton and primary cosmic radiation nucleus interactions with the nuclei of air atoms within the energy range  $10^{14}$  -  $10^{16}$  eV.

The complex will consist of the following basic parts (see Fig.1):

1. Shower part of the complex for the measurement of the shower electron-proton component (N°3,4,5,8).

2. Mobile master device (N°9).

3. The installation for the investigation of hadron nuclear interactions EAS- "ЯBA" (N°1,6).

4. "Video EAS" installation (N°2,7).

5.  $\mu$ -detector installation (Fig.2, N°6).

The shower part is an installation of central type including scintillation and ionization sensors for the measurements of the energy and direction of the particle generating an EAS, the avalanche age, the spatial behaviour of its basic components, EAS axis restoration.

The dimensions of scintillators (3 cm thick) used in the central part are  $0.5 \times 0.5$  m<sup>2</sup> the information pick-

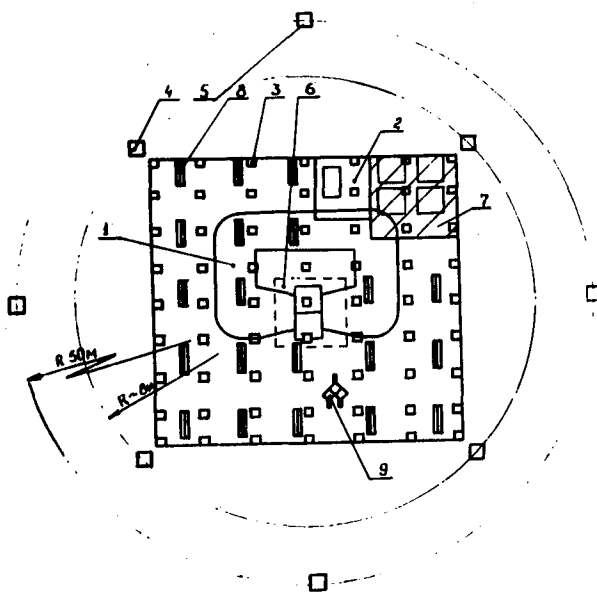


Fig.1

up from the detector corner.



The scintillators are 1.5 m distant from each other, filling an area of  $\sim 160 \text{ m}^2$ . It is also planned to locate on this area paired ionization chambers  $\sim 5 \text{ m}$  distant from each other (see Fig.1). Thus, a sufficiently detailed reproduction of the EAS central part is achieved.

The periphery of the shower part of the complex consists of two groups of scintillation detectors. One of them (4 detectors) will be situated along a circumference with a radius of 8 m centered in the geometric centre of the complex, while the second similar group of detectors will be situated at a radius of  $\sim 50 \text{ m}$  with respect to the geometric centre (see Fig.1). In the peripheric scintillators, the detectors  $3 \text{ cm}$  thick with the dimensions of  $1 \times 1 \text{ m}^2$  are used, with the information pick-up from the top.

II. Mobile master device represents three scintillation counters close to each other and switched for coincidence with the dimensions  $0.5 \times 0.5 \times 0.5 \text{ m}^3$  (Fig.1, N°9), which will detect the atmospheric showers with the energy  $E \geq 10^{14} \text{ eV}$  and define the axis position.

Moving the singling-out system within the distance of  $0 + 15 \text{ m}$  from the spark chambers, one may obtain the averaged spatial distribution of EAS components by measuring the particle density in spark chambers.

III. The installation "ЯБА" has been working at the station for 10 years serving for the investigation of hadron interaction with nuclei within the energy range  $0.1 + 10 \text{ TeV}$ . This unit includes a magnetic spark spectrometer (MSS) and a "small" ionization calorimeter (SIC). Spark chambers (Fig.1, N°5, Fig.2, N°1,5) intervalled with targets  $0.1$  nuclear interaction length thick are situated in the upper part of the magnet gap. This unit serves to determine the direction of an incident charged hadron and the characteristics of secondary particles.

IV. "Video EAS" apparatus is intended for a detailed investigation of EAS characteristics near the axis, as well as correlations between them, using spark and ionization chambers. The apparatus contains a large ionization calorimeter (BIC) (Fig.2, N°3), and its depth is supposed to reach  $1000 \text{ g/cm}^2$ . At present,  $\sim 200 \text{ g/cm}^2$  of the absorber is laid, and one layer of ionization chamber with a total number of the registration channels equal to 16 is mounted.

A part of the spark chambers of the "Video EAS" apparatus is mounted under the large ionization calorimeter (Fig.2, N°4) and serves for the simultaneous observation of hadron and muon EAS components. In the course of the experiment, muon registration threshold will be increasing beginning from  $E \geq 0.5 \text{ GeV}$  at the BIC thickness of  $0.2 \text{ kg/cm}^2$ . (Hadron registration threshold are approximately 50 times higher).

In the other part of spark chambers located in the immediate vicinity of BIC, the electron-photon EAS component with the energy threshold of  $\sim 2 \text{ MeV}$  is registered. The upper and lower walls of the chambers are transparent,

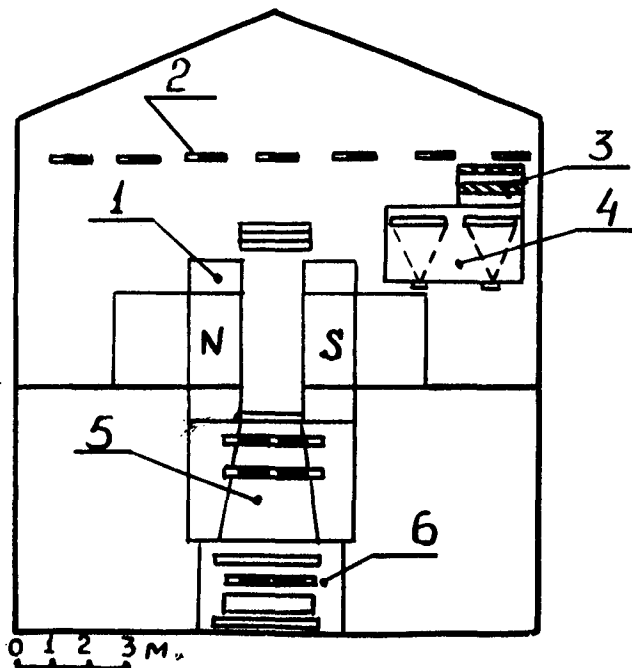
and the inner volume is photographed with the cameras.

V.  $\mu$ -detector is located under the SIC of apparatus and consists of two-spark chambers interleaved with magnetized iron (the magnetic field intensity is  $\sim 2$  T) and scintillation starting device. The distance between the layers of chambers is  $\sim 145$  cm. The photographing will be accomplished using the cameras RFK-5 constituting stereopairs, which is necessary to restore the spatial pattern and momentum measurements. The energy threshold of registration depends on  $\mu$ -meson direction and varies within  $3 + 10$  GeV.

VI. At the Institute of Physics of the Academy of Sciences of the Georgian SSR, a two-level system of using microcomputer "Electronics-60" at the first level and the computer "SM-4" at the next one is developed. According to our plans, the computer "Electronics-60" will be carry out the calibration of scintillators and ionization chambers, the spectra treatment, etc., while the total complex treatment of the whole system will be carried out by the computer SM-4.

VII. The problems, solved using the above complex.

The complex character of the device permits to study a wide range of nuclear-physical, cosmophysical and astrophysical problems.



It is planned to study the character of transverse pulse behaviour near the axis, momentum and angular correlations between hadrons and muons and each other, to investigate the secondary particle composition (the relationships between neutron and charged components) and to study  $\mu$ -meson group fluctuations in order to obtain the information on the primary composition, to study in detail the behaviour of primary particle and nuclei spectra within the energy range of  $10^{14} + 10^{16}$

Fig.2

Each unit of the complex described above has been tested. It is planned to put Tskhra-Tskaro installation in operation by the end of 1986.

A NEW STUDY OF SHOWER AGE DISTRIBUTION IN NEAR  
VERTICAL SHOWERS BY NBU AIR SHOWER ARRAY

N. Chaudhuri, D.K. Basak, G.C. Goswami and B. Ghosh  
Department of Physics  
North Bengal University  
Darjeeling - 734430, India

The air shower array has been developed since it started operation in 1931. The array covering an area of 900 m<sup>2</sup> now incorporates 21 particle density sampling detectors around two muon magnetic spectrographs. The air showers are detected in the size range 10<sup>4</sup> to 10<sup>6</sup> particles. A total of 11000 showers has so far been detected. Average values of shower age have been obtained in various shower size ranges to study the dependence of shower age on shower size. The core distance dependence of shower age parameter has also been analysed for presentation in the conference.

1. Introduction The age parameter which was calculated by fitting a particular shower with a given structure function is not constant over all core distances and shower sizes. Moreover the lateral distribution function does not fit well over all distances with the single age parameter. The age determination has been done using NKG as a reference function and also the forms of Hillas et al<sup>1</sup>, and Lagutin et al<sup>2</sup>. In all the cases of shower analysis it has been found that the age lies between 0.3 to 1.7 for various shower sizes in the range 10<sup>4</sup> to 10<sup>6</sup> particles. In the present study the shower size 'N<sub>e</sub>' and shower age 's' (average and local shower age) have been determined through standard  $\chi^2$  - method using NKG and various structure functions.

2. Methods In an array of 21 detectors covering an area of 900 m<sup>2</sup>, the density of the particles is estimated from the printed recording of the shower particles in each detector.

The shower age which is estimated by fitting the shower densities  $(r)$  with the help of the  $\chi^2$ -minimization method is shown in the figures for showers falling within zenith angle 0° - 30°. The fitting of NKG function for extensive air shower lateral electron distribution for a single age parameter gives some systematic errors. Hence the term 'local age parameter' (l.a.p.)  $S(r)$  is defined by Capdevielle et al<sup>3</sup> as

$$S(r) = \frac{1}{2x+1} \left[ (x+1) \frac{\partial \ln f}{\partial \ln x} + (2 + \beta_0) x + 2 \right]$$

which gives the best fit in the neighbourhood of  $r$  for a given structure function  $f$ . Where  $\beta_0 = 4.5$  if  $f$  is NKG function and  $X = r/r_0$ ,  $r_0 =$  Moliere radius.

The value of  $S(r)$  is numerically estimated in a small band of distance  $[r_i, r_j]$

$$S_{ij} = \frac{\text{Ln} [F_{ij} X_{ij}^2 Y_{ij}^{4.5}]}{\text{Ln} [X_{ij} Y_{ij}]}$$

where  $F_{ij} = f(r_i)/f(r_j)$ ,

$X_{ij} = r_i/r_j$  and  $Y_{ij} = (X_i + 1)/(X_j + 1)$

and  $S_{ij} \rightarrow S(r)$  if  $r_i \rightarrow r_j$   
with  $r = (r_i + r_j)/2$ .

### 3. Results

3.1. Age distribution The age is calculated over a particular shower size range and a typical age 's' distribution is shown in Fig.1. We find that for showers falling within zenith angle  $30^\circ$  having sizes in the range  $10^4 - 2 \times 10^4$  particles the individual shower age lies between 0.3 and 1.25.

### 3.2. Variation of 1.a.p. with core distance

The 1.a.p. distribution is shown in Figs. 2.1 and 2.2 in the core distance range 1-20m. For showers in the size range  $4.0 < \log N_e < 4.5$ , the 1.a.p. increases with the increase of core distance, whereas for showers in the size range  $4.6 < \log N_e < 5.3$ , the 1.a.p. decreases very slowly from 2.5m to 10m and then increases from 10m to 20m.

### 3.3. Variation of 1.a.p. with the shower size

The 1.a.p. distribution is shown in Fig.3 for core distances in the range from 3-10m and from 10-20m. It has been found that the 1.a.p. decreases as the shower size increases from  $10^4$  to  $10^5$  particles for both the distance ranges.

### 3.4. Variation of average age parameter distribution with shower size

The average age for a shower group was determined and plotted as a function of shower size as shown in Fig.4 along with the similar data of Kristiansen et al<sup>4</sup>, Asakimori et al<sup>5</sup>, Abdullah et al<sup>6</sup> and Gerhardy et al<sup>7</sup>. The average age is nearly constant over a shower size range  $10^4 - 10^6$  particles.

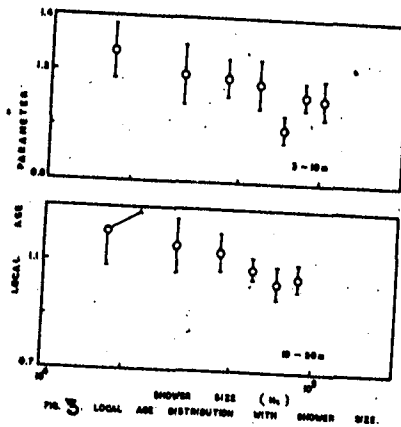
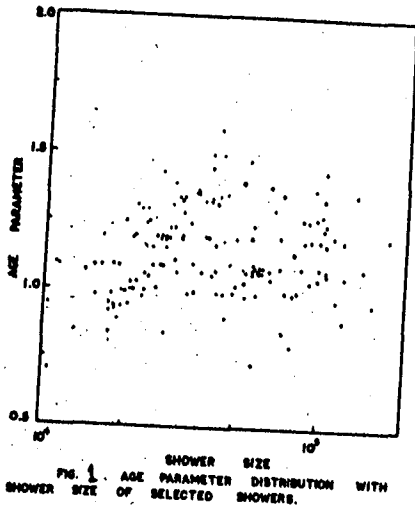
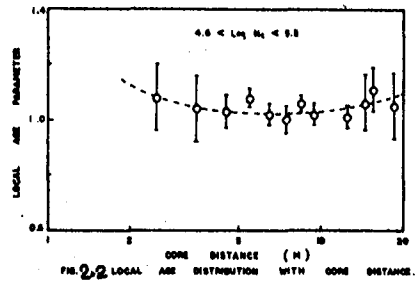
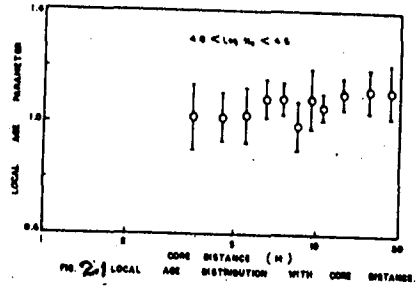
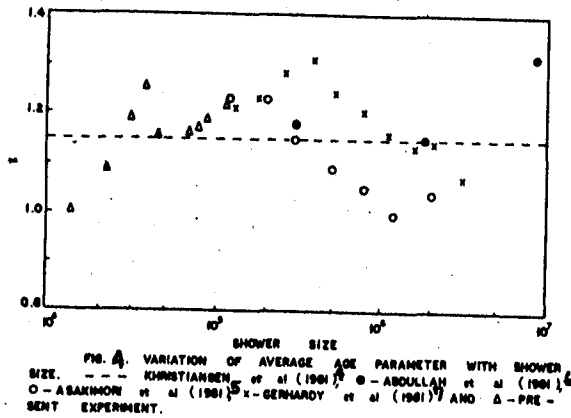
4. Discussion Each shower was fitted to the Hillas function to obtain the core coordinates and shower age. The average age for a shower group is consistent with other experiments. The present data on the 1.a.p. shown in Figs. 2.1 and 2.2 show the constancy of 1.a.p. in the core distance range 2-20m. The dependence of 1.a.p. on shower size in two core distance regions shown in Fig. 3 shows near constancy of 1.a.p. in the size range  $10^4 - 10^5$  particles.

5. Conclusions It can be concluded from the plotted data that the determination of average age and 1.a.p. from the present experiment is consistent with the measurements of other workers mentioned above.

6. Acknowledgements The Department of Atomic Energy, Govt. of India is thanked for the financial assistance for the DAE Project at North Bengal University.

#### References

1. Hillas, A.M. et al (1977), Proc. 15th ICRC, Plovdiv, 8, 450.
2. Lagutin, A.A. et al, (1979), Proc. 16th ICRC, Kyoto, 7, 13.
3. Capdevielle, J.N., (1933), Proc. 13th ICRC, Bangalore, 11, 303.
4. Khristiansen, G.B., et al, (1931), Proc. 17th ICRC, Paris, 6, 39.
5. Asakimori, K., et al, (1931), Proc. 17th ICRC, Paris, 11, 301.
6. Abdullah, M.M., et al, (1931), Proc. 17th ICRC, Paris, 6, 151.
7. Gerhardy, P.R., et al, (1931), Proc. 17th ICRC, Paris, 6, 152.



A NEW STUDY OF MUONS IN AIR SHOWERS  
BY NBU AIR SHOWER ARRAY

N. Chaudhuri, N. Mukherjee, S. Sarkar  
D. K. Basak and B. Ghosh

Department of Physics  
University of North Bengal  
Darjeeling - 734 430, India

The NBU air shower array has been in operation in conjunction with two muon magnetic spectrographs. The array incorporates 21 particle density sampling detectors around the magnetic spectrographs covering an area of  $900 \text{ m}^2$ . The layout of the array (Basak et al<sup>1</sup>) is based on the arrangement of detectors in a square symmetry. The array set up on the ground level is around a 10 m high magnetic spectrograph housing. This magnetic spectrograph housing limits the zenith angular acceptance of the incident showers to a few degrees. The array of detectors is sensitive to air showers initiated by cosmic primaries of energy in the range  $10^{14}$ - $10^{15}$  eV. The detectors are scintillator counters made of plastic scintillators of two different sizes :  $0.25 \text{ m}^2$  and  $0.125 \text{ m}^2$ . Each scintillator is of 5 cm thick mounted firmly within a box made of aluminium sheets. A DUMONT 6364 photomultiplier tube mounted suitably to view the scintillator forms a detector. The pulses from the detectors are digitised by an analog-to-digital converter and the density information from all the detectors is printed out on a paper tape by a line printer. Two muon magnetic spectrographs at a separation of 4 m have been installed in a housing which is located near the centre of the array of detectors.

A 2-metre neon flash tube (NFT) chamber which has been used as a low energy muon detector in the NBU air shower array consists of 9 layers of neon flash tubes installed in a chamber with a cover of 5 cm of lead to get rid of electrons. Each layer contains 54 tubes arranged in such a way that a single muon passing through the flash chamber must discharge the tubes lying on the trajectory of the particle. The NFT chamber covers an area of 1 m x 1 m for the localisation of muon trajectories.

An absorber of  $1000 \text{ gm/cm}^2$  of concrete on the roof about 1 m above the spectrograph units is provided to remove the electronic component. Additional lead absorber could be placed above the top tray of the spectrograph for this purpose. The information on muon triggered neon flash tube glows for the location of particle trajectory is obtained

by a set of cameras. From the recorded coordinates of the passing muon at the four levels of detection in the spectrograph, its deflection in the magnetic field is calculated. The momentum of a muon is determined from the relation

$$P = 21.96/\Delta \text{ GeV/c}$$

where  $\Delta$  is the deflection in t.s.unit (1 t.s. = 1.999 + 0.0002 cm) and the constant in the numerator is the product of the geometrical factor of the spectrograph and the line integral of the magnetic induction.

Three hundred muons in the fitted showers of size range  $10^4 - 10^5$  particles have so far been scanned and the momenta determined in the momentum range 2 - 440 GeV/c. More than 1500 recorded showers are now in the process of scanning and fitting. Shower records that will be obtained till June '85 will be incorporated. A lateral distribution of muons of energy greater than 300 MeV in the shower size range  $10^5 - 7 \times 10^5$  has been obtained from the record of NFT chamber.

The Department of Atomic Energy, Govt. of India, is supporting the air shower work at North Bengal University.

#### References

1. Basak, D.K. et al, (1984), Nucl. Instr. Meths., 227, 167.



## Lateral Distribution of Electrons of Air Showers

K.Asakimori and T.Maeda

Department of physics,

Kobe University, Nada-Ku, Kobe 657, Japan

T.Kameda

Kobe Women's University, Suma-Ku, Kobe 654, Japan

K.Mizushima

Kobe Women's Junior College, Chuo-Ku,

Kobe 650, Japan

Y.Misaki

Research Center for Nuclear Physics,

Osaka University, Ibaraki,

Osaka 567, Japan

## ABSTRACT

Lateral distribution of electrons (abbreviated to LDE) of the air showers of size  $10^5 \sim 10^6$  was studied within one MU.

The results are summarized as follows:

- i) LDE of the air showers observed is well represented by NKG function except for vicinity of the core,
- ii) LDE measured by thin scintillators does not differ from that measured by thick ones of 50mm thickness.

1 Introduction. Lateral distribution of shower particle is usually approximated by NKG function. However, several authors reported recently that the lateral distribution is not expressed by NKG function of single age parameter, and that number of particles measured by scintillator of 50 mm thickness distorts remarkably the lateral distribution near the core of air showers because of multiplication of the particles in scintillator (1)(2). Basing on these results, change of age parameter with distance from the core and its physical meanings are discussed among some researchers of air showers.

LDE of the air showers within one MU from the core and the effect of thickness of the scintillators on the lateral distribution were studied by the air shower array of Kobe University. The latter is investigated by means of scintillators of various thickness. From the results obtained by these measurements; change of age parameter with the distance from the core (local age parameter) is obtained.

2. Experiment and Results. Nine plastic scintillators of area  $1 \text{ m}^2$  and thickness of 50 mm and 67 plastic scintillators of area  $0.25 \text{ m}^2$  and thickness of 50 mm were used for the measurement of densities of charged particles of air showers of size  $\geq 10^5$ , within 1 MU from the core. In addition to these scintillators, scintillators of various thickness were placed among

them to study the effect of the thickness of scintillators on densities of particles (3).

Assuming LDE is expressed by NKG function, NKG function of best fit for individual shower was obtained. The shower array of Kobe University and the method of best fit were reported in detail elsewhere (4).

About ten thousands showers were observed during the period from December 1983 to June 1984.

The average LDE of showers of size  $10^5 \sim 10^6$  and less than  $30^\circ$  of zenith angle normalized to the showers of size  $10^6$  are shown in Fig.1 for several sections of age parameter. Solid line in the figure is NKG function of mean age parameter for the showers classified in each section. Number of particles is corrected for the transition effect using the correction formulae (4).

From the figure, it is pointed out that LDE is well represented by NKG function except for the showers of  $1.4 \leq s \leq 1.6$  and for distance within 3 m from the core. Large disparity of showers of the latter from NKG function of the same age parameter is considered to be caused by any small samples of showers, or the inadequateness of the method of best fit for these showers, or any physical reason, but nothing is known now definitely.

In Fig.2, are shown the average LDE of showers, which are measured by thin scintillators and have size  $\geq 10^5$ , zenith angle  $\leq 30^\circ$ , and age parameter  $1.0 \leq s < 1.2$ . The figure indicates that LDE is not different from those in Fig.1.

This result obviously show that the effect of the thickness of scintillators on density measurement is so small that one may safely use thick ones of 50 mm thickness. The local age parameter defined by Capdevielle and Gawin is obtained basing on LDE in Fig.1 and Fig.2 (5). The results are shown in Fig.3 and Fig.4. Local age parameter decreases slowly with increasing distance from the core, and farther than 3 m it is nearly constant, and does not show any tendency of decrease. Furthermore, local age parameter obtained by thin scintillators does not show any remarkable difference from that obtained by the scintillators of 50 mm thickness.

These results reveal that the variation of thickness of the scintillators does not significantly affect the value of age parameter, and that NKG function approximates well LDE.

3. Conclusion. LDE of air showers is approximated well by NKG function except for the neighborhood of the core and for the showers of old age parameter. Change of local age parameter is not recognized but for the vicinity of the core, and this shows the validity of approximation of LDE by NKG function of single age parameter. LDE obtained by thin scintillators does not differ largely from that obtained by those of 50 mm thickness, and this result shows that multiplication and absorption of particles in the scintillators are not so large.

Our results are in disagreement with those of Akeno group with respect to the variation of local age parameter and the

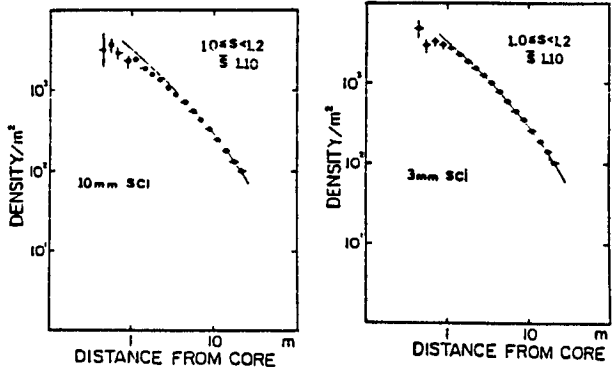
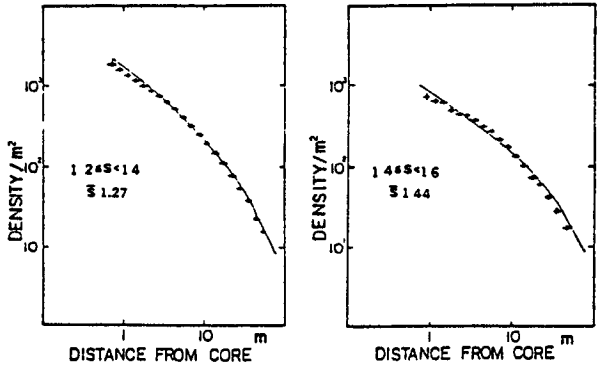
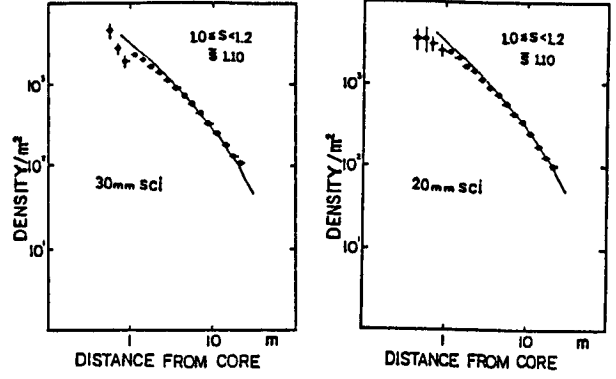
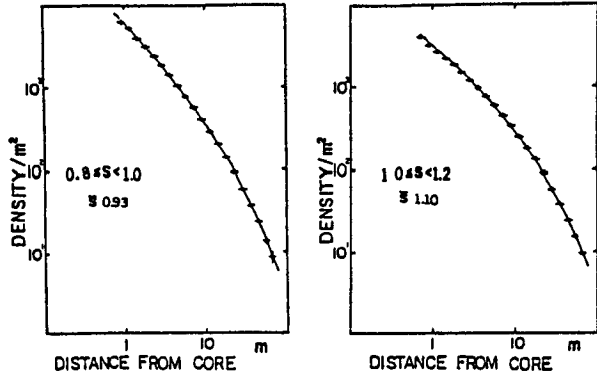


Fig.1

Fig.2

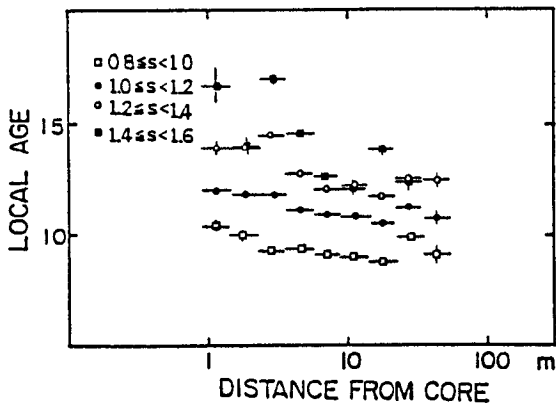


Fig.3

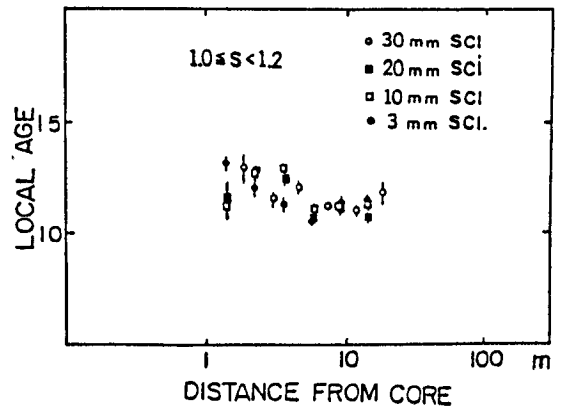


Fig.4

effect of the thickness of scintillators. Disagreement is considered to be caused by large spaces among detectors used by them, and it makes difficult to reveal the detailed information near the core. It is necessary to make spaces of detectors small as possible in order to determine precisely LDE near the core.

#### References

- (1) T.Kaneko et al.: Proc. 14th Int. Conf. on Cosmic Rays, Münch 8 (1975) 2747
- (2) M.Nagano et al.: J.Phys. Soc. Jpn. 53 (1984) 1667
- (3) K.Asakimori et al.: HE 4.4-9 of this conference.
- (4) K.Asakimori et al.: J.Phys. Soc. Jpn. 51 (1982) 2059
- (5) J.N.Capdevielle and J.Gawin: J.Phys. G(Nucl. Phys.) 8 (1982) 1317

DETAILED STUDIES OF THE ELECTRON LATERAL  
DISTRIBUTION IN EXTENSIVE AIR SHOWERS  
WITH ENERGIES AROUND  $10^{16}$  eV.

T.Dzikowski, J.Gawin and J.Wdowczyk

Institute of Nuclear Studies and  
University of Łódź, Cosmic Ray Laboratory  
90-950 Łódź 1, box 447, Poland.

I. The experimental procedure.

Using the Lodz extensive air shower array, we have performed detailed studies of the electron lateral distribution in extensive air showers. The showers were grouped according to their particle densities around 20 m from the core. The grouping was made in very narrow intervals of the densities. For every group of showers and for every distance interval /changing by 5 m/ histograms of the numbers of electron counters discharged have been obtained. The trays of G.M counters were located at following distances from the centre of the triggering detectors array : 16 m, 76 m, 117 m, 137 m, 141 m and 147 m, /Dzikowski et al., 1979/.

Every histogram then has been fitted with particle density spectrum described by the gamma distribution

$$P(\varrho) = \frac{b^p}{\Gamma(p)} \varrho^{p-1} \exp(-b\varrho)$$

taking into account the exact probabilities of the discharge of the given number of counters. The parameters  $p$  and  $b$  were calculated from the experimental histograms. Those parameters gives the average density and the width of fluctuations from the formulae /Dzikowski et al., 1977/.

$$\langle \varrho \rangle = \frac{p}{b} \quad \frac{\sigma}{\langle \varrho \rangle} = \frac{1}{\sqrt{p}}$$

In the present work we are analysing only the average densities as a function of the shower core distance.

The errors of the densities were obtained by Monte Carlo method following way. Taking the experimentally obtained distribution of densities in the form of the gamma function histogram of the expected discharged counters has been simulated. This procedure has been repeated 10 times. For every obtained histogram new values of the  $p$ ,  $b$  parameter have been obtained. The spreads of the parameters values have been taken as a measure of the errors.

## II. Results.

The obtained lateral distributions are compared in fig.1 with the commonly used Nishimura, Kamata, Greisen /N K G/ formula. As it is known the formula is /Greisen, 1956/

$$g(r) = \frac{N_0}{r_1^2} C(s) \left(\frac{r}{r_1}\right)^{s-2} \left(1 + \frac{r}{r_1}\right)^{s-4.5}$$

where  $s$  is the formal age parameter and  $r_1=79$  m the so called Moliere distance unit. The values of the obtained shower sizes and age parameters are given in table I.

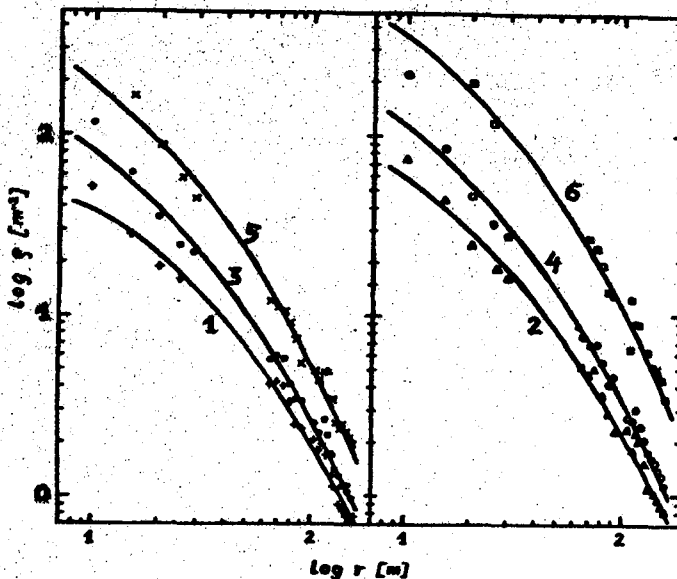


Figure 1. Experimental elektron lateral distribution for different shower sizes. The curves represent lateral distribution calculated from N K G formula for parameters summarised in table I.

Table I.

Number and symbol	$N_e$	s
1. +	$3.99 \times 10^5$	1.59
2. $\Delta$	$4.59 \times 10^5$	1.50
3. $\bullet$	$5.53 \times 10^5$	1.45
4. $\circ$	$7.07 \times 10^5$	1.42
5. $\times$	$1.13 \times 10^6$	1.39
6. $\square$	$2.26 \times 10^6$	1.41

It is interesting to note that the obtained lateral distributions are relatively wide /high value of the "s" parameters/ and that the NKG formula relatively well describes the lateral distributions at the distances above 50 meters from the core, whereas at the smaller distances the experimental distributions are slightly

steeper.

### III. Conclusions.

The electron lateral distribution at distances 60-150 m from the core seems to be well described by the NKG function with relative large values of the shower age parameter. The curves at smaller distances appear to go lower than the experimental points.

### References.

- Dzikowski, T. et al., J. Phys. G: Nucl. Phys., 3, 1591/1977/  
 Dzikowski, T. et al., Proc. XVI-th Int. C. R. Conf. Kyoto,  
8, 276 /1979/  
 Greisen, K., Progress in Cosmic Ray Physics, 3, 1 /1956/

STUDY OF MUONS NEAR SHOWER CORES AT SEA LEVEL  
USING THE E594 NEUTRINO DETECTOR

Goodman, J.A.,<sup>1</sup> Gupta, S.C.,<sup>1</sup> Freudenreich, H.,<sup>1</sup> Sivaprasad, K.,<sup>1</sup> Tonwar, S.,<sup>2</sup>  
Yodh, G.B.,<sup>1</sup> Ellsworth, R.W.,<sup>3</sup> Goodman, M.C.,<sup>4</sup> Bogert, D.,<sup>5</sup> Burnstein, R.,<sup>6</sup>  
Fisk, R.,<sup>5</sup> Fuess, S.,<sup>5</sup> Morfin, J.,<sup>5</sup> Ohska, T.,<sup>5</sup> Bofill, J.,<sup>7</sup> Busza, W.,<sup>7</sup>  
Eldridge, T.,<sup>7</sup> Friedman, J.I.,<sup>7</sup> Kendall, H.W.,<sup>7</sup> Kostoules, I.G.,<sup>7</sup> Lyons, T.,<sup>7</sup>  
Magahiz, R.,<sup>7</sup> Mattison, T.,<sup>7</sup> Mukherjee, A.,<sup>7</sup> Osborne, L.,<sup>7</sup> Pitt, R.,<sup>7</sup>  
Rosenson, L.,<sup>7</sup> Sandacz, A.,<sup>7</sup> Tartaglia, M.,<sup>7</sup> Taylor, F.E.,<sup>7</sup> Verdier, R.,<sup>7</sup>  
Whitaker, S.,<sup>7</sup> Yeh, G.B.,<sup>7</sup> Strongin, B.,<sup>7</sup> Abolins, M.,<sup>8</sup> Brock, R.,<sup>8</sup>  
Cohen, A.,<sup>8</sup> Ernwein, J.,<sup>8</sup> Perkins, G.,<sup>8</sup> Hatcher, R.,<sup>8</sup> and Werthmann, A.<sup>8</sup>

<sup>1</sup> Univ. of Maryland, College Park, MD

<sup>2</sup>Tata Inst. of Fundamental Research, Bombay, India

<sup>3</sup>George Mason University, Fairfax, Virginia

<sup>4</sup>Argonne National Laboratory, Argonne, Illinois

<sup>5</sup>Fermi National Lab., Batavia, Illinois

<sup>6</sup>Illinois Inst. of Technology, Chicago, Illinois

<sup>7</sup>Massachusetts Inst. of Technology, Cambridge, MA

<sup>8</sup>Michigan State University, East Lansing, Michigan

ABSTRACT

The E594 neutrino detector has been used to study the lateral distribution of muons of energy  $> 3$  GeV near shower cores. The detector consists of a 340 ton fine grain calorimeter with 400,000 cells of flash chamber and dimensions of 3.7 m x 20 m x 3.7 m (height). The average density in the calorimeter is 1.4 gm/cm<sup>2</sup> and the average Z is 21. The detector was triggered by four 0.6 m<sup>2</sup> scintillators placed immediately on the top of the calorimeter. The trigger required  $\geq 2$  p/m<sup>2</sup> in at least two of these four counters. The accompanying EAS was sampled by 14 scintillation counters located up to 15 m from the calorimeter.

Several off-line cuts have been applied to the data. Demanding five particles in at least two of the 'trigger' detectors, a total of 20 particles in all of them together, and an arrival angle for the shower  $< 45^\circ$  reduced the data sample to 11053 events. Of these in 4869 cases, a computer algorithm found at least three muons in the calorimeter. To take into account the failure of the computer algorithm to estimate the number of muons when the ionisation deposited in the calorimeter was very large, an upper limit on the total 'trigger' electrons was imposed. A limit of 100 electrons reduced the data set to 9657 events out of which 4803 events had more than three muons in the calorimeter. These cuts were also applied to the Monte Carlo simulated predictions (as described elsewhere at this conference) based on two different primary spectra; the first spectrum is dominated by heavy primaries while the second by protons. A preliminary comparison of the rates of predicted and observed triggers favors the first spectrum. Comparison of the detailed electron and muon numbers and their averages is carried out.



**CORRELATION OF HIGH ENERGY MUONS WITH  
PRIMARY COMPOSITION IN EXTENSIVE AIR SHOWER**

C.Cho, S.Higashi, N.Hiraoka, S.Ozaki, T.Sato,  
T.Suwada, T.Takahashi and H.Umeda

Department of Physics, Osaka City University

Osaka, Japan

**Abstract**

An experimental investigation of high-energy muons above 200 GeV in extensive air showers has been made for studying high-energy interaction and primary composition of cosmic-rays of energies in the range  $10^{14} \sim 10^{15}$  eV.

The muon energies are estimated from the burst sizes initiated by the muons in the rock, which are measured by four layers of proportional counters, each of area  $5 \times 2.6 \text{ m}^2$ , placed at 30 m.w.e. deep, Funasaka tunnel vertically below the air shower array. The air shower array, area of about  $30 \times 40 \text{ m}^2$  contains 21 plastic scintillation counters, of which five are for fast timing and all used for density determination.

The lateral distributions of high-energy muons above 200 GeV has been determined in the size range  $10^4 \sim 10^6$  particles and in the lateral range  $0 \sim 20 \text{ m}$ . These results are compared with Monte Carlo simulations based on the scaling model and the fireball model for two primary compositions, all proton and Mixed.

## 1. Introduction

High-energy muons in cosmic-rays keep information with characteristics of nucleus interaction and composition of primary cosmic-rays. An experimental investigation of high-energy muons in EAS with other components of the shower has been performed to take accurate information on both aspects. In this experiment the energies of muons are determined from the burst sizes initiated by them in the rock above the

detector and incoming directions are also determined by the use of the center of gravity of burst. By the use of this direction and the data from the shower array, we can determine the shower size  $N_e$ , age parameter  $S$  and distance between shower core and muon. Here we present results from an investigation of muon component ( $\geq 200$  Gev) of EAS in size range  $4 \times 10^4 \sim 10^6$  particles.

## 2. Experimental Arrangement and Method of Analysis

The apparatus consists of a scintillation counter array for the detection of air showers and four layers of proportional counters at the underground to observe bursts initiated by muons. Sixteen scintillation counters,  $1 \times 1$  m<sup>2</sup> and 10 cm thick, are used to record the densities correspond to 1 to 2000 particles. Five,  $50 \times 50$  cm<sup>2</sup> and 10 cm thick, counters are used for fast timing. These counters are distributed as shown in Fig. 1. Four layers of proportional counters are used to measure the size and the two dimensions lateral spread of the shower particles which are produced in the rock by high-energy muons. The area of each layer is  $2.6 \text{ m} \times 4.5$  m, the spatial resolution, i.e., distance of adjacent two particle array, and particle density;  $\bullet$ , and 10 cm along 4.5 m, and the distance between the top and

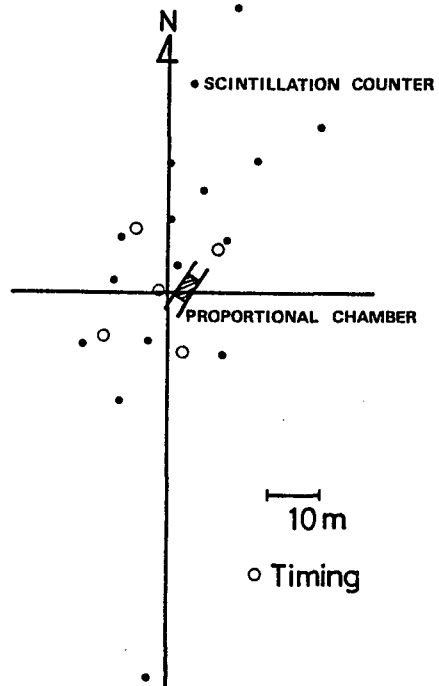


Fig.1 Plan of extended particle array.  $\circ$ , timing wires, are 5 cm along 2.6 m and particle density;  $\bullet$ , and 10 cm along 4.5 m, and the distance between the top and

the bottom layer is 94 cm. The burst detector is located inside the Funasaka Tunnel whose depth is 30 m.w.e. (1) and which is 18 m below the air shower array. Data are taken when each layer of the burst detector has more than 10 particles and any one of 16 scintillation counters has more than 6 particles. Lateral distribution of particles in observed burst is flat which is produced by multi-muon, or convex by a muon. Then convex bursts are selected by the following conditions which are determined on the basis of the analysis of bursts without air shower.

1)  $\beta_2 \geq 3$ ,  $\geq 30$  particles for each layer, where

$$\beta_2 = \mu_4 / (\mu_2)^2, \quad \mu_k = \sum f_i (r_i - \langle r \rangle)^k / n, \quad n = \sum f_i, \quad \langle r \rangle = \sum f_i r_i / n,$$

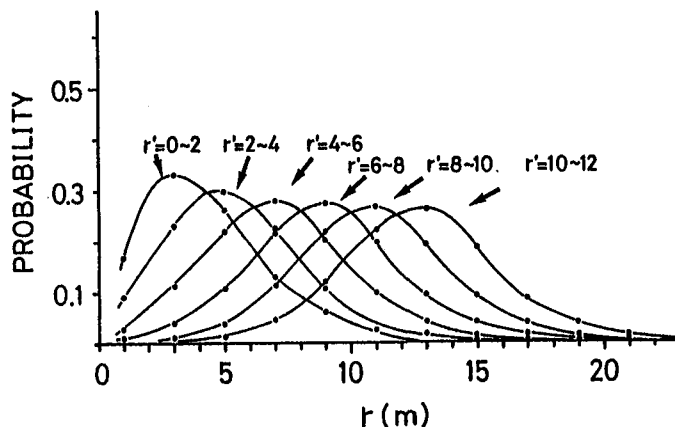
$f_i, r_i$  : particle number and position of  $i$ -th wire,  
 $\Sigma$  : sum of wires within a burst for each layer.

2) ratio of numbers of particles in a layer is  
 between 0.5 and 2.0.

For the selected data, center of gravity of burst size is calculated for each layer. Incoming direction of muon, namely, of air shower is determined from these 4 points. The energy of muon is determined from the burst size ( $N_b$ ) using the next equation:

$$E \text{ ( GeV )} = 0.67 N_b^{-1.03}.$$

Size ( $N_b$ ) is obtained from the average of four layers and zenith angle correction is applied. This equation is obtained from the conversion of burst size spectrum to energy spectrum. The air shower parameters, size ( $N_e$ ), core location ( $X, Y$ ) and age parameter ( $S$ ),



are determined by finding muon within interval  $r'$  for muon of a least square fit core distance  $r$ .

of observed densities to NKG

lateral distribution (2). We estimate the errors of these parameters,  $\sigma(X, Y) = \pm 2$  m and  $\sigma(\theta, \psi) = \pm 6^\circ$  from analysis of artificial showers. The probability of finding muon within interval  $r'$  for muon of core distance  $r$  is calculated by Monte Carlo method using the  $\sigma(X, Y)$  and  $\sigma(\theta, \psi)$ , and the result is presented in Fig. 2.

### 3. Results and Conclusion

During the 13666 hours, 2776 events have been obtained which are satisfied with burst conditions and air shower conditions. Only 103 events in which muon energy is  $\geq 200$

GeV are survived after next five conditions are applied.

- 1) air shower sizes  $N_e$  are in the range  $4 \times 10^4 \sim 10^6$  particles,
- 2) zenith angles  $\theta$  are in the range  $0 \sim 35^\circ$ ,
- 3) modified  $\chi^2$  values for lateral fit are in the range  $0 \sim 5$ ,
- 4) core distance are in the range  $0 \sim 20$  m.

Four conditions are on the basis of analysis of artificial showers. Under these conditions, correction factor of the acceptance-area is estimated to be 1. Relative densities of muon are obtained from 103 events by acceptance-area and finding probabilities. The density in the range 0 to 2 m becomes low because of flat lateral distribution of burst. Fig. 3 shows the lateral distribution of muons with energies more than 200 GeV in the associated shower size  $4 \times 10^4 \sim 10^6$  particles. Comparing the data curve with the predictions of Monte Carlo simulation (3), the data are normalized at the range 2 ~ 4 m. The figure shows that the primary composition of cosmic-rays in the energy interval  $10^{14} \sim 10^{14.5}$  eV is proton dominant. Data have errors due to energy estimation of air shower, short range of core distance and poor statistics, but the conclusion that the primary composition of cosmic-rays in the energy range till  $10^{14.5}$  eV are proton dominant, as other experiments suggest (4), may be correct. It is necessary to increase the range of shower size and core distance.

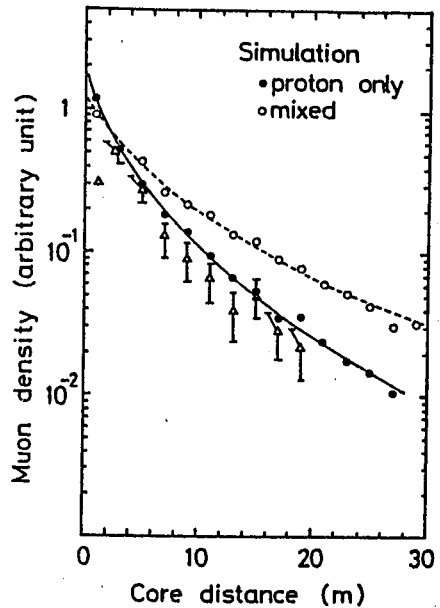


Fig.3  
Density distribution of muon above 200 GeV against core distance.

## References

- (1) Higashi, S. et al. ,16th ICRC, Kyoto, 10, 208, (1979).
- (2) This fitting program has been presented from the air shower group of Kobe University of Japan.
- (3) Mizutani, K. et al. , this Conference Paper, OG 5.2-9.
- (4) See, for example, Acharya, B.S. et al, 16th ICRC, Kyoto, 8, 304, (1979). ; Burnett, T. H. et al. , Phys. Rev. Lett., 51, 1010, (1983).

Measurement of Low Energy Muons in EAS at Energy Region Larger than  $10^{17}$  eV.

Y.Matsubara, T.Hara, N.Hayashida, K.Kamata, M.Nagano,  
H.Ohoka, G.Tanahashi and T.Teshima\*

Institute for Cosmic Ray Research, University of Tokyo,  
Tanashi, Tokyo, 188 Japan

\* Department of Physics, Kyoto University,  
Sakyo-ku, Kyoto, 606 Japan

#### Abstract

A measurement of low energy muons in EAS (threshold energies are 0.25, 0.5, 0.75 and 1.38 GeV) was carried out. The density under the concrete shielding equivalent to 0.25 GeV at core distance less than 500 m and 0.5 GeV less than 150 m suffers contaminations of electromagnetic components. Therefore the thickness of concrete shielding for muon detectors for the giant air shower array is determined to be 0.5 GeV equivalence. Effects of photoproduced muons are found to be negligible in the examined ranges of shower sizes and core distances. The fluctuation of the muon density in  $90\text{ m}^2$  is at most 25 % between 200 m and 600 m from the core around  $10^{17}$  eV.

#### 1. Introduction

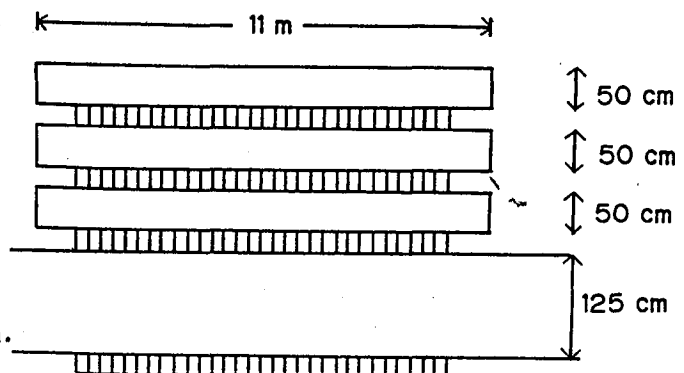
Construction of muon detectors for the giant air shower array starts from 1984 at Akeno. One of the purposes of this experiment is to determine the appropriate absorber thickness. Muons in EAS must be measured under the shielding in order to eliminate electromagnetic components. On the other hand, the thickness of shielding is desired to be as thin as possible from the economical point of view. Another purpose is to examine whether effects of photoproduced muons appear appreciably in giant air showers when we measure such low energy muons.

#### 2. Experiments and Data Analysis

The measurement was done by using a large calorimeter of  $100\text{ m}^2$  area (effective area  $90\text{ m}^2$ ) at the center of Akeno EAS Array (Hara et al. 1979), which consists of four layers of proportional counters under the concrete shielding as is shown in Fig.1. The threshold energies for muons at each layer correspond to 0.25,

0.5, 0.75 and 1.38 GeV respectively. Counters are made of iron square pipes of size  $10\text{ cm} \times 10\text{ cm} \times 500\text{ cm}$  filled with  $\text{P}10$  gas (Hayashida and Kifune 1980). The trigger condition is 7-fold coincidence with more than 4 particles out of 38 scintillation counters in Akeno EAS Array, which are arranged in lattice shape with mutual spacing of 120 m. 18000 showers are analyzed and the conditions for data

Fig.1 The structure of the calorimeter



selection are as follows; shower size larger than  $10^7$ , core distance larger than 50 m from the calorimeter and chi square for the fitting of shower sizes and directions reasonably small. Only vertical showers are examined in this paper except those shown in Fig.4. Present data are compared with those by other nine muon stations of 25 m<sup>2</sup> each, where the thickness of the concrete shielding corresponds to threshold energy 1 GeV .

### 3. Results and Discussions

The lateral distribution of muons of energy more than 1 GeV is given by Greisen's formula (Greisen, 1960)

$$\rho_{\mu}(R) = C(R/R_0)^{-0.75} (1+R/R_0)^{-2.5} \quad \dots (A)$$

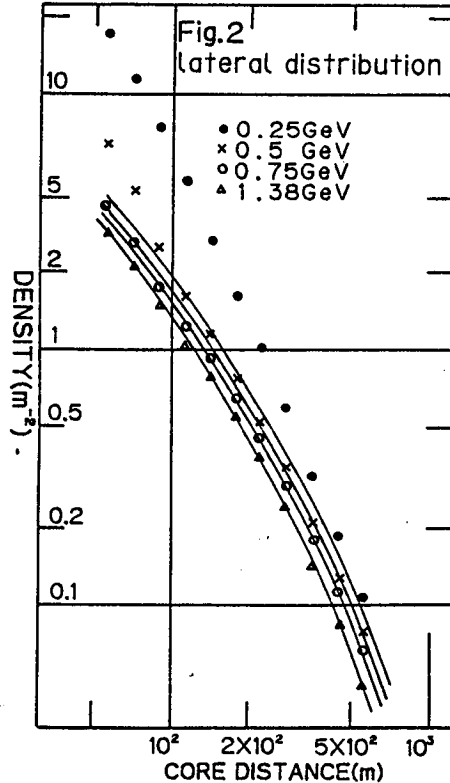
from the data of muon stations in Akeno EAS Array, where R is a core distance, C is a normalization factor depending on sizes and zenith angles, and  $R_0$  is a characteristic distance which varies with zenith angles (Hara et al. 1983). Greisen presents also the lateral distribution as a function of muon energy  $E_{\mu}$  as follows (Greisen 1960)

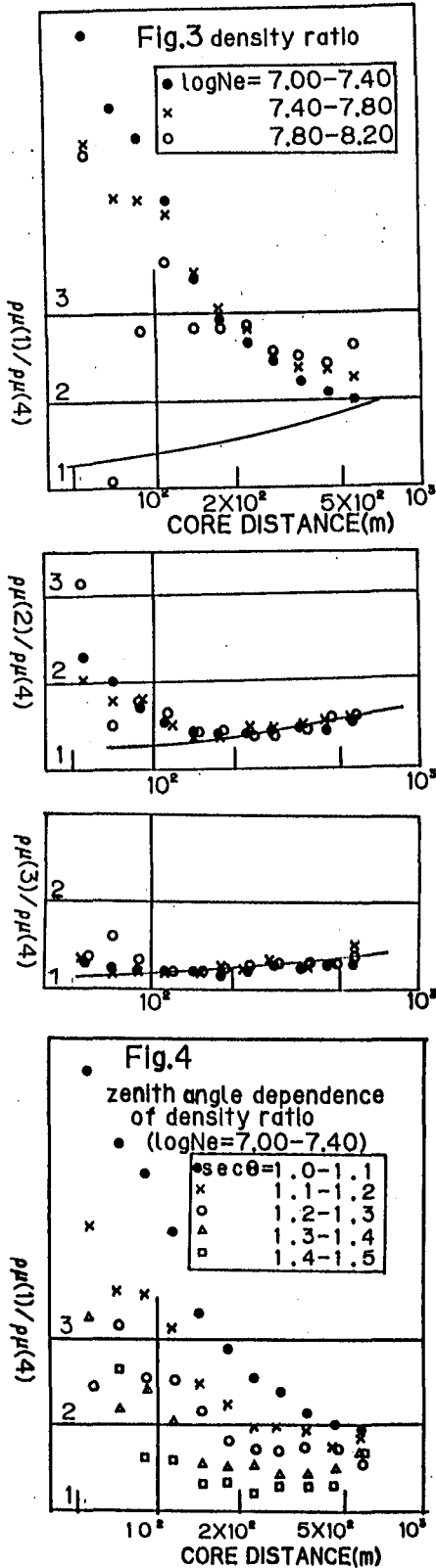
$$\rho_{\mu}( > E_{\mu}, R) = \rho_{\mu}(R) \times (51/(50+E_{\mu})) \times (3/(2+E_{\mu}))^{f(R)} \quad \dots (B)$$

where  $f(R) = 0.14 \times R^{0.37}$ . We use this function as a reference, though the Greisen's formula were derived from the data of lower sizes and larger energy regions of muons than are considered now.

#### (1) Lateral distribution

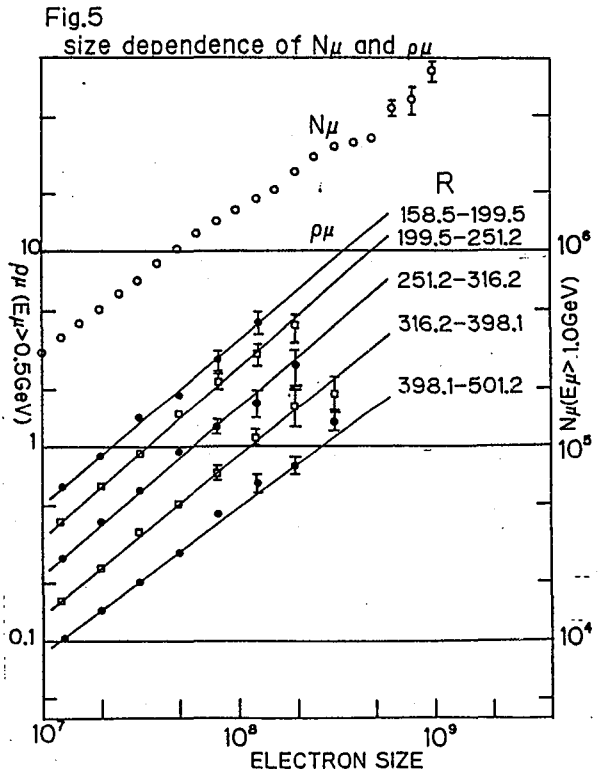
Fig.2 shows the lateral distribution of the density at each layer for vertical showers. Curves are those given by the formula (B) with  $R_0=280$  m. Densities under shieldings equivalent to 0.5, 0.75 and 1.38 GeV at more than 150 m from the core can be fit well to this formula, but those under the shielding equivalent to 0.25 GeV show larger values than this curve. The lateral distribution of the density ratio of each layer to the fourth layer in three shower sizes is shown in Fig.3, where the density of the lowest layer is taken as a reference value. Curves are given by the formula (B). It is suggested from both figures that the concrete shielding equivalent to 0.25 GeV can not prevent the leakage of electromagnetic components at the core distance less than 500 m, and 0.5 GeV less than 150 m also. Fig.4 is the zenith angle dependence of this ratio for the concrete shielding equivalent to 0.25 GeV  $\times \sec\theta$  at equal size. The higher the threshold energy becomes, the less the leakage of electromagnetic components is observed. We decide the thickness of concrete shielding for the observation of muons in giant air showers to be 0.5 GeV equivalence for safety, though the minimum absorber thickness is found to be 0.34 GeV (this is the case for  $\sec\theta = 1.3-1.4$ ) from Fig.4.



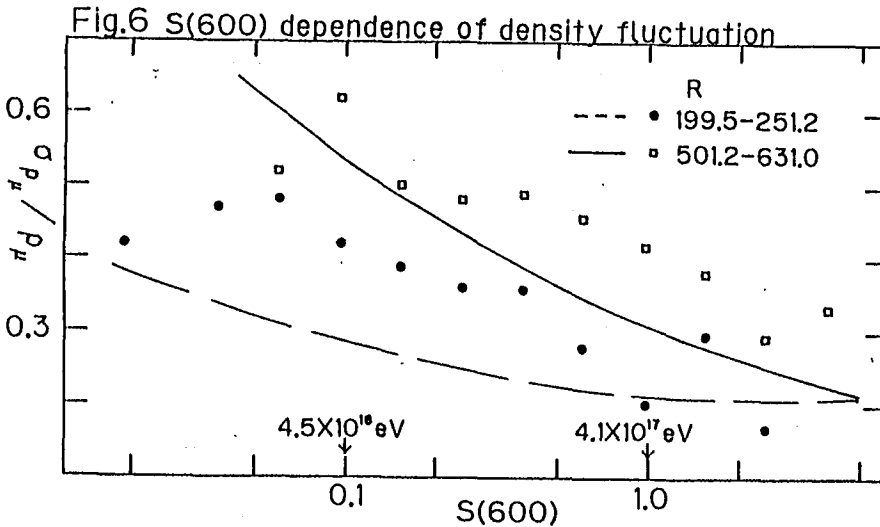


(2) Effects of photoproduced muons

The number of photoproduced muons in EAS is proportional to the primary energy  $E_0$ , while the number of muons in nuclear cascades to  $E_0^a$  ( $a < 1$ ). Therefore, the contribution of photoproduced muons to total muons becomes significant in larger shower sizes. According to the simulation (McComb et al. 1979), if the density of photoproduced muons takes over that from pionization, ' $\alpha$ ' in  $\rho \propto Ne^\alpha$  becomes 1. Fig. 5 shows the relation between the muon density and the shower size, and between the muon size and the shower size. There exists no significant tendency that the power ' $\alpha$ ' becomes larger as the shower size becomes larger. Effects of photoproduced muons may be negligible in the examined ranges of shower sizes and core distances.



## (3) Fluctuation of muons



It is important to know the fluctuation of the muon density in EAS. This value is related to not only the accuracy of muon size determination, but also to the primary mass composition. In Fig.6 are plotted the S(600) dependence of  $\sigma/\rho_\mu$  for two core distance ranges, where  $\rho_\mu$  is the

density of 0.5 GeV muons in  $90 \text{ m}^2$ ,  $\sigma$  is its fluctuation and S(600) is the electron density at 600 m from the core. S(600) is considered to have a good relation to the primary energy  $E_0$  as (Glushkov et al. 1979)

$$E_0 = 4.1 \times 10^{17} (S(600))^{0.96}$$

Curves in Fig.6 are the experimental errors which are derived from the data of Akeno EAS Array (Hara et al. 1981),

$$\sigma/\rho_\mu = (0.668/\rho_\mu^2 + 1.42/\rho_\mu + 0.04)^{1/2}$$

by using the average density in the corresponding S(600) and two core distance bins. Subtracting these experimental errors quadratically and considering the fluctuation of S(600) for the same primary energy, the fluctuation of the muon density is found to be at most 25% irrespective of the core distance examined for the primary energy around  $10^{17}$  eV.

#### Acknowledgements

The authors are indebted to the other members of Akeno group for obtaining and analyzing the data. The data analysis is done by FACOM M380 at the Computer Room, Institute for Nuclear Study, University of Tokyo.

#### References

- Glushkov A.V. et al. 1979, Proc. 16th ICRC(kyoto), 8, 158
- Greisen K. 1960, Ann.Rev.Nucl.Sci., 10, 63
- Hara T. et al. 1979, Proc. 16th ICRC(Kyoto), 8, 135
- Hara T. et al. 1981, Proc. 17th ICRC(Paris), 11, 231
- Hara T. et al. 1983, Proc. 18th ICRC(Bangalore), 6, 122
- Hayashida N. and Kifune T. 1980, NIM, 173, 431
- McComb T.J.L. et al. 1979, Proc. 16th ICRC(kyoto), 9, 126



MUON FLUCTUATION STUDIES OF EAS > 10<sup>17</sup> eV

P. R. BLAKE, M. LUKSYS, W. F. NASH and A. J. SEPHTON  
University of Nottingham, England.

1. Introduction Fluctuation studies need to compare a parameter which is sensitive to longitudinal fluctuations against a parameter which is insensitive. Cascade calculations indicate that the shower size parameter at Haverah Park,  $\rho(500)$ , and the muon density are insensitive while parameters that significantly reflect the longitudinal development of a particular EAS include the muon/water Cerenkov response ratio and the muon arrival time dispersion. This paper presents conclusions based on muon fluctuation studies of EAS measured between 1976 and 1981 at Haverah Park.

2. Description of Muon Detectors Three 10 m<sup>2</sup> shielded scintillators situated at 0, 150 m and 250 m from the centre of the Haverah Park array. Due to practical considerations the detectors had slightly different absorber thicknesses leading to calculated vertical muon thresholds of 317, 431 and 488 MeV respectively. Two of the muon detectors (those at 0 m and 150 m) had immediately neighbouring large area water Cerenkov detectors so that a local response ratio between the two detectors could be directly measured. The recording of the three detectors was triggered from the water Cerenkov 500 m array by the arrival of EAS with primary energies  $\geq 10^{17}$  eV.

3. Fluctuations in  $\mu/c$  Ratio The ratio of the density response of the muon detectors to the density of the water Cerenkov detectors (symbolised by  $\mu/c$ ) was used to study fluctuations between EAS. For a data set consisting of those EAS with two direct measurements of  $\mu/c$  an analysis of variance (AOV) was carried out in order to extract the between-EAS variance ( $\sigma_B^2$ ) from the total measured variance ( $\sigma^2$ ).

R(m)	sec $\theta$	Number of EAS	$\sigma_B/(\mu/c)$	F	P
120	1.0-1.1	61	22.4% ( $\pm 10$ )	2.44	<0.01
→220	1.1-1.2	36	19.7% ( $\pm 12$ )	2.57	<0.01
	1.2-1.3	28	24.7% ( $\pm 20$ )	2.23	0.01 < p < 0.025
220	1.0-1.1	83	0.0% ( $-0 +15$ )	0.74	>0.1
→320	1.1-1.2	52	19.9% ( $\pm 19$ )	1.46	0.05 < p < 0.1
	1.2-1.3	37	23.4% ( $\pm 12$ )	3.15	<0.01
320	1.0-1.1	54	0.0% ( $-0 +27$ )	0.94	>0.1
→420	1.1-1.2	36	1.1% ( $-1 +40$ )	1.00	>0.1
	1.2-1.3	23	4.4% ( $-4 +35$ )	1.02	>0.1

Table 1 Between-EAS fluctuations in  $\mu/c$ .

Because the different energy thresholds lead to different  $\mu/c$  ratios the AOV was carried out using standard residuals defined by  $S.R. = [(\mu/c) - (\bar{\mu/c})]/\sigma$ , where  $\mu/c$  is the normalised measured ratio,  $(\bar{\mu/c})$  is the average value and  $\sigma$  the standard deviation for the interval under consideration. The results of the AOV are presented in Table 1.

Also included in the table are the F ratio (mean square deviation between EAS to mean square deviation within EAS) and p, the probability that random variations in the data could account for the quoted between-EAS fluctuations. The results indicate that at core distances  $\sim 200$  m the magnitude of the between-EAS fluctuations is  $\sim 20\%$ . Such a result would be consistent with at least a 50% proton primary flux at  $\sim 10^{17}$  eV [eg. Marden et al, 1971].

4. Fluctuations in Muon Risetime The muon arrival timespread at each of the  $10 \text{ m}^2$  muon detectors is characterised by the time interval between 10% and 70% of the full pulse amplitude ( $T_{70}$ ). The instrumental response was found to be  $T_{70} = 32 \text{ ns}$ . For a specific R and  $\theta$ , fluctuations in  $T_{70}$  occur arising from fluctuations in the longitudinal development. AOV techniques allow between-shower fluctuations in  $T_{70}$  to be separated from within EAS fluctuations. Such analysis leads to a value of  $\sigma_B/T_{70} = 10.7(\pm 2) \text{ ns}/63 \text{ ns} = 17\%$  at 325 m, for  $\sec\theta = 1.1$ .

Detailed cascade model calculations relating to  $T_{70}$  fluctuations remain to be carried out. As a consequence the significance of the  $T_{70}$  fluctuations is treated in Section 7 in terms of fluctuations in the height of electromagnetic maximum

5. Correlations of  $\mu/c$  and  $\eta_C$  The water Cerenkov response lateral distribution function used by the University of Leeds group to analyse the EAS is of the form:

$$\rho_C = k R^{-(\eta_C + R/4000)}$$

It has been found that  $\eta_C$  is sensitive to EAS longitudinal development. Thus a strong correlation is expected between fluctuations in  $\mu/c$  and  $\eta_C$ . Table 2 gives the derived correlation coefficients for the data sets from two muon detectors and also the significance of the correlation.

Detector	sec $\theta$	N	r	P
A	1.0-1.1	190	0.449	<0.001
	1.1-1.2	81	0.342	<0.01
	1.2-1.3	40	0.420	<0.01
	1.3-1.4	20	0.598	<0.001
C	1.0-1.1	117	0.398	<0.001
	1.1-1.2	52	0.595	<0.001
	1.2-1.3	34	0.515	<0.01
	1.3-1.4	10	0.618	<0.1

Table 2 Correlation between fluctuation in  $\mu/c$  and fluctuation in  $\eta_C$ . r = correlation coefficient.

The strong correlation confirms that  $\mu/c$  and  $\eta_0$  are sensitive parameters to EAS development.

6. Correlation of  $\mu/c$  and  $T_{70}$  A small positive correlation is found between the values of  $SR(\mu/c)$  and  $SR(T_{70})$  at all zenith angles (see Table 3).

Detector	$\sec\theta$	No of EAS	r	P
A = $\mu/c$	1.0-1.1	20	0.032	>0.1
B = $T_{70}$	1.1-1.2	15	-0.306	>0.1
	1.2-1.3	4	0.541	>0.1
	1.3-1.4	7	-0.405	>0.1
A = $\mu/c$	1.0-1.1	32	0.016	>0.1
C = $T_{70}$	1.1-1.2	19	0.278	>0.1
	1.2-1.3	25	0.172	>0.1
	1.3-1.4	10	0.438	>0.1
C = $\mu/c$	1.0-1.1	44	0.203	>0.1
A = $T_{70}$	1.1-1.2	31	0.006	>0.1
	1.2-1.3	25	0.245	>0.1
	1.3-1.4	12	0.323	>0.1
C = $\mu/c$	1.0-1.1	15	0.122	>0.1
B = $T_{70}$	1.1-1.2	16	0.013	>0.1
	1.2-1.3	12	-0.197	>0.1
	1.3-1.4	9	0.382	>0.1

Table 3 Correlation between  $\mu/c$  and  $T_{70}$  fluctuations

Because of the different core distance dependences the two correlating parameters were measured simultaneously from two different muon detectors. The significance of the correlation coefficients in Table 3 is statistically limited due to the small amount of data available for the analysis.

7. Fluctuations in Depth of Electromagnetic Maximum Fluctuations in the depth of maximum ( $X_{max}$ ) are closely related to the mass spectrum of the primary particles. It is not possible to measure  $X_{max}$  directly at Haverah Park. However the fluctuation in  $X_{max}$  can be determined indirectly from the measurement of some shower parameters, eg.  $\mu/c$  which is sensitive to  $X_{max}$ . Assuming

$$\Delta X_{max} = \frac{X_{max} (\mu/c) - (\overline{\mu/c})}{X \quad \partial(\mu/c)/\partial X}$$

and using the AOV carried out on the  $\mu/c$  fluctuations observed at two detectors (for core distances  $120 \text{ m} < R < 220 \text{ m}$  and  $\sec\theta < 1.3$ ) yields:-

N	$\sigma_B(\text{g cm}^{-2})$	F	p
125	73.2	2.39	<0.01

The value of  $\sigma_B$  is the between-shower fluctuation (in  $\text{g cm}^{-2}$ ) obtained from the AOV and gives an initial estimate of the fluctuation in  $X_{\text{max}}$ . The values of F and p show that highly significant between-EAS fluctuations are present in the data. Removing the spurious contribution to  $\sigma_B$  from the pressure correction, the corrected fluctuations in depth of maximum,  $\sigma(X_{\text{max}})$  for EAS in the energy range  $10^{17} - 10^{18}$  eV is given by  $\sigma(X_{\text{max}}) = (71 \pm 12) \text{ g cm}^{-2}$ . Using a similar technique the fluctuations in  $T_{70}$  yield  $\sigma(X_{\text{max}}) = (69 \pm 28) \text{ g cm}^{-2}$ .

Measurement of  $\sigma(X_{\text{max}})$  at energies above  $10^{17}$  eV have been reported by other groups from a variety of studies. The values obtained above are in good agreement with these other measurements.

8. Conclusions It was stated in section 3 that the  $\mu/c$  fluctuations are consistent with at least a 50% proton primary flux at  $\sim 10^{17}$  eV. This conclusion is supported by the  $\sigma(X_{\text{max}})$  results. None of the different model predictions available give such a large  $\sigma(X_{\text{max}})$  value based on a pure iron primary beam [eg. Gaisser et al (1982), Chantler et al (1983)]. Since the value of  $\sigma(X_{\text{max}})$  measured in the present work,  $71 (\pm 12) \text{ g cm}^{-2}$ , is  $\sim 3.5 \sigma$  above even the largest calculated estimate for iron nuclei it is extremely unlikely that cosmic rays in the energy range  $10^{17} - 10^{18}$  eV are dominantly iron nuclei. This measurement of  $\sigma(X_{\text{max}})$  is however consistent with a pure proton mass composition on the basis of the calculations of Chantler et al (1983) [ $\sigma(X_{\text{max}}) = 60 \text{ g cm}^{-2}$ ].

Large fluctuations in  $X_{\text{max}}$  can arise if several masses are present in the primary beam. For a mixed composition in which P:He:(Mg:CNO):Fe is 50:19:19:12, it is found that  $\sigma(X_{\text{max}}) = 57 \text{ g cm}^{-2}$  based on Gaisser et al (1982).

In conclusion the fluctuation in  $X_{\text{max}}$  seen at energies in the range  $10^{17} - 10^{18}$  eV can be accounted for by a mass composition in which  $> 50\%$  of the primaries are protons. Primaries at these energies cannot be dominantly iron.

#### REFERENCES

- Chantler, M. P., Craig, M. A. B., McComb, T. J. L., Orford, K. J., Turver, K. E. and Walley, G. M. J. Phys. G 9 L27 (1983).
- Gaisser, T. K., Stanev, T., Freier, P. and Waddington, C. J. Phys. Rev. D, 25, 2341 (1982).
- Marsden, D. J., Hillas, A. M., Hollows, J. D. and Hunter, H. W. 12th Int. Cos. Ray Conf., Hobart p.1013 (1971).

AVERAGE FEATURES OF THE MUON COMPONENT OF EAS  $\geq 10^{17}$ eV

P. R. BLAKE, M. LUKSYS, W. F. NASH and A. J. SEPHTON  
University of Nottingham, England.

1. Method Three 10 m<sup>2</sup> liquid scintillators were situated at approximately 0 m, 150 m and 250 m from the centre of the Haverah Park array. The detectors were shielded by lead/barytes giving muon detection thresholds of 317 MeV, 431 MeV and 488 MeV respectively. During part of the operational period the 431 MeV threshold was lowered to 313 MeV for comparison purposes. For risetime measurement fast phototubes were used and the 10% to 70% amplitude time interval was parameterised by T<sub>70</sub>.

2. The Muon Density Lateral Distribution A muon lateral density distribution of the form  $\rho_{\mu}(R, \theta) = k[\rho(500)]^{0.94} 1/R(1 + R/490)^{-\eta}$  has been fitted to the data for 120 m < R < 600 m and 0.27 <  $\rho(500)$  < 2.55. The shower 'size' parameter  $\rho(500)$  is the water Cerenkov response at 500 m from the core of the EAS and is related to the primary energy (eg Hillas model A gives  $E_p = 3.87 \times 10^{17} [\rho(500)]^{1.018}$ ). Table 1 shows the best fit values of k and  $\eta$  to the data for near vertical EAS. The results show general consistency.

SEC $\theta$ RANGE	DETECTOR			UNCERTAINTY		
	THRESHOLD MeV	NO. OF EAS	BEST FIT k	UNCERTAINTY IN k	BEST FIT $\eta$	UNCERTAINTY IN $\eta$
1.0-1.1	313	320	2060	$\pm 150$	2.77	$\pm 0.15$
	317	1056	2000	$\pm 90$	2.69	$\pm 0.09$
	431	925	1980	$\pm 80$	2.96	$\pm 0.09$
	488	803	1890	$\pm 90$	3.11	$\pm 0.10$

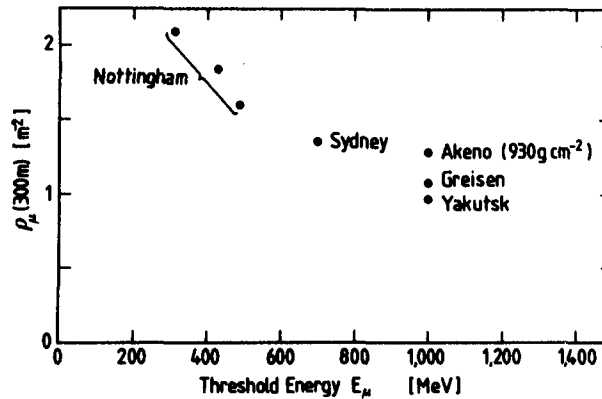
Table 1 Best fit values of k and  $\eta$  in the muon density lateral distribution.

Table 2 compares the values of muon density derived at 100 m core distance intervals from the Nottingham detectors for  $\rho(500) = 1.15$ . Also labelled are the data from other arrays where the intercalibration has been carried out on the basis of flux rates [Blake et al (1975) and (1981)]. The Akeno data is taken from Nagano et al (1984).

CORE DIST (m)	SYDNEY							
	NOTTM SCINT S-L	NOTTM SCINT S-L	NOTTM SCINT S-L	NOTTM SCINT S-L	SPARK CHAMB S-L	GREISEN (1960) S-L	YAKUTSK SCINT S-L	AKENO PROP 930gcm <sup>-2</sup> S-L
	313MeV	317MeV	431MeV	488MeV	700MeV	1GeV	1GeV	1GeV
100	14.00	13.80	13.00	12.10	-	6.60	6.90	8.50
200	4.55	4.54	4.10	3.72	2.86	2.29	2.20	2.82
300	2.09	2.10	1.83	1.63	1.35	1.09	0.96	1.28
400	1.12	1.14	0.96	0.84	0.72	0.60	0.52	0.70
500	0.67	0.69	0.56	0.48	0.42	0.37	0.30	0.42
600	0.43	0.44	0.35	0.30	0.26	0.24	0.20	0.27

**Table 2** Comparison of muon density lateral distribution (Muons  $m^{-2}$  for  $\theta < 25^\circ$  and  $E_p \sim 3.87 \times 10^{17}$  eV). [S-L = sea level]

Allowing for the different thresholds and altitudes the results show reasonably consistent agreement. Figure 1 plots the muon density data at 300 m as a function of threshold energy.



**Figure 1** Muon density at 300 m as function of threshold energy.

The errors on individual points are estimated as  $\sim 10\%$  and arise mainly from the intercalibration procedure.

Most nuclear cascade models yield distributions in agreement with the experimentally derived lateral distributions as regards slope.

Clearly absolute muon density predictions depend on both the primary mass composition assumed as well as the details of the cascade model.

**3. Muon-water Cerenkov Ratio** Figure 2 displays the muon-water Cerenkov density ratio as a function of  $R$  and  $\theta$  for  $\rho(500) = 1.15$  and  $E_\mu = 317$  MeV. Again, on the whole, models predict the observed shape of the observed lateral distribution with reasonable closeness. However whilst Hillas (1971) model A fits the absolute value of the ratio well with a 100% proton primary beam; the Gaisser et al (1978) predictions require  $A \sim 56$  to be compatible.

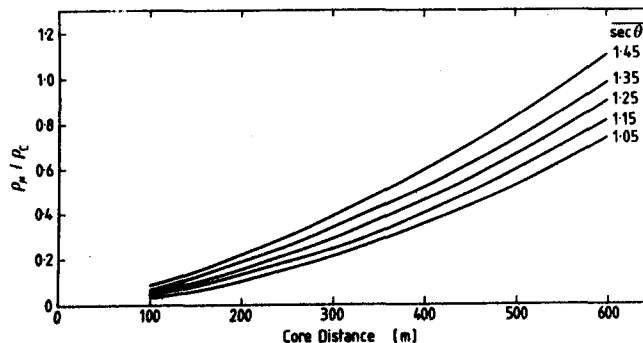


**Figure 2** Muon-water Cerenkov density ratio ( $\rho_\mu / \rho_c$ ) as a function of core distance and  $\sec\theta$ .

4. The Average Time Spread ( $\bar{T}_0$ ). Fast phototubes and electronics enable the time spread of the muons ( $T_{70} = 10\%$  to  $70\%$  full amplitude) to be determined including an instrumental response  $T_{70}=32$  ns.

Table 3 lists the derived values for  $T_{70}$  as a function of R for three of the threshold energies.

R(m)	313 MeV	431 MeV	488 MeV
200	57.9 ns	54.2 ns	53.4 ns
250	64.4 ns	59.2 ns	59.4 ns
300	70.9 ns	64.2 ns	65.4 ns
350	77.4 ns	69.2 ns	71.4 ns
400	83.9 ns	74.2 ns	77.4 ns
450	90.4 ns	79.2 ns	83.4 ns
500	96.9 ns	84.2 ns	89.4 ns

Table 3 Derived values of  $T_{70}$  for  $\rho(500) = 1$  and  $\sec\theta = 1$ .

Figures 3 and 4 compare the experimentally derived data for  $T_{70}$  (at 431 MeV threshold) with the cascade calculations of McComb and Turver (1981). Clearly the experimental data are faster than the predictions even assuming a 100% iron primary flux.

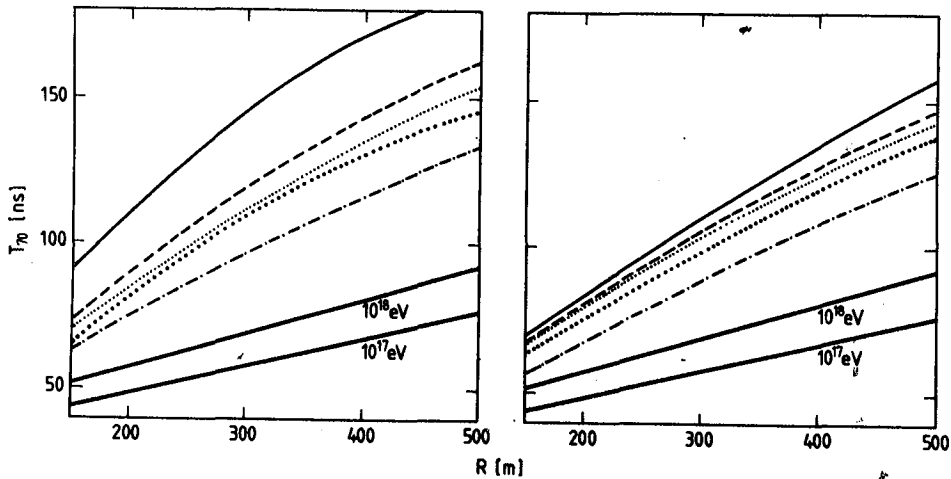


Figure 3 & 4 Comparison of predictions and experimental measurements of  $T_{70}$  as a function of R.  
 ————— Experimental data best fits. McComb and Turver (1981) simulations with  
 ————— scaling,  $\sigma = \text{const}$       - - - - - Landau,  $E^{1/4}$ ,  $\sigma = \text{const}$   
 ..... Landau,  $E^{1/3}$ ,  $\sigma = \text{const}$       ..... Scaling,  $\sigma = \ln^2 s$   
 - - - - - Landau,  $E^{1/3}$ ,  $\sigma = \ln^2 s$       Fig. 3 Proton      Fig. 4 Iron primaries

5. Elongation Length Both of the two parameters ( $\mu/c$  and  $T_{70}$ ) can be used to determine the 'elongation rate' of the EAS. The technique used has been described elsewhere (Blake et al, 1983). Calculations based on the data presented in this paper lead to an

elongation rate =  $66(\pm 10) \text{ g cm}^{-2} \text{ decade}^{-1}$  from  $(\mu/c)$  and  $73(\pm 23) \text{ g cm}^{-2} \text{ decade}^{-1}$  from  $T_{70}$ . These results are in substantial agreement with other experimental data in the same energy range.

6. Conclusions The average lateral distribution of both the density and time spread of muons in EAS have been measured. The density measurements fit in well with those from other arrays and thus serve successfully for cross-checking of array calibrations.

The fast average risetime of the muons indicates early EAS development and little contribution from photoproduced muons at these primary energies.

Both the muon density and muon time spread are sensitive to small changes in threshold detection energy (both ~6% per 100 MeV at ~400 MeV threshold). Both measurements yield 'elongation rates' ( $\sim 70 \text{ g cm}^{-2} \text{ decade}^{-1}$ ) in close agreement with other work.

These results support the general conclusion that the primary beam contains a significant proportion of light elements at these energies.

#### REFERENCES

- BLAKE, P. R., NASH, W. F., PRESCOTT, I. C. and STRUTT, R. B., 14th Int. Cosmic Ray Conf. Munich, 8, (1975).
- BLAKE, P. R., NASH, W. F., O'CONNELL, B., and STRUTT, R. B., 17th Int. Cosmic Ray Conf. Paris, 6, 8, (1981).
- GAISSER, T. K., PROTHEROE, R. J., TURVER, K. E. and McCOMB, T. J. L. Rev. Mod. Phys. 50 no.4 859 (1978).
- HILLAS et al. Proc. Int. Cos. Ray Conf., Hobart, 3, 1007 (1971).
- McCOMB, T. J. L. and TURVER, K. E., private communication (1981).
- NAGANO, M. et al. J. Phys. G 10, 1295 (1984).



Measurement of Shower Electrons and Muons  
using a Small Air Shower Array

S.K. Chan and L.K. Ng  
Physics Department, University of Hong Kong  
Hong Kong

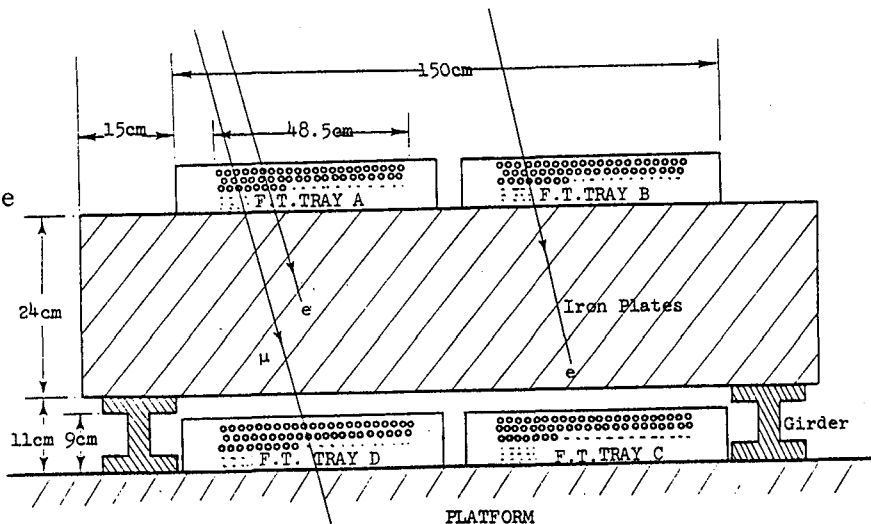
Abstract

A small air shower array has been used to measure the size spectrum of air showers at sea level in the size range  $6.10^3 - 10^6$ . The result fitted with the power law gives an index  $-2.79 \pm 0.11$  for the differential spectrum. Lateral distribution of electrons fitted with the well known NKG function results in an age parameter  $s = 1.35$  for core distances less than  $30\text{m}$  and  $s = 0.8$  for longer core distances. Lateral distribution of muons follows the general shape of Greisen's relation but is much higher in intensity. Muon and electron densities at the same observation point are also compared.

1. Introduction. Cosmic rays of energy around  $10^{14}\text{eV}$  are of particular interest with the present day availability of accelerator data. It was with this in mind that the present experiment was constructed.

The air shower array used has been described in a previous experiment (Chan et al 1979) and the accuracy of core location is typically  $\pm 6\text{m}$ . The present addition at the centre of the array is a flash tube assembly shown in figure 1. The upper trays of flash tubes (each  $1\text{m} \times 6.5\text{mm}$  diameter) are for measuring the total particle density, while the lower trays shielded by iron plates (threshold  $0.3\text{GeV}$ ) are for determining the muon density simultaneously. The maximum observable density is  $30\text{m}^{-2}$ .

Fig. 1  
Flash tube  
assembly



However, as the result below reveals, most air showers observed at sea level may be just old showers with primary energies greater than  $10^{14}$  eV, which are above the accelerator energy range. Nevertheless, it is still worthwhile to report on the measured results obtained.

2. The shower size spectra. The differential and integral size spectra in figures 2 and 3 respectively were computed from 6798 measured events taken in the period July - December, 1981. Fitting each spectrum with a power law gave agreeable slope indices,  $-2.79 \pm 0.11$  for the differential and  $-1.83 \pm 0.1$  for the integral. The latter is compared with other workers' results in figure 3.

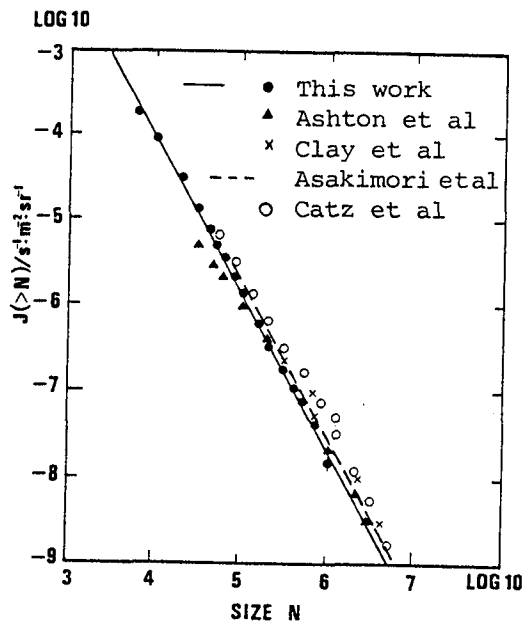
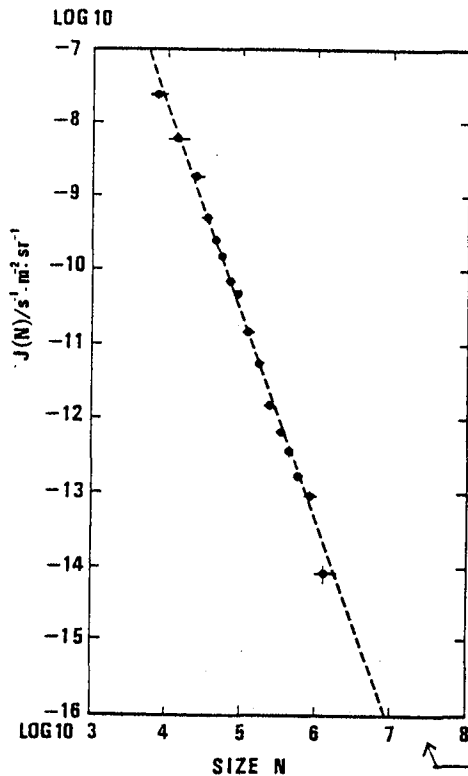


Fig.3 Integral size spectrum.

Fig.2 Differential size spectrum

3. Lateral distributions of electrons and muons. Results in the figures 4 and 5 are based on particle tracks observed from the flash tube assembly. Difference in track intensity between the upper and lower flash tube trays provides the electron density at a known location and known size of a shower. For showers in the size range  $10^4 - 4.1 \cdot 10^4$ , the results can be fitted with the well known NKG function with a single age parameter  $s = 1.3$ . Those in the size range  $4.1 \cdot 10^4 - 2.1 \cdot 10^6$  are more complicated, giving a fairly large age parameter ( $s \sim 1.35$ ) at smaller core distances, but a very small parameter ( $s \sim 0.8$ ) at larger core distances. A straight forward interpretation is that those falling close to our detection assembly were in fact old showers well

passed their point of maximum development, and those further away were developing young showers.

The data presented in figure 6 for the muon lateral distribution are based on the track count in the lower flash tube trays. Local bursts in the iron absorber were rejected since they were mostly hadron events. The distribution follows the general shape of the classical relation (Greisen 1960), but the intensity is about three times as large.

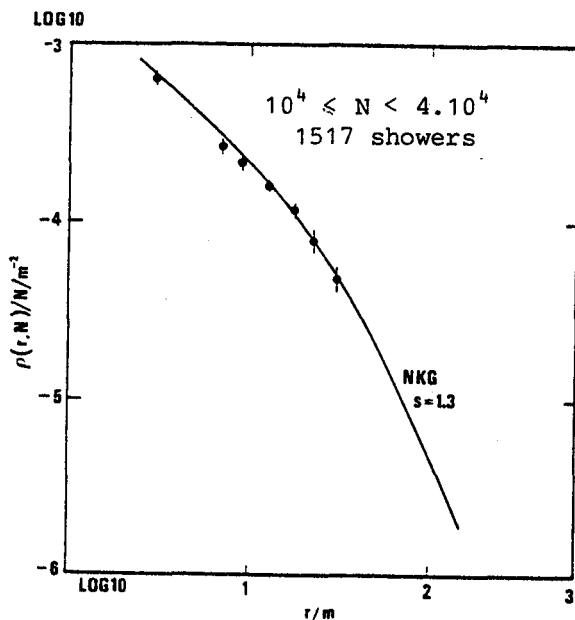


Fig. 4  
Lateral distribution  
of electrons.

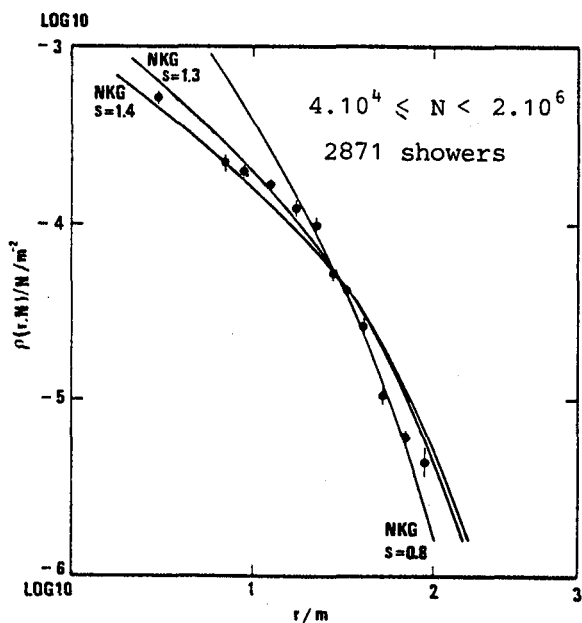


Fig. 5  
Lateral distribution  
of electrons.

4. Density ratios of muons to electrons. Figure 7 presents the density relation between shower muons and electrons at the same location from each core. The pioneer results due to Cocconi (Hayakawa 1969), and rough estimates based on Greisen's relation and the NKG function with mean shower size  $2.23 \cdot 10^4$  are also shown for comparison. Again our ratios are expected to be much higher.

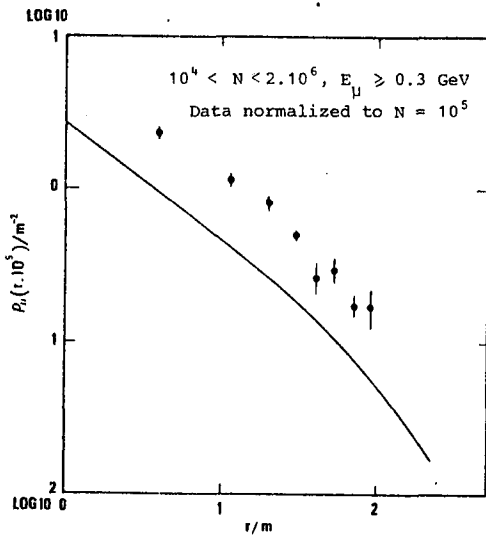


Fig.6 Lateral distribution of muons.

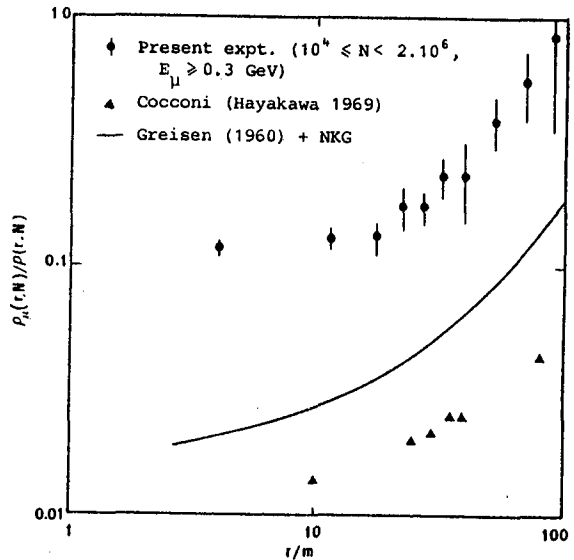


Fig.7 Density ratio of muons to electrons.

5. Discussions. If the observed shower events are either old declining showers ( $s \sim 1.3$ ) or very young developing showers ( $s \sim 0.8$ ), the smallness of the size is only phenomenological and may not have been initiated by primaries of small energies ( $\sim 10^{14}$  eV). High intensity of muon component in the showers supports that they were initiated by higher energy primaries.

Alternatively, if the richness in muon content is not due to the phenomenological factor, then this result would suggest that the primary cosmic rays at the energy range concerned are dominated by heavier components ( $A \sim 15$ ) and that p-p interaction at this energy range should possess multiplicity which rises with energy at least as fast as  $n_s \propto E^4$ .

#### References.

- Ashton F et al, Proc. 16th ICRC (Kyoto) 13 (1979) 243.  
 Catz P et al, Proc. 14th ICRC (Munich) 12 (1975) 4329.  
 Chan S K et al, Proc. 16th ICRC (Kyoto) 11 (1979) 149.  
 Clay R W et al, Aust. J. Phys. 35 (1982) 59.  
 Greisen K, Ann. Rev. Nucl. Sc. 10 (1960) 63.  
 Hayakawa S, Cosmic Ray Physics N.Y. Wiley-Interscience (1969).

THE LONGITUDINAL DEVELOPMENT OF MUONS IN  
COSMIC RAY AIR SHOWERS AT ENERGIES  $10^{15}$ - $10^{17}$  eV

T. Cheung and P.K. MacKeown  
Department of Physics  
University of Hong Kong  
HONG KONG

ABSTRACT

The relationship between longitudinal development of muons and conventional equi-intensity cuts is carefully investigated. The development of muons in EAS has been calculated using simulation with a scaling violation model at the highest energies and mixed primary composition. Profiles of equi-intensity cuts expected at observation altitudes of 550, 690 and 930  $\text{gcm}^{-2}$  can fit the observed data very well.

1. Introduction In recent years estimates of the longitudinal development of muons in EAS have been presented by several groups, based on equi-intensity cuts of muon size spectra following the method introduced 20 years ago by the BASJE group [1]. As is well known the relationship between such equi-intensity cuts and the profile of longitudinal development of the muons is not as straightforward as in the case of the electromagnetic component, and is particular to the altitude of observation. This arises because the muon longitudinal development itself depends on the zenith angle and the nature of the primary particle, moreover observations are made in general above a muon threshold energy which is zenith angle dependent. Some reported calculations when compared with measurements appear to show significant discrepancies [2],[3]. We report here calculations of equi-intensity curves, based on simulated showers, for different fractions of Fe nuclei in an otherwise pure proton beam using a model for hadronic interactions consistent with the degree of scaling violation discussed in [4].

2. Model Used in the Simulations A model for p-p collisions was adopted which incorporates scaling violation for interactions of the leading particle at  $E > 2 \cdot 10^{13}$  eV to the extent proposed in [4], with radial scaling assumed for all other interactions. Above  $10^{11}$  eV the cross-section for hadron air-nucleus interactions was assumed to rise as  $\sigma^{\text{inel.}} = \sigma_0(1+a\lambda n^2 E)$ , with values of the interaction lengths below this energy given by  $\lambda_{\text{p-air}} = 90 \text{ gcm}^{-2}$  and  $\lambda_{\pi\text{-air}} = \lambda_{\text{K-air}} = 120 \text{ gcm}^{-2}$ . For heavy nuclei incident we assumed  $\sigma_{\text{A-air}}^{\text{inel.}} = \pi r_0^2 (A^{1/3} + A_{\text{air}}^{1/3} - \delta)^2$ . The smaller elasticity [5] and larger multiplicity [6] reported for p-air nucleus collision was allowed for by taking  $\eta_{\text{p-air}} = 0.31$  and  $\langle m_{\text{p-air}} \rangle = 1.58 \langle m_{\text{pp}} \rangle$ . Although these additional particles arising from a nuclear target are in the central region and contribute little to the shower size they make a noticeable contribution to the muon component at low energies. A  $\Gamma$  distribution was taken for the transverse momentum, whose mean,  $\langle p_t \rangle$ , was assumed to vary with the density of particles in rapidity space, consistent with recent accelerator data [7].

Three dimensional Monte Carlo simulations were made for proton and Fe nucleus primaries at different energies, at the vertical and at zenith angles of  $30^\circ$ ,  $40^\circ$ ,  $50^\circ$  and  $60^\circ$ . In fig.1 we show the average

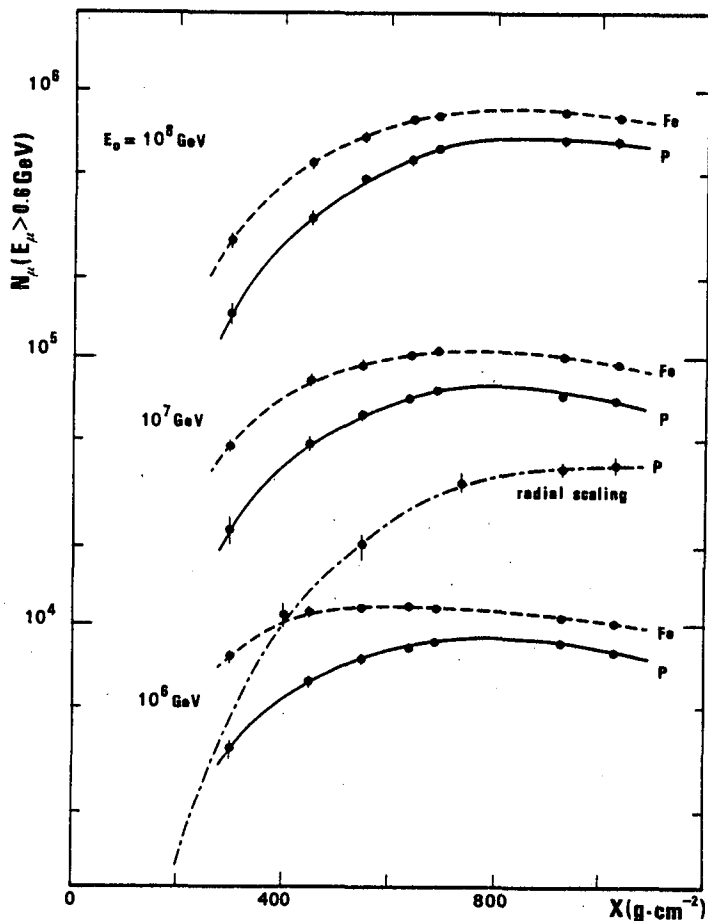


Fig.1 Expected muon longitudinal development at fixed primary energies initiated by protons (solid curves) and iron (dashed curves). The dot-dashed curve is for radial scaling model.

vertical longitudinal development of muons,  $N_{\mu}(E_0, \theta=0, x, \epsilon > 0.6 \text{ GeV})$  at fixed energies, the case for protons where radial scaling is assumed at all energies is also shown for comparison;  $\epsilon$  here is the muon threshold energy. These curves are generally similar to the calculations reported in [3].

3. Calculation of Equi-intensity Cuts To replicate the method used to derive equi-intensity cuts in the experiments would require the derivation of muon size spectra at different depths and zenith angles arising from particles selected from a primary spectrum of given slope and composition. This would involve an inordinate amount of computation, instead an approximate method is used. Because the muon decay probability depends on zenith angle, vertical longitudinal profiles cannot be used for constructing equi-intensity curves for comparison with experiment, unlike the case for the electron component. Longitudinal developments at different zenith angles at each depth must be used, in addition, as already mentioned, the relevant muon threshold energy must, in general, be taken as  $\epsilon_0 \text{Sec}\theta$  where  $\epsilon_0$  is the threshold for vertical muons. At a vertical depth  $x_0$ , when there is only one primary species present the experimental equi-intensity cuts correspond to  $N_{\mu}(E_0, \theta, x = x_0 \text{Sec}\theta, \epsilon > \epsilon_0 \text{Sec}\theta)$  — assuming a unique relationship between

the energy of the primary  $E_0$  and muon size at  $\theta$ ,  $J(N_{\mu}, x) = J(E_0(N_{\mu}, x))$  (fluctuations may be allowed for by considering instead root mean square sizes [8]). If we consider a primary beam containing two species, protons and Fe nuclei say, we have

$$J(N_{\mu}, x) = J_p(E_0^{(p)}(N_{\mu}, x)) + J_{Fe}(E_0^{(Fe)}(N_{\mu}, x)).$$

If the primary spectrum  $J(E_0) = AE_0^{-\gamma}$  is assumed to contain protons, with a constant fraction  $k$ , and Fe nuclei only an equi-intensity curve is defined by

$$AE_0^{(p)-\gamma} [k + (1-k)(E_0^{(p)}/E_0^{(Fe)})^{\gamma}] = J_{\mu}, \text{ a constant} \dots \dots \dots (1)$$

Since the range of primary energies of one species contributing to any one equi-intensity curve will not be very great we approximate  $N_{\mu}^{(p)}(E_0, x) = E_0^{\omega} g_p(x)$ ,  $N_{\mu}^{(Fe)}(E_0, x) = E_0^{\omega} g_{Fe}(x)$ , where  $\omega$  may depend on depth or zenith angle. Defining  $\Lambda(x) = (g_p(x)/g_{Fe}(x))^{1/\omega}$  and using (1) we may write  $N_{\mu}(x, J_{\mu}) = E_0^{\omega} g_p(x)$ , where  $E_0^{\omega} = E_0^{(p)}(N_{\mu}, x) [k + (1-k)\Lambda^{-\gamma}(x)]^{1/\gamma}$ .  $E_0^{(p)}(N_{\mu}, x) = (A/J_{\mu})^{1/\gamma}$ . Thus when  $k$  is not 0 or 1 equi-intensity curves' should be constructed from the simulated longitudinal developments, not at a fixed  $E_0$  but at values of  $E_0$  which depend on the depth.

4. Results Using the profiles simulated at different zenith angles values of the function  $\Lambda(x)$  could be obtained. Taking  $A = 2.5 \times 10^8$ ,

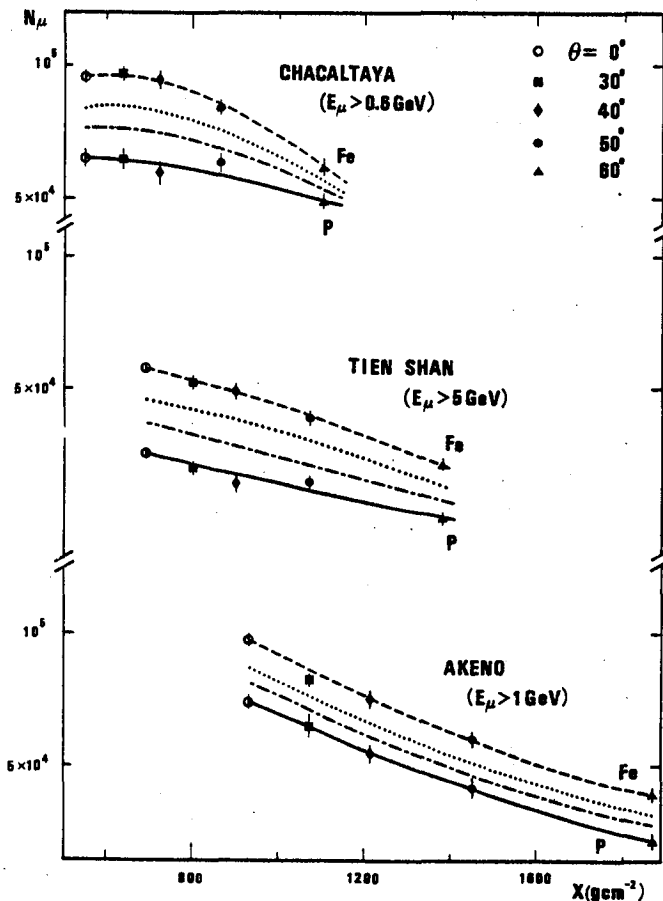


Fig.2 Expected muon longitudinal development for an integral intensity  $J = 2.5 \times 10^{-8} \text{m}^{-2} \text{s}^{-1} \text{sr}^{-1}$  at Chacaltaya, Tien Shan and Akeno. The dot and dot-dashed curves correspond to 50% and 25% of iron in primary cosmic ray.

$\gamma = 2$  [8], expected equi-intensity curves for  $J_{\mu} = 2.5 \cdot 10^{-8} \text{ m}^{-2} \text{ s}^{-1} \text{ sr}^{-1}$  at Chacaltaya, Tien Shan and Akeno have been calculated and are shown in fig.2, where a significant difference from the profiles at constant energy can be observed. Curves for 75%p, 25%Fe, normalised in each case to give a best fit to the data, are compared to experimental data from these experiments in fig.3. The relevance of these curves to the primary composition is noted in another paper (OG 5.2-12) at this conference.

Acknowledgments We are grateful to Director of Computer Services, H.K. University Centre of Computer Studies and Applications for the provision of computing facilities.

#### References

[1] Bradt H., Clark, G., La Pointe, M., Domingo, V., Escobar, I., Kamata, K., Murakami, K., Suga, K., and Koyoda, Y., (1965), Proc. 9th Int. Conf. Cosmic Rays, London, 2, 715-717.

[2] Aguirre, C. et al., (1979), J. Phys. G: Nucl. Phys. 5, 151-157.

[3] Honda, M. et al., (1983), 18th Int. Conf. Cosmic Rays, Bangalore, Conference Papers, 11, 350-353.

[4] Wdowczyk, J. and Wolfendale, A.W., (1984), J. Phys. G: Nucl. Phys. 10, 257-272.

[5] Jones, L.W., (1983), 18th Int. Conf. Cosmic Rays, Bangalore, Conference Papers, 5, 17-20.

[6] Tasaka, S. et al., (1982), Phys. Rev. D25, 1765-1785.

[7] Breakstone, A. et al., (1983), Phys. Lett. 132B, 463-466.

[8] Gaisser, T.K. and Hillas, A.M., (1977) 15th Int. Conf. Cosmic Rays Plovdiv, Conference Papers, 8, 353-357.

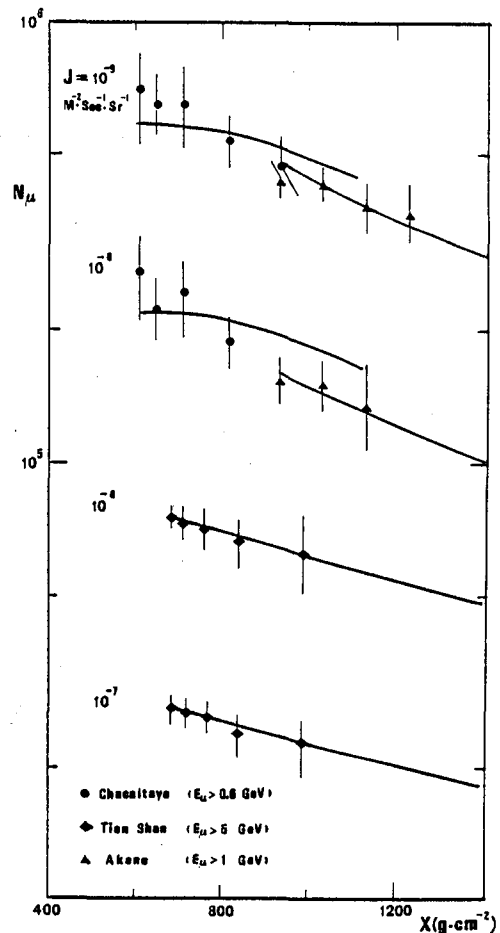


Fig.3 Normalised muon development curves (75%p, 25%Fe) compared with observations.



## TOPOLOGICAL ASPECTS OF AGE PARAMETER

J.N. Capdevielle

Laboratoire de Physique Théorique, Bordeaux, France

and

J. Gawin

Institute of Nuclear Studies, Lodz, Poland

1. Introduction

The well known NKG function is a very useful tool to describe the lateral extension of the electromagnetic component in EAS ; however, in spite of non negligible qualities (simplicity, normalization by beta-function), it doesn't correspond exactly to the natural shape of the lateral electron distribution. Several bias may occur in size estimation if NKG is used without correction, for instance, contradiction between lateral and longitudinal development the lateral parameter  $s_{\perp}$  being quite lower than the longitudinal one (1)(2). We emphasize here how the longitudinal age parameter  $s_{\parallel}$  can be correlated with the information obtained from the lateral electron densities according to the conditions of use of the NKG function.

2. Local age parameter phenomenology

The theoretical age parameter  $s_t$  illustrates the declining stage of a shower and is determined as the saddle point in the inverse Mellin transformation. We have postulated that the NKG function, derived from diffusion equations fails to describe EAS data, mainly because a uniqueness of parameter  $s$  was assumed, and we have admitted local agreement with NKG function in small bands of distance by introducing the local age parameter

$$s(r) = \frac{1}{2x+1} ((x+1) \frac{\partial \text{Ln } f}{\partial \text{Ln } x} + (6.5 x + 2)) \quad (f \equiv \text{NKG})$$

( $x = r/r_0$ ),  $r_0$  Molière radius. From two neighbouring points  $x_i, x_j$ , the lateral age parameter  $s_{ij}$  in  $[r_i, r_j]$  is given by

$$s_{ij} = \text{Ln} (F_{ij} X_{ij}^2 Y_{ij}^{4.5}) / \text{Ln} (X_{ij} Y_{ij})$$

where  $F_{ij} = f(r_i)/f(r_j)$ ,  $X_{ij} = r_i/r_j$ ,  $Y_{ij} = (x_i+1)/(x_j+1)$ .

If  $r_i \rightarrow r_j$ ,  $s_{ij} \rightarrow s(r)$  when  $r = (r_i+r_j)/2$ .

Different behaviour of lateral structure function were proposed from different analytical treatment of diffusion equations (3) or Monte-Carlo simulation of e.m. cascades (4). A convenient formula was advanced consisting to use NKG formula with a Molière radius reduced by a factor  $m = 0.78-0.21 s_t$  (for individual e.m. cascade). We observed for single e.m. cascade that  $s(r)$  had, versus (3) or (4) a behaviour similar to fig. 1 ; incorporating those results in EAS-3D simulation, we ascertained that this typical behaviour of  $s(r)$  survived in EAS lateral distribution for all sizes and levels.

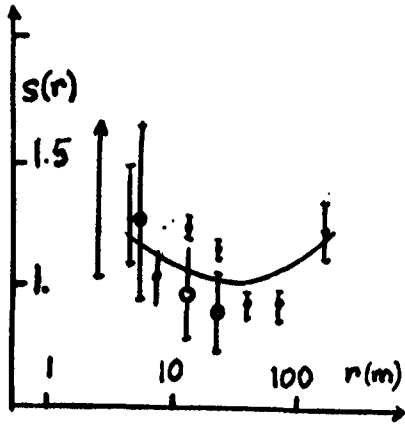


Fig. 1

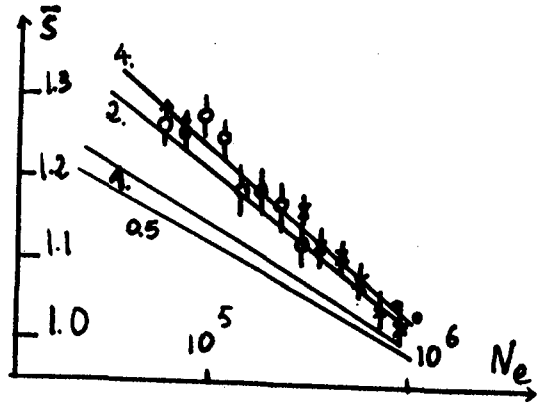


Fig. 2

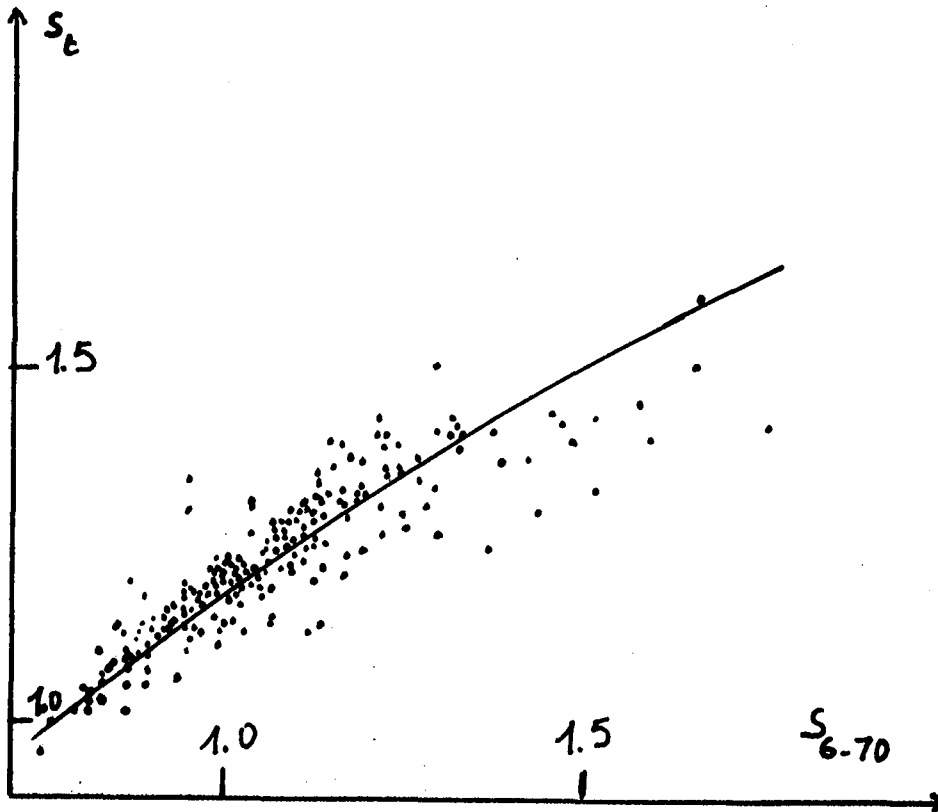


Fig. 3

Recently we developed a very detailed Monte-Carlo 3D-simulation, including all possible causes of deviation (for instance, the double body decay of each  $\pi^0$ , is completely described to produce energy and director cosines of each outgoing  $\gamma$ ,  $\langle p_t \rangle$ , is correlated with central rapidity density...); the model used for nuclear interaction is the multicluster phenomenological one described in HE 4.1-9,10. A surprising agreement is obtained with Akeno data (5) in favour of the parametrization (fig. 1)

$$s(r) = \alpha \xi^2 + \beta \xi + \gamma \quad , \quad \text{where } \xi = \text{Ln}(r/r_0)$$

For a uniform density of detectors, the answer of an experimental array will be averaged on all the shower disk seen by the array. The radius R of this shower disk depends on the detector area (or density threshold) and it comes :

$$\bar{s} = \frac{1}{R} \int_0^R s(r) dr = \frac{1}{X} (\alpha F_1(X) + \beta G_1(X)) + \gamma \quad \text{with } X = R/r_0$$

where  $F_1(X) = XLn^2 X - 2X(Ln X - 1)$  ,  $G_1(X) = XLn X - X$ . According to the shape of fig. 1, any attempt to estimate  $\bar{s}$  in [0 - 50 m] and [50 - 150 m] will give the same value of the integral (6).

### 3. Comparison with experiment

The variation of  $\bar{s}$  versus size has been calculated for MPM (nucleon primaries,  $\theta = 22^\circ 5'$ ) at Akeno level (fig. 2). Four values of R have been taken corresponding to 4  $e^-/m^2$ , 2, 1, 0.5  $e^-/m^2$ . The first value corresponding to 0.25  $m^2$  detector is in very good agreement with the experimental data. At Tian-Shan level, we have plotted the correlation between  $s_{6-70}$  and  $s_t$ , the first parameter being estimated by NKG function from numerical values simulated at 6 and 70 m (fig. 3) for different sizes between  $10^4 - 10^6$  particles. A general correlation appears :  $s_t = 1.434 s_{6-70}^{1/2} - 0.243$ .

The correspondance giving  $s_t$  at Akeno and Moscow altitudes has been also obtained as  $s_t = 1.246 \bar{s}^{1/2} + 0.044$  and  $s_t = 1.157 \bar{s}^{1/2} + 0.183$ . We note that with the present assumption included for e.m. cascade, the correlation is not independent on level (fig. 4).

### 4. Discussion

The behaviour versus r of s(r) is not smeared out by the hadronic cascade and survives in EAS (fig. 1). The agreement obtained previously with high multiplicity model is now obtained with the multicluster phenomenological model

(describing  $\bar{p}$ -p data) up to  $5 \cdot 10^6$  GeV (limit of our Monte-Carlo simulation) as well at Akeno for  $\bar{s}$  and s(r) as in Tian-Shan for  $s_{6-70}$ . The age parameter data doesn't suggest between  $2 \cdot 10^4 - 5 \cdot 10^6$  GeV any increase of primary mass and supports better a nucleon dominance in primary cosmic rays.

### References

1. S.C. Tonwar, 1981, Proc.17th Conf.on Cosmic Rays, Paris, rap. paper.
2. J.N. Capdevielle and J. Gawin, 1982, J.Phys. G8 (1982), 1317.
3. A.A. Lagutin, V.V. Uchaikin, 1979, Proc.16th Conf.on Cosmic Rays, Kyoto, 7, 18.
4. A.M. Hillas, 1981, Proc.17th Conf.on Cosmic Rays, Paris, 6, 244.

5. M. Nagano et al., 1984, J.Phys.Soc.Jap., 53, 1667.
  6. F. Ashton et al., 1983, Proc.18th Conf.on Cosmic Rays, Bangalore, 11, 181.
  7. M.V.S. Rao, 1983, Proc.18th Conf.on Cosmic Rays, Bangalore, 12, 449.
- M. Nagano, 1983, Proc.18th Conf.on Cosmic Rays, Bangalore, 12, 475.

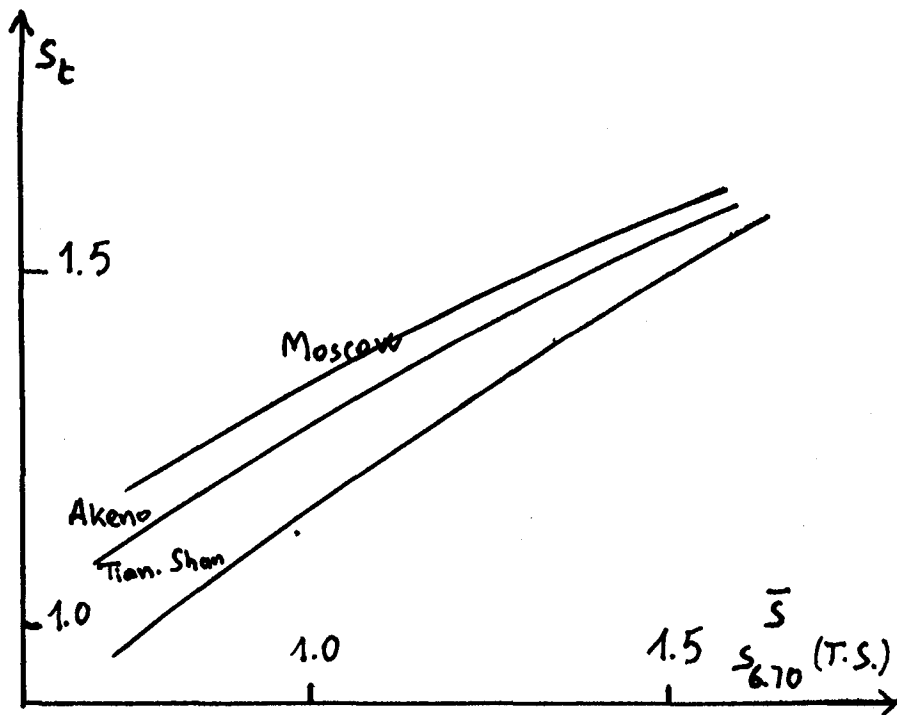


Fig. 4

MONTE CARLO SIMULATION OF E.A.S.  
GENERATED BY  $10^{14}$ - $10^{16}$  eV PROTONS

Fenyves, E.J. and Yunn, B.C.  
University of Texas at Dallas  
P.O. Box 830688  
Richardson, TX 75083-0688

Todor Stanev  
Bartol Research Foundation of the Franklin Institute  
University of Delaware  
Newark, DE 19716

### 1. Introduction

Detailed Monte Carlo simulations of extensive air showers to be detected by the Homestake Surface-Underground Telescope (1) and other similar detectors located at sea level and mountain altitudes have been performed for  $10^{14}$ - $10^{16}$  eV primary energies. The results of these Monte Carlo calculations will provide an opportunity to compare the experimental data with different models for the composition and spectra of primaries and for the development of air showers (2).

In the present paper we report on the results obtained for extensive air showers generated by  $10^{14}$ - $10^{16}$  eV primary protons.

### 2. Monte Carlo Simulation of the Hadronic Cascade

The interaction model used assumed inelastic cross sections increasing with energy as  $\ln^{1.8}s$ , which corresponds to a  $\ln^2s$  rise of the inelastic p-p cross section. The x distribution obeys radial scaling and is realized through the splitting technique suggested by A.M. Hillas. The K/ $\pi$  ratio is 0.09 and energy independent.

Transverse momentum distribution is of the form  $p_{\perp} \exp(-Kp_{\perp})$  and includes the "sea gull" effect. For  $x < 0.2$ ,  $K = \frac{2}{x + 1/4}$ , while

for  $x > 0.2$  we used a constant exponent of -4.44 for pions.

The secondary particles are followed until they reach certain threshold energy levels: 1.7 TeV for muons, 0.01 and 0.1 TeV for electrons, gammas, and 0.1 TeV for hadrons.

### 3. Simulation of the Electromagnetic Cascades

The electromagnetic cascades generated by gammas and electrons are propagated to the height of detection by applying the parametrized analytical formulas for the longitudinal development and lateral distribution of the electron component obtained by Fenyves and Yunn in previous Monte Carlo simulations of electromagnetic cascades (3). The threshold energy levels for the electromagnetic cascade generating gammas and electrons were: 0.01 TeV for  $10^{14}$  and  $10^{15}$  eV primary protons, and 0.1 TeV for  $10^{16}$  eV protons. The average number of gammas and electrons above the threshold per shower is given in Table 1. (Muons above 1.7 TeV are also included in the Table.)

Table 1

$E_p$ (eV)	$N_\gamma$	$N_e$	$N_\mu$
$10^{14}$	$361 \pm 8$	$3.9 \pm 0.3$	$0.30 \pm 0.06$
$10^{15}$	$2612 \pm 61$	$31.9 \pm 1.1$	$1.54 \pm 0.17$
$10^{16}$	$3015 \pm 78$	$34.9 \pm 1.2$	$8.20 \pm 0.50$

From the extrapolation of the gamma spectra below the threshold levels correction factors were calculated for the missing low energy elec-

tromagnetic cascades. The correction factors for the total number of electrons of the air shower are dependent on the depth and the primary proton energy varying between 1.010 and 1.021.

The geomagnetic effect was included in the calculation by stretching the east-west axis of each vertical electromagnetic cascade by  $[1 + 0.05(\cos \lambda / P)^2]^{1/2}$  where  $\lambda$  is the geomagnetic latitude and P the pressure in atmospheres (4). The individual cascades were then folded together to form the electron component of the extensive air shower.

#### 4. Results

We have run a total of 220 extensive air showers generated by  $10^{14}$ ,  $10^{15}$  and  $10^{16}$  eV primary protons in a standard atmosphere. As expected the longitudinal development of these showers could not be approximated well with the standard formula used for the electron component of electromagnetic cascades generated by single gammas (3)

$$N_e(E_0, E, t) = \frac{A(E, s) 0.31}{\sqrt{y}} \exp [t(1 - 1.5 \ln s)] \quad (1)$$

where  $t$  is the depth measured in radiation lengths ( $37.1 \text{ g/cm}^2$ ),  $y = \ln E_0 / \epsilon_0$  ( $\epsilon_0 = 81 \text{ MeV}$ ),

$$s = \frac{3t}{t + 2y} \quad (2)$$

and  $A(E, s)$  is the fraction of electrons having energies larger than the electron threshold energy,  $E$ . ( $E=5\text{MeV}$  and  $A(5\text{MeV}, s)=0.67$  were used in the present study (3).)

We could, however, fit  $N_e^{\max}$  and  $t_{\max}$  calculated from Eq.(1) simultaneously to the corresponding average values obtained for the  $10^{14}$ ,  $10^{15}$  and  $10^{16}$  eV showers by varying  $E_0$ , the energy of the cascade generating gamma. The longitudinal development of the simulated air showers was, however, increasing faster before  $t_{\max}$ , and decreasing slower after  $t_{\max}$  than the values calculated from Eq.(1). This is expected because the electromagnetic component of the air shower starts with a large number of gammas, and dies out slower after the maximum due to new electromagnetic cascades generated by the hadronic core.

According to this we modified Eqs.(1) and (2) simply by replacing  $t$  in both equations by

$$t' = t + \beta(t_{\max} - t)t^\gamma \quad (3)$$

where  $\beta$  and  $\gamma$  are constants depending on the primary proton energy, and the second term increases or decreases the effective  $t'$  values as compared to  $t$  before or after the maximum, respectively.

The optimum  $E_0$ ,  $\beta$  and  $\gamma$  values obtained for this parametrization for  $E_p=10^{14}$ ,  $10^{15}$  and  $10^{16}$  eV are given in Table 2. Fig. 1 shows the good agreement between the Monte Carlo simulated average values (dots with error bars) and the smooth curves calculated by using Eqs.(1) and (2) modified by Eq.(3) with the parameter values given in Table 2.

Table 2

$E_p$ (eV)	$E_0$ (eV)	$\beta$	$\gamma$
$10^{14}$	$5.2 \cdot 10^{13}$	0.0100	1.00
$10^{15}$	$6.4 \cdot 10^{14}$	0.0173	0.75
$10^{16}$	$6.9 \cdot 10^{15}$	0.0300	0.50

Eqs.(1), (2) and (3) can also be used to describe moderately inclined showers ( $\theta \leq 30^\circ$ ). Then  $t$  in Eq.(3) is the slant depth measured from the top of the atmosphere. The energy of

the single gamma,  $E_0$ , simulating the longitudinal development of the air shower is increasing with  $E_p$ , the energy of the shower as expected because of the increasing probability of charged pions and kaons to produce nuclear interactions rather than decay. The  $\beta$  and  $\gamma$  values can be easily interpolated for intermediate  $E_p$  values when plotted on a log-log or lin-log scale vs.  $E_p$ , respectively.

The lateral distribution of electrons of air showers generated by  $10^{14}$ ,  $10^{15}$  and  $10^{16}$  eV protons was compared with the modified NKG formula

$$f\left(\frac{r}{r'_M}\right) = C(s) \left(\frac{r}{r'_M}\right)^{s-2} \left(\frac{r}{r'_M} + 1\right)^{s-4.5} \quad (4)$$

where  $r'_M$  is about half of the Molière length length,  $r_M$ , as suggested by A. M. Hillas (5), and  $s$  is calculated by Eq.(2) modified by Eq.(3) with the parameters given in Table 2. A good agreement was found for not too large distances from the core, from  $r=1m$  to about 300m, as illustrated in Figs. 2, 3 and 4 for  $850 \text{ g/cm}^2$ , the height of the Homestake Telescope where  $r'_M=45m$  (3). Similarly good agreement was found for other heights too. At larger distances from the core, however, even the modified the NKG formula fails to agree with the Monte Carlo simulated data. Corrections for this effect will be discussed in a forthcoming paper.

The geomagnetic effect is relatively small at sea level but increasing with altitude. The east-west axis of vertical showers is stretched by a factor of 1.013 at sea level, and 1.019 at  $850 \text{ g/cm}^2$ . The relative difference between the  $f(r/r'_M)$  values averaged in a cone  $\pm 45^\circ$  around the east-west axis and in a cone  $\pm 45^\circ$  around the north-south axis is increasing with  $r$  from about  $-0.015$  at  $r=1m$ , to about  $-0.075$  at  $r=1000m$ .

### 5. Acknowledgements

The authors are indebted to N. R. Davis, S. S. Liao and D. J. Suson for their valuable cooperation. This work has been supported by the National Science Foundation.

### References

- (1) Cherry, M.L. et al., (1981), 17th Int. Cosmic Ray Conf., Paris, 11, p. 421.
- (2) Fenyves, E.J. and Cherry, M.L., (1983), Proc. Cosmic Ray Workshop, Utah, p.173.
- (3) Fenyves, E.J., Lee, C.J. and Yunn, B.C., (1983), 18th Int. Cosmic Ray Conf., Bangalore, 11, p. 240.
- (4) Greisen, K., (1956), Progr. in Cosmic Ray Phys., Vol. III, p.1.
- (5) Hillas, A.M., (1983), private communication.

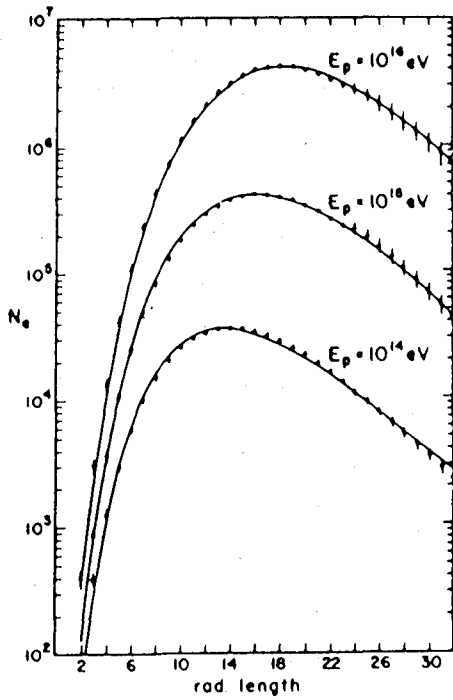


Fig. 1

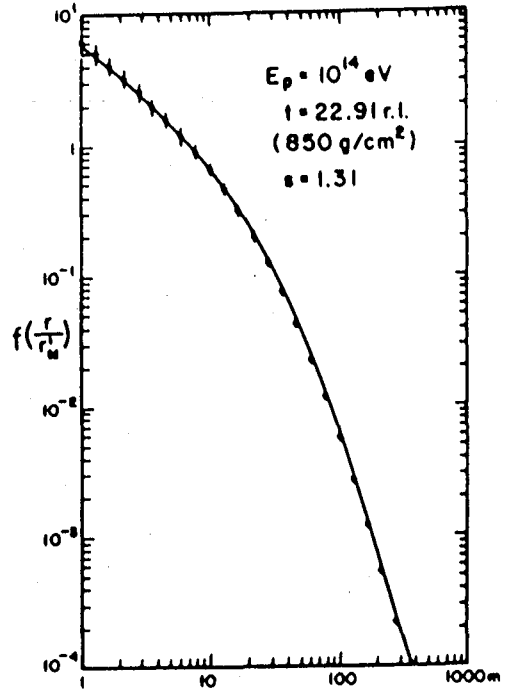


Fig. 2

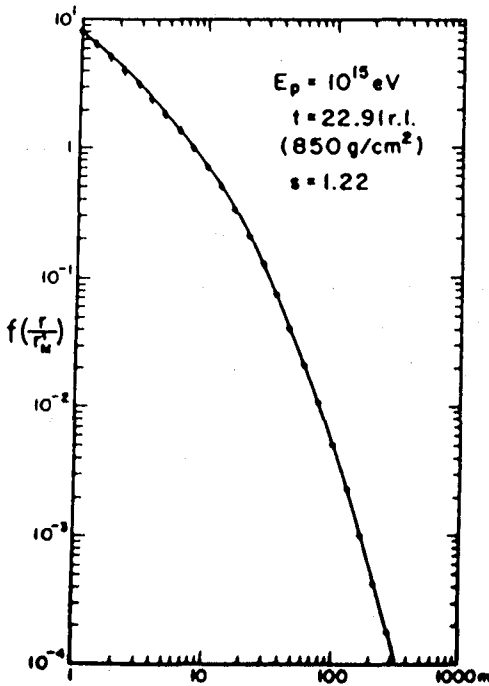


Fig. 3

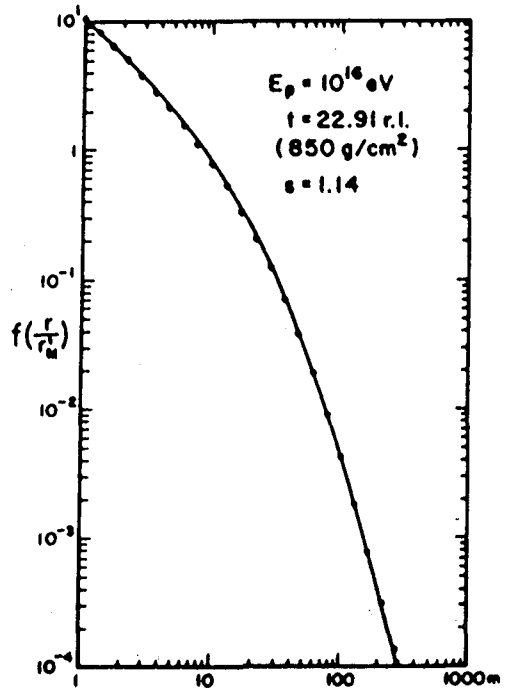


Fig. 4



## LATERAL DISTRIBUTION OF CHARGED PARTICLES IN EAS

Dedenko L.G., Kulikov G.V., Solovjeva V.I., Sulakov V.P.  
 Institute of Nuclear Physics, Moscow State University,  
 Moscow 119899, USSR

1. Introduction. The calculations of lateral distribution of charged particles which allow for the finiteness of energy of  $\gamma$ -quanta /1-3/, the inhomogeneity of the atmosphere /3,4/ and the experimental selection of EAS /5/ are needed to interpret correctly the experimental data /6,7/.

In /8,9/ calculations have taken into account the effect of finiteness of energy of  $\gamma$ -quanta which produce the partial electron-photon cascades by substituting  $KR_m$  instead of  $R_m$  in NKG approximation where  $K$  has been found to be 0.56 from comparison with the experimental data. In /5,10-12/ new results on the lateral distribution of electrons in the partial cascades from  $\gamma$ -quanta have been obtained. The analysis /5/ of results /11,12/ showed that the coefficient  $K$  can be regarded as a constant with the error of 5-10%. In /5/ the calculations have been carried out for such values of  $K$  as 0.75; 1, and  $K = 1 - 0.5(1 - y/16)$  for  $y \leq 16$  and  $K=1$  for  $y > 16$  where  $y = \ln(E_\gamma/1 \text{ GeV})$ . The last approximation of  $K$  was found to be most adequate from the comparison with the experimental data /6/ and it is used in this calculation. In /5/ the inhomogeneity of the atmosphere, muons and experimental selection were taken into account. In /5/ the calculation were done for EAS with size  $N_e = 10^7$  at sea level. In this paper we extend the calculation on  $N_e$  from  $10^5$  to  $10^7$  for sea level and for Akeno level ( $920 \text{ g.cm}^{-2}$ ).

2. Model and Method. The calculations were carried out in terms of the quark-gluon string model for hadron-hadron interactions /13-15/. The lateral distributions were calculated for primary protons and nuclei with  $A = 4, 14, 31, 56$  and the normal composition  $\Sigma$ . The energy spectrum index

was taken  $\chi_1 = 1.7$  at  $E_1 \leq 3 \cdot 10^{15}$  eV and  $\chi_2 = 2.2$  at  $E_2 \geq 10^{16}$  eV with smooth change between these two energies. The method includes the calculations of the two-dimensional functions and correlation matrixes for fixed  $E_0$  following by use of Bayes theorem and gaussian approximation for calculated functions to get the functions for fixed  $N_e$  and the zenith angle  $\theta$  /16,17/. To allow for experimental selection the calculated functions for fixed  $N_e$  and  $\theta$  were integrated on  $N_e$  and  $\theta$  /5/. The experimental errors were taken into account by summing the physical correlation matrix with the matrix of errors, which consist of errors of  $\sigma_{N_e}/N_e = 25\%$ ,  $\sigma_{\rho}/\rho = 15\%$  and  $\sigma_r/r = 10\%$  where  $\rho$  - density of electrons and  $r$  is distance from the shower axis. The approximation  $R_m = 1.1 R_m$  have been used to allow for the inhomogeneity of the atmosphere. The density of  $> 0.3$  GeV muons and additional 27% of muon density to take into account the decay electrons and  $\delta$  -electrons ( according to our analysis and /18/) were added to electron density to get charged particle density.

3. Results and Conclusions. In Fig. 1 the calculated lateral distributions of charged particles for sea level are shown together with the experimental data /6/. One can see that in the limits of experimental errors the normal and proton primary compositions may agree with the experimental data /6/. Fig. 2 shows the analogous calculated functions for  $920 \text{ g/cm}^2$  and Akeno experimental results /7/. To get the better agreement this time one should use a more steep electron lateral distribution in pure electron-photon cascades from  $\gamma$ -quanta than we have used. But our conclusion about primary composition made for sea level data is kept.

The authors wish to thank Prof. G.B. Kristiansen for informative discussions.

#### References

1. Gujavin V.V., Ivanenko I.(1960), Proc. 6th ICRC, Moscow v.2, p.253
2. Nishimura J. (1967) Handbuch der Physik, XL, VI/2.

3. Ivanenko I.P. et al. (1982) *Izv. Akad. Nauk SSSR, ser. phys.*  
v.46, p.2433
4. Osipova L.N., Paskhalov Yu.I. (1979), *Proc. 16th ICRC,*  
Kyoto, v.9, p.232
5. Dedenko L.G. et al. (1985), *Izv. Akad. Nauk SSSR, ser. phys.*  
v. 49, No. 7
6. Khristiansen G.B. et al. (1983), *Proc. 18th ICRC,*  
Bangalore, No. v.11, p.197.
7. Nagano M. et al. *J. Phys. Soc. Japan, 1984*
8. Dedenko L.G. et al. (1975), *Proc. 14th ICRC, München, v.8,*  
p. 2731.
9. Dedenko L.G. et al. (1976), *Brief Repts. on Physics,*  
FIAN, No.1, p. 30
10. Hillas A.M., Papikens J. (1977), v.8, p.460, *ICRC, Plovdiv*
11. Lagutin A.A. et al. *Proc. 16th ICRC, Kyoto, v.7, p.18*
12. Vorobjev K.V. et al. (1982), *Izv. Akad. Nauk SSSR, ser.*  
*phys. v.46, p.2437*
13. Kaidalov A.B., Ter-Martirosjan K.A. (1984), *Jadernaja*  
*Physika, v.39, p.1545*
14. Anisovich V.V. et al. (1978), *Jadernaja Physika, v.28,*  
p. 1063
15. Kalmykov N.N., Khristiansen G.B. (1983), *Proc. 18th*  
*ICRC, Bangalore, v.11, p.330.*
16. Dedenko L.G. (1964), *ZhETF, v.46, p.1859*
17. Dedenko L.G., Zatsepin G.T. *Proc. 6th ICRC, Moscow,*  
1960, v. 2, p.222.
18. Hayakawa S., (1969), *Cosmic Ray Physics, part 1,*  
Ed. by R.E. Marshak, v. XXII, John Wiley & Sons,  
New York.

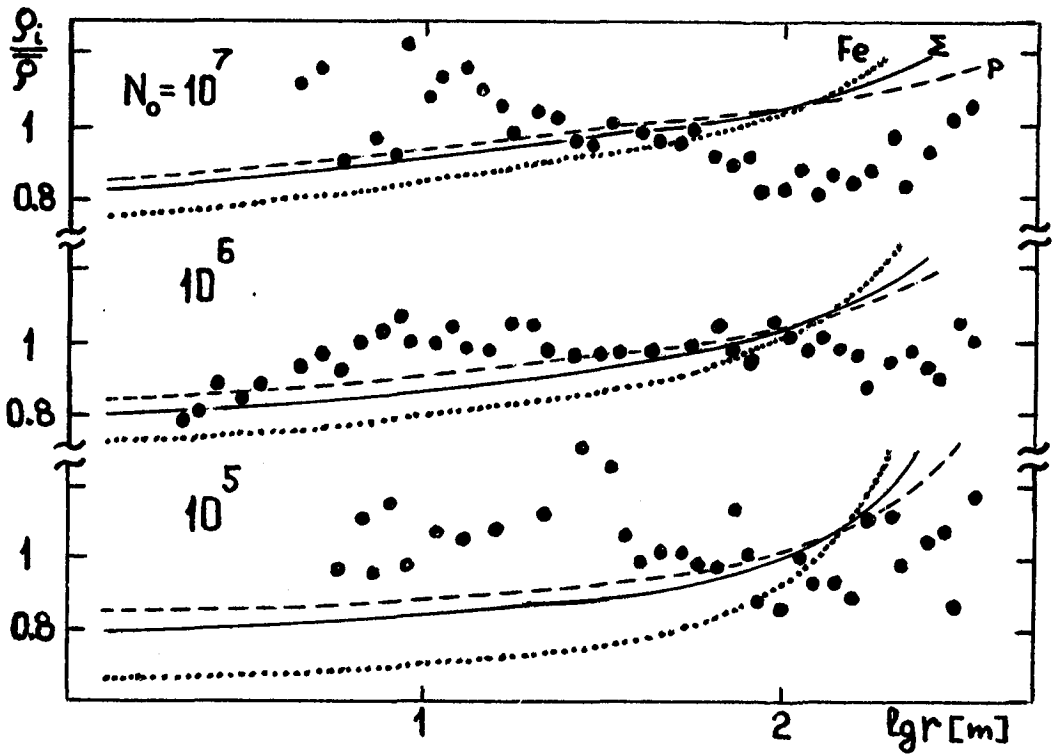


Fig. 2. The lateral distribution of charged particles at  
 $920 \text{ g cm}^{-2}$   
 $(\bar{\rho} \sim (r/r_0)^{-\alpha} (1+r/r_0)^{-\beta}, \alpha=0.96, \beta=3.06, r_0=91.6 \text{ m})$

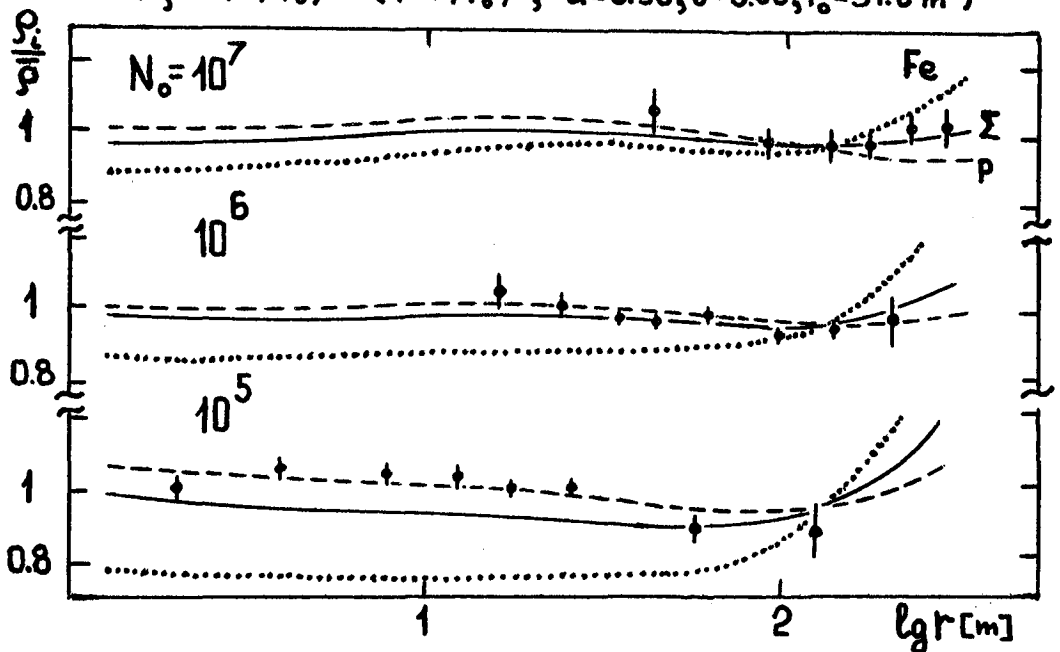


Fig. 1. The lateral distribution of charged particles at  
 sea level  
 $(\bar{\rho} \sim (r/r_0)^{-\alpha} (1+r/r_0)^{-\beta}, \alpha=0.9, \beta=2.8, r_0=80 \text{ m})$

LATERAL DISTRIBUTION OF HIGH ENERGY MUONS IN EAS  
OF SIZES  $N_e \approx 10^5$  and  $N_e \approx 10^6$ .

Bazhutov Yu.N., Ermakov G.G., Fomin Yu.A., Isaev V.I.,  
Jarochkina Z.V., Kalmykov N.N., Khrenov B.A., Khristian-  
sen G.B., Kulikov G.V., Motova M.V., Proshkina I.P., Ruko-  
vichkin V.P., Solovjeva V.I., Sulakov V.P., Shkurenkov A.V.  
Trubitsyn A.V. and Vashkevich V.V.

Institute of Nuclear Physics, Moscow State University,  
Moscow, 119899, USSR.

Muon energy spectra and muon lateral distribution in EAS are investigated with the help of the underground magnetic spectrometer working as a part of the Moscow State University EAS array [1,2,3]. Before going to new results on EAS muons a general concept of the measurement shall be mentioned. For every registered muon the data on EAS are analysed and the following EAS parameters are obtained: size  $N_e$ , distance  $r$  from the shower axis to muon, age parameter  $s$ . So the number of muons with energy over some threshold  $E_r$  associated to EAS of fixed parameters are measured:  $I_{reg}$ . To obtain traditional characteristics—muon flux densities as a function of the distance  $r$  and muon energy  $E_r$ , i.e. muon lateral distribution and energy spectra which are widely discussed in terms of hadron-nucleus interaction model and composition of primary cosmic rays one should use the equation:

$$\frac{\Delta I_{reg}}{\Delta N_e \Delta r \Delta s} = t \cdot 2\pi r \int_0^{\theta_0(\psi)/2\pi} \int_0^{\theta_0(\psi)} d\cos\delta d\psi I(\theta, \psi) F(N_e, s) W_{reg}^{EAS}(N_e, r, s, \theta) \cdot W_{reg}^{\mu}(E_r, N_e, r, s, \theta, \psi) \quad (1)$$

where  $F(N_e, s)$  is known spectrum of EAS,  $W_{reg}^{EAS}(N_e, r, s, \theta)$  is probability to register the EAS of specified parameters,  $W_{reg}^{\mu}$  is probability to register muon of energy over  $E_r$  in magnetic spectrometer with effective area  $\sigma(\theta, \psi, E_r)$ ,  $I(\theta, \psi)$  is angular distribution of EAS,  $\theta_0(\psi)$  is spectrometer geometry limit on zenith angle  $\theta$ ,  $t$  is operation time. In our case probability is equal

$$W_{reg}^{\mu} = \{1 - \exp[-\rho_{\mu}(E_r, N_e, r, s, \theta) \cdot \sigma(\theta, \psi, E_r)]\} \approx \rho_{\mu}(E_r, N_e, r, s, \theta) \cdot \sigma(\theta, \psi, E_r) \quad (2)$$

where  $\rho_{\mu}(E_r, N_e, r, s, \theta)$  is muon flux density.

For final analysis only showers with  $W_{reg}^{EAS} \geq 0,9$  ( $0,9 \leq s \leq 1,6$ ) are selected. In this case the densities  $\rho_{\mu}$  derived from experimental data are unbiased on age parameter. So equation (1) transforms to

$$\frac{\Delta I_{reg}}{\Delta N_e \Delta r \Delta s} = t \cdot 2\pi r \cdot F(N_e, s) \cdot \rho_{\mu}(E_r, N_e, r, s, \theta) \cdot \sigma'(E_r); E_r, \text{Gev} \sim \bar{\theta} = 90^\circ \quad (3)$$

where  $\sigma'$  equal to  $\sigma' = \int_0^{\theta_0(\psi)/2\pi} \int_0^{\theta_0(\psi)} I(\theta, \psi) \cdot \sigma(\theta, \psi, E_r) d\cos\delta d\psi$  is geometry factor  $\sigma(\theta, \psi) = 14 \text{ m}^2$ . In Table 1 the numbers of registered muons for threshold energies  $E = 10, 200$  and  $500$  Gev are presented. EAS size ranges are:  $N_1 - 1.3 \cdot 10^4 - 10^5$  ( $\langle N_1 \rangle = 6 \cdot 10^4$ ),  $N_2 - 10^4 - 3 \cdot 10^5$  ( $\langle N_2 \rangle = 1,6 \cdot 10^5$ ),  $N_3 - 3 \cdot 10^5 - 10^6$  ( $\langle N_3 \rangle = 5 \cdot 10^5$ ),  $N_4 - \geq 10^6$  ( $\langle N_4 \rangle = 3 \cdot 10^6$ ).

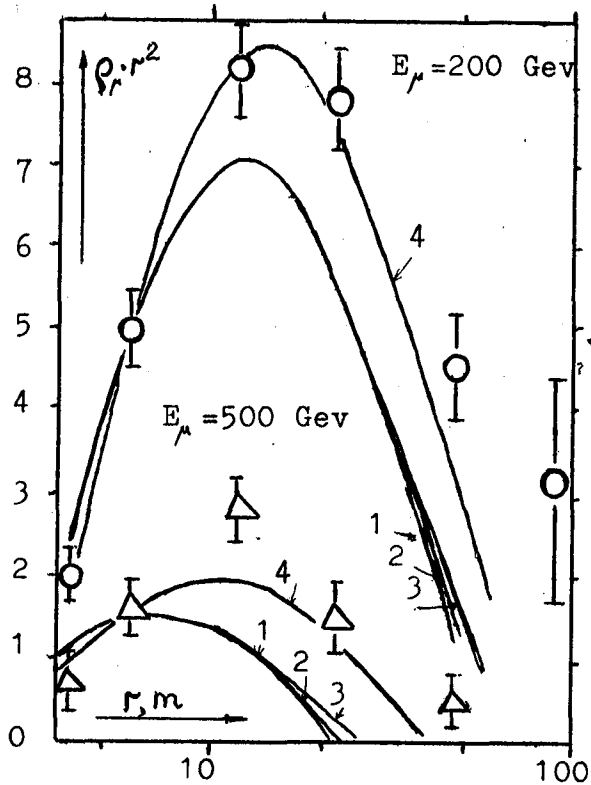


Fig. 1 a

The data for muon threshold energies  $E_\mu = 200$  and  $500$  Gev are corrected for MDM as in [1]. Muon lateral distribution (LD) shows weak dependence on EAS size. The following formula approximates the obtained data

$$\rho_\mu = K \cdot \left(\frac{N_e}{10^6}\right)^\alpha \cdot r^{-n} \cdot \exp\left[-\frac{r}{r_0} \left(\frac{N_e}{10^6}\right)\right]$$

where parameter  $\alpha$  is equal

$E_\mu$ , Gev	50	100	200	500
$\alpha$	0,78	0,77	0,76	0,77
$\pm$	0,04	0,05	0,06	0,1

and

$$k = 1,3 \cdot 10^4 / (E_\mu + 250)^{1,4}$$

$$n = 0,55 \cdot \left(\frac{E_\mu + 2}{12}\right)^{0,1}$$

$$r_0 = \begin{cases} 80 \cdot \left(\frac{E_\mu + 2}{12}\right)^{-0,62} \cdot \left(\frac{N_e}{10^6}\right)^{0,05 \pm 0,05} & 50 \leq E_\mu \leq 200 \\ 10 \pm 3 \text{ m} & E_\mu = 500 \end{cases}$$

In Fig. 1a the average LD of muons with  $E_\mu = 200$  and  $500$  Gev are presented for  $\langle N_e \rangle = 2 \cdot 10^5$ .

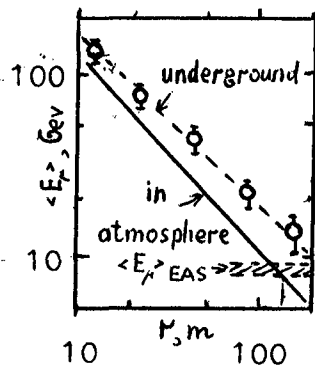


Fig. 1 b

The mean muon energy as a function of distance  $r$  is presented in Fig. 1b. Experimentally measured underground muon energy spectra were transformed to muon spectra in atmosphere. Solid line in Fig. 1b presents mean muon energy in atmosphere at sea level. At the distance  $r = 120 + 12$  m mean muon energy is equal to mean over EAS energy of muons,  $\langle E_\mu \rangle = 8 \pm 1$  Gev, [3]. The ratio of positive and negative muon numbers was analysed for various distances  $r$ . Numbers of muons in differential ranges of energy are presented in Table 2. It is seen that the ratio  $I_+/I_-$  does not deviate from 1 in statistical errors.

Table 1. Numbers of registered muons.

$E_\mu$ , Gev	$r=0-8$ m			$r=8-16$ m			$r=16-32$ m			$r=32-64$ m			$r=64-128$			$r \geq 128$	
	10	200	500	10	200	500	10	200	500	10	200	500	10	200	500	10	200
A11	359	94	35	556	92	30	980	87	21	952	29	5	301	3	1	55	0
W09	359	94	35	484	81	28	625	46	10	508	12	2	112	2	0	10	0
$N_{e-1}$	224	60	22	259	42	14	177	18	5	-	-	-	-	-	-	-	-
$N_{e-2}$	84	23	12	131	19	7	273	18	3	207	3	1	-	-	-	-	-
$N_{e-3}$	41	8	1	77	17	5	139	7	2	205	5	1	33	1	0	-	-
$N_{e-4}$	10	3	0	17	3	2	36	3	0	96	4	0	79	1	0	10	0

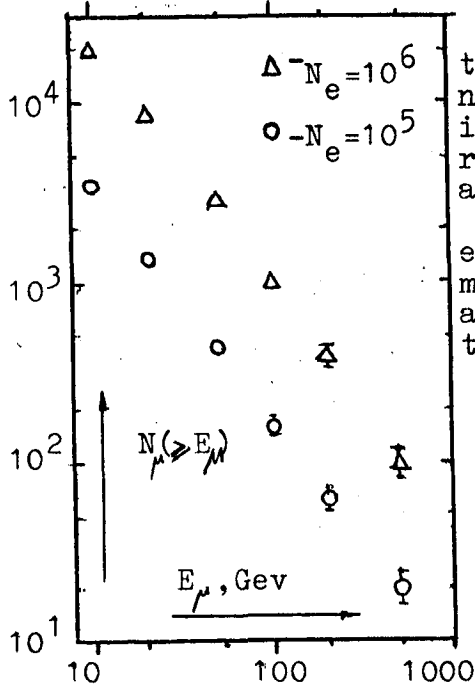


Fig. 2 a.

Comparison of LD of muons registered in E-W sectors of earth magnetic field and of muons registered in N-S sectors does not show difference in statistical errors ( of about 10-20 % ) for muon densities.

It proves that for vertical showers deflection of muons in earth magnetic field is much less than angular spread of muon parent particles in acts of their generation.

Full numbers of muons  $N_\mu (> E_\mu)$  in EAS of size  $N_e = 10^5$  and  $N_e = 10^6$  are presented in Fig.2a. The dependence  $N_\mu(N_e)$  for the range of muon threshold energies  $E_\mu = 10-500$  Gev and EAS of sizes  $N_e = 6 \cdot 10^4 - 3 \cdot 10^6$  can be presented in form

$$N_\mu(N_e) \sim N_e^\alpha$$

with  $\alpha = 0,78$  in experimental errors presented above.

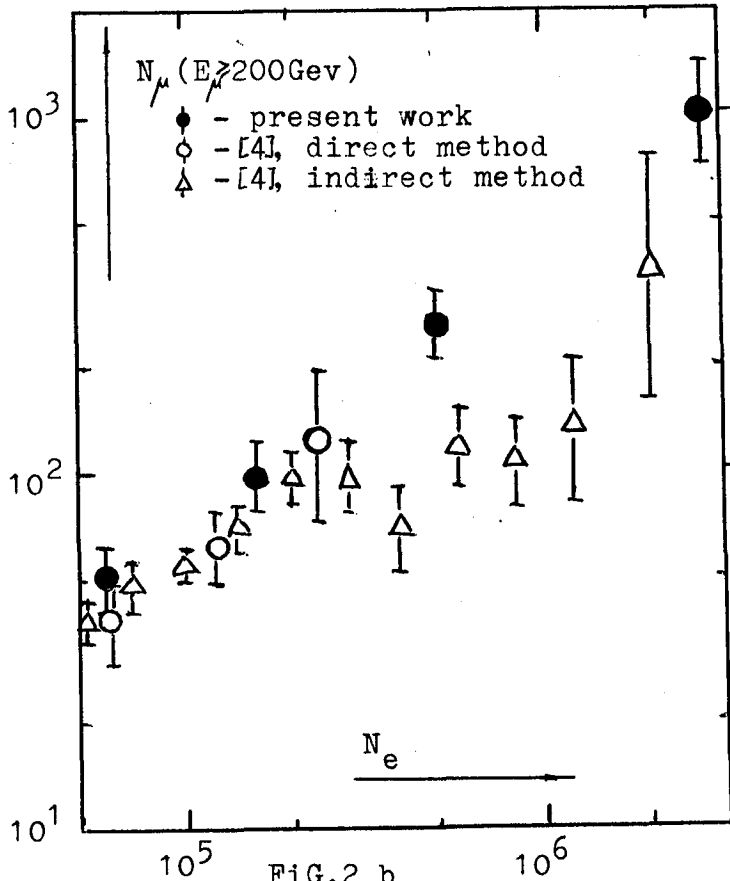


FIG.2 b

In Fig.2b our data on muons of threshold energy  $E_\mu = 200$  Gev are compared to the data[4] of Indian group. The data[4] is recalculated to sea level taking the dependance  $N_e$  on depth  $x$  in atmosphere as

$$N_e \sim \exp(-x/180)$$

where  $x$  is in  $g/cm^2$

One can see that our data do not confirm the change of the exponent  $\alpha$  in  $N_\mu(N_e)$  dependance obtained by indirect method in[4].

Table 2. Numbers of positive  $I_+$  and negative  $I_-$  muons.

$E_\mu$ Gev		10-50	50-100	100-200	200-500	500-1000
$r < 16$ m	$I_+$	161	97	77	57	9
	$I_-$	164	91	82	56	9
$r = 16-32$ m	$I_+$	174	75	51	18	4
	$I_-$	159	68	43	15	0
$r \geq 32$ m	$I_+$	224	69	16	6	0
	$I_-$	206	61	15	6	1

Experimental results presented above were compared to results of Monte-Carlo calculations based on the quark-gluon string theory of hadron-nucleon interactions[5]. This theory explains accelerator data including recent SPS collider data. In[6] this theory was applied to hadron-nucleus interactions. Calculations of EAS were carried out for muon production through pion and kaon decays for primary protons and various primary nuclei in assumption of "superposition" model of nucleus-nucleus interactions. The composition of primaries was suggested as follows

A	1	4	14	21	56
%	40	15	15	15	15

Results of the calculations are presented in Fig.1a curves 1. One can see that for the highest measured muon threshold energies  $E_\mu = 200$  and 500 Gev the theory does not agree with the experiment. To make agreement better there were carried out calculations taking into account muon production through decays of charm particles. Cross-section of charm production was taken as in[7]. Curves 2 present the results of this calculations. Soft jet production[8] was also checked as a reason for additional spread of muons. ( curves 3 in Fig.1a ). Both processes do not change LD of muons of threshold energies  $E_\mu = 200-500$  Gev in the range of distances  $r$  close to median radius as is experimentally measured. Muon LD proved to be more sensitive to the model of nucleus-nucleus interaction. The "fragmentation" model in which nucleons not included in heavy fragments interact with target nucleus gives better agreement with the experimental data. In Fig1a curves 4 present results of the calculations taking into account this "fragmentation" model. Primary composition is as before.

#### References.

1. Khrenov B.A., et al ,ICRC-16, Kyoto, 8,351, 1979.
2. Grishina N.V.,et al ,ICRC-17, Paris, 6, 3 , 1981.
3. Atrashkevich V.B., et al,ICRC-18,Bangalore,11,229,1983.
4. Rao M.V.S., ICRC-18, Rapp. paper, 1983.
5. Kaidalov A.B. & Ter-Martirosjan K.A., Jadernaja Phys.; 39,1514, 1983 and 40,211,1984 .
6. Kalmykov N.N. & Khristiansen G.B., ICRC-18,Bangalore, 11, 330, 1983.
7. Slavnov D.A., Jadernaja Phys., 41, 213, 1985.
8. Gribov L.V., Levin E.M., Ryskin M.V., Phys.Lett.,121B;65, 1983.



## ENERGY CALIBRATION OF THE FLY'S EYE DETECTOR

Baltrusaitis, R.M., Cassiday, G.L., Cooper, R., Elbert, J.W., Gerhardy, P.R., Ko, S., Loh, E.C., Mizumoto, Y., Sokolsky, P. & Steck, D.

Department of Physics, University of Utah, Salt Lake City, UT 84112

## ABSTRACT

The methods used to calibrate the Fly's Eye detector in order to evaluate the energy of EAS is discussed below.

1. Introduction. The energy of extensive air showers (EAS) as seen by the Fly's Eye detector are obtained from track length integrals of observed shower development curves(1). eg

$$E_{em} = \frac{\epsilon_0}{X_0} \int N_e(x) dx$$

where  $E_{em}$  is the total energy of the shower dissipated in the electromagnetic channel,  $\epsilon_0/X_0$  is the ratio of the critical energy of electrons to their radiation length in air(2) and  $N_e(x)$  is the observed size of the EAS as a function of atmospheric slant depth  $x$ . The energy of the parent cosmic ray primary is estimated by applying corrections to account for undetected energy in the muon, neutrino and hadronic channels (3,4). These corrections amount typically to about 10% in the energy range 0.1-100 EeV (1 EeV =  $10^{18}$  eV). Clearly, absolute values for  $E$  depend most critically upon the measurement of shower sizes  $N_e(x)$ . Knowledge of three essentially different processes are involved in leading to a measurement of  $N_e(x)$ . (i) An assessment of those factors responsible for light production by the relativistic electrons in an EAS and the transmission of light thru the atmosphere (ii) Calibration of the optical detection system, i.e., measuring and continually monitoring those factors required to convert measured electronic pulse integrals into absolute numbers of photons received by the Fly's Eye detector from the EAS light source and (iii) A knowledge of the trajectory of the shower which is necessary to convert apparent optical "brightness" into intrinsic optical brightness.

2. Light Production. The factors involving light production by EAS and transmission of light thru the atmosphere have been discussed in great detail in Ref.(1). These factors include:

(i) The Fluorescence Efficiency of Electrons in Air. Our values are taken from the work of Bunner(5).

$$\text{We find that } \frac{d^2N_\gamma}{dtd\Omega} = \frac{N_f N_e}{4\pi} \text{ where } N_f \text{ is the}$$

fluorescent yield in photons/electron/meter and  $N_e$  is the shower size. Roughly,  $N_f \approx 4-4.5$  photons/electron/meter depending on altitude and temperature(1).

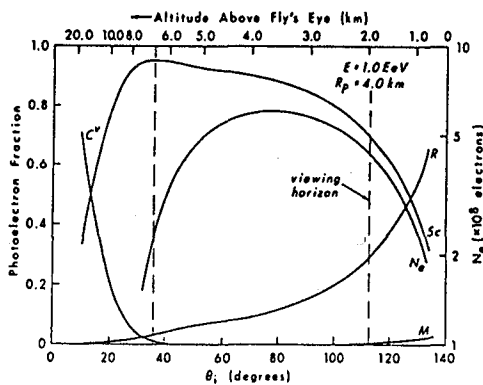
(ii) The Production of Cerenkov Light. This factor has been calculated most recently by Elbert(6) who finds that

$$\frac{d^2N}{d\Omega d\gamma} = \frac{dN}{d\gamma} \frac{\exp^{-\theta/\theta_0}}{2\pi \sin\theta} \quad \text{and} \quad \theta_0 \approx 0.83 E_t^{-0.67}$$

where  $dN/d\Omega$  is the Cerenkov photon yield per meter of air,  $\theta$  is the emission angle and  $E_t$  is the Cerenkov threshold energy in air in MeV. We have measured the angular distribution of Cerenkov light with the Fly's Eye by observing light from the same EAS source simultaneously at different emission angles by Fly's Eye I and Fly's Eye II (separated by 3.3 km). We find that at altitudes corresponding to threshold energies of about 30 MeV our measured value of  $\theta_0 = 5.0 \pm 0.5^\circ$  is in excellent agreement with the value  $\theta_0 = 4.87^\circ$  obtained from Elbert's above expression.

(iii) The Scattering of Light. Both Rayleigh and Mie Scattering affect the transmission of light thru air. Our estimates for these effects are based respectively on the work of Flowers(7) and Elterman(8), they are discussed in detail in Ref.(1).

Finally, we show in Figure 1 an example of calculated relative photoelectron yields obtained by the Fly's Eye detector as generated by the various light



production methods discussed above for a shower of size  $N_e(x)$  whose total energy was 1 EeV observed at an impact parameter of 4 km.

3. Optical Calibration. Converting measured pulse integrals into numbers of photons incident upon the Fly's Eye detector requires a knowledge of the overall efficiency-gain product  $\epsilon G_i$  of each of the approximately 1000 Fly's Eye data channels. An

Figure 1. Relative photoelectron yields as a function of altitude (upper scale) and observed shower emission angle (lower scale). Sc=scintillation light, C=direct Cerenkov, R=Rayleigh and M=Mie Scattered Cerenkov light.  $N_e$  is the shower size.

absolute measurement has been made on a single channel and the  $\epsilon G$  factors for all others determined by relative normalization. In situ Argon flash bulbs triggered on command by computer are used to continually monitor all  $\epsilon G$  factors during data taking at all times subsequent to the time of absolute calibration. Measured efficiency-gain factors are:  $\epsilon_{\text{pmt}} = 0.212 \pm 0.015$ ,  $\epsilon_{\text{cone}} = 0.80 \pm 0.05$  and  $\epsilon_{\text{mirror}} = 0.83 \pm 0.04$  giving an overall efficiency of  $\epsilon = 0.141 \pm 0.016$ . The gain factor  $G$  includes PMT gains, preamp transconductance, finite cable DC resistance, charge-integrator input impedance and voltage-time input to digitized output conversion factors. The resultant overall gain is  $G = 0.757 \pm 0.076$  mv/photoelectron. Hence, errors in absolute quanta measurements,  $\delta N_\gamma$ , are on the order of  $\pm 16\%$ .

4. Geometrical Reconstruction. The techniques of geometrically reconstructing an event seen either by Fly's Eye I alone or stereoscopically by Fly's Eyes I and II in coincidence have been discussed in Ref.(1). Essentially, the chief contribution of inaccurate geometrical reconstruction to uncertainty in energy measurement stems from inaccuracies in determining the shower impact parameter  $R_p$ , or distance of closest approach to the Fly's Eye I detector. These uncertainties are typically on the order of 5-10%. Hence, overall uncertainties in energy measurements from all factors listed above are expected to be on the order of  $\pm 20\%$ .

5. Tests. Several tests have been made to check the validity of all calculations and measurements of the energy determining factors described above.

(i) A Monte-Carlo simulation of the response of the Fly's Eye detector has been carried out in order to check the validity and self-consistency of the analysis procedure(1). Shown in Figure 2 is the Monte-Carlo response function for shower energies measured by the simulated detector. The effects of night sky noise fluctuations in measured pulse integrals have also been included. As can be seen from the plots, overall energy determinations appear to be accurate to within  $\pm 20\%$ .

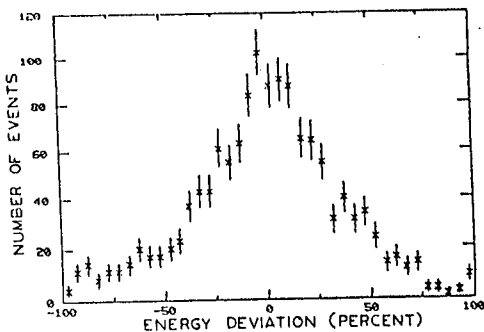


Figure 2. % Differences  
Between Measured Shower Energy  
and Known Monte-Carlo Input  
Energy.

(ii) A pulsed nitrogen laser was positioned at Fly's Eye I at a variety of different zenith, azimuth angles and impact parameters. The scattered light from the upward-going laser light pulse simulates light emission from an EAS. Absolute light yields measured by the Fly's Eye for each laser pulse can then be used to calculate the number of photons in the upward-going beam after reconstructing its trajectory and calculating the amount of light both Rayleigh and Mie scattered from the beam as outlined above. Resultant estimates of the laser's photon output based on Fly's Eye measurements agree with direct measurements of its output to within  $\pm 20\%$  and is virtually independent of scattering angles over a range of  $20^\circ < \theta < 120^\circ$ . The agreement implies that Fly's Eye optical calibration is well known and the treatment of Rayleigh and Mie scattering and light attenuation of a light beam propagating thru the atmosphere has been treated adequately.

(iii) About 500 showers have been observed stereoscopically i.e., by Fly's Eye I and Fly's Eye II (separated by 3.3 km) in coincidence. Shown in Figure 3 is an example of a shower reconstructed stereoscopically and whose longitudinal development sizes,  $N_e(x)$ , have been measured by data obtained by each detector. It is impossible to tell which data points belong to Fly's Eye I or Fly's Eye II. Again, since the light source was observed simultaneously from different emission angles as

well as optical path lengths, the implication is that the angular distribution of both direct and scattered Cerenkov light, its relative strength to fluorescence light, and the effects of the atmosphere on light propagation is being treated properly.

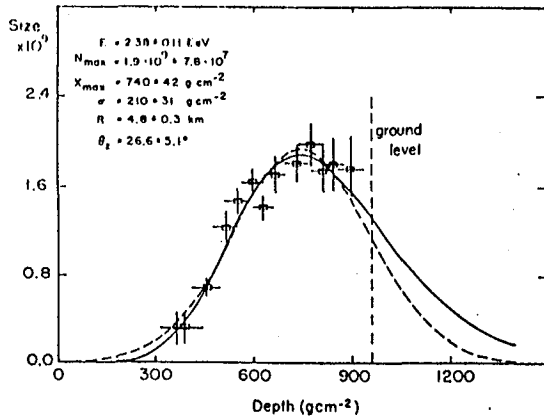


Figure 1. Longitudinal profile of an EAS observed by both Fly's Eye I and II simultaneously. Size estimates are composed of mixed data points, i.e., some from FEI, some from FEII.

(iv) During Fly's Eye prototype experiments, a direct intercalibration experiment of shower size measured by the Volcano Ranch experiment and the Fly's Eye optical detector was carried out at Volcano ranch(9). The obtained sizes in that experiment agreed to  $\pm 10\%$ . This intercalibration established the validity of the absolute values we currently use for the nitrogen fluorescence yield used to derive absolute shower sizes. It cannot, therefore, be argued that this normalization is in doubt. Any current systematic failure to properly assess energy could therefore only occur thru failures to properly calibrate the optical detector or reconstruct shower trajectories. We believe that we have demonstrated that errors inherent in these latter two procedures are well-understood.

6. Acknowledgements. We gratefully acknowledge the United States National Science Foundation for its generous support of this work under grant PHY8201089.

#### References.

1. NuclTear Instruments and Methods (submitted 1985).
2. Dozkenko, O.I. and Pomanskii, A.A., Soviet Physics JETP 18, 187 (1964)
3. Linsley, J., Spectra, Anisotropies and Composition of Cosmic Rays Above 1000 GeV, Proc. 18th Int. Conf. Cosmic Rays, Bangalore, India 12, 135 (1983).
4. Baltrusaitis, R.M., et al., paper HE 4.4-2 (this conference).
5. Bunner, A.N., The Atmosphere As a Cosmic Ray Scintillator, PhD Thesis, Cornell Univ., Ithaca, N.Y. (1964).
6. Elbert, J.W., et al., Proc. 18th Int. Conf. Cosmic Rays, Bangalore, India 6, 227 (1983).
7. Flowers, E.C., et al, J. Appl. Meterology 8, 955 (1969).
8. Elterman, L. and Toolin, R.B., Handbook of Geophysics and Space Environments, Chapt. 7, Air Force Cambridge Research Labs, Office of Aerospace Research, USAF (1965).
9. Bergeson, H.E., et al., Phys. Rev. Lett. 39, 847 (1977).

THE STRUCTURE OF EAS AT  $E > 0.1$  EeV

Baltrusaitis, R.M., Cassiday, G.L., Cooper, R., Elbert, J.W., Gerhardy, P.R., Loh, E.C., Mizumoto, Y., Sokolsky, P., & Steck, D.

Physics Department, University of Utah, Salt Lake City, UT 84112

## ABSTRACT

We have obtained the ratio of EAS total shower energy in the electromagnetic channel ( $E_{em}$ ) to the size of the shower at maximum development ( $N_{max}$ ) from a direct measurement of shower longitudinal development using the air fluorescence technique(1). The values obtained agree closely with those estimated by Linsley(2). However, they are not inconsistent with values based upon track length integrals of the Gaisser-Hillas formula for shower development(3) or the known relation between shower energy and size at maximum for pure electromagnetic cascades. Using Linsley's estimates for undetected shower energy(2) based on an analysis of a wide variety of cosmic ray data we obtain the following relation for total shower energy  $E$  vs  $N_{max}$ :  $E = 1.31 \pm .14 (N_{max}/10^9)^{0.990 \pm .005} \text{ GeV}$ . Using the Gaisser-Hillas implied undetected shower energy fractions, we obtain  $E = 1.53 \pm .16 (N_{max}/10^9)^{0.99 \pm .005} \text{ GeV}$ .

1. Introduction. The estimation of total EAS energy from shower size measurements at ground level depends, among other things, upon a knowledge of the conversion factor  $E/N_{max}$ (2,4). This factor has been derived by Linsley indirectly from a large body of existing cosmic ray data(2). In addition, it has been calculated from models of shower development incorporating scaling(3) and radial scaling(5). Values quoted range typically between 1.3 and 1.7 GeV/particle for EAS energies in the range .01-100 EeV (1 EeV =  $10^{18}$  eV) the precise value being dependent primarily upon estimates of undetected shower energy in the non-electromagnetic channel. We present below the results of the  $E_{em}$  vs  $N_{max}$  relationship obtained from a direct integration of EAS longitudinal development profiles as measured by the Fly's Eye detector. We then infer values for the total shower energy relationship to  $N_{max}$  based upon Linsley's estimates of undetected shower energy from cosmic ray data(2) as well as estimates inferred from the Gaisser-Hillas parameterization of shower longitudinal development(3).

2. Measurement. The Fly's Eye detector has been described in detail elsewhere(1). Essentially, the detector observes the passage of EAS thru the atmosphere via nitrogen fluorescence. Shower sizes vs depth are calculated from measured light yields and experimentally determined shower trajectories(1). Electromagnetic shower energy,  $E_{em}$ , and shower size at maximum  $N_{max}$  is determined by fits made to resultant longitudinal development curves. Shower energy is given by:

$$E_{em} = \frac{\epsilon_0}{X_0} \int N_e(x) dx$$

where  $N_e(x)$  is the shower size vs depth and  $\epsilon_0/X_0$  is the ratio of the critical energy of an electron to its radiation length in air, taken to be 2.18 MeV/electron g cm<sup>-2</sup> (6). We note that, if a shower development curve is represented by an equivalent Gaussian then

$$\frac{E_{em}}{N_{max}} = \sqrt{2\pi} \frac{\epsilon_0}{X_0} \sigma$$

where  $\sigma$  is the equivalent Gaussian width of the curve.

We have selected a sample of approximately 1150 showers observed during a 3 year interval whose equivalent Gaussian widths were measured to an accuracy of better than  $\pm 20\%$  and whose total observed track lengths subtended an angle in the sky of greater than  $60^\circ$ . This selection criterion ensured a sample of showers whose longitudinal profiles were well-known and whose subsequent ratios of  $E_{em}/N_{max}$  were determined to within  $\pm 20\%$ .

3. Results. Shown in Table 1 are the results of the measured  $E_{em}/N_{max}$  ratios as a function of total shower energy  $E_{tot}$ .

Table I.  $E/N_{max}$  vs  $E_{tot}$

Method	$E_{tot}$ (EeV)			
	.01	0.1	1.0	10.0
	$E_{em}/N_{max}$ (GeV/electron)			
E&M Cascade(8)	1.12	1.18	1.25	1.31
Gaisser-Hillas(3)	1.13	1.20	1.28	1.34
Linsley(2)	1.06	1.12	1.17	1.22
Measured	1.11 $\pm$ .09	1.17 $\pm$ .10	1.19 $\pm$ .10	1.20 $\pm$ .10
	Missing Energy (% of $E_{tot}$ )			
Linsley(2)	19	13	9	6
Gaisser-Hillas(3)	31	27	22	18
	$E_{tot}/N_{max}$ (GeV/electron)			
Measured(L)	1.37	1.34	1.31	1.28
Measured(GH)	1.16	1.60	1.53	1.46

In addition, we also show values of  $E_{em}/N_{max}$  derived in the following ways: (a) Pure electromagnetic cascades initiated by an electron (or photon) of energy  $E_{tot}$ , i.e.

$$N_{max} = \frac{0.31 E_{em}/\epsilon_0}{\sqrt{\ln(E_{em}/\epsilon_0) - 0.37}} \quad (7)$$

(b) By integrating the Gaisser-Hillas shower development curve(3) we obtain:

$$\frac{E_{em}}{N_{max}} = \frac{\epsilon_0}{X_0} \lambda \alpha^{-\alpha} \exp^{\alpha} \Gamma(\alpha+1)$$

where  $\lambda = 70$  g cm<sup>-2</sup> and  $\alpha = 0.51 \ln(E/\epsilon_0) - 1$

(c) Linsley's estimated values quoted in ref.(2).

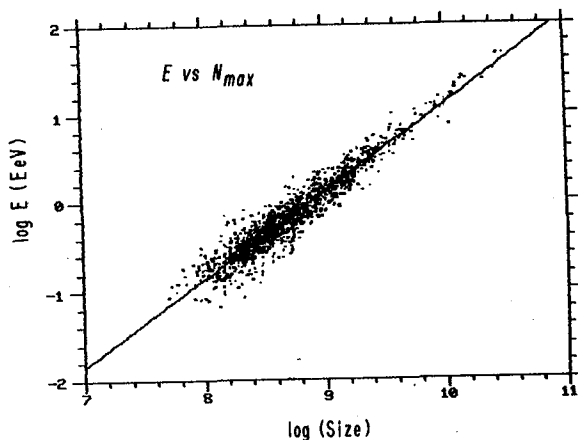
We note that the Gaisser-Hillas method yields  $E_{em}/N_{max}$  values remarkably close to those obtained from purely electromagnetic cascades. We also note that our measured values of  $E_{em}/N_{max}$  are in excellent agreement with the above estimates.

Finally, in order to convert  $E_{em}/N_{max}$  to  $E_{tot}/N_{max}$ , corrections for undetected shower energy (energy in the form of muons and neutrinos, undetected hadrons and nuclear excitation) must be applied. We have made such corrections in two ways primarily for the purposes of illustrating the uncertainties currently involved in accounting for total unobserved energy and thus obtaining the correct factors necessary to convert shower size measurements (or measurements of any other parameter basically dependent on the number of electrons in EAS) into total primary energy. The first estimate of missing energy is obtained directly from Linsley(2) who derives estimates of missing shower energy in a quite clever empirical fashion directly from measured electron and muon size spectra and the total assessed energy content of these respective components of the EAS. We have parameterized Linsley's estimates in the following way:

$$E_{em}/E_{tot} \cong 0.99 - .0782E_{tot}^{-0.175} \quad E_{tot} \text{ in EeV}$$

This parameterization is valid for  $1 \text{ PeV} < E < 100 \text{ EeV}$  and the resultant undetected energy percentages listed in Table 1.

Finally, we note that the amount of undetected energy based on the Gaisser-Hillas formula for shower development can be obtained directly from the values listed in Table 1 for  $E_{em}/N_{max}$  and noting that the Gaisser-Hillas formula is based on a constant value for  $E_{tot}/N_{max}$  of  $1.64 \text{ GeV/electron}$ . Thus the apparent undetected energy percentages inferred from the Gaisser-Hillas parameterization are as shown in Table 1. Finally, we also list in Table 1 the resultant  $E_{tot}/N_{max}$  ratios based on applying each of the above missing energy percentages corrections to the resultant measured values of  $E_{em}/N_{max}$  obtained directly from Fly's Eye data.



We note that the Gaisser-Hillas parameterization with its large amount of implied missing energy is based on fits to simulated showers which incorporate a simple scaling model with constant cross section for EAS development. Such models tend to generate penetrating showers in which the amount of undetected energy would be anticipated to be less than for those models

Figure 1. Scatter Plot of Total Shower Energy vs Shower Size at Maximum as Measured by the Fly's Eye Detector.

which led to more rapid shower development.

Finally, we show in Figure 1 a scatter plot of  $E_{\text{tot}}$ , assuming the Linsley estimates of missing shower energy, vs  $N_{\text{max}}$ . The best fit line is given by:

$$E_{\text{tot}} = 1.31 \pm .14 (N_{\text{max}}/10^9)^{0.990 \pm .005} \text{ GeV}$$

the scatter in the data points is due both to detector resolution as well as intrinsic fluctuations. Future work will concentrate upon an extraction of the detector resolution function in order to determine how much intrinsic scatter there is in  $N_{\text{max}}$  and thus its effect on total energy measurements which depend essentially on a measure of that parameter.

4. Acknowledgements. We gratefully acknowledge the United States National Science Foundation for its generous support of this work under grant PHY8201089.

#### References.

1. Nuclear Instruments and Methods (submitted 1985).
2. Linsley, J., Spectra, Anisotropies and Composition of Cosmic Rays Above 1000 GeV, Proc. 18th Int. Conf. Cosmic Rays, Bangalore, India 12, 135 (1983).
3. Gaisser, T.K., and Hillas, A.M., Proc. 15th Int. Conf. Cosmic Rays, Plovdiv, Bulgaria 8, 353 (1977).
4. Bower, A.J. et al. J. Phys. G: Nucl. Phys. 9, L53 (1983).
5. Hillas, A.M., Proc. of the Cosmic Ray Workshop, Univ. of Utah, ed. T.K. Gaisser, Bartol Res. Foundation of the Franklin Inst. Univ. of DE, Newark, DE 16 (1983).
6. Dozhenko, O.I., and Pomanskii, A.A., Soviet Physics JET P 18, 187 (1964).
7. Rossi, B., High Energy Particles, Prentice-Hall Inc., Englewood Cliffs, N.J., Chapt. 5 (1952).



## STANDARD VALUE FOR THE RADIATION LENGTH IN AIR

John Linsley  
 Department of Physics and Astronomy  
 University of New Mexico, Albuquerque, NM 87131  
 USA

## ABSTRACT

Following the Paris ICRC I did some additional research on the radiation length in air, which was reported in *Proceedings of the Paris Workshop on Cascade Simulations*. However no standard value was recommended because a few calculations remained undone. These have now been finished. They give new values for  $t_o$  in atomic oxygen and nitrogen which are entirely free of dependence on the Thomas-Fermi approximate model. With the usual small corrections for atmospheric A and CO<sub>2</sub>, these give  $t_o|_{\text{air}} = 37.15 \text{ g cm}^{-2}$ , in close agreement with a value recommended by Dovzhenko and Pomanskii, but in contrast to  $t_o|_{\text{air}} = 36.66 \text{ g cm}^{-2}$  obtained by Tsai using the Thomas-Fermi approximation.

1. Introduction. This concludes an inquiry concerning the radiation length in air, motivated by the importance of that unit in applying cascade theory to the interpretation of cosmic ray air shower data. The preceding installments provide background and more complete references (Linsley 1981a, 1981b).

2. Definitions. The radiation length  $t_o$  is customarily defined as follows:

$$(t_o)^{-1} = (N\sigma_o/A) [Z^2(L_{\text{rad}} - f) + ZL_{\text{rad}}'] , \quad (1)$$

where N is Avagadro's number,  $\sigma_o = 4\alpha r_o^2$  ( $\alpha$  the fine-structure constant,  $r_o$  the classical radius of the electron), A is the atomic weight and Z is the atomic number of the target atom, f corrects for use of the Born approximation,  $L_{\text{rad}}$  is the usual radiation logarithm given by

$$L_{\text{rad}} = \int_0^1 \frac{1}{(1-F)^2} \frac{dq}{q} + 1 , \quad (2)$$

where q is the momentum transfer in units of  $m_e c$  and F(q,Z) is the atomic form factor, and  $L_{\text{rad}}'$ , a quantity analogous to  $L_{\text{rad}}$ , takes into account collisions in which the scattering system is left in an excited state.

$$L_{\text{rad}}' = \int_0^1 \frac{1}{S} \frac{dq}{q} + 1 , \quad (3)$$

where S(q,Z) is the so-called incoherent scattering function. There is general acceptance of the Bethe-Maximon formula for f:

$$f(z) = z \sum_{n=1}^{\infty} n(n^2+z) \sim 1.202z - 1.0369z^2 + 1.008z^3 / (1+z) , \quad (4)$$

where  $z = (Z/137)^2$ . For N and O,  $f = 0.0031$  and  $0.0041$ , respectively.

3. Evaluation of Structure Dependent Terms. The effect of atomic structure on  $t_o$  is expressed mainly through  $L_{rad}$ . It was shown by Bethe (1934) that the Z-dependence of  $L_{rad}$  is given essentially by

$$L_{rad} = \ln(aZ^{-1/3}), \quad (5)$$

where  $a$  is called the elastic screening coefficient. Using the Thomas-Fermi model he obtained the widely quoted value 183 for  $a_{TF}$ .<sup>\*</sup> Recognizing the hazard in relying on a statistical model for an atom as light as N, Wheeler and Lamb (1939) recalculated  $L_{rad}$  for that element (and for hydrogen) using self-consistent wave functions of the Hartree-Fock type, obtaining a result equivalent to  $L_{rad}|_{SCF} = 4.56$ .

The need for taking into account inelastic scattering was noted first by Landau and Rumer (1938). Their estimate  $L_{rad}' \sim L_{rad}$  underestimates  $L_{rad}'$  by about 20% in case of elements as light as N and O, leading to errors in  $t_o$  of about 3%. A correct quantum mechanical formula equivalent to Eq. 3 was given by Wheeler and Lamb (1939). They used it to calculate  $L_{rad}'$  for N (and for hydrogen) using both the Thomas-Fermi model and self-consistent wave functions. Their result in the latter case was equivalent to  $L_{rad}'|_{SCF} = 5.47$ .

More recently, values of F and S based on accurate self-consistent wave functions have been tabulated for all the elements over a complete range of q-values (Hubbell et al. 1975). Using these data and Eq's (2) and (3) I have calculated  $L_{rad}|_{SCF}$  and  $L_{rad}'|_{SCF}$  for O as well as N, obtaining 4.490, 5.253 for O, and 4.554, 5.347 for N (in good agreement with the results of Wheeler and Lamb), respectively.

4. The Radiation Length in Air. The radiation length in a complex substance is given by the following expression (Rossi 1952):

$$(t_o)^{-1} = \sum_i p_i / (t_o)_i, \quad (6)$$

where  $p_i$  is the fraction by weight of the i-th atomic species. The data

---

\* The alternative value 191, frequently quoted although it is erroneous, apparently entered the literature through being recommended by Oppenheimer to Serber (1938, 1981). (In Serber's 1938 paper it is attributed to Bartlett, who visited Oppenheimer's group at Caltech about the time the paper was being written.) The value of  $a$  has been recalculated recently, but it is questionable whether the new result,  $a_{TF} = 184.15$  (Tsai 1974), is any more accurate than Bethe's, since the new calculation used an approximate parametrization of the Thomas-Fermi potential.

adopted here for calculating  $t_o|_{\text{air}}$  are given in Table 1. The present result is  $t_o|_{\text{air}} = 37.15 \text{ g cm}^{-2}$ .

Table 1. Calculation of Radiation Length in Air

i	$p_i$	$Z_i$	$A_i$	$f_i$	$(L_{\text{rad}})_i$	$(L_{\text{rad}}')_i$	note
1	0.05	6	12.0111	0.0019	4.618	5.403	(a)
2	75.52	7	14.0067	0.0031	4.554	5.347	(b)
3	23.14	8	15.9994	0.0041	4.490	5.253	(b)
4	1.29	18	39.9480	0.0204	4.252	5.081	(a)

note (a):  $L_{\text{rad}} = L_{\text{rad}}|_{\text{TF}} = \ln(183Z^{-1/3})$ ,  $L_{\text{rad}}' = L_{\text{rad}}'|_{\text{TF}} = \ln(1194Z^{-2/3})$  (Tsai 1974)

note (b):  $L_{\text{rad}} = L_{\text{rad}}|_{\text{SCF}}$ ,  $L_{\text{rad}}' = L_{\text{rad}}'|_{\text{SCF}}$

5. Comparison with Previous Results. Values of  $t_o$  for C, N, O and A, as well as air, are compared in Table 2 with values recommended in widely quoted reviews: 1) by Dovzhenko and Pomanskii (1964), and 2) by Tsai (1974). (Tsai's article is the authority for values given in the *Particle Properties Data Booklet*.) The results by Tsai are based entirely on the Thomas-Fermi model. Dovzhenko and Pomanskii used their own SCF calculations of  $L_{\text{rad}}$ . For  $L_{\text{rad}}'$  they used interpolated values based on Wheeler and Lamb's results for N.

Table 2. Radiation Length in C, N, O, A and air (units  $\text{g cm}^{-2}$ )

material	Dovzhenko & Pomanskii	Tsai	present work
C	43.3	42.70	43.33
N	38.6	37.99	38.53
O	34.6	34.24	34.83
A	19.7	19.55	19.57
air	37.1	36.66	37.15

6. Remaining Questions. Out of 7 questions listed previously (Linsley 1981b) there are 2 which have not been given definitive answers:

- 1) How great is the molecular binding effect in  $\text{N}_2$  and  $\text{O}_2$ ?

- 2) What is the relation between  $t_0$  defined by Eq. 1 and the electromagnetic cascade unit  $X_0$  defined by  $X_0 = X_{\max} / \ln(E/E_c)$ , where  $E_c$  is the critical energy and  $X_{\max}$  is the average depth of maximum development of simple cascades with energy  $E$ ?

Regarding (1): Using the conventional definition of  $L_{\text{rad}}$  (Eq. 2), the value I reported previously for molecular nitrogen (Linsley 1981a) becomes 4.50, 1.2% less than the best SCF value for atomic nitrogen. On the other hand, Bernstein and Panofsky (1956) showed that in the complete screening limit the effect of molecular binding in hydrogen is to increase  $\sigma_{\text{pair}}$  by 2.8%.

Regarding (2): The point of the distinction is that the quantity appearing in the elongation-energy relation should logically be  $X_0$  rather than  $t_0$ . Clearly,  $X_0/t_0$  is independent of the stopping medium to a high degree of accuracy. Landau and Rumer (1938), for approximation A, and Snyder (1949), for approximation B of electromagnetic cascade theory, give  $X_0/t_0 = 1.01$ . From tables given by Messel and Crawford (1970) I find  $X_0/t_0 = 1.04 \pm 0.02$ . Can additional results of this kind be derived from existing work?

## 7. References.

- Bernstein, D. and Panofsky, W. K. H. 1956, *Phys. Rev.* 102, 522.
- Bethe, H. A. 1934, *Proc. Cambr. Phil. Soc.* 30, 524.
- Dovzhenko, O. I. and Pomanskii, A. A. 1964, *Sov. Phys. JETP* 18, 187.
- Hubbell, J. H., Veigele, W. J., Briggs, E. A., Brown, R. T., Cromer, D. T., and Howerton, R. J. 1975, *J. Phys. Chem. Reference Data* 4, 471.
- Landau, L. and Rumer, G. 1938, *Proc. Roy. Soc. (London)* A166, 213.
- Linsley, J. 1981a, *Proc. 17th ICRC (Paris)* 11, 246.
- 1981b, *Proc. Paris Workshop on Cascade Simulations*, eds. J. Linsley and A. M. Hillas (Texas Center for the Advancement of Science and Technology, Albuquerque) p. 23.
- Messel, M. and Crawford, D. F. 1970, *Electron-Photon Shower Distribution Function Tables* (Oxford, Pergamon Press).
- Rossi, B. 1952 in *High Energy Particles* (Englewood Cliffs, NJ, Prentice-Hall).
- Serber, R. 1938, *Phys. Rev.* 54, 317.
- 1981, private communication.
- Tsai, Y-S. 1974, *Rev. Mod. Phys.* 46, 815.
- Wheeler, J. A. and Lamb, W. E. 1939, *Phys. Rev.* 55, 858, erratum 101, 1836 (1956).

## LONGITUDINAL TRIAL FUNCTIONS AND THE COSMIC RAY ENERGY SCALE

John Linsley

Department of Physics and Astronomy  
 University of New Mexico, Albuquerque, NM 87131  
 USA

## ABSTRACT

Formulae which have been proposed for representing the longitudinal profiles of cosmic ray air showers are compared, and the physical interpretation of the parameters they contain is examined. Applications to the problem of energy calibration are pointed out. Adoption of a certain especially simple formula is recommended, and its use is illustrated by means of examples.

1. Introduction. At all primary energies above  $\sim 10^3$  GeV, incoming cosmic ray nuclei deposit more than half of their energy via the soft component. At the highest observed energies the fraction  $E_{EM}/E$  approaches 90-95%, where  $E_{EM}$  is the energy deposited by the composite electron-photon cascade resulting primarily from  $\pi_0$  decay  $\gamma$ -rays. The single most important step, therefore, in determining the cosmic ray energy scale for  $E > 10^6$  GeV, where experiments above the earth's atmosphere currently give way to experiments using air showers, is measurement of  $E_{EM}$ .

The use of simple mathematical formulae to represent the *lateral* structure of extensive air showers began at an early stage in the study of shower phenomena (cf. Bethe quoted by Williams 1948), and such formulae continue to be useful tools. Analogous formulae for the *longitudinal* structure developed much later, possibly because accurate experimental data have taken much longer to obtain, and possibly because analytical methods have tended to be supplanted in recent years by Monte Carlo calculations.

With the advent of techniques for directly measuring the longitudinal profiles of individual air showers (Hammond *et al.* 1978, Grigoriev *et al.* 1979, Cassidy 1981, Cady *et al.* 1983) it seems an appropriate time to re-examine formulae that have been used to describe these profiles (Greisen 1956, Linsley 1967, Longo and Sestili 1975, Gaisser 1976 and 1979, Gaisser and Hillas 1977, Sass and Spiro 1978, Dyakonov *et al.* 1981). By analogy to formulae used for describing the lateral structure of various air shower components I will call them 'trial functions'. In case of lateral structure such functions have had an important role in comparing results of different experiments. One expects longitudinal trial functions to be useful in the same way. In case of the lateral structure of electrons, trial functions are also used in the conduct of experiments, to derive from raw data on shower density a global measure, the shower size  $N$ , as well as core location, age, and measures such as  $S_{600}$ . The corresponding step in dealing with profile data is to find  $N_m$ , long recognized as being one of the most reliable estimators of primary energy (Clark 1962), from data on  $N$  vs  $x$ . This step also yields  $x_m$ , the shower elongation, and may also yield the profile width  $\sigma_x$ . In case of the electronic lateral structure, trial functions are formulated in such a manner as to reflect the physical processes that govern cascade develop-

ment. Thus core distances are expressed in Molière units, and steepness is controlled by a parameter relating plausibly to shower age. One aspires to achieve similar success in case of the longitudinal structure.

2. Electromagnetic cascades. The longitudinal trial function proposed by Greisen (1956) provides a good illustration:

$$N = (0.31/\beta_0^{\frac{1}{2}}) \exp[t(1 - \frac{3}{2} \ln s)], \text{ where } s = 3t/(t + 2\beta_0). \quad (1)$$

Clearly its structure was influenced in several ways by theoretical results obtained with diffusion equations (see Rossi 1952):

- 1) Thickness is measured in units of the radiation length ( $t = x/x_0$ ).
- 2) Primary energy is measured in units of the critical energy  $E_C$  ( $\beta_0 = \ln(E/E_C)$ ).
- 3) There is a built-in elongation-energy relation,  $x_m = x_0\beta_0$ , which is approximately correct.
- 4) There is a built-in  $N_m$  relation,  $N_m = (0.31E/E_C)/[\ln(E/E_C)]^{\frac{1}{2}}$ , which is also approximately correct.
- 5) The shower age  $s$  is incorporated in an approximately correct manner.

The price paid for (5) is mathematical inconvenience. Expressions for  $N$ ,  $Nt$  and  $Nt^2$  cannot be integrated in closed form, so simple formulae for the track length integral, the average depth  $\langle x \rangle$  and the profile width  $\sigma_x$ , provided by the exact theory, must be patched on *ad hoc*.

An alternative form is the gamma distribution, recommended in the current *Particle Properties Data Booklet* for representing results from EGS, a well known Monte Carlo program for simulating electronic cascades. Gamma distributions have been chosen independently by several workers to represent air shower profiles as well. Indeed, the choice has been unanimous, and this is the choice recommended here.

3. Mathematical properties of gamma distributions. I will write this distribution in the form

$$N = N_0 \xi^q e^{-q\xi}, \quad (2)$$

calling the numerical constant  $q$  the 'index'. The optimum values of  $\xi$  and  $N$  are given by

$$\xi_m = 1, \quad (3) \quad N_m = N_0 e^{-q}, \quad (4)$$

while the mean value and variance are given by

$$\langle \xi \rangle = \frac{q+1}{q}, \quad (5) \quad \sigma_\xi^2 = \frac{q+1}{q^2}. \quad (6)$$

The normalization is given by  $\int N d\xi = \Gamma(q+1)/q^{q+1}$ , (7)

which admits approximation using Stirling's theorem

$$\int N d\xi \approx N_0 (2\pi/q)^{\frac{1}{2}} e^{-q} = N_m (2\pi/q)^{\frac{1}{2}}. \quad (8)$$

I propose to determine the parameters of (2) by using

- 1) the elongation-energy relation,  $x_m$  vs  $\ln E$  (note from (3) that  $\xi = x/x_m$ ),
- 2) a relation due to Kraushaar (1957) between the typical profile of an individual proton shower and the average profile of proton showers,
- 3) experimental data on  $\sigma_x$ , and on  $E_{EM}/E$ , the fraction of primary energy given to electrons.

First, however, I will show that (2) provides an excellent fit to electromagnetic cascade profiles.

4. Electromagnetic cascades revisited. Results of cascade theory in approximation B are (Rossi 1952):

$$x_m = x_0 (1.01\beta + A), \quad \langle x \rangle = x_0 (1.01\beta + B), \quad \sigma_x^2 = x_0^2 (1.61\beta + C), \quad (9)$$

where  $\beta = \ln(E/E_C)$  and A, B, C are constants  $\sim 1$  whose exact values depend on whether the primary particle is an electron or photon. Using (3) and substituting in (6) I solve for the index

$$q = 0.63 + D, \quad (10)$$

where  $D = -0.4, 0.2$  for primary electrons and photons, respectively.

Substituting this result in (5), I find

$$\langle x \rangle - x_m = 1.6x_0, \quad (11)$$

expressing the fact that the profile is unsymmetrical. To conserve energy the track length integral must equal E. Thus

$$\int (E_C/x_0) N dx = E. \quad (12)$$

Using (8), which I solve for  $N_m$ , and again substituting for q and  $x_m$ ,

$$N_m = (0.31E/E_C) / [\ln(E/E_C) - F]^{\frac{1}{2}}, \quad (13)$$

where  $F = 1.7, 1.0$  for primary electrons and photons, respectively. Results (11) and (13) are almost exactly the same as given by the detailed theory.

5. Application to air showers. One begins as in the preceding example, by letting  $\xi = x/x_m$ , where  $x_m$  is given by the elongation-energy relation. A reasonable choice for this is

$$x_m = A + D_{10} \log E \quad (14)$$

with  $A = 159 \text{ g/cm}^2$  and  $D_{10}$  (elongation rate per decade) =  $65 \text{ g/cm}^2$  (Linsley and Watson 1981; E is in GeV). The index q can be found as in the preceding example, using (6), but first I will show an alternative method illustrating a deep connection between gamma distributions and cascade processes.

It was pointed out by Kraushaar (1957) that the average number of electrons N at atmospheric depth x arising from a primary particle incident upon the top of the atmosphere is related as follows to the average number  $N_1$  of electrons at thickness  $x'$  below a nuclear interaction of such a particle:

$$N(x) = \int_0^x N_1(x') \exp[-(x-x')/\lambda] dx' / \lambda, \quad (15)$$

$$N_1(x) = [1 + \lambda(\partial/\partial x)]N(x), \quad (16)$$

where  $\lambda$  is the interaction mean free path of the particle, assuming that there are no fluctuations other than those in the starting level. Applying these, it is readily shown that the condition for N and  $N_1$  to be self similar; meaning in this case for one to be a gamma distribution if the other one is, is the following:

$$q = x_m / \lambda. \quad (17)$$

Substituting (17) in (6) one obtains a very interesting result,

$$\sigma_x^2 = \lambda^2 + \lambda x_m, \quad (18)$$

which can be combined with (14), giving

$$\sigma_x^2 = (\lambda^2 + A\lambda) + \lambda D_{10} \log E. \quad (19)$$

This says that if the energy dependence of  $\lambda$  is neglected, the energy dependence of  $\sigma_x^2$  has the same form as that of  $x_m$ , just as it does in case of electromagnetic cascades. The energy dependence is described by a rate, analogous to the elongation rate, which is in fact proportional to the elongation rate. This new rate, which might be called the 'width rate' or 'spreading rate', is equal to  $\lambda D_{10}$ .

An experimental result on  $\sigma_x$  has recently been reported by the Fly's Eye group. The value given,  $220 \pm 33$  g/cm<sup>2</sup> at  $10^9$  GeV (Baltrusaitis et al. 1985), agrees very well with a value derived from an average profile published by Grigoriev et al. 1983 for a slightly lower energy. Substituting the average of these results, and values of A and  $D_{10}$ , in (19), one finds  $\lambda = 58$  g/cm<sup>2</sup>.

This is appreciably greater than the mean free path for proton-air inelastic collisions found by other methods (see conference paper HEL.1-1). It is reasonable to assume that  $\lambda$  is greater than  $\lambda_{pa,inel}$  for the same reason that holds in similar cases: neglect of development fluctuations. This needs further study. Pending results of such a study, a reasonable estimate of  $\sigma_x^2$  for energies other than  $10^9$  GeV is obtained by assuming that  $\lambda$  is constant with the value found above. Then

$$q = 3.36 + 1.12 \log E, \quad (20) \quad \text{and} \quad \sigma_x^2 = 1.5 \cdot 10^4 + 3.8 \cdot 10^3 \log E \quad (21)$$

The remaining parameter in (2),  $N_0$ , is found in the same manner as for electromagnetic cascades, using (7) or (8), keeping in mind, of course, that the track length integral equals  $E_{EM}$ , not E. The relation between  $E_{EM}$  and E is discussed in conference paper OG5.1-5 (or see Linsley 1983). A convenient formula representing results of that work is

$$E_{EM}/E = 1 - 2.8E^{-0.17} \quad (E \text{ in GeV}) \quad (22)$$

References. BALTRUSAITIS et al. 1985, Phys. Rev. Lett. 54, 1875; CADY et al. 1983, Proc. 18th ICRC 11, 412; CASSIDAY 1981, *Proton-Antiproton Collider Physics* (Am. Inst. Phys.: New York) p. 528; CLARK 1962, J. Phys. Soc. Japan 17, Suppl. A-III, 286; DYAKONOV et al. 1981, Proc. 17th ICRC 6, 106; GAISSER 1976 private communication; 1979, *Proc. Air Shower Workshop Univ. Utah* (Bartol Foundation, Newark NJ) p. 57; GAISSER and HILLAS 1977, Proc. 15th ICRC 8, 353; GREISEN 1956, *Progress in Cosmic Ray Physics* (North-Holland: Amsterdam) Vol. 3; GRIGORIEV et al. 1979 ZhETP 30, 747; 1983, Proc. 18th ICRC 6, 204; HAMMOND et al. 1978, *Nuovo Cimento* 1C, 315; KRAUSHAAR 1957, *Nuovo Cimento Suppl.* 8, 623; LINSLEY 1967, Rev. Sci. Instrum. 38, 1268; 1983, Proc. 18th ICRC 12, 135 (see also paper OG5.1-4, this conference); LINSLEY and WATSON 1981, Phys. Rev. Lett. 46, 459; LONGO and SESTILI 1975, Nucl. Instrum. Meth. 128, 283; ROSSI 1952, *High Energy Particles* (Prentice-Hall: Englewood Cliffs NJ); SASS and SPIRO 1978, CERN pp Tech. Note 78-32; WILLIAMS 1948, Phys. Rev. 74, 1689.



EAS Development Curve at Energy of  $10^{16} - 10^{18}$  eV Measured by Optical Cerenkov Light

T.Hara, M.Daigo\*, M.Honda, K.Kamata, T.Kifune, Y.Mizumoto\*\*, M.Nagano, Y.Ohno and G.Tanahasni

Institute for Cosmic Ray Research, University of Tokyo, Tokyo, 188 Japan

\* Wakayama Medical College, Wakayama-shi, Wakayama, 649-63 Japan

\*\* Fujitsu Limited, 1-17-25, Shinkamata, Ohta-ku, Tokyo, 144 Japan

The data of optical Cerenkov light from extensive air shower observed at the core distance more than 1 Km at Akeno are reexamined. Applying the new simulated results, we reconstruct the shower development curves for the individual events. For the showers of  $10^{17}$  eV the average depth at the shower maximum is determined to be  $660 \pm 40$  gcm<sup>-2</sup>. The shower curve of average development is found to be well described by a Gaisser-Hillas shower development function with above shower maximum depth.

1. Introduction. The Cerenkov light from EAS is one of the most important observables to know the EAS development. In order to know the shower maximum depth for EAS of  $10^{16} - 10^{18}$  eV, the Cerenkov pulse shapes from EAS's at more than 1Km from the core are observed at Akeno air shower array by using 3 large telescopes(1). The data were analyzed by using the relation between the characteristics of Cerenkov pulse and the average development of showers in previous paper(2). In this paper we reanalyze the data for the construction of shower development curve by taking into account the first interaction depth, which is found to be important in interpretation of Cerenkov pulse shape.

2. Simulation results. The calculation of pulse shape of Cerenkov light from EAS was carried out with the same assumptions and procedures for showers of average development as in ref.3 except the model of atmospheric attenuation of Cerenkov light. The fraction of light reaching the observation level can be expressed by  $\exp(-x/\Lambda)$ , where x is the path length of Cerenkov light in the atmosphere. A constant value  $\Lambda$  (18Km) was assumed in the previos paper but here we use the same model as

that of Hillas(4), which is a function of atmospheric depth. The effect of the first interaction depth of primary cosmic rays to Cerenkov pulse shape was calculated with various interaction models. In this calculation, observation level is taken to be 700m a.s.l., where the telescopes are set in Akeno air shower array.

2-1. Cerenkov yield per particle at the depth of photon source.

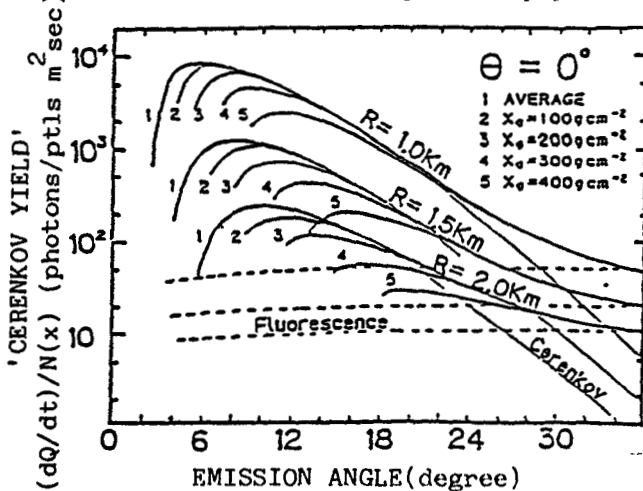


Fig.1 'Cerenkov yield' and photons from fluorescence.

In fig.1 is shown 'Cerenkov yield',  $(dQ/dt)/N(x)$ , observed number of Cerenkov photons

divided by the electron size at the light source level in the atmosphere. As shown in the previous paper the 'Cerenkov yield' is independent of the interaction models at 1 - 2 Km from the core. This is also indicated by Ivanenko et al. up to less core distance(700m)(5). This value is a function of the height of photon emission in the atmosphere(x), zenith angle of the shower( $\theta$ ), distance from the core(R) and also the first interaction depth of the primary cosmic ray( $X_0$ ). The abscissa of fig.1 is the emission angle of Cerenkov light to the shower axis. The fluorescent light from EAS is also shown in fig.1. If above parameters are experimentally determined we can construct the shower curve in the atmosphere from the Cerenkov pulse shape using the relation of fig.1. 2-2. The EAS path length in the atmosphere corresponding to the full

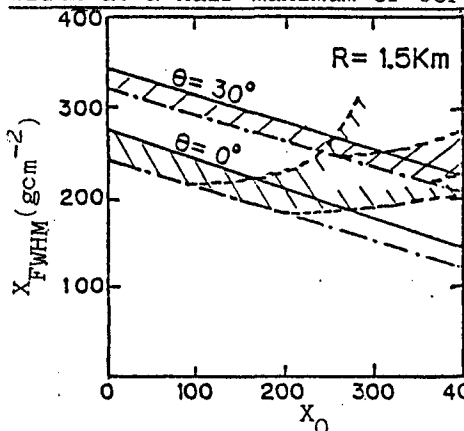


Fig.2 Relation between  $X_0$  and  $X_{FWHM}$ .

width at a half maximum of Cerenkov pulse is well known to have a good relation to the longitudinal development of EAS, especially to the shower maximum depth, but it has a poor relation to  $X_0$ . Here we find a parameter which has a good relation to  $X_0$ , that is,  $X_{FWHM}$ , the atmospheric depth which the EAS passes through during the time of FWHM of Cerenkov pulse. Fig.2 shows the relation between them. The parameter of  $X_{FWHM}$  is a function of  $\theta$ , R,  $X_0$  and the shower maximum depth( $X_{max}$ ). Our calculation is made in the range of  $X_{max}$  from  $450gcm^{-2}$  to  $800gcm^{-2}$  for showers of average development. In fig.2 solid and chain lines show the relation of  $X_{FWHM} - X_0$  for showers of extremely fast and slow development respectively in our calculation. The contribution of fluorescent light from EAS is also shown by broken lines for two extremely developed showers. Consequently showers concerned in the present paper distribute in the hatched regions in fig.2. If we know the value of  $X_{FWHM}$  we can estimate  $X_0$  with an error of about  $100gcm^{-2}$  for such showers that Cerenkov light photons exceed the fluorescent light.

### 3. Data analysis and results.

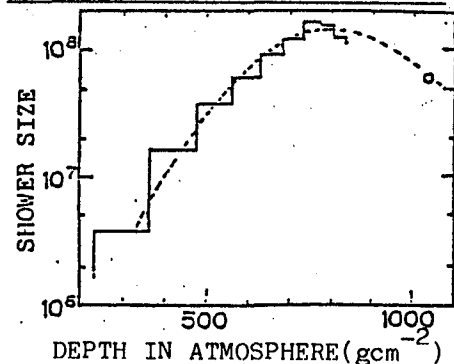


Fig.3 An example of shower curve determined from Cerenkov pulse wave.

The data taken in 1981 and 1982 are reanalyzed. In the measurement of Cerenkov pulse, the time resolution is 100ns and the space resolution in the atmosphere is  $4.5^\circ \times 4.5^\circ$ . Details of the experiment are described in ref.2. Finally 62 events were analyzed in order to determine  $X_{max}$  of EAS. Among them 38 events which have clear Cerenkov signals in more than 4 phototubes are selected.

First of all, for each event  $X_{FWHM}$  is determined from the Cerenkov pulse shape using shower parameters from the particle array and then  $X_0$  is estimated in most case within the error of about  $100gcm^{-2}$  by using the relation of fig.2. If we know  $X_0$  we can construct the shower development

curve in the atmosphere from the Cerenkov pulse shape by using the relation of fig.1. Fig.3 shows an example of the shower development curve thus determined. In this experiment the space resolution in the

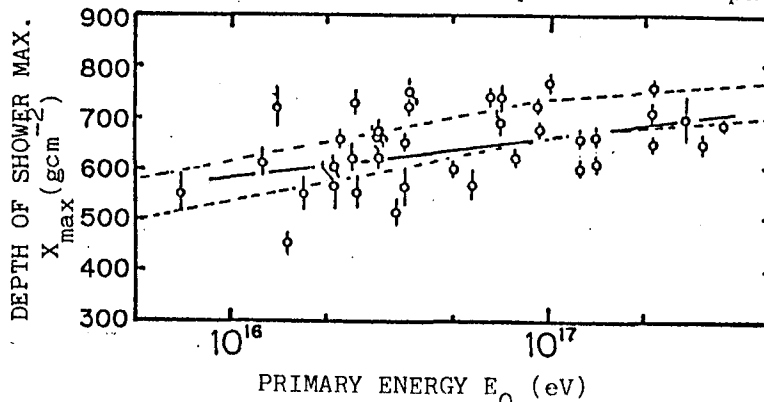


Fig.4 Shower Maximum depth determined by Cerenkov events.

atmosphere is limited by the time resolution of the registration system(100ns) for the Cerenkov pulse shape. In fig.3 open circle shows the shower size determined by the particle array for the event and broken line is a curve smoothly connected the data. From fig.3 we can determine both the depth of shower

maximum and the maximum shower size( $N_{max}$ ). The primary energy( $E_0$ ) is obtained by multiplying  $N_{max}$  by a constant value of  $1.4\text{GeV}(5)$ .

Fig.4 shows the relation between  $X_{max}$  and  $E_0$  for all events determined by the same procedure. The values of  $X_{max}$  for events which apparently penetrate in the atmosphere( $X_0 > 100\text{gcm}^{-2}$ ) are corrected by subtracting of  $X_0$ . The determination error of  $E_0$  is estimated to be about  $\pm 20\%$  which is mainly due to the uncertainty of the background contribution to the data. In fig.4 solid line shows the least square fit for these data. Two broken lines show the region where almost all other experimental results are distributed(7). Our results seem to be consistent with other results. From fig.4 the average value of  $X_{max}$  at the primary energy of  $10^{17}\text{eV}$  is  $660 \pm 40\text{gcm}^{-2}$ .

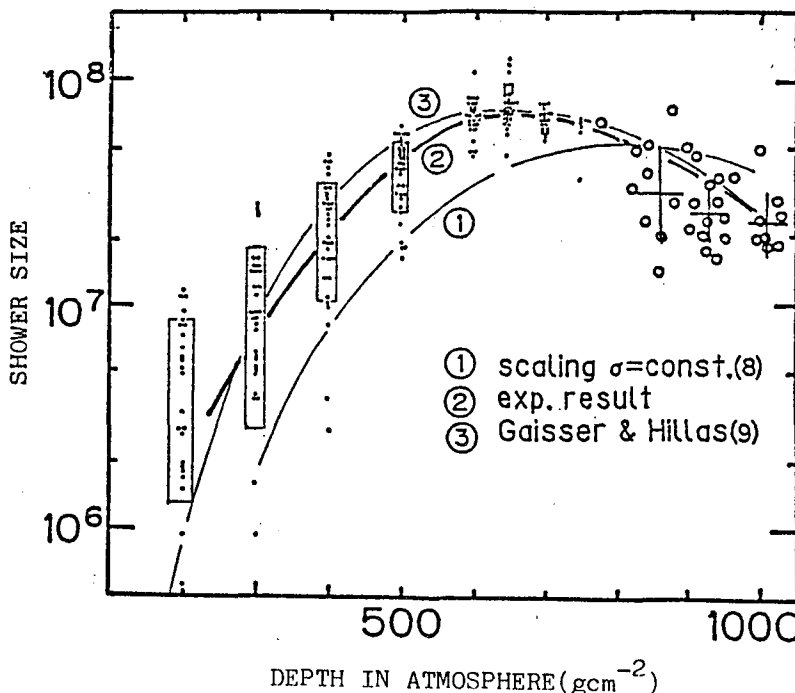


Fig.5 Shower development curve.

In order to know the average longitudinal development curve of showers, all data are normalized to the primary energy of  $10^{17}\text{eV}(E_{17})$  and to the maximum depth of  $660\text{gcm}^{-2}$  using the average relation in fig.4 as follows.

(1) First the shower maximum depth of each event is moved to the average one of the same primary energy( $E$ ) in fig.4 and then the each atmospheric depth of the

shower curve is normalized to that of the primary energy of  $10^{17}$  eV.

(2) Secondly each shower size(N) at each atmospheric depth determined from the Cerenkov pulse is normalized to that of the primary energy of  $10^{17}$  eV by dividing a constant factor of  $(E/E_{17})$ .

Fig.5 shows normalized shower developments of 38 events (small points). In fig.5 squares show the one standard deviation of data distribution in shower size of  $\log(N)$  and the ambiguity of the atmospheric depth determination. Open circles are shower sizes at Akeno level determined by the particle array. Crosses show the average and one standard deviations for the shower size determined by the particle array. Thick solid line is the curve smoothly connected to the average points of shower size distributions at each atmospheric depth except that of  $200\text{gcm}^{-2}$  where the effect of backgrounds seems to be serious. Then, thick solid line (denoted by ②) is the average development curve of showers of  $10^{17}$  eV normalized to the depth at the maximum development.

In comparison with data two curves are shown in fig.5. One is the simulation by Ivanenko et al. with the assumption of primary proton and constant cross section with scaling law(8) and the other is the shower development function by Gaisser and Hillas(9) with  $660\text{gcm}^{-2}$  for  $X_{\text{max}}$ . In most case, theoretical average curves are averaged over different starting points, and so can not directly be compared with our experimental one which is normalized at the depth of shower maximum. But when the depth of shower maximum is moved to the same one, the shape of shower development curve can be compared with our result except that in deep atmosphere. From fig.5 the average development of showers of energy  $10^{17}$  eV is well described by the Gaisser-Hillas development function.

4. Acknowledgments. The authors would like to thank the member of Akeno group for their help. Analysis and calculation were done by FACOM M380 at the computer room of Institute for Nuclear Study, University of Tokyo.

#### References

- 1) Y.Mizumoyo and T.Hara Proc. of Cosmic Ray Workshop, Univ. of Utah p99(1983)
- 2) M.Daigo et al. 18th ICRC 11 406(1983)
- 3) T.Hara et al. 15th ICRC 8 308(1977)
- 4) A.M.Hillas J. Phys. G;Nucl. Phys. 8 1475(1982)
- 5) I.P.Ivanenko et al. 16th ICRC 9 88(1979)
- 6) A.M.Hillas Proc. of Cosmic Ray Workshop, Univ. of Utah p16(1983)
- 7) M.Nagano 18th ICRC 12 425(1983)
- 8) I.P.Ivanenko et al. 16th ICRC 9 83(1979)
- 9) T.K.Gaisser and A.M.Hillas 15th ICRC 8 353(1977)

MISSING ENERGIES AT PAIR CREATION

Ahmed Abu El- Ela  
Department of Physics, Faculty of Science  
Mansoura University, Mansoura, Egypt  
Soad Hassan and Erich R. Bagge  
Institut fuer Reine und Angewandte Kernphysik  
der Universitaet Kiel, Olshausenstrasse 40-60  
2300 Kiel, W.-Germany

ABSTRACT

Wilson cloud chamber measurements of the separated spectra of positrons and electrons produced by gamma quanta of 6.14 MeV are differing drastically from the theoretically predicted (identical) spectra by BETHE and HEITLER, but are in good conformity to those of a modified theory of pair creation by one of the authors (B).

1. The experimental arrangement

A Wilson cloud chamber of the Blackett type (30 cm in diameter, 6 cm illuminated depth), filled with Helium at 1.2 bar gas pressure and a water alcohol mixture was operated to investigate pair creation by gammas of 6.14 ; 6.90 ; 7.11 and 8.87 MeV. These quanta will be emitted after irradiation of UREA (produced with highly enriched N15-nuclei) by the neutrons in the tangential hole of the 18 MW swimming pool reactor of the GKSS-Research-Centre Geesthacht near Hamburg. The cylindrical glass ring of the cloud chamber had a hole of 1 cm diameter, covered by a thin plexiglass foil to allow the gammas entering of the expansion room without passing the glass. Two Helmholtz coils produced inside the chamber a nearly homogeneous magnetic field of 703 Gauss (deviations from the homogeneity less than 1% within the illuminated volume). Helium was used to reduce the stopping power of the gas and also its motions due to its small expansion ratio (1.07 for  $\kappa=1.67$ ). By this way positrons of energies above 30 KeV became measurable. But also below this limit pairs were still recognizable and could be distinguished from Compton electrons although the energies could not be determined precisely enough to present credible values.

The cloud chamber was installed at a distance of about 6 m from the reactor behind its 3.5 m concrete radiation shield. After an irradiation for at least one minute in the middle of the tangential hole a cartridge filled with 0.7 g UREA was transported within 3.2 sec to a lead bloc at the cloud chamber by a pressurised pipe line. A hole in the lead bloc "focussed" the gammas to a 25  $\mu$ m gold foil inside the chamber.(Fig.1)



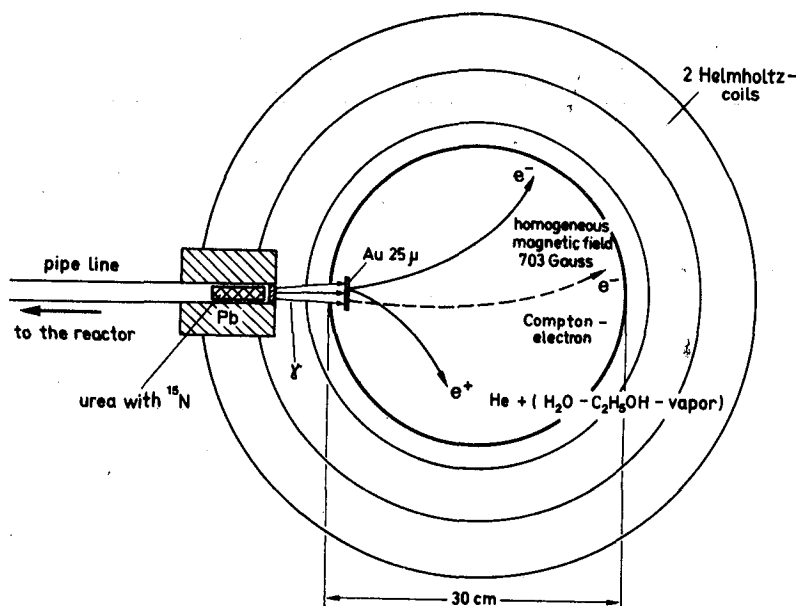


Figure 1. The Wilson cloud chamber arrangement with the Helmholtz coils, the pipe line for the cartridge transport and the 25  $\mu$ m gold foil as target for the pair production.

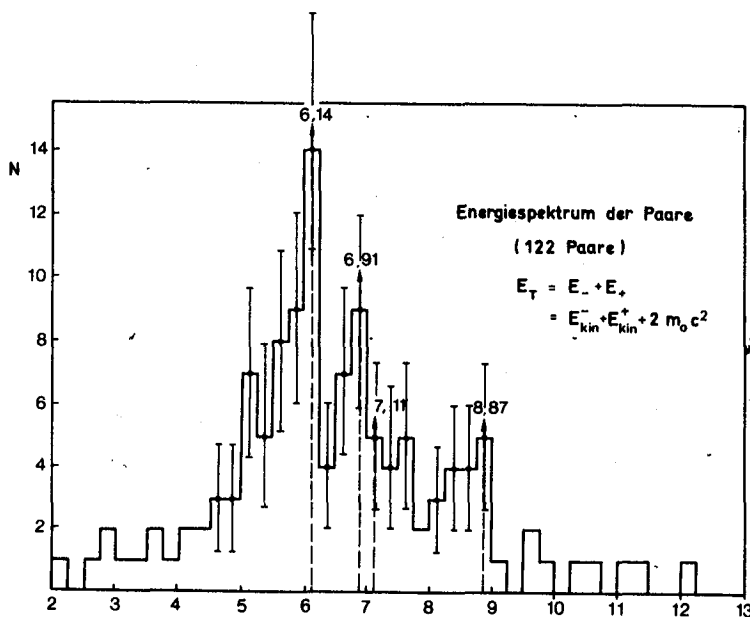


Figure 2. The energy sum spectrum of the positron-electron pairs produced by gamma quanta of 6.14; 6.90; 7.11 and 8.87 MeV. These quanta are emitted by  $^{16}\text{O}$ -nuclei, generated by irradiation of  $^{15}\text{N}$ -nuclei with the thermal neutrons of a swimming pool reactor and a subsequent  $\beta$ -decay of 7.13 sec lifetime.

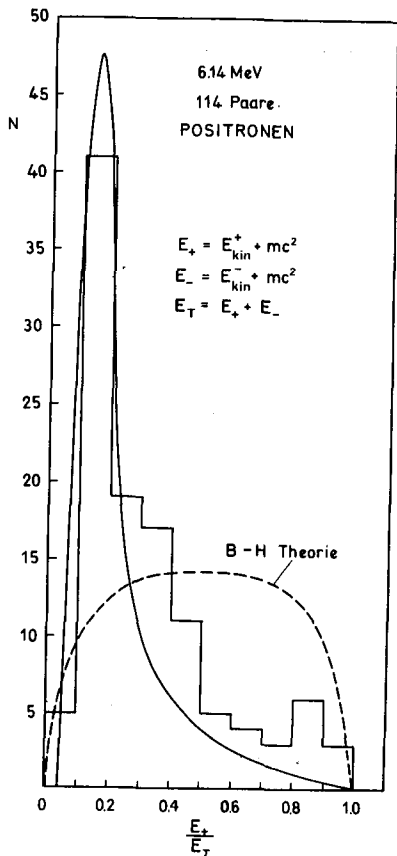


Figure 3.

The positron spectrum of 114 pairs created by 6.14 MeV quanta alone. Noteworthy is the high frequency of low kinetic energy positrons in full contradiction to BETHE and HEITLER's theoretically predicted (dotted) curve [2].

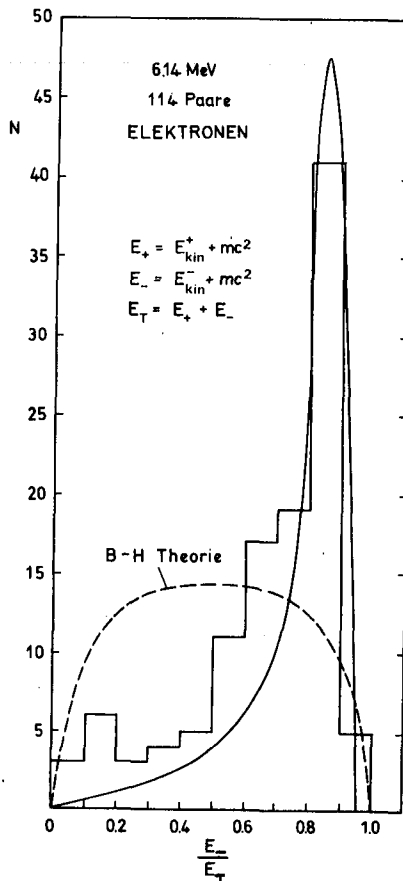


Figure 4

Here the corresponding electron spectrum of the same pairs as in figure 3 shows that these particles received mainly the highest possible energies at pair creation by the 6.14 MeV-quanta. There is no chance to say that positrons have identical spectra as BETHE and HEITLER's theory did it. The solid curves in the two figures 3 and 4 are derived in a modified theory of pair creation by BAGGE [3].



Transition Effect of Air Shower Particles in  
Plastic Scintillators

K.Asakimori and T.Maeda

Department of physics, Kobe University,  
Nada-Ku, Kobe 657, Japan

T.Kameda

Kobe Women's University, Suma-Ku, Kobe 654, Japan

K.Mizushima

Kobe Women's Junior College, Chuo-Ku,  
Kobe 650, Japan

Y.Misaki

Research Center for Nuclear Physics,  
Osaka University, Ibaraki,  
Osaka 567, Japan

ABSTRACT

Transition effect of air shower particles in the plastic scintillators near the core was measured by scintillators of various thickness. The air showers selected for the measurement were of size  $\geq 10^5$ . Results obtained are as follows:

- i) The multiplication of shower particles in the scintillators is less than 20% for that of 50mm thickness.
- ii) Dependence of the transition effect on age parameter is not recognized within the experimental errors.

1. Introduction In order to obtain an accurate density of air shower particles, it is essential to know the distortion caused by the materials which compose the detector and the surrounding container.

The transition effect of the shower particles due to plastic scintillators and iron plate of the container was investigated in detail (1), and multiplication of 10% was recognized near the core of air showers for the plastic scintillators of 50mm thickness.

However, some group reports that multiplication of  $> 50\%$  for the scintillator of 50mm thickness exists near the core compared to that of 3mm thickness, and that the transition depends remarkably upon the age parameter (2).

To reveal the contradiction, transition effect in the scintillators was studied by comparison of the response of each scintillator of different thickness which piled up in layer above and below.

2. Experiment and Results. Four sets of detectors composed of two plastic scintillators of different thickness piled up above and below, were placed in the air shower array of Kobe University. All scintillators are of  $0.25\text{m}^2$  area. The thickness of the plastic scintillators of each set is listed in Table 1. Measurement was carried out during the period from December 1983 to June 1984 and about 6000 showers which

had size of  $\geq 10^5$  and zenith angle less than  $30^\circ$  were selected. Using these showers, the transition effect of the shower particles near the core (within 30m from the core) was studied.

Table 1 Combination of Thickness of scintillators (mm)

upper scintillator	30	10	3	3
lower scintillator	50	20	50	50

A multiplication (or absorption) factor was obtained by dividing particles of lower scintillator by those of upper one. Fig. 1 shows mean values of the multiplication factors as a function of distance from the core of the showers, having size  $\geq 10^5$  and age parameter  $0.5 \leq s < 1.5$ . In every case, mean value of multiplication factors exceeds one near the core, and decreases gradually as the distance increases, and becomes less than one at distance farther than 10m. None of the cases shows a multiplication factor exceeding by 20% near the core. Rate of multiplication (or absorption) is largest for the combination (30mm, 50mm), and combinations (3mm, 50mm) and (10mm, 20mm) are in order of decrease. These trends are well explained considering the cascade of electron components in the showers.

To study a dependence of shower age on the transition effect, showers were divided into 3 groups showers of age parameter  $0.8 \leq s < 1.0$ ,  $1.0 \leq s < 1.2$ , and  $1.2 \leq s < 1.4$ , and for each group multiplication factor on the distance from the core were obtained.

Fig. 2 represents the results, and the figure shows that any obvious dependence does not exist within the experimental errors

3. Discussion Four sets of detectors give us consistent values of multiplication factors each other, and we can safely say that the results mentioned above are in accordance with those obtained previously for scintillators of thickness 50mm does not exceed by 20%.

Our results are in disagreement with those of Akeno group. Disagreement may be caused by the different arrangement of detectors. We used the scintillators piled up directly, and they placed the thin scintillators independently among the array. Accordingly, their results reflect sharply the accuracy of location of the cores, compared to our cases.

Applying the results obtained by us and approximating the lateral distribution to NKG function, use of the plastic scintillators of thickness 50mm give us smaller value of age parameter by 0.03 independent of the values of age parameter, and it gives little effect on the shower size.

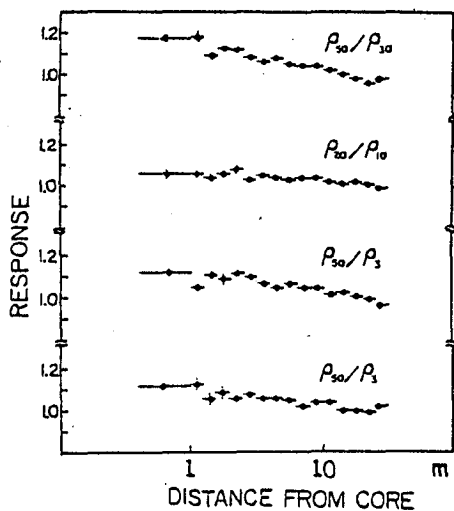


Fig. 1

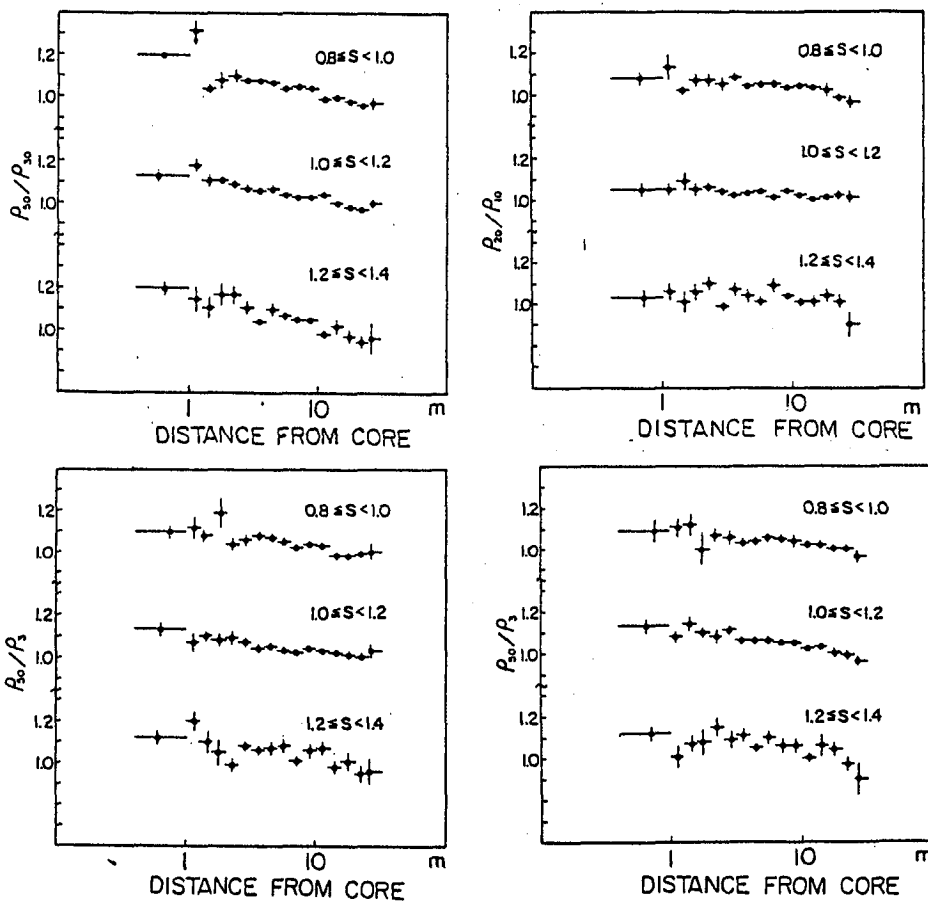


Fig. 2

## Reference

- (1) K.Asakimori et al.: Proc. 16th Int. Conf. on Cosmic Rays,  
Kyoto 8 (1979) 252
- (2) M.Nagano et al.,: J.Phys. Soc. Jpn. 53 (1984) 1667

## THE SYSTEM OF EAS TIME ANALYSIS

A.Z.KHALAFYAN, V.M.MKHITARYAN, J.S.OGANEZOVA

Yerevan Physics Institute, Markarian st. 2  
375036, Yerevan, Armenia, USSR

G.L.BASHINDJAGHYAN, N.B.SINEV, L.I.SARYCHEVA

Institute of Nuclear Physics,  
Moscow State University,  
117234, Moscow, USSR

## ABSTRACT

In studying the extensive air showers (EAS) it is important to have information for determining the EAS front shape, angle of incidence, disk thickness, particle distribution along the shower, on the delayed and EAS front advancing particles. The suggested system of the EAS time analysis allows one to determine the whole EAS longitudinal structure at the observation points. For this purpose the whole information from the detectors is continuously recorded in the memory with the memory cell switching in 5 ns, this enabling one to fix the moment of pulse input from the detector with an accuracy to  $\pm 2.5$  ns. Along with the "fast" memory, a "slow" memory with the cell switching in  $1\mu\text{s}$  is introduced in the system, this permitting one to observe relatively large time intervals with respect to the trigger (master) pulse with an appropriately lower accuracy ( $\pm 0.5\mu\text{s}$ ).

The methods of EAS structure analysis used at present are based on measuring the mutual delays between the operations of separate detectors or detector groups. One of the detectors switches on the time counter, and the other switches it off.

The suggested system principally differs from the existing ones by the fact that the information from each detector of the system is recorded continuously in the memory with memory cell switching in 5 ns.

At present, the system model connected to the EAS four detectors is tested on the PION installation.

As the memory capacity of each channel is limited, after filling all its cells (128 in the model) the further information is again recorded in the first cell, then in the second, and so on. Thus, every time moment in the channel memory there is an information on the particles striking the detector for the previous  $128 \times 5 = 640$  ns.

After the input of the trigger, the output of which is determined by the experiment conditions, the memory cells switch for another 320 ns, the readout being feasible after that. The information about all the particles that passed through the system detectors before and after the trigger within  $\pm 320$  ns is received by the computer. This time range may be extended by increasing the memory volume.

To extend the system possibilities, along with the "fast" memory a "slow" memory with cell switching in  $1 \mu s$  is introduced in it (the time interval in the model is  $\pm 64 \mu s$  with respect to the trigger).

Apparatus. The signal from the scintillation detector photomultiplier (PMT) is fed to the amplifier-limiter A (fig.1) located in the close proximity to it, and then

over the coaxial cable - to the memory block, where through the peaker P and shaper S is received by two shift registers Rg1 and Rg2.

Simultaneously, from the control unit CU the stable-frequency pulses are received, which in the phase inverter PI are separated into pulses of the same polarity, but out of phase by  $\frac{1}{2}$  period, that control the operation of Rg1 and Rg2 (K500UP141).

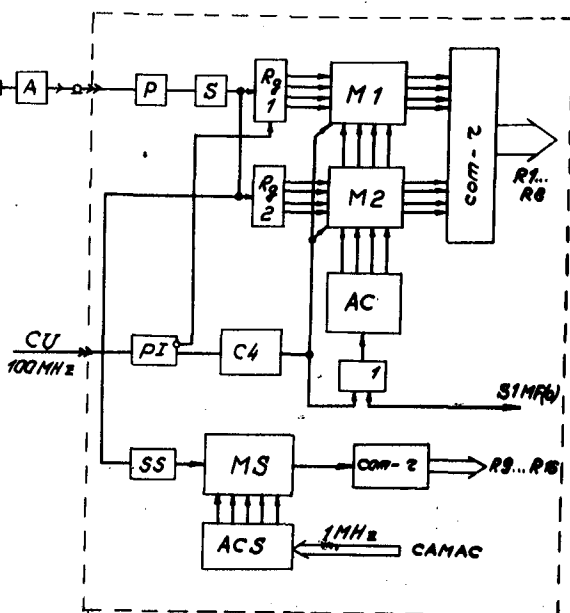


Fig.1. Block diagram of the time channel.

The real frequency of recording rises up to 200 MHz owing to register alternation. The recording from the registers in the memories M1 and M2 (K500PY145) of 64-bit capacity each is realized after filling the registers of 25 MHz frequency. (In the future, with appearance of more speedy microcircuits it will be possible to operate without shift registers and to record the information directly in the memory.) The record permitting pulses are received from the counter C4, and the simultaneous switching of M1 and M2 addresses - from the address counter AC.

The slow memory is organized analogously, but without shift registers. The address counter controlling the MS operation receives 1 MHz stable frequency pulses from the control unit.

The control unit (fig.2) is located in a separate module and is intended for the control of one crate memory blocks.

The quartz generator G produced 100 MHz pulses which are applied to the memory blocks through the key K and splitters. The fast shower master is received by the "stop" input of the control trigger CT. Having counted off 64 pulses of the generator G, the counter C64 closes the key K through the key K1, owing to which the information continues to be recorded in the memory cells for another 320 ns after the fast master

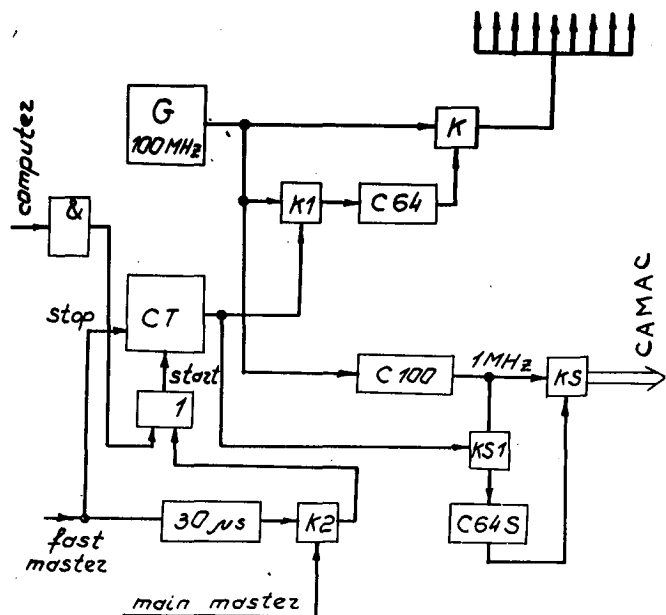


Fig.2. Control unit.

input. If during  $30\mu s$  the main shower master is not received by the other CU input, then in  $30\mu s$  the fast master pulse will be applied to the CT "start" input. The key K

opens and the information from the detectors again starts to be recorded in the memory cells. And the main master input closes the key K2 and the CT remains in the "stop" position until from the computer a record permitting pulse is received that returns the CT to the "start" position.

The receipt of switch pulses to the slow memory is organized analogously. The keys KS and KS1 together with the counter C64S allow to generate 64 pulses more after the fast master input.

In reading, a fixed number of address switching pulses (64) from the computer is received by the same address counters. This allows one to start the readout from the cell in which the information was recorded at the most remote moment of time ( $-320$  ns). The pulse number unambiguously reflects the information advance or delay time with respect to the master, this allowing one to operate without introducing the memory cell addresses and, particularly, the master address, into the computer.

The authors are very grateful to V.V.Avakyan for the problem statement and active assistance in the work, to E.A.Mamidjanyan for the support as well as to A.S.Beglar-yan and K.S.Gabrielyan for the help in drawing up the programmes of information detection and processing.



ON THE DETERMINATION OF THE DEPTH OF EAS DEVELOPMENT  
MAXIMUM USING THE LATERAL DISTRIBUTION OF CERENKOV LIGHT  
AT DISTANCES  $< 150$  m FROM EAS AXIS

N. Aliev, T. Alimov, M. Kakhkharov, B.M. Makhmudov,  
N. Rakhimova, R. Tashpulatov  
Samarkand State University, Samarkand, USSR

N.N. Kalmykov, G.B. Khristiansen, V.V. Prosin  
Institute of Nuclear Physics, Moscow State University,  
Moscow 119899, USSR

ABSTRACT

The Samarkand EAS array was used to measure the mean and individual lateral distribution functions (LDF) of EAS Cerenkov light. In the interval of distances  $r = 20-150$  m, the functions are approximated to take the form  $q(r) \sim \exp(b \cdot r/10^4)$ . The analysis of the individual parameters  $b$  has shown that the mean depth of EAS maximum and the variance of the depth distribution of maxima of EAS with energies of  $\sim 2 \times 10^{15}$  eV can properly be described in terms of Kaidalov-Martirosyan quark-gluon string model (QGSM).

The Samarkand EAS array has been described in detail in /1/. The present work uses the experimental data obtained in 1983 when the EAS array consisted of 13 Cerenkov light detectors, each of which included from 7 to 10 FEU-49 photomultiplier tubes, arranged at distances of 15-120 m from the array center and 18 scintillators of  $0.5-2$  m<sup>2</sup> area each arranged at distances of 15-60 m from the array center. The showers were selected on the basis of their Cerenkov light. The events were selected for the analysis in which  $\theta \leq 30^\circ$  and the Cerenkov light flux density  $q \geq 8$  photon/cm<sup>2</sup>·eV in 6 detectors located at 60m and  $q \geq 5$  photon/cm<sup>2</sup>·eV in 3 detectors at 120 m.

The EAS axis positions and sizes were inferred from the scintillator data. The shower energy was derived from the Cerenkov light flux density at a 100-m distance from EAS axis. The analysis were made for the showers whose

axes fell within a 60-m radius circles and the selection probability was  $> 90\%$ .

During 45 hours of the array operations, 500 showers satisfying the above requirements were selected. The shower energies were from  $10^{15}$  to  $10^{16}$  eV.

Fig. 1 shows the mean LDF for  $E_0 = 3 \times 10^{15}$  eV. Fig. 2 exemplifies the individual LDF of Cerenkov light.

The LDF at small distances was proposed in /2,3/ to describe by the function of the form

$$q(r) \approx \exp(-r/10^4) \quad (1)$$

We used this approximation with one parameter  $b$  to describe the mean and individual LDF. From Figs 1 and 2 it is seen that the approximation (1) can properly describe the experimental functions at distances of 20-150 m from EAS axis.

The Samarkand EAS array permits from 8 to 12 dots to be obtained in an individual shower at the above mentioned distances. In such a way, individual parameter  $b$  was found in each of 500 showers.

The results were interpreted quantitatively by mathematical simulation of experimental data. The EAS axis position and direction, energy, and depth of maximum were simulated as main parameters. The rest parameters, namely, EAS size  $N_e$ , the LDF parameters of Cerenkov light and charged particles, and densities in individual detectors, were treated as functions of the main parameters. The calculations allowed for the errors in measuring the angles and the flux densities of Cerenkov light and charged particles. The relationship of LDF to EAS maximum depth was taken from the calculations made in terms of the supracritical pomeron model described in detail in /4/. The parameter of the maximum depth distribution were taken from the calculations made in terms of the same model for mixed chemical composition of primary cosmic rays (40% of p and 15% of nuclei with  $A = 4, 15, 31, \text{ and } 56$  each):

$$\begin{aligned} \bar{X}_m &= 504 + 75 (\lg E_0 - 15) \text{ g/cm}^2 \\ G(X_m) &= 85 \text{ g/cm}^2 \end{aligned}$$

640 artificial showers were simulated. The simulation has shown that the accuracy of determining  $b$  in individual cases is  $\Delta b = 18$ .

To make sure that the LDF form reflects the depth of the maximum of an individual shower, we examined the correlation of the parameter  $b$  with the independent parameter, the particle number-to-energy ratio, which must also be sensitive to the depth of EAS maximum. Fig. 3 shows the experimental dots of the dependence  $b$  on  $\lg(N_e/E_0)$ . The correlation coefficient is  $0.55 \pm 0.03$ . The curve in the figure is the regression line:

$$b = 153 + (102 \pm 7) \cdot (\log_{10}(N_e/E_0) + 9.7)$$

Fig. 4 shows the  $b$  distribution of individual showers with  $E_0 = 2 \times 10^{15}$  eV. In the distribution,  $\bar{b} = 154 \pm 2$  and  $\sigma(b) = 35 \pm 1$ . The dashed line is the distribution obtained by simulating experimental data. In the distribution,  $b = 154 \pm 2$  and  $\sigma(b) = 33 \pm 1$ . The experimental data coincide in practice with the calculation results for the above mentioned parameters of the maximum-depth distribution.

To test the sensitivity of the  $b$  distribution to the fluctuations of the maximum depth, the experimental data were repeatedly simulated at  $\zeta(X_m) = 65 \text{ g/cm}^2$ , but at the same shape of the cascade curve. In this case  $\sigma(b) = 26 \pm 1$ , i.e. is much different from the experimental value.

It should be noted in conclusion that the procedure of finding  $X_{\max}$  from LDF of Cerenkov light is in principle dependent on the model determining the cascade curve shape in the lower atmosphere.

#### References

1. Kalmykov et al. (1983), Proc. 18th ICRC, Bangalore, 11, 383
2. Kuhlmann J. Det al. (1981) J. Phys. G, 7, 183.
3. Petterson J.R., Hillas A.M. (1983), J. Phys. G. preprint
4. Kalmykov N.N., Kristiansen G.B. (1983) Proc. 18th ICRC Bangalore, 11, 330.

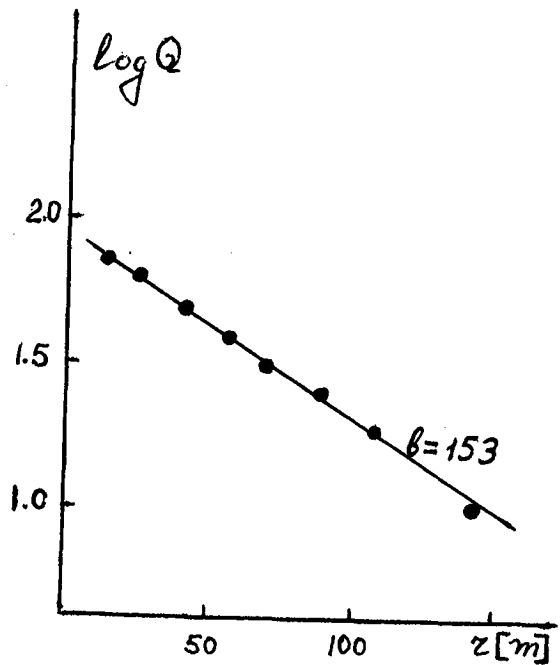


Fig 1.

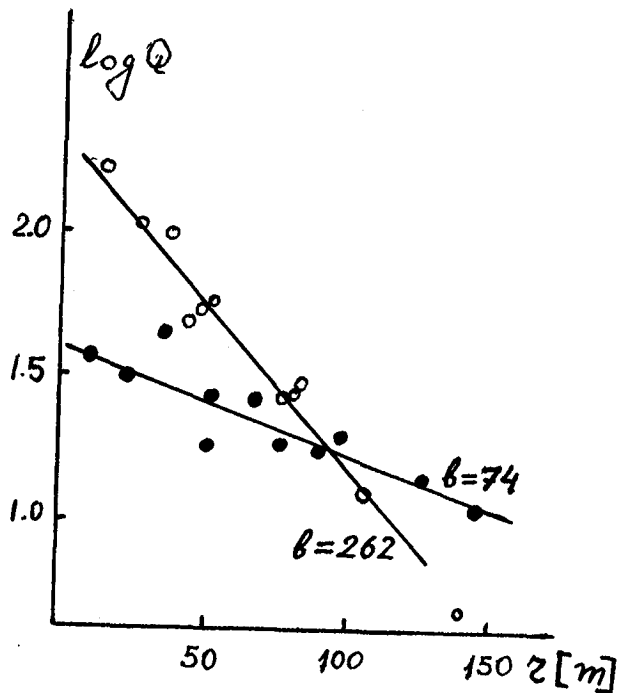


Fig 2.

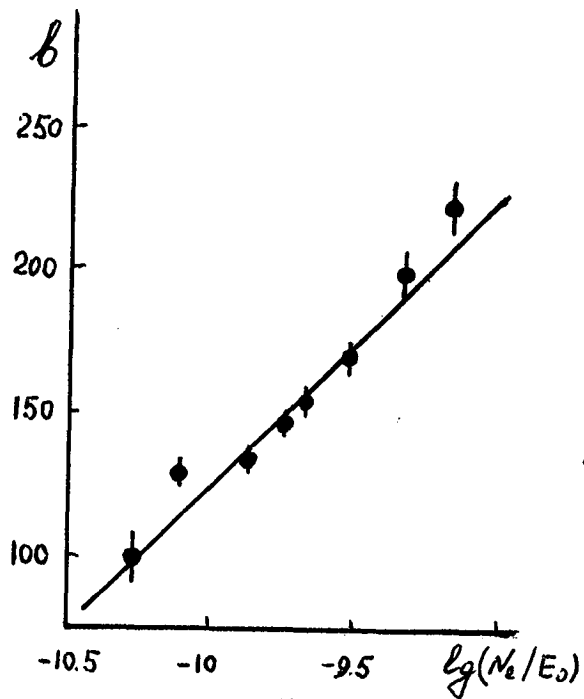


Fig 3.

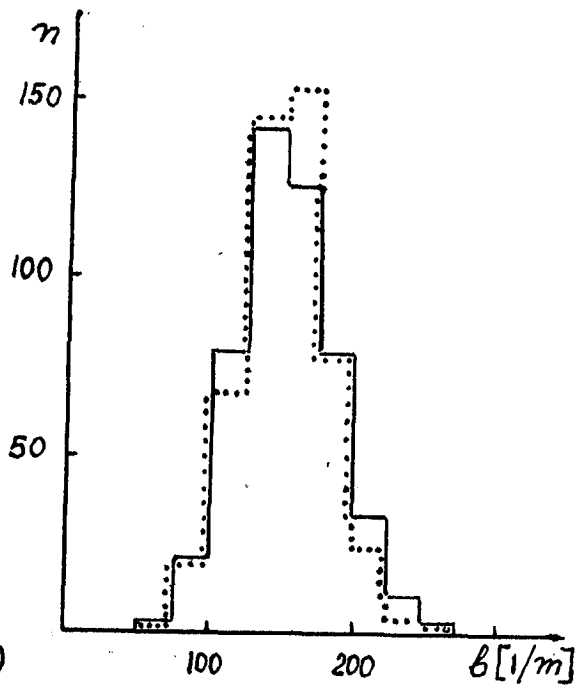


Fig 4.

STUDY OF THE ENERGY SPECTRUM OF PRIMARY COSMIC  
RAYS; EAS SIZE FLUCTUATIONS AT A FIXED PRIMARY  
ENERGY

N. Aliev, T. Alimov, N. Kakhharov, N. Khakimov, N. Rakhimova,  
R. Tashpulatov

Samarkand State University, Samarkand, USSR

G.B. Khristiansen

Institute of Nuclear Physics, Moscow State University,  
Moscow 119899, USSR

During the initial period of the Samarkand EAS array operations (1981) the showers were selected on the basis of charged-particle flux density [1], and during the subsequent periods (1982-1983) the showers were selected on the basis of Cerenkov light flux density [2]. Such a procedure has made it possible to measure the shower energy, to estimate the EAS size fluctuations at a fixed primary energy, and to experimentally obtain the scaling factor  $K(N_e, E_0)$  from the EAS size spectrum to the primary energy spectrum. In 1983 six scintillators of area  $S = 2 \text{ m}^2$  each were added to the array. The scintillators were placed at the vertices of a right hexagon at 60-m distances from the EAS array center. The fluctuations of EAS sizes in the showers of fixed primary energies and the scaling factors  $K(N_e, E_0)$  were inferred from the data obtained in 1983.

The showers with zenith angles  $\leq 30^\circ$  were selected. The EAS axis positions were inferred from the amplitude data of the scintillators. The primary energy  $E_0$  was determined by the method of least squares for the known EAS axis position (inferred from the scintillator data) using the data of the Cerenkov detector located at 80-150 m (100m on the average) from EAS axis. In this case the NKG function was taken to be the mean lateral distributions function (LDF) of charged particles, while the Cerenkov light LDF was assumed to be of the form proposed in [3] with the parameters found using the Samarkand EAS array.

The calculations [4] have shown that the Cerenkov light

flux fluctuations at 100 m from EAS axis,  $q_{100}$ , do not exceed 10% at a fixed EAS energy, so the parameter  $q_{100}$  may be used to estimate the EAS-generating primary particle-energy.

Fig. 1 compares between the calculated and experimental data on the fluctuations of sizes  $N_e$  of EAS with fixed  $E_0$ . The mean energy of such showers is  $3 \times 10^{15}$  eV. The standard deviation  $\lg N_e$  is  $\sqrt{D(\lg N_e)} = 0.31 \pm 0.02$ . The figure also shows the distribution calculated in terms of the supracritical pomeron model (SPM) allowing for the difference between the hadron-nucleon and hadron-nucleus interactions (the solid line). The calculations were made in case of mixed chemical composition (40% of p and 15% of nuclei with  $A=4, 15, 31, \text{ and } 56$  each) distributed through the  $0^\circ - 30^\circ$  zenith angles. To imitate the instrumental errors, each values of  $N_e$  was added a random number distributed normally with a variance equaling the squared instrumental error. The instrumental error in the values of  $N_e$ ,  $\sigma_{N_e}$ , was taken to be  $0.15 N_e$ .

The so obtained distribution shows the standard deviation  $\sqrt{D(\lg N_e)} = 0.31 \pm 0.01$  (for the pure proton composition of primary cosmic rays,  $\sqrt{D(\lg N_e)} = 0.34 \pm 0.01$ ).

Fig. 2 shows the  $N_e$  dependence of the scaling factor from  $N_e$  to  $(N_e, E_0)$  in the showers with fixed values of  $E_0$  and  $N_e$ . Also shown are the results of the model calculations of the scaling factors in case of complex chemical composition for various models of EAS development. The SPM gives a good agreement with experimental data.

The  $N_e$  spectrum was scaled to the primary spectrum using the  $K(N_e, E_0)$  approximation of the form

$$K(N_e, E_0) = E_0/N_e = (0.57 \pm 0.06) \times 10^6 (N_e/10^6)^{-0.1 \pm 0.02}$$

The approximation was obtained as follows. Experimental data were used to find only the absolute value of  $K(N_e, E_0)$ , while the  $N_e$  dependence of  $K(N_e, E_0)$  was inferred from the SPM calculations.

During 160 hours of its operations (at clear moonless nights), the EAS array detected 10240 showers which gave 7-fold coincidences in the scintillators located at 30 m (see / 1/) from the array center. Out of the events detected, the showers were

selected in which the charged-particle density was at least 2 particle/m<sup>2</sup> in the scintillators at 30 m from the array center. A 6 particle/m<sup>2</sup> density was required in the central scintillator. After such a selection, 7233 showers remained. Of them, 3380 showers were with zenith angles  $\leq 30^\circ$ . For the purposes of final analysis the showers were selected whose detection probability is  $> 0.9$  within a 20-m circle for  $N_e = (2.5-4.0) \times 10^5$  and within a 30-m circle for  $N_e = 4 \times 10^5$ . Such showers amounted to 920 and were used to construct the EAS size spectrum. This spectrum can be approximated by the the functions

$$F(>N_e) = (3.45 \pm 0.20) \times 10^{-10} (N_e/10^5)^{-1.47 \pm 0.05} \text{ cm}^{-2} \text{ s}^{-1} \text{ sr}^{-1}$$

for  $2.5 \times 10^5 \leq N_e < 6 \times 10^5$  and

$$F(>N_e) = (1.15 \pm 0.30) \times 10^{-9} (N_e/10^5)^{-2.10 \pm 0.09} \text{ cm}^{-2} \text{ s}^{-1} \text{ sr}^{-1}$$

for  $9.0 \times 10^5 \leq N_e < 3.2 \times 10^6$ .

The experimental scaling factor found in the showers with fixed  $N_e$  was used to scale from the measured EAS size spectrum to the primary EAS energy spectrum which can be approximated by the functions.

$$F(>E_0) = (1.9 \pm 0.3) \times 10^{-10} (E_0/10^{15})^{-1.63 \pm 0.09} \text{ cm}^{-2} \text{ s}^{-1} \text{ sr}^{-1}$$

for  $1.5 \times 10^{15} \leq E_0 < 3.5 \times 10^{15}$  eV and

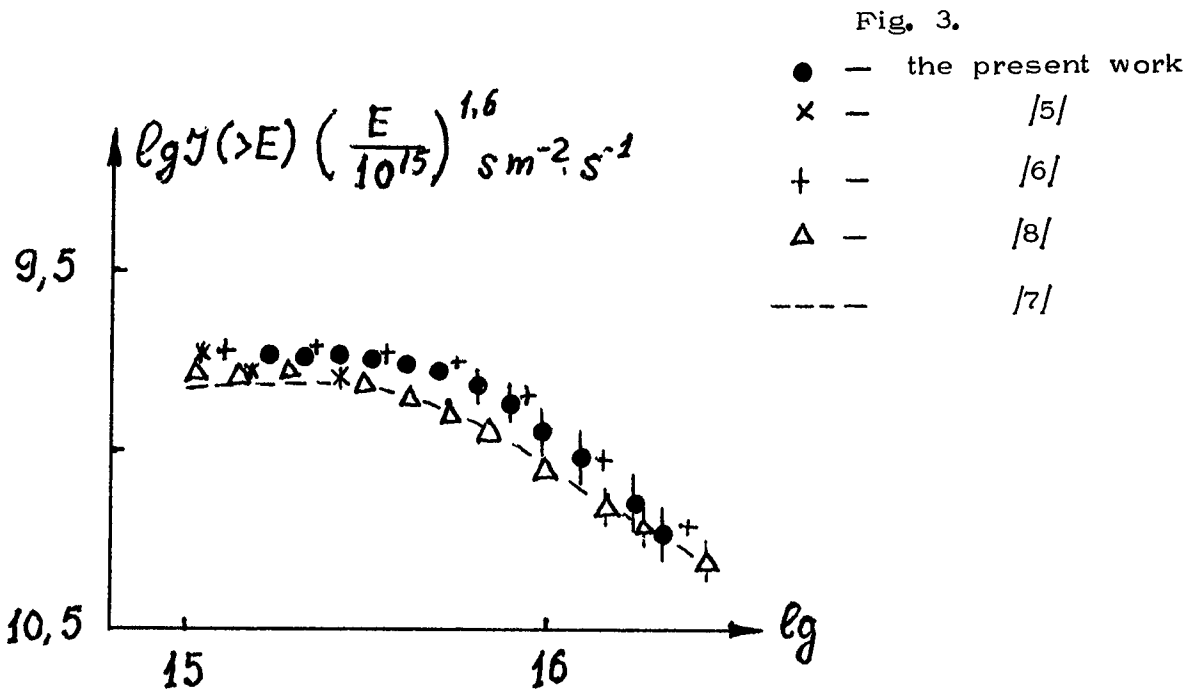
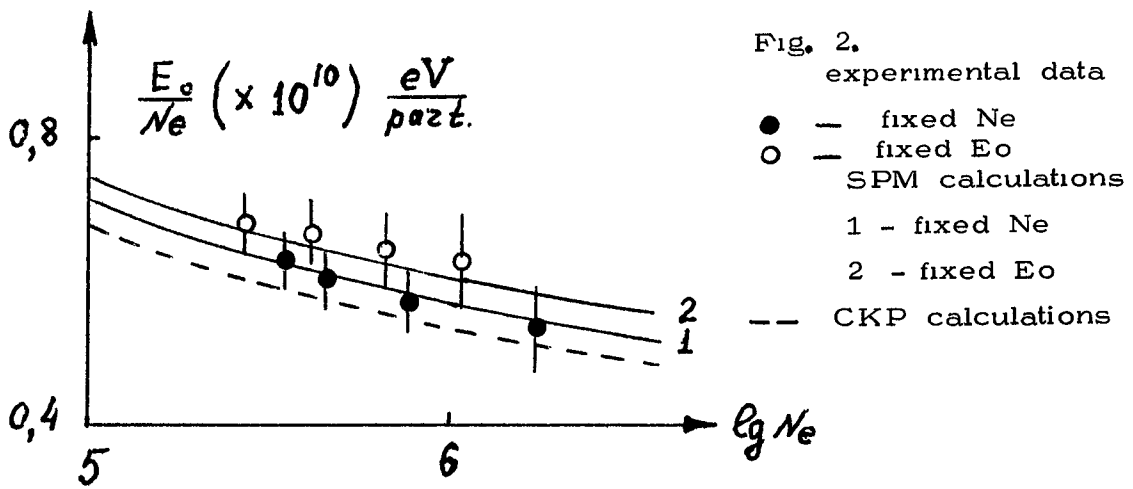
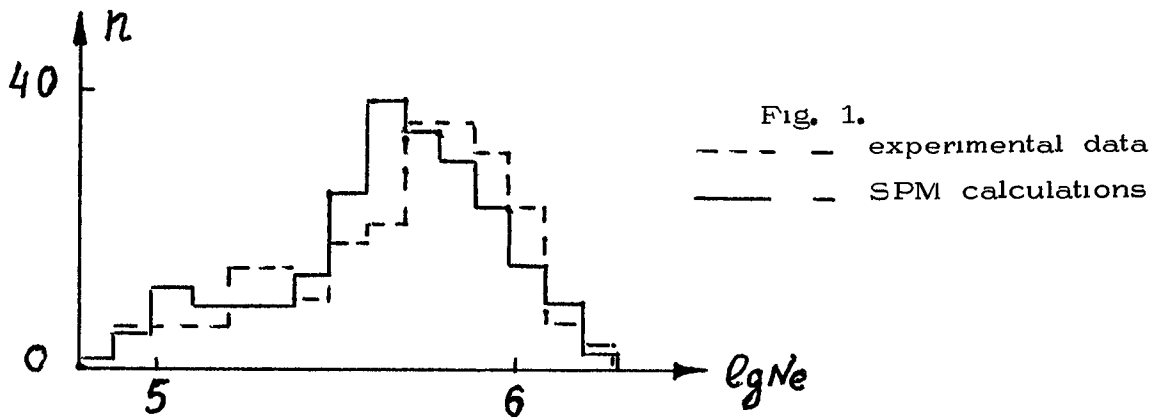
$$F(>E_0) = (5.2 \pm 0.8) \times 10^{-10} (E_0/10^{15})^{-2.30 \pm 0.12} \text{ cm}^{-2} \text{ s}^{-1} \text{ sr}^{-1}$$

for  $5.2 \times 10^{15} \leq E_0 < 2.0 \times 10^{16}$  eV.

Fig. 3 shows the primary cosmic ray spectra obtained with the Samarkand EAS array and elsewhere [5-8].

#### REFERENCES

1. Makhmudov B.M. et al. (1979) Proc. 16th ICRC, Kyoto, v.9, p.61
2. Kalmykov N.N. et al. (1983) Proc. 18th ICRC, Bangalore, v.11, p.383.
3. Diminstein O.S. et al. (1981) Proc. 17th ICRC, v.11, p.242, Paris
4. Alimov T.A. et al. (1982) Izv. Acad. Nauk SSSR, ser. fiz. 46, 1815.
5. Grigorov N.L. et al. (1972) Research XII Akademie Verlag, Berlin
6. Vernov S.N., Khristiansen G.B. Proc. 13th ICRC, PA, p.345, 1969
7. Nagano M. et al. (1984). J. Phys. G. Nucl. Phys. 10, 1295.
8. Kirov I.N. et al. (1982). Iyv. Akad. Nauk SSSR, ser. fiz. 46, 1827.





STUDY OF THE SHOWER MAXIMUM DEPTH BY THE METHOD  
OF DETECTION OF THE EAS CERENKOV LIGHT PULSE SHAPE

N. Aliev, T. Alimov, M. Kakhkharov, N. Khakimov,  
B.M. Makhmudov, N. Rakhimova, R. Tashpulatov

Samarkand State University, Samarkand, USSR

G.B. Khristiansen, V.V. Prosin, V.Yu. Zhukov

Institute of Nuclear Physics, Moscow State  
University, Moscow 119899, USSR

ABSTRACT

The report presents the results of processing the data on the shape of the EAS Cerenkov light pulses recorded by the EAS array of the Samarkand University in 1983. The pulse FWHM is used to find the mean depth of EAS maximum.

In 1983 the Samarkand EAS array consisted of 13 integral detectors of Cerenkov radiation arranged as was described in /1/ and 18 scintillators arranged symmetrically around the array center, with 6 instruments located on each of the circles of 15, 30, and 60-m radii. The detector of Cerenkov pulse shape was installed at 250 m from the array center and included 13 photomultiplier tubes of the XP-2041 type. The detector is described in more detail in /2/.

The pulse shape was recorded with a 6LOR-04 oscillographic recorder, as described in /2/, and sometimes with the AFI-16 digital analyzer of pulse shape described in /3/. The digital analyzer recorded the instantaneous values of the pulse amplitude at 16 points with a 2-6 ns step which was selected automatically depending on the detected pulse duration. The digital analyzer threshold was above the oscillograph threshold.

The total resolution time of the recorders was estimated as the minimum duration at half-maximum of the Cerenkov light pulses whose amplitude is 2 times as high as the threshold amplitude.

Such duration proved to be 7.5 ns for the oscillograph and 6.5 ns for AFI-16.

The showers were selected using their Cerenkov light. Some 2500 showers accompanied by the oscillograph pulses and about 1500 showers accompanied by the digital analyzer pulses were detected.

For the purpose of processing we selected EAS with  $\theta < 30^\circ$  and the photon flux densities in 6 detectors at the 60-m distance from the array center  $q > 8$  photon/cm<sup>2</sup>.eV, at the 120-m distance from the array center  $q > 5$  photon/cm<sup>2</sup>.eV, in the pulse shape detector  $q > 3$  photon/cm<sup>2</sup>.eV for the oscillographic recording and  $q > 5.3$  photon/cm<sup>2</sup>.eV for the digital recording.

The EAS arrival directions were inferred from the readings of the detectors at  $r = 60$  m. The axis coordinates and the EAS size were determined from the readings of the scintillators. The energy was found from the Cerenkov light flux density at a 100-m distance from EAS axis. The processing procedure is described in detail in /4/.

The results were obtained using the showers whose axes fall inside the array ( $r < 60$  m) at a  $> 200$  m distance from the pulse shape detector. The selection probability calculated allowing for the fluctuations of the Cerenkov light LDF is  $> 0.9$ . In such a way, we have selected 55 events recorded with the oscillograph and 28 events recorded with the digital analyzer. The FWHM of the pulses were measured for all the events. The depths of the individual shower maxima were inferred from the duration and the distance from EAS axis using the method described in /2/.

In terms of energy, all the events were broken into three groups. The mean depths of the maxima for the three groups are shown in Fig. 1 which also presents the results obtained earlier with the EAS arrays at Samarkand /2/, Yakutsk /5/, Tien-Shan /6/, in Japan (Akeno)/7/, and Australia (Adelaide) /8/.

A certain systematic shift of the dots obtained with

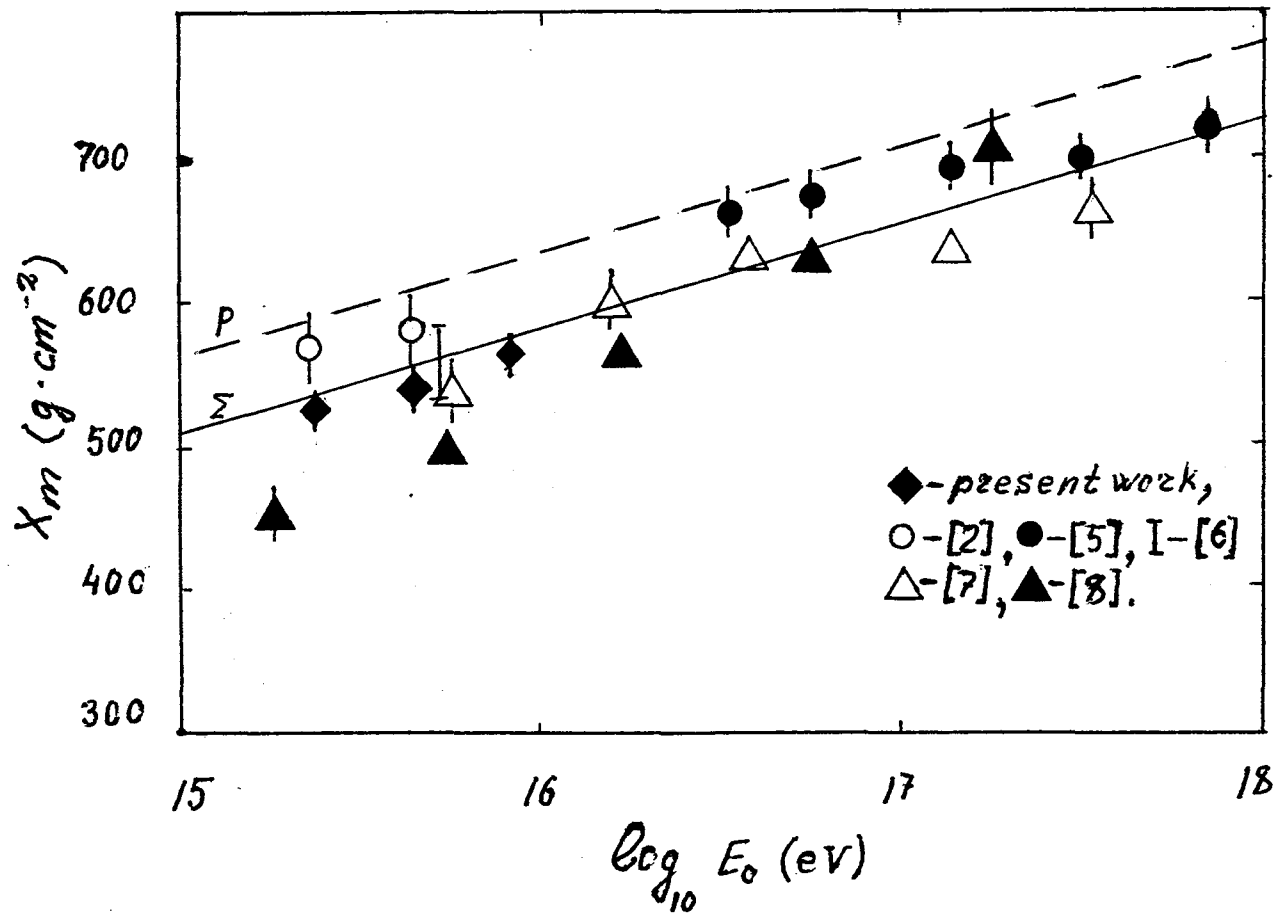
the Samarkand EAS array may be explained by the transition from the density-based selection of showers at  $r=60$  m from the array center /2/ to the density-based selection at  $r=120$  m. Our calculations /11/ have shown that the latter selection is closer to the selection of showers with a fixed energy.

A good agreement is observed with the data obtained at Tien-Shan and in Japan. The data of /8/ may be significantly distorted by the shower selection effects, as was noted in the work /9/ carried out using the same EAS array.

Fig. 1 shows the results of calculating the depths of EAS maxima in terms of the supracritical pomeron model described in /10/ for primary protons and complex chemical composition (40% of p and 15% of nuclei with  $A=4, 15, 31$ , and 56 each). A good agreement of the dots of this work and of the dots obtained in /6,7/ with the theoretical dependence for the complex chemical composition can be seen. The dots obtained with the Yakutsk EAS array at  $E_0 > 10^{17}$  eV do not contradict the dependence either. At lower energies the Yakutsk dots deviate from the dependence by 2 statistical errors. This is probably due to the poor allowance for the errors arising from the application of the photomultiplier tubes of a high time resolution ( $\sim 23$  ns) for EAS with  $E_0 < 10^{17}$  eV.

#### REFERENCES

1. Kalmukov N.N., et al. (1983). Proc. 18th ICCR, 11, 383, Bangalore.
2. Alimov T.A. et al. (1983). Proc. 18th ICCR, 11, 387, Bangalore.
3. Sazansky V.Ya., Sheingezicht A.A., Preprint Inst. Nucl. Phys., Sob. Brunch, Acad. Sci. USSR, Novosibirsk
4. Alimov T. et al., Proc. This Conference
5. Prosin V.V. (1980). Thesis for Candidate Degree, MGU.
6. Kvashnin A.N., et al. (1983). 18th ICCR, 11, 394, Bangalore.
7. Inone N., et al. Proc. 18th ICCR, 11, 402, Bangalore.
8. Thornton G.J., R.W. Clay, J. Phys. Rev. Lett. 43, p. 16#22, 1979.
9. Liebing D.F. et al. (1984) J. Phys. G. Preprint
10. Kalmykov N.N., G.B. Kristiansen, (1983), Proc. 18th ICCR, 11, 330, Bangalore.
11. Aliev N.A. et al. (1983) Proc. 18th ICCR, 11, 391, Bangalore.



ANALYSIS OF CERENKOV PULSES  
RECORDED SIMULTANEOUSLY AT TWO SITES.

D.F. Liebing\* and J.R. Patterson

Physics Department, University of Adelaide,  
Adelaide, South Australia, 5001.

\*Present address: Physics Department,  
Iowa State University, Ames, Iowa.

ABSTRACT

The agreement between measured distances to maximum for  $\sim 49$  simultaneous Cerenkov pulse profiles from different sites is  $\pm \sim 0.1$  km near 4.5 km and  $\pm 0.5$  km near 7 km. Uncertainty in depths of maximum are  $\sim \pm 10$  g cm<sup>2</sup> and  $\pm 30$  g cm<sup>-2</sup> respectively. Usually the Hillas-Patterson simulation is able to fit both pulse shapes satisfactorily using a single  $N(x)$  profile.

1. Introduction. Measurement of the widths of optical Cerenkov pulses from cosmic ray air showers has proved to be a most useful means of studying shower development, in particular the distance to maximum. Several theoretical studies have been published including that by Patterson and Hillas<sup>1</sup> (1983) which forms the basis of the present study. Because of a lack of published data on simultaneous measurements on individual cosmic ray showers, the theories have not previously been tested for consistency of measured distances or for the goodness of the fit with a single longitudinal development curve,  $N(x)$ .

2. Experimental Data. We make use of part of an extensive data set obtained by Liebing<sup>2</sup> at Buckland Park in 1981-82 in which detectors were located at 200 m North of the centre of the air shower array and 200 m South East. The Cerenkov pulses were obtained in coincidence with showers recorded by the array for which a full NKG shower analysis giving directions, core locations, and hence radial distances, and shower sizes was available. Each detector comprised a 125 mm diameter fast-response photo-multiplier (Philips XP2040, with S11 response) and mechanically collimated at 45° from the zenith, the cut-off being sharp. Few showers detected have greater inclinations than 40°. Short wide-band ( $> 400$  MHz or 2 ns rise time) cables (with no preamplifiers) and independently triggered storage oscilloscopes (Tektronix 7834) were used with photographic recording. Impulse responses ( $\sim 5.0$  and 5.7 ns FWHM, non-oscillatory and non-Gaussian<sup>1</sup>) were routinely checked for each system using the narrowest sky pulses. Because of a 2s dead time associated with each oscilloscope trigger, a dead time  $\sim 30\%$  was associated with each system.

Of  $\sim 138$  analysed pulses recorded at the 200 m N site and 166 at the 150 m N site, and  $\sim 170$  at the 200 m SE site, a subset of 49 showers were observed with analysable pulses in two sites. A full analysis of these data treating the systems as quite independent and looking at the

variation of depths of maximum with shower size is given in ref. 3. It clearly showed the effect of array selection effects in the data which arise because of the limited dynamic range of the optical detectors and the array bias. However, these are not relevant to the present discussion, except to say that many pulses were lost either because they went off scale or did not trigger the oscilloscopes.

Three representative showers were studied in detail and fits to the experimental profiles are given in figures 1, 2 and 3. They were chosen because the radial distances from the two detector sites were markedly different. Few usable pulses were observed further than 250 m from the shower axis; and sensitivity of the pulses to shower development becomes much less inside 150 m. We also imposed the requirement that for reliable shower analysis, the core should fall inside the perimeter of the array. On the figures the full lines are the oscilloscope traces and show the effect of sky background pulses especially at the more distant site.

3. Theoretical Fits. Hillas<sup>4</sup> has described a method of mapping back from the pulse profiles to the  $N(x)$  profiles using absolute timing, not available in these cases. However, a timing zero can be fixed for each pulse by using the width of the pulse to determine the distance to maximum first. In a preliminary investigation we found the  $N(x)$  profile derived from the data very sensitive to the sky noise and divergent below the maximum. This was not surprising as Patterson and Hillas<sup>1</sup> showed that the pulse profile was very insensitive to large changes in shower attenuation. The alternative approach adopted therefore was, knowing the measured distance to maximum, to select the closest match from a library of previously simulated  $N(x)$  profiles by Hillas<sup>4</sup> which varied in depth of maximum but not very much in shape. Primary energies of  $10^{15}$ ,  $10^{16}$  and  $10^{17}$  eV were available, but do not markedly affect the shape.

The simulation calculation of pulse shape was then performed including the photomultiplier resolution for angles  $0^\circ$ ,  $15^\circ$ ,  $30^\circ$  or  $40^\circ$  and radial distances increasing by 25 m steps. The simulations are not very sensitive to zenith angle so the closest angle was chosen. However, the shape appropriate to the measured radial distance was interpolated graphically from the calculation. The results are fairly sensitive to the radius, which is subject to  $\pm 5$  m errors and small changes in distance to maximum.

The theoretical fits are shown as dashed lines and enable the agreement with experiment to be checked over the full profile, whereas it is more usual to be only concerned with the Full Width at Half Maximum. For this comparison the theoretical pulse has been normalized to the experiment at the peak and the relative times adjusted to give the best fit.

The agreement in shape on the rising edge and near the top of the pulse is considered fairly satisfactory. There is a tendency for the theory to underestimate the flux in the tail. This cannot be attributed to a slower attenuation in the  $N(x)$  profile because the preliminary study showed the required  $N(x)$  to diverge. It arises partly because of

the limitation in the simulation to 10 GeV subshowers. The simulation in fig. 1 using 100 GeV subshowers improves the fit in the tail of the pulse.

**4. Conclusion.** Comparison of simulation fits for a single  $N(x)$  development profile to experimental pulses at the different sites has shown satisfactory agreement with the Patterson-Hillas simulations. Independent estimates of distance to maximum indicate errors of  $\pm \sim 0.1$  km near 4.5 km and  $\pm 0.5$  km near 7.0 km, again consistent with predictions<sup>1</sup>. These correspond to errors in depth of maximum of approximately  $10 \text{ g cm}^{-2}$  and  $30 \text{ g cm}^{-2}$  respectively.

**Acknowledgements.** We acknowledge the contribution of colleagues including Dr. A.M. Hillas, University of Leeds, and Drs. Gerhardy, Gregory and Clay. The work was supported by the Australian Research Grants Scheme.

### References.

1. Patterson, J.R. and Hillas, A.M., (1983), J. Phys. G., 9, 323.
2. Liebing, D.F., (1983), PhD Thesis, University of Adelaide.
3. Liebing, D.F., Clay, R.W., Gregory, A.G. and Patterson, J.R. (1984), J. Phys. G., 10, 1283.
4. Hillas, A.M., (1982) J. Phys. G., 8, 1475.

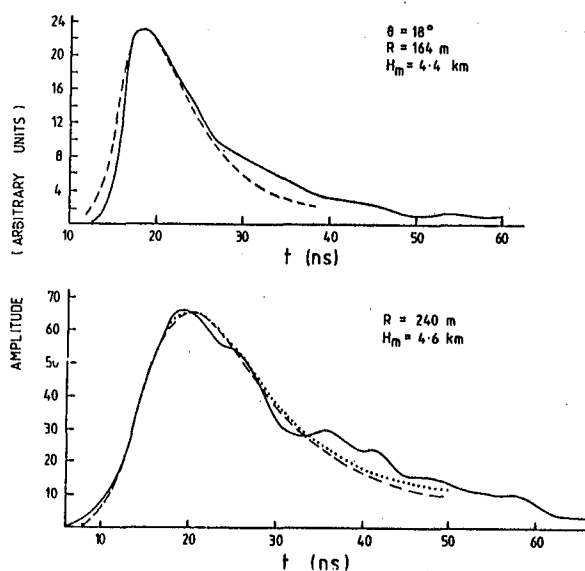


Fig. 1 shows a comparison of the experimental trace (full lines) for a shower with  $N_e = 4.6 \times 10^6$ ,  $E = 2 \times 10^{16}$  eV and  $S=1.28$ , and the Patterson-Hillas simulation using 10 GeV subshowers (dashed lines) and 100 GeV subshowers (dotted). The  $N(x)$  profile used<sup>1</sup> has  $H_m = 4.5$  km, and depth of maximum  $640 \text{ g cm}^{-2}$ .

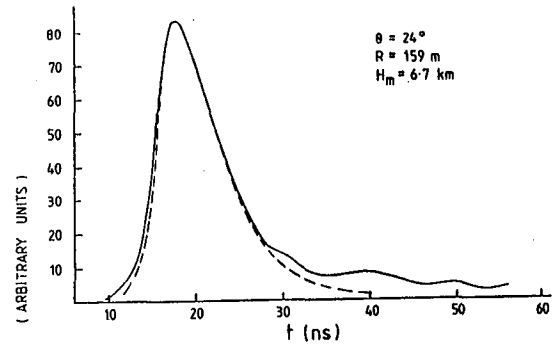


Fig. 2. shows a comparison of experiment and simulation for a shower with  $N_e = 6 \times 10^5$ ,  $E = 8 \times 10^{15} \text{ eV}$  and  $S = 1.56$ . The  $N(x)$  profile has  $H_m = 7.4 \text{ km}$  and depth of maximum  $470 \text{ gcm}^{-2}$ .

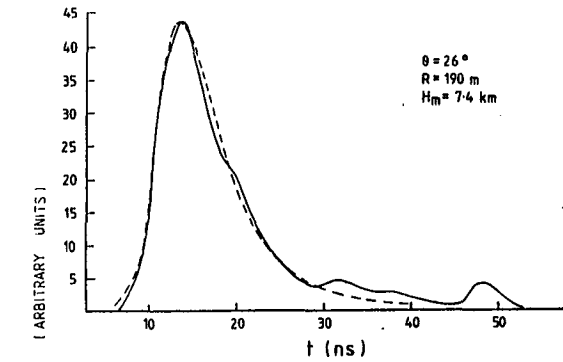
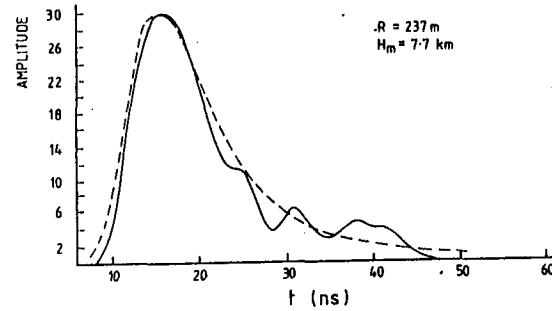
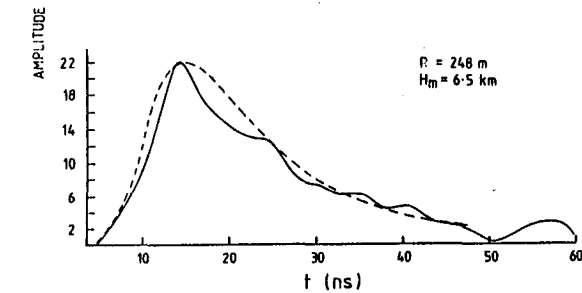


Fig. 3 shows a comparison and experiment and simulation for a shower with  $N_e = 1.7 \times 10^6$ ,  $E = 3 \times 10^{16} \text{ eV}$  and  $S = 1.19$ . The  $N(x)$  profile has  $H_m = 7.4 \text{ km}$  and depth of maximum  $490 \text{ gcm}^{-2}$ .





PRELIMINARY RESULTS OF THE CERENKOV EAS FLASHES  
OBSERVATIONS ON THE MULTI-MIRROR INSTALLATION OF  
THE CRIMEAN ASTROPHYSICAL OBSERVATORY

B.M.Vladimirsky, Yu.L.Zyskin, Yu.I.Neshpor,  
A.A.Stepanian, V.P.Fomin, V.G.Shitov

Crimean Astrophysical Observatory  
p/o Nauchny, 334413, Crimea, USSR

Abstract

A short description of the facility designed for the study of angular resolution of light in the EAS flashes is communicated. The threshold energy of the facility is about  $3 \times 10^{16}$  eV. The data on the angular distribution of light in a flash and the ratio of the flux in the UV ( $\lambda < 300$  nm) and visual region as a function of the distance to the axis of a shower are given. Obtained results are compared to the published computations.

1. Introduction.

It is commonly assumed, that the main obstacle to increase the sensitivity of Cerenkov EAS detectors for gamma-quanta registration is the charged particles background.

It was Grindlay [1] who made the first attempts to reduce the registered background of cosmic rays. Turver [2] suggested to reduce the background by using spaced detectors. The experiments in Tata institute, India, showed, that spaced detectors permit to determine the direction of the primary particle (or quantum) on the sky with the accuracy up to  $0.3^\circ$  [3].

In [4] we proposed a method of discrimination of gamma-showers from proton-showers. This method is based in principle on different angular dimensions of these showers. But since the difference is rather scanty, it needs an optical system which allows to obtain the image of the flash with high (minimum  $0.1^\circ$ ) angular resolution. Besides, we suggested in [4] to use the difference in UV region of shower light spectrum ( $\lambda < 300$  nm) for gamma and proton showers.

2. Description of the facility located at the Crimean observatory.

The facility was described in short in the Proceedings of Ban-

galore Conference [5]. The results given hereafter are obtained on the installation consisting of six similar elements. Each of them comprizes 4 spherical mirrors 1.2-m in diameter. Nineteen PMs are located in the focal plane of each of the four elements (see Fig.1). The light is transmitted to the photocathodes by means of light conductors. The signals from 4 elements being directed in parallel are summarized within each channel, digitized and then stored in the computer memory. Any 2-channel coincidence from 7 central was adopted as a muster-pulse.

Two other telescopes also being directed in parallel were used for UV region of flash spectrum with solar-blind PM. Summarized signal yeild from these two elements is also digitized and recorded in the computer memory. The diameter of the light spot from the point source at the focal plane is  $0.1^{\circ}$ .

### 3. The results of the observations.

The observations of the EAS flashes were carried out in November - December, 1984. More than 1000 Cerenkov flashes have been registrated. But for the further analysis only those were selected whose maximal amplitude coincided with one of 7 central pixels.

The final sampling constituted 644 events. The energies of primary particles responsible for a flash lie, according to estimations within the range  $(3-6) \times 10^{12}$  eV.

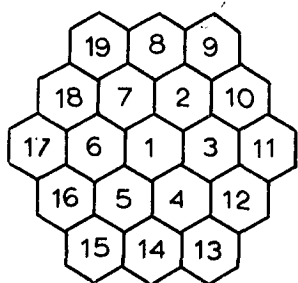
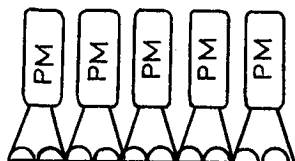


Figure 1.

The configuration of pixels with PM at the focal plane.

We have calculated the values of  $\alpha^2 = \sum_{i=1}^{19} (x_i - \bar{x})^2 A_i$  and  $\beta^2 = \sum_{i=1}^{19} (y_i - \bar{y})^2 A_i$  where  $A_i$  is the amplitude of flash in the  $i$ -channel,  $x$  is the coordinate axis directed along the large axis of ellipsoid of Cerenkov flash, and  $y$  is the coordinate

axis along the small axis; that gives  $\bar{x} = \sum_{i=1}^{19} x_i \frac{A_i}{\sum A_i}$  and  $\bar{y} = \sum_{i=1}^{19} y_i \frac{A_i}{\sum A_i}$

Fig.2a shows the frequency distribution with respect to  $a$  and Fig.2b gives the value of  $b/a$ . The mean value of  $a$  equals to  $0.40 \pm 0.02$  and  $(b/a) = 0.69 \pm 0.01$ .

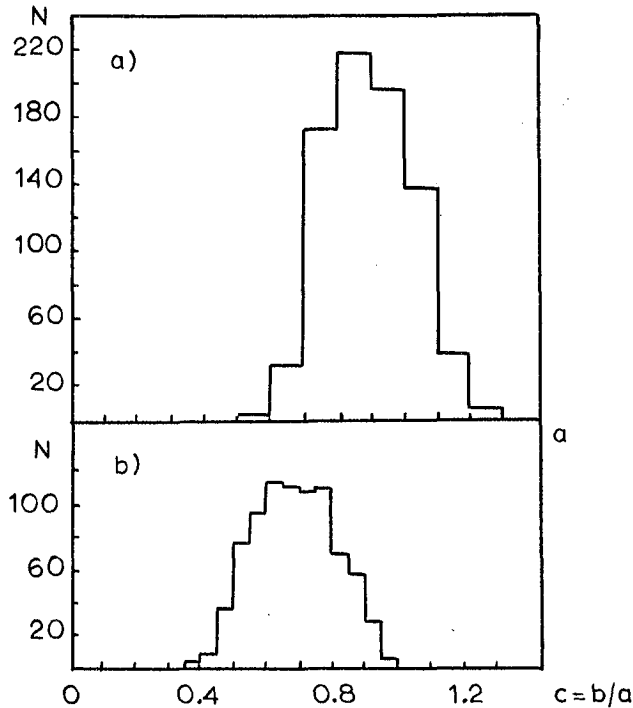


Figure 2.

Frequency distribution :

a) of the effective dimension of the large semiaxis of the flash ellipsoid,

b) of the semiaxis ratio.  
"N" corresponds to the number of flashes.

For the given values of  $b/a$  the flashes amplitudes ratios were obtained for the rim  $A_e$  zone to central  $A_c$  zone. Here the central zone is adopted as a pixel with maximum amplitude together with the adjacent pixel having the highest amplitude. All other pixels are considered as "rim". Therefore  $A_e/A_c$  parameter can be considered as a characteristic of angular distribution of light in a flash. It approaches to "y" computed in [4] .

The obtained distribution is presented on Fig.3a. According to this distribution, the mean value of  $A_e/A_c$  depends on  $b/a$  variation. The value  $b/a$  is distance-dependent: the larger the distance from detector to the axis, the smaller the value of  $b/a$ . Here one can see the magnitude of dispersion  $D(A_e/A_c)$  of individual estimates. It corresponds to (30-40)% of the estimated value.

Fig.3b shows the ratio of the UV flux  $A_u$  to the flux in visual region  $A_v$  as a function of  $b/a$ . The dispersion of  $A_u$  amplitude is high and compatible with the mean value within the given interval. The error of the mean value of  $A_u/A_v$  is presented here.

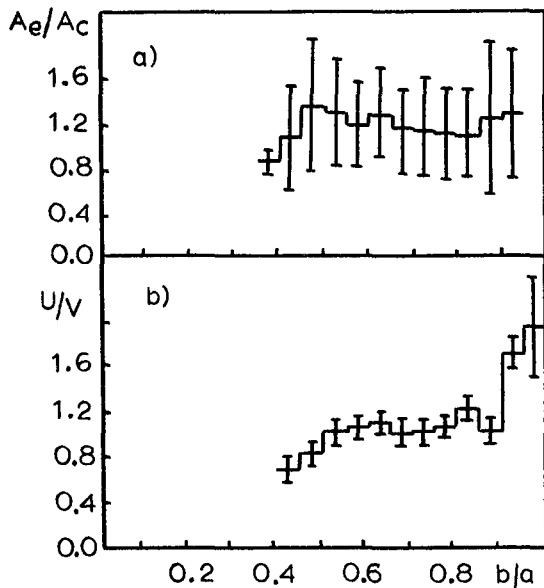


Figure 3.  
The dependence of the semiaxes ratio  $b/a$  :

- a) the amplitude ratio  $A_e/A_c$   
b) the ratios of amplitudes in UV and "visible" flashes at random units.

#### EAS

Near the axis the UV flux is much stronger than at large distances. We should note, that detailed information on UV flashes needs further enlargement of mirror surfaces detecting UV-light.

#### 4. Discussion and results.

The obtained data on flash angular dimension are in good agreement with our earlier calculations [4]. These measurements are compatible with the data of Plyasheshnikov and Bignami [6], the accord is rather high. For instance, according to [6]  $a=0^{\circ}.42$  and in our computations  $a=0^{\circ}.40$ , although our data is still crude.

As far as we know, the UV flashes have never been registered so far. So, just the fact of their registration seems to be of importance. We think, that the perspective of gamma and proton showers discrimination is realistic.

#### References.

1. Grindlay J.E. 1975, Smithsonian Astrophys.Obs.Spec.Rep. N 334.
2. Gibson A.I. et al., 1981, Phil.Trans.R.Soc.Lond. A 301, 635.
3. Gupta S.K. et al., 1982, Proc. of Intern.Workshop on VHE Gamma-Ray Astronomy, Ootacamund, Sept.20-25, 1982, p.295.
4. Stepanian A.A., Fomin V.P., Vladimirovsky B.M. 1983, Izv. Krimsk. Astrophys. Obs., 66, 234.
5. Fomin V.P. et al., Proc. 18-th Intern. Cosmic-Ray Conf. Bangalore, India, 1983, v.6, p.223.
6. Plyasheshnikov A.V., Bignami G.F. Nuovo Cim. 1985, in press.

THE EXPERIMENTAL CASCADE CURVES OF EAS AT  $E_0 > 10^{17}$  eV  
OBTAINED BY THE METHOD OF DETECTION OF CHERENKOV PULSE SHAPE

Yu.A. Fomin, N.N. Kalmykov, G.B. Khristiansen, M.V. Motova,

Yu.A. Nechin, V.V. Prosin, V.Yu. Zhukov

Institute of Nuclear Physics, Moscow State University,

Moscow II9899, USSR

N.N. Efimov, V.M. Grigoriev, E.S. Nikiforova,

Institute for Cosmophysical Research and Aeronomy,

Yakutsk 677891, USSR

Since recently we have systematically studied the individual cascade curves of EAS with  $E_0 > 10^{17}$  eV /1-3/ by the method of detection of EAS Cherenkov light pulses proposed initially in /4/.

The scintillators located at the center of the Yakutsk EAS array within a 500-m radius circle were used to select the showers and to determine the main EAS parameters (the axis coordinates, the azimuthal and zenith angles  $\psi$  and  $\theta$ , and the primary energy  $E_0$ ) /5/. The individual cascade curves  $N(t)$  were obtained using the EAS Cherenkov light pulses satisfying the following requirements: (1) the signal-to-noise ratio  $f_m/\sigma_n \geq 15$ , where  $f_m$  is the amplitude of pulse,  $\sigma_n$  is the r.m.s. value of night sky noises, (2) the EAS axis-detector distance  $r_1 \geq 350$  m, (3) the zenith angle  $\theta \leq 30^\circ$ , (4) the probability for EAS to be detected by scintillators  $W \geq 0.8$ . Condition (1) arises from the desire to reduce the amplitude distortion of Cherenkov pulses due to noise and determines the studied range of EAS sizes,  $N(t)$ . The resolution times of the Cherenkov pulse shape detectors are  $\tau_0 \approx 23$  ns which results in distortion (broadening) of a pulse during the process of the detection. The restrictions  $r_1 \geq 350$  m and  $\theta \leq 30^\circ$  permit to select the Cherenkov pulses with relatively high  $\tau_{0.5}$  (the half-width of non-distorted pulses). We estimated the distortion of pulses due to the finiteness of  $\tau_0$  value. It was shown that the rise

time of pulse becomes greater as  $\tau_{0.5}/\tau_0$  ratio decreases; at the same time the tail does not vary within 5% accuracy. The results were used in order to correct the experimental pulses.

Since the moment of intersection of the observation level and the EAS axis is not fixed experimentally, the Cherenkov pulse is measured on the scale of relative time  $\tau$ . In order to determine the absolute time  $\tau_A$  it is necessary to use the results of theoretical calculation /6/ which permit to find the difference of values  $\tau_{mA}^N$  and  $\tau_{mA}^f$ , where  $\tau_{mA}^N$  is the time moment when the light corresponding to EAS maximum is detected and  $\tau_{mA}^f$  is the time corresponding to the Cherenkov pulse maximum:  $\Delta\tau_m(t_m, r_\perp) = \tau_{mA}^N(t_m, r_\perp) - \tau_{mA}^f(t_m, r_\perp)$ , where  $t_m$  is the EAS maximum depth in the atmosphere. The value of  $t_m$  can be determined from the half-width  $\tau_{0.5}$  of the given pulse /7/ and can be used to find  $\tau_{mA}^N$  in accordance with formulae of /2,3/. Then one obtains the time  $\tau_{mA}^f = \tau_{mA}^N - \Delta\tau_m$  corresponding to the maximum of experimental Cherenkov pulse. The theoretical functions /2,3/ used for the transformation of the Cherenkov pulse  $f(\tau_A, r_\perp, \theta)$

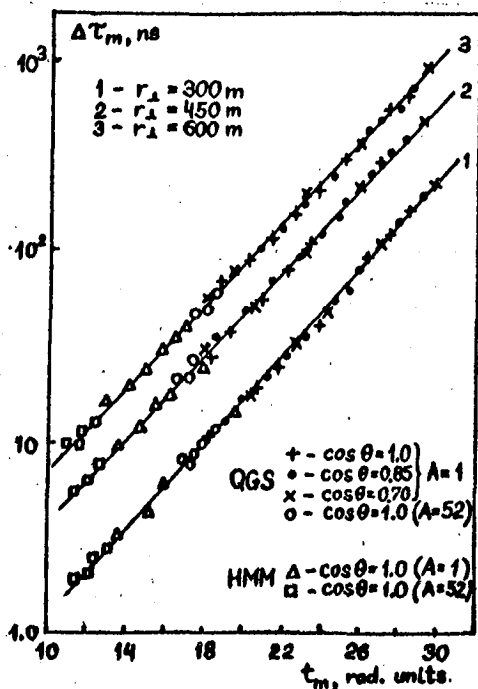


Fig. I

to the cascade curve  $N(t)$  are independent, to within a 5% accuracy, on the adopted model of EAS development and the primary composition. This is illustrated by the function  $\Delta\tau_m(t_m, r_\perp)$  shown in Fig. I for the high-multiplicity model (HMM) and for the quark-gluon strings (QGS) model for a primary proton ( $A=1$ ) and a primary iron nucleus ( $A=52$ ) /6,8/. These functions depend only on the angle distribution of EAS electrons /7/.

26 showers with Cherenkov pulses satisfying to above men-

tioned requirements were selected. It should be noted that 10 showers out of 26 exhibited the Cherenkov pulses in two detectors at different distances from EAS axis under condition  $f_m/b_h \geq 15$ . For these events the r.m.s. errors  $\delta_m = \sqrt{D(t_{m1} - t_{m2})} = 1.2$  radiation units, where  $t_{m1}$  and  $t_{m2}$  are depths of EAS maximum determined from two Cherenkov pulses. The errors  $\delta_{0.25}$  for the depths corresponding to the points on the ascending branch of the cascade curve at the 0.25  $N_m$  level ( $N_m$  is the EAS size in the maximum)  $(t_{0.25})_1$  and  $(t_{0.25})_2$  is somewhat higher and is about 1.6 radiation units.

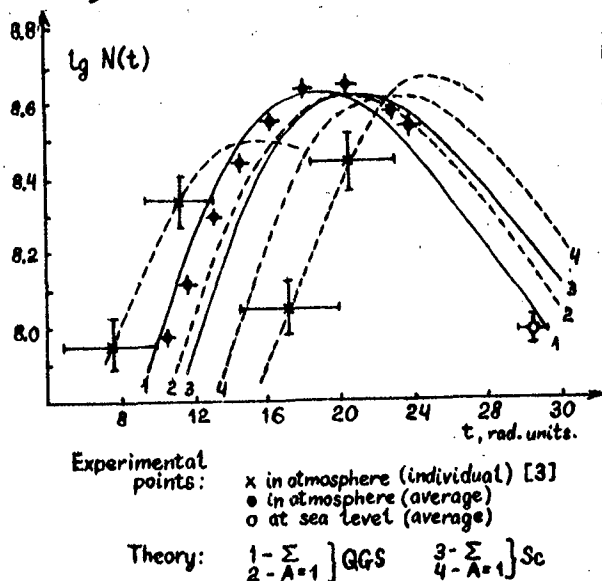


Fig. 2

ted by the time-integral Cherenkov light detectors of the Yakutsk array /5/;  $S = mP_c$ , where  $S$  [mm, ns] is the Cherenkov pulse area measured initially on millimetre scale of amplitudes and on nanosecond sweep of oscillograph,  $m$  is calibration factor (which permits to express the amplitudes of pulses in units of flux density [ $\text{cm}^{-2}\text{ns}^{-1}\text{eV}^{-1}$ ]). After that, using the theoretical functions /2,3/ one obtains the cascade curves  $N(t)$  for the number of shower electrons. The accuracy of the calibration factor  $m$ , hence of the EAS size  $N(t)$ , is 25% and arises mainly from the accuracy of the absolute calibration of the integral detectors. The EAS size in the maximum of the mean cascade curve is  $\overline{N}_m = (4.5 \pm$

Fig. 2 presents the mean cascade curve constructed using 26 individual cascade curves in EAS size units  $N(t)$ . To construct the cascade curves in the absolute units  $N$ , the detectors of Cherenkov pulse shape were calibrated by comparing the pulses detected in them with the Cherenkov light flux densities  $P_c$  [ $\text{cm}^2\text{eV}$ ] detected

± I.I). $10^8$ . Fig. 2 also shows the point corresponding to the mean EAS size at sea level  $\bar{N}_s = (0.95 \pm 0.06) \cdot 10^8$  inferred from the data of the Yakutsk EAS array scintillators. The energy of individual cascade curves was also determined on the basis of the parameter  $\rho_{600}$  /9/. The mean cascade curve energy is  $\bar{E}_0 = (7.0 + 2.0) \cdot 10^{17}$  eV. The correlation coefficient between  $E_0$  and  $N_m$  inferred from 26 experimental cascade curves is  $\bar{K} = (E_0/N_m) = (1.60 \pm 0.08) \cdot 10^9$  for r.m.s. error 30% related mainly to the apparatus errors of determination of  $E_0$  and  $N_m$ .

The comparison by the Pearson method between the experimental cascade curve and the theoretical curves calculated in terms of the scaling model (Sc) /6/ and the QGS model /8/ under various assumptions concerning the chemical composition of primary cosmic rays exhibits a better agreement of the experimental data with the QGS model for complex chemical composition (QGS,  $\Sigma$ ) ( $P(\chi^2) = 0.07$ ). Other versions of the theory are in a poorer agreement with the experimental data ( $P(\chi^2) \leq 0.01$ ).

## References

1. Grigoriev V.M. et al. Pis'ma ZhETF (1979) 30, II, 747
2. Kalmykov N.N. et al. Proc. 17th ICRC (1981) 6, II4
3. Grigoriev V.M. et al. Proc. 18th ICRC (1983), 9, 204.
4. Fomin Yu.A., Khristiansen G.B. Sov.Nucl.Phys. (1971) 14, 642.
5. Glushkov A.V. et al. Characteristics of EAS from Ultrahigh energy cosmic rays, Yakutsk, 1976, p.45
6. Grishina N.V. et al. Proc. 16th ICRC (1979) 9, I.
7. Berezhko I.A. et al. Sov.Nucl.Phys. (1979), 30, 415.
8. Kalmykov N.N., Fomin Yu.A., Khristiansen G.B. Sov.Nucl. Phys. (1985) 41, 947.
9. Vasiliev I.V. et al. Cosmic Rays of Energies above  $10^{17}$  eV Yakutsk, 1983, p.19.



LATERAL-ANGULAR AND TEMPORAL CHARACTERISTICS OF EAS  
OPTICAL RADIATION

Chuykova T.A., Galkin V.I., Ivanenko I.P., Roganova T.M.  
Institute of Nuclear Physics, Moscow State University,  
Moscow 119899, USSR

The paper presents characteristics of the direct and scattered components of electron-photon shower optical radiation for distances  $R \geq 500$  m from the shower core to a detector, allowing for the Cerenkov and fluorescent mechanism of photon generation. The results of calculations can be employed to clarify the techniques for determination of the shower parameters detected by both installations registering fluorescent light and those recording Cerenkov light.

1. Introduction. Optical radiation has been used for many years to investigate the lateral EAS development/1,2/. Each new more accurate and/or detailed consideration of the optical component leads, as a rule, to decreasing uncertainties in the determination of shower parameters and sometimes allows finding new characteristics of the shower optical image, which are more sensitive to the nuclear interaction parameters at superhigh energy or to the shape of the primary cosmic ray spectrum than those used earlier/3/.

One of these improved considerations has been reported in /4,5/ where "contamination" of the fluorescent component of EAS optical radiation by scattered Cerenkov light has been examined, and both lateral-angular and temporal characteristics of the shower optical image has been presented. The author of /4,5/ divides the Cerenkov light registered by a detector into three components: direct (non-scattered) light, scattered light, and fluorescent light, thus assuming that fluorescent photons, unlike to Cerenkov ones, would not scatter in the atmosphere (i.e. the fluorescent light being always only direct). When considering the scattered component, the author confines himself to a single scattering; as a model of longitudinal development of EAS with  $E_0 = 10^{17} - 10^{18}$  eV the author have used a cascade curve of a shower induced deep in the atmosphere by a gamma-ray of  $E_0 = 2 \cdot 10^{11}$  eV, with the hope that this simplification would not considerably distort the relative contributions of various optical radiation components. The papers /4,5/ furthermore have not presented the temporal characteristics of a direct Cerenkov component. Since the results obtained using the above noted approximations, on one hand, are only preliminary and, on the other hand, seem to be important and interesting, we attempted to consider this group of phenomena with the help of simulating program of a different type.

2. The present paper approach. A separate consideration of the Cerenkov and fluorescent components undoubtedly gives an additional information of their relative contributions, however most of modern installations are incapable of dis-

tinguishing the nature of photons arriving at a detector.

We performed calculations for a 3000-8000Å wavelength-band. Since large distances ( $R \geq 500\text{m}$ ) from the core to a detector are considered at which the characteristic temporal scale of a pulse is  $\sim 100\text{ ns}$ , the time of fluorescent photon reemission can be neglected in the first approximation. Thus, in the situation of interest for us the differences between the two components reduce to their angular characteristics which practically do not affect the simulation algorithmic aspect. So, a unified source of photons is used composed of Cerenkov and fluorescent sources with appropriate angular characteristics and intensities, and the photon transfer from this source to a detector is considered as usually introducing the photon time delay:

$$CT = r - r_0 + H_0 \gamma_0 \left( \frac{\exp(z/H_0) - 1}{\cos \theta} - \frac{\exp(z_0/H_0) - 1}{\cos \theta_0} \right), \text{ where } H_0 = 7.5\text{km} \quad (1)$$

is the exponential atmosphere depth;  $\gamma_0 = 2.9 \cdot 10^{-4}$  is the diversity from a unity of an atmosphere refraction index at sea level;  $\vec{r}_0 = (r_0, \theta_0, \psi_0)$  being the shower generation point;  $\vec{z}_0 = r_0 \cos \theta_0$ ;  $\vec{r} = (r, \theta, \psi)$  is the point under consideration;  $z = r \cos \theta$ ; the spherical coordinate system is bound to a detector.

As far as a large core distances region is concerned a simple shower model—that of a moving point—is valid, i.e. we neglect the electron lateral distribution and take into account their angular distributions only. The direct optical radiation component is calculated on average. Use is made of a model of the angular distribution /6/,  $f(\theta)$  where  $\alpha$  is calculated using moments  $\overline{\theta^2}$  also present in /6/. The cascade curve approximation used is  $N(\epsilon_0, \epsilon, s) = \frac{\epsilon_0 s}{(1+\epsilon)s} \cdot \frac{1}{q(s)}$  (2)

where  $\epsilon = ED(s)/\beta$ ,  $\epsilon_0 = E_0 D(s)/\beta$ ,  $\beta = 81\text{ MeV}$ ,  $D(s)$  and  $q(s)$  are the known cascade functions from /7/.

For the Cerenkov component  $E$  is the threshold energy of Cerenkov light, and for the fluorescent component  $E = 0$ . A charged particle is assumed to produce 5 photons over a meter of path due to the fluorescent mechanism. The scattered component was Monte-Carlo simulated. Over each segment of the shower trajectory, approximately 0.1 c.u. long,  $6 \times 13$  photons (6 cells over the azimuth and 13 cells over the polar angle) were radiated and followed till their arrival at a detector, till their absorption by the Earth's surface, till their leaving the atmosphere or till their departure from a detector to a distance larger than some value. When arriving at a detector, a photon was given a weight factor proportional to the overall light amount radiated by the shower electrons over a fixed trajectory segment and to the weight of angular cell from which centre of mass the photon has been radiated. The differential cross section of scattered light was, as in /4,5/, proportional to  $(1 + \cos^2 \chi)$ , where  $\chi$  is the scattering polar angle. The data on the scattering length (molecular Rayleigh and aerosol) were taken from /8/. The detector comprised 200 temporal bins each of 10 ns and one integral bin for delays  $> 2000\text{ ns}$ . The angle  $2\pi$  ster was divided into 120 bins (12 equal-size bins over the azimuth angle  $\times 10$  equal-size bins over the polar angle) covering

different solid angles (.04 ster to .08 ster). Though the program can simulate inclined showers, the present paper reports on the results for the vertical electron-photon showers with  $E_0=10^{17}$  eV for distances  $R=.5, 2.0, 8.0$  km from detector. For a better comparison with the results of /4,5/ we considered production depth  $119 \text{ g/cm}^2$  ( $H=16.1$  km) that yields  $t_m=896 \text{ g/cm}^2$  and the same distance  $H_{\text{obs}}-H_m=1.2$  km, as in /4,5/. For each  $R$  the data on scattered light were obtained by averaging over 10 showers.

3. Simulation results. The lateral-angular distribution of the light in Fig.1 (the solid curves are for the present calculation, the dash-dot ones - /4,5/- the sum of direct Cerenkov and fluorescent photons, the dashed curves are for scattered Cerenkov light /4,5/). All the data are divided by detector solid angles; The data /4,5/ are furthermore multiplied by  $5 \cdot 10^7$  to allow for the differences in primary energies. The present paper data were selected from the bins facing the shower core. Unlike to the data /4,5/, our curves for scattered light do not reveal such an abrupt rise with zenith angle, though an increase of scattered light in the overall flux is noticeable even at  $R=.5$  km that is explained by a decreasing contribution of the Cerenkov mechanism. At  $R=8$  km, the two sets of data are the most similar, though some differences in intensity are observed which can be explained by the diversity between the cascade curves and solid angles of detectors in /4,5/ and present paper.

Fig.2 shows the data on FWHM  $\tau$  of scattered light pulses. FWHM of the scattered component, according to our calculation, is noticeably broader than that of the direct one (multiple scattering really matters) and increases with  $R$ , though slower than FWHM of the direct component. In the present paper FWHM increases with zenith angle similar to that in /4/. Fig.3 shows typical pulses for the direct and scattered components (integrated over all bins facing the shower core).

### References

1. Jelly J. Cerenkov radiation, Moscow, 1960.
2. Nesterova N.M., Chudakov A.E., 1962, JETP, 42, vyp6, 1622.
3. Galkin V.I., Makarov V.V., 1983, 18th ICRC, v.6, 236.
4. Protheroe R.J., 1982, J. Phys. G., v.8, L165.
5. Protheroe R.J., 1983, Proc. 18th ICRC, v.6, 240.
6. Belyaev A.A. et al. Electron-photon showers in cosmic rays at superhigh energies, 1980, Moscow.
7. Belenky S.Z. Avalanche processes in cosmic rays, 1984, Moscow.
8. Martynov A.Ya. Course of applied astrophysics, 1964, Moscow.

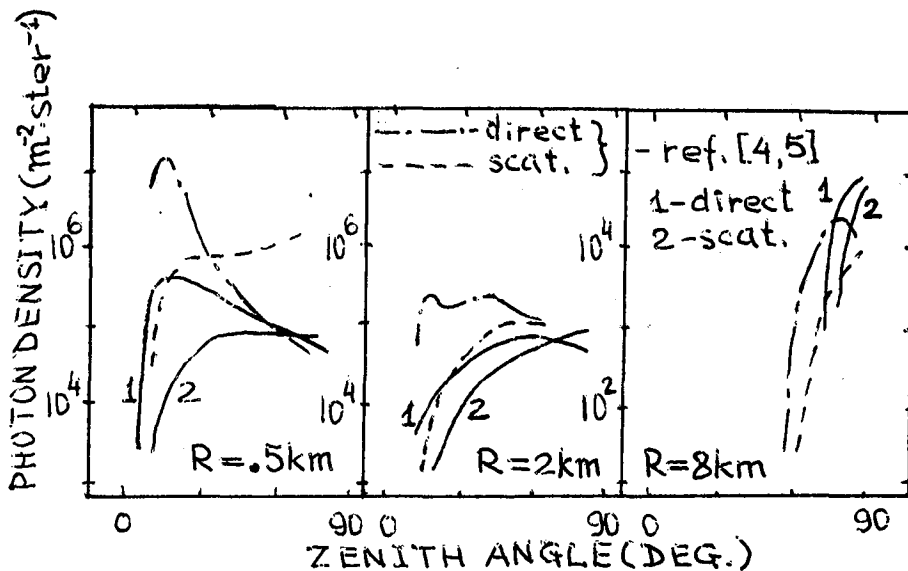


FIG. 1

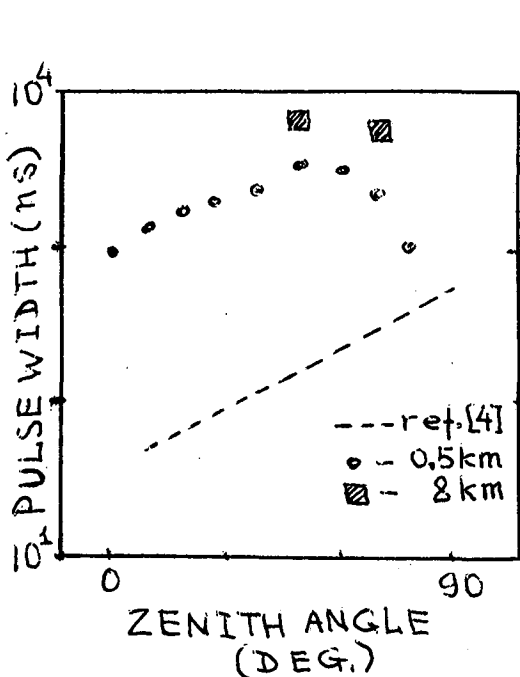


FIG. 2

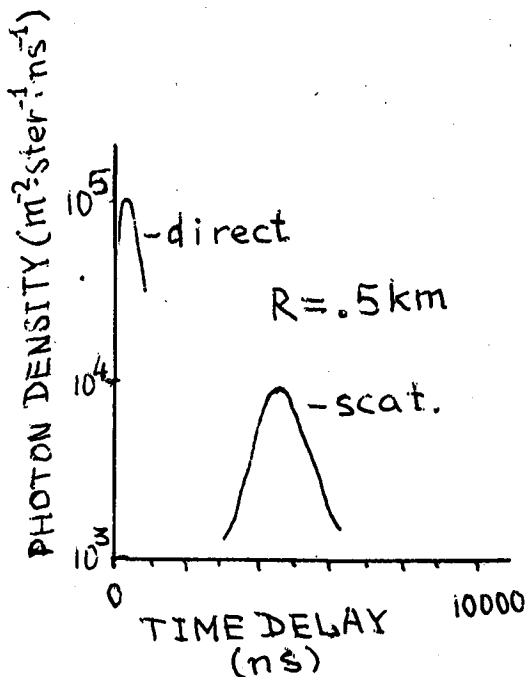


FIG. 3

THE IDENTIFICATION OF GAMMA RAY INDUCED EAS

P. R. BLAKE and W. F. NASH

Department of Physics, University of Nottingham, U.K.

Abstract

Recently Stanev et al have suggested that some of the penetrating particles in "gamma-induced" EAS from Cygnus X-3 observed by the Kiel EAS group using a single layer of flash-bulbs under 880 g cm<sup>-2</sup> concrete, may be "punched through" photons rather than muons. This paper presents an analysis of the shielded flash-tube response from EAS detected at Haverah Park. The penetration of the electromagnetic component through 20 cm of Pb has been observed at core distances  $\lesssim 10$  m.

1. Introduction Experiments carried out by the Kiel group [1] indicated an excess of showers of size  $N \geq 10^5$  arriving from the direction of Cygnus X-3. Further, these showers exhibited the 4.8 hour modulation characteristic of well-determined X-ray measurements. The excess EAS were assumed to be primary  $\gamma$  induced. Simulations by Wdowczyk et al [2], and McComb et al [3] comparing the muon densities from proton and gamma initiated showers of the same primary energy predicted that gamma induced showers would produce about 10% of total muons compared with proton induced showers.

Samorski and Stamm [4] (1983) used the Kiel array to investigate the muon content of the EAS produced by these "gammas" in the range  $10^{15}$  -  $10^{16}$  eV. The EAS detector consisted of 28 scintillator detectors of 1 m<sup>2</sup> each at distances up to 100 m from the centre of the array. A neon hodoscope of effective area 21.5 m<sup>2</sup> under 880 gm/cm<sup>2</sup> of concrete was used as a muon detector for muons of energy  $> 2$  GeV.

In comparing the average number of muons in "on" and "off" source showers at core distances of approximately 10 m, they concluded that the difference in muon content of the two kinds of EAS was very small ( $< 20\%$ ). The densities of muons in the source showers appeared to increase more rapidly with shower size and fell more rapidly with core distance than normal showers.

Recently Stanev et al [5] carried out simulations in an attempt to explain this apparent discrepancy in the behaviour of "gamma induced" showers. Their calculations agreed with the work of McComb et al [3] in that only at  $E_p > 10^{18}$  eV will photo production contribute a significant number of muons. In the primary energy range of the Kiel experiment, however, the number of photoproduced muons should still be very significantly less than the muon number in hadronic showers. Consequently Stanev et al investigated the number of photons that might "punch through" the 880 gm/cm<sup>2</sup> of concrete shield at approximately 10 m from the shower core. They concluded that only 30% of the muon density might be explained in

terms of "punch through" gammas, assuming an overall detection efficiency for gammas of 40% for the neon flash bulbs.

2. Experimental Arrangement For several years the Nottingham group working at the Haverah Park EAS Array operated a detector of crossed neon flash tubes interleaved with lead absorber in order to identify and measure the arrival directions of muons.

The detector is shown in Figure 1. The top two boxes of crossed flash tubes ( $3.34 \text{ m}^2$ ) have 5 cm of lead between them. The next two layers of flash tubes ( $4.18 \text{ m}^2$ ) were covered by a further 5 cm and 10 cm of lead. Thus not only could the muons be clearly identified but the degree of accompaniment under 5, 10 and 20 cm of lead could be observed. The threshold energy for muons to penetrate the whole stack was approximately 350 MeV. Although this was less than that of the Kiel group, the number of cascade lengths of the total lead absorber was not significantly different.

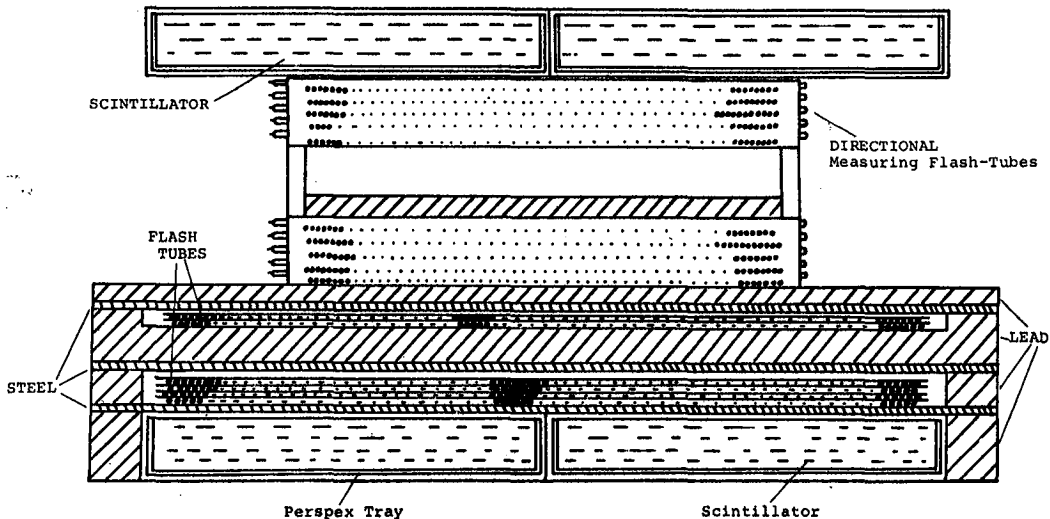


FIGURE 1 The neon-flash tube muon detector

3. Analysis of Data Normally EAS with  $E_p \geq 10^{17}$  eV were recorded and for this "punch through" study EAS have been selected with well determined core distances such that  $20 \text{ m} < R < 100 \text{ m}$ . The sandwich of flash tubes and absorber enabled the muons to be unambiguously identified. The number of muons detected in the shower was measured along with the degree of electromagnetic punch through accompaniment (excluding obvious muon-induced knock-ons and bursts), under 5, 10

and 20 cm of lead. The water Cerenkov response at the same position in the EAS was also measured.

Figure 2 shows the frequency distribution of the electron accompaniment per muon capable of penetrating at least 5 cm of lead for two core distances, viz  $20 \text{ m} < R < 35 \text{ m}$  and  $20 \text{ m} < R < 100 \text{ m}$ . It is seen that within the statistical limits of the sample there is no significant change with limitation of the core distance to 35 m. The detected accompaniment per muon per flash tube layer under 5, 10 and 20 cm of Pb was found to be 2.48, 0.14 and 0.02 respectively. It is seen therefore from these observations that the degree of "punch through" from "normal" showers for 10 cm and 20 cm of lead is insignificant beyond 20 m from the axis. However this result may be attributed to the low photon energies found in EAS at these core distances.

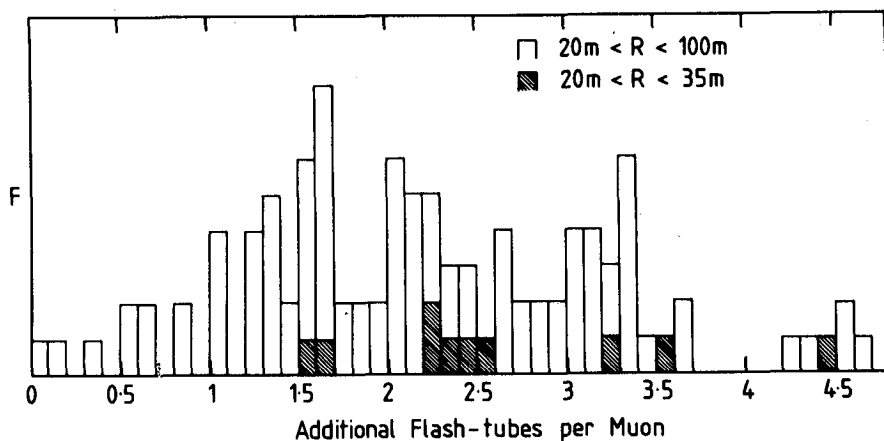


FIGURE 2 Frequency distribution of electron accompaniment/muon

It should be noted that the Kiel measurements applied to core distances around 10 m and the Stanev calculations were for such small core distances. It is in this region of the EAS that photons of energies 10-100 GeV have a significant probability of causing punch-through effects. For a period of time, apart from being triggered by the 500 m Air Shower Array at Haverah Park the muon flash tube detectors were also triggered from large bursts (detected by the fully-shielded scintillator) in "local" showers. The details of these showers was not determined directly but it was possible by determining the muon/electron density ratio to identify EAS falling within about 10 m of the core.

For these events the ratio of the number of detected accompanying "punch-through" particles to the number of muons was found to be approximately 2:1. With the limitations of the technique it would appear that the degree of accompaniment capable of "punching through" 20 cm of lead is significant at core distances  $\leq 10 \text{ m}$ .

4. Conclusion Analysis of the data obtained with a crossed flash tube/scintillator array indicates that the degree of "punch-through" accompaniment of muons from EAS of  $E > 10^{17}$  eV for  $R > 20$  m capable of penetrating 20 cm of lead and being detected by flash-tubes is negligible. However there is a strong indication that within a core distance  $R \lesssim 10$  m there is a significant increase in such accompaniment. Thus in order to reduce the possible contamination of observations from such an effect it is therefore clear that observations of the muon content of showers should be made at core distances  $\gtrsim 20$  m. If observations are to be made at core distances of  $< 10$  m then the detector must be capable of unambiguously identifying muons.

#### References

- [1] M. Samorski and W. Stamm, Ap. J. 268 L17 (1983).
- [2] J. Wdowczyk, Proc. 9th ICRC, London, 2 p.691 (1965).
- [3] T. S. L. McComb, R. J. Protheroe and K. E. Turver, J. Phys. G 5 1613 (1979).
- [4] M. Samorski and W. Stamm, Proc. 18th ICRC, Bangalore, 11 p.244 (1983).
- [5] T. Stanev, T. K. Gaisser and F. Halzen (private communication) 1984.



## Muons in gamma showers

*Todor Stanev\* and Ch. P. Vankov\**

Bartol Research Foundation of the Franklin Institute, University  
of Delaware, Newark, DE 19716

*Francis Halzen*

Department of Physics, University of Wisconsin-Madison, Madison,  
WI 53706

### ABSTRACT

We study muon production in gamma-induced air showers, accounting for all major processes. For muon energies in the GeV region the photoproduction is by far the most important process, while the contribution of  $\mu^+\mu^-$  pair creation is not negligible for TeV muons. The total rate of muons in gamma showers is, however, very low.

### 1. Introduction

There are two types of processes involved in generation of muons in electromagnetic showers: photoproduction and direct creation of muon pairs. In the photoproduction muons are generated through production and subsequent decay of mesons, thus in addition to the photoproduction cross-section one has to account for the meson interaction cross-section and the interaction-decay competition. At higher energies and in dense atmosphere mesons interact rather than decay and the resulting muon spectrum is steeper than the photoproduction one by one power of the energy. Directly produced muons are not affected by the production depth and their spectrum is a convolution of the photon energy spectrum and the pair creation cross-section.

We shall briefly discuss the cross-sections of both types of processes, introduce the techniques used in the calculations and show the muon production spectra for fixed primary energy. We shall use such spectra to estimate the total muon rates resulting from the observed gamma-ray fluxes of point sources.

### 2. Photoproduction and muon pair creation cross-sections.

Figure 1<sup>a</sup> shows the energy dependence of the photoproduction cross-section in air used in the calculation. It interpolates gamma-proton data and assumes a  $A^{0.91}$  dependence on atomic number. After the resonance region below 1 GeV the cross-section shows a very slow logarithmic rise with the incident photon energy. A constant diffractive cross-section of  $194 \mu b$  is assumed to result in  $\rho$  production. The electron photoproduction cross-section is shown on the same graph with dash line. Although this process has a significant cross-section, it does not contribute much to the muon production because the spectrum of the radiated virtual photons is very soft and the energy loss to photoproduction is small.

The lower part of the figure shows the cross-section for direct production of  $\mu^+\mu^-$  pairs by photons in air. This process is analogous to the creation of electron-positron pairs and in the asymptotic case of full screening of the nucleus field by the atomic electrons  $\sigma_{\mu^+\mu^-}/\sigma_{e^+e^-}=(m/\mu)^2$ . In addition to that the screening parameter  $\xi_\mu=\xi_e(\mu/m)^2$  and the asymptotic cross-section for muon pairs is achieved for  $E_\gamma \gg 1$  TeV. In the very interesting region between 1 and 10 TeV the cross section increases by a factor of two. The corresponding process

of muon pair production by electrons is of higher order and its cross-section is smaller at least by a factor of  $\alpha$ .

All cross-sections shown on Fig. 1 are very small. Even at 1000 TeV their values are 2.4 and 2.1 mb for photoproduction by photons and electrons and 11.7  $\mu b$  for muon pairs compared to the 502 mb cross section for  $e^+e^-$  pairs. Only a very small fraction of the shower energy goes into these channels and we can still use the cascade theory to estimate the shower size.

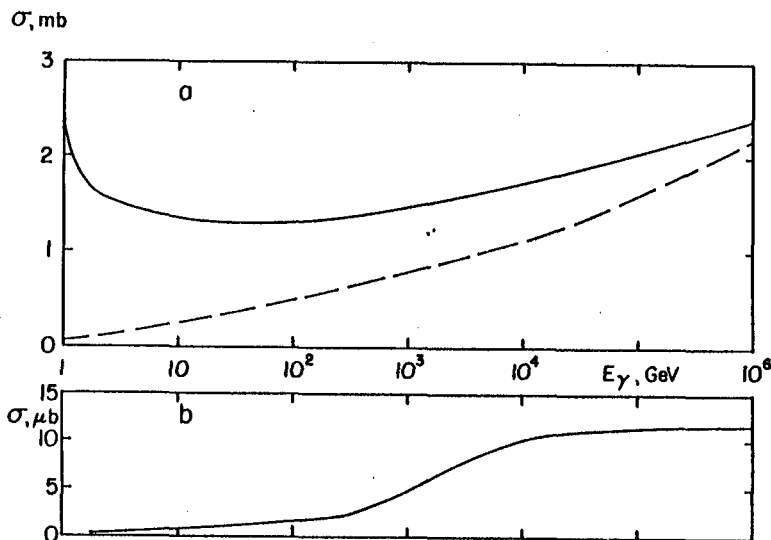


Fig. 1. Cross-sections for photoproduction by photons and electrons (dash line)<sup>(a)</sup> and for muon pairs creation<sup>(b)</sup> in air. Note the difference in the units (mb for photoproduction and  $\mu b$  for pair creation).

### 3. Computational technique.

We have used two methods to calculate the muon production in gamma showers due to photoproduction. An electromagnetic Monte Carlo program was used to calculate the photoproduction at fixed primary gamma ray energy and all photoproduction events were recorded. Then the data files were treated with a hadronic Monte Carlo simulation program, which followed the muon production and propagation to the appropriate threshold energies. Results from these runs for GeV muons were discussed in Ref. 1. The same approach was used in Ref. 2 to calculate the number of TeV muons in gamma showers.

A numerical integration including the photoproduction energy spectrum and the three first generations in the hadronic cascades was also performed to check the Monte Carlo calculation and to extend the results for GeV muons to higher primary energies.

To calculate the number of muons with energy greater than  $E_\mu$  in gamma showers of primary energy  $E_0$  due to creation of muon pairs one has to evaluate the integral

$$N(>E_\mu) = \int_{E_\mu}^{E_0} \int_{E_\mu}^{E_\gamma} \frac{dN_\gamma(E_0, E_\gamma)}{dE_\gamma} \sigma_{\mu^+\mu^-}(E_\gamma, E) dE dE_\gamma$$

where  $dN/dE_\gamma$  is the total number of  $\gamma$  rays in the shower. We evaluated the integral using the tracklength (total number of particles with energy  $E_\gamma$  in the

cascade) given by Rossi <sup>3</sup>  $g_0^{(\gamma)}(E_0, E_\gamma) = 0.572 E_0 / E_\gamma^2$ .

#### 4. Results

The calculation confirmed that the number of GeV muons in gamma showers is at least one order of magnitude smaller than the number of muons in hadronic showers. For muon energy  $> 2$  GeV we obtained a factor of 25 in the muon content of hadronic and electromagnetic showers for shower sizes between  $10^5$  and  $10^6$  particles at sea level. We also found that the fluctuations in the muon production are very large and most of the gamma showers will have only half of that amount of muons.

At muon energies below 1 GeV, where the muon decay is extremely important, the number of photoproduced muons grows in the same shower size region faster than linearly with the energy. We agree with the conclusions of McComb et al. <sup>4</sup> that at energies around  $10^{18}$  eV the photoproduction will significantly contribute to the number of low energy muons.

Fig. 2 compares the production spectra of muons by photoproduction and muon pair creation in gamma showers with primary energy of  $10^6$  GeV. Photoproduced muons have integral energy spectrum of  $E^{-2}$  and directly created muons of  $E^{-0.80}$ . If the same trend continues at higher muon energies the production spectra will cross over at muon energies 10 TeV. At energy 3 TeV directly produced muons contribute about 1/4 of the total muon number.

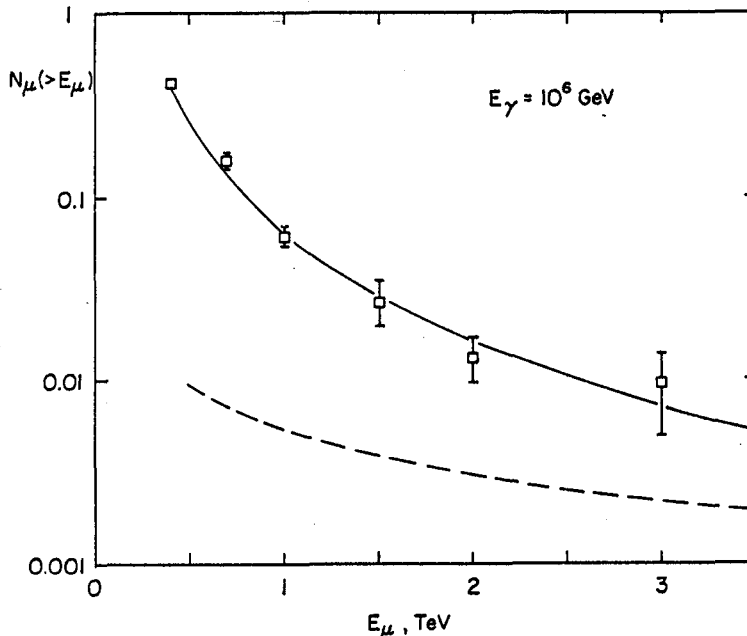


Fig 2. Muon production spectrum in  $10^6$  GeV showers through photoproduction and muon pairs creation (dash line).

#### 5. Discussion and conclusion.

One can now use the flux of high energy  $\gamma$  rays measured at Kiel <sup>5</sup>  $N(>E_\gamma) = 6 \times 10^{-7} E_\gamma (\text{GeV})^{-1.11} \text{photons.cm}^{-2} \cdot \text{s}^{-1}$  with cut-off at  $10^7$  GeV as suggested by the measurement at Haverah Park <sup>6</sup> and calculate the flux of muons at different depths underground due to both photoproduction and pair creation. The vertical muon flux resulting from this photon flux at depths 2 and 4 km.w.e. underground are respectively  $1.60 \times 10^{-13}$  and  $2.05 \times 10^{-14} \text{cm}^{-2} \times \text{s}^{-1}$ . These rates

are very low and the expected muon rates in a  $1000 \text{ m}^2$  detector are respectively 45 and  $6 \text{ yr}^{-1}$ . For the 0.92 yrs running time of the  $9 \text{ m}^2$  Soudan <sup>7</sup> detector the expected number of muons from gamma showers is 0.4.

Gamma showers are inefficient in producing muons in the TeV as well as in the GeV region. The photon induced air showers are "mu-poor" and this feature can be used as identification signature. It is not possible to understand the underground muon signals from point sources<sup>7</sup> as a result of photon showers in the atmosphere.

### Acknowledgements

The authors gratefully acknowledge the participation of T.K. Gaisser in this work through numerous discussions and reading the manuscript.

This work was funded in part by the U.S. Department of Energy under contract DE-AC02-76ER00881 (F.H.) and by the National Science Foundation under Grant PHY-8410989 (T.S.) and the U.S.-Bulgaria Cooperative Research Program (Ch.P.V.). Ch.P.V. would like to thank Bartol Research Foundation for its hospitality.

### References

- (\*) Permanent address: Institute for Nuclear Research and Nuclear Energy, Sofia 1184, Bulgaria.
- (1) T. Stanev, T. K. Gaisser and F. Halzen, Bartol report 85-10, Submitted to Phys.Rev.D.
- (2) T. Stanev and Ch. P. Vankov, Bartol report 85-22, To be published in Phys.Lett.B.
- (3) B. Rossi, *High-Energy Particles*, Englewood Cliffs, N.J. (Prentice-Hall, 1952).
- (4) R. J. Protheroe and K. E. Turver, J. Phys. G: Nucl. Phys. 5, 1613 (1979).
- (5) M. Samorski and W. Stamm, Ap J 268, L17 (1983).
- (6) J. Lloyd-Evans *et al.*, Nature 305, 784 (1983).
- (7) M. L. Marshak *et al.*, Phys. Rev. Lett. 54, 2079 (1985) Rev. Lett.

## MUON SPECTRUM IN AIR SHOWERS INITIATED BY GAMMA RAYS

S.A. Stephens  
Tata Institute of Fundamental Research  
Homi Bhabha Road, Bombay 400005, India

R.E. Streitmatter  
NASA/GSFC, Maryland 20771, U.S.A.

## ABSTRACT

We have derived an analytic representation for the invariant cross-section for the production of charged pions in  $\gamma$ P interactions by making use of the available cross-sections. Using this the abundance of muons in a gamma ray initiated air shower is calculated.

1. Introduction. Total hadronic cross-section of  $\gamma$ -rays at energies greater than a few GeV is about two hundred times smaller than hadron inelastic cross-section. Therefore, hadron production by  $\gamma$ -ray showers in the atmosphere is neglected for the study of muons. However, the discovery of pure  $\gamma$ -ray air showers from Cygnus X-3 [1] has renewed interest in this study, because of the observed muon content in these air showers is not very small compared to those from hadron showers. We have attempted in this paper to derive an analytic representation for the invariant cross-section for the production of charged pions in  $\gamma$ -P interaction, using the available data. Making use of this, the pion production spectrum in the atmosphere is calculated for an air shower initiated by  $\gamma$ -rays and muon spectrum at different depths is determined.

2.  $\gamma$ -P Inclusive Cross-section. The frame in which particle production is symmetric in  $\gamma$ -P interaction is found to be the one in which the ratio,  $Q$ , of the target momentum to the beam momentum is larger than 1. Experiments performed at energies  $>$  a few GeV show that the value of  $Q$  lies between 2 and 3 [2-5]. However, at low energies, where  $P_{33}$  and  $D_{13}$  resonances dominate, the threshold is consistent with that of centre of mass system (CMS) with  $Q = 1$ . Therefore, we assume in our investigation that  $Q$  is energy dependent of the form

$$Q = 1. + 2. \exp(-m_p/E_\gamma) \quad (1)$$

From a study of the observed invariant cross-section for the production of charged pions, we obtained a representation of the type

$$E \frac{d^3\sigma}{dp^3} = f(E_\gamma) \exp(-C_1\mu) \cdot \exp(-C_2\tilde{x}^{-1.5}) / \{1 + C_3/(1-p^*/p_{\max}^*)\} \dots \quad (2)$$

Here  $\tilde{x} = \sqrt{\{x_{11}^{\prime 2} + Q(p_{\perp}^2 + m_\pi^2)/S\}}$  and  $\mu = \sqrt{(p_{\perp}^2 + 9m_\pi^2)}$ , where  $x_{11}' = p_{11}'/p_{\max}'$ ,  $C_1$ ,  $C_2$  and  $C_3$  have values 6.93, 3.4 and 0.03 respectively. The longitudinal momentum in the  $Q$ -system is given by

$$p_{11}' = \{p(S' + m_p^2) - E(S' - m_p^2)\} / 2m_p \sqrt{S'} \quad \dots \quad (3)$$

In the above expressions  $S = m_p(m_p + 2E_\gamma)$ , the square of the invariant mass and  $S' = m_p(m_p + 2QE_\gamma)$ . The last term in Eqn. (2) makes sure that the momentum of pions  $p^*$  in CMS does not exceed the maximum allowed momentum  $p_{\max}^*$ . It is clear that Eqn. (2) is symmetric in Q system except at large values of  $x$  due to this restriction.

We have shown in Figure 1, the invariant cross-section for the production of  $(\pi^+ + \pi^-)$  as a function of  $x_{11}^* = p_{11}'/p_{\max}^*$  for various values of  $p_\perp$  at  $E_\gamma$  values 18 and 6 GeV [3,6]. The general fit to this data using Eqn. 2 is very good. Notice that the invariant cross-section does not peak at  $x_{11}^* = 0$ . The measured  $2/E(d^3\sigma/dp^3)_\perp dp_\perp$  is shown in Fig. 2, for various  $p_\perp$  intervals. The filled circles, triangles and squares correspond to respectively data from 9.3, 4.7 and 2.8 GeV. The data plotted in this figure relate to  $\pi^-$  production only. Here again one finds that the overall fit to the data is remarkably good.

The form of the function  $f(E_\gamma)$  is  $A[1+g(E_\gamma)]$ . In order to evaluate this, we have adopted the following procedure. In the energy region between about 2.5 and 20 GeV, we have made use of the measured cross-sections given in Figures 1 and 2 and the observed  $\pi^+/\pi^-$  ratio of  $\approx 1.1$  [2,3,6]. For the rest of the energy region, we have made use of the observed multiplicity in PP collisions with the assumption that multiplicity depends only on the available energy in CMS. It is found that at large  $E_\gamma$  values the observed  $\langle m_\pi \rangle$  agrees well with that calculated using PP data [7,8]. However, in the region, where  $\rho$  production dominates, the  $\langle m_\pi \rangle$  in  $\gamma P$  interaction is larger. Therefore, at low energies, we have smoothly fitted from the observed data at 2.8 GeV to one pion production region. By setting  $\langle m_\pi^\pm \rangle \sigma_T = 2\pi \int p^* (Ed^3\sigma/dp^3)_\perp dp_\perp / E^*$  and using the observed  $\sigma_T$  values [9,10], we found that  $A=4.7$  and  $g(E_\gamma)$  as

$$\begin{aligned} g(E_\gamma) &= 3350 (E_\gamma + 10)^{-3.5} & E_\gamma \geq .86 \text{ GeV} \\ &= 125 \exp(-5.6 E_\gamma) & .725 \leq E_\gamma \leq .86 \\ &= 3.5 E_\gamma^{1.5} & .625 \leq E_\gamma \leq .725 \quad \dots \quad (4) \\ &= 1.73 & .49 \leq E_\gamma \leq .625 \\ &= 1620 \exp(-14E_\gamma) & .315 \leq E_\gamma \leq .49 \end{aligned}$$

The above expressions approximately characterize  $\Delta(1232)$ ,  $N(1520)$  and  $N(1680)$  resonances well within a few percent.

From our investigation, we need to know the cross-section for  $\gamma$ -air nuclei interactions. In order to obtain information on this, we have examined the asymptotic total cross-sections for  $\gamma P$ ,  $\gamma D$ ,  $\pi P$ ,  $\pi D$ ,  $KP$ ,  $KD$ ,  $PP$ ,  $PD$ ,  $\bar{P}P$  and  $\bar{P}D$  interactions [10]. It is found that photo-hadron cross-section scales exactly as other hadron-hadron cross-sections with atomic number of the target. Therefore, we made use of the scaling for proton interactions and obtained  $\gamma$ -air inclusive cross-section as  $\sigma_T < A >_{\text{air}} / 1.8$ .

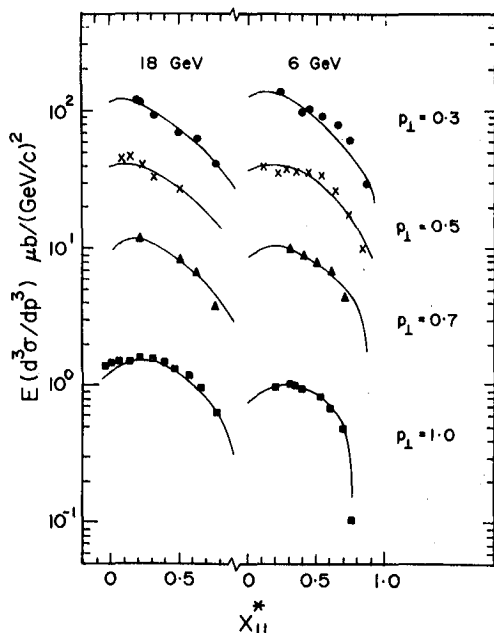


Fig. 1 Invariant cross-section for  $(\pi^+ \pi^-)$  is shown as a function  $x_{11}^*$  for  $E_\gamma = 18$  and  $6$  GeV

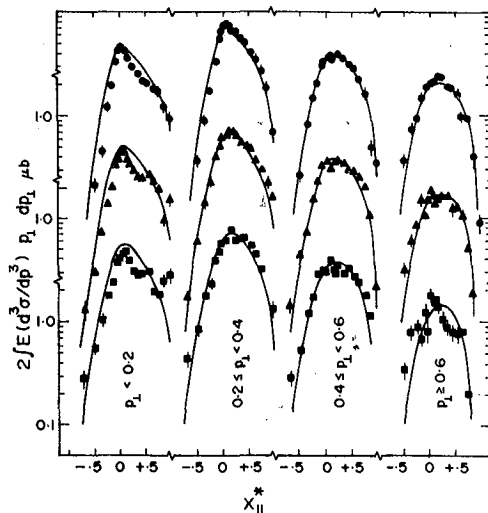


Fig. 2  $\pi^-$  invariant cross-section integrated over  $p_\perp$  is shown for different  $p_\perp$  intervals. The filled circles, triangles and squares correspond to  $E_\gamma = 9.3$ ,  $4.7$  and  $2.8$  GeV respectively.

3. Muon Production in  $\gamma$ -ray Showers. Pion production spectrum in the atmosphere is given by

$$P_\pi(E, x) = \iint J_\gamma(E_\gamma, x) dE_\gamma \cdot \{2\pi (E d^3\sigma/dp^3) p_\perp d\theta \dots \quad (5)$$

Here, the photon spectrum  $J$  is obtained using one dimensional propagation of cascade initiated  $\gamma$ -rays in the atmosphere without approximations [11]. From this the spectra of pions and muons in the atmosphere are calculated by taking into account the decay, energy loss processes and the 2nd generation of pions as described by Stephens [12].

In Figure 3, we show the preliminary results based on a representation of invariant cross-section, which has the same form as that for  $\pi^0$ -inclusive production. The integral flux muons is shown as a function of primary  $\gamma$ -ray energy for different energy thresholds and for a few sample depths. It is seen that the total muon flux is small at all depths and therefore, the observed large flux of muons with  $\gamma$ -ray showers associated with Cygnus X-3 [1] could be due to other reasons.

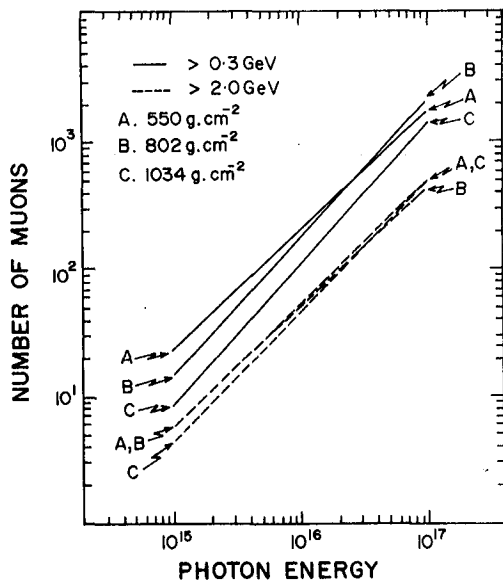


Fig.3 Total muons above .3 and 2 GeV are shown as a function of primary  $\gamma$ -ray energy at 3 atmospheric depths.

One of the possible explanation for this anomaly is that some of the air shower electrons and photons, which continue their propagation are registered by the muon detectors.

#### References

- [1] M. Samorski and W. Stamm, *Ap.J.*, 268, L17 (1983)
- [2] P. Rankin, Ph.D. Thesis, Imperial College, London (1982)
- [3] A.M. Boyarski et al., *Phys. Rev.*, D14, 1733 (1976)
- [4] K.C. Moffeit et al., *Phys. Rev.*, D5, 1603 (1972)
- [5] G. Alexander et al., *Phys. Rev.*, D8, 712 (1973)
- [6] H. Burfeindt et al., *Nuclear Phys.*, B74, 189 (1974)
- [7] G.D. Badhwar et al., *Phys. Rev.* D15, 820 (1977)
- [8] S.A. Stephens and G.D. Badhwar, *Ap.Sp. Sci.*, 76, 213 (1981)
- [9] T.A. Armstrong et al., *Phys. Rev.*, D5, 1640 (1972)
- [10] M.A. Benitez et al., *Rev. Mod. Phys.*, 56, No.2 (1984)
- [11] R.E. Streitmatter and S.A. Stephens (This Conference)
- [12] S.A. Stephens, *Proc. 16th ICRC (Kyoto)*, 10, 90 (1979)



DEVELOPMENT OF ELECTROMAGNETIC CASCADES IN THE ATMOSPHERE  
INCLUDING THE LANDAU-POMERANCHUK-MIGDAL EFFECT

R. E. Streitmatter and S. A. Stephens\*  
NASA/Goddard Space Flight Center, Greenbelt, MD 20771, U.S.A.

ABSTRACT

Numerical solutions have been obtained for the one-dimensional atmospheric electromagnetic cascade diffusion equations, including the LPM and screening effects. Spectra produced by primary gamma rays of various energies are given at a number of depths in the atmosphere.

1. Introduction. As the first step in a program to calculate the muon content of gamma-ray-induced atmospheric showers (1), we have carried out numerical solutions of the 1-dimensional electromagnetic cascade diffusion equations (2).

We have attempted to carry out a calculation with a minimum of approximation. The Landau-Pomeranchuk-Migdal (LPM) effect (3,4) on pair-production and bremsstrahlung cross sections has been included. The LPM cross sections were calculated using the formalism of Bowen *et al.* (5). Atmospheric densities were taken from the U. S. Standard Atmosphere. Constant collisional energy loss was included. Lastly, the effects of incomplete screening (6) were included.

The diffusion equations were integrated using the Runge-Kutta method. An initial condition of a single gamma ray vertically incident on the atmosphere was used. Electron and photon spectra down to 10 MeV were found throughout the atmosphere. Solutions have been obtained for incident gamma ray energies ranging from  $10^{14}$  to  $10^{19}$  eV. As a check, the LPM and incomplete screening effects can be removed, yielding the classical complete screening cross sections. In this case, the solutions obtained agree with Approximation B.

Figure 1 shows the atmospheric development of the integral electron spectra above 10 MeV for 6 incident gamma ray energies. Generally, the effects of the LPM cross sections on the integral spectrum are most pronounced at shallow atmospheric depths. For a  $10^{19}$  eV incident gamma, at 550 g/cm<sup>2</sup> the ratio of the Approximation B integral spectrum (not shown here) above 10 MeV to the integral spectrum of Figure 1 is 1.56. At 1034 g/cm<sup>2</sup>, the same ratio is 0.95.

Figures 2 and 3 show the differential electron spectra at 550, 700, 800, 900, and 1034 g/cm<sup>2</sup> for incident  $10^{14}$  and  $10^{16}$  eV gammas, respectively. While there are differences between this spectra and the corresponding Approximation B spectra at the 15 percent level, only above  $10^{18}$  eV do the differential electron and photon spectra sharply and progressively deviate from the Approximation B spectra. Figure 4a shows the differential electron spectra induced by a  $10^{19}$  eV gamma,

\* Tata Institute of Fundamental Research, Bombay, INDIA

again at the same 5 atmospheric depths as the previous figures. Figure 4b, plotted to the same scale, shows the Approximation B spectra.

### References

1. Stephens, S. A., and Streitmatter, R. E., This Conference, HE 4.5-4.
2. Rossi, B., 1952, High Energy Particles, 214.
3. Landau, L. and Pomeranchuk, I., Dokl. Akad. Nauk SSSR, 1953, 92, 535.
4. Migdal, A. B., Phys. Rev., 1956, 103, 1811.
5. Bowen, T., et al., 1979, At. Data Nucl. Data Tables, 24, 495.
6. Bernstein, I. B., 1956, Phys. Rev., 80, 995.

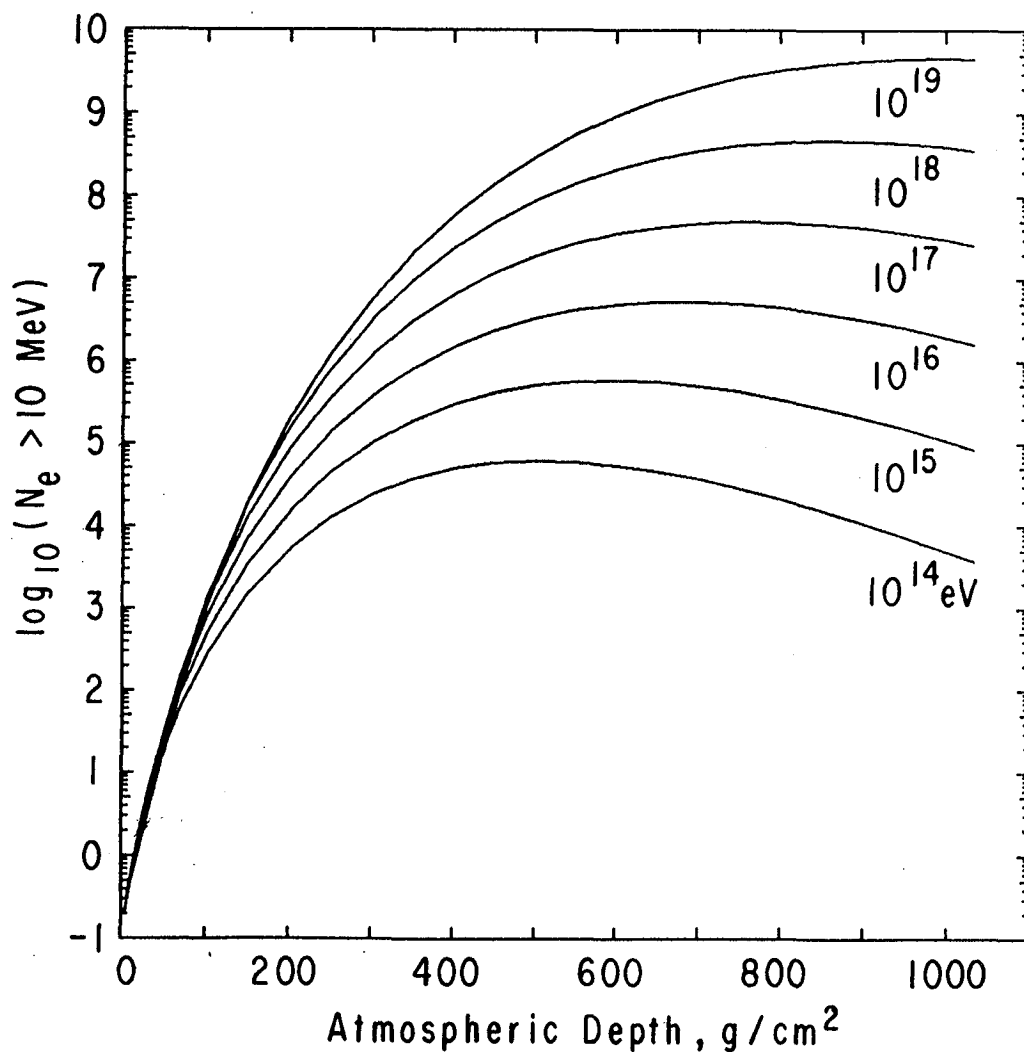
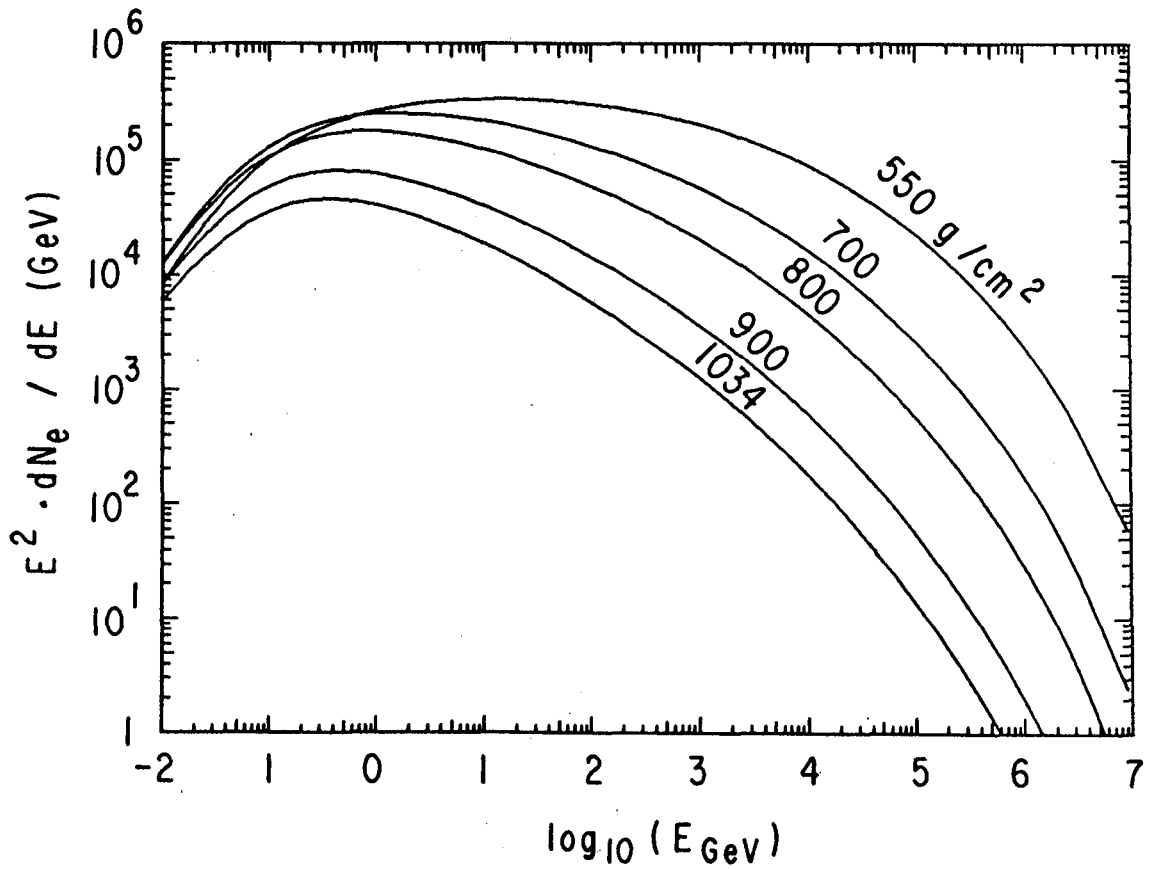
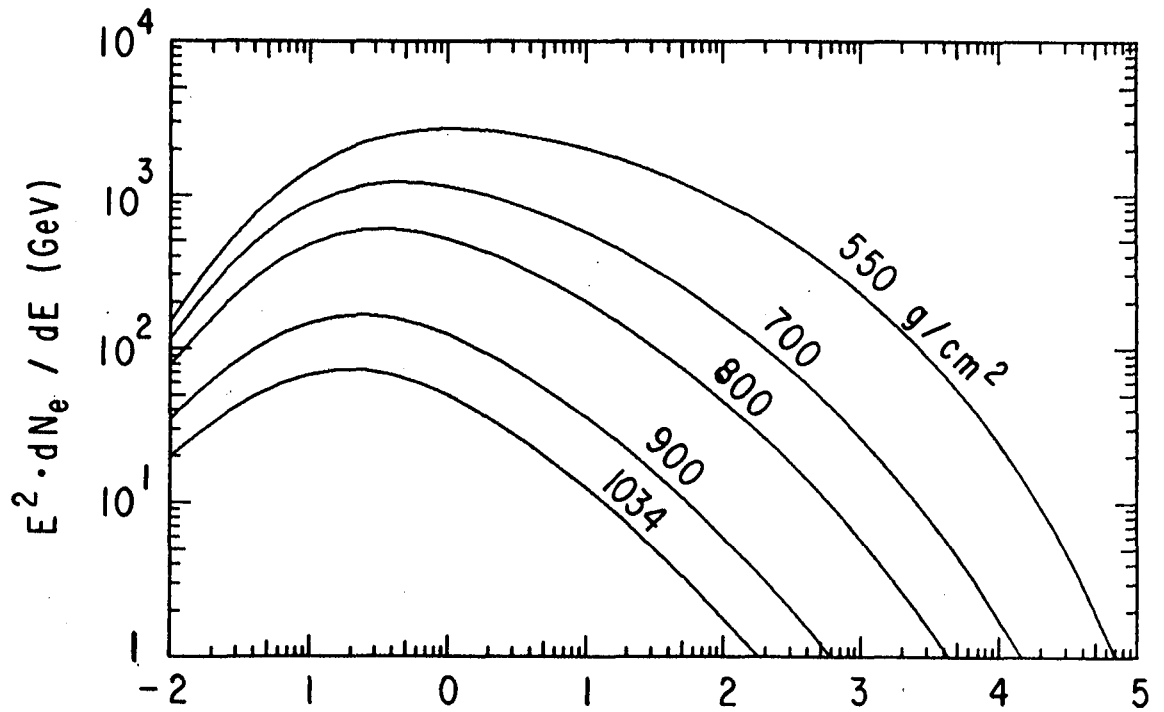


Figure 1.



Figures 2 (above) and 3 (below) for  $10^{14}$  and  $10^{16}$  eV, respectively

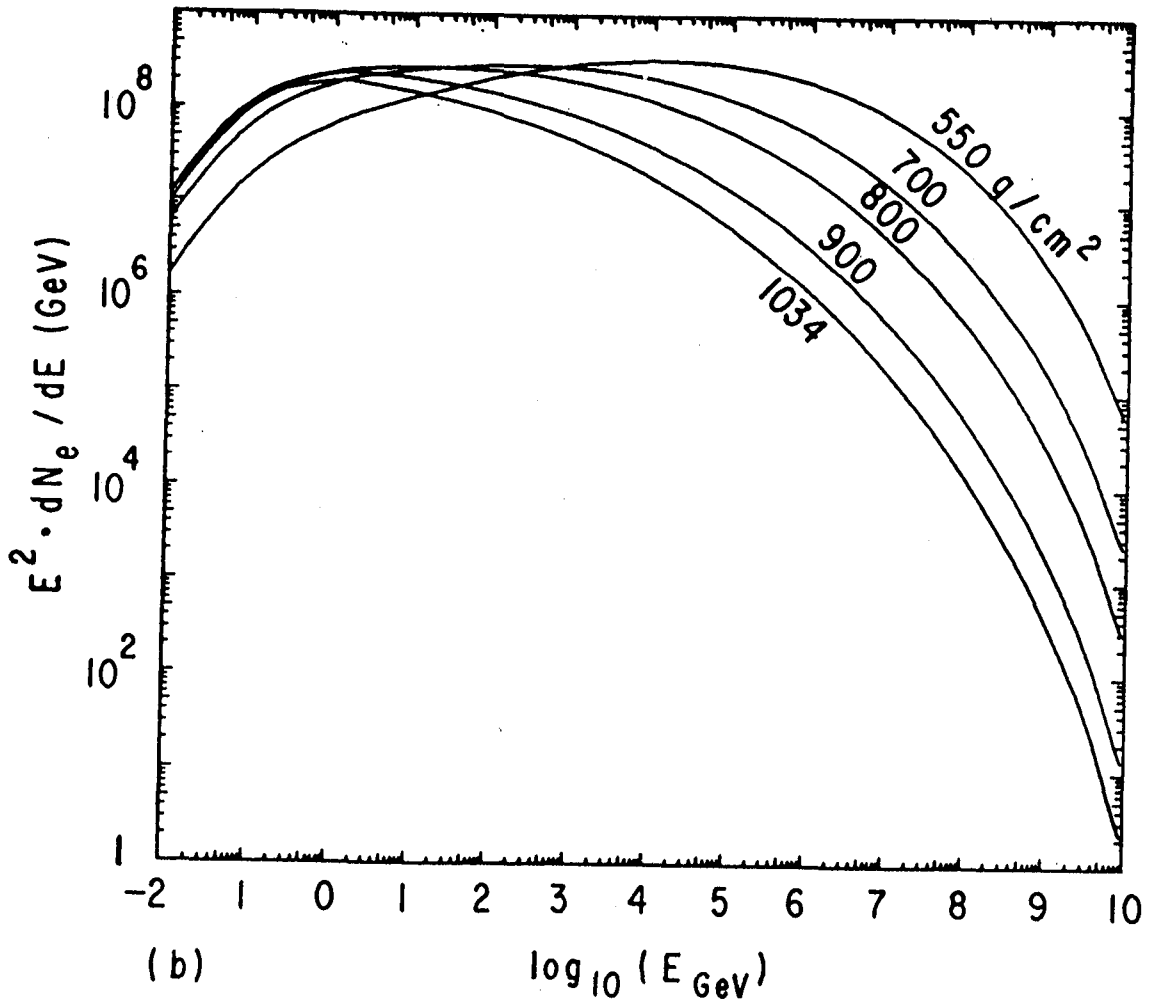
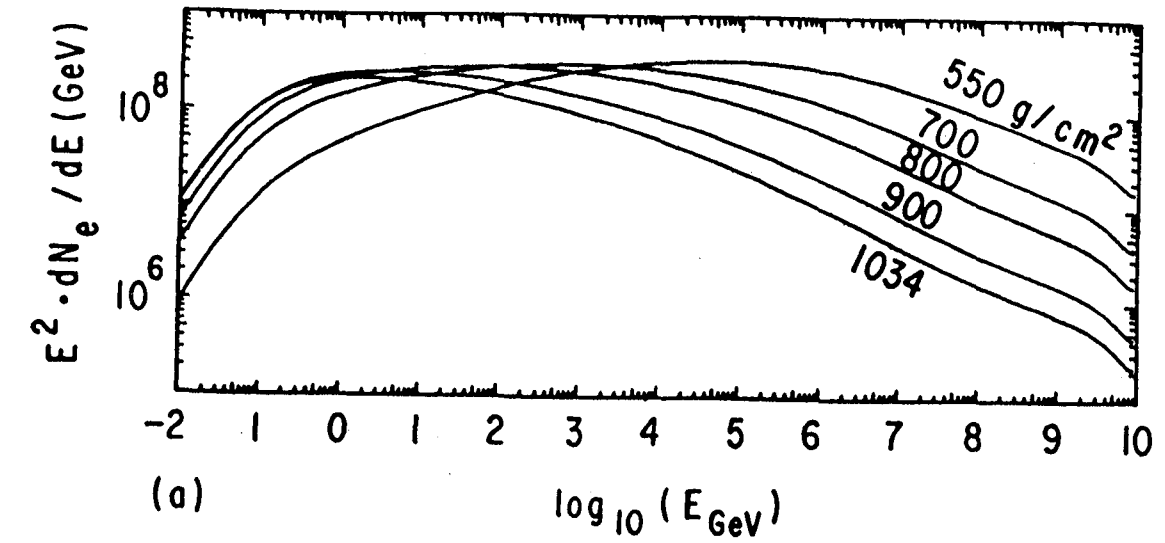


Figure 4

ELECTROMAGNETIC AND MUONIC STRUCTURE OF SHOWERS INITIATED  
BY GAMMA-RAYS AND BY HADRONS

A. M. Hillas  
Physics Department, University of Leeds,  
Leeds LS2 9JT, UK

ABSTRACT

(a) If photon cascades develop by the usual mechanisms, there should indeed be notable differences between the structure of showers due to photon and hadron primaries, as regards muon densities and lateral distributions of some detector signals.

(b) The muon content of showers from Cygnus X-3, observed at Kiel, cannot be understood in this way. One remedy is to postulate arbitrarily a strong hadronic interaction of photons in the TeV region. This would utterly change the nature of electromagnetic cascades, but surprisingly does not at first sight seem to be in conflict with air shower observations.

1. Two questions concerning gamma-ray initiated showers

(i) Can the structure of extensive air showers ( $10^{15}$  -  $10^{16}$  eV) be used to distinguish those that are initiated by primary gamma-rays from the normal proton- or nucleus- initiated showers? This would help in observations of point sources such as Cygnus X-3. The low muon content of gamma showers has been regarded as their most obvious hallmark, with different shower "age" as another possible distinguishing feature. However,

(ii) can one understand the observation by Samorski & Stamm (1) that showers from Cygnus X-3 (whose primaries are undeflected and stable, and hence presumably photons) have about 2/3 of the normal density of penetrating particles (muons of 2 GeV or more) at  $\sim 10$  m from the shower axis?

If the directional particle fluxes being reported from various proton decay experiments are confirmed, they indicate that the radiation from Cygnus X-3 has important interactions that are not yet understood.

2. Calculation of shower development

A 3-dimensional Monte-Carlo simulation is used to follow all particles (electrons, photons, nucleons, pions, muons - but omitting kaons) down to 0.05 MeV, and to determine the signals produced in 5-cm-deep scintillators and 120-cm-deep water Cerenkov detectors (as used at Haverah Park). (The average response of such detectors - covered by a thin wood roof - to the relevant particles and energies was calculated beforehand, but, as a check, the shower particles were followed into a 120-cm-deep lake on reaching the ground, where their Cerenkov emission was noted and the ionization loss in the top layer was also noted to check the scintillator response.)

*Assumptions about hadronic interactions of photons:* Up to several GeV,  $\sigma(\gamma, \text{air nucleus} \rightarrow \text{hadrons}) = 6.4 \sigma(\gamma, \text{deuteron})$ . The intermediate states produced in the well-known resonances below 1 GeV were taken to decay isotropically (in c.m.s.) as an approximation, in 2-body stages. However, these resonances are of little importance in EAS: most of the muons resulting (via pion decay) are of such low energy that they stop - and certainly none is above 2 GeV. From 10 GeV to 200 GeV the cross-section is taken to be 1.42 mb, and then to rise rather like p-p cross-sections - i.e.  $1.42 (1 + 0.0273u + 0.01u^2)$  mb, where  $u = \ln(E/200 \text{ GeV})$ . Interacting photons are taken to behave very much like pions.

*Assumptions about hadron interactions.* Two models of hadronic interactions are used: (a) a radial scaling model (with rising hadron-nucleon cross-sections), based on detailed accelerator data up to 1 TeV, but making the approximation of working with scaling in the laboratory frame of reference (thus underestimating a little the particles below  $\sim 1$  GeV); (b) a modification in which a greater multiplicity of low-x particles is generated (but without a large reduction in the fragmentation-region particles) at collision energies above  $\sim 1$  TeV, and fewer leading pions are produced. These two variants are thought to bracket the true main features of interactions. Roughly speaking, the first model with a large content of very heavy nuclei in the primary beam, or the latter with largely protons, would account for many air shower features.

### 3. Proton-initiated and gamma-initiated showers

Figure 1 shows the apparent particle densities  $\rho$  at various axial distances, in showers produced by normal primaries of  $10^{14}$ ,  $10^{15}$ ,  $10^{16}$  and  $10^{17}$  eV per nucleon, and by gammas of  $10^{15}$  and  $10^{16}$  eV, all at  $15^\circ$  zenith angle. All are normalized to  $10^{16}$  eV energy, by plotting  $r^2\rho/E_{16}$ , where  $E_{16} = E_{\text{prim}}/10^{16}$  eV. Particle densities recorded by deep water tanks, and

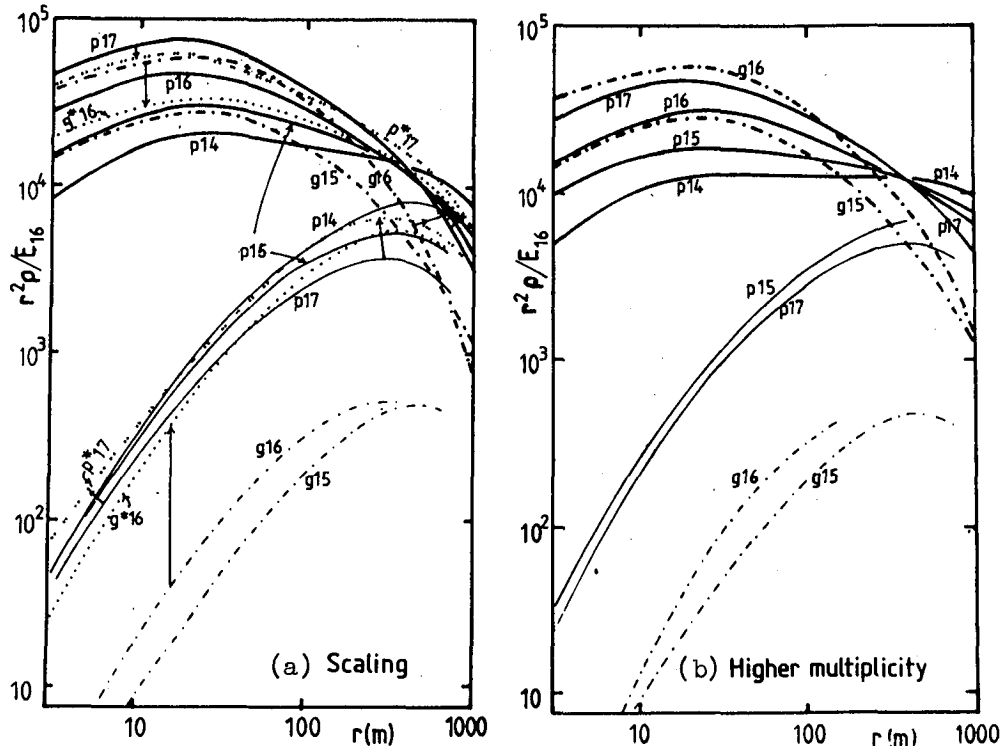


Figure 1: Particle densities (in water tank) and muon densities in proton and gamma-initiated showers at  $15^\circ$  to vertical (Sea level).

muon densities above 0.4 GeV (as at Haverah Park). Graphs 1(a) and 1(b) use the two different hadronic interaction models. Muon densities, in the lower part of the graphs, are shown by thinner lines. The gamma showers (---) differ from the proton showers by having a very much lower muon density — as expected from calculations by Wdowczyk long ago (2), and this helps to make the overall particle density fall more steeply beyond 200m — though this effect is less marked in scintillators.

As an alternative to muon detection may be to compare particle densities recorded by deep and shallow detectors, the ratio of (120 cm) water tank signal (ptcle. density) to (5 cm) scintillator density is plotted in Figure 2 for  $10^{16}$  eV proton showers (line and dashed curve show results

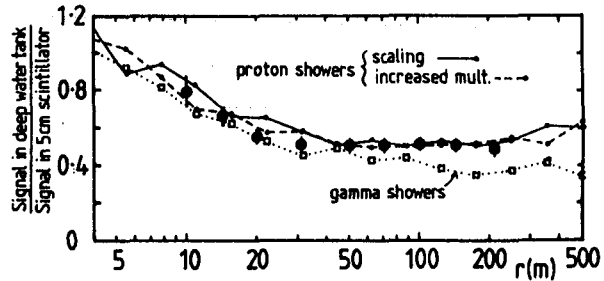
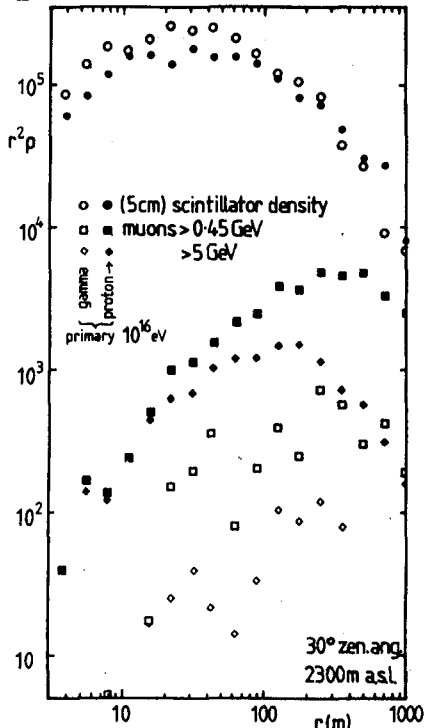


Figure 2 (↑). Ratio of particle densities recorded by two detectors in proton and gamma showers at various axial distances. (Sea level: zenith angle  $15^\circ$ : energy  $10^{16}$  eV or thereabouts.)

← Figure 3. Predicted particle densities  $\rho$  in proton (filled symbols) and gamma showers (open symbols) of  $10^{16}$  eV at high altitude site (2300 m). Showers at  $30^\circ$  zenith angle. Detectors are 5-cm scintillators.

from the two models) and gamma showers (dotted curve). Mean ratios in showers of  $\sim 3 \times 10^{16}$  eV at  $\sim 13^\circ$  zenith angle have been observed for ordinary real showers (filled circles: J. Perrett & A. A. Watson, private communication), and agree fairly well with expectation. (The sensitivity to the proportion of heavy nuclei is not calculated here, but is not a major factor in the present comparison.) Measurements are required beyond 100m with very large detector areas to make use of the expected peculiarities of individual gamma showers.

Figure 3 shows what is expected (from the scaling model) at a high level observing station (2300m altitude), looking at  $10^{16}$  eV gamma showers and proton showers at  $30^\circ$  zenith angle (typical for Cygnus X-3). Scintillator particle densities are plotted. The statistical accuracy of this simulation run for gamma showers is too low to give a good determination of their muon densities, though the shape of the muon curve should be very similar to the curves in Figure 1.

#### 4. Do gamma-rays produce hadrons much more frequently?

This would, of course, invalidate the previous graphs.

Figure 4 shows the density of muons above 2 GeV at 10m from the shower axis, interpolated from the calculations for protons (line p - both models agree here) and gammas (line g). A line for iron primaries (Fe) is also shown. The Kiel results (1) for nuclear and (presumed) gamma showers are marked. There is a huge discrepancy. So, do electrons or photons of high energy generate pions or muons readily by some unknown process? Would this not wreck all interpretations of air showers?

To begin an exploration of the latter question, a quite arbitrary large addition has been made to the hadronic cross-section for photons at

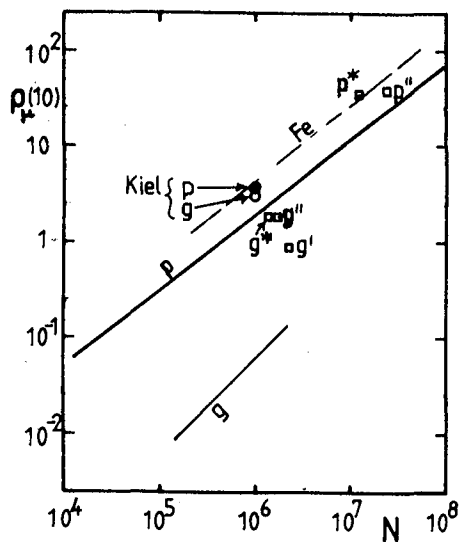


Figure 4. Densities of muons ( $>2$  GeV) at 10 m from shower axis in nuclear (p, Fe) and gamma (g) showers.

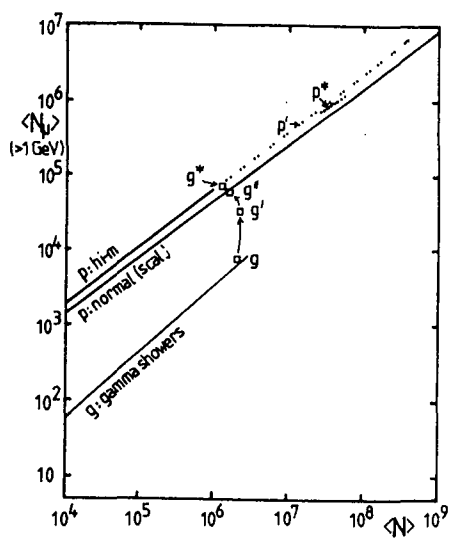


Figure 5. Number of muons ( $>1$  GeV) & total shower size  $N$ . See text.

high energy (no change below 1 TeV) — either (i) a very broad resonance at a few TeV, the interaction m.f.p. at its peak being  $100 \text{ g cm}^{-2}$  (result: muon density in gamma showers shown as  $g'$ ) — or (ii) the same but with m.f.p.  $40 \text{ g cm}^{-2}$  at peak ( $g''$ , and point  $p''$  for  $10^{17}$  eV proton EAS) — or (iii) cross-section having threshold above 1 TeV, and m.f.p. remaining at  $100 \text{ g cm}^{-2}$  above 10 TeV ( $g^*$  and, for proton showers,  $p^*$ ). Clearly, gamma showers are now hardly distinguishable from proton showers by their muon content — and their lateral distributions become more similar. (See Fig. 1: the line ..... shows the modified  $10^{16}$  eV gamma showers,  $g^*$ , and the line .. .. shows the resulting change to the structure of ordinary  $10^{17}$  eV proton showers. The latter are in fact a surprisingly good fit to observations!)

One would expect the  $N_{\mu}$ - $N_e$  relationship for showers to be spoiled — perhaps  $N_{\mu} \propto N_e$  now? Figure 5 shows that this is not the case. (The mean  $N_{\mu}$  ( $E_{\mu} > 1 \text{ GeV}$ ) is plotted against total number of particles ( $N$ ) in the shower. For the purpose of this simple test only the averages  $\langle N \rangle$  for fixed  $E_{\text{primary}}$  are plotted, without applying the small correction for primary spectrum selection bias.) Such an (arbitrary) assumption about photon interactions would also be expected to ease the problem of accounting for the ratio of multi-TeV hadrons and gammas in the atmosphere.

The alternative of considering direct muon production, or production via charm rather than by pions, has not been explored. Pions have the advantage of putting their energy into many lower-energy muons, after cascading.

Such a large hadron-like cross-section has no theoretical justification: can it really be possible? It would perhaps not have been noticeable in emulsion calorimeters with short (Pb) radiation lengths.

#### References

1. Samorski, M. & Stamm, W. (1983) 18th Int. C. R. Conference, Bangalore, 11, 244-7.
2. Wdowczyk, J. (1965) 9th Int. Conf. on Cosmic Rays, London, 2, 691-3



## THE MUON CONTENT OF GAMMA-RAY SHOWERS

P.G. Edwards and R.J. Protheroe  
 Department of Physics, University of Adelaide  
 Adelaide, South Australia 5001

*Abstract.* We report the result of a calculation of the expected number of muons in  $\gamma$ -ray initiated and cosmic ray initiated air showers using a realistic model of hadronic collisions in an effort to understand the available experimental results and to assess the feasibility of using the muon content of showers as a veto to reject cosmic ray initiated showers in ultra-high energy  $\gamma$ -ray astronomy. We also consider the possibility of observing very-high energy  $\gamma$ -ray sources by detecting narrow angle anisotropies in the high energy muon background radiation.

1. *INTRODUCTION.* With the recent observation of ultra-high energy (UHE)  $\gamma$ -rays from Cygnus X-3 (Samorski and Stamm, 1983a; Lloyd-Evans *et al.*, 1983), Vela X-1 (Protheroe *et al.*, 1984) and LMC X-4 (Protheroe and Clay, 1985), together with the detection of excess air showers from the direction of the Crab Nebula (Dzikowski *et al.*, 1983; Boone *et al.*, 1984), it is timely to examine the muon content of extensive air showers (EAS) initiated by primary  $\gamma$ -rays to investigate the possibility of: (a) using a "normal" muon content to veto some fraction of cosmic ray (CR) showers; and (b) detecting  $\gamma$ -ray sources at very-high energies through observing narrow angle anisotropies in the muon background radiation.

Measurements of the muon content were made in two of the recent source observations, that of Cygnus X-3 by the Kiel group (Samorski and Stamm, 1983b) and that of the Crab by the Lodz group (Dzikowski *et al.*, 1983). Early predictions of muons in  $\gamma$ -ray EAS (Karakula and Wdowczyk, 1963; Wdowczyk, 1965; Braun and Sitte, 1965) together with later work on muons of photoproduction origin in CR EAS by McComb *et al.* (1979), had led us to expect that at  $10^{18}$ - $10^{19}$  eV energies  $\gamma$ -ray initiated EAS would have a muon content about one tenth of that of proton-initiated EAS. The ratio of muon number in the excess EAS to that in CR EAS was measured to be somewhat higher in the two recent experiments, however: about 0.6 for the observation of the Crab and about 0.7 for the Cygnus X-3 observation. This surprising result appeared to preclude the possibility of using a "normal" muon content to veto CR events in UHE  $\gamma$ -ray astronomy.

A number of deep underground muon detectors are now being commissioned to search for muons produced by the interaction of extraterrestrial neutrinos and an estimate of the flux and neutrino light curve for Cygnus X-3 has recently been made by Gaisser and Stanev (1985). If a significant number of muons are produced in the atmosphere as secondaries by  $\gamma$ -ray showers at very-high energies, it may also be worth searching for narrow angle anisotropies in the sea-level muon background radiation as an alternative to the atmospheric Cerenkov technique. Searches of this type were conducted some years ago (Allkofer *et al.*, 1981) although not specifically for  $\gamma$ -ray sources.

To consider these questions we have recently performed a new calculation of the muon content of  $\gamma$ -ray initiated EAS using a realistic model of high energy hadronic interactions. Details of the calculation are given by Edwards *et al.* (1985).

## 2. MUONS IN GAMMA-RAY SHOWERS.

The integral energy spectra of muons we obtain at an atmospheric depth of  $1130 \text{ g cm}^{-2}$  are given in Fig. 1 for average  $\gamma$ -ray and proton initiated EAS for primary energies in the range  $10^{11} - 10^{17} \text{ eV}$  and  $10^{10} - 10^{17} \text{ eV}$

respectively. The atmospheric depth chosen is appropriate to the Kiel (sea level) observation of Cygnus X-3. In the Kiel and Lodz experiments, the muon measurements were obtained at fixed shower size rather than at fixed primary energy. For a realistic comparison, then, we have calculated the mean muon number for showers of given size by performing a numerical integration over primary energy taking account of fluctuations in longitudinal development.

For primary CR a broken power law energy spectrum was adopted with a differential exponent of  $-2.7$  steepening to  $-3.1$  above  $3 \times 10^{16} \text{ eV}$ . For  $\gamma$ -rays, the spectrum adopted had a differential exponent of  $-2$  and was cut off at  $10^{17} \text{ eV}$ . The results are given in Fig. 2 and show that the ratio of the muon number in  $\gamma$ -ray initiated EAS to that in proton initiated EAS is about 0.1. If the primary composition at  $10^{10} - 10^{17} \text{ eV}$  energies is mixed or is enriched in heavy nuclei, however, the ratio would be less than 0.1. From these results then it would appear that the muon component of EAS could usefully be employed to veto against CR initiated EAS in UHE  $\gamma$ -ray astronomy.

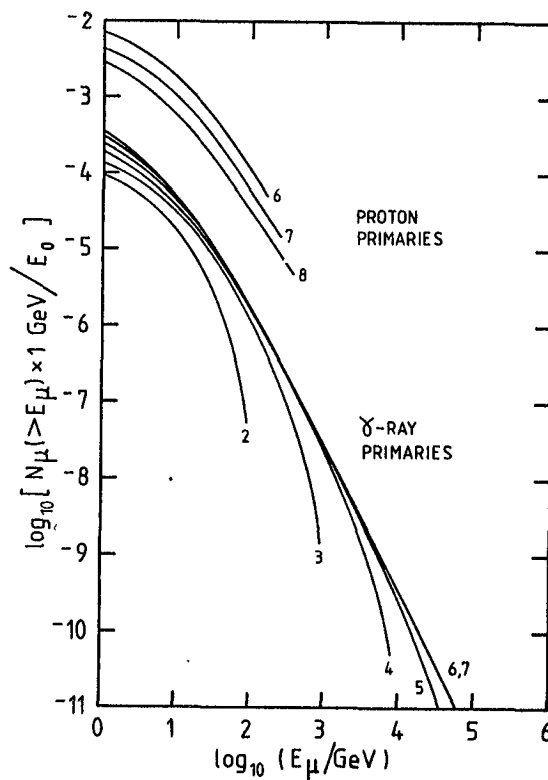


Fig. 1. Integral energy spectrum of muons in average proton and  $\gamma$ -ray initiated EAS divided by primary energy  $E_0$ . Numbers attached to the curves are  $\log_{10}(E_0/\text{GeV})$ .

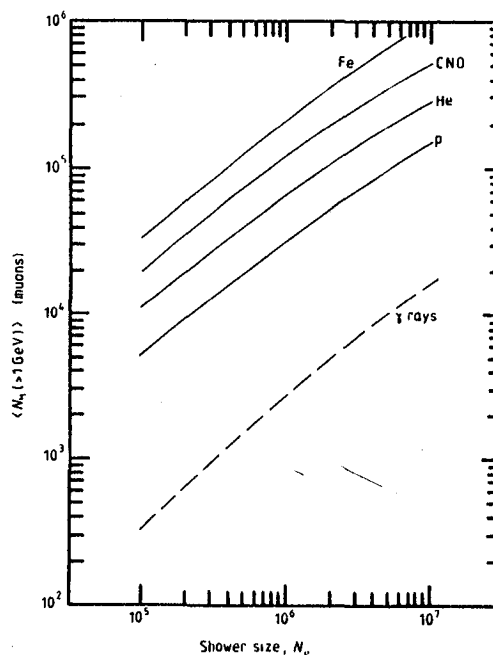


Fig. 2. Average muon number ( $>1 \text{ GeV}$ ) at fixed shower size at an atmospheric depth of  $1130 \text{ g cm}^{-2}$  in  $\gamma$ -ray and nucleus initiated EAS. (Reproduced from Edwards et al., 1985).

3. **GROUND LEVEL MUON FLUX.** The flux of atmospheric muons due to  $\gamma$ -rays from Cygnus X-3 has been calculated by convolving the muon energy spectra in  $\gamma$ -ray showers (Fig. 1) with the  $\gamma$ -ray energy spectrum of Cygnus X-3. For this we took an  $E^{-2}$  differential photon spectrum normalised to the integral flux above  $3 \times 10^{16}$  eV reported by Lloyd-Evans *et al.* (1983):

$$N(E) = 4.5 \times 10^{-4} (E/\text{GeV})^{-2} \quad (\text{photons m}^{-2} \text{ s}^{-1} \text{ GeV}^{-1}). \quad (1)$$

The resulting integral muon spectrum is shown in Fig. 3 assuming the  $\gamma$ -ray spectrum of equation (1)

continues to a cut-off energy of: (a)  $10^{16}$  eV; (b)  $10^{17}$  eV; (c)  $10^{18}$  eV. Whether this muon flux can be seen significantly above the background for a given exposure (area  $\times$  time) depends on the accuracy with which the muon directions recorded reflect the  $\gamma$ -ray arrival directions. The angular uncertainty is likely to be made up of two parts for high energy muons: (i) uncertainty in muon track reconstruction in the detector; and (ii) angular spread due to transverse momentum imparted to parent pions. For the background muon intensity summarised by Allkofer *et al.* (1971), and assuming that  $\gamma$ -rays are present over 1/100th of the orbital period, the exposure required to detect muons due to  $\gamma$ -rays from Cygnus X-3 with 99% confidence is shown in Fig. 4 for various detector track resolutions.

4. **DISCUSSION.** From the present calculations the Kiel and Lodz results are inconsistent with the excess EAS detected by these groups being due to  $\gamma$ -rays. For the nearer of the two sources, the Crab, Dzikowski *et al.* (1983) have already suggested the possibility that the excess EAS are due either to neutrons

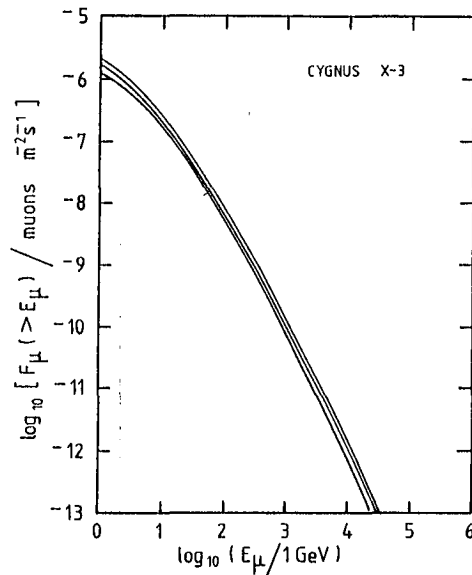


Fig. 3. Integral flux of atmospheric secondary muons due to gamma-rays from Cygnus X-3. The three curves given correspond to different assumptions about the high energy cut-off energy in the  $\gamma$ -ray spectrum (see text).

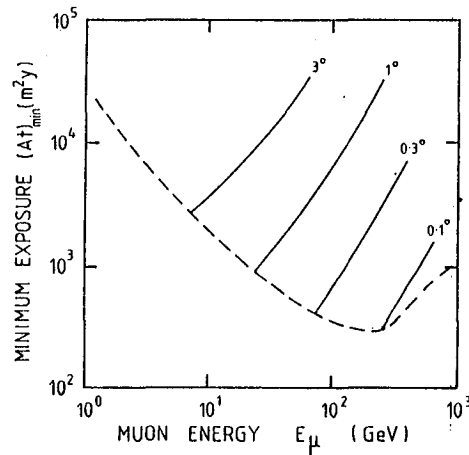


Fig. 4. Minimum exposure required as function of muon energy threshold and muon track reconstruction accuracy (the numbers attached to the curves). A lower limit is imposed by the angular spread of muons due to transverse momentum (assumed to be:  $\theta \sim \langle p_{\perp} \rangle / E_{\mu}$ ) and by Poisson statistics and is indicated by the broken line.

or protons, energetics arguments strongly favouring the latter alternative. The present calculations would also favour the excess EAS being due to protons or light nuclei: a ratio of 0.7 could easily be obtained if the excess events are due to protons and light nuclei from the Crab Supernova and if the galactic CR are of mixed composition at these energies (i.e. the CR's produced during the Crab supernova had a somewhat lighter composition than average). For Cygnus X-3, protons or nuclei can be ruled out because the excess EAS are observed in phase with the orbital motion of the system and it appears fairly certain that the excess EAS from Cygnus X-3 are indeed due to  $\gamma$ -rays. The observed ratio of muons in these EAS to that in CR EAS of 0.7 is then very difficult to explain. We conclude then that the discrepancy is likely to be due either to a systematic effect in the experiment (e.g. array triggering biases, etc.) or alternatively, may indicate that the nature of hadronic interactions at  $10^{14}$  -  $10^{16}$  eV energies differs from our current expectations. If the first possibility turns out to be correct, then the observation of a "normal" muon content in an EAS could be used to veto CR initiated EAS in UHE  $\gamma$ -ray astronomy. A similar conclusion has been reached independently by Stanev *et al.* (1985).

We turn now to the possibility of observing  $\gamma$ -ray sources through detecting atmospheric muons. From Fig. 4 the best energy range to examine appears to be that above 100 GeV for which a detector with a  $0.1^\circ$  track reconstruction accuracy would require an exceptionally large exposure, in excess of 300  $\text{m}^2$ -years when the source was in the field of view, in order to detect a significant excess from Cygnus X-3. While technically such an experiment may be feasible, there appear to be few (if any) advantages of such a system over over more conventional methods of very-high energy  $\gamma$ -ray astronomy (i.e. the atmospheric Cerenkov technique).

*Acknowledgements.* This research is supported by the Australian Research Grants Scheme. P.G. Edwards acknowledges receipt of a Commonwealth Postgraduate Research Award.

#### REFERENCES

- Allkofer DC *et al.* 1971 Phys. Lett., 36B, 425  
 Allkofer DC *et al.* 1981 Proc 17th ICRC (Paris) 9, 174  
 Boone J *et al.* 1984 Ap. J. 285, 264  
 Braun D and Sitte K 1965 Proc. 9th ICRC (London) 2, 712  
 Dzikowski T *et al.* 1983 J. Phys. G:Nucl. Phys. 9, 459  
 Edwards PG, Protheroe RJ and Rawinski E 1985 J. Phys G: Nucl. Phys. (letter) in press.  
 Gaisser TK and Stanev T 1985 Bartol preprint BA-85-12  
 Karakula S and Wdowczyk J 1963 Acta Phys. Polonica 24, 231  
 Lloyd-Evans J *et al.* 1983 Nature 305, 784  
 McComb TJL, Protheroe RJ and Turver KE 1979 J. Phys. G:Nucl. Phys. 5, 1613  
 Protheroe RJ, Clay RW and Gerhardy PR 1984 Ap. J. 280, L47  
 Protheroe RJ and Clay RW 1985 Nature, in press. See also these proceedings paper DG2.6-10.  
 Samorski M and Stamm W 1983a Ap. J. 268, L17  
 Samorski M and Stamm W 1983b Proc 18th ICRC (Bangalore) 11, 244  
 Stanev T, Gaisser TK and Halzen F 1985 preprint  
 Wdowczyk J. 1965 Proc. 9th ICRC (London) 2, 691

## THE HUMP IN THE CERENKOV LATERAL DISTRIBUTION OF GAMMA RAY SHOWERS

S. Sinha and M.V.S. Rao  
Tata Institute of Fundamental Research, Bombay 400005, India

## ABSTRACT

The lateral distribution of atmospheric Cerenkov photons emitted by gamma ray showers of energy 100 GeV is calculated. The lateral distribution shows a characteristic hump at a distance of  $\sim 135$  meter from the core. The hump is shown to be due to electrons of threshold energy 1 GeV, above which the mean scattering angle becomes smaller than the Cerenkov angle.

Introduction : We have reported earlier<sup>1</sup> the calculation of the lateral distribution of Cerenkov radiation at sea-level emitted by showers initiated by gamma rays of energy 100 GeV incident at the top of the atmosphere. The lateral distribution shows a characteristic shoulder at a distance of  $\sim 125$  m from the core. This shoulder has been seen by various authors<sup>2-4</sup> but not by Browning and Turver<sup>5</sup>. Our calculation did not include the effect of Rayleigh and aerosol scattering and ozone absorption on the Cerenkov photons and the effect of the geomagnetic field on the electrons. Also the effect of temperature variation in the atmosphere was not included in this calculation.

Further calculations were done in which the effect of Rayleigh, aerosol scattering and ozone absorption have been included but not the geomagnetic field as the effect due to this is found to be small<sup>4</sup>. Also the effect of temperature variation is now included. The resulting lateral distribution still shows the hump at a distance of  $\sim 135$  m from the shower core. Investigations on the nature and origin of the shoulder are reported in the present paper.

Method of Calculation

The treatment of the soft cascade is essentially similar to calculations of Vatcha<sup>6</sup>. For photons both pair production and Compton scattering processes are considered while for electrons bremsstrahlung, multiple Coulomb scattering and ionisation losses are taken into account.

Everywhere corrections have been applied for the screening effect. The value of the radiation length in air used is 37.2 gms/cm<sup>2</sup>. For the atmosphere a realistic model is taken. The relation between the height  $h$  (in meters) and the depth  $x$  (gms/cm<sup>2</sup>) in the atmosphere is given by

$$h = (6740 + (2.5 \ln x)) \ln (1030/x)$$

The scale height is thus dependent on depth

The most important effect is that of multiple Coulomb scattering. Both the single and multiple Coulomb scattering are considered for particles of energy below 1 GeV and for particles with energy above 1 GeV only the multiple Coulomb scattering is taken into account since inclusion of single scattering term for these particles has negligible effect on the

Cerenkov photon lateral distribution. The refractive index,  $n$ , of air is given by

$$n = 1 + 0.0002926 (X/1030) (273.2/T) \quad \text{where } T, \text{ the atmospheric temperature (°K) is}$$

$$T = 204 + 0.091 X$$

Each photon and electron (or positron) is treated by Monte Carlo method from the point of its production to the next interaction point until either one of the following conditions is satisfied (a) its energy falls below 1 MeV, (b) it starts moving horizontally or backwards, or (c) it emerges below the observation level.

For the calculation of the Cerenkov emission it is assumed that the electron moves in a straight path to a certain distance (this distance varied for different sets of calculations) and does not suffer any energy loss in between. This energy loss, is, however, taken into account for following the electrons in the cascade.

The Cerenkov photon lateral distribution is calculated in the following manner. For each straight section of the electron path the Cerenkov photons emitted are confined between two cones having vertices at the two ends of the straight section. These two cones intersect the observation plane in two ellipses. The Cerenkov photon density is calculated by assuming uniform distribution within the two ellipses and is accumulated at some fixed points which happen to fall in between the two ellipses. The points lie along the X-axis at distances from 10 m to 220 m from the core. The average Cerenkov lateral distribution at sea-level for the wave length interval 300 nm to 650 nm is obtained, from a total of 100 showers.

Different sets of calculations have been carried out with and without including the effect of Rayleigh, aerosol scattering and ozone absorption of the Cerenkov photons. For this purpose, the data given by Eltermann<sup>7</sup> is used. A fourth degree polynomial is fitted to Eltermann's data for interpolation to intermediate distances.

### Results

The lateral distribution without absorption (a) and with absorption (b) are shown in Fig.1. The lateral distribution shows the characteristic hump at  $\sim 135$  m from the core. It is quite clear that inclusion of the effect of absorption does not reduce the prominence of the hump at all.

Such a hump in the lateral distribution was noticed in the calculations of Zatsepin and Chudakov and Patterson and Hillas whereas it is absent in that of Browning and Turver. The hump present in the calculation of Zatsepin and Chudakov is less prominent than in ours and Patterson and Hillas see a hump whose height is intermediate between ours and that of Zatsepin and Chudakov.

Patterson and Hillas suggest that the extraordinary prominence of the hump in our first calculation may result because of the fact that we have taken very large slab thickness ( $5 \times 10^{-4} \times E$  for  $E$  less than 1 MeV, 1 radiation length above 1 GeV) while treating the Coulomb scattering. In our present calculations we have used very small slab thickness, sometimes as small as 0.003 radiation length. Still the shape of the hump remains unchanged. (Fig.2)

We have calculated the Cerenkov photon lateral distribution produced

by particles with energy greater than 1 GeV and by particles with energy less than 1 GeV separately (Fig.2). The lateral distribution due to lower energy particles shows a very weak shoulder. The lateral distribution due to particles having energy greater than 1 GeV shows a very strong shoulder. These are the particles for which the r.m.s. scattering angle due to Coulomb scattering is less than the Cerenkov emission angle. The contribution to the lateral distribution from different depths in the atmosphere from electrons of energy greater than 1 GeV and less than 1 GeV is shown in Fig.3 (a) and (b) respectively.

The product of the height of production of the Cerenkov photons from electrons of energy greater than 1 GeV and the Cerenkov angle remains almost constant (between 110 and 140 m) for a fairly large range of the height of production of the Cerenkov photons (between 7 and 20 Km). The hump is essentially a consequence of this and is due to the contribution from particles of energy of greater than 1 GeV where the scattering angle becomes smaller than the Cerenkov angle.

### Conclusions

We have shown that the hump in lateral distribution of Cerenkov photons at sea level in electromagnetic cascades of energy 100 GeV, remains essentially unaffected even after taking into account the Rayleigh and aerosol scattering and ozone absorption, and reducing the atmospheric slab thickness to very small values in the treatment of scattering of high energy electrons. The hump is essentially due to particles of energy greater than 1 GeV where the mean scattering angle becomes smaller than the Cerenkov angle.

### References

1. B. S. Acharya et al., Proc. Intl. Workshop on Very High Energy Gamma Ray Astronomy, Ootacamund (Eds.P.V. Ramana Murthy and T. C. Weekes) 1982, p.303.
2. V. I. Zatsepin and A. E. Chudakov, Zh. Eksperim.I.Teor.Fiz,42,1622(1962) English Translation. Soviet Physics-JETP, 15,1126 (1962).
3. G. Rieke, Smithsonian Astrophysical Observatory Space Report No.301(1969).
4. J. R. Patterson and A. M. Hillas, J. Phys.G.Nucl.Phys. 9 (1983)1433-1452.
5. R. Browning and K. E. Turver, Nuovo Cimento, 38A,223 (1977).
6. R. H. Vatcha, Ph.D. Thesis, University of Bombay (1972).(Unpublished).
7. L. Elterman 1968 US Airforce Cambridge Research Laboratory Report AFCRL-68-0153.

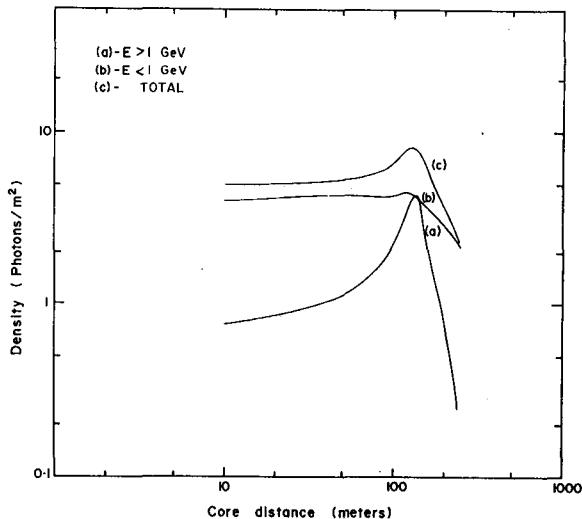
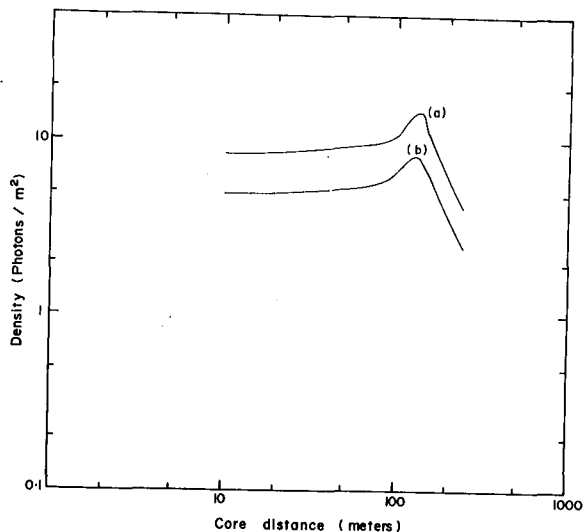


Fig. 1. Lateral distribution of Cerenkov photons (a) without absorption, (b) with absorption

Fig. 2. Lateral distribution of Cerenkov photons due to particles of energy (a)  $> 1$  GeV (b)  $< 1$  GeV and (c) total

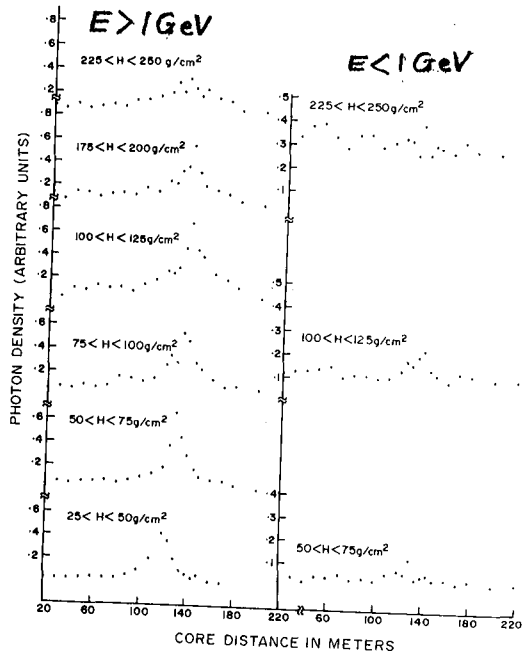


Fig. 3 Contribution to lateral distribution of Cerenkov photons from different depths in the atmosphere due to particles having energy (a)  $> 1$  GeV (b)  $< 1$  GeV.



## SIMULATION OF GAMMA-INITIATED SHOWERS

Yo. Stamenov and Kh. Vancov

Institute for Nuclear Research and Nuclear Energy

BG-1784 Sofia, Bulgaria

T. Vodenicharova

Department of Physics, Institute for Foreign Students

BG-1111 Sofia, Bulgaria

Abstract

The main average characteristics of muon, electron and hadron components of extensive air showers were calculated using a standard model of nuclear interaction. The obtained results are in good agreement with Tien Shan experimental data.

1. Introduction. The method of analysis of the anomaly in the development and structure of extensive air showers /EAS/ gives the real possibility<sup>[1]</sup> for experimental investigation of gamma-quanta with high energy in the primary cosmic radiation. On the basis of Tien Shan experimental data was shown<sup>[2]</sup>, that EAS poor in muons and high energy hadrons are initiated by gamma-quanta with energy -  $10^{15}$  eV.

2. Method. The development of electron-photon component with a threshold energy of 500 MeV in homogeneous atmosphere was simulated with help of Monte-Carlo method. The primary energy of the initiated photon was  $E_{\gamma} = 10^{15}$  eV.

The probability for realization of the cross-section:

$$\sigma_{\gamma p}(E) = 114.3 + 1.647 \ln^2(0.0213E) \quad , \text{ where } \xi_{\gamma p} \text{ is in } \mu b$$

and  $E$  in GeV.

It was supposed, that the nuclear cascade, initiated by a proton with the same energy as the correspondent photon energy, starts in the point of the photonuclear interaction. Further there were used the differential energy spectra of pions for different deepnesses in the atmosphere<sup>[4]</sup> in attempt to evolute the analogous spectrum for the observation level 700 g. cm<sup>-2</sup>. By this way were calculated the total number of muons with energy  $E_{\mu} > 5 \text{ GeV}$  too.

The energy flux carried by the electron-photon component of the same type of EAS was estimated with help of the lateral distribution function  $E_{ef}(\alpha, S)$ <sup>[5]</sup> of the average energy per electron. In this case the correspondent energy flux density

is:

$$P_E(\alpha, S) = P_e(\alpha, S) E_{ef}(\alpha, S) \\ = [N_e / (m R_M)^2] f_{NK}(\alpha / m R_M, S) \quad , \text{ where } P_e(\alpha, S) =$$

is the modified<sup>[6]</sup> NK function of the lateral distribution of electrons in a shower.

**3. Results.** The average energy of the hadron component  $E$  in EAS, initiated by a primary gamma-quanta with energy  $10^{15}$  eV was estimated for the threshold energy of the Tien Shan experimental data -  $E_{htr} > 3.8 \text{ GeV}$ :

$$E_{htr} (> 3.8 \text{ GeV}) = 1.62 \cdot 10^{12} \text{ eV}$$

Only  $\sim 3\%$  of the primary energy were transferred as energy of the electron-photon component and there are  $\sim 11.5$  GeV in each photonuclear interaction.

The number of muons with  $E_\mu > 5$  GeV in the same showers was estimated as  $N_{\mu\gamma}(E_\mu > 5 \text{ GeV}) = 555$ .

4. Discussion. The total number of muons  $N_{\mu\gamma}$  in gamma-initiated shower with energy  $\sim 6 \cdot 10^{14}$  eV was estimated with help of a semiempirical method<sup>[2]</sup> as 255 for the Tien Shan experimental data. Taken into account the  $N_{\mu}(E)$  dependence<sup>[4]</sup> we obtain  $N_{\mu\gamma}(6 \cdot 10^{14} \text{ eV}) = 361$ . The average relation between total numbers of muons in gamma-initiated  $N_{\mu\gamma}$  and normal  $N_{\mu A}$  showers was estimated as  $\left(\frac{N_{\mu\gamma}}{N_{\mu A}}\right) = 0.047$ . Taken into account the total muon fluctuations for the Tien Shan experiment<sup>[2]</sup> we can obtain the threshold value for the selection of muon poor showers:

$\left(\frac{N_{\mu\gamma}}{N_{\mu A}}\right) = 0.15$ , what is in good agreement with the semiempirical value 0.11<sup>[2]</sup>.

The energy of the electron-photon component transferred in the Tien Shan calorimeter<sup>[7]</sup> is:

$$E_{ec} = 2\pi \int_{0.2\pi}^{3\pi} dr r \rho(r, s) = 6.94 \cdot 10^{13} \text{ eV}$$

The correspondent part of the energy of hadron component was estimated as  $E_h = 3.7 \cdot 10^{11}$  eV, taken into account the results<sup>[7, 8]</sup> about the lateral distribution of hadrons with different energies. So is the average value of the relation<sup>[2]</sup>  $(E_h / E_e) = 5.3 \cdot 10^{-3}$  and including the total fluctuation of  $(E_h / E_e)$  for Tien Shan experiment<sup>[2]</sup> we obtain for the threshold value for hadron poor shower selection  $(E_h / E_e) = 1.5 \cdot 10^{-2}$ , which confirms the semiempirical value  $1.42 \cdot 10^{-2}$  too.

5. Conclusions. The results of the present calculation confirms the criteria, adopted by the analysis<sup>[2]</sup> of the Tien Shan experimental data, for selection of muon and hadron poor showers as gamma-initiated showers with energy  $\sim 10^{15}$  eV

6. Acknowledgments. The authors are thankful to Dr. A. Erlykin and Dr. S. Ushev for many fruitful discussions

References:

- 1/ Maze R. , Zavadzki A.; 1960, Nuovo Cimento, 17 5, 625-633
- 2/ Nikolsky S. , Stamenov Y. , Ushev S. , 1984, Adv. Spac. Res. v. 3, 10-12 , 131-134
- 3/ Bezrukov L. B. , Bugaev E. V. , 1981 Proc. ICCR, Paris, v. 7, 90-93
- 4/ Dedenko L. G. , 1965, Preprint FIAN A-69
- 5/ Danilova T. V. , Erlykin A. D. , 1984 Preprint FIAN N°15
- 6/ Dedenko L. G. , Nikolsky S. I. , Stamenov Y. N. , 1976 , Short Reports FIAN , 1 , 30
- 7/ Romakhin V. A. , Nesterova N. M; 1979, Trudy FIAN v. 109, 77-108
- 8/ Vernov S. N. et. al; 1970, Acta Sci. Hungaricae, 29 Suppl. v. 3, 429

PHENOMENOLOGICAL CHARACTERISTIC OF THE ELECTRON  
COMPONENT IN GAMMA-QUANTA INITIATED SHOWERS

Nikolsky S.I\*, Stamenov J.N\*\*, Ushev S.Z.\*\*

\* P.N.Lebedev Physical Institute, Moscow, USSR

\*\* Institute for Nuclear Research and Nuclear  
Energy, Sofia, Bulgaria

ABSTRACT

The phenomenological characteristics of the electron component in showers initiated by primary gamma-quanta were analyzed on the basis of the Tien Shan experimental data. It is shown that the lateral distribution of the electrons in gamma-quanta initiated showers can be described with NKG - function with age parameter  $\bar{S} = 0,76 \pm 0,02$ , different from the same parameter for normal showers with the same size  $\bar{S} = 0,85 \pm 0,01$ . The lateral distribution of the correspondent electron energy flux in gamma-quanta initiated showers is steeper as in normal EAS.

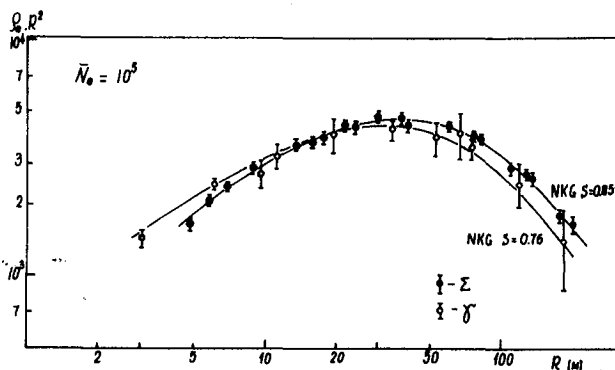
I. Introduction

The phenomenological characteristics of the electron component of EAS contains information about the primary particle which has initiated the shower /1,3/. Particularly, the muon and hadron components in the extensive air showers, generated by primary gamma-quanta, are practically absent because the photonuclear processes cross-section are relatively small in comparison with the hadron-hadron interactions cross-sections, which are responsible for the normal showers.

In our earlier papers /4-6/ the investigation results are discussed of primary gamma-quanta with energy of  $\sim 10^{15}$  eV with the help of the method of muon and hadron poor-shower selection on the basis of the Tien Shan experimental data, obtained during an effective running time  $\sim 1,8 \cdot 10^4$  h.

## 2. Results

The lateral distributions of the electron flux in the selected muon and hadron poor-showers were described in the distance interval  $5 \div 180$  m from the axis by means of standard NKG-function with age parameter  $\bar{S}_L = 0,76 \pm 0,02$ . On

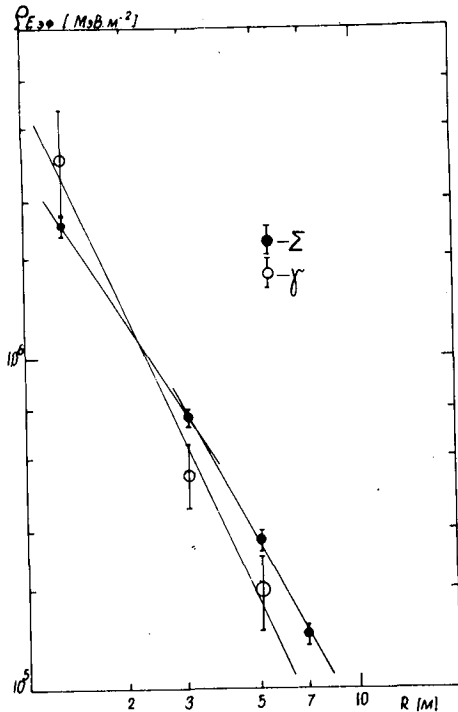


the other hand, the normal showers with the same size have electron lateral distribution, characterized with the age parameter  $\bar{S}_L = 0,85 \pm 0,01$ . In this case, the gamma-initiated showers are also younger than

the showers with the same size but generated by primary nucleons and nuclei. Taking into account the relation  $S = S_L + \Delta S$ , where  $\Delta S = 0,15 \div 0,20$  /7/, it is necessary to suppose that the development maximum of the gamma-initiated showers is localized deeper in the atmosphere. This supposition is confirmed by the comparison of the experimental data /8/ about the height of the maximum in proton initiated showers with energy  $10^{15}$  eV -  $X_{\max} \approx 450 \text{ g.cm}^{-2}$  with the cal-

calculation result for the electron-photon cascades in the atmosphere, assuming the same energy of the primary photon -  $X_{\max} \approx 600 \text{ g.cm}^{-2}$  /9/.

The lateral distribution of the electron energy flux in gamma-initiated and normal showers were analyzed too in the distance interval  $0,2 < r < 5 \text{ m}$  /fig.2/.



It is shown that the lateral distribution in normal proton or nuclei initiated showers were described by the same functions as in /10/:

$$\rho_{E_{ef}} \sim r^{-1,53} \quad 0,2 < r < 3 \text{ m}$$

$$\rho_{E_{ef}} \sim r^{-1,9} \quad 3 \text{ m} < r < 7 \text{ m}$$

but in gamma-initiated showers

$$\rho_{E_{ef}} \sim r^{-2,0} \quad 0,2 < r < 3 \text{ m.}$$

The absence of flattening of the lateral distribution of the energy flux in the central part of the pure electromagnetic showers is a natural consequence of the absence of transverse momenta of secondary hadrons in the high energy hadron interactions.

### References

1. Nikolsky S.I, (1970), Trudy FIAN, v.46, 900.
2. Stamenov J.N, (1982), Thesis of doctor, FIAN, Moscow.
3. Khristiansen G.B, Kulikov G.V et al, (1975), "Cosmicheskoe

- izluchenie sverhvisokoi energii", Moscow.
4. Stamenov J.N, Ushev S.Z et al, (1983), Proc. I8th ICRC, v.6, pp.54-57.
  5. Nikolsky S.I, Stamenov J.N, Ushev S.Z, (1984), Adv. Space Res, v.3, 10-12, pp.131-134.
  6. Nikolsky S.I, Stamenov J.N, Ushev S.Z, (1984), JETPh, v.87, I/7/, pp.18-36.
  7. Dedenko L.G, Nesterova N.M et al, (1975), Proc. I4th ICRC, v.18, 2731-2736.
  8. Antonov R.A, Ivanenko I.P, Tulinova Z.I, (1973), Yad. Phys., v.18, pp.554-559.
  9. Pljasheshnikov A.V, Lagutin A.A, Uchaikin V.V, (1979), Proc. I6th ICRC, v.7, pp.1-6.
  10. Aseikin V.S, Kirov I.N et al, (1976), Moscow, Prepr. FIANI42.



A Three-dimensional Monte Carlo Calculation of the Photon  
initiated Showers and Kiel Result

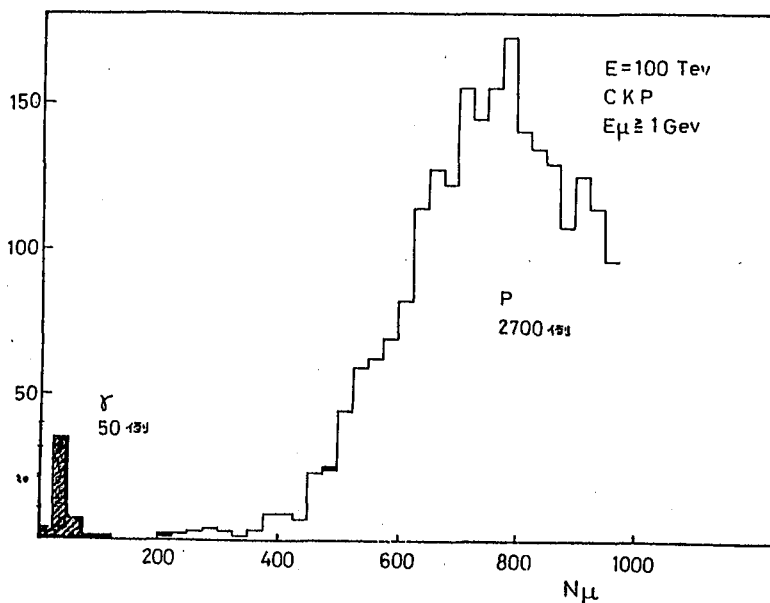
A. Okada and Y. Muraki

Inst. for Cosmic Rays, Univ. of Tokyo, Tanashi, Tokyo 188

abstract

The Kiel experimental results indicate an existence of the ultra high-energy gamma-rays coming from Cyg. X-3. However the result indicates that the number of the muons included in the photon initiated shower is the same as the number included in the proton initiated showers. According to our Monte Carlo calculation as shown in the graph of underpart, the number of muons included in the photon initiated showers should be less than 1/15 of the proton's [See also Proceed. 17th ICRC 7 (1983),54.].

The previous simulation was made under one dimensional approximation. This time we report the result of three dimensional calculation by oral and ICRR preprint.



## Construction of a Cosmic Ray Air Shower Telescope

L.K. Ng and S.K. Chan  
 Physics Department, University of Hong Kong  
 Hong Kong

## Abstract

The telescope under construction is mainly for the purpose of locating the arrival directions of energetic particles and quanta which generate air showers of sizes  $10^5 - 5.10^6$ . Both fast timing method and visual track method are incorporated in determining the arrival directions. The telescope is composed of four stations using scintillators and neon flash tubes as detectors. The system directional resolution is better than  $1.5^\circ$ .

1. Introduction. Application of medium-size shower arrays in astronomical observations is exemplified by the Kiel experiment<sup>1</sup> in the detection of high energy gamma rays from Cygnus X-3. This type of continuous observation using ground-base air shower arrays may yield more fruitful results, if it is participated by more stations spreading out at various latitudes. For long term observations, such telescope could be less elaborate than Kiel's. The requirements may just be high directional resolution and ability to measure the muon/electron density ratios of individual showers, in addition to the usual determination of lateral distributions and age parameter. This paper reports a simple air shower telescope which meets the above requirements.

2. Detection system. It consists of four detector assemblies (a required minimum), which are at sea level and arranged as shown in figure 1.

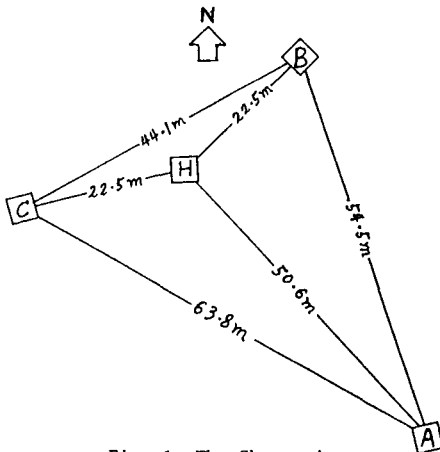


Fig. 1 The Shower Array.

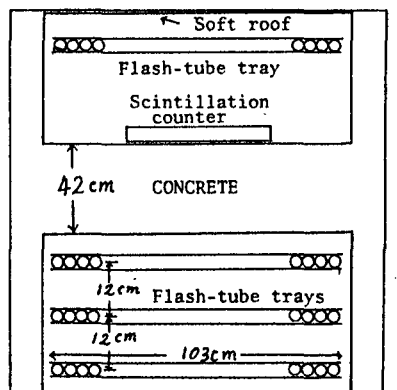


Fig. 2 The Detector Assembly.

Each detector assembly has a soft roof and contains a plastic scintillator, 4 trays of neon flash tubes and an absorber medium as shown in figure 2. The scintillator has

a minimum geometry of  $0.5\text{m} \times 0.5\text{m} \times 0.05\text{m}$  and is viewed by two 2" photomultipliers in contact with the scintillator. For precise arrival time determination, anti-jitter preamplifiers described in another conference paper (HE 4.7 - 9) are used.

Each of the four flash-tube trays consists of 48 close packed tubes. Each tube has a geometry of  $2\text{m} \times 1.9\text{cm}$  dia. and when it fires, its output electromagnetic signal is picked up by a latch. There are  $4 \times 48$  latch units in an assembly providing 24 bytes of data per shower per assembly. Clearly, the top tray is for shower density measurement and the bottom three trays are for muon density and direction measurements.

3. Electronics. For each shower, data required from the system include information from the flash tubes, the particle arrival times, and the event time and date. Block diagram of the electronic system is given in figure 3. Communication between each assembly and the central processing station is linked by transceiver buses throughout. A master pulse is produced by 4-fold coincidence of the scintillator outputs ( $2\mu\text{s}$  window). The master pulse is used to reset the flash-tube latches, to fire the flash tubes by triggering the UHT pulsing unit, and to start the data acquisition subroutine in the microcomputer.

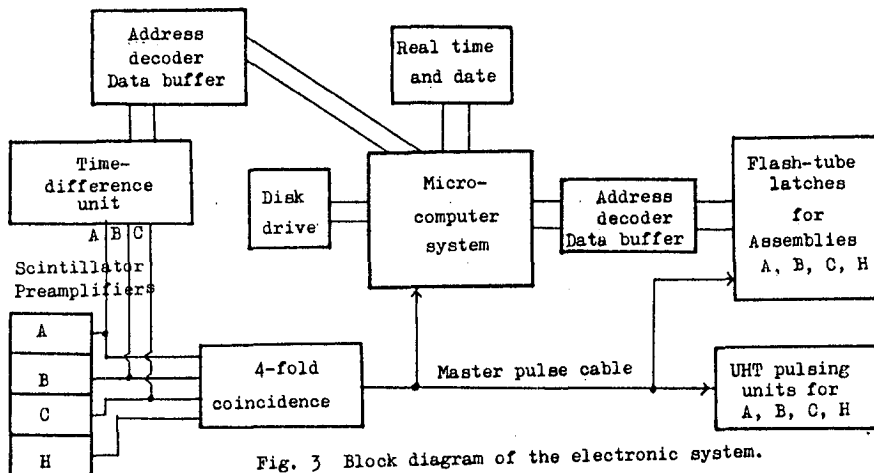


Fig. 3 Block diagram of the electronic system.

However, the key part of the electronic system is the time-difference unit which determines the relative arrival time of particles falling at the scintillators. The arrival time is precisely related to the leading edge of the output pulse from the anti-jitter preamplifier. This leading edge is free from distortion during transmission, because the signal cable is terminated by a matched pair of driver/receiver.

The time-difference unit contains three sets of time-to-amplitude converter (TAC) and analogue-to-digital converter (ADC). The leading edge of an input pulse from one

of the assemblies A, B, C is compared with a common time reference, and the difference is then digitized by the TAC and ADC. The TAC and time reference circuits are shown in figure 4.

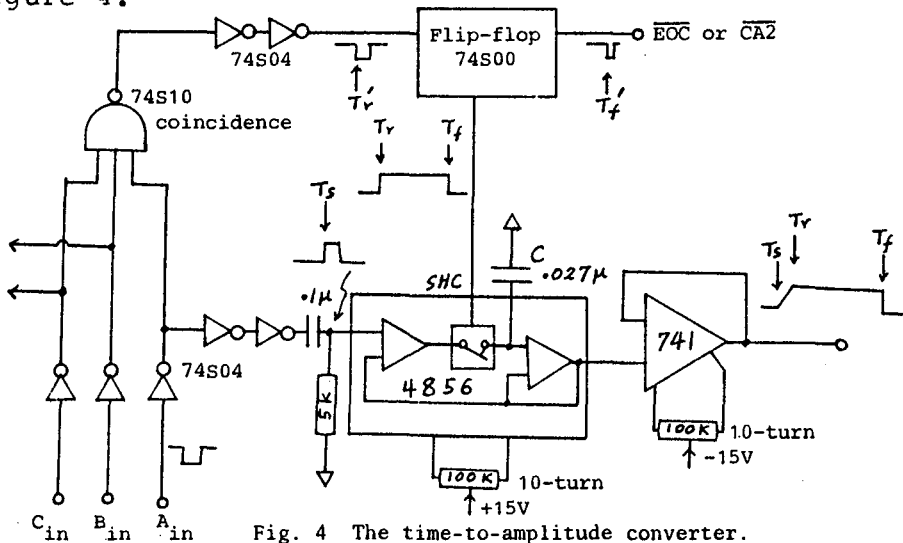


Fig. 4 The time-to-amplitude converter.

The TAC is a sample/hold chip (Teledyne Philbrick 4856) with a charging rate  $\sim 1.5$  V/ $\mu$ s and a drift rate  $\sim 0.8$  mV/s at the hold state, using a low leakage capacitor C of  $0.027$   $\mu$ f. The hold pulse (at SHC) is generated by a fast flip-flop as shown. Its leading edge  $T_r$  is the time reference corresponding to the latest leading edge of the three input pulses  $A_{in}$ ,  $B_{in}$ ,  $C_{in}$  (after triple coincidence). Its falling edge  $T_f$  corresponds to either the end of ADC conversion (EOC) or the end of computer processing ( $\overline{CA2}$ ), whichever is the last. When the chip is at the sample state, the capacitor C is being charged up starting from  $0$  V at time  $T_s$ , the leading edge of the input pulse. If there is a shower event, the hold pulse opens the switch at the reference time  $T_r$ . Hence C stores a voltage amplitude corresponding to the time difference ( $T_r - T_s$ ). It is held until the falling edge  $T_f$  sets in, and the chip starts to sample again.

Digitization is done by a slow but high precision ADC (MC14514) with a reference voltage  $+2.48$  V provided by a chip MC1403. This together with the TAC gives a full range of 1999 corresponding to a time difference of 1768 ns. Hence the time resolution is better than 1 ns. The unit is calibrated by using a fast CRO and a signal generator. The various fixed time delays are also determined similarly.

From the geometry in figure 1, a time difference of 2.9ns corresponds to  $\sim 1^\circ$  zenith angle. Hence the directional resolution is mainly determined by the time fluctuation in the scintillation counters, including photomultipliers and preamplifiers. The fluctuation is not expected to exceed 4ns. Therefore, the directional resolution is better than  $1.5^\circ$ .

4. Shower rate and efficiency. The minimum trigger density at each scintillator is  $4 \text{ m}^{-2}$ . Using the differential intensity spectrum<sup>2</sup>,

$$j(N) = 1.95 \cdot 10^6 N^{-2.7} ,$$

The shower rate is estimated by the expression,

$$\phi = \frac{2\pi}{\alpha+2} \int j(N)A(N)dN, \text{ with } \alpha = 8.6 \text{ at sea level,}$$

and is presented below.

Shower size (N - N+ $\delta$ N)	A( $\bar{N}$ )	$\bar{N}^{-2.7}$ A( $\bar{N}$ ) $\delta$ N
9.2 E4 - 1 E5	1.0 E1	0.03 E-7
1 E5 - 2 E5	3.0 E2	4.87 E-7
2 E5 - 3 E5	2.05 E3	6.31 E-7
3 E5 - 4 E5	4.10 E3	4.76 E-7
4 E5 - 5 E5	6.10 E3	3.47 E-7
5 E5 - 6 E5	8.00 E3	2.61 E-7
6 E5 - 7 E5	1.05 E4	2.16 E-7
7 E5 - 8 E5	1.24 E4	1.73 E-7
8 E5 - 9 E5	1.47 E4	1.46 E-7
9 E5 - 1 E6	1.67 E4	1.22 E-7
1 E6 - 2 E6	2.40 E4	7.78 E-7
2 E6 - 3 E6	4.20 E4	2.58 E-7
3 E6 - 4 E6	5.70 E4	1.32 E-7
4 E6 - 5 E6	6.80 E4	0.77 E-7
		Total 41.07 E-7

Hence the shower rate is  $\phi (>9.2 \cdot 10^4) = 4.7 \text{ hr}^{-1}$ .

The effective area of each flash-tube tray is  $1.73 \text{ m}^2$  and the expected efficiency of the tubes is  $\sim 85\%$ . Hence on the average, the minimum number of shower particles recorded from each tray is  $4 \times 1.73 \times 0.85 = 5.9$ . The directions of the muon tracks in a muon-rich shower can be used to check the shower direction obtained by the time-difference method.

5. Acknowledgement. The authors are grateful to Professor D.J. Newman for his support and encouragement.

#### References.

1. Samorski M and Stamm w, Ap.J. Lett. 268 (1983) L17.
2. Hillas A M et al, Phys. Reports, 20C (1975) 79.

An Underground Cosmic Ray Muon Telescope  
for Observation of Cosmic Ray Anisotropy

Y.W. Lee and L.K. Ng  
Physics Department, University of Hong Kong  
Hong Kong

Abstract

A telescope housed in a tunnel laboratory has an overburden of  $573 \text{ hg cm}^{-2}$  and is located under the centre of a saddle-shaped landscape. It is composed of triple layers of proportional counters, each layer of area  $\sim 4\text{m} \times 2\text{m}$  and their separation  $0.5\text{m}$ . Events are selected by triple coincidence and software track identification. The telescope is in operation for over a year and the overall count rate is  $1280 \text{ hr}^{-1}$ . The structure and operation of the system is reported.

1. Introduction. Construction of a cosmic ray muon telescope in a road tunnel laboratory on Hong Kong Island was proposed in 1979<sup>1</sup> for the purpose of measuring high energy cosmic ray sidereal variations in the light of similar experiments at Poatina<sup>2</sup> and Utah<sup>3</sup>. The work was delayed due to the tunnel construction, but was finally in operation since August 1983.

The laboratory site is under a saddle-shaped landscape with a vertical rock overburden of  $573 \text{ hg cm}^{-2}$  (including the atmospheric depth). Two hill peaks of height  $\sim 420\text{m}$  limits the East-West zenith view. The North-South profile of the 'saddle' is given in figure 1. With the detectors (proportional counters) placed along E-W direction, 23 directional bins are obtained in the N-S profile.

The experiment is expected to run continuously for three more years in order to obtain statistically significant data. A preliminary data analysis is given at this Conference (OG5.3-9). This paper only reports on the structure and operation of the system.

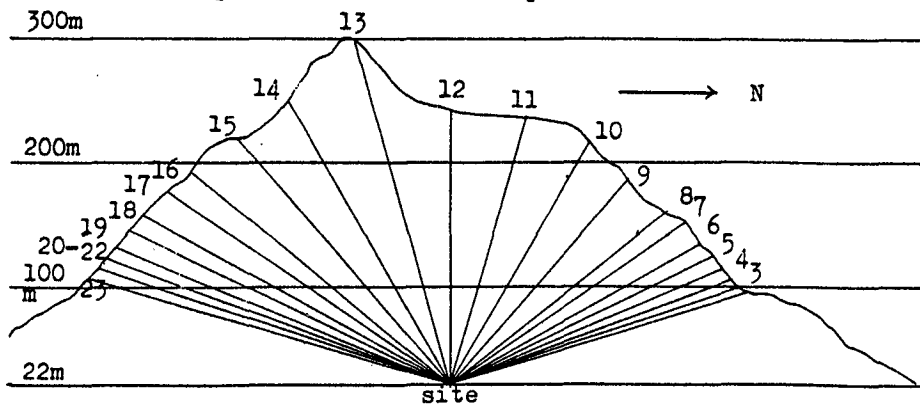


Fig. 1 The N-S profile of the landscape.

2. Detection system. Large area proportional counters (2m x 7.6cm dia.) are used. The counter body is made of 0.16cm thick stainless steel with 50  $\mu$ m stainless steel anode wire under 100g tension. The tube is filled with a standard P-10 gas at 1 atmospheric pressure. Figure 2 shows the arrangement of the counters with 48 tubes in one layer. The whole assembly is covered by lead sheets to minimize soft radiation from the tunnel rocks.

The counters are operated at the limited proportional region (EHT = +2600 V) and the single count rate is  $\sim 80 \text{ s}^{-1}$ . Operation of the counters is indicated hourly by a monitor spectrum described in later sections. Long term drift due to slow aging is found insignificant.

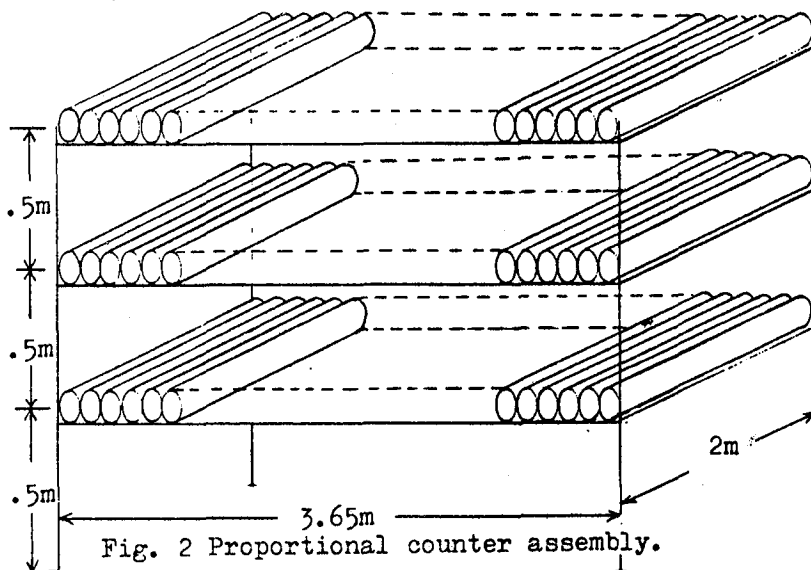


Fig. 2 Proportional counter assembly.

3. Electronics. Each proportional counter has its own pre-amplifier, and they are binned together with 4 counter in one bin shown in figure 3. For more precise track identification, counters in the middle layer are binned in two ways A and B as shown.

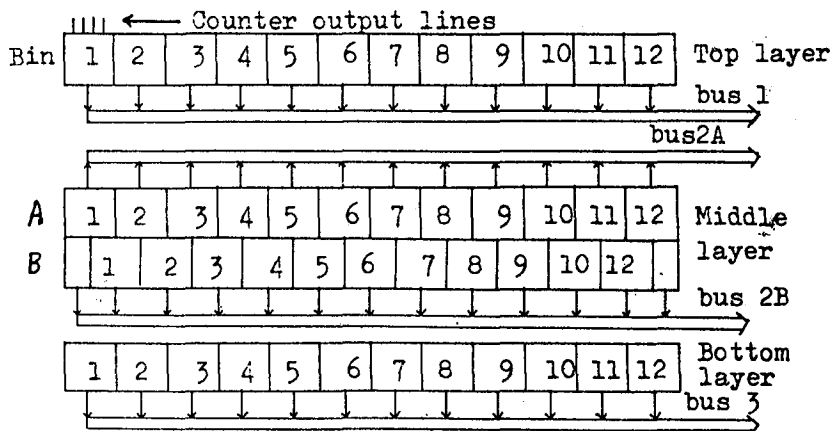


Fig. 3 Counter output bins.

The digital system mainly consists of counter latches, a triple coincidence system and three microprocessor systems MPS (Motorola 6800) as shown in figure 4.

The coincidence unit with window  $1.14 \mu\text{s}$  provides the required master pulse which commands holding of the counter information in the latches and starts a series of operations in the three MPS systems. The wires in each input bus to the coincidence unit are ORed before entering the unit. MPS1 reads the latched counter information and sends the raw data to the remote system MPS2. If MPS2 is busy, the data is temporarily held in the MPS1 output buffer. MPS2 accumulates hourly a muon directional spectrum and a monitor spectrum of individual bin counts. It also keeps time and date; and for visual checking, it can provide an option of slow video display of particle tracks in a current event. The triple coincidence rate, the two spectra and the time and date are finally transferred to MPS3 which stores them hourly in floppy disks and hard prints.

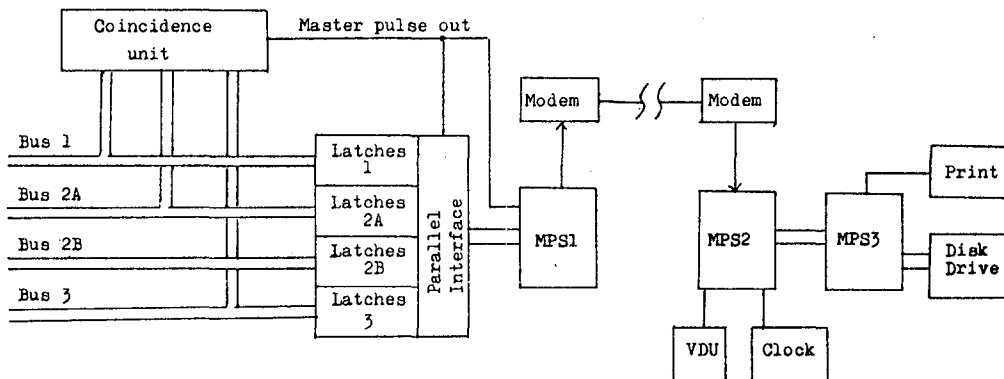


Fig. 4 The digital system.

4 Data collection. From the single count rate and the triple coincidence time window, the chance rate is about  $800 \text{ hr}^{-1}$ , which is very significant when compared with the corrected event rate of  $1280 \text{ hr}^{-1}$ . Hence software particle track identification is carried out in MPS2 as follows:

The counter bins in each layer are labelled from 1 to 12 (see figure 3). If a muon traverses Bin p on the top layer and Bin q on the bottom layer, the track direction is given by the number  $N = (p-q)$ . Thus the directional spectrum contains 23 bins ranging from  $N = -11$  to  $+11$ . The track identification criteria are (i) the top layer or the bottom layer should not have more than two bins fired. (When a bin fires, its latch stores a '1', otherwise a '0'); and (ii) the track must pass through a fired bin on the middle layer, either among bins in A if the number N is even, or in B if N is odd).

The monitor spectrum contains the accumulated counts during triple coincidence from each counter bin. The count



rate in each bin therefore depends on the bin location. But the spectral shape should not vary if the counters are operating normally. This determines the data reliability.

5. Comparison and discussion. The table below compares the experimental system with those at Utah and Poatina.

	Hong Kong	Utah	Poatina
Site latitude	22.2° N	40.6° N	41.8° S
Effective depth/hg cm <sup>-2</sup>	573	486	365
Vertical threshold muon energy/GeV	157	121	~80
Median regidity/GV	1915	1500	~1000
Effective area/m <sup>2</sup>	7	37	4
Total counts	1.27.10 <sup>7</sup>	1.52.10 <sup>8</sup>	--

From the particle track identification criteria, it is obvious that showers and local bursts are excluded and so are the chance events. However, the second particle identification criterion was considered to be too restrictive which could exclude some genuine events due to deviation in the counter alignment. This criterion was then relaxed by including the neighbouring bins on the middle layer. This relaxation only results in a chance coincidence of 1.4 counts per hour. The merit of this system over a scintillator system is that all particle tracks are identified first before acceptance.

6. Acknowledgement. We are grateful to the Hong Kong Royal Observatory for the continuous supply of meteorological data, the Public Works Department and the Transport Department of Hong Kong for the construction and maintenance of the tunnel laboratory.

#### References.

1. Ng L K et al, Proc. 16th ICRC (Kyoto) 4 (1979) 232.
2. Fenton A G et al, Proc. 15th ICRC (Plovdiv) 11 (1977) 242.
3. Bergeson HE et al, Proc. 16th ICRC (Kyoto) 4 (1979) 188.

NUCLEAR CASCADES IN ELECTROMAGNETIC SHOWERS PRODUCED  
BY PRIMARY GAMMA-QUANTA IN THE ATMOSPHERE.

Danilova T.V., Erlykin A.D., Mironov A.V., Tukish E.I.  
P.N. Lebedev Physical Institute, Leninski pr. 53,  
Moscow, 117924, USSR.

Distributions have been calculated for the number of electrons  $N_e$ , number of muons with the energy above 5 GeV  $N_\mu$  and the energy of hadron component  $E_h$  in electromagnetic showers, produced by primary gamma-quanta with energies  $10^{13} - 10^{16}$  eV, incident on the atmosphere at zenith angles  $\theta \leq 30^\circ$  and observed at the mountain level 700 g/cm<sup>2</sup>. The mean number of nuclear interactions of photons with the energy above 5 GeV is about 0.3 per each TeV of the primary energy and nuclear cascades take out in average about 2% of the total shower energy. The mean number of 5 GeV muons for the electromagnetic shower is (2-5)% from the number of muons in EAS with the same number of electrons at the observation level. Similar value for the total energy of hadron component is also (2-5)%.  $N_\mu$  and  $N_e$  values as well as  $E_h$  and  $N_e$  don't correlate at the fixed primary energy  $E_\gamma^0$ . Between  $N_\mu$  and  $E_h$  there is a positive correlation at the given  $E_\gamma^0$ .

Simulation of nuclear cascades arising when the electromagnetic shower propagates through the atmosphere has been undertaken in connection with the works on high energy gamma-astronomy carried out at the Tien-Shan EAS array /1/. Similar study is planned at ANI array /2/. The difference between the present set of calculations and that carried out in pioneer works of Wdowczyk /3/ is in their orientation onto Tien-Shan and ANI arrays, i.e. the observation of showers at the mountain level 700 g/cm<sup>2</sup>, higher muon threshold energy - 5 GeV and the usage of hadron component as an additional criterium for the selection of pure electromagnetic showers.

Electromagnetic showers were simulated for primary gamma-quanta with energies  $10^{13}, 10^{14}, 10^{15}$  and  $10^{16}$  eV, incident on the atmosphere isotropically in the zenith angle interval  $\theta \leq 30^\circ$ . The total number of electrons at the level 700 g/cm<sup>2</sup> was determined after the sampling of the first

interaction point and of the value  $\cos \theta$  by means of approximation formulae of Greisen /4/ or Klimakov-Pavlov /5/. Then the development of the electromagnetic shower in the atmosphere was followed by steps  $\Delta z = 10 \text{ g/cm}^2$ . The probability for photons  $\Gamma(E_\gamma^0, > 5 \text{ GeV}, z)$  to have photonuclear interaction in the step was estimated according to formulae of the Approximation A of the cascade theory:  $W = 1 - \exp(-\Gamma(E_\gamma^0, > 5 \text{ GeV}, z/\cos \theta) \cdot \sigma_{\gamma A} \cdot \Delta z/\cos \theta)$ . If this probability exceeded 0.1, then the step  $\Delta z$  was reduced by 2, and the procedure repeated. The cross-section of the photonuclear interaction with air atoms  $\sigma_{\gamma A}$  was taken constant and equal <sup>to 2 mb.</sup> When such a photonuclear interaction occurred, then the energy of the photon giving rise to the nuclear cascade was sampled within the photon spectrum at the depth  $z$ , calculated also by means of Approximation A formulae. The number of 5 GeV muons and the energy of the hadron component in that nuclear cascade, reaching the observation level  $700 \text{ g/cm}^2$ , were calculated on the base of simulation results, obtained for the "tails" of nuclear cascades with the help of the routine for small EAS simulation /5/. The result obtained for all partial nuclear subcascades in one and the same electromagnetic shower were summarized. For  $10^{13}$ ,  $10^{14}$  and  $10^{15}$  eV primary energy 1000 showers were simulated, for  $10^{16}$ -100.

$N_e$ -distributions for simulated showers are shown in the fig.1a. Arrows indicate mean values in these distributions. It is necessary to notice that approximation formulae /4/ give higher values of  $N_e$  compared with /5/, which differ by 1.35 at  $10^{13}$  eV and by 1.07 at  $10^{16}$  eV. In the fig.1a results are given, obtained by formulae /4/. It is interesting to note the change of the distribution shape, when  $E_\gamma^0$  increases. It is due to the shower maximum, approaching the observation level at  $E_\gamma^0 = 10^{16}$  eV and to the different impact of deep penetrations of primary gamma-quantum on  $N_e$ , when the shower in the mean is either after the maximum

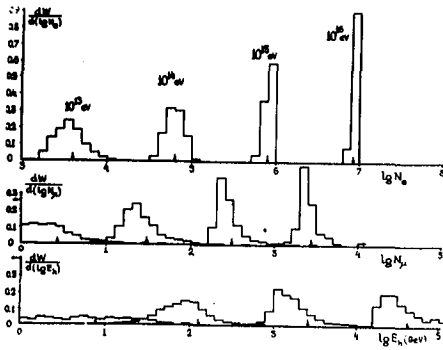


Fig. 1.

or in the maximum of its development.

The simulation showed that the number of photo-nuclear interactions with energies above 5 GeV is proportional to the primary energy  $E_p^0$  with a good accuracy. The proportionality coefficient is  $0.358 \text{ TeV}^{-1}$  at  $10^{13} \text{ eV}$  and  $0.247 \text{ TeV}^{-1}$  at  $10^{16} \text{ eV}$ , i.e. it is equal to about 0.3 interactions per each TeV of the primary energy. The same concerns the fraction of the total energy, carried out by photons, initiating nuclear cascades in the shower. It is 0.015 at  $10^{13} \text{ eV}$  and 0.027 at  $10^{16} \text{ eV}$ , i.e. about 2% of the primary energy in the average.

In figures 1b and 1c distributions are shown for the number of 5 GeV muons and the energy of the hadron component reaching the observation level  $700 \text{ g/cm}^2$ . Arrows indicate again mean values of  $\bar{N}_\mu$  and  $\bar{E}_h$  in the distributions. It is seen that the muon number fluctuates less than the energy of the hadron component. In the figure 2 distributions of the muon number and of the hadron energy in the electromagnetic shower with  $E_p^0 = 10^{15} \text{ eV}$  are shown in comparison with similar distributions for ordinary nuclear EAS with the same  $N_e$ . The latter distributions were obtained in the paper /6/. It is seen that  $N_\mu$  and  $E_h$  distributions for electromagnetic and nuclear EAS are principally rather well separated from each other. Ratios of their mean values, shown in the fig. 3, vary from 2.0% at  $10^{13} \text{ eV}$  up to 4.5% at  $10^{16} \text{ eV}$  for  $N_\mu$  and from 1.4% at  $10^{13} \text{ eV}$  up to 5.0% at  $10^{16} \text{ eV}$  for  $E_h$ , i.e. are about (2-5)% for both values. However since

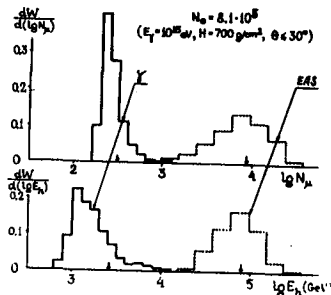


Fig. 2.

the absolute number of muons with the energy above 5 GeV in electromagnetic showers is relatively small ( $\sim 300$ ) for  $E_{\gamma}^0 = 10^{15}$  eV and they are widely spread over the area, then it is usually difficult to identify electromagnetic showers by muons. It is possible to make this only at

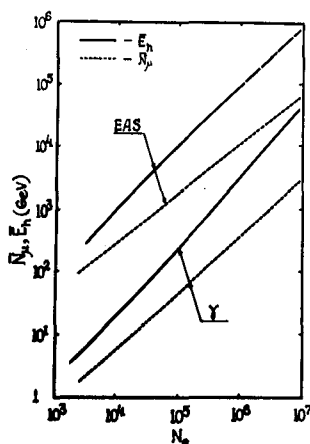


Fig.3

The simulation showed also that  $N_{\mu}$  and  $N_e$  values, as well as  $E_h$  and  $N_e$  don't correlate with each other at the fixed value of  $E_{\gamma}^0$ . At the same time there is a strong positive correlation between  $N_{\mu}$  and  $E_h$  at the fixed  $E_{\gamma}^0$ .

#### References.

1. Stamenov J.N., Ushev S.Z. et al. 18 ICRC, 1983, Bangalore, 6, 54; Adv. Space Res., 1984, 3, 10.
2. Danilova T.V. et al. 18 ICRC, 1983, Bangalore, 5, 520.
3. Wdowczyk J. IX ICRC, 1965, London, 2, 691.
4. Greisen K. in "Progress in Cosmic Ray Physics" ed. by J.G. Wilson, Amsterdam, 1954, 3.
5. Klimakov A.P., Pavlov A.A. "Elementary particles and cosmic rays", 1976, 4, 35, Moscow, Atomizd. (in Russian).
6. Danilova T.V. et al. 17 ICRC, 1981, Paris, 6, 146.

arrays with good resolution in the region of muon-poor showers, that is by means of large area of muon detectors about several hundreds of  $m^2$ . The identification of electromagnetic shower by the energy of the hadron component is more reliable, since this energy is considerably more concentrated around the shower core. The calorimeter area about several tens of  $m^2$  is enough for such identification.

ON THE POSSIBILITIES OF LARGE-SCALE RADIO  
AND FIBER OPTICS DETECTORS IN COSMIC RAYS,

G.A.Gusev, M.A.Markov, I.M.Zheleznykh  
Institute for Nuclear Research, the USSR  
Academy of Sciences, Moscow, USSR

ABSTRACT

Different variants of radio and fiber optics detectors for registration of super high energy cascades in the atmosphere and in dense media are discussed. Particularly the possibilities for investigation of quasi horizontal EAS and simulated muons from these EAS with the help of radio detectors and fiber optics detectors located on the ice surface are considered.

1. Introduction. The problems of super high energy physics and astrophysics not accessible by modern accelerators require creation of surface, under ground, and deep under water super large area and volume detectors. The particles with energy up to  $E \approx 10^{28}$  eV (particularly neutrino) could be created in the evolution of the stable (or long life-time) elementary black holes with Planck's masses and dimensions [1-3] which could have been formed in early Universe. Such absolutely cold black holes ( $T \rightarrow 0$ ) could have external mass ( $\sim 10^{28}$  eV) determined by the electric charge or the rotational moment.

2. Different Radio Detectors. In recent years several variants of super large radio detectors [3-7] were proposed based on the principle of the registration of the cascade coherent radio emission which was proposed as early as 1961 [8]. We note three possibilities.

The first possibility is founded on the reflection of EAS radio emission from the Earth and ionosphere producing the augmentation of the region where EAS radio emission may be received, up to  $10^4$ - $10^5$  km<sup>2</sup>. The second possibility is founded on some crust transparency for cascade radio emission created by the neutrino in the crust and spreading out in the atmosphere (RAMAND-A) [3,6,7]. The last possibility (RAMAND-I) [5,7] is founded on the use for example of antarctic ice in which radio emission absorption for frequencies up to 1 GHz is very small (for temperature  $-50^\circ$  C in the frequency band 0,5-1 GHz the attenuation is about 10 dB/km).

Particularly a radio detector with volume  $10^{11} \text{ m}^3$  could be used for determination of electron antineutrino fluxes in the energy region  $6 \cdot 10^{15} \text{ eV}$  with the help of the reaction  $\bar{\nu}_e + e^- \rightarrow W^- \rightarrow \text{hadrons}$  in the W-boson resonance region and for determination of  $P\bar{\nu}$ -neutrino fluxes [7,9] with energy  $\sim 10^{19} \text{ eV}$  (compare also optic registration of  $P\bar{\nu}$ -neutrino cascades spreading out in the atmosphere [10]).

3. Large-scale radio detectors for quasi horizontal EAS and muons. Here we consider the possibility of complex radio installation for EAS muons registration by its cascade radio emission in the ice simultaneously with the EAS radio emission. We also discuss the utilization of fiber optics detectors for EAS registration.

It is known that EAS muon spectra (see for example [11] have high energy muon component. Its cascades in the volume 1 km according to [11] have statistics of the order of 10 events per year per steradian for cascade energies above  $5 \cdot 10^{14} \text{ eV}$ . This allows to register simultaneously EAS with energy more than  $3 \cdot 10^{18} \text{ eV}$  and muon cascade with energy more than

$5 \cdot 10^{14} \text{ eV}$  (for effective noise temperature  $\sim 1000^\circ \text{C}$ ) with probability of the order of 1.

Complex radio detector is shown in Fig.1. Such radio detector has two parts: EAS radio detector (domain 1) and EAS muon cascade radio detector in the ice (domain 2). These parts are placed so that for EAS axg in the domain 1 in the zenith angle region  $60^\circ - 80^\circ$  the radio spot from the muon cascade with deepness of 500m is projected on the domain 2. The radio detector has 50 antennas (separated from each other on a distance of 500m) with the amplifiers in the frequency band of 30-70MHz, so 7-10 channels receive a signal as much as 30-20dB above the atmosphere noise for EAS energy of  $10^{19} \text{ eV}$  [3]. Muon cascade radio detector has 50 antennas (placed on a distance 250m) with the amplifiers in the frequency band of 200-100MHz, so for cascade energy about  $5 \cdot 10^{14} \text{ eV}$  10-20 channels receive the signal with signal noise ratio  $\sim 10\text{dB}$  [5].

We consider the possibility of changing EAS radio detector by fiber optics detector. The idea of such detector consists in the registration of the optic Cherenkov radiation of the electrons crossing the light guide. The optic emission guided in the fiber can propagate with small absorption at large

distances to the photomultiplier (with small photocathode). It is known that after passing the distance of 1 cm in dense matter an electron in the optic region sets 200 Cherenkov photons. For a fiber of the diameter 0,5 mm this will give 10 photons and for an aperture of 0,3 10% of photons will be guided excepting some EAS electrons coming from directions along and normally to the fiber. So one electron produces one photon guided in the fiber. For a cable consisting of 10 fibers of diameter 0,5 mm the calculation gives 200 photons at the photocathode, if the EAS axis is at distance of 250 m from the cable (EAS energy being  $\sim 10^{19}$  eV). If the photomultiplier effectiveness is roughly 10% then there will be registered 20 one electron pulses during some units microseconds. At Fig.2 the complex detector with EAS fiber optics detector (threshold is about  $10^{18}$  eV) is presented.

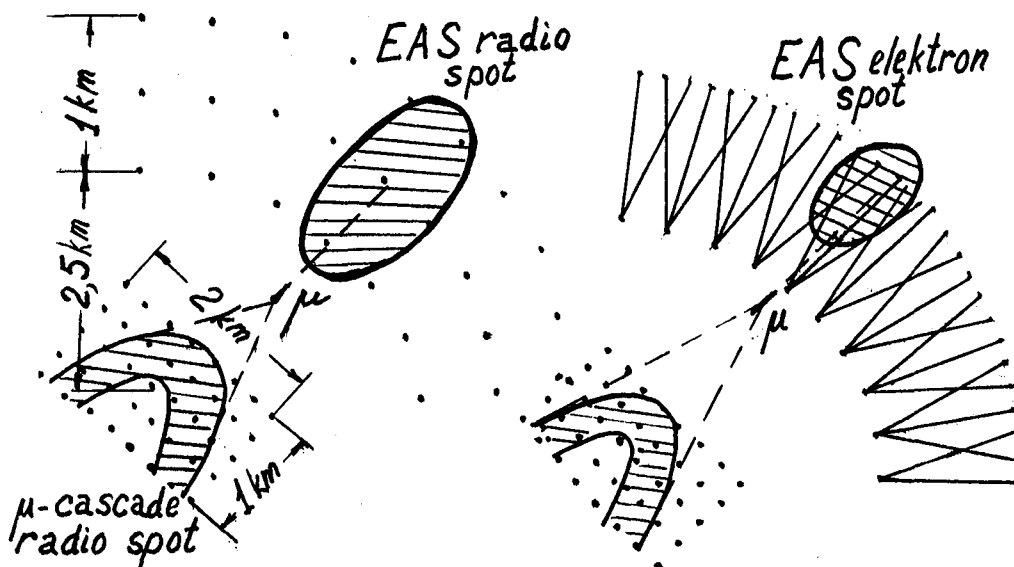


Fig.1. Complex Radio Detector for Quasi Horizontal EAS and Muons.

Fig.2. Complex Detector with EAS Fiber Optics Detector.

**4. Conclusion.** Complex detector placed on the ice surface may be important instrument for research of neutrino, primary composition of cosmic rays, prompt muon creation at super high energies and etc.

**5. Acknowledgements.** We wish to thank A.E.Chudakov and L.G.Dedenko for an useful discussion.



References

1. Markov M.A., On the Upper Limit of the Cosmic Ray Energy Spectrum (DUMAND-type experiments). Preprint INR.P-0197 Moscow 1981.
2. Markov M.A., Zheleznykh I.M. Proc. 1979 DUMAND Workshop at Khabarovsk and Lake Baikal (ed. J.Learned, Honolulu) p.177.
3. Dedenko L.G., Markov M.A., Zheleznykh I.M. Proc. 1981 Int.Conf. Neutrino Phys. and Astrophys.ed. R.Cense, E.Ma, A.Roberts, Maui, Hawaii, 1981, v.2, p.292.
4. Gusev G.A., Dedenko L.G., Markov M.A., Zheleznykh I.M. Pisma JETP, 1982, v.36, p.316.
5. Gusev G.A., Zheleznykh I.M. Pisma JETP, 1983, v.38, p.505.
6. Gusev G.A., Zheleznykh I.M. Uspekhi Fisich.Nauk, 1984, v.143, p.499.
7. Gusev G.A., Dedenko L.G., Zheleznykh I.M. Paper presented at Neutrino-84, Dortmund, 1984.
8. Askaryan G.A. JETP, 1961, v.41, p.616.
9. Gusev G.A., Krystev P., Zheleznykh I.M. Paper presented at Int. Seminar "Quark-84", 1984.
10. Linsley J. Paper presented at 18-th ICRC, India 1983.
11. Kitamura T. DUMAND Workshop at Khabarovsk and Lake Baikal, ed.J.Learned, 1979, p.234.

## Radio Signals from Very Large Showers

Suga K.\* and Kakimoto F.  
 Department of Physics, Tokyo Institute of Technology  
 Meguro, Tokyo 152, Japan

Nishi K.  
 The Institute of Physical and Chemical Research  
 Wako, Saitama 351, Japan

## ABSTRACT

Radio signals from air showers with electron sizes in the range  $1 \times 10^7$  to  $2 \times 10^9$  have been detected at 50kHz, 170kHz and 1,647kHz at large core distances in the Akeno  $20\text{km}^2$  air-shower array. The field strength is higher than that expected from any mechanisms hitherto proposed.

1. Introduction. An experiment is being made to detect low-frequency radio signals from air showers observed in the Akeno  $20\text{km}^2$  air-shower array at large core distances. The motivation is a discussion on the possibility made by one of the present authors(K.S) at the Bangalore Conference in 1983(1) to observe giant air showers by detecting the low-frequency radio signal radiated from the electric current of air-shower particles due to the negative excess during the longitudinal development. And the experiment is an effort in seeking a method to detect air showers at a great core distance, which provides a huge effective area suitable to observe super giant air showers of very low flux beyond the 2.7K Greisen-Zatsepin cut-off, even if exists(2).

2. Experimental. Antennas are located in the yard of a closed primary school at a distance of about 2km from the center of the Akeno  $20\text{km}^2$  air-shower array(3), and the receivers and recording apparatus are set in the classroom. The recording of radio signals is made by a master pulse from the array sent through an optical-fiber cable.

Following two kinds of antennas are operated simultaneously:

(a) Ball antenna(4). A inverted metal cup, whose capacity to the ground is about 10pF, is fixed to the top of vertical glass-fiber pole of 10m and the potential difference of radio signal between the cup and the ground is measured. The preamplifier is enclosed in the metal cup, and the frequency response is flat from several Hz up to 10MHz with a gain of unity.

(b) Vertical wire antenna. A thin wire is stretched vertically along a glass-fiber pole of 10m. The preamplifier is set just above the ground, and the input stage consists of a capacity of 100pF parallel to a resistor of  $20\text{M}\Omega$  to the ground. The frequency response is flat from a few kHz up to 10MHz with a gain of 2.5.

The output of the preamplifier is sent through a co-axial cable(3C2W) to a receiver in the classroom. Following three kinds of receivers are operated alternately:

(i) Sony CRF1 commercial radio receiver(10kHz-30MHz). The output signal

---

\*Present address: Department of Physics, Meisei University, Hodokubo 337, Hino-shi, Tokyo 191, Japan

from the AM detection circuit is recorded at frequencies of 50kHz, 170kHz and 1647kHz. The bandwidth is  $\pm 7\text{kHz}$  at  $-50\text{dB}$ .

(ii) Sony ICF2001 commercial radio receiver(150kHz-30MHz). The output signal from the AM detection circuit is recorded at frequencies of 170kHz and 1647kHz. The bandwidth is almost same as the above receiver(i).

Following three kinds of recorders are operated alternately:

(I) Storage oscilloscope (Tektronix 7834, 400MHz).

(II) Storage oscilloscope (Tektronix 466, 100MHz).

(III) 1-100kHz passive band pass filter(BPF), low noise amplifier( $\times 100$ , NF circuit LI75A), 17.4kHz active band elimination filter(BEF) and FFT (fast Fourier transform) signal analyser(100kHz, 12bit, Iwatsu SM-2100C). The display on CRT is made by a master pulse from the air-shower array and, then, the photograph is taken. The sensitivities of all combinations of the antennas and the commercial receivers are confirmed to be almost same at frequencies from 10kHz to 2MHz.

3. Recorded radio signals. Air showers accompanying radio signals observed well beyond the background noise at the output of commercial radio receiver are plotted with large open circles and those unaccompanying radio signals are plotted with small full circles in figure 1(170kHz) and figure 2(50kHz) for air showers with  $\sec\theta(\theta)$  smaller than 1.30( $40^\circ$ ).

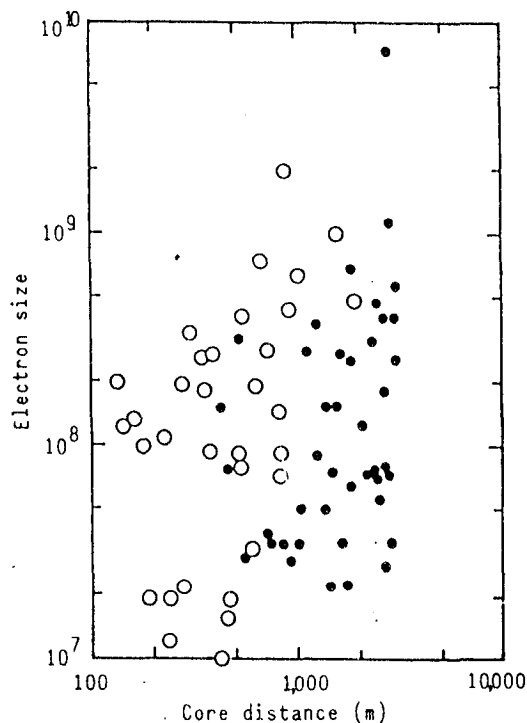


Fig. 1

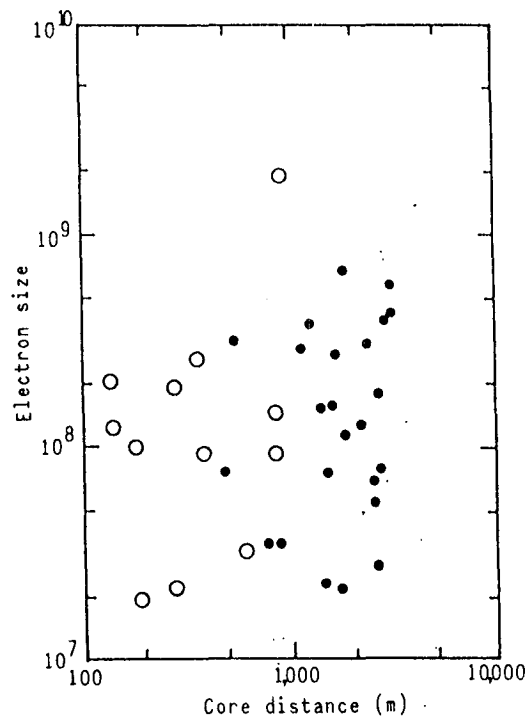


Fig. 2

The effective core distances for showers with zenith angles larger than  $40^\circ$  are somewhat longer. Radio signals were observed at 1647kHz up to almost same core distances as at 50kHz. The effective core distances seem to be independent of the weather condition, such as clear sky, fog, cloud, rain, snow, humidity, temperature, and radio signals have been observed stably during the intermittent operation in every months from December 1984 to May 1985.

The operation with the FFT signal analyser has been made in order to obtain information on the shape of radio pulse. The 1-100kHz BPF is used to cut intense local MF broadcasts and the 17.4kHz BEF an intense local VLF radio signal. A radio signal stored in the FFT signal analyser with a master pulse from the air-shower array undergoes the Fourier transform, and the real and imaginary parts at frequencies corresponding to man-made radio waves are erased. Then, after the inverse Fourier transform is applied, the reconstructed signal is displayed on CRT and is photographed. A wave packet was observed for a shower with the associated radio signal at the output of the commercial radio receiver. From these patterns of observed wave packets, the main component of frequencies of the radio signal associated with the air shower in the present experiment seems to be above 100kHz of the limit of the signal analyser, although the shape of the radio pulse is not known at present.

The field strength of the radio pulse observed in the present experiment can not be estimated accurately for lack of the knowledge of the pulse shape and due to an application of commercial radio receivers. However, the calibration of the radio receivers with pulses of various shapes and lengths seems to indicate that the field strength of the radio pulse peak may be higher than several mV/m at largest core distances where the radio signals were observed well beyond the background noise level as shown in figure 1 and figure 2.

**4. Discussion.** As is described in section 3, radio signals of 50kHz, 170kHz and 1,647kHz from the same air showers have been detected simultaneously at large core distances. The range of electron sizes is  $1 \times 10^7$  to  $2 \times 10^9$  and the effective core distance extends to about 2km. The detection was stable and seems to be independent of the weather condition. Clay et al already reported the detection of radio signals from air showers with primary energies in the range  $10^{15}$  eV to  $10^{16}$  eV at a frequency of 100kHz (bandwidth 80 kHz) (5). However, the detection was unstable (5) (6).

The field strength of the radio pulse detected in the present experiment seems to be at least 100 times higher than that expected from the electric current of air-shower particles due to the negative excess during the longitudinal development. The field strength seems to be also at least 10 times higher than that expected from local reduction of the atmospheric electric field (A.E.F.) due to the acceleration of electrons produced by ionization of air-shower particles in A.E.F. discussed by Wilson (7). A plausible mechanism to produce radio signals detected in the present experiment seems to be radiation from electrons produced by ionization of air-shower particles in the atmosphere due to the acceleration in A.E.F.. The field

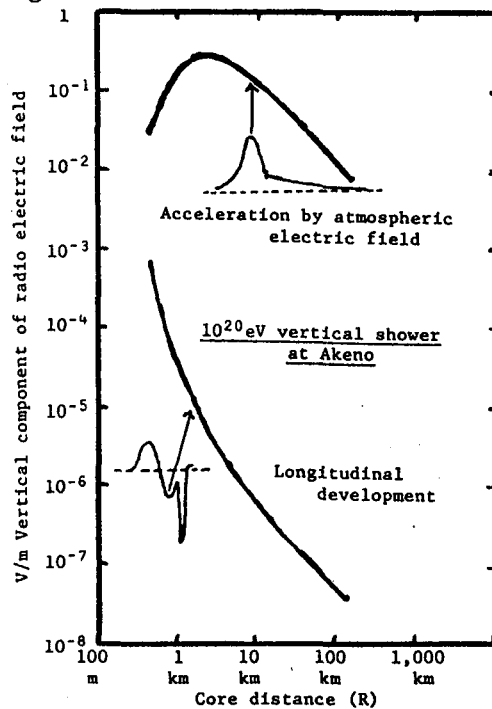


Fig. 3

strength of this radio pulse estimated for a vertical air shower with primary energy of  $10^{20}$  eV observed at Akeno is shown in figure 3, together with that of radio pulse expected from the net negative current of air-shower particles during the longitudinal development. The slow tail of the radio pulse also shown in the figure is due to the acceleration of ions produced by ionization of air shower particles in A.E.F. and contains a frequency component from several tens of Hz to 0.1Hz. This extremely low-frequency component is very important, since the frequencies of the Schumann resonance (earth-ionosphere cavity resonance) are 8Hz and 14Hz for the ground mode and the second mode, respectively. An experiment is undertaken with the ball antenna, a 20Hz passive low pass filter, the low noise amplifier, an active 5-20Hz BPF and the FFT signal analyser.

It is clear that further work to observe many air showers with electron sizes larger than  $10^9$  is required to examine whether this low-frequency radio method is promising for providing a huge effective area of detection. It is also important to check whether the mechanism tentatively suggested above is accepted. For that purpose, the shape of radio pulse will be examined with a wave form recorder (20ns sampling, 10 bit) connected to the FFT signal analyser.

5. Acknowledgments. The authors wish to express their sincere thanks to Prof. T. Ogawa of Department of Physics of Kōchi University for his suggestion of the ball antenna and to Prof. T. Kamata and Mr. H. Jindō of Institute for Atmospheric Research of the Nagoya University for their suggestion of the vertical wire antenna. The authors are deeply grateful to the staffs of the air-shower group of Institute for Cosmic Ray Research of the University of Tokyo, especially Prof. M. Nagano and Dr. M. Teshima, for their operation of the air-shower array and their analysis of the air-shower data.

#### References

1. Kaneko T. et al: Proc. 18th Int. Cosmic Ray Conf.(ICRC), Bangalore, 11 (1983) 428
2. Baltrusaitis R. M. et al: Phys. Rev. Lett. 54 (1985) 1875
3. Teshima M. et al: This Conference OG 9.4-8
4. Ogawa T.: Contr. Geophys. Inst., Kyoto Univ., 13 (1973) 111
5. Clay R. W. et al: Proc. 13th ICRC, Calgary, 4 (1973) 2420
6. Clay R. W. et al: Proc. 14th ICRC, München, 8 (1975) 3039
7. Wilson R. R.: Phys. Rev. 108 (1957) 155

ON THE PRODUCTION MECHANISM OF RADIO\_PULSES  
FROM LARGE EXTENSIVE AIR SHOWERS

Datta, Mrs. P. and Pathak, K.M.  
Department of Physics, Gauhati University,  
Gauhati - 781 014, ASSAM, INDIA.

1. Introduction : None of the theories (1,2,3 & 4) put forward so far to explain the radio-emission from EAS, has been successful to give satisfactory explanation of all the experimental data obtained from various laboratories over the globe. It is apprehended that emission mechanism at low and high frequencies may be quite different (5). This calls for new theoretical look into the phenomenon.

Using basic equations of Kahn & Lerche (1) and a much sophisticated model for shower structure, Castagnoli et al. (2) calculated the radiation field at a point outside the disc of charges. They, however, calculated the radiation field due to current and excess charge only. In this paper, the resultant field inside the disc of charges, due to current and dipole moment have been calculated afresh using the technique adopted by Castagnoli et al. (2), from very low to very high frequencies.

2. Methods : The radiation field at a distance  $R$  from the axis of the shower disc can be obtained by phase mixing the contributions from the various rings of charges. For a point lying inside the disc of charges of radius  $R_0$  at a distance  $R$  from the axis, the point will be an outer one w.r.t. the disc of radius  $R$  and an inner one w.r.t. the annular ring of inner radius  $R$  and an outer radius  $R_0$ . Accordingly, effects of the disc of radius  $R$  and the annular ring are to be taken into account.

The current field at a distance  $R$  from the axis  
(  $R < R_0$  ) :

(A) Current field due to the disc of radius R :

$$E_C'(R) = -\frac{k_e \times 10^5}{2C(29.4)^2} \times 2\pi \times 0.4N \times H_0^{(1)}(k\alpha R) \int_0^R J_0(k\alpha r) r^2 \left(\frac{r}{29.4}\right)^{-0.75} \left(\frac{r}{29.4} + 1\right)^{-3.25} \left(1 + \frac{r/29.4}{11.4}\right) dr \dots (1)$$

(B) Current field due to the annular ring of inner radius R and outer radius Ro :

$$E_C''(R) = -\frac{k_e}{2C} \frac{J_0(k\alpha R)}{(29.4)^2} \times 10^5 \times 2\pi \times 0.4N \int_R^{R_0} H_0^{(1)}(k\alpha r) r^2 \left(\frac{r}{29.4}\right)^{-0.75} \left(\frac{r}{29.4} + 1\right)^{-3.25} \left(1 + \frac{r/29.4}{11.4}\right) dr \dots (2)$$

The dipole field at a distance R from the axis ( $R < R_0$ ) :

(C) Dipole field due to the disc of radius R :

$$E_P'(R) = ik\alpha e r \pi \frac{0.4N \times 10^5}{40(29.4)^2} H_0^{(1)}(k\alpha R) \int_0^R J_0(k\alpha r) r^2 \left(\frac{r}{29.4}\right)^{-0.75} \left(\frac{r}{29.4} + 1\right)^{-3.25} \left(1 + \frac{r/29.4}{11.4}\right) dr \dots (3)$$

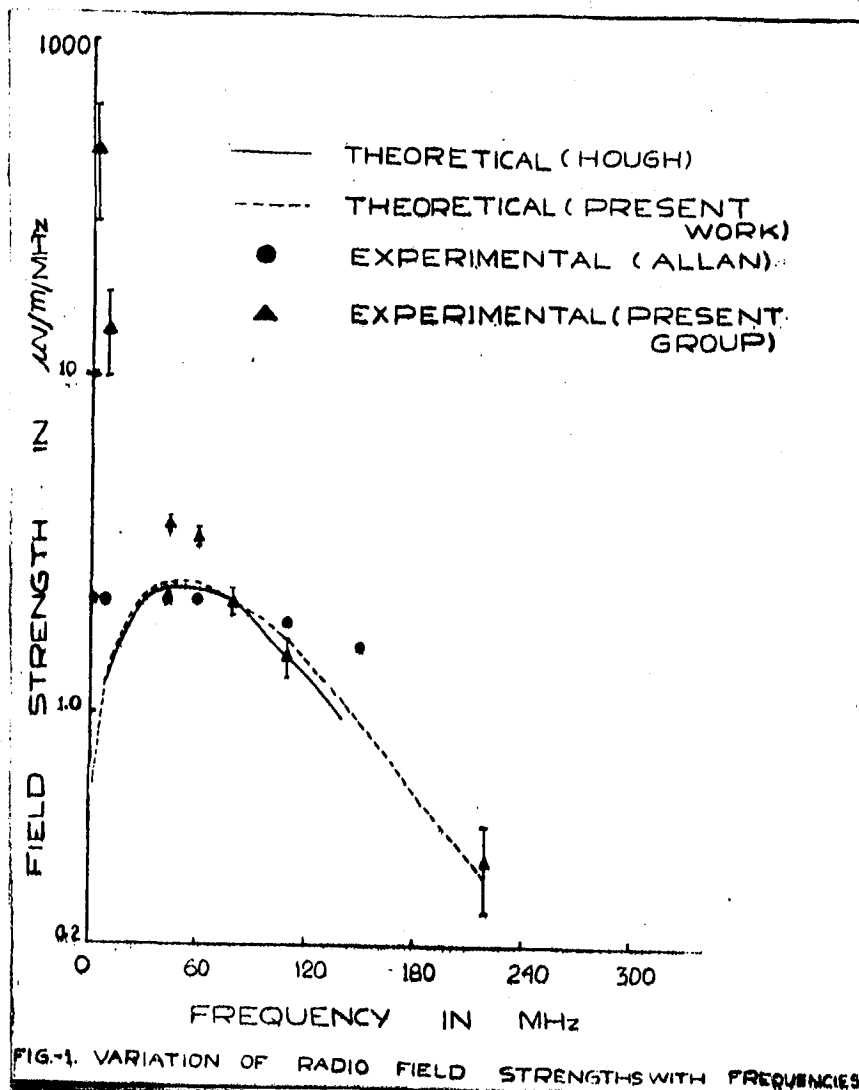
(D) Dipole field due to the annular ring of inner radius R and outer radius Ro :

$$E_P''(R) = ik\alpha e r \pi \frac{0.4N}{40(29.4)^2} \times 10^5 J_0'(k\alpha R) \int_R^{R_0} H_0^{(1)}(k\alpha r) r^2 \left(\frac{r}{29.4}\right)^{-0.75} \left(\frac{r}{29.4} + 1\right)^{-3.25} \left(1 + \frac{r/29.4}{11.4}\right) dr \dots (4)$$

The vector sum of  $E_C'$ ,  $E_C''$ ,  $E_P'$  &  $E_P''$  will give the resultant field.

3. Results : Equations (1) to (4) have been integrated numerically at various frequencies for  $R=40$  m,  $R_0=100$  m and  $E=10^{16}$  eV. Theoretical frequency spectra of (i) the present work, (ii) Hough, as well as the experimental data of different workers normalised at 80 MHz with the theoretical curve of Hough (4), are shown in Fig.1.

4. Discussion : Experimental results of different workers (6,7, 8) support the presence of a plateau region in the frequency range (40-60)MHz. For frequencies above 80 MHz, experimental data of the present group, within experimental error, agree with the present calculation. But in the low frequency region ( $< 10$  MHz), none of the experimental results support any of the theoretical predictions. It seems to indicate that below 80 MHz besides geomagnetic mechanism,



some other mechanism/s are also involved. Nature of variation of experimental data with frequency shows gradual decrease of the effect of the above unknown mechanism/s towards 80 MHz.

5. Conclusions : Theoretical as well as the experimental results of the present authors and also of other workers indicate that the frequency spectrum is rather flat in the frequency range (40-60)MHz. Above 80 MHz, the radio-emission can be explained with the help of geomagnetic mechanism. But at very low frequency (< 10 MHz), mechanisms other than geomagnetic are involved.



6. Acknowledgements : The authors thank the Department of Atomic Energy, ( BRNS ), Govt. of India for funding the project.

References :

1. Kahn, F.D. and Lerche, I., ( 1966 ), Proc. R. Soc. A 289, 206.
2. Castagnoli, C. et al., ( 1969 ), Nuo. Cim. LXIII B, N.I, 373
3. Allan, H.R., ( 1971 ), Prog. Elem. Part. & C.R. Phys., 10 , 171
4. Hough, J.H., ( 1973 ), J. Phys. A., 6, 892.
5. Borah, B. et al., ( 1983 ), Proc. ICRC, 6 , 249.
6. Borah, B. et al., ( 1983 ), Proc. ICRC, 6, 245.
7. Allan, H.R. et al., ( 1970 ), Nature, Lond. 227.
8. Mandolesi, N. et al., ( 1976 ), J. Phys. A., 9, 815.

===== X =====

A NEW STUDY ON THE EMISSION OF  
EM WAVES FROM LARGE EAS

PATHAK K.M. & MAZUMDAR G.K.D.  
Physics Department, Gauhati University,  
Gauhati-781014, Assam, INDIA

**1. Introduction.** Studies on Cosmic Ray Showers of energy  $E_p \gg 10^{16}$  eV have been continuously pursued since 1970 in Gauhati University, Assam (1). With an GM counters array. EM waves—both at optical Cerenkov and at Radio frequencies (from 2 to 220 MHz) - associated with the showers have been studied in this laboratory. Experimental results obtained reveal the following features:

- (i) Frequency spectrum of Radio as well as Cerenkov pulses decreases with increasing pulse heights.
- (ii) Field-strength of radio pulses decreases with increase in frequency.
- (iii) Radio pulses are polarised in E-W direction. The high value of polarization ratio at 9 MHz appears to confirm the predominance of geomagnetic effect on emission mechanism.
- (iv) Studies on the correlation coefficients of emission between radio pulses of different frequency pairs from the same shower indicate:
  - (a) There is no correlation between low ( $< 80$  MHz) and high ( $> 80$  MHz) radio frequencies.
  - (b) The positive correlation coefficient between the frequency pairs below 80 MHz (eg. 9-60 MHz) and negative correlation coefficient between any frequency pair below and above 80 MHz (eg. 9-220, 60-80, 60-110 MHz) confirm that the production mechanism of radio pulses below and above the cut off frequency ( $\sim 80$  MHz) may perhaps be different.
  - (c) There is no correlation between the emission of optical Cerenkov radiation and radio pulses at different frequencies.

The above observations have tempted us to repeat the whole experiment with a sophisticated particle detector array with facilities for corelocation and energy determination of individual showers. In this paper the new array and the core detection technique along with a few of the sampled parameters, obtained so far, are reported.

**2. Methods.** (a) The array. The present array consists of seven plastic scintillators (50cm x 50cm x 5cm each) the outermost is located at 100 m from the array centre. Fig 1 gives the schematic diagram of the array used along with

the positions of the antennas and Cerenkov detector.

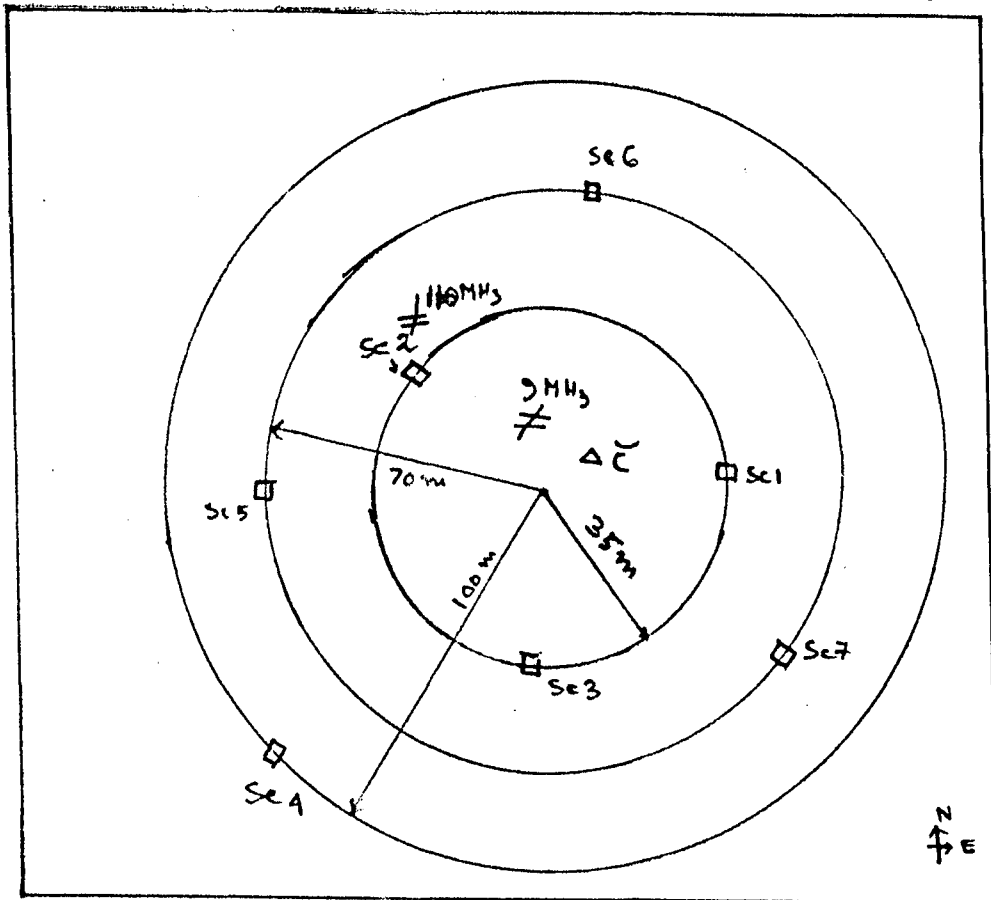


Fig 1. The array. Sc 1-Sc 7 - Positions of scintillators  
 $\neq$  -positions of Antennas,  $\Delta$  -position of C detector.

2.(b) Core location. Each shower can be specified by four parameters viz size ( $N$ ), co-ordinates of the core ( $x_0, y_0$ ) and the age ( $s$ ). Therefore, measurements of four particle densities are, in principle, enough to evaluate these parameters. We assumed NKG lateral distribution for particles given by  $\Delta = Nf(r,s)/R_1^2$ . It is evident from this that by taking the ratio of densities between any two detectors the parameter  $N$  can be eliminated. Numerical calculations using computer (Ellipse 316), give a set of curves i.e. locii of the shower axes producing different density ratios. With these sets of locii, assuming different 'S' values, one can locate the shower core within  $\pm 3.3$  metres.

The above method has been applied in locating the core of each individual shower. Using a microprocessor-based detecting system (2), the density distribution and hence, energy of each detected shower has been estimated.

HE 4.6-5  
 2. (c) Detection of Radio & Cerenkov pulses. Two antenna systems for detecting radio pulses at frequencies 9 MHz and 110 MHz have been set up. For detection of optical Cerenkov pulses associated with each shower, a parabolic reflector of 76 cm diameter, and 13 cm focal length viewed by a Dumont 6364 PMT has been used. The positions of the antennas and the Cerenkov detector in the array are shown in Fig 1.

For each shower, the detected outputs of the receivers (for radio pulses) and signals from the PMT (for Cerenkov pulses) are digitized using sample and hold (S/H) and A/D converter, triggered by the master coincidence pulse. The digitization and the storing of the informations are controlled by a 8085 A microprocessor (2).

3. Results. As the data can only be collected during clear moonless nights, the experiment is yet to be completed. However, a few of the sampled parameters, obtained so far, are presented in Table 1.

TABLE - 1

Event No.	Distances of the cores from the scintillators in metre				$E_p \times 10^{16}$ in eV	Pulse heights (arb.unit) $\times 10^{-2}$		
	$r_1$	$r_2$	$r_3$	$r_4$		9MHz	110MHz	Optical
1	55	60	10	80	4.30	75	26	58
2	50	45	28	80	3.57	96	20	40
3	80	53	56	30	0.80	67	26	44
4	65	13	65	105	6.70	80	16	60
5	64	64	105	68	5.90	60	26	30
6	60	60	10	71	0.50	50	20	28
7	62	58	40	68	3.20	70	28	30
8	70	65	40	80	1.20	60	30	40
9	68	60	25	68	4.80	78	30	26
10	45	50	20	65	0.70	65	20	37

$r_1, r_2, r_3, r_4$  are the distances of the core from Sc 1, Sc 2, Sc 3 and Sc 4 respectively.

4. Conclusions. The work is in progress and we hope to get adequate data within a couple of months or so to test our earlier observations as mentioned in the introduction.

5. Acknowledgements. The authors thank the Department of Atomic Energy (BRNS), Govt. of India for funding the project, and the TIFR, Bombay for some equipments. They also like to thank the Institute of Advance Studies in Science and Technology (Assam Science Society) for partial funding of the project.

References.

1. Pathak K.M. et al (1982) Proc. of the International workshop on V.H.E.G.R. Astronomy 309.
2. Mazumdar G.K.D. et al (1985) XIX ICRC Papers code HE 4.6-13

## AIR FLUORESCENCE DETECTION OF LARGE AIR SHOWERS BELOW THE HORIZON

Peter Halverson and Theodore Bowen  
Department of Physics  
University of Arizona, Tucson, AZ 85721, USA

In the interest of exploring the cosmic ray spectrum at energies greater than  $10^{18}$  eV, where flux rates at the earth's surface drop below  $100 \text{ yr}^{-1} \text{ km}^{-2} \text{ sr}^{-1}$ , cosmic ray physicists have been forced to construct ever larger detectors in order to collect useful amounts of data in reasonable lengths of time. At present, the ultimate example of this trend is the Fly's Eye system<sup>1</sup> in Utah, which uses the atmosphere around an array of skyward-looking photomultiplier tubes. The air acts as a scintillator to give detecting areas as large as  $5000 \text{ km}^2 \text{ sr}$  (for highest energy events). This experiment has revealed structure (and a possible cutoff) in the ultra-high energy region above  $10^{19}$  eV.<sup>2</sup>

The success of the Fly's Eye experiment provides impetus for continuing the development of larger detectors to make accessible even higher energies. However, due to the rapidly falling flux, a tenfold increase in observable energy would call for a hundredfold increase in the detecting area. But, the cost of expanding the Fly's Eye detecting area will approximately scale linearly with area.

It is for these reasons that the authors have proposed a new approach<sup>3</sup> to using the atmosphere as a scintillator; one which will require fewer photomultipliers, less hardware (thus being less expensive), yet will provide position and shower size information.

The Side-Looking Air Shower Detector. As shown in Fig. 1, the Side-Looking Detector (SLD) consists of an array of at least three SLD stations, each containing six photomultipliers, a large cylindrical focusing mirror, and some associated electronics such as PMT power supplies, digitizing modules, and communication equipment (to transmit the digital data to the base station).

Each SLD station would look almost horizontally, dividing the atmosphere into a stack of three wedges 60 degrees wide and 0.2 degrees thick. The three detector stations are identical and are located at the three corners of an equilateral triangle, so their fields of view overlap. Since the detector stations are expected to be able to detect  $10^{19}$  eV events up to 30 kilometers away, our detecting area would be about  $380 \text{ km}^2$ . If we can detect larger events up to 35 km away, then our detector area will grow to  $520 \text{ km}^2$ . A cosmic ray shower descending through the atmosphere above the detecting area successively passes through the three wedges of air, whereupon near-ultraviolet photons from excited nitrogen molecules are emitted.

As shown in Fig. 2, the photons are collected by the mirrors in the SLD stations and are focused onto long strips of acrylic that have been doped with the wavelength-shifting chemical BBQ. The BBQ absorbs the ultraviolet photons and re-emits them as green photons, which travel down the plastic strips to PMT's at each end. The PMT's convert the light from the BBQ to photoelectrons which, after being waveform digitized, are transmitted to the base station for data

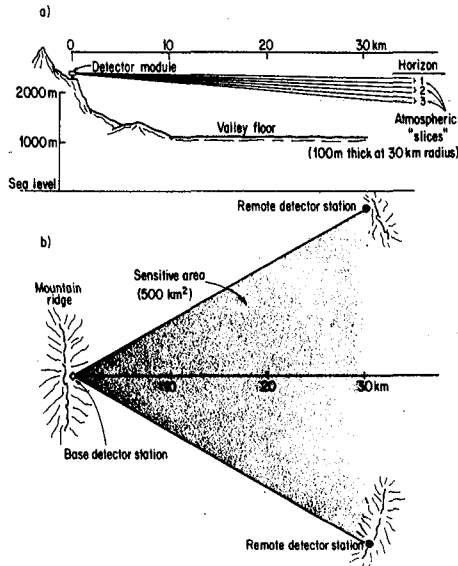


Fig. 1. Proposed side-looking air fluorescence detector to observe  $E \geq 10^{19}$  eV air showers. (a) Side view (Vertical scale:  $\times 10$ ), showing three slices or wedges (opening angles  $\sim 0.2^\circ$ ) viewed by each station. Viewing angles are set below the horizon to reduce background light; (b) Plan view, showing suggested triangular coverage of three stations, each having a horizontal viewing wedge angle of  $60^\circ$ .

analysis. The amplitude and timing information in the light pulses resulting from the passage of the cosmic ray shower contains information about the shower's location, orientation, and energy. The location and distance from the detector stations of the shower can be determined by accurately comparing the arrival times of the light pulses at each station and for each wedge. By comparing the arrival times of the photons in the upper and lower wedges at each station, the orientation of the shower may be determined. Once the distance of the shower from the SLD stations has been computed, the size of the light pulses can be used to compute the shower size. With stations located at the three corners of a triangle, the corrections required for atmospheric light attenuation can be computed from the data, as well as from calibration light flashes sent from one station to another. The calibration flashes would also synchronize the timing at the remote stations.

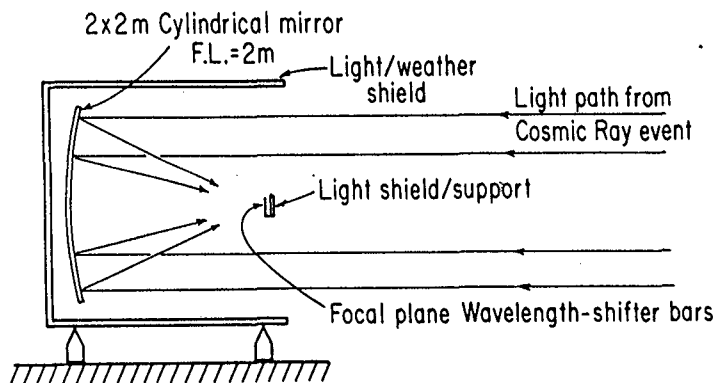


Fig. 2. Side view of proposed SLD station.

Design Equations. If  $S$  is the number of photoelectrons due to the shower, and  $b\tau$  is the number of photoelectrons due to background light in time interval  $\tau$ , then the fractional error is given by  $\sigma(S)/S = (S+b\tau)^{1/2}/S$ , which must be  $\ll 1$  for a useful measurement. It is convenient to define a figure of merit  $M$ , which is the square of the reciprocal of the fractional error;  $M \equiv S^2/(S+b\tau) \gg 1$  for a useful measurement. It can be shown that  $M = K_1 / [(1/\delta) + K_2(1+(\ell/r\delta)^2)^{1/2}]$ , where  $K_1 = [qN_e A \epsilon] / [4\pi \exp(\alpha r)]$ , and  $K_2 = [4\pi\beta I_{\text{sky}} \Delta\lambda \phi r^2 \exp(\alpha r)] / [qN_e c]$ . In these equations,  $q$  = no. of optical air fluorescence photons per meter of shower electron track ( $\sim 3$ ),  $N_e$  = no. of shower electrons,  $A$  = area of SLD mirror,  $\epsilon$  = combined wavelength shifter and photocathode efficiency,  $\alpha$  = attenuation coefficient for light transmission in air,  $r$  = distance from detector to shower,  $I_{\text{sky}}$  = no. photons/m<sup>2</sup>-s-sr-A in night sky ( $\sim 4 \times 10^8$ ),  $\beta$  = intensity reduction factor due to viewing below horizon ( $\sim 0.4$ ),  $\Delta\lambda$  = effective bandwidth of detector ( $\sim 90$  nm),  $\ell$  = lateral size of shower ( $\sim 100$  m),  $c$  = speed of light,  $\phi$  = horizontal opening angle of viewing wedge (1.047 rad), and  $\delta$  = its vertical opening angle. As  $\delta$  increases,  $M$  approaches a maximum possible value,  $K_1/K_2$ , because the time interval  $\tau$  increases with  $\delta$ . If  $A\epsilon$  is chosen to be  $0.25$  m<sup>2</sup> and  $N_e$  is  $8 \times 10^9$  electrons for an event at  $r = 30$  km, then  $K_1/K_2 = 9.3$  and  $M = 4.9$  if  $\delta = 0.2^\circ$  ( $\tau \sim 0.5$   $\mu$ s).

The Scintillation Efficiency of Air. We have carried out a small experiment using ground-level muons in the laboratory to confirm that the yield of photons per meter,  $q$ , into a PMT with bialkali response is  $3.2 \pm 0.5$  photons/meter. A black box was employed so Cherenkov photons would be absorbed; most ground-level muons are near or below the Cherenkov threshold in air, so the black walls appear to reduce the Cherenkov component to a negligible level relative to air fluorescence. The yield was obtained from the counting efficiency for single-photoelectron pulses in a 5 inch RCA 4522 PMT viewing 20.3 cm of path.

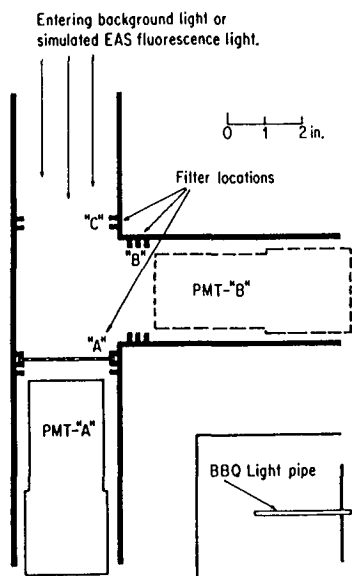


Fig. 3.

#### The Effect of Filters on Signal and Background.

The apparatus used in making these measurements is shown in Fig. 3. The transmission coefficient of each filter was measured by comparing the output current of an RCA 6655A photomultiplier having S11 response with and without the filter in place. Two sets of data were gathered: filter performance on background light, as observed from Mount Hopkins, and filter performance on light from each of the major air fluorescence lines, as produced by a monochromator. Table I shows the factor by which the figure-of-merit,  $M$ , is predicted to improve with the use of each filter. The emission spectrum predicted by Bunner<sup>4</sup> was employed in the calculations. The distance between the air shower and the detector must be specified because the attenuation due to Rayleigh scattering significantly modifies the source spectrum.

Since the signal-to-background ratio tends to be smallest for the most distant events, the UG-5 and U330 filters have the most favorable characteristics among those listed. Filtering also attenuates the signals; this must be considered along with the improvement factors. If a filter with  $\geq 70\%$  transmission for the 3914 and 4000 Å bands could be found, it would be better than any of those listed in Table I.



Table I. Expected figure-of-merit improvement factors for various filters.

Event Distance [km]	Filter:	UG-1	UG-5	U330	U340
0		5.0	4.8	4.6	4.1
4		4.4	4.5	4.2	3.3
16		2.7	3.5	3.3	1.4
32		1.6	2.8	2.7	0.5

The Effect of Viewing Below the Horizon. The background light intensity  $I_T$ , below the horizon at Mount Hopkins, Arizona was compared with the dark night sky intensity  $I_0$ . At each angle, the distance to the valley floor could be calculated. Figure 4 shows  $I_T/I_0$  as a function of the  $g/cm^2$  of air between the detector and the valley floor. As shown by the curves, the data seem to agree with a model in which the below-horizon background is due to Rayleigh-scattered light; for this model  $I_T/I_0$  approaches 0.5 for infinite air thickness.

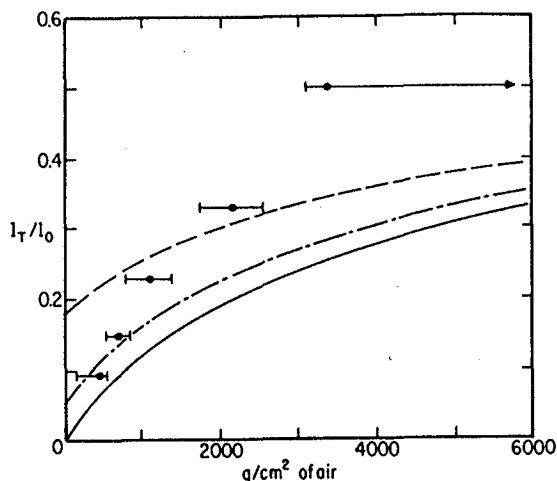


Fig. 4, Plot of scattered light observed at Mt. Hopkins as a function of air thickness to the ground. The theoretical curves are for 0%, 5%, and 18% (solid, dot-dashed, and dashed, respectively) ground reflectivities.

Conclusion. Filters and below-horizon viewing may offer important advantages for an economical side-looking air fluorescence detector.

Acknowledgments. The authors thank Charles Bridges for his assistance with the measurements. This work is supported by NSF Grant No. PHY-82-07697.

1. R. Cady et al., "The Fly's Eye," Report UUHEP-83/11, University of Utah, 1983.
2. R. M. Baltrusaitis et al., Phys. Rev. Lett. 54 (1985).
3. T. Bowen and P. Halverson, Proceedings of Workshop on Cosmic Ray and High Energy Gamma Ray Experiments for the Space Station Era, Baton Rouge, LA, 17-20 October 1984.
4. A. N. Bunner, "Cosmic Ray Detection by Atmospheric Fluorescence," Thesis, Cornell University, 1966.

## INVESTIGATION OF COSMIC RAYS IN VERY SHORT TIME SCALES

J. Peltonen, E. Valtonen, J.J. Torsti, H. Arvela, M. Lumme,  
M. Nieminen and E. Vainikka

Wihuri Physical Laboratory, University of Turku, and  
Department of Physical Sciences, University of Turku,  
SF-20500 Turku, Finland

## ABSTRACT

We have constructed a fast databuffer system, where cosmic ray events in the Turku hadron spectrometer, including particle arrival times, are recorded with time resolution of 100 ns. The databuffer can be read continuously by a microprocessor, which preanalyses the data and transfers it to the main computer. The time span, that can be analysed in every detail, is a few seconds.

The high time resolution enables a study of time correlated groups of high energy particles. In addition the operational characteristics of the spectrometer can be monitored in detail.

### 1. The spectrometer

The Turku hadron spectrometer consists at present of a double neutron monitor combined with plastic scintillators. The spectrometer has been used to measure the energy spectra of neutrons and protons in the energy range .05 - 1000 GeV. Detailed description of the apparatus and its future development is given in paper /1/ presented at this conference.

### 2. The data collection system

Two identical microprocessor units are used in the Turku hadron spectrometer to collect the cosmic-ray events. Both units can record the status of the spectrometer with time resolution of 50  $\mu$ s. This time resolution already enables a detailed study of very rapid cosmic-ray phenomena. It is also possible to study the spectrometer characteristics in detail.

The two microprocessor units have different tasks. Unit 1 calculates the hadronic spectra and monitors the hadron and muon flows through the spectrometer. Unit 1 is programmed to study energy dependent variations of hadron and muon intensities in time scales  $> 30$  s. A detailed description of the microprocessor 1 and of its software was given in /2/.

Unit 2 can be used parallel with unit 1. Its time resolution can be improved by adding a fast data buffer. This data buffer records spectrometer events, including particle arrival times, with time resolution of 100 ns.

The overall diagram of the data collection system is given in fig. 1.

### 2.1. A fast data buffer

The heart of the buffer memory is a DUALPORTED FIFO-memory type IDT-7201-S-80-C from Integrated Device Technology (identical to better known MK4501 from Mostek). This memory component is very handy in data buffering applications. The READ-WRITE-operations can be done truly asynchronously and independently. Besides, these new memories are fast (cycle time 100 ns or even better) and easily cascadable.

The schematics of the data buffer is given in fig. 2. The 8 parallel FIFOs form a memory of  $64 \times 512$ . This memory can be triggered from 6 sources. On every trigger the logic generates a common WRITE-pulse and 64-bits of data is latched in, including the data of the time counters. The status and control signals are connected to microprocessor, which can access the READ-side of the FIFOs.

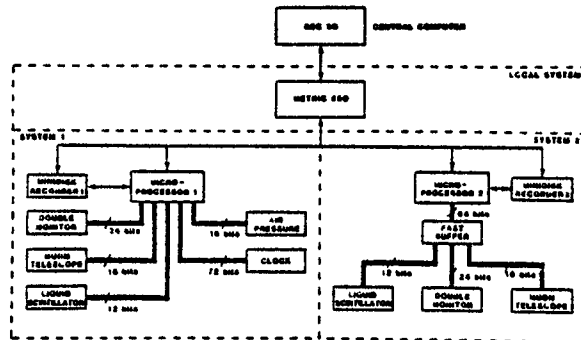


Fig 1. The overall diagram of the control system.

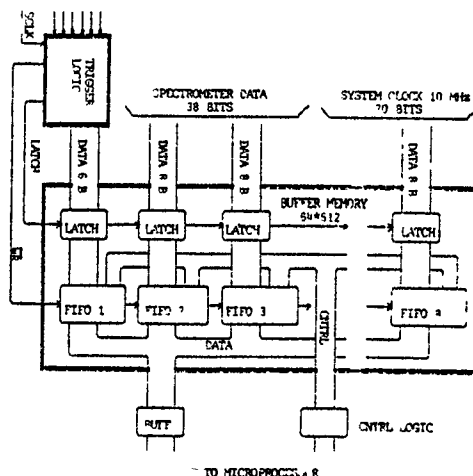


Fig. 2. Schematic of the data buffer.

### 3. Some results and discussion

Until now, the system 2 has been used only for some simple, mainly instrumental measurements. Two examples of these measurements are shown in figures 4 and 5. The study of more interesting problems, like long tails of extensive air showers and time behaviour and detection of high energy bursts (  $\gamma$ -ray bursts ) requires longer measurements.

In fig.3 , the measured time intervals between charged particles coming into our spectrometer are shown. According to Poisson-statistics we should have exponential distribution of the form  $A \cdot \exp(-kt)$  . As one can see from figure 3, the measured time distribution is strictly Poissonian when  $t > 20 \mu s$ . At shorter time intervals there is, however, an excess of events, compared with the Poisson distribution. We believe that most part of these events can be explained by afterpulses from the photomultipliers. The exact portion of afterpulses and the role of some other possible phenomena in these events are being investigated.

In fig. 4, there is shown the time distribution of charged particles that arrive at the spectrometer before the first evaporation neutron is registered in the monitors. It can be seen that most of the particles arrive at times  $t < 250 \mu s$ . This time distribution is important, since we separate muons from protons and pions by assuming certain maximum reaction delay.

The Turku hadron spectrometer will be used in future as a central detector of an air shower array /1/. In addition, there will be position and direction sensitive detectors in the spectrometer. With the fast recording system described and with some additional electronics we can analyse cosmic ray showers and bursts in detail.

### References

- /1/ E. Valtonen, J.J. Torsti, H. Arvela, M. Lumme, M. Nieminen, J. Peltonen and E. Vainikka, paper HE 4.6-8 in this conference,
- /2/ Lumme, M., Nieminen, M., Peltonen, J., Torsti, J.J., Vainikka, E., and Valtonen, E., Proc. 18th Int. Conf. Cosmic Rays, Bangalore, 8, 182-5 (1983).

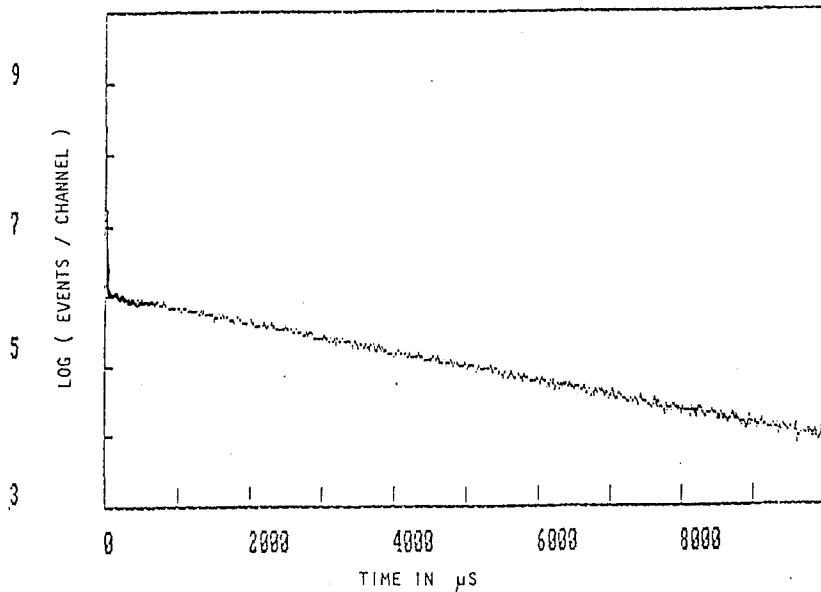


Fig. 3. The time interval distribution of charged cosmic-ray particles in the Turku hadron spectrometer.

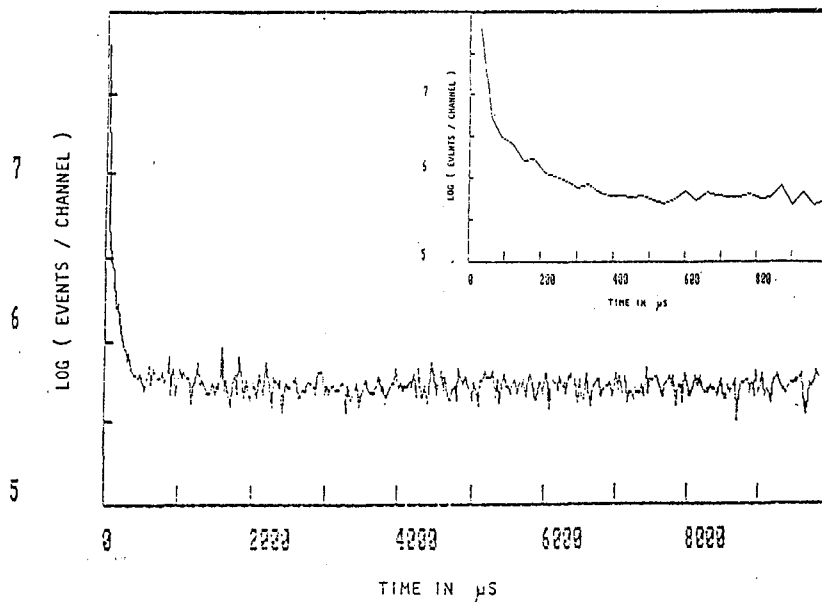


Fig. 4. The time distribution of charged particles arriving at the spectrometer before the first neutron is detected in the neutron monitors. This time distribution is used to separate protons and pions from muon background.

## A FACILITY FOR INVESTIGATION OF MULTIPLE HADRONS AT COSMIC-RAY ENERGIES

E. Valtonen, J.J. Torsti, H. Arvela, M. Lumme, M. Nieminen, J. Peltonen, and E. Vainikka

Wihuri Physical Laboratory, University of Turku and  
Department of Physical Sciences, University of Turku,  
SF-20500 Turku, Finland

## ABSTRACT

An experimental arrangement for studying multiple hadrons produced in high-energy hadron-nucleus interactions is under construction at the university of Turku. The method of investigation is based on the detection of hadrons arriving simultaneously at sea level over an area of a few square metres. The apparatus consists of a hadron spectrometer with position-sensitive detectors in connection with a small air shower array. The position resolution using streamer tube detectors will be about 10 mm. Energy spectra of hadrons, or groups of simultaneous hadrons produced at primary energies below  $10^{16}$  eV can be measured in the energy range 1-2000 GeV.

### 1. Introduction

Measurements of the exact shape of cosmic-ray hadron spectra give information on the properties of high-energy hadron-nucleus interactions. Recently, energy spectra of charged and neutral hadrons were measured at sea level in the range 0.05-1000 GeV /1/. Particularly interesting is the spectrum of pions, because the few previous measurements made at sea level have given contradictory results /2,3,4/. Nieminen et al. /1/ estimated pion spectrum assuming an identical shape of neutron and proton spectra above 5 GeV and a proton-to-neutron ratio of 1.05. Even then, above 50 GeV only upper bound was obtained for pion spectrum. This was due to simultaneous incidence of multiple hadrons, not necessarily pions.

Incidence of several simultaneous hadrons in sea-level detectors was earlier studied theoretically /5/. It was shown that the frequency of occurrence of multiple hadron events is noticeable above total hadron energies of about 100 GeV increasing with energy and is strongly dependent on the detector area. The role of multiple hadrons in the interpretation of air shower results was recently discussed by Sreekantan et al. /6/. At high energies the air shower results were found to be severely distorted if these events were not properly taken into account. The present report concerns an experimental arrangement for studying multiple hadron production.

### 2. Hadron spectrometer

Front view of the hadron spectrometer used in the experiment is shown in figure 1. Central part of the spectrometer is a double neutron monitor. Effective depth of the lead target in each monitor is  $270 \text{ gcm}^{-2}$ . Evaporation neutrons produced in hadron-lead-nucleus collisions are detected with 16  $\text{BF}_3$ -counters with an average efficiency of 12.5 % /7/. In addition to the double neutron monitor, five liquid scintillation counters ( $100 \times 100 \times 6.7 \text{ cm}^3$ ), viewed from two sides by photomultipliers, are used to measure the energy of electromagnetic cascades produced in the spectro-

meter. The thicknesses of the four iron absorbers shown in fig. 1 are 1.2 cm, 5 cm, 10 cm, and 10 cm, starting from the top. The total depth of lead and iron in the spectrometer is 4.5 interaction mean free paths of hadrons. The measurement of energy of incident hadrons is based on recording the multiplicities of neutrons produced in each monitor and on the pulse heights observed in the liquid scintillators due to electromagnetic cascades. The spectrometer can be used in the energy range 1-2000 GeV.

### 3. Position-sensitive detectors

Three layers of streamer tubes at the top of the spectrometer (fig. 1) are used to determine the number of simultaneously incident charged hadrons. The uppermost tube layer is unshielded while the other two are shielded against low-energy electrons by lead and/or iron layers. The active areas of these three detectors are 4.0, 1.7, and 1.0 m<sup>2</sup>. The streamer tubes are of the same type as those of the Mont Blanc detector described by Iarocci /8/. The basic element is an 8-cell plastic profile coated with graphite. The dimensions of a cell are 0.9x0.9x120 cm<sup>3</sup>. The diameter of the Be-Cu anode wires is 100 μm and the gas filling is a mixture of 75 % isobutane and 25 % argon. Two-dimensional read-out from each three tube planes by perpendicular induction strips enables the determination of positions and number of incident particles. To solve mirror ambiguities, the induction strips of successive tube planes are rotated by 45° with respect to each other. By using digital read-out, the position resolution will be about 10 mm. In addition, the angle of incidence of particles can be measured with an accuracy of about 2 degrees. The read-out electronics are based on commercial Camac system. A special circuit has been designed, which triggers the read-out in case a selected number ( $\geq 2$ ) of charged particles traverses the streamer tube layers.

A fourth layer of streamer tubes is installed between the two neutron monitors (fig. 1). This detector enables measurement of positions of showers produced in hadron cascades in the upper monitor. Thus, also the number of neutral hadrons incident on the spectrometer and interacting in the lead target can be determined.

### 4. Air shower array

The air shower array which will be constructed in connection with the hadron spectrometer is shown in figure 2. The shower parameters to be measured are core position, size, and arrival direction of a shower. The principal idea is to study hadrons near the shower core. The core position is determined using the method proposed by Bergamasco et al. /9/. This method enables the signals from the core detectors to be used as a master trigger for the other instruments in case the core falls in an

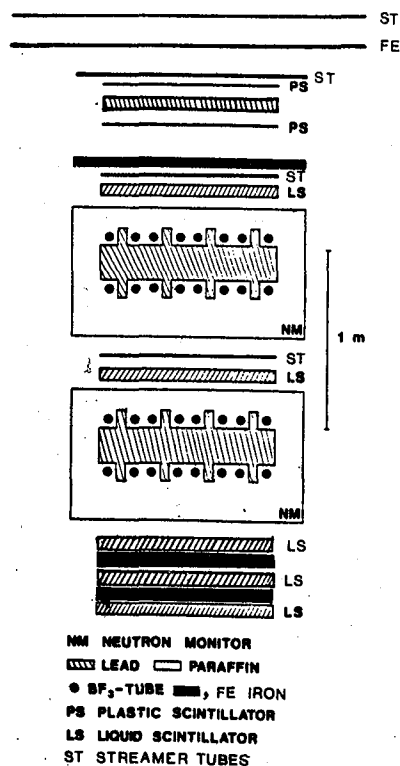


Fig. 1. Front view of the hadron spectrometer.

appropriate distance ( $\lesssim 20$  m) from the hadron spectrometer. There are in total four core detectors consisting of two plastic scintillators placed one on top of the other and separated by a lead layer with thickness of 5 cm. An example of such a detector are the two plastic scintillators at the top of the spectrometer (fig. 1). The measurement of the core position is based on the relative pulse heights observed in the two scintillators. Near the core the number of high-energy electrons undergoing multiplication in the lead is high.

Four liquid scintillators (DD in fig. 2) are used to measure the density of shower electrons and accordingly to estimate the shower size by using a theoretical lateral distribution function. Four plastic scintillators (FT in fig. 2) are equipped with fast photomultipliers.

With these detectors the arrival times of the shower front in each peripheral timing detector are measured with respect to the central detector. The arrival direction of the shower is then estimated using plane approximation of the shower front.

Electronic system used to measure all the pulse heights and time differences is based on Camac equipment. Microcomputers are used to read the data and store it on floppy disks. Hadron cascade model of Lumme et al. /10/ is being extended to include electromagnetic component in order to calculate response of the array as well as the accuracy of shower size, core position and arrival time measurements.

## 5. Discussion

Assuming that multiple cosmic-ray hadrons arriving simultaneously at sea level are produced in the last collision of a high-energy hadron in the atmosphere, the height of production will be a few hundred metres and particles detected over an area of  $1 \text{ m}^2$  at sea level are emitted into very narrow cone ( $\lesssim 1$  mrad). The higher is the collision point in the atmosphere, the narrower is the emission cone. Accordingly, such events of multiparticle production are detected, where the relative transverse momentum of the particles is very small. Using the experimental arrangement described above, intensities and energy spectra of groups with various numbers of hadrons can be studied. Restricting to single particles, the exact shape of energy spectra of cosmic-ray hadrons (e.g. pions) can be measured. Investigation of lateral distribution of particles produced in the same collision and emitted into a narrow cone is also possible, fixing the center of the group to the position of the most energetic particle. This can be estimated by determining the number of charged particles in hadron cascades observed under the first neutron monitor using analog read-out of the streamer tubes or possibly simply by observing the physical size of the clusters produced by the developing cascades.

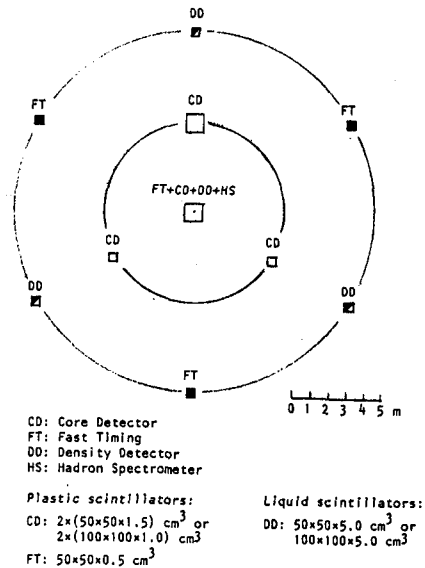


Fig. 2. Air shower array.



Multiple high-energy hadrons observed without accompanying air showers are thought to be produced in diffractive excitation processes. In these processes the primary particle retains most of its energy thus preventing the development of a shower. Recently, however, a model of coherent production of hadrons with small transverse momentum from nuclear targets was advocated by Berlad and Dar /11/. The mechanism was attributed to the decay of resonances produced in Coulomb excitation. By measuring intensities of groups of simultaneous hadrons, energy dependence of cross sections of coherent production can be studied and their possible contribution to the rising total cross section estimated. Even the relative contribution of single and double diffractive excitation can be studied on the basis of observed single and double clusters of particles.

Multiple hadrons have been earlier investigated in air showers /6/ and at very high energies ( $>1$  TeV) by several groups using emulsion chambers. In the present experiment occurrence of multiple hadron events is studied both in air showers and without accompanying air shower. Furthermore, also low-energy ( $\approx 1$  GeV) hadrons are taken into account. Primary energy range covered by the experiment is from 1 TeV upto about 10000 TeV. Properties of multiple production in air showers are of great importance and could explain, at least in part, for example the observed increase of transverse momentum with energy.

#### References

- /1/ Nieminen, M., Torsti, J.J., Valtonen, E., Arvela, H., Lumme, M., Peltonen, J., and Vainikka, E., J. Phys. G 11, 421 (1985).
- /2/ Brooke, G., Meyer, M.A., and Wolfendale, A.W., Proc. Phys. Soc. 83, 871 (1964).
- /3/ Diggory, I.S., Hook, J.R., Jenkins, I.A., and Turver, K.E., J. Phys. A 7, 741 (1974).
- /4/ Ashton, F. and Saleh, A.J., Proc. 14th Int. Conf. Cosmic Rays, Munich, 7, 2507 (1975).
- /5/ Arvela, H., Lumme, M., Nieminen, M., Peltonen, J., Torsti, J.J., Vainikka, E., and Valtonen, E., J. Phys. G 10, 695 (1984).
- /6/ Sreekantan, B.V., Tonwar, S.C., and Viswanath, P.R., Phys. Rev. D 28, 1050 (1983).
- /7/ Arvela, H., Torsti, J.J., and Valtonen, E., Nucl. Instrum. and Methods 192, 467 (1982).
- /8/ Iarocci, E., Nucl. Instrum. and Methods 217, 30 (1983).
- /9/ Bergamasco, L., Castagnoli, C., Dardo, M., and Saavedra, O., Nuovo Cimento 2C, 453 (1979).
- /10/ Lumme, M., Nieminen, M., Peltonen, J., Torsti, J.J., Vainikka, E., and Valtonen, E., J. Phys. G 10, 683 (1984).
- /11/ Berlad, G. and Dar, A., Phys. Rev. D 21, 3133 (1980).

A POSSIBLE EAS ARRAY ABOVE THE  
SOUDAN II DETECTOR

K. Sivaprasad  
Department of Physics & Astronomy  
University of Maryland  
College Park, MD 20742  
( On leave from TIFR, Bombay, India )

ABSTRACT

Multiple high energy muons, when studied with a large area detector, can be useful in the study of the composition of Cosmic Rays at energies  $\sim 10^{14}$  eV. The Soudan II detector, primarily designed to detect nucleon decay, is located  $\sim 600$  m deep underground and has dimensions 16m X 8m X 5m(height), and is made up of drift tubes. The minimum muon energy needed to penetrate that depth is  $\sim 500$  GeV.

We have used a set of simulated EAS to calculate the rate of muon associated events, using a trigger array with the number of detectors varying from 37 to 127 ( the radius of acceptance varying from 50m to 100m). The number of simulated showers, initiated by different nuclei (mass A) used in the calculations, is given in the following table.

A	$E_0$	50 Tev	100 Tev	400 Tev	1600 Tev
1		711	917	711	-
4		-	306	1100	-
14		-	-	686	120
24		-	-	629	149
56		-	-	1100	88

The association rate is seen to be a strong function of the multiplicity of muons in the detector. The difference in the rates of association of proton and nuclei induced showers rises rapidly with multiplicity. More detailed decoherence studies, which is possible with this high resolution detector, and correlation with shower characteristics is under progress. Flux considerations dictate that a minimum radius of 100m for the EAS array is essential for the method to be useful.

## FAST SCINTILLATION COUNTER SYSTEM AND PERFORMANCE

Sasaki,H., Nishioka,A., Ohmori,N., Kusunose,M.

Kochi University, Kochi, Japan

Nakatsuka,T.

Konan University, Kobe, Japan

Horiki,T.

The Institute of Physical and Chemical Research, Woko, Japan

Hatano,Y.

Institute for Cosmic Ray Research, University of Tokyo, Tokyo, Japan

## §1. Introduction.

At the investigation of the arrival time distribution, it is very important to measure the pulse wave-form precisely as much as possible and still the observation by fast pulse technique has attracted the attention of many researchers.(1),(2),(3),(4)

Experimental study of the fast scintillation counter(FS) system to observe a shower disk structure at Mt.Norikura are described in this paper, especially on the system performance and a pulse wave-form by a single charged particle. Some improvements were made on a few points. As reported at the previous conference, the photomultiplier tube pulse (PT-pulse, at Bangalore called a knot pulse) is appeared at the leading edge of the main pulse. To remove this PT-pulse from the main pulse, we changed the frame of the scintillator vessel (1) and have made the fast triggering system to decrease the dead time which came from the use of the function of the self triggering of the storage oscilloscope(OSC). To provide a new field on the multi-parameter study of the EAS, the system response of our FS system also improved as a results of many considerations.

## §2. Experimental.

For the fast triggering system, four  $0.25\text{m}^2$  trigger fast scintillation counters (TFS) were used for the air shower trigger and two  $0.0625\text{m}^2$  TFS used for the identification of a single particle at the present work, where the photomultiplier is the same one for the FS(R329-02,Hamamatsu). A block diagram of developed fast trigger system and the FS system is shown in Fig. 1. Four constant fraction timing discriminators (CFTD) were added last year, where its propagation delay is  $\sim 10\text{nS}$ , time walk is  $\sim 1.5\text{nS}$  and the out put pulse width was set to  $80\text{nS}$ , because of the usage for the EAS trigger.

Used plastic scintillators for the FS to measure pulse wave-forms, are the polymerization type ternry plastic scintillator plates( $50\text{x}50\text{x}5\text{cm}^3$ ) with the same lot(CI LTD). To avoid diffused reflection, the inside wall of the scintillator vessel is covered with a sheet of black paper except for the bottom. The signal outputs from the FS were connected to a storage oscilloscope(TS8123,IWATSU) with a  $15\text{m}$  10D2V cable and a  $5\text{cm}$  58 U/G cable and terminated to  $50\Omega$  by the terminator(BB50M1 frequency range is  $\text{DC}\sim 3\text{GHz}$ ) at the entrance of the storage main amplifier. Coincidence output signal triggers the storage OSC of the external trigger mode, first of all, and when the service request signal through GPIB control Bus is transmitted from the storage OSC to the personal computer, the computer begins to control the GPIB data Bus. It takes about 12 seconds per one record.

By the way, the definition of the pulse wave-form parameters, such as

a rise time, FWHM and FWTM, are illustrated in Fig. 2. As the FWTM represents a thickness of shower disk, we must pay attention to the definition.

### §3. Performance of the FS system.

As the measuring method of the time response of the system, we adopted the Cerenkov light signal observation from the acrylic acid resin plate ( $50 \times 50 \times 5 \text{ cm}^3$ ) with the same vessel and the photo-tube as for the FS scintillator. Fig.3(a) shows the arrangement of the Cerenkov detector. A single charged particle does not pass through the photo-tube, so the influence of the PT-pulse (e.g.  $\bar{C}$  light signal at the photocathode made by borsillicate glass with a concave surface, 1mm to 6.7mm thick) is avoidable. Most of the obtained pulse wave-form have a small ringing pulse train, gradually decreasing their amplitude, at the trailing edge of the main pulse which may be due to high frequency component contained in the main pulse. But the pulse height of the first ringing pulse is less than 10% of the main peak. The result of the time response is tabulated in Table 1.

### §4. Pulse wave-form of the FS by a single charged particle.

On the pulse wave-form measurement of the scintillation counter had been done mainly by the time spectrometer with a time to pulse height converter (TPHC) and the results show a smooth curve. (5) This pulse wave-form is an averaged one, so we must be handle with caution. On the other hand, the single particle response of the system must be known at the time when we discuss the arrival time distribution of the shower particles. Then, we observed the pulse wave-forms for single particles with the detector arrangement shown in Fig.3(b). TFS1, and TFS2 were installed as to avoid the PT-pulse occurrence.

The experimental results are shown in Fig.4. Various time response data in this work are listed in Table 1, where parenthesized values show

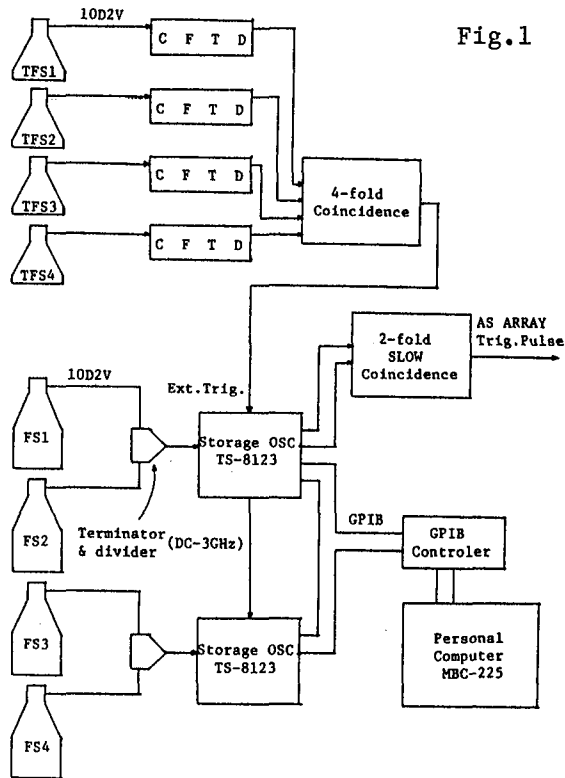
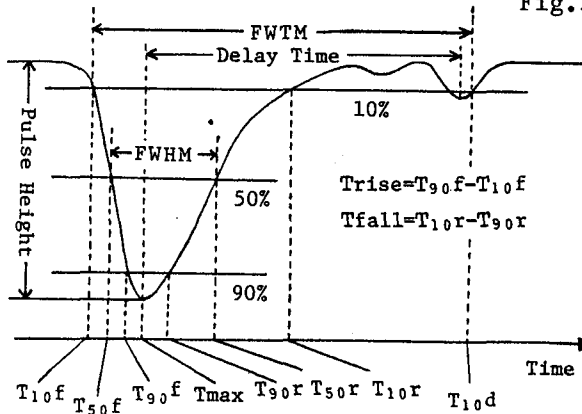


Fig. 2



The experimental results are shown in Fig.4. Various time response data in this work are listed in Table 1, where parenthesized values show

the standard deviation. Our data are quite sufficient one, because the maximum rise time of the storage OSC 3.5nS (Commercial data) is larger than our Cerenkov data.

Fig.3(a)

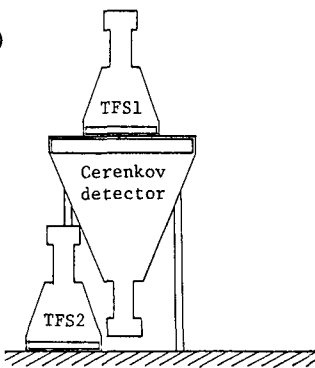


Fig.3(b)

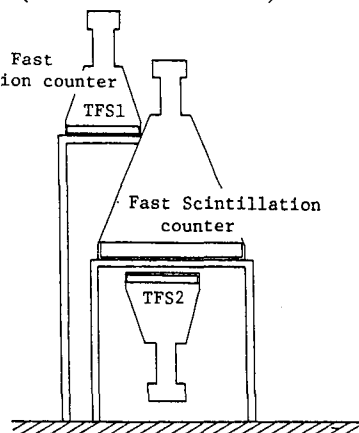
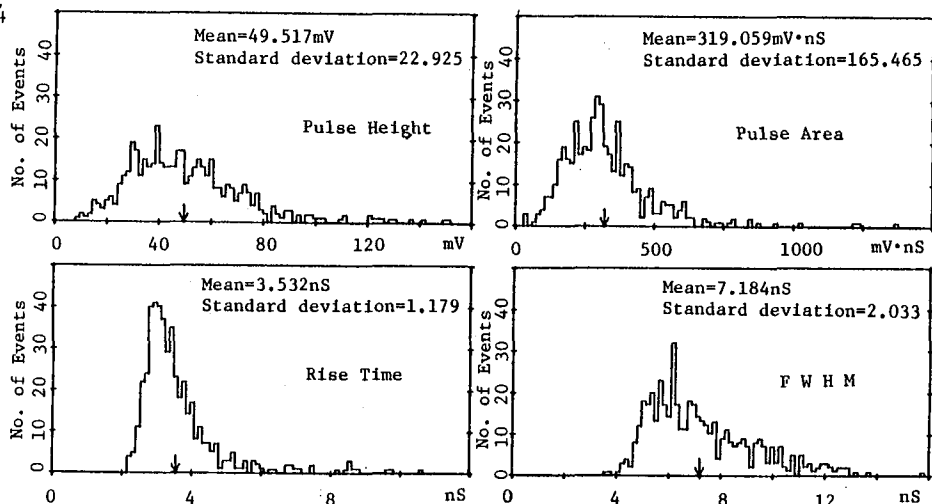


Table 1

Mode of Experiment	Rise Time (nS)	F W H M (nS)	Comment
Cerenkov Detector	2.68 ( $\pm 0.3$ )	4.31 ( $\pm 0.15$ )	present work
PT pulse	2.51 ( $\pm 0.2$ )	4.37 ( $\pm 0.2$ )	present work
Single particle	3.54 ( $\pm 1.18$ )	7.18 ( $\pm 2.03$ )	present work
Averaged Single particle	3.57	7.43	present work
PT pulse	2.5~3.5	5.2~5.5	Kobe Group Ref(2)
Single particle	4.3~4.5 (0.9~1.3)	8.6~8.8 (1.7~1.8)	Kobe Group Ref(2)

Fig.4

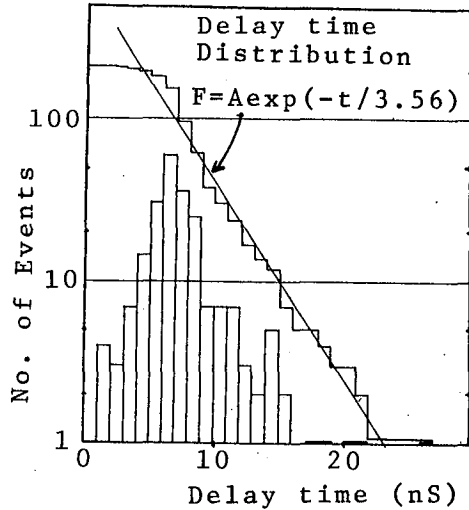


The fluctuation of the pulse wave-form from the plastic scintillator is larger than what we expected and this tendency is obvious at glance of individual pulse profile. The rate of subpeaks, at the condition that the peak height of a subpeak is greater than the 10% of the average peak height, is about 82%, and at the condition that larger than the 33% of the main the rate is about 48%. In the former case that is  $P.H.(subpeak) \geq 0.1 \times P.H.(mainpeak)$ , the rate is affected by the small ringing pulse. At the case  $P.H.(sub) \geq 0.33 \times P.H.(main)$ , the influence by the ringing pulse is small and the delay time distribution of subpeaks in this case is shown in Fig.5. This delay time distribution is expressed as

$$F = A \exp(-t/\tau_0) : \tau_0 = 3.56 \text{ nS}$$

the value  $\tau_0 = 3.56 \text{ nS}$  is quite reasonable as compared with the fall time measurement.(6)

Fig.5



### §5. Simulation of the pulse wave-form.

To give an effective and practical comment at the data analysis of the shower disk, we simulated pulse wave-forms at their density 10, 20 and 40 particles/ $0.25 \text{ m}^2$  using a sample arrival time distribution function :

$$f(t) = \frac{1}{\sqrt{2\pi}\sigma} \exp\left(-\frac{(x-m)^2}{\sigma^2}\right)$$

, where  $\sigma = 0.5 \text{ nS}$  and  $m = 1.5 \text{ nS}$ , and observed pulse wave-form data for a single particle whose values of area are within 17% of that of the average area distribution. The number of simulated pulse wave-forms for density 10, 20 and 40 are 21, 23 and 16 events, respectively.

The average values of the obtained rise time, and the FWHM, are somewhat larger than those of the measured for a single particle. Analysis shows, also,

that the ratio of the sub peaks to total number of simulated events whose pulse height is larger than 1 particle, are 38%, 59% and 81%, respectively. Those high rate may come from the ringing pulses at the trailing edge of a single particle's pulse profile. While as an analysis of the subpeaks whose densities larger than 2 particles/ $0.25 \text{ m}^2$ , they are quite small and are 10%, 27% and 6% for each density.

### §6. Conclusions.

From the facts described above, we obtained satisfying results on the system performance and it becomes clear that the behavior of the pulse wave-form of the thick(5cm) plastic scintillator by a single charged particle.

On the other hand, with respect to the pulse wave-form simulation there are still many problem as a selection of the sample arrival time distribution function. And in future we must devise that how to decrease the effect of the PT pulse and the ringing pulses technically.

### References.

- (1) Sasaki, H. et al :in this conference HE 4.7-1.
- (2) Yoshida, M. et al :J.Phys. Soc. JAPAN, 53(1984)1983
- (3) Sakuyama, H. et al :Proc. 18th Int. Cosmic Ray Conf, Bangalone 11(1983)88
- (4) Mincer, A.I. et al:Proc. 18th Int.Cosmic Conf, Bangalone(1983)264
- (5) Moszynski, M. and Bengttson, B. N.I.M. 158(1979)1
- (6) Yates, E.C. and Crandall, D.G.: IEEE TRANS. Nuclear Science June(1966)153

Performance of a local electron density trigger to select extensive air showers at sea level.

T. Abbas, J. Madani and F. Ashton

Dept. of Physics, Durham University, Durham, England.

Abstract

Time coincident voltage pulses in the two closely spaced (1.6m) plastic scintillators have been recorded. Most of the recorded events are expected to be due to electrons in EAS whose cores fall at some distance from the detectors. This result is confirmed from a measurement of the frequency distribution of the recorded density ratios of the two scintillators.

Introduction. A threshold local electron density selection requirement is the simplest method of detecting extensive air showers. With this system the minimum shower size (and hence primary energy) that produces a threshold trigger is reasonably well defined but for a given recorded density, showers with a wide spread of core distance and shower size can satisfy the trigger requirement. Near the shower core (<1m) the electron density is believed to increase more rapidly with decreasing core distance than at larger core distances and it is possible that small core distance showers could be selected by a density ratio requirement.

Experimental arrangement and results. EAS were selected by a twofold coincidence  $\Delta_A$  ( $>27.5\text{m}^{-2}$ ),  $\Delta_B$  ( $>27.5\text{m}^{-2}$ ) between two plastic scintillators A and B each of area  $80 \times 50 \text{ cm} = 0.4\text{m}^2$ , their long sides being parallel and their centres being separated by a distance of 1.6m. For each trigger the number of particles  $N_A$  and  $N_B$  traversing each scintillator was recorded using a computerised data acquisition unit and figure 1 shows the frequency distribution of the density ratio  $N_A/N_B$  and also  $N_B/N_A$ . It is seen that the most probable value of the frequency ratio is close to unity in both cases and that the distributions show a long tail. The peaking of the density ratio at a value close to unity is consistent with the known slope of the electron density lateral structure function as a function of core distance and the estimates of the median core distance of showers that produce a local electron density greater than some threshold value are shown in table 1 (Ashton and Parvaresh, 1975).

The data can also be used to evaluate the integral density spectrum of electrons at sea level and the result is shown in figure 2 where the minimum of the two recorded densities was used in evaluating the integral spectrum. For density thresholds in the range  $2\text{-}40\text{m}^{-2}$  the integral spectrum was measured directly by counting the rate of twofold coincidences. It is seen from figure 2 that the present measurements are consistent with the best estimate given by Greisen (1960) for  $\Delta > 27.5\text{m}^{-2}$  but that for smaller densities a somewhat larger rate is observed. Also shown in figure 2 is the response of the two counters A and B measured individually to the global cosmic ray flux where the output pulse height from either detector is plotted in terms

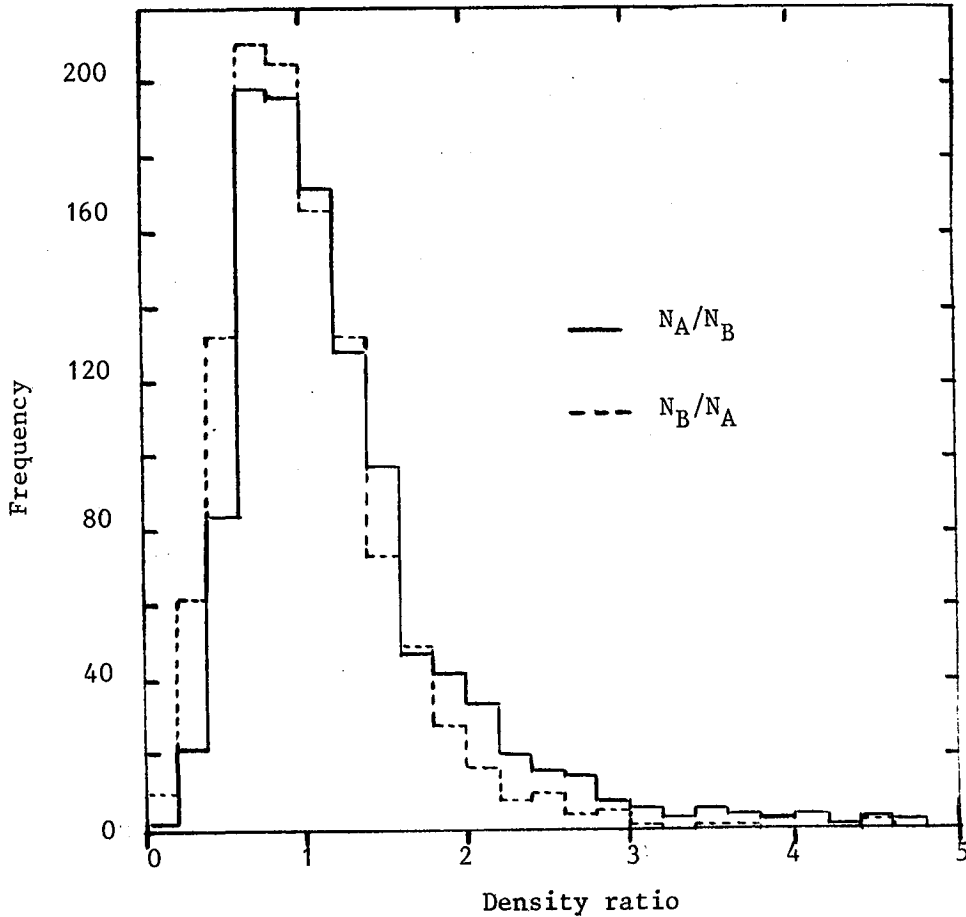


Figure 1. Frequency distribution of the ratio  $N_A/N_B$  where  $N_A$ ,  $N_B$  are the number of particles traversing scintillators A and B which each have area  $0.4\text{m}^2$ . EAS were selected by requiring  $\geq 11$  particles to traverse both scintillators simultaneously and the ratio  $N_A/N_B$  is evaluated if both  $N_A$  and  $N_B$  satisfy  $11 \leq N \leq 134$  as the passage of  $> 134$  particles through either scintillator saturated the recording system. Total number of shower triggers = 1184. Number of evaluated density ratios = 1122. i.e. 62 shower triggers saturated at least one channel of the recording system. Number of observed triggers with  $N_A/N_B > 5$  and hence not plotted in the figure = 10 ( $N_A/N_B = 8.1, 10.3, 7.6, 8.1, 5.5, 6.4, 7.7, 8.6, 6.2, 6.4$ ). Also plotted is the ratio  $N_B/N_A$  (dashed histogram). Number of observed triggers with  $N_B/N_A > 5 = 2$  ( $N_B/N_A = 6.2, 5.7$ ).

of the equivalent density of particles traversing it. Extrapolating the measured distributions suggests that for  $\Delta \geq 600\text{m}^{-2}$  EAS could be selected using only a single detector rather than the coincidence between two detectors as used in the present work.



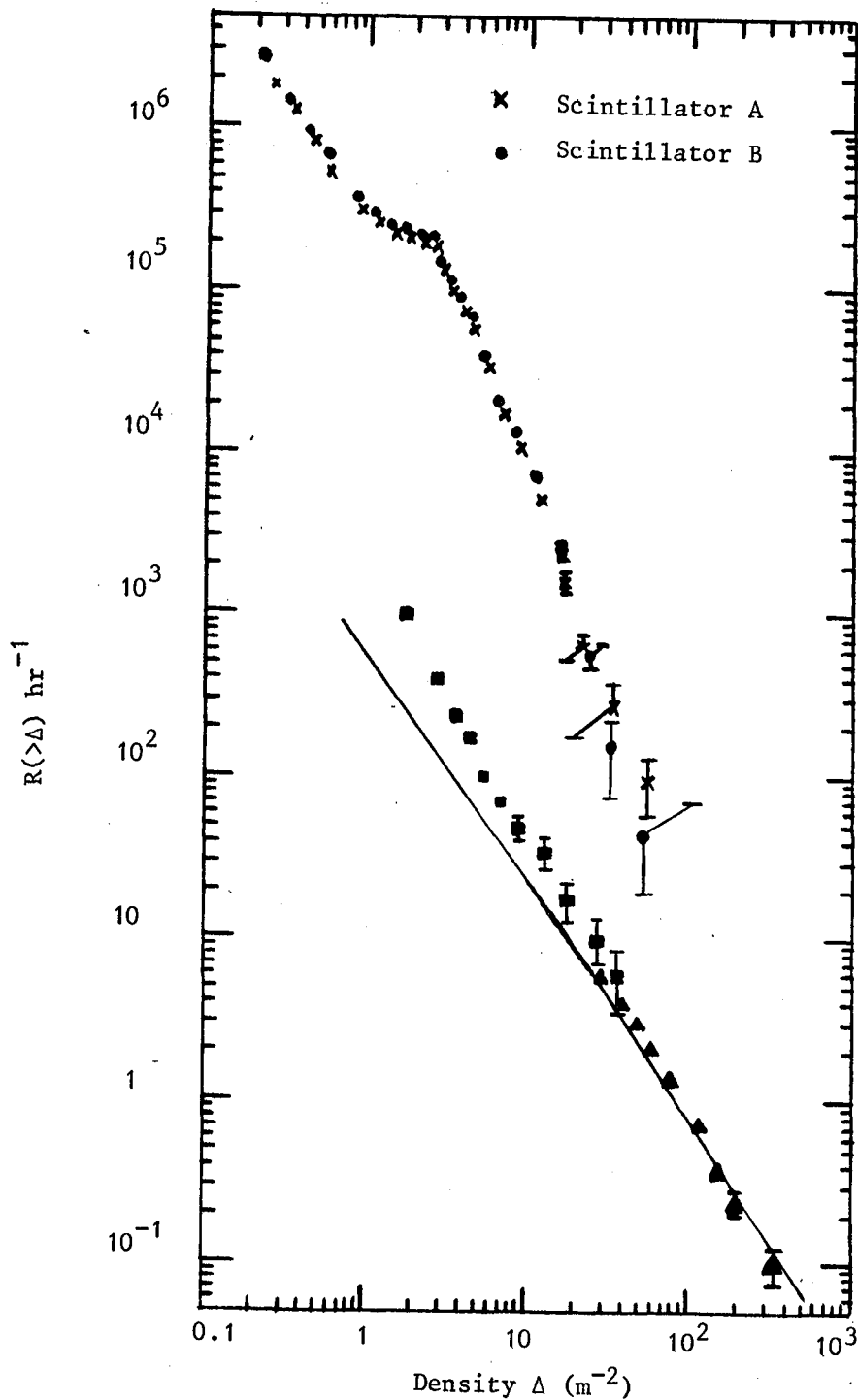


Figure 2. Integral rate response of scintillators A and B (each of area  $0.4\text{m}^2$ ) to the global cosmic ray flux. The pulse heights recorded by each scintillator have been converted to the number of equivalent particles traversing the scintillator at normal incidence and then expressed in terms of the density of equivalent particles incident on the scintillator. The traversal of the scintillator by single particles

Caption to Figure 2 continued.

corresponds to a density of  $2.25\text{m}^{-2}$ . Also shown is the electron density spectrum measured using a twofold coincidence requirement. At small densities (■) the measurements were made by twofold coincidence counting while at high densities (▲) a computerised data acquisition unit was used. The solid curve is the expression.

$$R(>\Delta) = 540 \Delta^{-(1.3+0.055\log_{10}\Delta)} \text{hr}^{-1}$$

for the sea level electron density spectrum given by Griesen (1960).

Threshold density ( $\text{m}^{-2}$ )	Median core distance (m)	Median shower size	Minimum shower size
1	30	$3.5 \cdot 10^4$	$8.0 \cdot 10^2$
10	15	$1.5 \cdot 10^5$	$1.7 \cdot 10^3$
40	11	$2.1 \cdot 10^5$	$5.5 \cdot 10^3$
300	6	$7.0 \cdot 10^5$	$3.0 \cdot 10^4$
1,000	3.5	$1.5 \cdot 10^6$	$8.0 \cdot 10^4$

Conclusion. The value of almost unity for the most probable value of the density ratio is consistent with the core distance of most of the showers falling at distances large compared with the separation (1.6m) of the counters A and B. The events observed in the tail of the distribution are interpreted as having a decreasing core distance, the larger the value of the density ratio.

#### References.

- Ashton, F., and Parvaresh, A., 1975, Proc. 14th Int. Cosmic Ray Conf. (Munich), 8, 2719 - 2724.
- Griesen, K., 1960, Ann.Rev.Nuc.Sci., 10, 63 - 108.

## MICROPROCESSOR -BASED SINGLE PARTICLE CALIBRATION OF SCINTILLATION COUNTER

MAZUMDAR G.K.D. & PATHAK K.M.  
Department of Physics, Gauhati University  
Gauhati -781014, ASSAM, INDIA

### ABSTRACT

A microprocessor-based set-up is fabricated and tested for the single particle calibration of the plastic scintillator. The single particle response of the scintillator is digitized by an A/D converter, and a 8085 A based microprocessor stores the pulse heights. The digitized informations are printed with a printer. Facilities for CRT display and cassette storing and recalling are also made available.

The details of fabrication along with some results are presented in this paper.

**1. Introduction.** The system described here is designed to calibrate the plastic scintillators used in an EAS array in Gauhati University, Assam. The different aspects and significance of the study are already reported elsewhere (1). In this paper the design and the experimental set-up relating to the detection and recording of the scintillator responses due to single muons are reported.

**2. Methods.** Fig. 1 shows the experimental set-up for the calibration of the scintillators.

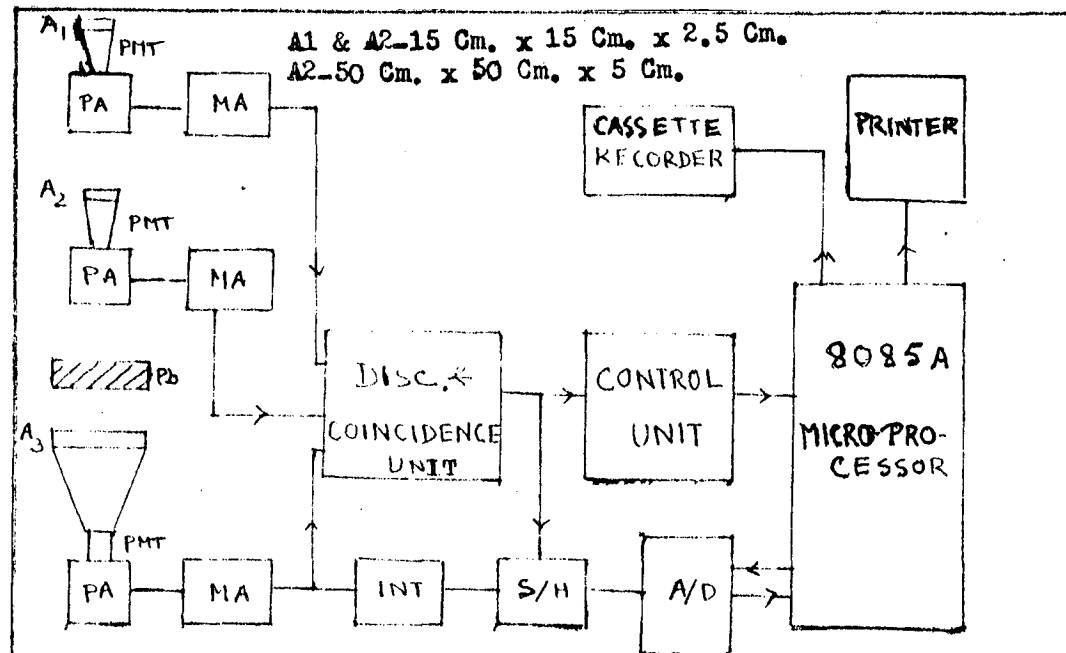


Fig.1:- The Experimental set-up .

It consists of three plastic scintillators A1, A2, & A3. The Scintillator A3 which is to be calibrated, is placed under a 20 Cm. thick lead block. Each scintillator is viewed by a 6364 PMT of 12.5 Cm. diameter.

The analog signals from each PMT are taken out from an inverting pre-amplifier (PA) fabricated using a MOSFET 2N 200 and two HF transistors BF115. The details of the amplifier system including sample-and-hold are reported elsewhere (2).

The output from the PA is input to the main amplifier (MA) by low loss cables. The MA output is integrated by an integrator (INT) and the integrated signal is sampled and held by a sample-and-hold (S/H) consisting of two LF 398 and 74 series TTL circuits. The S/H is actuated by a logic step derived from the Discriminator & coincidence unit. This unit comprises of three discriminators using Three 710 & one CD 4068. This unit is triggered by the MA output. The analog output of the S/H is digitized by an A/D converter 0816 and is controlled by a 8085 A microprocessor.

The microprocessor controls the detection and recording of the events.

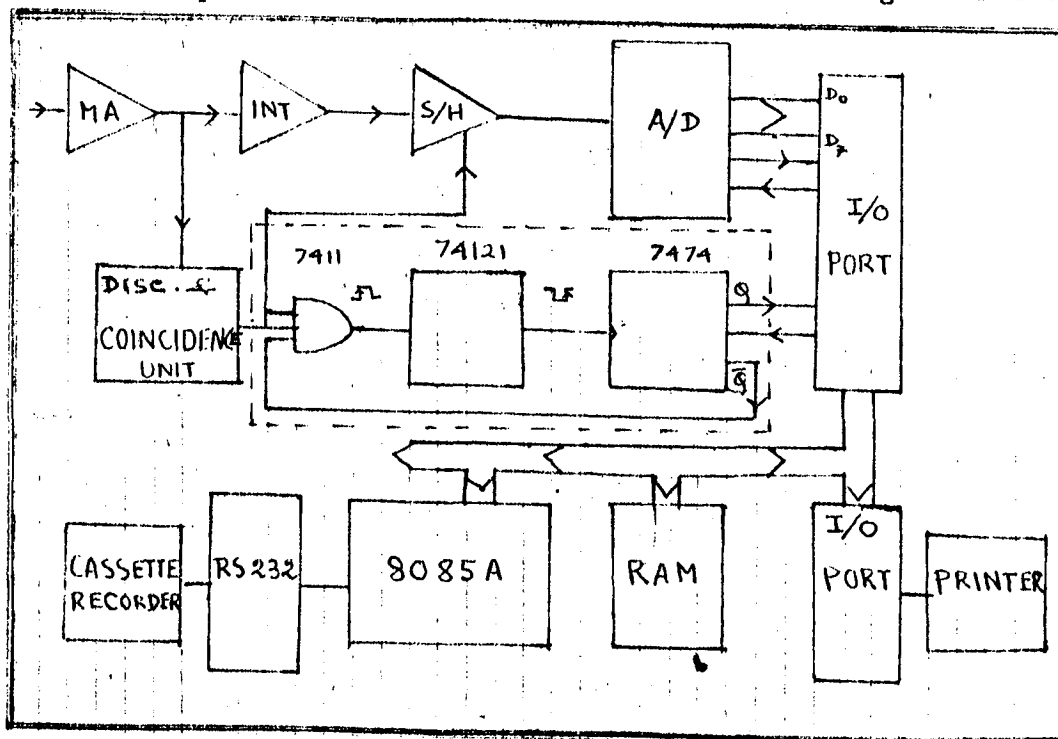


Fig. 2 Block Diagram of A/D conversion & recording electronics.

The electronics of the conversion & storing are shown in fig.2.

When A1, A2, and A3 are traversed by a vertical muon, the coincidence pulse is generated. On receipt of the coincidence pulse, the S/H holds the input analog signal and at the same time a positive pulse is generated by the AND gate 7411 of the control unit. The rising edge of this pulse triggers a monoshot 74121 to give a negative pulse at the output.

This pulse is connected to the clock input of the flipflop (F/F) 7474 and Q and  $\bar{Q}$  are set to high and low states respectively. Q is connected to the other input of the AND gate and it does not give any pulse till Q is reset to high state.

The high output of the F/F interrupts the microprocessor and it sends a start conversion pulse to the A/D. The 8-bit data bus of the A/D is coupled to the one of the I/O ports of the processor. The microprocessor sends a clear pulse after storing the digitized information in a RAM and it resets the F/F to be ready for the next event.

With the help of another port, the stored informations are printed out. The interface RS 232 is provided for cassette recording / CRT display.

**3. Results & Discussion.** Fig. 3 shows the pulse height distribution obtained with the present set-up. The most probable pulse height for single porticle is found to be  $0.45 \pm .05$  Volts.

The number of electrons collected at the anode of the PMT is calculated using the relation  $Q = NPM$  where N is the number of photon produced by the incident particle of energy E which dissipates  $dE$  energy in scintillator. P is photon transfer efficiency. M - over all gain of the PMT. Q is also calculated from the most probable pulse height and it is found to tally with the theoretical value within experimental error.

The response of the scintillator over different regions is also studied and is found to have variation less than 10% with a slight decrease towards the edge.

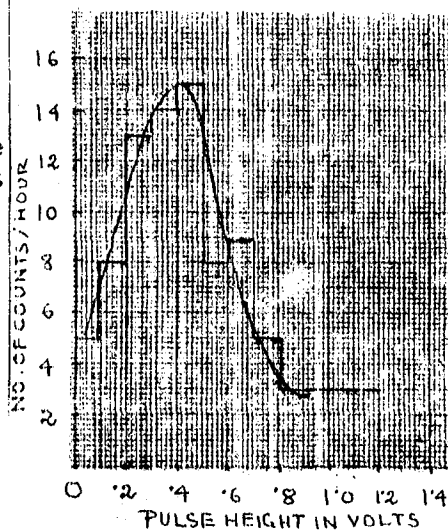


**Fig. 3** Pulse height distribution

**4. Conclusions.** The technique developed has been used in estimating the number density in an air shower array for studying emission of EM waves from EAS.

The method, which can be very well used in place of an expensive Multichannel-Pulse-height-analyser (MCPHA), is useful for small laboratories.

**5. Acknowledgements.** The authors thank the Department Atomic Energy (BRNS), Govt. India for funding the project, and the TIFR, Bombay for some equipments. They also like to thank the Institute of Advance Studies in Science and Technology (Assam Science Society) for partial funding of the project.

#### References

1. Pathak K.M. et al (1982) Proc. of the International Workshop on V.H.E.G. R. Astronomy 309.
2. Mazumdar G.K.D. et al (1982) Proc. XVIII ICRC T 8 204.

**SAMARKAND COMPLEX SETUP FOR INVESTIGATION OF  
COSMIC RAY VARIATION IN THE ENERGY RANGE OF  
 $7 \cdot 10^9 - 10^{15}$  eV**

Dorman L.I.

Institute of Terrestrial Magnetism, Ionosphere and Radio  
Wave Propagation, USSR Academy of Sciences, I42092 Troitsk,  
Moscow Region, USSR

Valikhodzhaev F., Makhmudov B.M., Sirodzhev N., Tashpulatov R.  
Samarkand State University, Uz.RRS, Samarkand, USSR

**I. Abstract.** The Samarkand complex setup is aimed at the study of cosmic ray variations in a wide energy range from  $7 \cdot 10^9$  eV (which corresponds to the geomagnetic threshold in the region of Samarkand) up to  $\sim 10^{15} - 10^{16}$  eV. The setup consists of four 6-counter sections of neutron supermonitor with counters SNM-15 and 48 scintillator detectors ( $1 \text{ m}^2$  each) placed under and above the supermonitor. The effective area of the setup for recording neutrons and muons is  $24 \text{ m}^2$ . The setup can register time variations of the following cosmic ray components: 1) the total neutron counting rate, 2) counting rates for neutrons of different multiplicity, 3) soft-muon fluxes, 4) hard-muon fluxes at various zenith and azimuth angles, 5) electron-photon component, 6) extensive air showers (EAS) induced by primary particles in a wide energy range and accompanied or not accompanied by muons and neutrons.

**2. Description of the setup.** The complex setup consists of four 6-counter sections of neutron supermonitors which are compactly placed at a height of 1 m. Under and above each section there are 6 scintillator detectors with an effective area of  $1 \text{ m}^2$  each. The dimensions of each section are  $315 \times 222 \times 52 \text{ cm}^3$  and the weight is about 13 tons. The generator of neutrons is made of lead (an effective area in one section is  $-6.21 \text{ m}^2$ ), and the retarder and reflector of neutrons was made of polyethylene. Neutrons are detected by Soviet neutron counters SNM-15 (effective length -200 cm, diameter-15 cm, filled with a gas  $\text{BF}_3$  up to a pressure of 20 cm Hg, the concentration of  $^{10}\text{B}$  isotope in boron reaches 80 %, operating voltage - 2600-2800 B, proper radioactive background  $\leq 1$  %). Plastic scintillators with reflectors and photomultipliers placed at the top of reflectors are used as detectors of charged particles (electrons, muons, protons). After amplification, formation, and discrimination, pulses from detectors come to the general logic scheme in which different components are selected (neutron, electron-photon, muon, EAS with different accompanying). The results of the selection come into a multichannel recorder with a punch out on the paper tape and digitizer.

3. Recording of single and multiple neutrons. The developed electronics makes it possible to sort out events induced by single and multiple neutrons and to block pulses from electrons and muons in neutron counters /I/. Bearing in mind the coupling coefficients for single and multiple neutrons one can say that the Samarkand neutron supermonitor is sensitive to primary cosmic rays in the energy range from 7 to several tens of GeV, with an effective energy of about 15 GeV. The total counting rate for neutrons is expected to be about  $10^6$  pulses/hr, which corresponds to the rms statistical error  $\sigma = 0.1\%/hr$ ; for 5-minute data this corresponds to  $\sigma \sim 0.3-0.4\%/5 \text{ min.}$ , which is quite sufficient for statistical investigation of cosmic ray scintillations. The counting rate for neutrons of multiplicity  $m=2$  is  $\sim 1.3 \cdot 10^5$  pulses/hr, which provides  $\sigma \sim 0.3\%/hr$ ; for  $m=3$  the counting rate is  $\sim 4 \cdot 10^4$  pulses/hr, which gives  $\sigma \sim 0.5\%/hr$ ; for the sum  $m=4$  and 5 the counting rate is  $\sim 2 \cdot 10^4$  pulses/hr and  $\sigma \sim 0.7\%/hr$ , and for  $m=6$  the counting rate is  $\sim 4 \cdot 10^3$  pulses/hr and  $\sigma \sim 2\%/hr$ . These accuracies show that the data on high multiplicities can be used only for the investigation of long-period variations and statistical analyses, and also of short-time variations with a large amplitude (powerful Forbush decreases, effects of solar flares).

4. Recording of soft muons. It is well known (see the review /I/) that in a neutron supermonitor about 7 % of pulses are induced by soft negative muons which form on lead nuclei the mesonic atoms with a subsequent capture of muons and a formation of several neutrons. Such events can be discriminated by pulse anticoincidence in the upper and lower scintillators and by retarding pulse coincidence in a neutron supermonitor. The expected counting rate for soft muons is about  $1.3 \cdot 10^5$  pulses/hr, which corresponds to  $\sigma \sim 0.3\%/hr$ . This will make it possible to study in detail the meteorological variations of soft muons which are of great theoretical and practical interest.

5. Recording of the electron-photon and muon components. Summation of the counting rates of upper scintillators provides information on time variations of the total ionizing component with a high statistical accuracy ( $\sigma \sim 0.02\%$  for a 5-minute interval). Subtraction from this counting rate of the flux of hard and soft muons gives data on variations of the electron-photon component. Further, the use of a scintillator system for selecting the respective double coincidences between individual upper and lower scintillator detectors gives exclusively valuable information about time variations of hard muon fluxes which arrive at different zenith and azimuth angles. After the quality of the work is analyzed, analogous

channels of coincidences which correspond to one and the same zenith and azimuth angles are summed up. The large effective area of the setup allows us to obtain observational data with so small statistical errors (smaller than 1 % for 5-minute data) that we can very reliably use the recording even at large zenith angles which correspond to primary cosmic rays with an energy  $\geq 10^2$  GeV. The data on time variations of hard muon fluxes from different directions yield much information about variations of atmospheric, geomagnetic and extraterrestrial origin with an energy of  $10^{10} - 10^{12}$  eV.

#### 6. Recording of different types of extensive air showers.

Pulses from each of the 48 upper and lower scintillators, as well as from 24 neutron SNM-15 counters come to a logic system which sorts out the following events: a) various combinations of coincidences only of upper scintillators - recording of counting rate for EAS of different power which correspond to primary particles of energies  $10^{13} - 10^{16}$  eV; b) recording of EAS of different power accompanied by muons; c) recording of EAS of different power accompanied by neutrons.

#### 7. Meteorological and coupling coefficients.

With an account of the geometry of the setup and its geographical position, each of the components mentioned above in 3-6 is characterized by the following coefficients:  $\beta_i$ ,

a barometric coefficient for the i-th component of a setup;  $\lambda_i(h)$ , the density of temperature coefficient, where h is pressure at a corresponding isobaric level;  $W_i(R)$ , the coupling coefficient depending on the rigidity R of primary particles (see /1/, /2/, /3/).

8. Application of generalized spectrographic method for the analysis of observational data. A continuous recording of fluxes of single and multiple neutrons, soft muons, electron-photon component, fluxes of hard muons from different directions and frequencies of different types of EAS with essentially different meteorological coefficients and different coupling coefficients makes it possible to use the generalized spectrographic method /4/ for obtaining separate information about variations of atmospheric, geomagnetic, and extraterrestrial origin. The method consists in the fact that for each i-th component recorded by a complex setup for each time moment t one derives an equation for an observed variation of the counting rate

$$\frac{\delta I_i(t)}{I_{i0}} = \beta_i \delta h_0(t) + \int_0^{h_0} \lambda_i(h) \delta T(h,t) dh - \delta R \frac{W_i(R_0)}{D_i(R)} + \frac{\delta D_i(R)}{D_i(R)} \frac{W_i(R)}{W_i(R_0)} (I)$$



where the intensity variation  $\delta I_i(t) = I_i(t) - I_{i0}$ , variation of the air column mass above the setup may differ considerably from the pressure  $\delta h_0(t) = h_0(t) - h_0$ , temperature variation  $\delta T(h,t) = T(h,t) - T_0(h)$ , variation of geomagnetic cutoff rigidity  $\delta R_C(t) = R_C(t) - R_C$  and variation of the primary spectrum  $\delta D(R,t) = D(R,t) - D_0(R)$ . Here the first two terms on the right imply variations of atmospheric origin, the third term determines variations of geomagnetic origin, and the fourth term - variations of extraterrestrial origin. The solution of a system of equations of the type (I) by the method described in /4/ for the above-mentioned set of components of a complex setup allows us to obtain continuously the information about  $\delta h_0(t)$ ,  $\delta T(h,t)$ ,  $\delta R_C(t)$  and  $\delta D(R,t)/D_0(R)$ , i.e. in the end, about the processes in the atmosphere /2/ and magnetosphere /5/ of the Earth and in cosmic space /6/; the information of space-time variations of the energy spectrum of primary CR will be obtained in a wide energy range from  $7 \cdot 10^9$  eV to  $10^{15} - 10^{16}$  eV.

#### REFERENCES

1. Dorman L.I. Experimental and Theoretical Principles of Cosmic Ray Astrophysics. Nauka, 1975.
2. Dorman L.I. Meteorological effects of cosmic rays. Nauka, 1972.
3. Dorman L.I. Cosmic Rays: variations and space exploration. Amsterdam, 1974.
4. Dorman L.I. Proc. 15-th ICRC, vol.4, 281, Plovdiv, 1977.
5. Dorman L.I., Smirnov V.S., Tyasto M.I. Cosmic rays in the magnetic field of the Earth. Nauka, 1971.
6. Dorman L.I. Variations of galactic cosmic rays. Izd. MGU, 1975.

RADIO WAVE EMITTED BY AN EXTENSIVE AIR  
SHOWERS IN 10KHZ TO 1MHZ REGION

Jun Nishimura

The Institute of Space and Astronautical Science  
Komaba, Meguro, Tokyo, Japan

ABSTRACT

An importance of radio wave in a frequency range less than 1MHz has been discussed by Suga at the time of the Bangalore Conference. In this paper, an estimate of radio intensities at 10KHz, 100KHz and 1MHz has been made on the basis of the Kahn-Lerche theory. An emphasis is made that negative charge excess in a shower gives main contribution for low frequency radio emission, in spite of the importance of the contribution of transverse current in the geomagnetic field in higher frequency range. An estimate is also made for radio intensity produced when the shower hits the ground. Contribution of this process seems to be important at large distance say beyond 1km from the shower axis.

1. INTRODUCTION

The radio wave emitted from extensive air showers has been studied since 1965 in the frequency range of 30 to 60MHz. However, since lateral spread of the radio wave intensity was found to be steep, such studies have not been considered to be promising to detect low frequency large showers. In a low frequency range around 1MHz, only a few studies have been reported. Moscow and Yakutsk group (V.B.Atrashkevich et al: 1973) reported that strong radio wave of 1.9MHz with 1 to 25 micro V./M.MHz were observed for showers of  $6 \times 10^6 < N_e < 1.7 \times 10^8$  at distances from 600m to 1300m.

Suga proposed possible detection and importance of radio wave at frequency range less than 1MHz (K.Suga: 1983). He discussed contribution of charge excess in an extensive air shower for emission of the radio wave in this range, and also discussed possible emission process when this excess charge hits the ground. Similar treatment to estimate the contributions of these processes have also been performed recently by Sakata. ( T.Sakata: 1985).

Since these results seem to be promising to detect low frequency large showers, we examined the contribution on the basis of Kahn-Lerche treatment, in which we can estimate radio intensity more easily, such as to include effect of emission angle of the radio wave from shower axis. The comparison is made for the degree of the each contribution by excess charge, dipole and transverse current, and shows

excess charge gives the most important contribution between these processes in frequency range less than 1MHz. Radio wave emission when the excess charge hit the ground is also treated by using the formulae of the transition radiation. Contribution for the radio intensity by this process is much larger than other processes below 1MHz. We estimate a few times of 100 micro V/M.MHz or more at 1km from the shower axis for a shower of  $10^{20}$  eV.

## 2. RADIO WAVE EMISSION IN A LOW FREQUENCY RANGE.

The radio wave emission from an extensive air shower has been treated by Kahn and Lerche on the basis of the Maxwell equation.(F.D.Kahn and I.Lerche:1965). They discussed the contributions from three process, i.e. charge excess, dipole and transverse current in the geomagnetic field. They obtained a fourier transformed field strength due to each process as, in the notation of their paper:

a) Charge excess

$$E(k) = -ie\Delta/2 \cdot (k\alpha) J_0(k\alpha a) H_0^{(1)}(k\alpha r) \quad (1)$$

b) Dipole

$$E(k) = -iM/2 \cdot (k\alpha)^2 J_0(k\alpha a) (H_0^{(1)}(k\alpha r)/k\alpha r + H_0^{(1)}(k\alpha r)) \quad (2)$$

c) Current

$$E(k) = -J/2 \cdot k J_0(k\alpha a) H_0^{(1)}(k\alpha r). \quad (3)$$

Here  $\Delta$ ,  $M$  and  $J$  are the excess charge, dipole moment and current in an extensive air shower.  $k$ ,  $\alpha$ ,  $a$ , and  $r$  are the wave number, Cerenkov angle, radius of shower disk and the distance of the observation point from the shower axis.

If the number of the shower particles changes with altitude as  $\exp(-Lx)$ , where  $L$  and  $x$  are the absorption coefficient and depth of the atmosphere measured in unit of length, another process for emission of radio wave arises.

$k\alpha$  in eq.(1) should be replaced, in this case, as

$$((k\alpha)^2 + 2ikL + L^2)^{1/2}. \quad (4)$$

The relative importance of each term in eq(4) depends on the radio concerned. Since  $L$  is of the order of  $1/1\text{km} = 10^{-5}/\text{cm}$ ,  $\alpha = .024$  and  $k = 2 \times 10^{-4}/\text{cm}$  at 1MHz, contribution of  $k\alpha$  in eq.(4) becomes small in these frequency range. Thus the radio emission is mainly due to the charge acceleration rather than the Cerenkov process as illustrated in Fig.1. The effect of change of number of shower particles with altitude becomes predominant in the low frequency radio waves.

Due to this situation, degree of the contribution of charge excess becomes important compared with that of other process in the low frequency range as seen from formulae (1),(2) and (3). The emission angle  $\alpha$  is also changed to about  $(L/K)^{1/2}$ , giving a large angle spread compared with Cerenkov angle. This results wide lateral spread of radio pulse, and gives us a possibility to detect large extensive air showers efficiently. The relative importance of each process for

intensities at various frequencies are shown in Table 1.

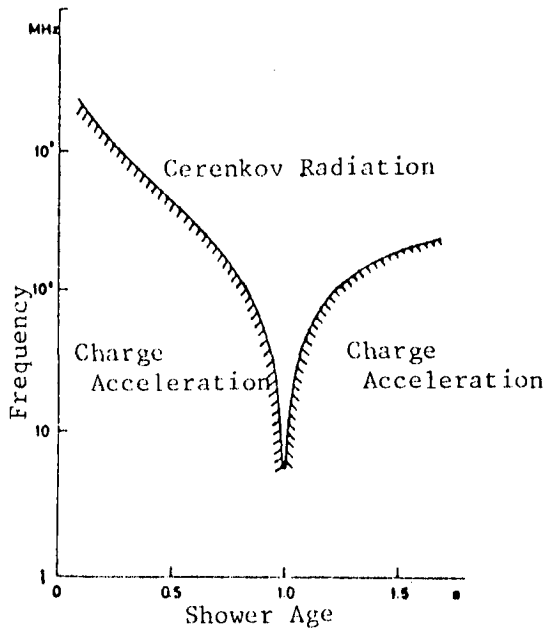


Fig.1. Relative importance of Cerekov emission and charge acceleration.

Table 1  
Relative contribution of each process (  $L = 10^{-5} / \text{cm}$  )

Freq.(MHz)	Excess charge	Dipole	Current
100	1	0.57	2.2
1.0	1	0.053	0.24
0.1	1	0.0169	0.074

Here we refer to the values of  $\Delta$ ,  $M$  and  $J$  in the paper ( M. Fujii and J. Nishimura: 1968 ). This clearly indicates the importance of the charge excess in the low frequency range, and we can estimate the radio intensity by only taking this process.

### 3. RADIO PULSE WHEN SHOWER PARTICLES HIT THE GROUND

When shower particles hit the ground, radio pulse is emitted by excess charge in the shower. This is just the same process known as the transition radiation. Since the shower disk hits the ground with a time duration of 0.1 to 1 micro sec. depending on the inclination of the shower axis. Only the radio wave of frequency less than 1 to 10MHz are emitted coherently. The radio pulse intensity is

$$W(f, \theta) d\theta d\Omega = e^2 / \pi c \cdot |\cos \theta| d\theta d\Omega, \quad (5)$$

where  $f$  is the frequency of the radio wave, and  $\theta$  is the zenith angle of the shower axis. If  $N$  charged particles are involved,  $e$  in the eq.(5) should be replaced by  $Ne$ .

## 4. NUMERICAL RESULTS AND DISCUSSIONS

Referring to the formula in section 2, 3, numerical evaluations are made and shown in Fig 2, 3. Here we assume number of shower particles changes with altitude as :

$$N = N_0 \cdot \exp(-x^2/2(\sigma c)^2),$$

where  $\sigma$  is around 5 micro sec. for a vertical incident shower. The calculated radio intensity is 100 to 1000 micro V/m.MHz for a shower of  $10^{20}$  eV and is similar to those orders of magnitude obtained by Suga and Sakata.

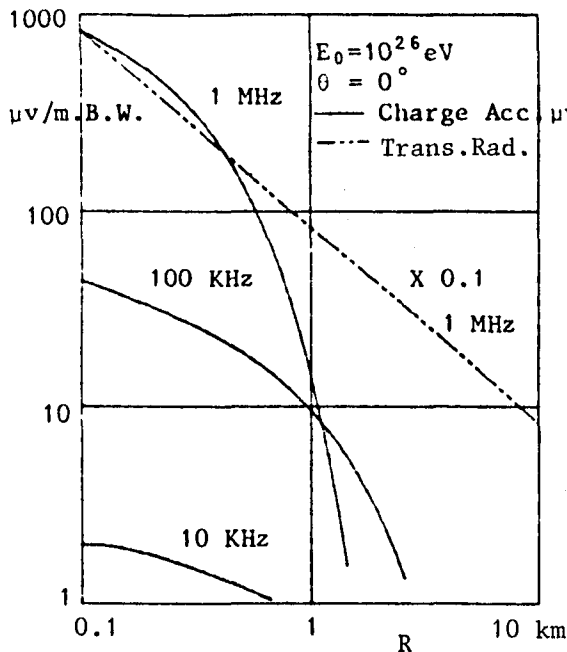


Fig.2. Radio intensity per band width of each Frequency. Vertical incident Shower.

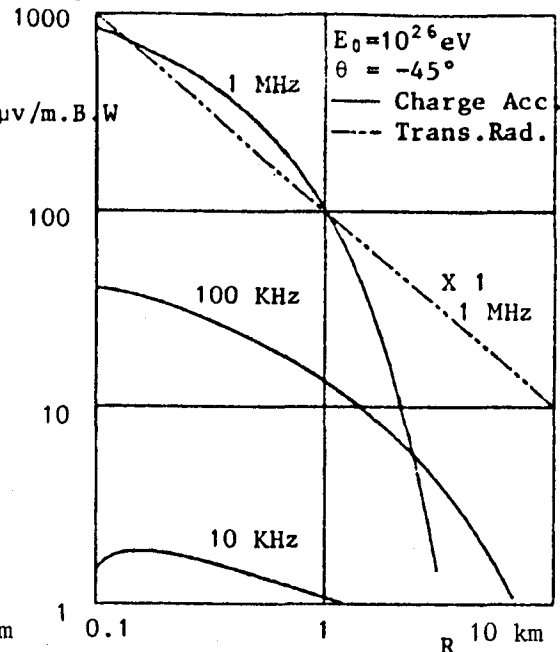


Fig.3. Radio intensity of shower with Zenith angle of -45 degrees.

The transition radiation emitted by charge excess in shower gives the most predominant contribution at a distance beyond 1km. Since the intensity of transition radiation is known to be changed as  $(\sqrt{\epsilon} - 1/\sqrt{\epsilon} + 1)$ , where  $\epsilon$  is a dielectric constant of the ground, which indicate that radio intensity is affected by condition of the ground. Other processes to emit the radio wave are proposed by Suga and Sakata. Contribution of those processes will be discussed at the time of the conference.

## References

- Atrashkevich, V.B. et al : 1973, Proc. 13th ICRC 2399  
 Fujii M. and Nishimura, J. : 1968, Proc. 11th ICRC 710  
 Kahn F.D. and I. Lerche : 1966 Proc. Roy. Soc. A289, 206  
 Sakata T.: 1985, in this issue  
 Suga K. : 1983, Proc. 18th ICRC Vol 11. 428.

THE STRUCTURE OF THE SHOWER DISK OBSERVED  
AT MT. NORIKURA

Sasaki, H., Nishioka, A., Ohmori, N., Kusunose, M.  
Kochi University, Kochi, Japan  
Nakatsuka, T.  
Konan University, Kobe, Japan  
Horiki, T.

The Institute of Physical and Chemical Research, Wako, Japan  
Hatano, Y.

Institute for Cosmic Ray Research, University of Tokyo, Tokyo, Japan

### §1 Introduction.

It is very important to find out parameters describing the air shower phenomena, so the fine measurement of the structure of the shower disk, that is, the arrival time distribution of the all charged particles (mainly electron component) near the core of the small or middle size EAS were planned at Mt. Norikura since 1982.(1)

Pulse wave-form measurement of the electron and muon component of the EAS had been made by several groups (e.g.(2)) and also with respect to delayed hadrons in the EAS. (e.g.(3)) Up to now, however, the structure of the shower disk does not studied precisely, especially at near the core of a small or middle size EAS.

At the previous conference, the preliminary study on the pulse wave-form was reported with some problems, such as the effect of the PT-pulse(4), and the existence of the abnormal pulse wave-form. These observed data by the same apparatus as this work were affected the effect of the PT-pulse and not so good time response appeared in the value of the FWHM for a single muon. As mentioned in another paper at this conference (4), we made some improvements on the fast scintillation counter (FS) system (i.e. on the fast trigger scintillation counter (TFS) system) and on the system response of the FS.

### §2 Experimental.

Four fast scintillation counters whose area is  $0.25\text{m}^2$  and four TFS have been added to Mt. Norikura EAS array as shown in Fig. 1. The triggering requirement for this run was that four TFS counters show the pulse height greater than 4 particles/ $0.25\text{m}^2$  at the same time whose allowable time delay is 80ns for each TFS.

Approximately 6200 showers were caught for this work in last summer.

Digitized data by storage oscilloscope were transmitted to the personal computer through the GPIB bus and were recorded on the floppy disk. To measure the rise time of the pulse, some improvements were made. First, we change the design of the FS vessel to as shown in Fig. 2, because this change means the increase of

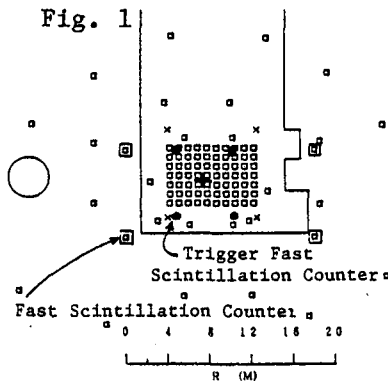
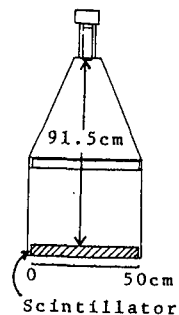


Fig. 2



time difference between the prompt PT-pulse and the main scintillation pulse. So we can easily eliminate such a pulse shape data that affected by the PT-pulse. Secondary, the dynode chain of the resistance (i.e. voltage distribution ratio) for the photo-tube was improved to that for the pulse linearity measurement, consequently, the effect of a saturation of pulse height was avoided. Finally, we changed a high voltage to feed the photo-tube up to about 1900 volts, from 1550 volts at the previous experiment, and if the time response characteristics has the same tendency as for the photo-tube 931A, circular cage type, the rise time of the photo-tube (R329-02) may be improved about 0.5nS (i.e. the rise time become 2.1nS).

The definition of the various parameters of the pulse wave-form are reported in another paper at this conference (4). About the definition of the FWHM, care must be taken, because only when the time of the 50% of the main peak pulse height is found at the trailing edge of the main peak, the FWHM is obtained.

### §3 Experimental Results.

#### 3.1 Rise time, FWHM and FWTM

Fig. 3 (a),(b),(c) show the rise time, the FWHM and the FWTM distributions of the fast scintillation counter FS1 against the lateral distance from the shower axis to FS1, where size region is  $10^6$  to  $2 \cdot 10^6$ , age is greater than 0.2 and zenith angle is less than  $30^\circ$ , the core distance

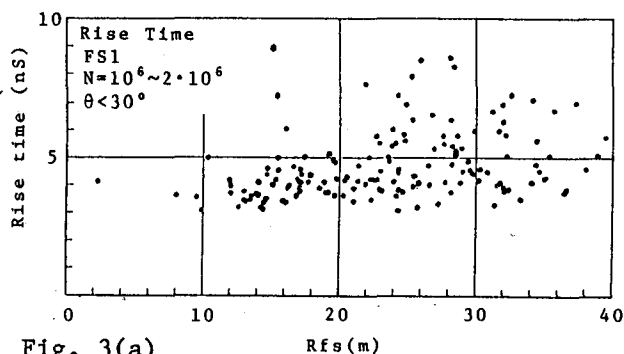


Fig. 3(a)

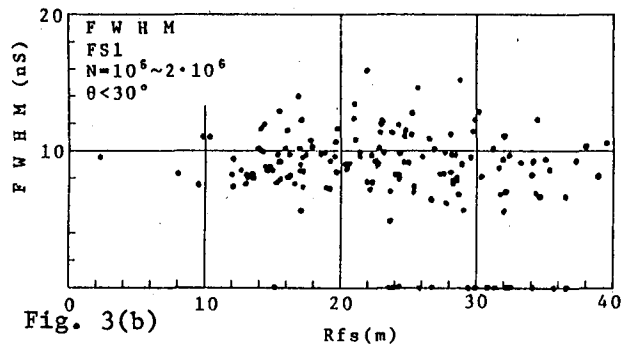


Fig. 3(b)

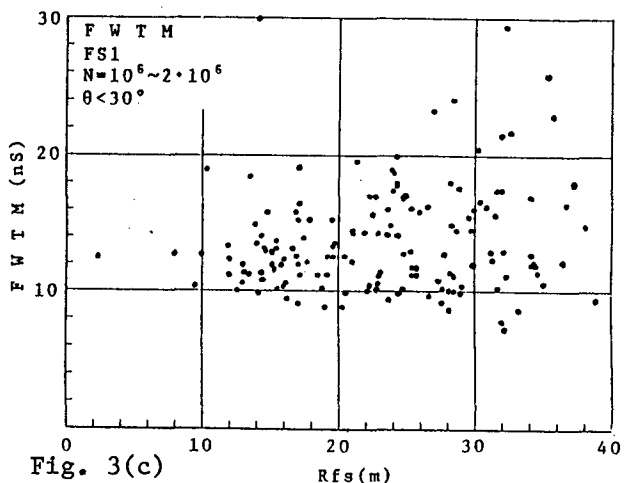


Fig. 3(c)

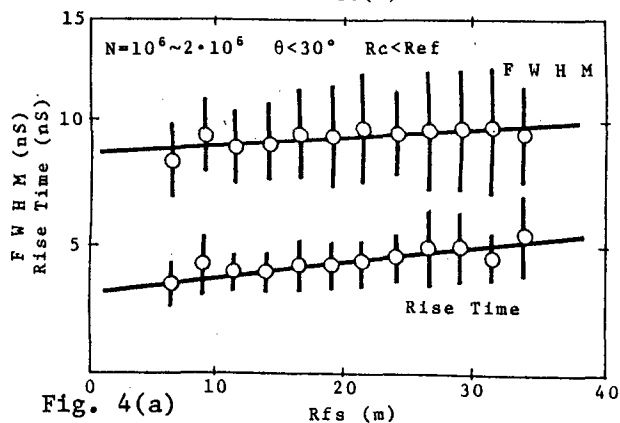


Fig. 4(a)

(between the axis and the trigger center)  $R_c$  is less than the effective distance Ref. At the selection of the pulse wave-form data, we considered how to eliminate the PT-pulse events as shown in Fig. 5 and the pulse wave-form data which have a ringing tail at the trailing edge of the main pulse. Considerable such events were omitted by the adoption of the condition with respect to the rise time, that is  $T_{\text{rise}} \geq 3.0 \text{ nS}$ .

What is evident from the figures is that the fluctuation of the rise time and the FWTM become large with the lateral distance but the distribution of the FWHM is not so broad.

3-2. Structure of the shower disk.

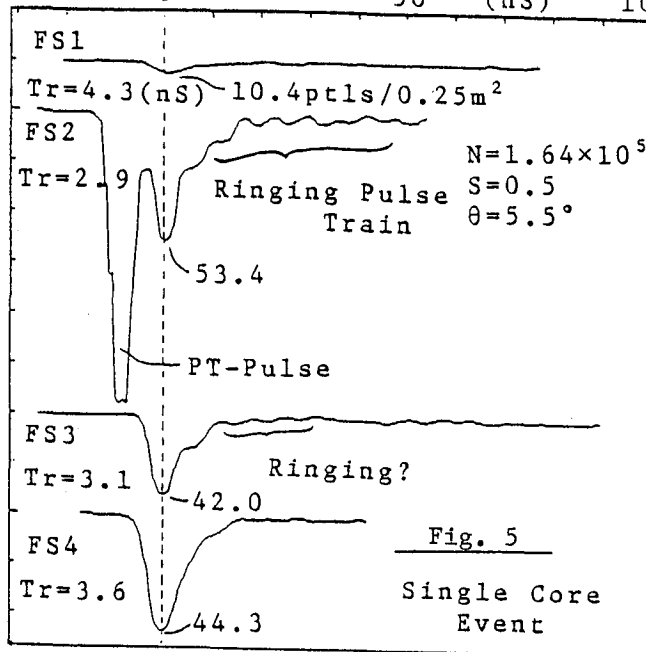
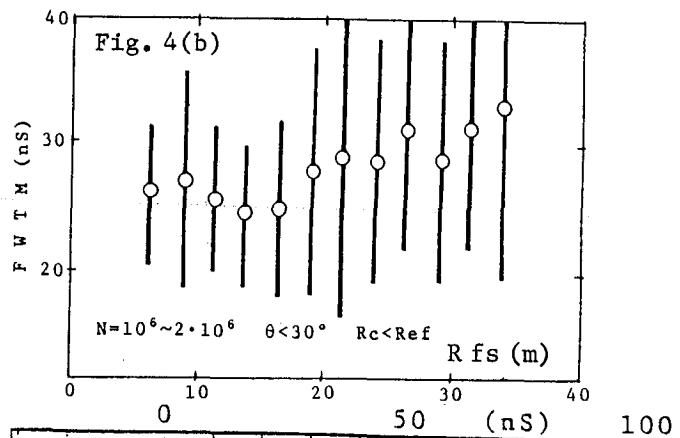
All the data of every FS were summarized and we obtained an average feature of shower disk as in Fig. 4 (a),(b),(c), where the error bar represents a standard deviation. From these figures the

following become clear as an average structure of the EAS disk. (A) The rise time shows an increasing tendency with a lateral distance from 3.5 nS to 5.4 nS. (B) The FWTM, also shows the same tendency as that of the rise time and it changes from 25 nS to 33 nS. (C) The FWHM has slight dependence on the lateral distance. (D) All the parameters of the pulse wave-form show large fluctuations for each shower.

Similarly, the average parameters for the EAS whose size region is  $10^5$  to  $2 \cdot 10^5$  were obtained. Compared with above results, size dependence of these parameters may be described as follows. (A) The rise time of the size  $10^6 \sim 2 \cdot 10^6$  is less than that of  $10^5 \sim 2 \cdot 10^5$ . (B) The FWHM of the size  $10^6 \sim 2 \cdot 10^6$  has greater value than that of  $10^5$ . (C) The variation of the FWTM with the distance from the axis for the size region  $10^5 \sim 2 \cdot 10^5$  is larger than that for the size  $10^6 \sim 2 \cdot 10^6$ .

3-3. Observed pulse wave-form and its core structure.

All pulse wave-form data obtained were printed again by a computer and we found various types of pulse profiles. The core maps of interesting events, also, were obtained and 40 showers whose core hit





the central array were analysed up to now, together with the pulse data. Fig. 6 shows an example of the multi-core event that all of the pulse wave-form of this event have a subpeak at time=26.0nS~27.4nS delayed from the main peak time. On the other hand, an example of the single core event is shown in Fig. 5. The pulse wave-form from the FS2 has a PT-pulse and also has a ringing pulse train. This event has not any coincident subpeak whose time allowance was 2.5nS around the time of the biggest subpeak.

#### §4 Conclusions.

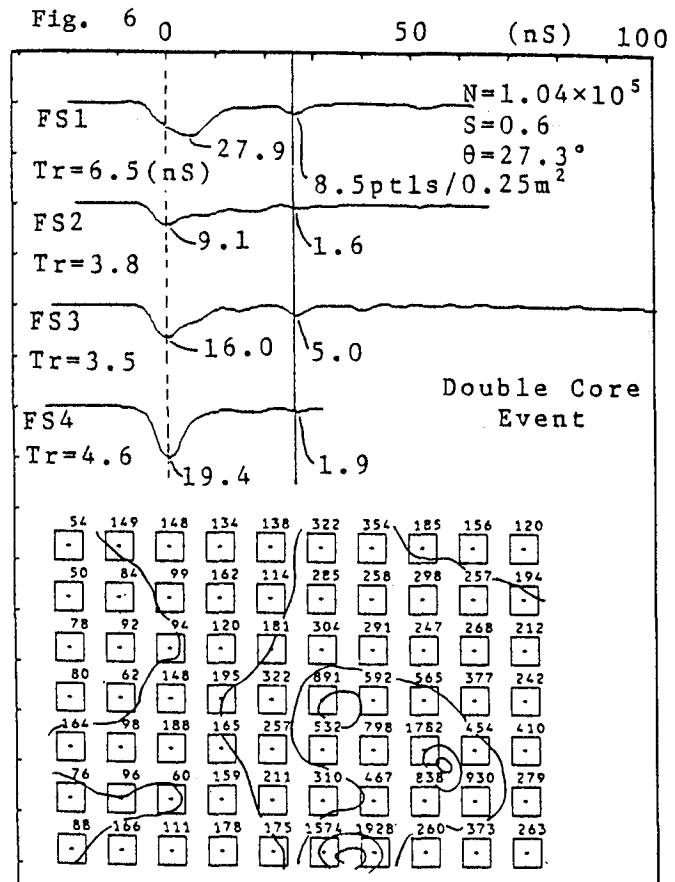
(A) The average structure of the shower disk became clear and further analysis will be continued with respect to the size and age dependence of the pulse wave-form parameters.

(B) Considerable pulse wave-forms of the electron component observed have two decay constant and the simulated pulses reported in another paper (4) also have same tendency.

(C) Rough analysis on the correlation between the core and time structure, it seems that about 1/3 of the core event have 3 or 4 coincident subpeaks where the limit of the pulse height of subpeak is 1 particle. And the rate of a multi-cored shower was ~60% out of them at the size  $10^5 \sim 10^6$ . Simulation work and further technical development will be necessary, because small subpeak less than 10% of the pulse height may be under the influence of the ringing pulse appeared in the single particle pulse.

#### References

- (1) Sasaki, H. et al.: Proc. 18th Int. Cosmic Ray Conf., Bangalore 11(1983) 205
- (2) Tamura, T. et al.: Proc. 18th Int. Cosmic Ray Conf., Bangalore EA-1.2 18(1983) 133
- (3) Mincer, A.I. et al.: Proc. 18th Int. Cosmic Ray Conf., Bangalore 11(1983) 264
- (4) Sasaki, H. et al.: in this conference, HE 4.6-10



## STRUCTURE OF AIR SHOWER DISC NEAR THE CORE

Inoue, N., Kawamoto, M.

The Graduate School of Science and Technology, Kobe University,  
Japan

Misaki, Y., Maeda, T., Takeuchi, T., Toyoda, Y.

Department of Physics, Kobe University, Japan

## ABSTRACT

The longitudinal structure of air shower disc has been studied by measuring the arrival time distributions of air shower particles for showers with electron size in the range  $3.2 \times 10^{5.5}$  to  $3.2 \times 10^{7.5}$  in the Akeno air-shower array (930 gcm<sup>-2</sup> atmospheric depth). The average FWHM as a parameter of thickness of air shower disc is increasing with core distances at less than 50m. At present stage, it cannot be seen the dependence on electron size, zenith angle and air shower age. The average thickness of air shower disc within core distance of 50m is almost determined by electromagnetic cascade starting from lower altitude.

### 1. Introduction

The experiment to search for long-lived massive particles in extensive air showers has been carried out in the Akeno air-shower array, using twelve fast scintillation detectors at intervals of 5m, will be discussed in a separate paper (HE 6,2-10). The time profile of the signal from photomultiplier (PMT) reflects the arrival time distribution of air shower particles, namely the longitudinal structure of air shower disc. Hitherto, the lateral structure of air shower particles is rather well known through basically measurement of lateral density of air shower particles and also nuclear cascade theory. However, informations on the longitudinal structure near the core ( $\leq 50$ m) are not abundant in spite of recent improvement of recording apparatus and additive parts for nano second measurement. Only, C P Woldneck et al (1975) measured the longitudinal particle distribution from the time delay measurement, so far. It is interested in studying the thickness, the curvature of air shower disc and also their fluctuations in order to discuss the longitudinal development of air shower and primary compositions. The preliminary results on average thickness of air shower disc and its dependence on zenith angle and air shower age are presented in this paper.

### 2. Experimental

Twelve scintillation detectors were located at the S2 area in the Akeno air-shower array at intervals of 5m as described in separate paper (HE 6,2-10). The group A consisted of two 0.25m<sup>2</sup> scintillation detectors with 2" fast PMTs and a 1m<sup>2</sup> scintillation detector with 5"

fast PMT. Signals fed to an adding circuit through co-axial cables (11C4AF) with different length of 50m, 63m and 75m, and then added signals were recorded by a 100MHz storage oscilloscope. The group B and C were also same systems as mentioned above. The time response of the whole 0.25 m<sup>2</sup> scintillation detector system for single relativistic particle was 4.9ns in rise time ( $t_r$ : time from 10% to 90% of the maximum signal) and 10.6ns in Full Width at Half Maximum ( $t_w$ ). That of the whole 1m<sup>2</sup> scintillation detector system was also 6.2ns and 15.2ns in  $t_r$  and  $t_w$ , respectively.

The work was performed in conjunction with the air-shower array. Signals from each groups were stored in three storage oscilloscopes if the heights of three signals from the triggering detectors (A-1, B-1 and C-1) were higher than a given level and coincided in time with one another. The stored signals were read out to a floppy disk by simultaneous master pulse from the air-shower array.

### 3. Analysis and Result

Observation was made from May to October of 1984. Total running time was 88 days and the total number of events triggered was about 6300. The analysis was made on 2142 events recorded by B-2 detector. The arrival direction ( $\theta$  and  $\phi$ ), the electron size ( $N_e$ ), the core location and the age parameter ( $s$ ) of an air shower were determined according to the procedure adopted by the air-shower group of Institute for Cosmic Ray Research of the University of Tokyo. We excluded the signals whose peaks of some showers were out of the storage oscilloscope frame and also whose peaks were smaller than given level corresponding to four relativistic particles. In this paper, the arrival time distributions of air shower particles with  $N_e$  in the range  $3.2 \times 10^{5.5}$  to  $3.2 \times 10^{7.5}$  and sec  $\theta$  in the range 1.0 to 1.3 are reported.

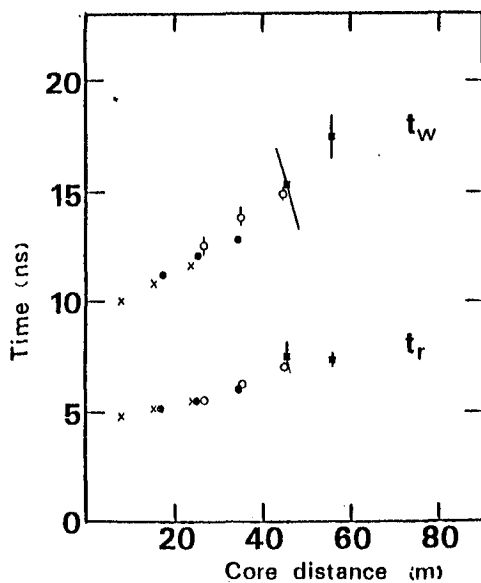


Figure 1. Average  $t_r$ s and  $t_w$ s against core distance for showers with sec  $\theta$  of 1.0-1.2 and  $N_e$  of  $3.2 \times 10^{5.5}$  ( $\times$ ),  $1.0 \times 10^{6.0}$  ( $\times$ ),  $1.0 \times 10^{6.5}$  ( $\bullet$ ),  $3.2 \times 10^{6.5}$  ( $\circ$ ),  $1.0 \times 10^{7.0}$  ( $\circ$ ) and  $1.0 \times 10^{7.0}$  ( $\square$ ),  $3.2 \times 10^{7.5}$  ( $\blacksquare$ ).

As is seen in this figure, both values increase with increase in core distances. On the other hand, dependence of these values on  $N_e$  cannot be seen from this figure. As often pointed out, average  $t_w$ s have some biases at core distances larger than those presented here in each  $N_e$  bins. They are caused by small number of incident particles (less than about ten particles), and consequently, average  $t_w$ s are estimated to be rather small values. We have been confirmed carefully unbiased regions of core distances in regard to each  $N_e$  bins.

The average values of  $t_r$  and  $t_w$  plotted against core distances are shown in figure 1. As is seen in this figure, both values increase with increase in core distances. On the other hand, dependence of these values on  $N_e$  cannot be seen from this figure. As often pointed out, average  $t_w$ s have some biases at core distances larger than those presented here in each  $N_e$  bins. They are caused by small number of incident particles (less than about ten particles), and consequently, average  $t_w$ s are estimated to be rather small values. We have been confirmed carefully unbiased regions of core distances in regard to each  $N_e$  bins.

Figure 2(a) shows the average values of  $t_w$  for showers with  $N_e$  in the range  $3.2 \times 10^{6.5}$

to  $1.0 \times 10^{7.0}$ , core distances in the range 20m to 50m and sec  $\Theta$  in the range 1.0 to 1.1, 1.1 to 1.2 and 1.2 to 1.3. Figure 2(b) shows dependence of average  $t_w$  on  $s$  for showers with sec  $\Theta$  in the range 1.0 to 1.2, and same  $N_e$  and core distance bins as figure 2(a). Average number of incident particles to the detector in these three core distance bins is about 50, 25 and 12 for sec  $\Theta$  in the range 1.0 to 1.2 and for  $s$  in the range 0.75 to 1.25. Average particle number adopted in figure 2(a), (b) is the same values within errors regardless of different  $s$  and sec  $\Theta$ .

These quantities ( $t_r$  and  $t_w$ ) derived from recorded signal shape are distorted due to the decay time of plastic scintillator, the transit time spread in PMT and the response in storage oscilloscope. Accordingly, the average signal shapes have to be reduced to a system with zero time response in order to discuss the true thickness of air shower disc. We assume the function  $V_e$  for the arrival time distribution of air shower particles as

$$V_e(t) = \exp(-a(t)) \times (1 - \exp(-b(t)))$$

The average signal shape derived from the recorded signals,  $V_o$ , can express as the convolution of the two functions  $V_e$  and  $V_s$  which is average shape corresponding to single relativistic particle.

$V_o(t) = \int_0^t V_s(t-t') \times V_e(t') dt'$  Here,  $V_o$  is an expected signal shape. Calculation was made by two parameter (a and b) fit, and then determined these parameters giving the minimum value of  $\sum (V_o(t) - V_e(t))^2$ . Figure 3 shows the corrected arrival time distributions of air shower particles for showers with sec  $\Theta$  in the range 1.0 to 1.2, and different  $N_e$  and core distance bins as showed in figure caption. These distributions presented here are normalized their areas to be same value, namely to same number of incident particles. The distribution at core distance of 10m to 20m have a large ambiguity when correct to zero time response, because the average signal shape is as narrow as the average shape of single particle. In figure 4, corrected average  $t_w$ s are presented against core distances derived from the procedure mentioned above.

#### 4. Discussion

The average thickness of air shower disc presented as the value of  $t_w$  is increasing with core distances. Apparently, the effects of multiple Coulomb scattering and transvers momenta of the particles contribute to broaden the thickness with increase in core distances. On the other hand, the contribution of high energy interaction and primary compositions through the longitudinal development of air shower particles to the value of  $t_w$  is not obvious as is seen in figure 2(a) and (b). It seems

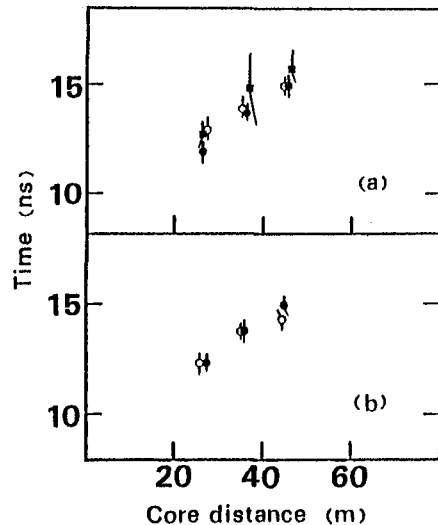


Figure 2. Average  $t_w$ s against core distance for showers with  $N_e$  of  $3.2 \times 10^{6.5}$   $1.0 \times 10^{7.0}$ . (a) shows the dependence of average  $t_w$  on sec  $\Theta$ ; 1.0-1.1 (○), 1.1-1.2 (●) and 1.2-1.3 (■). (b) shows the dependence of average  $t_w$  on age parameter ( $s$ ); 0.75-1.0 (○) and 1.0-1.25 (●).

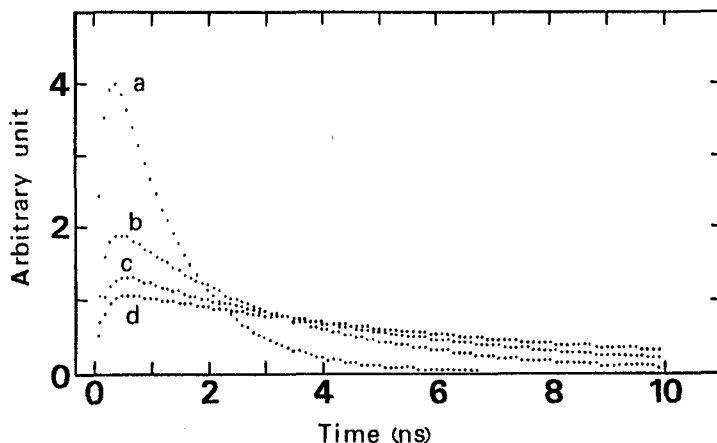


Figure 3. Corrected arrival time distributions of air shower particles for showers with sec  $\theta$  of 1.0-1.2 and  
 (a)  $N_e$  of  $3.2 \times 10^{5.5}$  -  $1.0 \times 10^{6.0}$  for core distances 10m-20m  
 (b)  $N_e$  of  $1.0 \times 10^{6.0}$  -  $3.2 \times 10^{6.5}$  for core distances 20m-30m  
 (c)  $N_e$  of  $3.2 \times 10^{6.5}$  -  $1.0 \times 10^{7.0}$  for core distances 30m-40m  
 (d)  $N_e$  of  $1.0 \times 10^{7.0}$  -  $3.2 \times 10^{7.5}$  for core distances 40m-50m

that the thickness at core distance less than 50m is almost determined by electromagnetic cascade starting at lower atmosphere. However, the detailed discussions should be done after a comparison of the whole shape of arrival time distribution, especially on the part of tail and also those at larger core distances, which are seemed to include the information of upper atmosphere. Furthermore, it is necessary to compare with an elaborate three-dimensional shower simulation.

We are going to process the data obtained simultaneously in an air shower by twelve detectors in order to expect higher accuracy and also to study the uniformity of thickness.

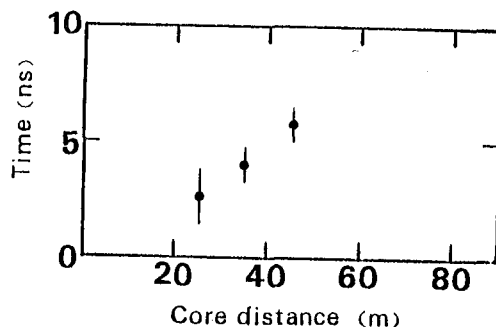


Figure 4. Corrected average  $t_w s$  against core distance derived from the arrival time distributions shown in figure 3.

#### References

- Kawamoto, M. et al; HE 6,2-10 of this conference.  
 Woidneck, C.P. et al: J.Phys. A:Math.Gen. 8(1975)997.

## Properties of $10^{18}$ - $10^{19}$ eV EAS at far core distance

M.Teshima\*, M.Nagano, T.Hara, Y.Hatano, N.Hayashida, C.X.He\*\*  
 M.Honda, F.Ishikawa, K.Kamata, Y.Matsubara\*, M.Mori\*,  
 H.Ohoka and G.Tanahashi

Institute for Cosmic Ray Research, University of Tokyo, Tokyo, 188 Japan

\*Department of Physics, Kyoto University, Kyoto, 606 Japan

\*\*Institute of High Energy Physics, Academia Sinica, Beijing, China.

### Abstract

Properties of  $10^{18}$ - $10^{19}$ eV EAS such as the electron lateral distribution, the muon lateral distribution ( $E > 1\text{GeV}$ ), the ratio of muon density to electron density, the shower front structure and the transition effects in scintillator of 5cm thickness are investigated with the Akeno  $4\text{km}^2/20\text{km}^2$  array at far core distances between 500m and 3000m. The fluctuation of densities and arrival time increase rapidly at the core distances farther than 2km.

### 1. Introduction

The  $4\text{km}^2$  array has been in continuous operation for two years[1] and the expanded array of  $20\text{km}^2$ [2] from the end of 1984. Properties of  $10^{18}$ - $10^{19}$ eV extensive air shower(EAS) at far core distances are studied with  $4\text{km}^2/20\text{km}^2$  array in conjunction with the data of the dense Akeno  $1\text{km}^2$  array[3] which consists of 151 scintillation counters of  $1\text{m}^2$  area and 9 muon stations of  $25\text{m}^2$  area. The results are important not only for determining electron size, muon size and arrival direction of the large showers and estimating their errors, but also for designing the future huge surface array of  $100\text{km}^2$  area. The reliability of the Linsley proposal for the detection of giant air shower with "mini array"[4] is also discussed using the data obtained.

The data observed with  $4\text{km}^2$  array during a period between Dec. 1982 and Oct. 1984 and with  $20\text{km}^2$  between Sep. 1984 and May. 1985 are analyzed. During this operation time about 250 EAS of energies above  $10^{18}$ eV are observed.

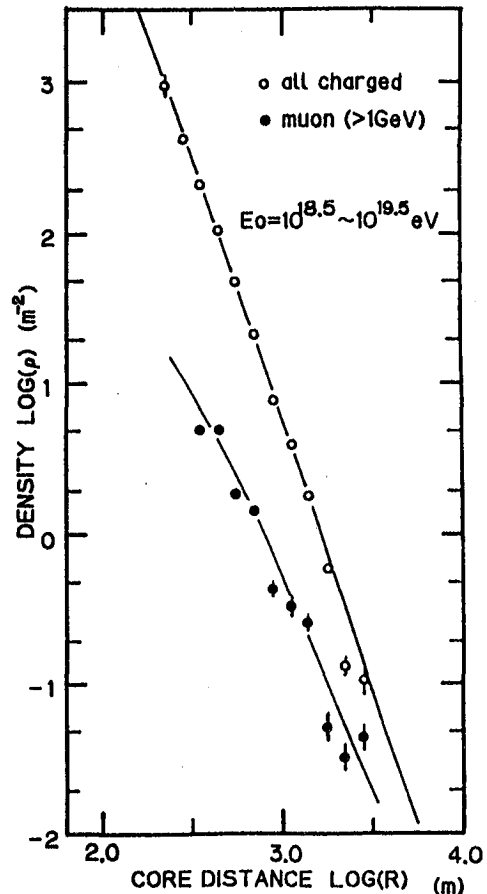


Fig.1 The lateral distribution of electrons and muons.

### 2. The lateral distribution of electrons(LDE)

The LDE is expressed by the function with two parameters  $\alpha$  and  $\eta$  [5].

$$\rho e(R) = C(R/R_m)^{-\alpha} (1+R/R_m)^{-(\eta-\alpha)}. \quad R_m = 91.6\text{m}; \text{Moliere unit. ---(1)}$$

$\alpha$  is 1.2, to which our experiments is not sensitive.  $\eta$  can be measured precisely with many detectors. For the EAS of  $3 \times 10^{18}$  eV  $\eta$  is about 3.8. The LDE becomes steeper as the energy increases and is expressed by

$$\eta = 3.80 \pm 0.05 + (0.10 \pm 0.05) \text{LOG}(E/10^{19} \text{eV}) \quad \text{-----}(2)$$

between 100m and 1000m. This energy dependence is a little larger than the result reported by Linsley[6].

At core distances above 1km, the LDE becomes steeper than the extrapolation of the above formula. In fig.1 the average LDE of  $10^{18.5}$  eV -  $10^{19.5}$  eV for vertical EAS is shown.

The fluctuations of electron densities after subtracting statistical ones (Poisson) are shown by solid lines in fig.2(a) and expressed as a function of core distances as follows.

$$\Delta \rho_e(R) / \rho_e(R) = 0.20 \times (1 + R/1500)^{2.0}. \quad \text{-----}(3)$$

At core distances near 2km, the fluctuations become about 100%.

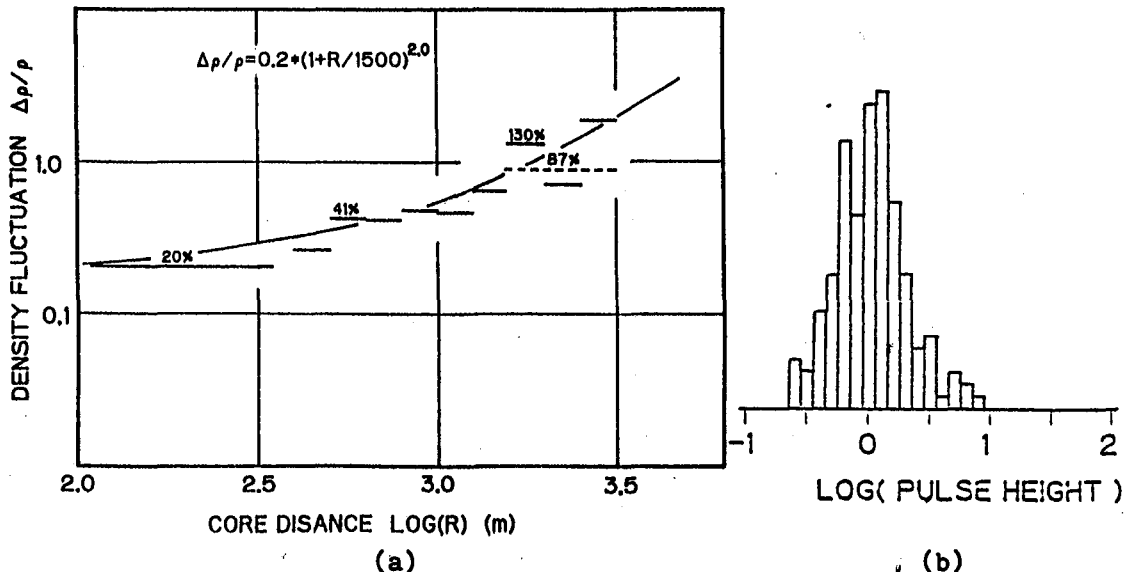


Fig.2 The fluctuation of electron densities(a). The broken line is derived from pulse height distribution of single particles. That is shown in (b).

### 3. Ionization losses in scintillator at far core distances

At far core distances the fluctuations of electron densities become larger. The following causes are possibly related to its increment; the transition effect in scintillator, slow neutrons, large core angle distributions of electrons or broad arrival time distribution of electrons. The last one is important when the densities are measured by one detector of large area.

The transition effect in scintillator is examined by comparing the ionization losses of 16 scintillation detectors of  $1 \text{m}^2$  area with 5cm thickness and those of 25 detectors of  $0.25 \text{m}^2$  area with 0.3cm thickness. The ratio of them is  $1.05 \pm 0.05$  and the transition effect is negligible.

The slow neutrons may be partly responsible, since the delayed pulses are frequently observed at far from the core[7].

We are measuring the density with the logarithmic amplifier by discriminating the exponential pulse of decay constant 10  $\mu$ sec. Therefore the successive particle incidence with broad arrival time distribution described in section 5 may contribute to the fluctuation. The fluctuation due to this is estimated to be about 5% at 1km and 60% at 2km, which are less than the observed values. The pulse height distribution of a single particle which traverse the scintillator is measured at core distances around 2km and is shown in fig.2(b). This distribution is obtained with 151 scintillators of 1km<sup>2</sup> array when the average density is smaller than 0.2 per detector. Therefore this distribution shows the energy loss distribution of a single particle and is free from the pile up of the exponential pulses. The FWHM is about 100% and is the same with the value of Eq(3). This shows that the large density distribution is not due to the spurious one of the used amplifier.

The large core angle distribution of electrons is expected to be originated from multiple scattering, which is also concerned with time structure of shower front reported in section 5.

#### 4. The lateral distribution of muons(LDM) and the ratio of muon density to electron

The LDM(>1GeV) between 200m and 3km is well expressed by Greisen's formula[6].

$$\rho_{\mu}(R) = C(R/R_0)^{-0.75} (1+R/R_0)^{-2.5}. \quad R_0=280m \quad \text{-----(4)}$$

The average LDM for vertical EAS of 10<sup>18.5eV</sup>-10<sup>19.5eV</sup> is shown in fig.1.

The average ratio of muon density to electron is shown by horizontal bars as a function of core distances between 100m and 3km in fig.3. The points with error bars are the individual events which are observed by using the detectors of 1km<sup>2</sup> array triggered by 20km<sup>2</sup> array. The average ratio at core distances between 2km and 3km is 0.20 $\pm$ 0.01, but the fluctuation of each event is large.

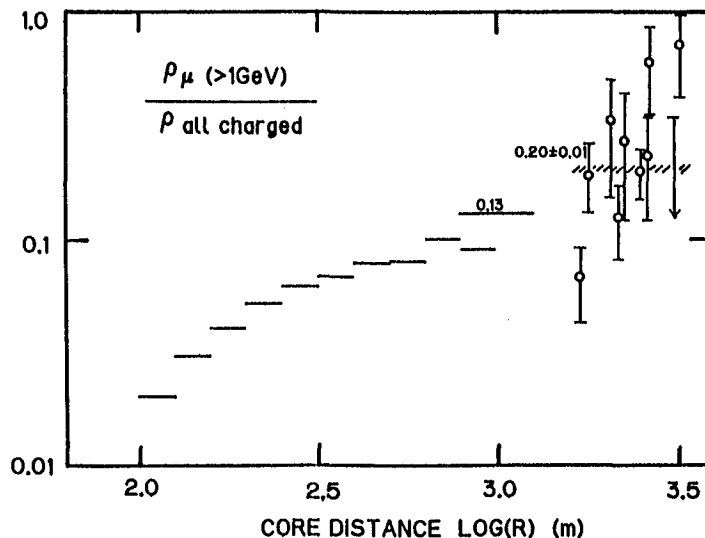


Fig.3 The ratio of muon density to electron.

#### 5. The time structure of shower front

The arrival time of the fastest particle of each detector is measured to determine the arrival direction of EAS. There are 53 fast timing channels with 10nsec resolution in 1km<sup>2</sup> array and 23 channels with 20nsec in 20km<sup>2</sup>. The time structures of shower front are studied by using these 76 channels. Our information is the arrival time of the fastest particle,



but it gives the shower front structure at far from the core where the average density per detector is less than 1.

In fig.4 the dispersion of arrival time is shown. The dispersion increases rapidly at core distances above 2km, and deviates from the extrapolation of the formula given by Linsley[4]. The curvature of shower front shows the similar tendency.

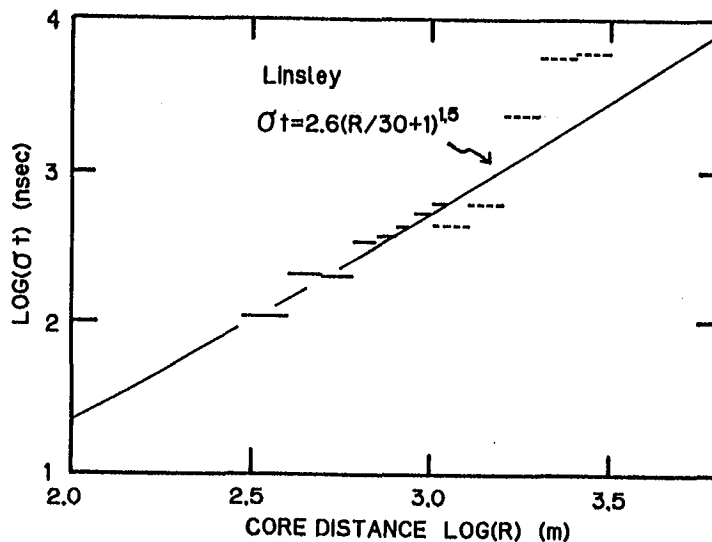


Fig.4 The thickness of shower front.

## 6. Discussion and Conclusion

At core distances above 1km, the LDE becomes steeper than the extrapolation of that within 1km. The density fluctuation increases with distances and exceeds 100% above 2km. The causes of the increment of fluctuations are possibly related to the broad arrival time distribution and the large core angle distribution originated from multiple scattering of electrons. The curvature and the thickness of shower front increase more rapidly above 2km. Therefore, it is necessary to arrange the detectors within 1km spacing.

The observation of Giant Air Shower with "mini array" proposed by Linsley[4] has serious limitations, because the lateral distribution of electrons becomes steeper and its fluctuations become large above 1km. Furthermore fraction of low energy muons to total charged particles fluctuate largely in shower to shower. This method requires the detectors of large area.

## Acknowledgements

The authors wish to thank the other members of Akeno A.S. Group for their help and fruitful discussions. The analysis was carried out with FACOM M380 at the Computer Room of Institute for Nuclear Study, University of Tokyo.

## Reference

- [1] T. Hara et al., Proc. 18th ICRC, Bangalore 11 (1983) 276.
- [2] M. Teshima et al., This conf., La Jolla OG 9.4-8
- [3] T. Hara et al., Proc. 16th ICRC, Kyoto 8 (1979) 135.
- [4] J. Linsley, Proc. 18th ICRC, Bangalore 12 (1983) 135.
- [5] J. Linsley, Proc. 15th ICRC, Plovdiv 12 (1977) 56.
- [6] K. Greisen, Ann. Rev. Nucl. Sci. 10 (1960) 63.
- [7] F. Kakimoto et al., This conf., HE4.7-5.

Longitudinal development of muons in large air showers  
studied from the arrival time distributions measured  
at 900m above sea level

Kakimoto, F., Tsuchimoto, I., Enoki, T. and Suga, K.\*  
Department of Physics, Tokyo Institute of Technology,  
Meguro, Tokyo 152, Japan

Nishi, K.  
The Institute of Physical and Chemical Research,  
Wako, Saitama 351, Japan

#### ABSTRACT

The arrival time distributions of muons with energies above 1.0GeV and 0.5GeV have been measured in the Akeno air-shower array to study the longitudinal development of muons in air showers with primary energies in the range  $10^{17}$ eV to  $10^{18}$ eV. The average rise times of muons with energies above 1.0GeV at large core distances are consistent with those expected from very high multiplicity models and, on the contrary, with those expected from the low multiplicity models at small core distances. This implies that the longitudinal development at atmospheric depths smaller than  $500\text{gcm}^{-2}$  is very fast and that at larger atmospheric depths is rather slow.

Comparison of the mean arrival times of muons with energies above 0.5GeV and the calculation made by McComb et al suggests no serious contribution of muons arising from photon-nucleus collisions to the arrival time distributions of muons with energies above 0.5GeV.

#### 1. Introduction

The Bolivian Air Shower Joint Experiment (BASJE) group and the Tokyo Institute of Technology group carried out a series of experiments to study the longitudinal development of electrons and that of muons by measuring the arrival time distributions both of atmospheric Cerenkov light and of muons, at widely separated atmospheric depths of  $550\text{gcm}^{-2}$  (Mt. Chacaltaya) and  $930\text{gcm}^{-2}$  (Akeno). The longitudinal development of muons derived from the experiment at Chacaltaya and that of electrons derived from both experiments at Chacaltaya and at Akeno have already been published<sup>(1),(2),(3)</sup>.

In the present paper, we report on the arrival time distributions of muons with energies above 1.0GeV in air showers with primary energies in the range  $10^{17}$ eV to  $10^{18}$ eV observed in the Akeno air-shower array. Also reported in the paper are arrival time distributions of muons, with a lower threshold energy of 0.5GeV, in air showers around  $10^{18}$ eV. On this basis an estimate is made of the contribution of muons arising from photon-nucleus collisions (photoproduced muons) to the arrival time distributions of muons with energies above 0.5GeV, by comparing the mean arrival times of muons calculated by McComb et al<sup>(7)</sup> with those measured in the present experiment.

#### 2. Experimental

The first run (May 1981-December 1982) was made to measure the arrival time distributions of muons with energies above 1.0GeV in air showers with primary energies around  $10^{17}$ eV. The result of this run was already reported<sup>(4)</sup>.

---

\*Present address: Department of Physics, Meisei University,  
Hodokubo 337, Hino-shi, Tokyo 191, Japan

In the second run (January 1983–October 1984) the measurement was made both at the M4 muon station ( $E_\mu > 1.0\text{GeV}$ ) and at the ME3 muon station ( $E_\mu > 0.5\text{GeV}$ ), which were separated by 100m from each other. Four  $4\text{m}^2$  shielded scintillation detectors were operated along with a  $4\text{m}^2$  unshielded scintillation detector at each station (hereafter called muon detector and electron detector, respectively). The inside wall of muon detector was covered with black paper while that of electron detector was painted white, and a 5in fast photomultiplier with 14 stages (Hamamatsu Photonics R1250) viewed a scintillator in the detector. Signals from four muon detectors were added in a circuit through a coaxial cable (11C4AF). A signal from the electron detector was delayed by  $1.8\mu\text{s}$  through a coaxial cable (8C4AF) and then added in the circuit. This combined signal was fed to a waveform recorder (Biomation 8100) with a sampling interval of 20ns. When the local trigger pulse generated by the passage of at least one particle through the electron detector was coincident with a master pulse from the Akeno  $4\text{km}^2$  air-shower array<sup>(5)</sup>, which observed an air shower with electron size larger than  $10^{7.5}$ , the combined signal was stored in the recorder.

The time response of the whole system was 16.2ns for rise time between 20% and 70% of the integrated full signal from the muon detector ( $T_{20-70}$ ).

### 3. Arrival time distributions of muons with energies above 1.0GeV

In figure 1 average values of  $T_{20-70}$  for muons with energies above 1.0 GeV in the second run are presented against core distances, where the data are free from biases arising from the requirement for the local trigger and the limited dynamic range of the pulse height in the recording system. Also shown in the figure are values of  $T_{20-70}$  calculated from four models for primary protons with energies of  $10^{18}\text{eV}$  and  $\sec\theta$  of 1.1. As is seen in the figure, the average values of  $T_{20-70}$  at small core distances are consistent with those calculated from low multiplicity models, while high multiplicity models reproduce the present  $T_{20-70}$  consistently at large core distances, indicating that the observed values of  $T_{20-70}$  at all core distances seem not to be explained by any single model as in the case of lower primary energies<sup>(4)</sup>. Since the showers observed in the present experiment were classified by their electron sizes, the sample of showers with a given electron size observed in the Akeno array contains showers initiated at the top of the atmosphere with a particular primary energy as well as those from lower primary energies starting at the deeper atmosphere. This fact was already confirmed from the measurement of atmospheric Cerenkov light at Akeno<sup>(3)</sup>. Considering this fluctuation, a model with an enhanced  $E^{1/2}$  multiplicity law reproduces the observed values of  $T_{20-70}$  better than a model with an  $E^{1/2}$  multiplicity law at largest core distances.

### 4. Comparison of both arrival time distributions of muons above 0.5GeV and 1.0GeV

The average values of  $T_{20-70}$  for muons with energies above 0.5GeV are longer than those with energies above 1.0GeV by about 50% for showers with electron sizes in the range  $10^{8.0}$  to  $10^{8.5}$  and  $\sec\theta$  in the range 1.0 to 1.2, as shown in figure 2. It is worth noting that the average values of  $T_{20-70}$  for muons above 0.5GeV are almost consistent with those above 0.42GeV obtained by the Nottingham group in the Haverah Park array<sup>(6)</sup>, if the differences of the system time response and the threshold energy of

muons in the two experiments are allowed for.

In figure 3 the mean arrival times of muons above 0.5GeV and those above 1.0GeV were calculated from observed muon signals and are compared with those estimated from the mean arrival times and lateral distributions of photoproduced and normal muons above 0.3GeV at sea level calculated by McComb et al<sup>(7)</sup> using a scaling model for proton and iron-initiated showers. After allowing for differences of the threshold energy of muons and the atmospheric depth between the calculation and the present experiment, we would conclude that the longitudinal development of muons in air showers with primary energies around  $10^{18}$ eV is faster than that calculated by McComb et al using a scaling model and primary iron, furthermore the proportion of photoproduced muons to all muons above 0.5GeV must be much smaller than that calculated by these authors.

### 5. Discussion and conclusions

The observed values of  $T_{20-70}$  at small core distances are consistent with those calculated from low multiplicity models while at large core distances these observed values of  $T_{20-70}$  are well explained by high multiplicity models. According to the present calculation, the average production depth of muons arriving at the time intervals of  $T_{20-70}$  decreases with increasing core distance. We may conclude, therefore, that the longitudinal development of muons in air showers with primary energies in the range  $10^{17}$ eV to  $10^{18}$ eV is as fast as expected from an enhanced  $E^{1/2}$  multiplicity law from  $200\text{gcm}^{-2}$  to  $500\text{gcm}^{-2}$  and is rather slow beyond that atmospheric depth. This conclusion is consistent with that derived from the arrival time distributions of muons in air showers with primary energies above  $10^{17}$ eV observed at Chacaltaya<sup>(1)</sup> and of atmospheric Cerenkov light from air showers with primary energies in the range  $5 \times 10^{15}$ eV to  $2 \times 10^{17}$ eV observed at Akeno<sup>(3)</sup> as well as at Chacaltaya<sup>(2)</sup>.

The fact that photoproduced muons appear to make no significant contribution to the arrival time distributions of muons with energies above 0.5GeV means that the character of particle interactions may be conveniently studied by measuring the arrival time distributions of muons above 0.5GeV, instead of 1.0GeV, and comparing them with calculations for normal muons. This way is important to reduce the cost of the shielding material of muon stations with large area in a large air-shower array.

### References

- (1) F. Kakimoto et al: J. Phys. G: Nucl. Phys. 5(1983)339.
- (2) N. Inoue et al: J. Phys. G: Nucl. Phys. 11(1985)669.
- (3) N. Inoue et al: J. Phys. G: Nucl. Phys. 11(1985)657.
- (4) T. Tamura et al: Proc. of 18th ICRC, Bangalore, 6(1983)133.
- (5) T. Hara et al: Proc. of 18th ICRC, Bangalore, 11(1983)276.
- (6) P.R. Blake et al: J. Phys. G: Nucl. Phys. 8(1982)1605.
- (7) T.J. McComb et al: J. Phys. G: Nucl. Phys. 5(1979)1613.

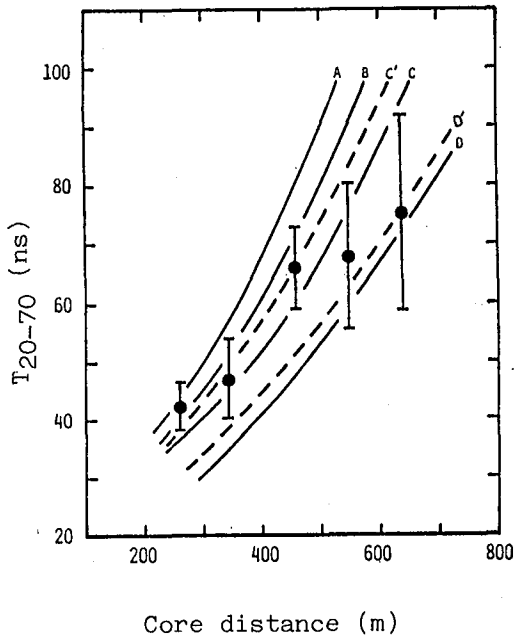


Figure 1. The average  $T_{20-70}$  of the arrival time distributions of muons with energies above 1.0 GeV for showers with  $N_e$  of  $10^{8.0}-10^{8.5}$  and  $\sec\theta$  of 1.0-1.2 compared with those calculated from A: scaling model, B: a model with an  $E^{1/4}$  multiplicity law, C: a model with an  $E^{1/2}$  multiplicity law and D: a model with an enhanced  $E^{1/2}$  multiplicity law and with first-interaction depths of  $40\text{gcm}^{-2}$  for A-D and  $120\text{gcm}^{-2}$  for C'-D'.

Figure 3. Mean arrival times of muons with energies above 0.5 GeV ( $\square$ ) and those above 1.0 GeV ( $\blacksquare$ ) for showers with  $N_e$  of  $10^{8.0}-10^{8.5}$  and  $\sec\theta$  of 1.0-1.2 against core distances compared with those of muons above 0.3 GeV estimated for primary protons (—) and for primary irons (---) with energies of  $10^{18}$  eV and  $\sec\theta$  of 1.0.

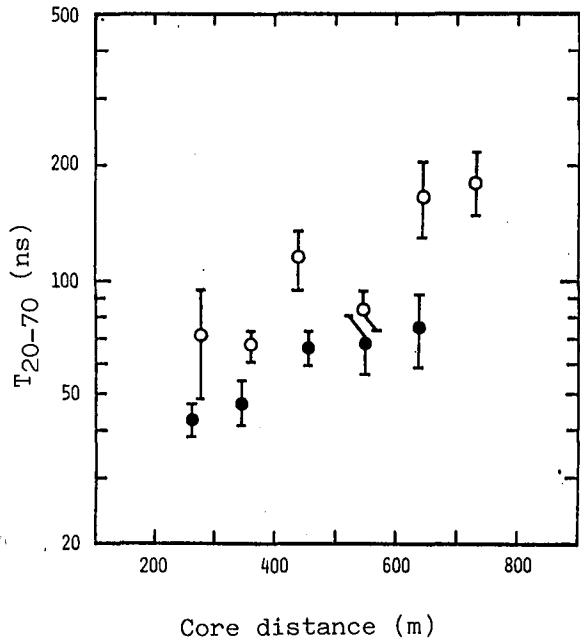
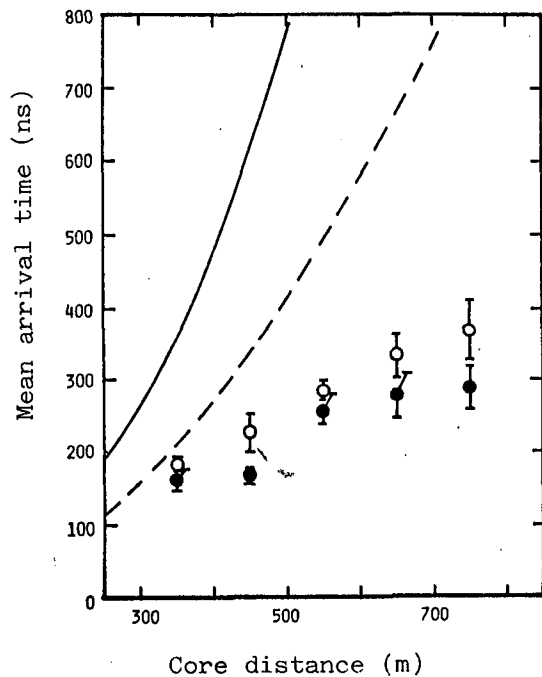


Figure 2. The average  $T_{20-70}$  of the arrival time distributions of muons with energies above 0.5 GeV ( $\square$ ) and those above 1.0 GeV ( $\blacksquare$ ).



Arrival time distributions of electrons in air showers  
with primary energies above  $10^{18}$  eV observed  
at 900m above sea level

Kakimoto, F., Tsuchimoto, I., Enoki, T. and Suga, K.\*  
Department of Physics, Tokyo Institute of Technology,  
Meguro, Tokyo 152, Japan

Nishi, K.

The Institute of Physical and Chemical Research,  
Wako, Saitama 351, Japan

## 1. Introduction

Detection of air showers with primary energies above  $10^{19}$  eV with enough statistics is extremely important in an astrophysical aspect related to the Greisen cut off and the origin of such high energy cosmic rays. Recently, Linsley proposed a method to observe such giant air showers by measuring the arrival time distributions of air-shower particles at large core distances with a mini array<sup>(1)</sup>.

We started experiments to measure the arrival time distributions of muons in 1981 and those of electrons in early 1983 in the Akeno air-shower array ( $930\text{gcm}^{-2}$  atmospheric depth, 900m above sea level). During our observation, the detection area of the Akeno array was expanded from  $1\text{km}^2$  to  $4\text{km}^2$  in 1982<sup>(2)</sup> and to  $20\text{km}^2$  in 1984. Now the arrival time distributions of electrons and muons can be measured for showers with primary energies above  $10^{19}$  eV at large core distances.

In this paper, the possibility of Linsley's proposal is examined on the basis of the arrival time distributions of particles measured with unshielded scintillation detectors for following three points:

- (1) Is the time dispersion as proposed by Linsley a suitable parameter?
- (2) How large area is needed for the detector?
- (3) Are core distances and shower sizes determined accurately enough?

Also reported in this paper are signals delayed by longer than  $1\mu\text{s}$  from the shower front, together with a discussion on the nature of these signals.

## 2. Experimental

In the first run from January 1983 to October 1984, the arrival time distributions of air-shower particles was measured using a  $4\text{m}^2$  unshielded scintillation detector with a 5in fast photomultiplier (Hamamatsu Photonics R1250) located above both the M4 and ME3 muon stations in the Akeno array. Details of the measurement are described in the preceding paper<sup>(4)</sup> (hereafter called paper I).

Since the detection area of the Akeno array was expanded from  $4\text{km}^2$  to  $20\text{km}^2$  in October 1984<sup>(3)</sup>, the scintillation detectors located at the M4 and ME3 muon stations were rearranged. In this second run four  $4\text{m}^2$  unshielded scintillation detectors were installed near the center of this new  $20\text{km}^2$  array and two  $4\text{m}^2$  scintillation detectors were located above the M4 muon station, separated by about 2km from the center of the new array. The added signal from these detectors was stored in the waveform

---

\*Present address: Department of Physics, Meisei University,  
Hodokubo 337, Hino-shi, Tokyo 191, Japan

recorder (Biomation 8100) with a sampling interval of 50ns in each station, when the local trigger pulse generated by a passage of at least one particle through any one of the detectors was coincident with a master pulse from the array to observe air showers with electron sizes larger than  $10^{8.0}$ .

The time response of the whole system in the first run was 39ns for rise time between 20% and 70% of the integrated full signal ( $T_{20-70}$ ), while this value in the second run became larger due to the larger sampling interval of the recorder but this is not serious for observation of the arrival time distributions of particles at large core distances.

### 3. Arrival time distributions of particles at large core distances

On the basis of the observed arrival time distributions, the time dispersion ( $\sigma$ ) proposed by Linsley as well as the rise time ( $T_{20-70}$ ) were calculated for each shower. Average values both of  $\sigma$  and  $T_{20-70}$  are plotted against core distances in figure 1(a) and (b), respectively, for air showers with electron sizes from  $10^{8.0}$  to  $10^{8.5}$  and  $\sec\theta$  from 1.0 to 1.2 in the first run. Also shown in figure 1(a) is the value of  $\sigma$  given by Linsley's empirical formula. Although the average values of  $\sigma$  obtained at core distances smaller than 500m are larger than the value of  $\sigma$  by Linsley, those at large core distances are consistent with each other. As is seen in figure 1(b) average values of  $T_{20-70}$  show a steeper dependence on the core distance than those of  $\sigma$ .

Though the sample of showers is limited at present, time dispersions for showers with electron sizes above  $10^{9.0}$  observed in the two runs are plotted against core distances in figure 2. A large fluctuation in  $\sigma$  is seen at given core distances. The distribution of  $\sigma$  depends upon the number of observed particles. For a sample of showers with electron sizes of  $10^{8.0}$ - $10^{8.5}$  at core distances of 500-600m, the standard deviation of  $\sigma$  is 100ns for more than 10 particles while 30ns for more than 30 particles.

### 4. Signals delayed by longer than $1\mu\text{sec}$

Signals, which correspond to the passage of more than 0.5 particles, delayed by longer than  $1\mu\text{s}$  from the shower front have been seen in 15% of arrival time distributions measured for showers with electron sizes larger than  $10^{8.0}$ . Figure 3 shows the delay time distribution for air showers with electron sizes from  $10^{8.0}$  to  $10^{8.5}$  and  $\sec\theta$  from 1.0 to 1.2. The frequency decreases monotonously up to  $4\mu\text{s}$  with delay time while, after that time, this frequency is almost constant up to  $10\mu\text{s}$ . The frequency of accidental signals is as low as  $8 \times 10^{-4} (4\text{m}^2 \cdot 1\mu\text{s})^{-1}$ . Moreover, during first run, we observed five interesting showers in which one or successive delayed signals appeared in both the arrival time distribution of muons and that of electrons with almost same delay times, one of which is shown in figure 4(a), and observed one shower in which four successive delayed signals appeared in both arrival time distributions of electrons with almost same delay times at the M4 and ME3 muon stations separated by 100m from each other, which is shown in figure 4(b).

### 5. Discussion and conclusion

From the fluctuation in the time dispersions ( $\sigma$ ) shown in figure 2, we may tentatively argue that the core distance and the shower size would be determined within an accuracy of 100-150m and  $\pm 120\%$ , respectively, if the number of particles observed in the detectors exceeds ten and the core

distance is around 1.5km. However, it should be mentioned from the present analysis that the value of time dispersion ( $\sigma$ ) is more sensitive to the existence of delayed particles than that of  $T_{20-70}$  and the values of  $T_{20-70}$  show a steeper dependence on core distance than that of  $\sigma$ . Needless to say, it is most important to accumulate the sample of showers and examine further the dependence of the dispersion on the electron size and the zenith angle to make a final conclusion on the possibility of the proposal made by Linsley.

The delayed signals observed in the present experiment seem to be explained qualitatively as originated from low-energy neutrons which made interactions in the scintillator. However, the successive delayed signals as described at the end of §4 look very interesting and more samples should be necessary to clarify their origin.

#### References

- (1) J. Linsley: Research Reports UNML-6/11/83, UNML-6/15/83 and UNML-6/20/83(1983)
- (2) T. Hara et al: Proc. of 18th ICRC, Bangalore, 11(1983)276.
- (3) M. Teshima et al: OG 9.4-8 in this Conference.
- (4) F. Kakimoto et al: HE 4.7-4 in this Conference.

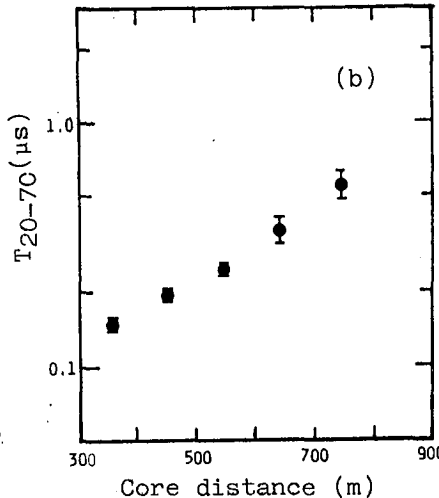
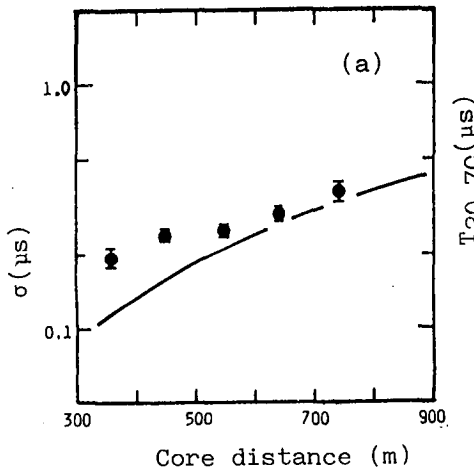


Figure 1. The average  $\sigma$  (a) and  $T_{20-70}$  (b) of the arrival time distributions of particles in the first run for showers with electron sizes from  $10^{8.0}$  to  $10^{8.5}$  and  $\sec\theta$  from 1.0 to 1.2. A curve in (a) is given by Linsley's empirical formula ( $\sigma(\text{ns}) = 2.6(1+R/30\text{m})^{1.5}$ , R: core distance)

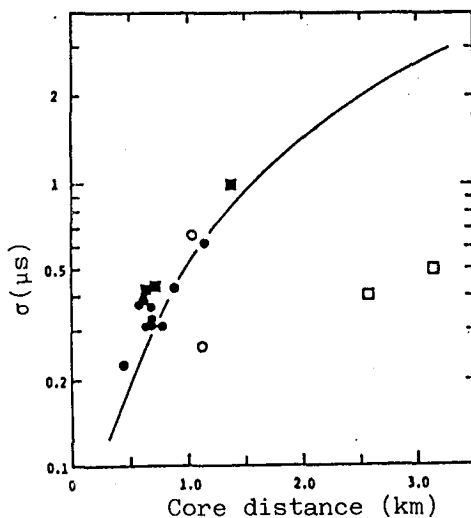
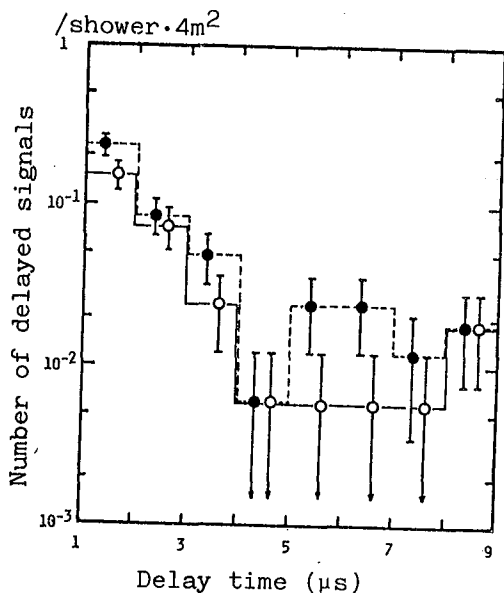


Figure 2. Time dispersions ( $\sigma$ ) of the arrival time distributions of particles for showers with electron sizes above  $10^{9.0}$  observed in the first run (●, ○) and in the second run (■, □). The number of particles observed in the unshielded detectors:  $\geq 10$  for ● and ■;  $< 10$  for ○ and □. Time intervals in the arrival time distributions of particles, within which time dispersions were calculated;  $2.4\mu\text{s}$  for ● and ○;  $10\mu\text{s}$  for ■ and □. A curve is given by Linsley's formula.

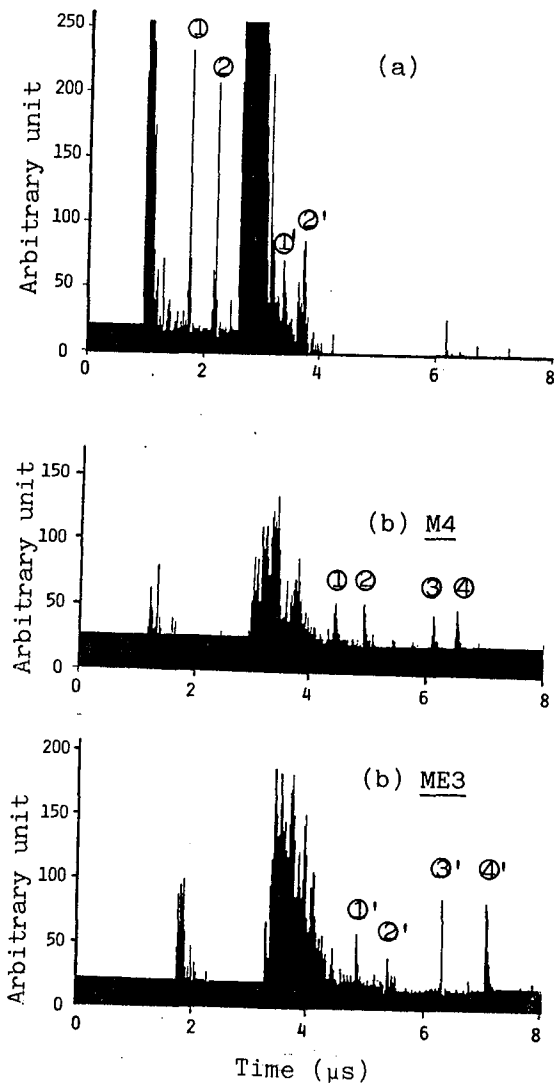




**Figure 4(a).** Delayed signals observed both in the shielded detectors ( $\textcircled{1}$ :  $t_d=0.76$ ,  $n_d=14.8$ ;  $\textcircled{2}$ :  $t_d=1.18$ ,  $n_d=15.7$ ) and in the unshielded detector ( $\textcircled{1}'$ :  $t_d=0.70$ ,  $n_d=2.6$ ;  $\textcircled{2}'$ :  $t_d=1.12$ ,  $n_d=3.2$ ) at ME3 station for air shower with  $N_e$  of  $3.7 \times 10^8$ ,  $\theta$  of  $15.2^\circ$  and  $R$  of  $327.3\text{m}$ .  $t_d$ : delay time in  $\mu\text{s}$  and  $n_d$ : the number of delayed particles. Time between both signals from the shielded detectors and the unshielded one is  $1.8\mu\text{s}$  as described in paper I. Under-shoot in the figure is due to overloading in the amplifier of the recorder.

**(b).** Delayed signals observed in the unshielded detector both at M4 station ( $\textcircled{1}$ :  $t_d=1.48$ ,  $n_d=2.3$ ;  $\textcircled{2}$ :  $t_d=2.00$ ,  $n_d=2.4$ ;  $\textcircled{3}$ :  $t_d=3.16$ ,  $n_d=1.7$ ;  $\textcircled{4}$ :  $t_d=3.56$ ,  $n_d=2.0$ ) and ME3 station ( $\textcircled{1}'$ :  $t_d=1.56$ ,  $n_d=1.5$ ;  $\textcircled{2}'$ :  $t_d=2.04$ ,  $n_d=0.9$ ;  $\textcircled{3}'$ :  $t_d=3.00$ ,  $n_d=1.6$ ;  $\textcircled{4}'$ :  $t_d=3.76$ ,  $n_d=4.4$ ) for air shower with  $N_e$  of  $2.8 \times 10^9$ ,  $\theta$  of  $8.1^\circ$  and  $R$  of  $697.3\text{m}$  from M4 and of  $665.6\text{m}$  from ME3.

**Figure 3.** Delay time distribution of signals delayed by longer than  $1.0\mu\text{s}$  observed in the arrival time distributions of particles for air showers with electron sizes from  $10^{8.0}$  to  $10^{8.5}$  and  $\sec\theta$  from  $1.0$  to  $1.2$ .  $\textcircled{1}$ : more than  $0.5$  particles;  $\textcircled{2}$ : more than  $1.0$  particle.



THE THICKNESS OF THE SHOWER DISC AS OBSERVED IN SHOWERS  
PRODUCED BY PRIMARIES ABOVE  $10^{19}$  eV

M.A. Lawrence, A.A. Watson and A.A. West  
Department of Physics, University of Leeds, LEEDS 2.

ABSTRACT

The thickness of the shower disc has been measured in showers initiated by primaries of energy  $> 10^{19}$  eV using the large area water Cerenkov detectors of the Haverah Park array. Results are presented which (a) provide supporting evidence for the accuracy of our analysis procedures in giant showers, (b) offer an evaluation of Linsley's mini-array technique for the detection of giant showers and (c) extend earlier work on developmental fluctuations above  $10^{19}$  eV.

1. Introduction. A unique feature of the Haverah Park shower array is the large area ( $34 \text{ m}^2$ ) of the water-Cerenkov detectors of the 500 m array. These have been used in a succession of studies (Watson and Wilson 1974, Lapikens 1977, Walker and Watson 1981, 1982 and 1983) to provide measurements of the thickness of the shower disc as a function of core distance ( $r > 250 \text{ m}$ ), zenith angle ( $\theta < 40^\circ$ ) and energy ( $E > 2 \times 10^{17} \text{ eV}$ ). In particular these measurements were amongst the first to be used to demonstrate the reality of shower-to-shower fluctuations in large showers. Here we describe further results which have been deduced about giant showers produced by primaries with  $E > 10^{19} \text{ eV}$ .

2. Check on the accuracy of core location above  $4 \times 10^{19} \text{ eV}$ . There is considerable contemporary interest in the shape of the cosmic ray energy spectrum above  $10^{19} \text{ eV}$  (e.g. Hill and Schramm 1985) and, despite considerable experimental effort world-wide, the shape of the spectrum remains in dispute (e.g. Bower et al 1983, Diminstein et al 1982, Horton et al 1983, Linsley 1983). In particular the Yakutsk group have reported no events of energy  $> 10^{20} \text{ eV}$  while the other three groups all claim events  $> 10^{20} \text{ eV}$ . The Yakutsk group have suggested that errors in core location and inadequate knowledge of the water-Cerenkov structure function have lead to gross over-estimates of the energy of some Haverah Park events (Vasilev et al 1983). We briefly describe a simple check, based on our detailed studies of shower disc thickness, which refute this hypothesis. This check has in fact been used in our work for many years and has been alluded to before (e.g. Lapikens 1977, Cunningham et al 1981).

It is found that the thickness of the shower disc increases with distance from the shower axis independent of detector type (Linsley and Scarsi 1962, Baxter, Watson and Wilson 1965). This arises because the source of particles at a large axial distance is essentially a line source. Furthermore as the shower energy increases the 'line-source' moves deeper in the atmosphere so that at a given distance the disc will become thicker.

These features, and others, have been quantified in the Haverah Park work through the measurement of  $t_1$ , the risetime of the signal in the water-Cerenkov detectors between 10 and 50% of full height. So far all of the work has been done with  $34 \text{ m}^2$  detectors and the majority of data is derived from measurements on oscilloscope records.

The easiest and most common way to over-estimate the size of an air-shower is to misplace the core at greater than the correct distance from the centre of the array. The steepness of the lateral distribution, combined with the wide-spacing of detectors, make this an important and well-recognized problem. The shower disc thickness allows a check on the accuracy of the assigned core: if the core is placed too far from the array centre then the measured risetime will appear to be anomalously fast. The risetime of the pulse thus acts as an independent check on the core location analysis.

Figure 1: Plot of risetime against distance for events listed in Table 1.

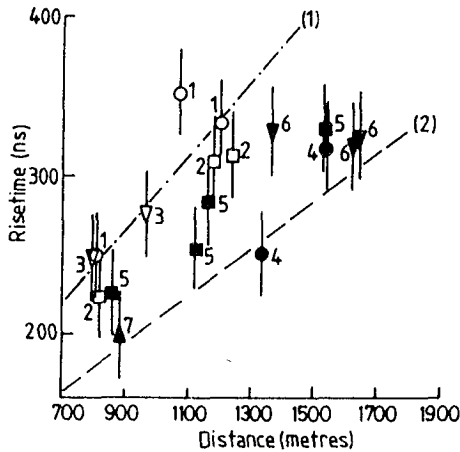


Table 1

	MR	$\theta$	1D	$E_p/eV$
(1)	9597348	$11^\circ$	1	$6.7 \times 10^{19}$
	19384465	$9^\circ$	2	$5.1 \times 10^{19}$
	21220296	$13^\circ$	3	$4.2 \times 10^{19}$
(2)	9160073	$30^\circ$	4	$1.6 \times 10^{20}$
	12701723	$29^\circ$	5	$1.4 \times 10^{20}$
	16632298	$34^\circ$	6	$1.1 \times 10^{20}$
	17684312	$35^\circ$	7	$9.8 \times 10^{19}$

Events included in the Haverah Park energy spectrum (Brooke et al OG5.1-3) with  $\theta < 40^\circ$ ,  $E > 4 \times 10^{19}$  eV and for which risetime measurements are available are shown in Figure 1. The lines are for  $11^\circ$  and  $32^\circ$  but are appropriate to the 139 events with  $5 \times 10^{18} < E < 4 \times 10^{19}$  eV ( $\log E = 19.0$ ) from which the regression relation

$$t_{\frac{1}{2}} \text{ (ns)} = ((0.71 \pm .01) - (0.47 \pm .10) \sec \theta) r + (55 \pm 8)$$

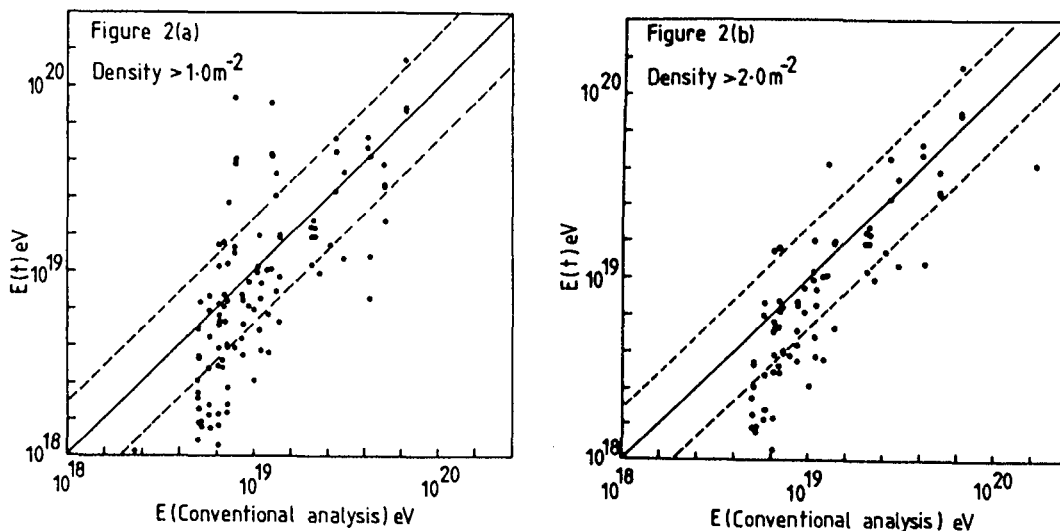
was derived. The points, on average, lie above this line as expected; specifically  $\Sigma \sigma(\theta, r) / \sigma_m(t_{\frac{1}{2}})$  is +8.3 for the 18 risetimes measured in 7 events. Checks made in this way on the vast majority of showers with  $E > 5 \times 10^{18}$  eV and  $\theta < 40^\circ$  underpin our confidence in the existence of primary cosmic rays above  $5 \times 10^{19}$  eV.

3. The mini-array method. Linsley (1983 and this conference OG-9) has proposed a cheap and novel method of detecting giant air-showers through the simultaneous measurement of shower disc thickness, density and direction at a small ( $\sim 50$  m) shower array. His proposal was based on empirical data from the Volcano Ranch array obtained by averaging over many showers. We find this idea attractive and are presently instrumenting the peripheral arrays at Haverah Park for this purpose (Brooke et al 1983). As an interim step we have attempted to evaluate the potential of the method using existing data.

Events of known primary energy  $> 5 \times 10^{18}$  eV and with at least one risetime measurement were selected. Using the zenith angle determined from the 500 m array detectors and the known regression line for giant showers (section 2 above) the distance of the core from each detector was estimated and hence, from the known density and assumed lateral distribution, the primary energy was derived. In Figure 2 the primary energy,

$E(t)$ , derived from risetime measurement is compared with that from our normal analysis, the dashed lines indicating factors of two about the 1:1 line. Data for two threshold density cuts are shown.

Figure 2: Plots of energy derived from risetime against energy derived from conventional analysis.



An unweighted straight line fit to the points above  $10^{19}$  eV yields gradients of  $0.9 \pm 0.2$  and  $1.2 \pm 0.2$  and the rms scatters about these lines are 100% and 75% for the two threshold density cuts respectively. A number of factors contribute to the spread in  $E(t)$  and some of these will be discussed in the context of risetime measurement at 1 km in a  $10^{19}$  eV shower at  $30^\circ$ .

(a) Zenith angle uncertainty. For the showers used above the typical zenith angle uncertainty is about  $3^\circ$ . However for realistic mini-arrays (such as those already set up at Haverah Park)  $\Delta\theta \approx 5^\circ$  (Brooke et al 1983). For a density recorded at 1 km this leads to an uncertainty in  $E(t)$  of about 30%. It is possible that with suitable calibration improved zenith angle uncertainties might be achieved. Present work in optimizing angular resolution for UHE  $\gamma$ -ray astronomy might have spin-off here.

(b) Density threshold. The density threshold for the events in Figure 2(a) was set at  $> 1 \text{ m}^{-2}$  (34 vertical equivalent muons). A detailed analysis of measurement errors shows that for the reference shower being discussed here  $\sigma \approx 20$  ns with the major contribution coming from the finite size of the density sample. This leads to an rms error in  $r$  of about 100 m and to an rms error in  $E(t)$  of about 35%. The error in the risetime from this cause will vary as  $1/\sqrt{\rho}$ , where  $\rho$  is the density.

(c) Between shower variations. There are fluctuations in the longitudinal development of individual air-showers. These are unavoidable and cannot be overcome by new experimental techniques. For the reference shower  $\sigma \approx 20$  ns so that again the error in the deduced  $E(t)$  is  $\sim 35\%$ .

These three factors when combined in quadrature predict an rms spread in  $E(t)$  of  $\sim 60\%$  for a  $10^{19}$  eV observed at 1 km and  $30^\circ$  with water-Cerenkov detectors of  $34 \text{ m}^2$  area. With smaller area detectors the situation will

be worse, but we propose to evaluate the problem using the sub-arrays at Haverah Park which are located 2 km from the centre of the array. Each, consisting of  $4 \times 13.5 \text{ m}^2$  water-Cerenkov detectors, spaced at 50 or 150 m, is presently used to record small local showers ( $> 10^{15}$  or  $10^{16}$  eV) as well as being slaved by the giant array trigger. A single mini-array will have a collecting area of  $\sim 6 \text{ km}^2$  at  $10^{20}$  eV for a  $1 \text{ m}^2$  threshold so that a x3 enhancement of our present system will be achieved at low cost. The uncertainties in energy measurement discussed above suggest that the mini-array technique will be more useful in the investigation of anisotropy at the highest energies than for the accurate determination of the cosmic ray spectrum.

The above evaluation refers to the use of  $t_{\frac{1}{2}}$  to measure the disc thickness. In fact Linsley (1983) proposed the use of the dispersion and there will be differences of detail between an evaluation of that parameter and the present one.

4. Developmental Fluctuation. We have used our sample of 51 events above  $10^{19}$  eV to estimate the fluctuation in the mean depth of maximum at  $3 \times 10^{19}$  eV. Details will be given elsewhere but the method is essentially that discussed in Walker and Watson (1983). The rms fluctuation in  $X_m$ ,  $\{X_m\}$ , is found to be  $33 \pm 8 \text{ g cm}^{-2}$ , consistent with our previous work. The tendency for  $\{X_m\}$  to decrease with energy and the conclusion that pure Fe can be excluded above  $10^{19}$  eV are reinforced.

5. Acknowledgements. Extensive discussion with Bob Reid is gratefully acknowledged as is the financial support of the Science and Engineering Research Council.

### References

- Baxter, A.J., Watson, A.A. and Wilson, J.G. (1965) Proc. 9th Int. C.R. Conf. (London) 2, 724.
- Bower, A.J. et al (1983) J. Phys. G 9, L53.
- Brooke, G. et al (1983) Proc. 18th Int. C.R. Conf. (Bangalore) 9, 420.
- Cunningham, G. et al (1981) Proc. 16th Int. C.R. Conf. (Paris)
- Diminstein, O.S. et al (1982) Bull. Naush. Info. Yakutsk 9, 537.
- Hill, C.T. and Schramm, D. (1985) Phys. Rev. D31, 564.
- Horton, L. et al (1983) Proc. 18th Int. C.R. Conf. (Bangalore) 2, 128.
- Lapikens, J. (1977) Proc. 15th Int. C.R. Conf. (Plovdiv) 8, 1978.
- Linsley, J. (1983) Proc. 18th Int. C.R. Conf. (Bangalore) 12, 135.
- Linsley, J. and Scarsi, L. (1962) Phys. Rev. Lett. 9, 123.
- Vasilev, I.V. et al (1983) 'Cosmic Rays with Energy  $> 10^{17}$  eV', published by Yakutsk Branch of Academy of Science USSR, EDK537.591, p.19.
- Walker, R. and Watson, A.A. (1981) J. Phys. G 7, 1297.
- Walker, R. and Watson, A.A. (1982) J. Phys. G 8, 1131.
- Walker, R. and Watson, A.A. (1983) Proc. 18th Int. C.R. Conf. (Bangalore) 6, 114.
- Watson, A.A. and Wilson, J.G. (1974) J. Phys. A 7, 1199.

## METHODS FOR ROOF-TOP MINI-ARRAYS

Wayne E. Hazen and Eric S. Hazen\*

Randall Laboratory of Physics, University of Michigan  
Ann Arbor, MI 48109, USA

\*ETC Inc., Middleton WI 53562, USA

1. Introduction. In order to test the idea of the Linsley effect mini array (1) for the study of giant air showers, it is desirable to have a trigger that exploits the Linsley effect itself. In addition to the trigger, it is necessary to have a method for measuring the relative arrival times of the particle swarm selected by the trigger. Since the idea of mini- arrays is likely to appeal to small research groups, it is desirable to try to design relatively simple and inexpensive methods, and methods that utilize existing detectors.

Thus far we have designed for clusters of small detectors where the operation is in the local particle density realm where the probability of  $>2$  particles per detector is small. Consequently, we can discriminate pulses from each detector and thenceforth deal mainly with logic pulses.

This report describes the key circuits that have been built and the results of preliminary tests. Results from a preliminary run with a small shower array are presented in another conference paper (2). Expected rates of data collection are calculated in paper HE 4.7-8.

2. Method. Pulses from the photomultiplier (PM) of each detector are fed to discriminators (after preamplification if desirable). The discriminators can be single level or double level (CFD) if desirable enough to warrant the extra circuitry. The discriminator outputs are then "shaped" to 20 ns length and combined by an OR element. The OR'd output is fanned-out to the trigger circuit and to a 100 MHz time shift register.

For a study and utilization of the Linsley effect itself a time window of 2  $\mu$ s is sufficient, but we can also provide an additional 2  $\mu$ s of analog display (with lower time resolution) by means of a 30 MHz pulse form digitizer,<sup>3</sup> if we want to look for delayed pulses. Both of the above are also readily lengthened by adding more shift-register IC's.

(A) The trigger circuits are of two sorts. The first is digital and simply counts the number of pulses that arrive within a 2  $\mu$ s gate that is opened by each pulse. (With the "singles" counting rates we need in order to have satisfactory particle detection efficiency, the accidental rates can be kept manageable.) If the number of pulses within the window satisfies the preset requirement, a trigger is generated at the end of the 2  $\mu$ s gate. The circuit is shown in Fig. 1.

The above trigger has the advantage of simplicity, but it cannot count pulses that are closer together than 30 to 40 ns. There-

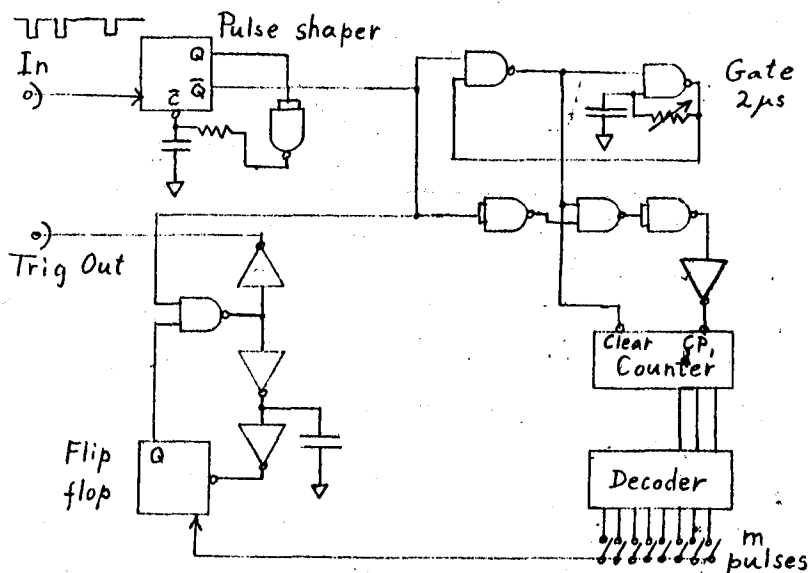


Fig. 1 Pulse-train trigger; digital.

fore, we have built a second type of trigger. Again, each arriving particle, i.e., pulse on the OR line, opens a  $2 \mu\text{s}$  gate. But this time the gate is for an analog device that integrates the time occupied by following pulses (if any). This system has the advantage of partially "resolving" overlapping pulses. The circuit is shown in Fig. 2. Again, a trigger is generated at the end of the  $2 \mu\text{s}$  gate if the preset requirement is met.

(B) The relative time record is obtained from a 100 MHz time shift register that holds  $2 \mu\text{s}$  of information. The register is stopped and read out when a trigger is received from (A). The register is composed of four 25 MHz elements with a 50 ns multitap TTL delay IC to phase shift among the registers. The circuit is shown in Fig. 3.

3. Applications. The above circuit elements are being used by the cosmic ray group of L.K. Ng at Hong Kong (2) in conjunction with a cluster of eight  $1/4 \text{ m}^2$  scintillators. There are plans underway to use this method in parallel with the main shower experiment of the Cosmic Ray Group of the Institute of High Energy Physics at Beijing. We also hope to use it for calibrations at some of the existing large shower arrays.

This work has been supported by grants from the Rackham Graduate School of the University of Michigan and the U.S. Department of Energy.

#### References

- <sup>1</sup>Linsley, J (1983) Research Report UNML 6/83.
- <sup>2</sup>Ng, LK et al., Paper at this conference.
- <sup>3</sup>Crosby, DA and MacAdam KB (1981), Rev. Sci. Inst. 52(2) 297.

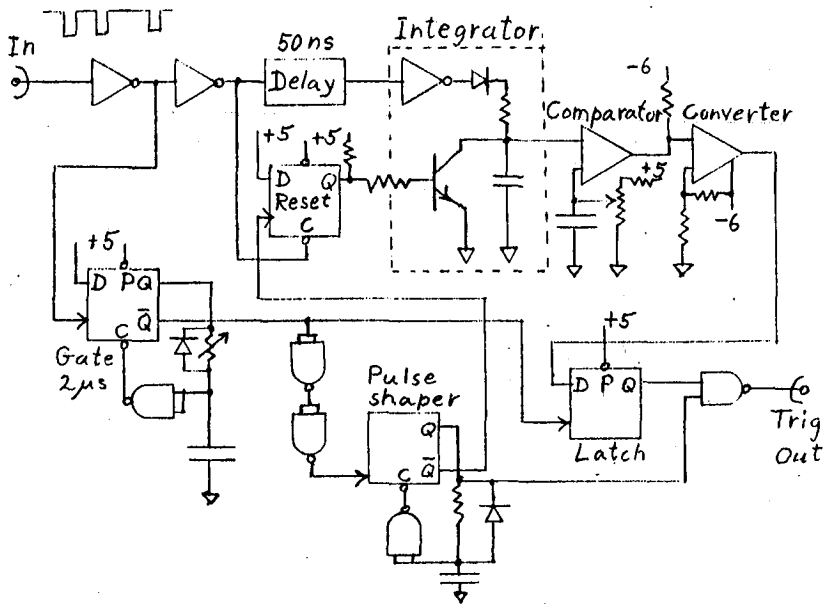


Fig. 2 Pulse-train trigger; integrated width.

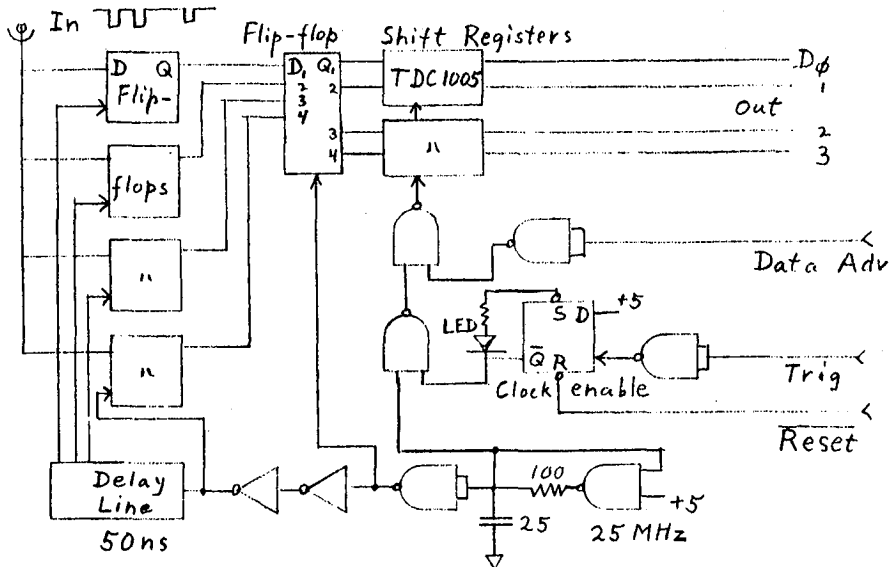


Fig. 3 100 MHz shift register.



## EXPECTED RATES WITH MINI-ARRAYS FOR AIR SHOWERS

Wayne E. Hazen  
 Randall Laboratory of Physics  
 University of Michigan  
 Ann Arbor, MI 48109, USA

1. Introduction. As a guide in the design of mini-arrays used to exploit the Linsley effect in the study of air showers, it is useful to calculate the expected rates. The results can aid in the choice of detectors and their placement or in predicting the utility of existing detector systems. Furthermore, the potential of the method can be appraised for the study of large showers. Specifically, we treat the case of a mini-array of dimensions small enough compared to the distance of axes of showers of interest so that it can be considered a point detector.

The input information is taken from the many previous studies of air showers by other groups. The calculations will give: (a) the expected integral rate,  $F(\sigma, \rho)$ , for disk thickness,  $\sigma$ , or rise time,  $t_{1/2}$ , with local particle density,  $\rho$ , as a parameter; (b) the effective detection area  $A(N)$  with  $\sigma(\min)$  and  $\rho(\min)$  as parameters; (c) the expected rate of collection of data  $F_L(N)$  versus shower size,  $N$ . The latter is flatter than the number spectrum because the detection area increases with  $N$ .

2. Method. The required input relations are:

- (a) the shower disk thickness,  $\sigma \approx Br^\beta$  (1), which is a passable form for the large values of core distance,  $r$ , of interest here;
- (b) the particle density distribution,  $\rho \approx CNr^{-n}$  (2), where  $N$  is the total number of particles and, again, the simple form is adequate for our purposes;
- (c) the number spectrum,  $F(N) = DN^{-\gamma}$ , or  $f(N) = -\gamma DN^{-\gamma-1}$  (3), where a constant value of  $\gamma$  is an approximation adequate to our purposes.

(A) The frequency of Linsley events is obtained from

$$F(\sigma, \rho) = \int_{N(\min)}^{\infty} A(N)f(N)dN \quad (4)$$

where

$$A(N) = \pi(r_{(\max)}^2 - r_{(\min)}^2) \quad (5)$$

and  $r(\min) = (\sigma/B)^{1/\beta}$  from (1) (6) and  $r(\max) = (CN/\rho)^{1/n}$  from (2) (7) and, finally,  $N(\min) = (1/C)B^{-n/\beta} \sigma^{n/\beta} \rho$  (8) which comes from  $A(N(\min)) = 0$  (see (5) above).

The result is:

$F(\sigma, \rho) = \pi C \gamma B^{(n\gamma-2)/\beta} D(1-\gamma/(\gamma-2/n)) \rho^{-\gamma} \sigma^{(2-n\gamma)/\beta}$  (9), where the constants are defined in (1), (2), and (3) above.

(B) The effective detecting area,  $A(N)$ , obtained from (5), (6), and (7), is  $A(N) = \pi C^2/n \rho^{-2/n} N^{2/n} - \pi B^{-2/\beta} \sigma^{2/\beta}$  (10).

(C) The expected rate of collection of data versus shower size is

$$F_L(N) = \int_N^{\infty} A(N)f(N)dN \quad (11)$$

which gives:  $F_L(N) = \pi C^2/n_D (\gamma/(\gamma-2/n)) \rho^{-2/n} N^{-\gamma+2/n} - \pi B^{-2/\beta} D \sigma^{2/\beta} N^{-\gamma}$  (12).

The Haverah Park Group reduce their data to energy of the incident primary and, therefore, give an energy spectrum,  $F(E)$ , rather than a shower size spectrum,  $F(N)$ . The rate calculations above are directly applicable with  $N$  replaced by  $E$ , since the approximations are about equally valid.

3. Numerical Results. In order to get a tentative idea of actual rates, values for the constants were obtained from a brief survey of the literature.

For (1), we have Linsley's fit to his Volcano Ranch data<sup>1</sup>, which has been corroborated by others as far as average values are concerned. Thus  $\sigma = 2.6(1 + r/30)^{1.5}$  (nsec) gives  $\sigma \approx 1.58 \times 10^{-2} r^{1.5}$  (nsec) that is,  $B = 1.58 \times 10^{-2}$  and  $\beta = 1.5$ .

For (2), the Akeno Highlands data with scintillators reported at Bangalore<sup>2</sup> seem appropriate since they are for large showers and extend out to  $r > 1000m$ . The constants in (2), for large  $r$ , are  $C = 853$  and  $n = 3.8$  for  $\rho$  to be in particles/m<sup>2</sup>.

For (3), the reviews by Hillas<sup>3</sup> give summaries of determinations of the frequency shower-size spectrum. The constants obtained for (3) for large showers are  $D = 318$  and  $\gamma = 1.7$ .

The above are plotted in Figs. 1 and 2. Some rates for accidentals (see below) are also shown.

In the case of the deep water Cerenkov detectors of Haverah Park,  $t_{1/2}$  replaces  $\sigma$  in (1). The constants in (1), determined from the data in the World Catalogue<sup>4</sup>, are  $B = 0.14$  and  $\beta=1$ . The constants obtained<sup>5</sup> for (2) are  $C = 7.8 \times 10^{-9}$  and  $n = 3.5$ . As stated earlier, it is convenient to do (3) in terms of  $E$  (of the primary) in place of shower size,  $N$ . The constants become<sup>5</sup>  $D = 3.5 \times 10^{27}$  and  $\gamma = 2.17$ , when  $E$  is in eV. The results are also plotted in Figs. 1 and 2.

4. Accidental Rate. A basic limitation to the sensitivity of the method is due to accidental time clustering of pulses that are unrelated. The accidental rate,  $R$ , of occurrence of  $m$  pulses within a time window  $\tau$  when the rate is  $f$  can be written  $R = f^m \tau^{m-1}$ .

The particle rate  $J \times S$  (where  $J$  is the omni-directional flux and  $S$  the total detector area) can be a good approximation to  $f$  with the usual sort of detectors used in shower studies. There is generally a shoulder in the free running pulse height distribution and consequently a minimum pulse height,  $P_v$ , can be chosen such that the particle detection efficiency is high and signal/noise is also high (Fig. 3). The pulse rate is then approximately equal to the particle rate. Since  $\sigma$  is the FWHM value, the effective window width,  $\tau$ , is, say,  $\sim 1.5\sigma$ .

We then have  $R = (JS)^m (1.5\sigma)^{m-1}$  (13). In Fig. 1, we show examples for  $m=4$  and two areas,  $S=2$  or  $4m^2$ , that we are using in exploratory runs. The particle densities are then  $\rho=1$  or  $2m^{-2}$ , and the singles rates  $f \approx 300$  or  $600 s^{-1}$ . (The accidental rate for  $m=3$  is dominated by  $\mu \rightarrow e$  plus a single!)

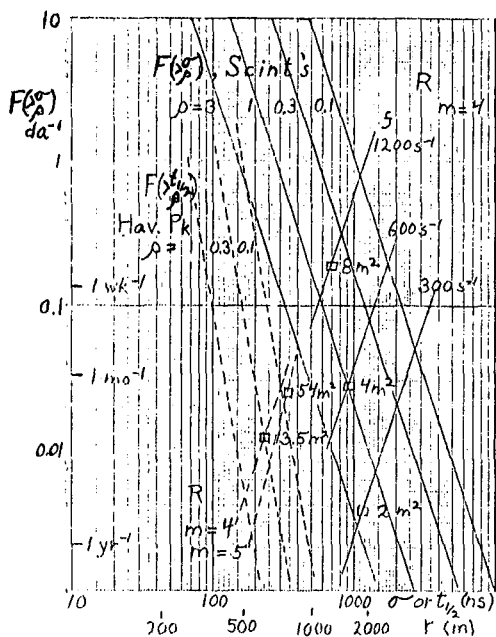


Fig. 1

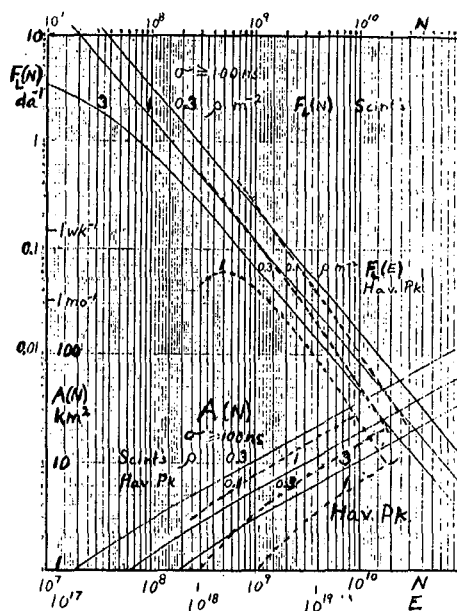


Fig. 2

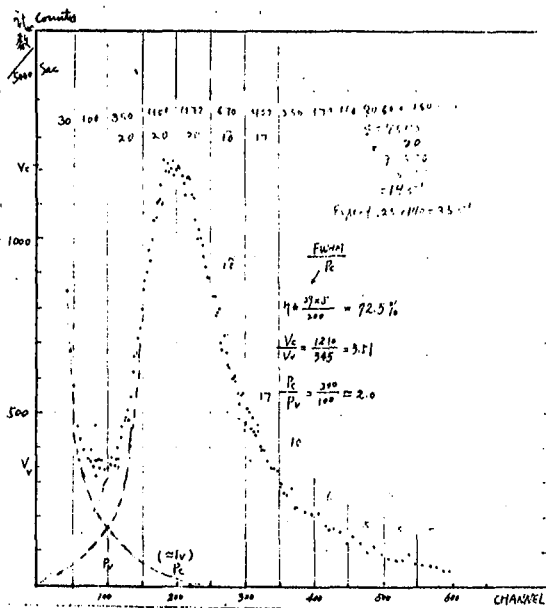


Fig. 3

5. Conclusions. The above predictions show that it is necessary to go down to low particle densities,  $\rho$ , in order to get a good rate for large showers. But, to limit the uncertainties, the size of the particle sample,  $\approx m$ , cannot be too small. Thus, the total detector area,  $S (=m/\rho)$  must be as big as feasible. However, as the area is increased, the "singles" rate increases with consequent increase in accidental rate.

The relationships among the above are implicit in Fig. 1. It may be more graphic to use total detector area,  $S$ , as abscissa with  $m$  and  $\sigma$  as parameters. This is done in Fig. 4, with shower rate  $F(S)$ , solid lines, and accidental rate  $R(S)$ , dashed lines, as ordinates. Numerical values of the parameters,  $m$  and  $\sigma$ , are written near the lines.



Fast Scintillation Counter Preamplifier  
for the Observation of Linsley Effect

L.K. Ng  
Physics Department, University of Hong Kong  
Hong Kong

Abstract

A fast preamplifier circuit has been designed and thoroughly tested for the purpose of observing the air shower arrival directions including the Linsley effect. The circuit intends to eliminate the time jitter due to variation of scintillation counter signal amplitudes. It assumes that the output signals from one counter system have the same rise time. On this basis, error arising from time jitter is removed by voltage discrimination at about half signal amplitudes. Detailed description of the circuit is reported.

1. Introduction. In the investigation of cosmic ray extensive air showers, it is often required to determine the particle arrival time at various detection stations of a shower array, in order to find the shower arrival direction. This applies to our observation of the Linsley effect in large air showers described in a paper (HE 4.7-10) at this conference, and to the determination of the shower arrival directions incident on our shower telescope given in another paper (HE 4.5-14) at this conference.

Large area plastic scintillators are commonly used for the above purpose because of their fast response to traversing shower particles. However, the signals obtained from a scintillation counter has a finite rise time typically in the range of 10 ns - 100 ns. Its magnitude depends chiefly on the counter geometry which affects the optical paths, and on the quality of the photomultiplier. This finite rise time gives rise to time jitter when signals of varying amplitudes are subjected to a constant voltage discrimination as illustrated in figure 1. Hence, for precise arrival time measurement, this time jitter cannot be overlooked. An anti-jitter preamplifier is therefore designed.

2. Design principles. Two criteria are adopted for the present design: (i) the rise time of counter output signals is assumed to be a constant characteristic of the counter system, and (ii) there is no signal pile-up at the counter output with proper choice of the output RC coupling. These criteria ensure that the pulses to be processed by the preamplifier are of proper shape. From criterion (i), if each pulse is discriminated at its half signal amplitude, the time relation between the incidence of a particle and the leading edge of the discriminated output pulse is a

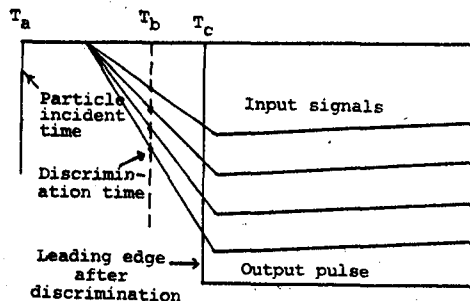
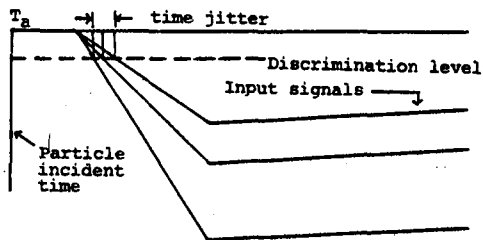


Fig. 1 Time jitter due to fixed voltage discrimination.

Fig. 2 Discrimination at the half signal amplitude.

constant as illustrated in figure 2. The time relation is indicated by the particle incident time  $T_a$ , the time at half amplitude  $T_b$  and the leading edge  $T_c$  of the discriminated output. The delay time ( $T_c - T_a$ ) is a constant independent of signal amplitudes. The discrimination is done at half signal amplitudes, because the slope of the leading edge of the input signal is sharpest at this position.

To achieve the above result, the the following design is carried out:

- a. In order to provide a reference voltage equal to the half amplitude of an input signal, one branch of the input is connected to a simple 1:1 potential divider, so that the signal amplitude is halved and its peak level can then be used as a reference voltage.
- b. Since the reference voltage must be established before the arrival of the input pulse at the discriminator input, another branch of the input is connected to a long coaxial cable in order to delay the input signal for a fixed interval of time  $t_d$ . The time relation between the reference voltage signal and the delayed signal is shown in figure 3.

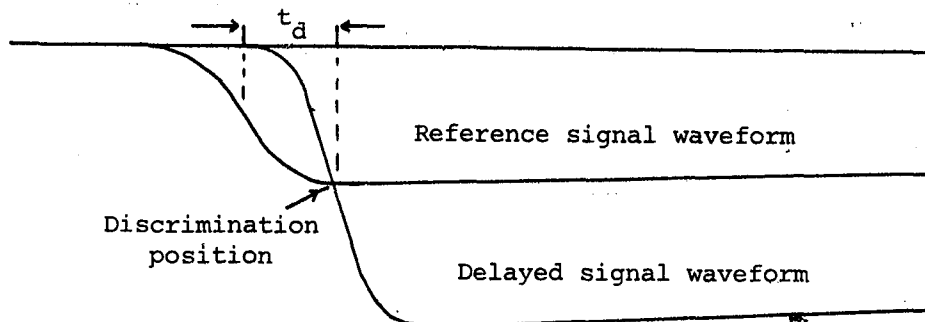


Fig. 3 The time relation of the signal waveforms.



shifters provide sufficient power to drive the coaxial cable and the potential divider respectively.

The fixed reference voltage of the discriminator B is controlled by the potentiometer P3. Output pulses from B are shaped by a monostable shaper and the strobe pulses obtained then gate the discriminator A as required.

4. Discussions. It should be noted that in the discriminator A, the base line voltage of the signal input must be slightly higher than that of the reference voltage input for the discriminator to work. This fixed voltage difference causes slight deviation of the reference voltage from the true half amplitude level. Since the difference is not proportional to the input signal amplitude, a jitter can therefore be introduced. This jitter obviously depends on the rise time of the photomultiplier signals, but is very small, (well within 5 ns for a large rise time of 100 ns).

It should also be pointed out that the circuit is sensitive to high frequency ringing. Therefore, decoupling capacitors are found at various power supply points. The shortest ground path is required for each of these capacitors. The recommended layout of the printed board is to have the circuit on one side of the board only and the other side a ground plane.



## A Mini-array for Large Air Showers

L.K. Ng and S.K. Chan  
Physics Department, University of Hong Kong  
Hong Kong

W. Hazen and E. Hazen  
Physics Department, University of Michigan  
U.S.A.

## Abstract

A mini-array that utilizes the Linsley effect is proposed for the measurement of large air showers. An estimate of the detectable shower rates for various shower sizes is made. Details of the detection and data collection systems are also described.

1. Introduction. Interest in the measurement of large air showers has been enhanced by the conflicting result reported in 1982 (Yakutsk<sup>1</sup>). However, since intensities of large air showers are extremely low and only a few large centres are able to do the measurement, it was proposed by J. Linsley<sup>2</sup> that more independent measurements could be done with rooftop mini-arrays by making use of the particle arrival time distributions (Linsley effect). This idea has been pursued by us, and the present proposed system is the result after looking into various problems associated with such mini-arrays.

2. Theoretical estimation. To be able to measure the arrival time distribution, at least two particles per event are required. With a mini-array of  $2 \text{ m}^2$ , a threshold density of the shower particles arriving at this mini-array should be  $\rho_1 = 1 \text{ m}^{-2}$ . Using the differential intensity expression,

$$j(N, \theta) = j(N) \cos^{\alpha} \theta ,$$

with  $\alpha = 8.6$  at sea level, the shower rate for large showers with size  $N$  to  $N + \delta N$  should be

$$\begin{aligned} \phi(N) \delta N &= 2\pi j(N) A(N) \delta N \int_0^{\pi/2} \cos^{\alpha+1} \theta \sin \theta d\theta \\ &= \frac{2\pi}{\alpha+2} j(N) A(N) \delta N, \end{aligned}$$

where  $A(N)$  is the area containing the cores of all the air showers detected by the mini-array. Hence the integral shower rate is

$$\phi(>N_{\min}) = \frac{2\pi}{\alpha+2} \int_{N_{\min}}^{\infty} j(N) A(N) dN.$$

The area  $A(N)$  is an annular ring with its outer radius determined by the density threshold  $\rho_1 = 1 \text{ m}^{-2}$  and its inner radius determined by the minimum time spread  $\sigma_1$  selected. Therefore, it has the form,

$$A(N) = \pi \left[ \left( \frac{CN}{\rho_1} \right)^{2/n} - \left( \frac{\sigma_1}{B} \right)^{2/\beta} \right]$$

Hillas' integral intensity spectrum<sup>3</sup>,

$$J(>N) = 8.10^{-12} (N/10^8)^{-1.7} \text{ m}^{-2} \text{ sr}^{-1} \text{ s}^{-1}$$

is used to determine  $j(N)$ , and Linsley's empirical formula<sup>2</sup>,

$$\sigma(\text{ns}) = 2.6 \left( \frac{r}{30} + 1 \right)^{1.5} \text{ with } r \text{ in m}$$

is used to relate the time spread  $\sigma$  to the core distance  $r$  from the mini-array. The lateral distribution of electrons at Akeno<sup>4</sup> for large showers,

$$\rho = 5.10^{-5} N (r/r_0)^{-3.8} \text{ with } r_0 = 79 \text{ m}$$

is used to relate  $\rho$  to  $r$ .

The final expression for the shower rate is given by

$$\phi(>\sigma_1, >\rho_1) = 9.07 \cdot 10^6 \rho_1^{-1.7} \sigma_1^{-2.97} \text{ day}^{-1},$$

and the values are tabulated below.

$\rho_1 (\text{m}^{-2})$	$\sigma_1 (\text{ns})$	$N_{\min}$	Shower rate ( $\text{day}^{-1}$ )
1	50	$9.07 \cdot 10^5$	81.6
1	100	$6.25 \cdot 10^6$	10.4
1	200	$3.04 \cdot 10^7$	1.33
1	300	$8.49 \cdot 10^7$	0.40
1	400	$1.76 \cdot 10^8$	0.17

Table I

3. Detection system. From the estimation given in Table I, it is clear that a mini-array so constructed should be able to pick out the very few large air shower events from a swarm of irrelevant events including the counter noises, the background soft radiations and the small air showers. Fast electronics is also required for the determination and collection of the arrival time spread.

In order to eliminate the large number of small air showers, a minimum time spread  $\sigma_1$  has to be assigned. According to Table I, for a mini-array of  $2 \text{ m}^2$ , a minimum acceptable shower size of  $9.07 \cdot 10^5$  requires a minimum time spread  $\sigma_1$  equal to 50 ns.

A mini-array of 2 m<sup>2</sup> is then assembled which consists of 8 pieces of plastic scintillators each with dimensions 0.5m x 0.5m x 0.05m. In view of the small particle density encountered, each scintillator is not expected to receive more than one particle at a time from a shower.

Each scintillator is viewed by two 5" photomultipliers, the signal coincidence of which practically eliminates all the counter noises. In order to exclude the background soft radiations, the array is shielded by thin sheets of galvanized iron (0.5mm thick). Particle track identification may be found necessary at a later stage to ascertain genuine large shower events. This can be done by sandwiching the array by 4 layers of small diameter proportional counters.

The mini-array is placed in another small air shower array system, which may provide additional information on the nature of showers received.

4. Fast electronics. Precise measurement of the particle arrival time is essential in this experiment, and hence an anti-jitter preamplifier per counter is employed to remove the time jitter between the particle arrival time and the signal output time. The preamplifier as shown in figure 1 is a slightly modified version of the circuit described in another paper (HE 4.7 - 9), and the modification provides another coincidence input from a second photomultiplier.

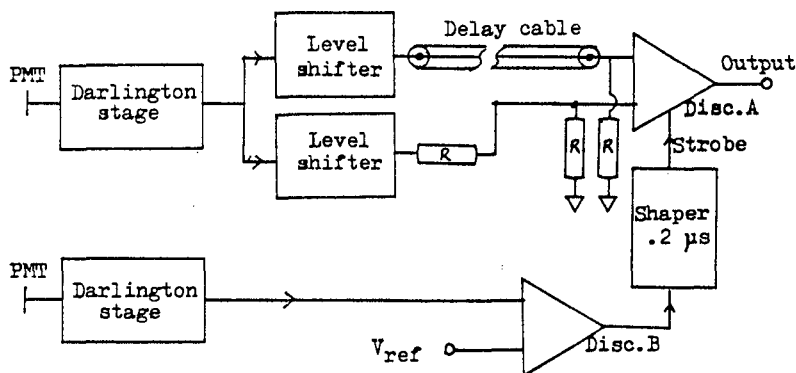
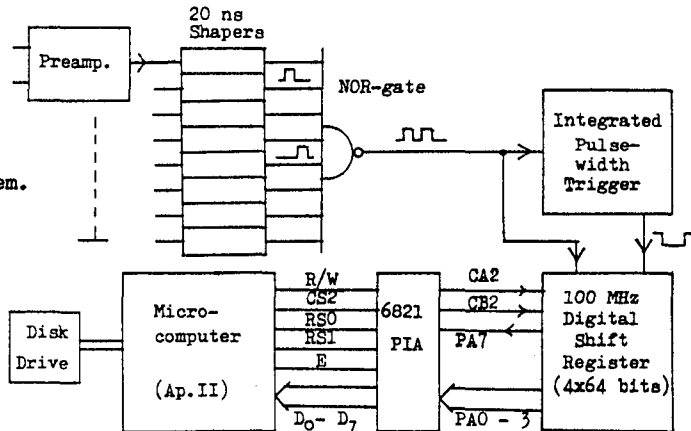


Fig. 1 Counter preamplifier.

Outputs from the eight counter preamplifiers are individually shaped to narrow pulses of 20 ns each, and then combined together to give a train of narrow pulses per shower. The time delay in each of the 8 channels from the particle arrival to the pulse output after combination has been equalized by adjusting the length of the delay cable in each preamplifier. The number of pulses in the train depends on the number of counters giving out particle signals, and the relative positions of the pulses in the train depend on their particle arrival time. The circuit block diagram is given in figure 2.

Fig. 2 The electronic system.



The pulse train is temporarily stored in a set of four shift registers. The shift registers have  $4 \times 64$  bits in total and hence can readily store  $2 \mu\text{s}$  of information. The clock rate for accepting the pulse train is equivalent to  $100 \text{ MHz}$ . Consequently, it provides a time resolution of  $10 \text{ ns}$  in the measurement of particle arrival time.

The criteria for recording a pulse train temporarily stored in the shift registers are (i) at least two pulses are found in the train, and (ii) the time spread of the pulses should not be less than  $\sigma_1$ . Criterion (i) is dealt with by means an integrated pulse-width trigger circuit. Its basic element is given in figure 3. The charge accumulated in the capacitor  $C$  is proportional to the number of pulses in the train. A trigger pulse can be produced from the circuit at a pre-selected discrimination level. The trigger pulse then transfers data to the microcomputer shown in figure 2. Criterion (ii) is conveniently handled by software means after the data is read into the microcomputer.

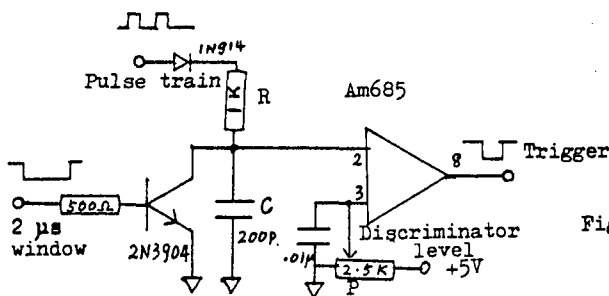


Fig.3 The integrator.

The above system has been assembled and thoroughly tested.

#### Reference.

1. Diminstein O S et al, 8th Eur.Cosmic-ray Symp. (Rome), 1982
2. Linsley J, (preprint).
3. Hillas A M et al, Phys. Reports, 20C (1975) 79.
4. Hara T et al, Proc. 18th ICRC (Bangalore), 11 (1983) 276.

A NOTE ON SOME STATISTICAL PROPERTIES OF RISE TIME  
PARAMETERS USED IN MUON ARRIVAL TIME MEASUREMENTS

D.J. van der Walt and E.J. de Villiers  
PU-CSIR Cosmic Ray Research Unit,  
Department of Physics,  
Potchefstroom University for CHE,  
Potchefstroom, 2520.  
South Africa.

## 1. Introduction

Most investigations of the muon arrival time distribution in EAS during the past decade made use of parameters which can collectively be called rise time parameters. We will follow the definition of Blake et al. (1981) and define the rise time parameter  $T_{A/B}$  as the time taken for the integrated pulse from a detector to rise from A% to B% of its full amplitude. The use of these parameters are usually restricted to the determination of the radial dependence thereof. This radial dependence of the rise time parameters are usually taken as a signature of the particle interaction characteristics in the shower. As these parameters have a stochastic nature, it seems reasonable to us that one should also take notice of this aspect of the rise time parameters. The aim of this paper is therefore to present a statistical approach to the rise time parameters, as this has not been done in the past.

## 2. Order statistics and rise time parameters

From the definition of  $T_{A/B}$  it is reasonable to assume that on the average A% of the total number of particles which gave rise to the output pulse from the detector have arrived in the time  $T_{0/A}$ . A sample quantile of order  $p$  is defined as follows: Let  $(X_1, X_2 \dots X_n)$  be a random sample of size  $n$  of a random variable  $X$  with probability density function (pdf)  $f(t)$ . Let  $(X_1^{(n)}, X_2^{(n)} \dots X_n^{(n)})$  be an arrangement of  $(X_1, X_2 \dots X_n)$  such that  $X_1^{(n)} \leq X_2^{(n)} \leq \dots \leq X_n^{(n)}$ .  $X_i^{(n)}$  is called the  $i$ -th order statistic. The sample quantile of order  $p$ ,  $0 < p < 1$ , is defined to be the order statistic  $X_k^{(n)}$  for which  $k = [np] + 1$ , where  $[np]$  is the greatest integer not larger than  $np$ . This definition states that a fraction  $p$  of the sample values is less than  $X_k^{(n)}$ . This corresponds exactly to the definition of  $T_{0/A}$ . The rise time parameter  $T_{A/B}$  corresponds therefore to the difference between two order statistics of the sample. The statistical properties of  $T_{A/B}$  can therefore be determined from the properties of the difference between two order statistics.

We now give a number of properties which are very useful. The following notation is used:  $f_k^{(n)}(t)$  is the pdf of  $X_k^{(n)}$ ,  $w_{k\ell}^{(n)}(t)$  is the pdf of  $X_\ell^{(n)} - X_k^{(n)}$ ,  $F(t)$  is the distribution function of the random variable  $X$ , i.e.  $F(t) = P(X \leq t)$ , and  $g^{(n)}(t)$  is the pdf of the arrival times of muons with respect to the first detected muon.

- (i)  $f_k^{(n)}(t) = C f(t) [F(t)]^{k-1} [1-F(t)]^{n-k}$  with  $C = n! / (k-1)!(n-k)!$
- (ii)  $w_{k\ell}^{(n)}(t) = C \int_0^\infty f(t)f(x+t) [F(t)]^{k-1} [F(x+t)-F(x)]^{\ell-k-1} [1-F(x+t)]^{n-k} dx$   
with  $C = n! / (k-1)!(n-k)!(\ell-k-1)!$

(iii)  $\lim_{n \rightarrow \infty} P(|X_k^{(n)} - a_p| \geq \epsilon) = 0$  for  $\epsilon > 0$ ,  $k = [np] + 1$ , and  $a_p$  is the

population quantile of order  $p$ .

(iv)  $\lim_{n \rightarrow \infty} f_k^{(n)}(t) = N\left(a_p, \frac{p(1-p)}{nf^2(a_p)}\right)$  (Fisz(1963))

(v)  $\lim_{n \rightarrow \infty} W_{k\ell}^{(n)}(t) = N\left(a_q - a_p; \frac{p(1-p)}{nf^2(a_p)} + \frac{q(1-q)}{nf^2(a_q)} - \frac{a_p a_q}{nf(a_p)f(a_q)}\right)$   
(Swanepoel (1985)).

(vi)  $\lim_{n \rightarrow \infty} g^{(n)}(t) = f(t)$  (Van der Walt (1984)).

Property (iii) states that the sample quantile converges stochastically to the population quantile. Properties (iv), (v) and (vi) give the limiting distributions of  $f_k^{(n)}(t)$ ,  $W_{k\ell}^{(n)}(t)$  and  $g^{(n)}(t)$ . The rise time parameters will then also have the above properties.

The significance of these results is further that it is possible to examine specific properties of the rise time parameters without having to simulate air showers. It must be made clear at this point that points (i) to (vi) does not add directly to the understanding of the physics involved in shower development. We feel, however, that it gives one a firm basis from which one can understand the properties of the measured rise time parameters.

### Discussion

Consider, for example, property (iii). For the case of EAS, the arrival of the hypothetical shower front can be considered as the time  $t=0$  from which timing measurements can be made. In this case  $f(t) = 0$  for all  $t \leq 0$ , and we can allow  $p$  to be equal to zero. Then  $X_1^{(n)}$ , corresponds to the zeroth order sample quantile while  $a_p = a_0 = 0$ . We then have  $\lim_{n \rightarrow \infty} P(|X_1^{(n)} - 0| \geq \epsilon) = 0$ , which means that the arrival time of the first detected muon with respect to the shower front converges stochastically to zero. This means that for large samples one can consider the first detected particle as the time  $t = 0$ . Property (vi) is equivalent to what has just been said.

In figure 1 we show the arrival time distribution of muons together with the arrival time distribution of muons when the first detected muon was taken as the time  $t = 0$ . The difference at small delays is due to the fact that the sample size was only ten.

In figure 2 we present the relationship between  $\langle X_5^{(5)} - X_1^{(5)} \rangle$  and  $\langle X \rangle$  for the case when  $f(t)$  is a gamma density function. The same relationship was found to exist for larger samples. It is also possible to show that this linear relationship exists for a wide variety of density functions. In figure 3 we present the relationship between  $\langle X_{10}^{(10)} - X_1^{(10)} \rangle$  and  $\langle X \rangle$  for shower simulation data.  $X_i^{(10)}$  is the  $i$ -th order statistic for a sample of 10 muon arrival times measured in a detector and  $\langle X \rangle$  is the mean muon arrival time. It can be seen that the relationship is also linear even though we do not know the parametric form of the muon arrival time distribution. This example also illustrates that it is not necessary to

determine the properties of the rise time parameters through the simulation of air showers. It should also be noted from figure 2 that  $\langle X_k^{(n)} - X_k^{(n)} \rangle$  does not determine  $\langle X \rangle$  uniquely. This is an example of some of the limitations of rise time parameters.

### Conclusion

With the above examples we have tried to illustrate that there exist a statistical basis for the rise time parameters. We believe that the statistical properties of rise time parameters may be of use not only for the analysis of experimental data but also for the planning of experiments.

### References

1. Blake, P.R.; P.J. Connor, D.M. Mann, W.F. Nash, B. O'Connell and R.B. Strutt: Nuclear Instruments and Methods, 188 (1981).
2. Fisz, M.: Probability Theory and Mathematical Statistics, 3rd edition, John Wiley and Sons (1963).
3. Swanepoel, J.W.H. (1985). Personal communication.
4. Van der Walt, D.J. (1984). D.Sc.Thesis, Potchefstroom University.

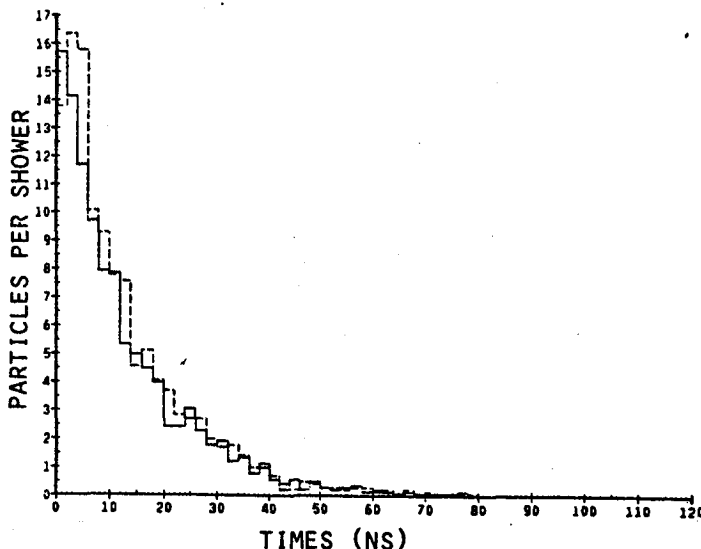


Figure 1 Comparison between  $g^{(10)}(t)$  and  $f(t)$  for 14 Fe-initiated showers. —  $f(t)$ , ---  $g^{(10)}(t)$ .  $110m \leq R \leq 120m$ ,  $E_{\mu} \geq 1 \text{ GeV}$

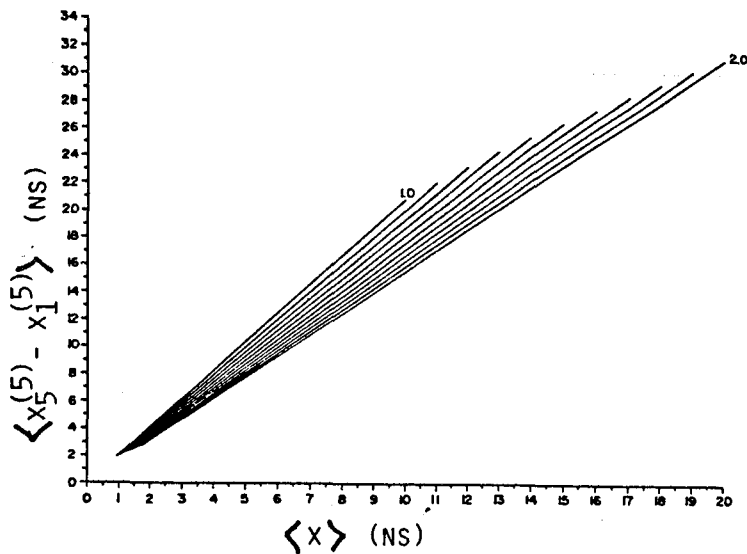


Figure 2 Relationship between  $\langle X_5^{(5)} - X_1^{(5)} \rangle$  and  $\langle X \rangle$  for a number of gamma random variables for which  $1 \leq \langle T \rangle^2 / \sigma_T^2 \leq 2$ .

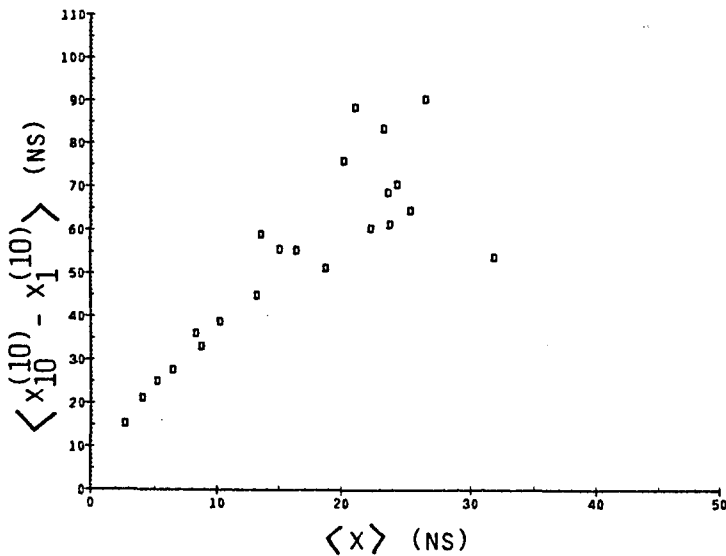


Figure 3 Relationship between  $\langle X_{10}^{(10)} - X_1^{(10)} \rangle$  and  $\langle X \rangle$  for 14 Fe-initiated showers.  $E_\mu > 1$  GeV.



## SUB-LUMINAL PULSES FROM COSMIC RAY AIR SHOWERS

John Linsley  
Department of Physics and Astronomy  
University of New Mexico, Albuquerque, NM 87131  
USA

## ABSTRACT

Some of the signals produced by air showers in scintillators possess a distinctive feature, a 'sub-luminal pulse' (SLP) following the normal one with a time delay of approximately 1.5 r/c. The average amplitude of the SLP corresponds to an energy deposit of about 50 MeV, three times as much as is deposited in a typical scintillator by vertical minimum ionizing muons. The SLP account for approximately 5% of the energy deposited in the atmosphere by air showers with energy  $> 10^{10}$  GeV at impact parameters  $> 1$  km. Assuming with Greisen that these pulses are due to neutrons travelling with a speed slightly less than  $c$ , they provide a unique means of estimating  $E_h$ , the energy deposited by slow hadrons, in showers of this very high energy. On the other hand, if not allowed for properly, these pulses are liable to cause errors in estimating the impact parameters of large showers from pulse width observations.

1. Introduction. There are two reasons for regarding the phenomenon reported here as more than a mere curiosity: 1) it may prove to be useful as an additional indicator of primary mass, and 2) if it is not taken into account properly it can cause errors in estimating shower size from measurements of particle density and arrival time spread by means of a mini array (Linsley 1983).

When air showers (AS) were first observed at very large values of the impact parameter it was found that signals produced in thin scintillators were unexpectedly broad (Linsley *et al.* 1961, Linsley and Scarsi 1962). Recently some of the records of the experiment were re-examined in connection with a controversy about very large AS with  $E > 10^{10}$  GeV (Bower *et al.* 1982, 1983). Such records (oscilloscope photographs) still exist for more than 500 events registered during 1962-63, including 16 which were qualified, by satisfying the above energy condition, for inclusion in the *Catalogue of Highest Energy Cosmic Rays* (Linsley 1980). The experimental method as it relates to the present discussion is described by Linsley and Scarsi (1962); for a complete bibliography see (Linsley 1980).

2. Observations. It was noticed that the scintillator signals from these AS frequently possess a sort of after-pulse, called for reasons explained below an SLP (sub-luminal pulse). To account for the name, signals with delays  $< r/c$  can be produced by 'luminal' particles travelling at essentially the speed of light. Almost all particles in AS are of this type. Signals with greater delays require that the observed energy be transported from the shower core at 'sub-luminal' velocities appreciably  $< c$ . For  $r > 1$  km such signals are easily recognized in the Volcano Ranch data

(double pulse resolving time  $\sim 3 \mu\text{s}$ ). Sixteen of them were discovered while re-examining the events listed in the Catalogue. Tracings are shown in Fig. 1, together with tracings of a typical bandwidth-limited (BWL) test pulse and a typical train of 1 MHz timing pulses.

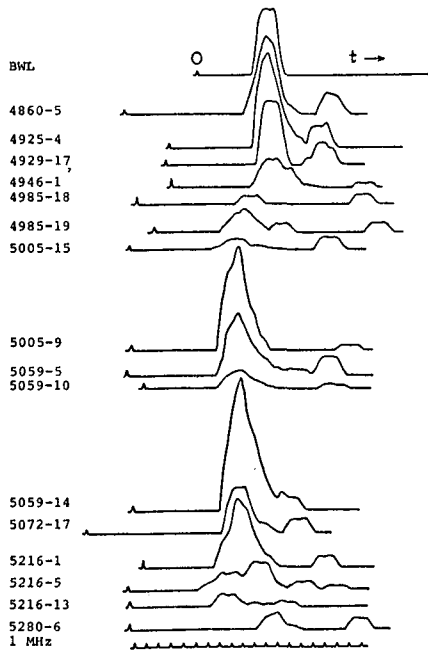


*Fig. 1. Scintillator signals showing SLP, identified by event No. and channel No., with a typical bandwidth-limited test pulse (BWL) and a typical train of 1 MHz timing pulses.*

identical to pulses of the same size from smaller showers, the differences there are, in average pulse duration, fail to account for the strong shower size dependence seen in Fig. 2. Ignoring therefore the differences there are, in pulse duration, I take it that the fraction of DP in small-shower pulses gives an upper limit for the percentage of DP that might be spurious. I conclude that no more than 10% of the DP in large showers (size  $N > 10^9$ ) are in fact instrumental, or accidental.

In case of very large showers (highest 3 bins) about half of the DP are sub-luminal. The trend seen in Fig. 2 can be explained as follows:

In order to rule out instrumental effects such as photomultiplier after-pulsing as the source of delayed pulses, the following tests were made:

1) All 1962-63 AS signals in the same size range as signals preceding the Fig. 1 SLP were scanned for the presence of delayed pulses. (The pulses preceding the SLP have integrated charge values 4 to 40 times the average for vertical minimum ionizing muons.) In 132 cases out of 1648 the prompt pulse was followed after 3 to 10  $\mu\text{s}$  by a well defined delayed pulse (DP). It was determined that the fraction of DP was the same within statistical errors for all 19 channels corresponding to the 19 scintillators making up the Volcano Ranch array.

2) The 1648 DP candidates were then sorted according to shower size, using bins a factor of 2 in width. It was found that the showers in the two lowest-size bins (41 candidate pulses) had no DP, and that showers in the next higher bin (169 candidates) had only 3 DP. The fraction of DP in larger showers increased steadily as shown in Fig. 2, reaching a value  $\sim 0.2$  for the highest 3 bins.

While it is not quite true that pulses of a given size from large showers are

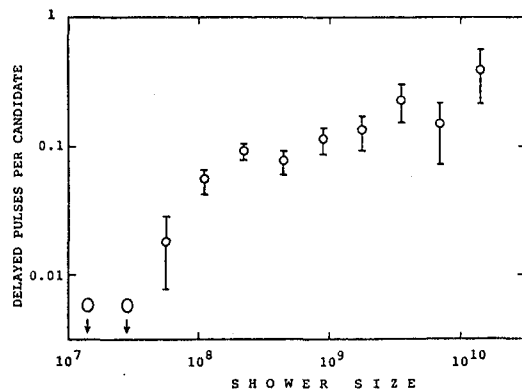


*Fig. 2. Fraction of signals with delayed pulses vs shower size, for densities 4-40 particles per  $3.26 \text{ m}^2$  scintillator area.*

as one goes from very large showers to smaller ones (right to left in the figure) the impact parameter corresponding to the accepted range of pulse amplitudes decreases, and so does the critical delay separating the luminal and sub-luminal regimes. By the time one reaches shower size  $3 \cdot 10^8$ , nearly all DP (which are required to have delays  $> 3 \mu\text{s}$  so as to be clearly resolved) are sub-luminal. As one goes to still smaller sizes the SLP begin to merge with the prompt pulses, until finally (for  $N < 3 \cdot 10^7$ ) all of them have merged, and no more DP are found using the definition adopted here.

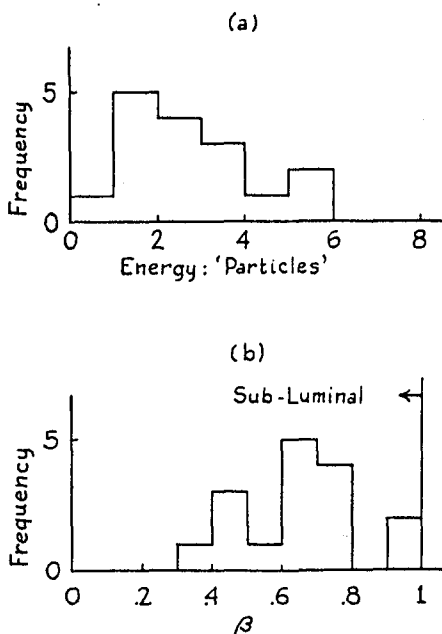


Fig. 3. Distribution of deposited energy (a) and transport velocity (b) for 16 SLP.

latest pulse is a superposition of 2 BWL signals. Only the later, larger one satisfies the condition: delay (with respect to the shower plane)  $> r/c$ . With two exceptions, the one just noted and 5059-14, the SLP seem to be completely resolved from the normal particles by that condition alone. Additional evidence that SLP are a distinct phenomenon is given by Fig. 3b. The most frequent examples are not the ones that just marginally satisfy the selection condition, they are those with time delay  $\sim 1.5 r/c$  ( $\beta \sim 0.7$ ).

Fig. 4 shows the ratio of SLP to normal particles in various  $r$  intervals, for all signals with particle density  $< 10 \text{ m}^{-2}$  (hence sufficiently undistorted by the electronic system for DP to be recognizable) and  $r > 1 \text{ km}$ . The average ratio is  $(1.6 \pm 0.4)\%$ , and there is no evidence of any  $r$  dependence. This fact, and the fact that SLP occur in AS with zenith angles in a broad range ( $7^\circ$  to  $55^\circ$  for this sample) suggests that the component which causes them is in equilibrium with the normal particles. Under this assumption the energy deposited in the form of SLP amounts to about 5% of the primary energy. (The scintillation plastic

**3. Results and discussion.** The amplitudes of the Fig. 1 SLP (apparent particle densities) show that the average amount of energy deposited in the scintillators is about 50 MeV, 3 times as much as is deposited by a vertical minimum ionizing muon (see Fig. 3a). If the scintillations are produced by heavily ionizing secondaries, as the low transport velocity suggests may be the case, then the actual deposited energy will be somewhat higher because the response of the plastic scintillator to heavily ionizing particles is nonlinear (Korff 1962).

The time at which the earlier pulse begins (see Fig. 1) corresponds to passage of the shower plane, a plane perpendicular to the axis through the central portion of the particle swarm, determined by means of detectors at relatively small core distances. In most cases the SLP (latest pulse) has no structure; its shape indicates that the energy is deposited in a time interval too small to be resolved. Exceptions are 5216-5 and possibly 4860-5. In case of 4929-17 the

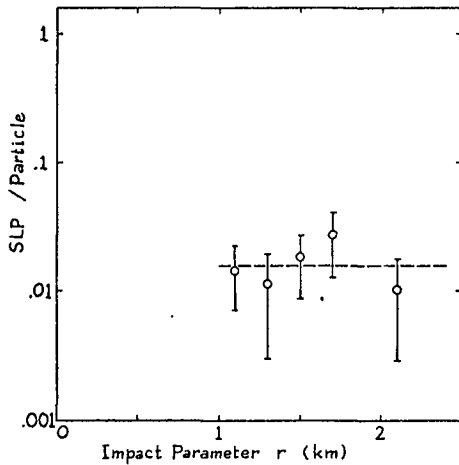


Fig. 4. Abundance of SLP vs impact parameter.

which agrees at face value with the estimate from Fig. 4. But the equilibrium hypothesis needs further testing. In any case, one must still explain the amplitude and delay distributions (Fig. 3). Aside from the present work the only experimental evidence on low energy nucleons in showers with energy  $> 10^6$  GeV is from data taken with a neutron monitor at the Yakutsk array (Kozlov et al. 1981).

**Acknowledgement.** The re-examination of old records was started during a visit to the University of Leeds, assisted by the Science and Engineering Research Council (UK) through the award of a Senior Visiting Fellowship. Discussions with Alan Watson, Michael Hillas and other members of the Leeds AS group played an important part in gaining an understanding of SLP. Rosalind Mendell kindly provided information about the response of organic scintillators to recoil protons. This work was supported in part by the National Science Foundation.

**References.** BOWER, A.J., REID, R.J.O. and WATSON, A.A. 1982, Proc. 8th European Cosmic Ray Symposium (Rome) paper B 1.4; BOWER, A.J., CUNNINGHAM, G., LINSLEY, J., REID, R.J.O. and WATSON, A.A. 1983, J. Phys. G: Nucl. Phys. 9, L53; GREISEN, K. 1956, *Progress in Cosmic Ray Physics*, ed. J.G. Wilson (North-Holland: Amsterdam) 3, 1; 1962, Proc. 5th Interamerican Seminar on Cosmic Rays (Lab. Fisica Cosmica, UMSA, La Paz, Bolivia) 2, XLVII-2; KORFF, S. 1962, *ibid.* (same page); KOZLOV, V.G., KUZMIN, A. I., MIGUNOV, V.M., SKRIPIN, G.V. and UPOLNIKOV, A.A. 1981, Proc. 17th Int. Cosmic Ray Conf. (Paris) 6, 210; LINSLEY, J., SCARSI, L. and ROSSI, B. 1961, Phys. Rev. Lett. 6, 485; LINSLEY, J. and SCARSI, L. 1962, Phys. Rev. 128, 2384; LINSLEY, J. 1980, *Catalogue of Highest Energy Cosmic Rays*, ed. M. Wada (Inst. Phys. Chem. Res., Tokyo: World Data Centre C2) 1, 3; 1983, Proc. 18th Int. Cosmic Ray Conf. (Bangalore) 12, 135; ZATSEPIN, G. T., NIKOLSKII, S.I. and KRISTIANSEN, G.B. 1963, Proc. 8th Int. Cosmic Ray Conf. (Jaipur) 4, 100.

has a composition similar to air.) The explanation of Fig. 2 offered above is based on the same assumption.

**4. Conclusions.** Commenting on the result of Linsley and Scarsi (1962) in the light of his own observations using similar equipment, Greisen opined that "some of the delayed pulses with large delays...are due to neutrons travelling at a speed slightly lower than light" (Greisen 1962). Assuming that SLP and the pulses referred to by Greisen are the same, and accepting his suggestion as to their cause, one notes that for AS with much lower total energies  $\sim 10^6$  GeV the percentage dissipated by low energy hadrons is estimated to be 4 or 5% (Greisen 1956, Zatsepin et al. 1963),

## THICKNESS OF THE PARTICLE SWARM IN COSMIC RAY AIR SHOWERS

John Linsley

Department of Physics and Astronomy

University of New Mexico, Albuquerque, NM 87131

USA

## ABSTRACT

The average dispersion in arrival time of air shower particles detected with a scintillator at an impact parameter  $r$  is described with accuracy 5-10% by the empirical formula  $\langle \sigma \rangle = \sigma_{t0}(1 + r/r_t)^b$ , where  $\sigma_{t0} = 2.6$  ns,  $r_t = 30$  m and  $b = (1.94 \pm 0.08) - (0.39 \pm 0.06) \sec \theta$ , for  $r < 2$  km,  $10^8 < E < 10^{11}$  GeV, and  $\theta < 60^\circ$ . ( $E$  is the primary energy and  $\theta$  is the zenith angle.)

The amount of fluctuation in  $\sigma_t$  due to fluctuations in the level of origin and shower development is less than 20%. These results provide a basis for estimating the impact parameters of very large showers with data from very small detector arrays (mini-arrays). The energy of such showers can then be estimated from the local particle density. The formula also provides a basis for estimating the angular resolution of air shower array-telescopes (conference paper OG9.5-6).

1. Introduction. The particles making up an air shower (AS) travel in a swarm which is remarkably compact near the shower axis. Within 10 m of the axis the thickness is only a meter or two (Bassi *et al.* 1953). But when the thickness was measured at much greater distances it was found unexpectedly to be much greater, tens to hundreds of meters (Linsley *et al.* 1961, hereafter LSR; Linsley and Scarsi 1962, hereafter LS). This result, like the earlier one, was derived from arrival time measurements with scintillators. In reporting it primary emphasis was given to  $t_{\frac{1}{2}}$ , the median delay with respect to the shower plane. This is a plane perpendicular to the axis through the central portion of the particle swarm, determined from timing data at relatively small distances. It was shown that for a given impact parameter  $r$ , the median delay decreases with increasing zenith angle  $\theta$ , and it was pointed out that by a simple kinematic argument the median time delay of the essentially unscattered muon component (observed in the same experiment using a shielded scintillator) provides an estimate of the median production height of the muons (LS).

This behavior at large distances was soon confirmed by J.G. Wilson and his collaborators using an array of deep water Cerenkov detectors at Haverah Park. Painstaking studies showed that  $t_{\frac{1}{2}}$  measured with these detectors depends not only on  $\theta$  but also on primary energy (Baxter *et al.* 1965, Walker and Watson 1981). They showed, moreover, that for given  $\theta$  and  $E$ ,  $t_{\frac{1}{2}}$  fluctuates, presumably as a result of variability in starting points and subsequent development of AS, possibly also because of differences in mass of the primary particles (Walker and Watson 1982).

The early results near the axis have been confirmed (Woidneck and Böhm 1975, Sakayama and Suzuki 1981), but until recently no further results had been reported on arrival times measured with scintillators at large distances, nor had data been published on measures of thickness other than  $t_{\frac{1}{2}}$  (and  $\langle t \rangle$ , the average particle delay). Presently there is

renewed interest in AS thickness at large core distances for 3 reasons:

- 1) a disagreement between the S(600) spectrum (equivalent to the primary cosmic ray energy spectrum) reported by a group in Yakutsk (Diminstein et al. 1982) and similar results obtained in the Volcano Ranch and Haverah Park experiments (Bower et al. 1983). It has been suggested that this may result from some peculiarity of the Yakutsk electronic system related to signal durations (Bower et al. 1982),
- 2) the presence of so-called SLP's (sub-luminal pulses) observed with scintillators, apparently caused by the low energy nucleon component of AS (Linsley 1984),
- 3) a suggestion for using pulse widths to measure AS impact parameters, increasing by an order of magnitude the area that can be made sensitive to  $10^{20}$  eV cosmic rays for a given cost (Linsley 1983, Brooke et al. 1983, Hazen and Hazen 1983, Clay and Dawson 1984).

In response to this interest, records from the Volcano Ranch experiment (oscilloscope photographs) have been re-examined. Given here are results from this re-examination, together with new results derived from previously published Volcano Ranch data (LSR, LS).

2. Arrival Time Dispersion. In some applications, notably (3) above, the shower plane may not be well determined by the data, so an appropriate measure of shower thickness is the separate event arrival time dispersion defined by  $\sigma_t = [\int (t - \langle t \rangle)^2 p(t) dt]^{1/2}$ , rather than  $t_{1/2}$ , where  $p(t)$  is the probability of a particle arriving in time interval  $dt$ . Volcano Ranch records provide 3 avenues by which estimates of  $\sigma_t$  can be obtained:

- 1) a previously published set of signals from a certain unusually large AS, notable because they afford good statistical accuracy at quite large impact parameters,
- 2) previously published arrival time histograms for single particles in smaller AS, affording good statistical accuracy at smaller impact parameters,
- 3) original photographic records of 16 especially large AS from 1962-63.

It is shown that an empirical formula which fits the data at smaller impact parameters (average small AS, data set 2 above) is consistent with the data at larger impact parameters (set 1). It is then shown by means of the previously unpublished data (set 3) that the single large AS is in fact typical, and that pulse width fluctuations are tolerably small. Data set 3, containing events with  $\theta$  ranging from  $7^\circ$  to  $55^\circ$ , also yields the zenith angle dependence of  $\langle \sigma_t \rangle$ .

Data set 1 consists of 8 graphically deconvoluted signals from scintillators at impact parameters  $> 1.3$  km. The estimates of core location, size and energy for this event (LSR) have since been revised on the basis of a detailed study of shower structure (Linsley 1977). The final values used here are given in the *Catalogue of Highest Energy Cosmic Rays*, together with values of many subsidiary quantities for the same event, No. 2533 (size  $1.1 \cdot 10^{10}$  particles,  $E = 5.6 \cdot 10^{19}$  eV,  $\theta = 42^\circ$ ; Linsley 1980). For the present purpose the signals were sorted into 2 groups according to  $r$ , and those in each group were combined. For each group the dispersion is given in Table 1 with standard estimates of the statistical error.

Table 1. Width of signals, AS No. 2533

av. r (km)	No. of parti- cles	mean delay (ns)	dispersion (ns)
1.45	91	840 ± 60	610 ± 45
1.80	33	1260 ± 200	1140 ± 140

small. If this is correct then the dispersion values given in Table 1 will be consistent with those obtained by the method of LS, in which distributions for various  $r$  intervals were built up from single particle delays for many AS with widely ranging values of  $N$  (shower size) and  $\theta$ . Results on dispersion were not given in that article, so they have now been calculated from the single particle delay histograms that were given. The new results are listed in Table 2. Inspection shows that they are reasonably consistent with those for the one large event (Table 1), and that all of the data, including data at small core distances referred to in the Introduction, can be represented by the empirical formula

$$\langle \sigma_t \rangle = \sigma_{t0} (1 + r/r_t)^b \quad (1)$$

with  $\sigma_{t0} = 2.6$  ns,  $r_t = 30$  m, and  $b \sim 1.5$ . When these fixed values are taken for  $\sigma_{t0}$  and  $r_t$ , the value of  $b$  controls the fit at large distances. A best value for  $b$  will be determined next from data set 3.

The original records for all years of Volcano Ranch operation except the last one (1962-1963) have been lost, so it is not possible to re-examine the record of event No. 2533. Records still exist, however, for more than 500 large AS, including 16 which satisfied the condition ( $E > 10^{19}$  eV) for being listed in the *Catalogue of Highest Energy Cosmic Rays*. The proposed method of determining  $r$  (and hence  $E$ ) from  $\sigma_t$  and  $S$  (integrated particle density) at a single location was tested using these 16 events (Linsley 1983). An intermediate result of the test is another set of  $\sigma_t$  values given in Table 3. Because they belong to different events these values will reveal whether fluctuations of  $\sigma_t$  are likely to be troublesome. By agreeing fairly well on average with Table 1 they show that No. 2533 is indeed typical of AS with  $E > 10^{19}$  eV. By agreeing on average with Table 2 they show that  $\langle \sigma_t \rangle$  hardly changes between  $10^{17}$  and  $10^{19}$  eV.

The Volcano Ranch array consisted of 19 detectors. For events such as these most of them were struck by one or more particles. The first step was to select in an unbiased manner one pulse per event. It should not be too small because of statistical errors nor too large because of electronic distortion. The one chosen in each case is the one with greatest  $S$  such that  $S < 7 \text{ m}^{-2}$ . The number of particles contributing to the various AS pulses ( $n = A \cos \theta$ , where  $A$  is the de-

It was stated in LSR that this event is typical, meaning that 1) to first order the arrival time distribution is independent of shower size or zenith angle, depending only on  $r$ , and 2) for given  $N$ ,  $\theta$ ,  $r$  the fluctuations in this distribution due to variability in starting points, development, etc. are relatively

Table 2. Width of single particle arrival time distribution

r (km)	No. of parti- cles	mean delay (ns)	dispersion (ns)
0.46	62	238 ± 20	152 ± 10
0.55	202	271 ± 17	242 ± 12
0.65	289	307 ± 16	280 ± 12
0.75	193	330 ± 24	329 ± 17
0.85	161	534 ± 35	448 ± 25
0.95	167	475 ± 39	508 ± 28
1.10	169	649 ± 50	671 ± 36
1.35	88	683 ± 73	660 ± 50

Table 3. Width of separate event arrival time distributions

serial number	$\theta$ (deg)	r (km)	No. of particles	dispersion (ns)
4827	28	1.3	17	490 $\pm$ 80
4835	31	1.7	10	1040 $\pm$ 230
4860	12	1.3	19	710 $\pm$ 120
4882	40	2.0	9	880 $\pm$ 200
4906	25	1.1	19	1090 $\pm$ 180
4925	7	1.3	12	690 $\pm$ 140
4929	55	1.4	11	200 $\pm$ 40
4946	37	1.2	13	760 $\pm$ 150
4985	39	1.3	9	690 $\pm$ 170
5005	23	1.3	10	860 $\pm$ 190
5051	40	1.2	9	350 $\pm$ 80
5059	31	1.6	6	1550 $\pm$ 450
5072	32	0.9	18	540 $\pm$ 90
5171	54	1.2	10	380 $\pm$ 90
5216	16	1.3	22	920 $\pm$ 140
5280	52	1.5	8	750 $\pm$ 190

tector area, 3.26 m<sup>2</sup>) ranges from 6 to 22, averaging 12. The values of r range from 0.9 to 2.0 km, averaging 1.4 km.

The AS pulses and a bandwidth-limited (BWL) test pulse were digitized and the dispersions were calculated. The dispersion of the input signal was taken as  $(\sigma_{\text{obs}}^2 - \sigma_{\text{BWL}}^2)^{1/2}$ . Sub-luminal pulses, present in 2 cases, were disregarded in calculating  $\sigma_{\text{obs}}$ . Thanks to an astute anonymous reviewer it was noted that the data of Table 3 contain useful information about the zenith angle dependence of  $\langle\sigma_t\rangle$ . A convenient way to express this is through the parameter b in (1), by letting  $b = b_1 + b_2 \sec\theta$ . By use of least squares one obtains  $b = (1.94 \pm 0.08) - (0.39 \pm 0.06) \sec\theta$ . Using this expression in (1), there is excellent agreement between Tables 1, 2 and 3. The individual

values of  $\sigma_t / \langle\sigma_t\rangle_{\text{calc}}$  have about 3 times the variance expected from the simple statistical errors. The excess variance is due in part to systematic differences in primary energy and possibly primary mass, in part to random instrumental errors, and in part to AS fluctuations. By neglecting the first two types of contribution one obtains an upper limit of 20% for the amount of fluctuation in  $\sigma_t$  due to fluctuations in level of origin and shower development.

3. Conclusions. Eq. 1 with  $\sigma_{t0} = 2.6$  ns,  $r_t = 30$  m, and  $b = (1.94 \pm 0.08) - (0.39 \pm 0.06) \sec\theta$  represents the average dispersion in arrival time of AS particles as measured with scintillators when SLP's are excluded. The dispersion is not strongly energy dependent over the range  $10^8 < E < 10^{11}$  GeV. The fluctuation in  $\sigma_t$  due to fluctuations in level of origin and shower development is less than 20%.

References. BASSI et al. 1953, Phys. Rev. 92, 441; BAXTER et al. 1965, Proc. 9th ICRC 2, 724; BOWER et al. 1982, Proc. 8th European Cosmic Ray Symposium, paper B-1.4; BOWER et al. 1983, J. Phys. G: Nucl. Phys. 9, L53; BROOKE et al. 1983, Proc. 18th ICRC 8, 140; CLAY and DAWSON 1984, Aust. J. Phys. 37, 309 (includes data for intermediate distances); DIMINSTEIN et al. 1982, Bull. Nausho-technithekoj Informasii (Yakutsk) 9, 537 and Proc. 8th European Cosmic Ray Symposium, paper B-1.2; HAZEN and HAZEN 1983, Proc. 18th ICRC 6, 14; LINSLEY et al. 1961, Phys. Rev. Lett. 6, 485; LINSLEY and SCARSI 1962, Phys. Rev. 128, 2384; LINSLEY 1977, Proc. 15th ICRC 12, 56, 62, 89; 1980, Catalogue of Highest Energy Cosmic Rays, ed. M. Wada (Tokyo: World Data Centre C2) 1, 3; 1983, Univ. New Mexico Research Note UNML-6/20/83; 1984, J. Phys. G: Nucl. Phys. 10, L191; SAKAYAMA and SUZUKI 1981, Proc. 17th ICRC 11, 309; WALKER and WATSON 1981, J. Phys. G: Nucl. Phys. 7, 1297; 1982, J. Phys. G: Nucl. Phys. 8, 1131; WOJDNECK and BÖHM 1975, J. Phys. A: Math, Nucl. Gen. 8, 1004.



STUDY OF THE TIME-DIFFERENTIATED PARTICLE FLUX DENSITY AT  
VARIOUS DISTANCES FROM EAS AXIS

V.G. Atrashkevich, R.J. Chernykh, Yu.A. Fomin, G.K. Garipov,  
G.B. Khristiansen, G.V. Kulikov, A.P. Lebedev, S.J. Matsenov,  
V.J. Nazarov, A.A. Silaev, V.J. Solovyeva, V.P. Sulakov,  
A.V. Trubitsyn, O.V. Vedeneev  
Institute of Nuclear Physics, Moscow State University,  
Moscow 119899, USSR

This work is devoted to studying the EAS time structure with the enlarged EAS array of the Moscow State University. The array was described earlier in /1,2/.

The time measurements are made using 22 scintillators which form 13 rectangles of  $180 \times 190 \text{ m}^2$  size covering the entire array area. The array was triggered by a signal of 4-fold coincidences of the pulses from the detectors forming each of the rectangles.

The data presented below were obtained during 2200 hours of the array operation in 1984. 816 showers to which at least 14 of 22 scintillator detectors responded were selected among all the detected showers. The coordinates of the EAS axis in the observation plane and the EAS sizes were determined by the maximum likelihood method using a computer /1/ on the assumption that the electron LDF is of the NKG form. 492 showers in the interval of EAS size  $N_e = 5 \times 10^6 - 2 \times 10^8$  ( $\bar{N}_e = 1.7 \times 10^7$ ) with zenith angles  $\theta \leq 45^\circ$  and axes within the array were analyzed.

The spatial orientation of the shower axis was determined using only the data of four scintillators included in the rectangle containing shower axis (it is called central system). The shower axis angles  $\theta, \varphi$  were found on the assumption of a plane shower front /2/. The front plane was drawn through the central system detector with the maximum detected density of the charged particle flux. The delays of the particle arrivals at the detectors  $\tau$  were

treated with respect to front plane. The r.m.s. error of the distribution of the delays with respect to the front plane in the central system is  $\sigma = 8$  ns for 492 showers as the whole. To have a sufficiently reliable determination of the shower front plane, we selected the events in which the maximum delays in the central system detectors did not exceed 10 ns. (The r.m.s. error of the distribution derived from the analysis of the showers with  $N_e \geq 7 \cdot 10^7$  proves to be  $\sigma = 5$  ns). At the above mentioned value of the maximum delay (10 ns),  $\sigma$  of the distribution is 4 ns and the spreads of angles are  $\Delta\theta \leq 1.6^\circ$  and  $\Delta\varphi \leq 5.6^\circ$ . This criterion was used to select 341 showers.

To obtain the distribution  $f(\tau)$  of the delays in the times of particle arrival at the detector relative to the shower front we examined the showers with  $N_e = (0.5-2) \times 10^7$  and made allowance for the delays accompanied by the respences of not more than  $m=5$  Geiger counters (the value  $m=5$  corresponds in average to the passage of a single particle through a scintillator). Analysis of the dependence  $f(\tau)$  on  $m$  shows that  $f(\tau)$  does not depend on  $m$  for  $m \leq 5$  in the present statistics (see also /2/).

The distributions of the delays  $f(\tau)$  for three intervals of distances  $\Delta R_l$  from shower axis are given in Fig. 1. The negative delays in the distributions of the particle arrival times are contingent on the errors in determining the angles  $\theta, \varphi$  and, probably, on the mesons moving ahead of EAS electrons at large Lorentz factors. The distributions exhibit durable falls which extend at the level of several events up to the delays of  $\sim 2$  mcs (at  $R_l = 300-600$  m) and cannot be accounted for by random particles. The fraction of such events is  $\sim 3\%$  of all events.

From the fig. 1 it is seen that when moving away from EAS axis the mean delay  $\bar{\tau}$  and the r.m.s. error  $\sigma$  increase while the relative shower disc depth  $\sigma/\bar{\tau}$  does not vary within the errors. The value of  $\bar{\tau}$  may be used to estimate the shower curvature radius. At the mean distances

from the axis of 270 m, 350 m and 470 m, the curvature radii are obtained to be ( in km)  $1.43 \pm 0.06$ ;  $1.5 \pm 0.07$ ;  $1.57 \pm 0.06$ , respectively.

It is seen that there is a tendency for increasing of curvature radius with increasing the distance from shower axis. The values obtained are much below the curvature radii when many particles traverse a detector ( see below). The difference may be accounted for by the fact that the high values of the curvature radii observed at high densities are determined by the fastest particles produced high in the atmosphere which are probably muons /3/ or electrons from the photons converted near the array. In case of the passage of single particles through a detector the curvature radius characterizes the altitude where the major bulk of the particles are produced.

The dependence of the distribution  $f(\tau)$  on the shower age  $S$  was studied for two intervals of distances from EAS axis. With this purpose, the examined showers were broken into two groups with  $S < 1.45$  ( $\bar{S} = 1.35$ ) and  $S \geq 1.45$  ( $\bar{S} = 1.55$ ). The values of  $\bar{\tau}$ ,  $\sigma$  and  $\sigma/\bar{\tau}$  are presented in the Table. From the Table it follows that in each of the intervals of distances from EAS axis, as the shower age increases, the mean delay of particle arrivals  $\bar{\tau}$  decreases slightly, while the values of  $\sigma$  and  $\sigma/\bar{\tau}$  are within the errors. The more statistics is required to obtain the final result on the dependence  $f(\tau)$  on  $S$ .

15 showers with  $N_e \geq 7 \times 10^7$  were selected for estima-

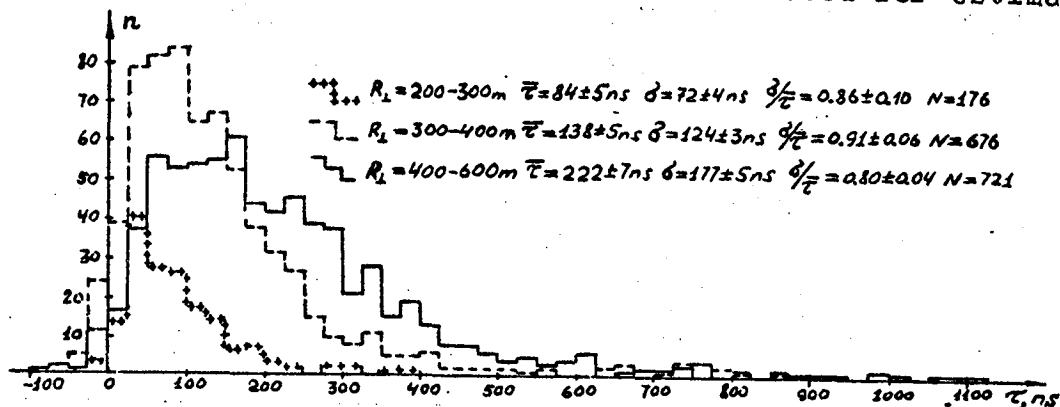


Fig. 1

$R_1, m$	300-400			400-600		
	$\bar{\tau}, ns$	$\mathcal{Z}, ns$	$\mathcal{Z}/\bar{\tau}$	$\bar{\tau}, ns$	$\mathcal{Z}, ns$	$\mathcal{Z}/\bar{\tau}$
$S \geq 1.45$	$129 \pm 6$	$121 \pm 6$	$0.94 \pm 0.08$	$207 \pm 8$	$172 \pm 6$	$0.83 \pm 0.06$
$S < 1.45$	$148 \pm 7$	$127 \pm 5$	$0.86 \pm 0.08$	$246 \pm 11$	$184 \pm 8$	$0.75 \pm 0.06$

measuring the shower front curvature. The curvature radius was calculated from the readings of individual detectors and was determined using the formula  $R_c = R_1^2 - (C\tau)^2 / 2C\tau$  ( $C$  is speed of light,  $R_1$  is the detector-shower axis distance). One can obtain the distribution  $f(R_c)$  for not so big  $R_c$ , this is a consequence of errors in  $\tau$ . Therefore, the values of  $R_c > 10$  km (which corresponds to  $\tau = 2\mathcal{Z}$ ,  $\mathcal{Z} = 5$  ns) are excluded. Fig. 2 shows the resultant curvature radius distributions for three intervals of distances from shower axis. From the values presented it follows that the mean curvature radius of shower front does not vary within the errors at distances of 200-500 m from shower axis.

It should be noted that the distribution  $f(R_c)$  does not arise because of different  $R_c$  for different EAS. The distribution exists also in individual showers. This result means that there are big fluctuations in different altitude contribution to the flux of shower-front particles at a given distance from the axis.

#### References

1. Vernov S.N. (1979), et al. ICRC, Kyoto, v.8, p.129.
2. Atrashkevich V.B. et al. (1985), Izv. Akad. Nauk SSSR, ser. fiz. v.49, No.7.
3. Hillas A.M. (1966), ICRC, London, v.2, p. 758.

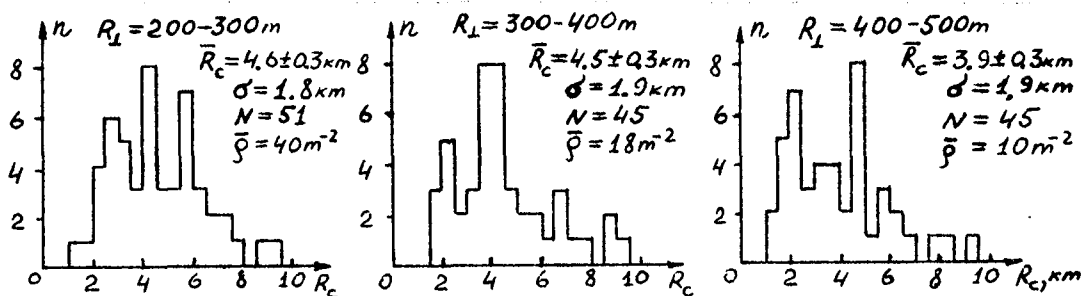


Fig. 2.

367  
AUTHOR INDEX

ABBAS, T  
297

ABOLINS, M  
114

ALIEV, N  
191,195  
187

ALIMOV, T  
191,195  
187

ANTONOV, RA  
52

ARVELA, H  
284,288

ASAKIMORI, K  
64,107,179

ASH, AG  
81,89,93  
94

ASHTON, F  
297

ATRASHKEVICH, VG  
363

BAGGE, ER  
175

BAI, GZ  
60

BALTRUSAITIS, RM  
159,155

BASAK, DK  
56,101,105

BASHINDJAGHYAN, GL  
183

BAZHUTOV, YUN  
151

BERDZENISHVILI, OL  
98

BLAKE, FR  
123,127  
215

BOFILL, J  
114

BOGERT, D  
114

BOWEN, T  
280

BOYAADJIAN, NG  
32

BROCK, R  
114

BULL, RM  
81

BURNSTEIN, R  
114

BUSZA, W  
114

CAPDEVIELLE, JN  
139,20,24

CASSIDAY, GL  
159,155

CHAN, SK  
131,252  
347

CHAUDHURI, N  
56,101,105

CHERNYKH, RJ  
363

CHEUNG, T  
135

CHO, C  
115

CHUBENKO, AP  
40

CHUYKOVA, TA  
211

COHEN, A  
114

COOPER, R  
159,155

DAIGO, M  
171

DAKE, S  
69

DALLAKYAN, PYU  
32

DANILOVA, TV  
40,260

DATTA, P  
272

DE VILLIERS, EJ  
351

DEDENKO, LG  
147,48

DORMAN, LI  
304

DUBOVY, AG  
40

DZIKOWSKI, T  
111

EDWARDS, PG  
235

EFIMOV, NN  
48,207

EL-ELA, AA  
175

ELBERT, JW  
159

ELBERT, R

368  
AUTHOR INDEX

ELBERT, R		GROMOV, YA	
	155		98
ELLSWORTH, RW		GUPTA, SC	
	114		114
ENOKI, T		GUSEV, GA	
	324,328		264
ERLYKIN, AD		HALVERSON, P	
	40,260		280
ERMAKOV, GG		HALZEN, F	
	151		219
ERNWAIN, J		HARADA, K	
	114		69
FENYVES, EJ		HARA, T	
	143		77,119,171
FISK, R			320
	114	HASSAN, S	
FOMIN, VP			175
	203	HATANO, Y	
FOMIN, YUA			77,293,320
	363,151		312
	207	HATCHER, R	
FREUDENREICH, H			114
	114	HAYASHIDA, N	
FUESS, S			77,119,320
	114	HAZAMA, M	
FUKUSHIMA, Y			69
	73	HAZEN, ES	
GALKIN, VI			336,60,347
	211,52	HAZEN, WE	
GARIPOV, GK			336,60,339
	363		347
GARYAKA, AP		HE, CX	
	32		320
GAWIN, J		HEIN, LA	
	139,20,24		52
	111	HIGASHI, S	
GENG, QX			115
	60	HILLAS, AMM	
GERHARDY, PR			231
	159,155	HIRAOKA, N	
GHOSH, B			115
	101,105	HODSON, AL	
GLUSHKOV, AV			81
	48	HONDA, M	
GOODMAN, JA			171,320
	114	HORIKI, T	
GOODMAN, MC			293,312
	114	INOUE, K	
GOSWAMI, GC			68
	101	INOUE, N	
GRIGORIEV, VM			316
	207	ISAEV, VI	
GROCHALSKA, B			151
	24	ISHIKAWA, F	

369  
AUTHOR INDEX

ISHIKAWA, F	320	LEBEDEV, AP	363
IVANENKO, IP	211,52	LEE, YW	256
JAROCKINA, ZV	151	LIEBING, DF	199
KAKHHAROV, N	191	LI, GJ	60
KAKHKHAROV, M	195,187	LING, J	60
KAKIMOTO, F	268,324	LINSLEY, J	167,359
	328		355,163
KALMYKOV, NN	187,44,151		163
	207	LIU, JG	60
KAMATA, K	119,171	LIU, ZH	60
	320	LOH, EC	159,155
KAMEDA, T	64,107,179	LUKSYS, M	123,127
KANEVSKY, BL	52	LUMME, M	284,288
KAWAMOTO, M	69,316	MACKEDOWN, PK	135
KHACHATURYAN, LS	98	MADANI, J	297
KHAKIMOV, N	191,195	MAEDA, T	64,107,179
KHALAFYAN, AZ	183		316
KHRENOV, BA	151	MAGAHIZ, R	114
KHRISTIANSEN, GB	191,195	MAKAROV, IT	48
	187,363,44	MAKHMUDOV, BM	304,195
	151,207		187
KIFUNE, T	77,171	MAMIDJANIAN, EA	32
KOSLOV, VD	155	MARKOV, MA	264
KOTLYAREVSKI, DM	98	MATSENOV, SJ	363
KUBIAK, G	16	MATSUBARA, Y	119,320
KULIKOV, GV	363,147	MATTISON, T	114
	151	MAZUMDAR, GKD	276,301
KUSUNOSE, M	293,312	MIRONOV, AV	260
KUZMIN, VA	52	MISAKI, Y	64,107,179
LAWRENCE, MA	332		

370  
AUTHOR INDEX

MISAKI, Y	316	NISHIOKA, A	293,312
MIZUMOTO, Y	159,155	NOVALOV, AA	98
	171	OGANEZOVA, JS	183
MIZUSHIMA, K	64,107,179	OHMORI, N	312
MKHITARYAN, VM	183	OHNO, Y	171
MORFIN, J	114	OHOKA, H	119,320
MORI, M	320	OHSKA, T	114
MOTOVA, MV	44,151,207	OKADA, A	251
MUKHERJEE, A	114	OSBORNE, L	114
MUKHERJEE, N	105	OZAKI, S	115
MURAKI, Y	251	PATHAK, KM	272,276
NAGANO, M	77,119,171		301
	320	PATTERSON, JR	199
NAKATSUKA, T	293,293	PAZIASHVILI, IV	98
	312	PELTONEN, J	284,288
NASH, WF	123,127	PERKINS, G	114
	215	PITT, R	114
NAZAROV, VJ	363	POPOVA, L	85
NECHIN, YUA	207	PRAVDIN, MI	48
NESHPOR, YI	203	PROCUREUR, J	9
NESTEROVA, NM	40	PROSHKINA, IP	151
NG, LK	256,131	PROSIN, VV	195,187
	252,343		207
	347	PROTHEROE, RJ	235
NIEMINEN, M	284,288	RAKHIMOVA, N	191,195
NIKIFOROVA, ES	207		187
NIKOLSKY, SI	247	RAO, MVS	239
NISHI, K	268,324	ROGANOVA, TM	211
	328	ROSENSON, L	
NISHIMURA, J	308		
NISHIOKA, A			

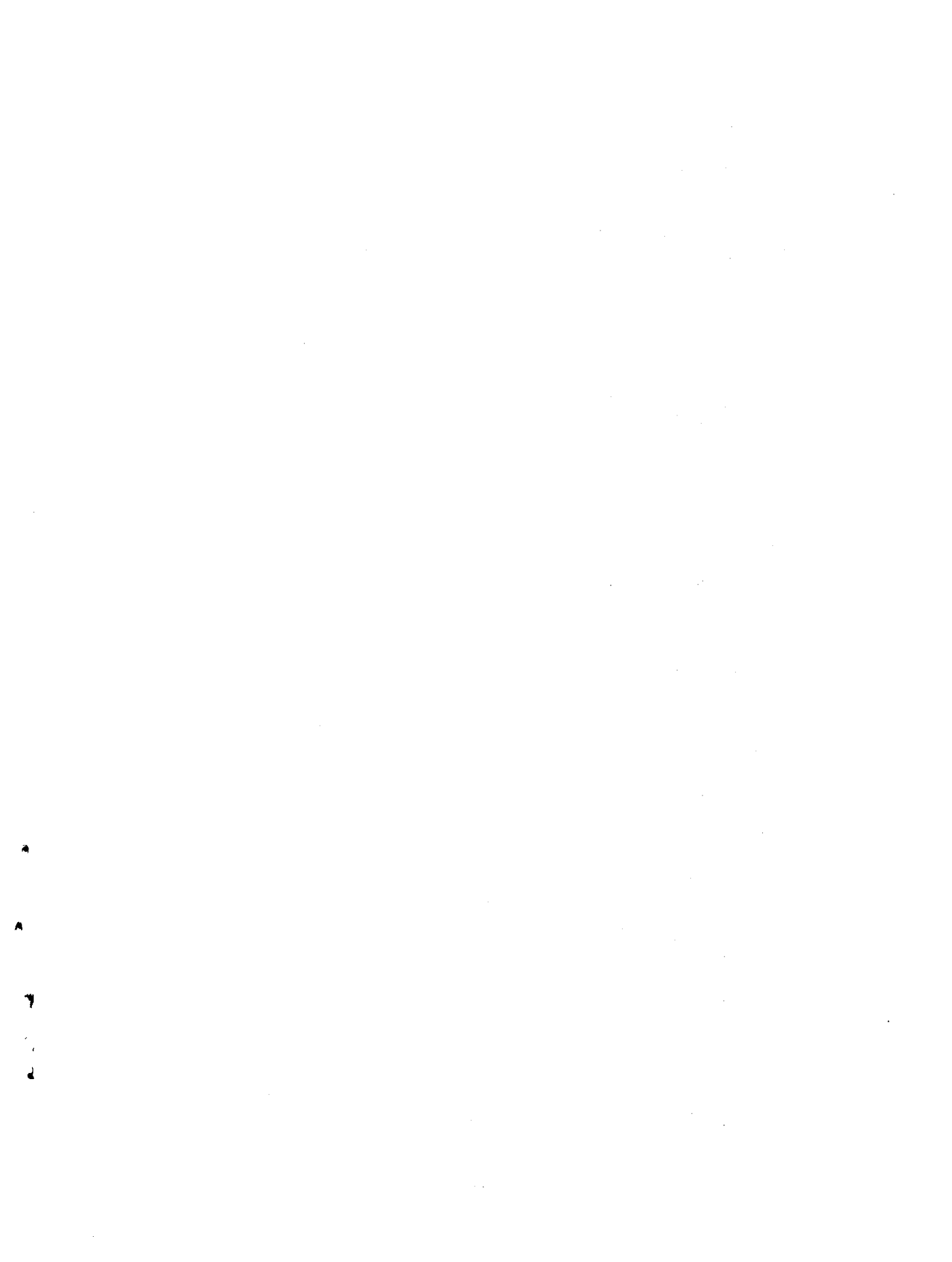


371  
AUTHOR INDEX

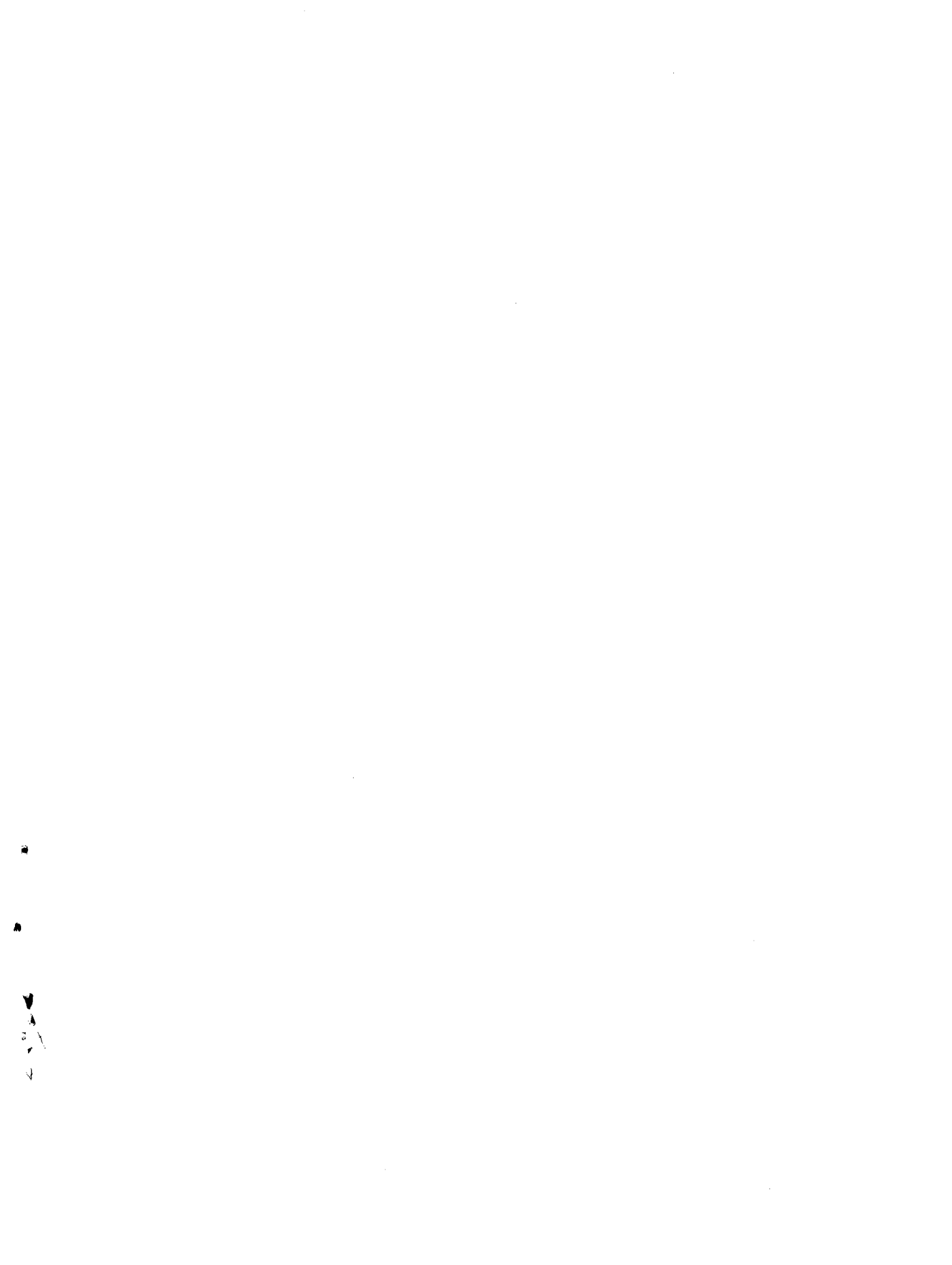
ROSENSON, L  
114  
ROY, S  
36  
RUKOVICHKIN, VP  
151  
RUSISHVILI, NS  
98  
SAITO, T  
73  
SAKATA, M  
69,73  
SAKUYAMA, H  
68  
SANDACZ, A  
114  
SARKAR, S  
105  
SARYCHEVA, LI  
183  
SASAKI, H  
293,312  
SATO, T  
115  
SEPHTON, AJ  
123,127  
SHARVADZE, ZS  
98  
SHIMA, M  
73  
SHITOV, VG  
203  
SHKURENKOV, AV  
151  
SILAEV, AA  
363  
SINEV, NB  
183  
SINHA, M  
36  
SINHA, S  
239  
SIRODZHEV, N  
304  
SIVAPRASAD, K  
114,292  
SOKOLSKY, P  
159,155  
SOLOVJEVA, VI  
147,151  
SOLOVYEVA, VJ  
363  
STAMENOV, JN  
9,243,247  
STANEV, T  
143,219  
STAVREV, PV  
9  
STECK, D  
159,155  
STEMANETYAN, GZ  
98  
STEPANIAN, AA  
203  
STEPHENS, SA  
223,227  
STREITMATTER, RE  
223,227  
STRONGIN, B  
114  
SUGA, K  
268,324  
328  
SUGIHARA, T  
69  
SULAKOV, VP  
363,147  
151  
SUWADA, T  
115  
SUZUKI, N  
68  
SUZUKI, T  
68  
SZABELSKI, J  
16  
TAKAHASHI, T  
115  
TAKEUCHI, T  
316  
TANAHASHI, G  
5,77,119  
171,320  
TARTAGLIA, M  
114  
TASHPULATOV, R  
191,304  
195,187  
TAYLOR, FE  
114  
TESHIMA, M  
320  
TESHIMA, T  
119  
TONWAR, SC  
28,114  
TORSTI, JJ  
284,288

372  
AUTHOR INDEX

TOYODA, Y 316  
TRUBITSYN, AV 363,151  
TSMAYA, PV 98  
TSUCHIMOTO, I 324,328  
TUKISH, EI 260  
UMEDA, H 115  
USHEV, SZ 9,247  
VAINIKKA, E 284,288  
VALIHODZHAEV, F 304  
VALTONEN, E 284,288  
VAN DER WALT, DJ 351  
VANCOV, K 243  
VANKOV, CP 219  
VASHKEVICH, VV 151  
VEDENEEV, OV 363  
VERBETSKI, YG 98  
VERDIER, R 114  
VLADIMIRSKY, BM 203  
VODENICHAROVA, T 243  
WATSON, AA 332  
WADOWCZYK, J 16,111  
WERTHMANN, A 114  
WEST, AA 332  
WHITAKER, S 114  
WROTNIAK, JA 1,12  
YAMAMOTO, Y 73  
YEH, GB 114  
YERSHOV, AA 183  
YODH, GB 1,12,114  
YUNN, BC 143  
ZHELEZNYKH, IM 264  
ZHUKOV, VV 207  
ZHUKOV, VYU 195  
ZYSKIN, YL 203







# BIBLIOGRAPHIC DATA SHEET

1. Report No. NASA CP-2376 Volume 7	2. Government Accession No.	3. Recipient's Catalog No.	
4. Title and Subtitle 19th International Cosmic Ray Conference Conference Papers		5. Report Date August 1985	
		6. Performing Organization Code 665	
7. Author(s) Frank C. Jones, compiler		8. Performing Organization Report No.	
9. Performing Organization Name and Address Laboratory For High Energy Astrophysics Goddard Space Flight Center Greenbelt, MD 20771		10. Work Unit No.	
		11. Contract or Grant No.	
		13. Type of Report and Period Covered  Conference Publication	
12. Sponsoring Agency Name and Address National Aeronautics and Space Administration Washington, D. C. 20546		14. Sponsoring Agency Code	
15. Supplementary Notes			
16. Abstract These volumes contain papers submitted for presentation at the 19th International Cosmic Ray Conference, held on the campus of the University of California, San Diego, in La Jolla, CA., August 11-23, 1985. The conference is held every other year. The present volume contains papers with Paper Codes HE 4.1 through HE 4.7 and deals with various aspects of extensive air showers (EAS), produced by energetic particles and gamma rays.			
17. Key Words (Selected by Author(s)) EAS theories and simulations, EAS cores, EAS density spectra, EAS muons, EAS electrons, Cerenkov radiation, energy calibration, gamma rays, EAS arrival times, mini-arrays		18. Distribution Statement Unclassified - Unlimited  Subject Category - 93	
19. Security Classif. (of this report) Unclassified	20. Security Classif. (of this page) Unclassified	21. No. of Pages	22. Price*





National Aeronautics and  
Space Administration

**Goddard Space Flight Center**  
Greenbelt, Maryland 20771